frontiers | Research Topics

Novel approaches to prevention, diagnosis, and treatment of bacterial and viral infections of clinical relevance

Edited by
George William Carnell, Leon G. Leanse and Claudia Maria Trombetta

Published in
Frontiers in Microbiology

ISSN 1664-8714
ISBN 978-2-8325-2296-7
DOI 10.3389/978-2-8325-2296-7

About Frontiers

Frontiers is more than just an open access publisher of scholarly articles: it is a pioneering approach to the world of academia, radically improving the way scholarly research is managed. The grand vision of Frontiers is a world where all people have an equal opportunity to seek, share and generate knowledge. Frontiers provides immediate and permanent online open access to all its publications, but this alone is not enough to realize our grand goals.

Frontiers journal series

The Frontiers journal series is a multi-tier and interdisciplinary set of open-access, online journals, promising a paradigm shift from the current review, selection and dissemination processes in academic publishing. All Frontiers journals are driven by researchers for researchers; therefore, they constitute a service to the scholarly community. At the same time, the *Frontiers journal series* operates on a revolutionary invention, the tiered publishing system, initially addressing specific communities of scholars, and gradually climbing up to broader public understanding, thus serving the interests of the lay society, too.

Dedication to quality

Each Frontiers article is a landmark of the highest quality, thanks to genuinely collaborative interactions between authors and review editors, who include some of the world's best academicians. Research must be certified by peers before entering a stream of knowledge that may eventually reach the public - and shape society; therefore, Frontiers only applies the most rigorous and unbiased reviews. Frontiers revolutionizes research publishing by freely delivering the most outstanding research, evaluated with no bias from both the academic and social point of view. By applying the most advanced information technologies, Frontiers is catapulting scholarly publishing into a new generation.

What are Frontiers Research Topics?

Frontiers Research Topics are very popular trademarks of the *Frontiers journals series*: they are collections of at least ten articles, all centered on a particular subject. With their unique mix of varied contributions from Original Research to Review Articles, Frontiers Research Topics unify the most influential researchers, the latest key findings and historical advances in a hot research area.

Find out more on how to host your own Frontiers Research Topic or contribute to one as an author by contacting the Frontiers editorial office: frontiersin.org/about/contact

Novel approaches to prevention, diagnosis, and treatment of bacterial and viral infections of clinical relevance

Topic editors

George William Carnell — University of Cambridge, United Kingdom
Leon G. Leanse — University of Gibraltar, Gibraltar
Claudia Maria Trombetta — University of Siena, Italy

Citation

Carnell, G. W., Leanse, L. G., Trombetta, C. M., eds. (2023). *Novel approaches to prevention, diagnosis, and treatment of bacterial and viral infections of clinical relevance*. Lausanne: Frontiers Media SA. doi: 10.3389/978-2-8325-2296-7

Table of contents

frontiers | Frontiers in Microbiology

TYPE Editorial
PUBLISHED 13 April 2023
DOI 10.3389/fmicb.2023.1192435

OPEN ACCESS

EDITED AND REVIEWED BY
Axel Cloeckaert,
Institut National de recherche pour l'agriculture, l'alimentation et l'environnement (INRAE), France

*CORRESPONDENCE
Leon G. Leanse
✉ leon.leanse@unigib.edu.gi

SPECIALTY SECTION
This article was submitted to Infectious Agents and Disease, a section of the journal Frontiers in Microbiology

RECEIVED 23 March 2023
ACCEPTED 24 March 2023
PUBLISHED 13 April 2023

CITATION
Leanse LG, Trombetta CM and Carnell GW (2023) Editorial: Novel approaches to prevention, diagnosis, and treatment of bacterial and viral infections of clinical relevance. *Front. Microbiol.* 14:1192435. doi: 10.3389/fmicb.2023.1192435

Editorial: Novel approaches to prevention, diagnosis, and treatment of bacterial and viral infections of clinical relevance

Leon G. Leanse[1,2]*, Claudia Maria Trombetta[3] and George W. Carnell[4]

[1]Health and Sport Sciences Hub, University of Gibraltar, Europa Point Campus, Gibraltar, Gibraltar, [2]Wellman Center for Photomedicine, Massachusetts General Hospital, Harvard Medical School, Boston, MA, United States, [3]Department of Molecular and Developmental Medicine, University of Siena, Siena, Italy, [4]Department of Veterinary Medicine, University of Cambridge, Cambridge, United Kingdom

KEYWORDS

bacterial diagnosis, viral diagnosis, infection treatment, vaccination, novel application

Editorial on the Research Topic
Novel approaches to prevention, diagnosis, and treatment of bacterial and viral infections of clinical relevance

In the era of antimicrobial resistance, infectious diseases are ranked among the most serious global health threats. This concern continues to be perpetuated by the current COVID-19 pandemic which has reinvented the scientific, cultural, and sociological paradigm that drives daily life, illuminating the fact that the ongoing emergence and re-emergence of pathogenic microorganisms place a burden on public health. Considering that the ongoing emergence and re-emergence of pathogenic microorganisms place a burden on public health, therapeutic antimicrobials and vaccines are essential approaches to control infections and prevent pandemic occurrences. However, as new pathogens emerge, therapeutic and vaccine approaches are not always readily available. This is further complicated by pathogens that express variable antigenicity, rendering effective vaccine development difficult. The treatment of pathogens is similarly convoluted in that many infection syndromes present with similar constellations of symptoms, which can obscure the selection of appropriate treatment methods. The current gold-standard methods for diagnosis of bacterial and viral infections often take hours or days to give accurate results that would permit healthcare providers to initiate appropriate treatment, potentially increasing the chances of adverse effects. More worryingly, even with an accurate diagnosis, the ubiquity of pathogens that are resisting conventional therapeutics coupled with those complex pathogens that have no effective or gold-standard treatment within the clinical pipeline (e.g., SARS-CoV-2) makes controlling infectious diseases more difficult. Thus, the development of novel prevention, diagnosis, and treatment methods that effectively control infectious diseases is essential for integration into the clinical pipeline.

Our special issue entitled 'Novel approaches for diagnosis, prevention, and treatment of bacterial and viral infections of clinical relevance' tackles these very concerns listed above. With a total of 13 articles published within our special issue, many of the research articles are one step closer to adjusting the clinical pipeline to improve current prevention, diagnostic, and treatment platforms against a myriad of bacterial and viral infections of clinical importance.

A study by Rua et al. attempted to improve the diagnosis of bacterial and fungal infections. They utilized Positron emission tomography (PET), which is a non-invasive imaging technique to identify the sites of infection. The authors identified that 2-deoxy-2[^{18}F]fluoro-D-glucose: [^{18}F]FDG, a commonly used radiotracer used in PET, demonstrated uptake at regions of inflammation. However, it does not discriminate between sterile and infectious inflammation. Thus, they evaluated two infection-specific radiotracers 2-deoxy-2-[^{18}F]-fluoro-D-sorbitol ([^{18}F]FDS) and 2-[^{18}F]F-ρ-aminobenzoic acid ([^{18}F]FPABA using 19 bacterial and fungal (yeast) species *in vitro* or within a mouse model with myositis infection. They found that non-lactose fermenters were unable to take up [^{18}F]FDS *in vitro*. Impressively, [^{18}F]FDS could be visualized in *Escherichia coli in vivo*. In addition, it could discriminate between yeasts that have differential sorbitol assimilation capabilities. Conversely, uptake of [^{18}F]FPABA was possible in all bacterial and fungal species. Additionally, it could adequately discriminate between inflammation and infection in the myositis model. The authors concluded that the PET approach using [^{18}F]FPABA may offer an approach to assist in the diagnosis of bacterial and fungal infections.

A complimentary manuscript by Ting et al. touched upon the difficulties associated with the diagnosis of infectious keratitis (IK). They explained how IK is the 5th leading cause of blindness, and how timely diagnosis is essential to mitigate any adverse reactions. They stated that this is not always possible due to clinical delays complicated by a lack of education and the use of medicinal eye drops. A low culture yield, the long turnaround time for culture results, undifferentiated clinical phenotypes, or polymicrobial infection has been shown to further complicate timely diagnosis. They described potential solutions targeted at improving the timeliness of diagnosis. For example, the use of digital innovations such as artificial intelligence-directed imaging techniques to identify an ocular infectious burden. They discussed the use of metagenomic next-generation sequencing (NGS) methods, initially touching upon the use of polymerase chain reaction (PCR) as a strategy to diagnose infectious diseases. With the advancement in NGS technologies, they provided evidence that NGS can identify IK even when the sample in the culture is negative or if the patient was pre-treated with antimicrobials. They concluded that further advancement of digital and NGS methods may change the current IK diagnostic framework. They remain, however, cognizant of the feasibility related to implementing these methods based on accessibility and cost effectiveness.

In another "diagnosis-driven" review, Raeisi et al. touched upon the use of rapid-format recombinant antibody-based methods for the diagnosis of *Clostridiodes difficile* as an effective way to provide a timely diagnosis to limit the rate of infection recurrence and improve the clinical outcome. They touched upon the traditional diagnostic method [i.e., detection of TcdA/TcdB toxins *via* enzyme-linked immunosorbent assay (ELISA)] given that studies demonstrated that their expression is restricted to pathogenic strains. Other methods of diagnosis include cell-culture cytotoxicity neutralization assay, and PCR. The authors suggested that the currently used methods suffer from drawbacks in the form of specificity/sensitivity issues such as long turnaround times, use of polyclonal (pAb) and monoclonal antibodies (mAb) for applications in immunofluorescence, and ELISA, and the methods are more advantageous relative to conventional antibodies given their accurate and reliable production. They are also beneficial as they can be fused with other proteins (i.e., detector enzymes) that increase the rate of reaction and assay sensitivity, thus improving on current gold-standard methods (e.g., ELISA). The authors concluded that recombinant antibodies (rAb) could be a "future trend" when designing highly sensitive diagnostic methods for *Clostridiodes* difficile infection.

Sohail et al. touched upon the role of infectious diseases on Diabetes Mellitus (DM) pathogenesis, specifically patients with DM who are at a high risk of hospitalization and/or death from infectious diseases, with inadequate control of blood glucose levels driving a myriad of infection syndromes. Thus, the authors proposed that a timely infection diagnosis coupled with appropriate glycemic control may be the key to limiting these adverse effects. They suggested that novel high-throughput blood-based immunoassays capable of detecting both infection and hyperglycemia are warranted. The authors presented the most common infections linked to DM and the disease pathogenesis and the use of immunoproteomics in an early infection diagnosis, concluding that the use of antibody screening should be a standard procedure with infection/diabetic screening.

In line with the above-mentioned studies, Wei et al. evaluated a novel rapid nucleic acid amplification method, chips for complicated detection (CCID) based on Loop-mediated isothermal amplification (LAMP), to diagnose elderly patients suffering from pneumonia. In their study on 81 patients, where 57 samples were isolated *via* sputum/airway secretion and 35 from bronchoalveolar lavage, they found the CCID results to be available in 50 min with a limit of detection of 500 copies/reaction. Additionally, they found the sensitivity of CCID to supersede conventional microbiological tests (CMTs), with the percentage of positive results in patients pre-treated with antibiotics for >3 days similarly higher in CCID vs. CMT (91.9% vs. 64.9%). The authors concluded that CCID may offer a rapid approach in the detection of pneumonia in older patients, with the added benefit of being highly sensitive even in patients treated with antibiotics.

In another study by Zhang et al., another novel method, targeted nanopore sequencing (TNPseq), to identify pathogens (and antimicrobial resistance (AMR) genes) causing lower respiratory tract infections (LRTIs) was applied. They recruited 146 patients with suspected LRTIs (median age: 61 years) and used traditional culture or TNPseq to identify pathogens and their associated AMR genes. In 91.1% (133/146) of patients, they identified at least one pathogen using TNPseq. Conversely, using traditional culturing, they only identified pathogens in 37/146 samples (25.3%), illustrating a higher sensitivity of TNPseq, relative to culture. Additionally, TNPseq detected more bacteria and mixed infections, compared to culture. Lastly, TNPseq was effective in detecting AMR genes, such as bla_{TEM}. The authors concluded that TNPseq can efficiently detect pathogens early, thus, providing patients with accurate and timely treatment of LRTIs.

As the COVID-19 pandemic continues, novel diagnostic and treatment regimens continue to be developed such as a study by Pratelli et al. who developed a pooling strategy of real-time

PCR (RT-PCR) to detect SARS-CoV-2. The authors postulated that the detection of SARS-CoV-2 within pooled samples would be a suitable and rapid approach for the mass monitoring of COVID-19 within a population. In their study, they used 17 patients who had previously tested positive for COVID-19 and 19 who were negative, using retested nasal swabs (NS) for their pooling strategy. For the test, one swab from a positive patient was mixed with 19 negative samples (20 NS in total). The pooling strategy detected SARS-CoV-2 to a similar extent to individual tests, demonstrating that even a low viral load is detectable. The authors concluded that this may be a suitable approach to routinely monitor SARS-CoV-2 within a population with low prevalence.

A study by Yu et al. sought to identify biomarkers that indicate liver injury as a result of chronic hepatitis B (CHB). Due to the incidences of hepatocellular carcinoma (HCC) that is associated with CHB, the inability to treat with a hepatectomy, which is the only treatment, increases the importance of identifying liver injury early. Given that expression of cytokines within the liver microenvironment has been shown to mediate liver damage, the authors investigated whether there is a correlation between five specific chemokines (CXCL8, CXCL9, CXCL10, CXCL11, and C-X-C-motif) to see if they may be used as predictors of liver injury. In their study, they recruited 28 healthy patients, 45 patients that suffer from CHB, and 20 patients that do not have HBV infection but have alanine aminotransferase (ALT) concentrations that are comparable to CHB patients. The authors concluded that CXCL8, 9, 10, and 11 can be used as biomarkers to forecast liver injury as a result of HBV infection.

Within the prevention component of our Research Topic, we have a study by Ren et al. that is concerned with the development of an influenza vaccine that confers heterologous protection with H5N1 and H9N2 subtypes. They constructed a replication-deficient recombinant influenza virus, WM01ma-HA(H5), that expresses a chimeric hemagglutinin (HA) protein from H5N1 and H9N2, with flanking neuraminidase (NA) sequence from A/Mink/Shandong/WM01/2014(H9N2)(WM01ma). The authors found this recombinant influenza strain to induce a significant immune response with complete immune protection (following intranasal inoculation), which was observed within a mouse model with H9N2 or H5N1 influenza infection. The authors hope their recombinant candidate vaccine will be effective in preventing future influenza pandemics.

A novel investigation by Xu et al. was performed that evaluated the efficacy mechanism of the Lianhua Qingwen capsule (LHQW), a traditional Chinese medicine, to promote immune function in a mouse model with influenza A infection. Specifically, they aimed to look at the role of intestinal microbiota in reducing pneumonia caused by influenza A infection. In infected mice, they detected influenza within the lungs; histologically evaluated tissue from the lungs and small intestine and biochemical inflammatory indices assessments were performed to assess the severity of the infection and potential amelioration. Additionally, they used 16s rRNA analyses to look at the intestinal microbiota, and network pharmacology techniques were implemented to validate the targets of LHQW. The authors found significant symptoms within the infected group (body weight reduction, and lung/mucosal barrier injury). The intestinal microbiota was similarly perturbed, with observed decreases in *Streptococcus* spp. These symptoms (and viral load) were ameliorated by LHQW. Network pharmacology revealed six putative compounds that may influence the population of microbiota as well as inhibit inflammatory responses *via* Toll-like receptor/nuclear factor kB lung signaling pathways. From the data, the authors inferred that LHQW can be used effectively as a treatment for the symptoms caused by influenza A and the mechanism involved in the regulation of the above-mentioned pathways.

In a clinically focused study, Salomão et al. investigated the role of the placenta in the transmission of chikungunya virus (CHIKV), as the vertical transmission had been reported previously. They studied five placentas of women who were infected with CHIKV during their pregnancy. Findings showed that within 4/5 formalin-fixed placenta samples, there was a positive RT-PCR result for CHIKV. In the 5th case, however, there was a positive RT-PCR in the mother's and baby's serum, validating vertical transmission. Histopathology of the placenta revealed deposits, villus edema, and villous necrosis. Within the placentas that revealed infection, there were increases in $CD8^+$ and $CD163^+$ cells and proinflammatory (IFN-γ and TNF-a) and anti-inflammatory cells (TGF-B and IL-10) cytokines, relative to non-infected placentas. Additionally, CHIKV was detected in trophoblastic cells and decidual cells. The authors concluded that CHIKV alters the placental histology as a result of perturbing its homeostasis, resulting in a potentially harmful fetal environment.

A study by Singh et al. revealed HupB, a nucleoid-associated protein, to be vital for the survival of *Mycobacterium tuberculosis,* in conjunction with being important to tolerate host-mediated stressors and first-line antibiotics. In their investigation, they revealed that HupB can aid in *M. tuberculosis* survival following macrophage attack, such as *via* nutrient depletion, pH alterations, and oxidative/nitrosative stress. They found a *hupB M. tuberculosis* mutant to be highly susceptible to all the stressors mentioned above. Furthermore, the authors revealed that *M. tuberculosis* can appropriately modulate the expression of HupB in order to mitigate the damage associated with these stressors. The authors also reported that HupB can assist in the generation of resistance to both rifampicin and isoniazid, with the *hupB* mutant illustrating increased susceptibility to both these antibiotics even during a short exposure. When the authors overexpressed HupB, they found *M. tuberculosis* to be significantly more tolerant to macrophage-induced stressors. Interestingly, it was observed that in the mutant devoid of HupB, the permeability of the cell wall was reduced as was the efflux pump expression, which led the authors to suggest that this may play a role in increasing susceptibility to host-mediated stress and antibiotic susceptibility. Lastly, the authors found that when HupB was targeted by a small molecule inhibitor, SD1, *M. tuberculosis* became significantly more susceptible to first-line antibiotics. The authors concluded that HupB may be a potential therapeutic target for combination with first-line antibiotics.

A study performed by Liu et al. aimed to investigate the anti-*Staphylococcus* activity of an organic acid extract of *Portulaca oleracea* (OAPO) *in vitro* and *in vivo*. *S. aureus* is an important clinical pathogen and can be responsible for a variety of infections at different sites in humans and livestock. However, due to the occurrence of methicillin-resistant strains and the introduction of strict laws on antibiotic usage in animals in China, new methods are needed to reduce antibiotic usage to kill S. *aureus*. Using a series of experiments, the authors examined the antibacterial activity of the organic acid of OAPO against *S. aureus*.

In vitro antibacterial mechanisms were evaluated based on the integrity and permeability of the cell wall and membrane, scanning electron microscopy, and soluble protein content. A mouse skin wound recovery model was used to assess the antibacterial effects of OAPO on *S. aureus in vivo*. The results showed that the extract of P. oleracea not only inhibits methicillin-resistant *S. aureus* activity *in vitro* but also inhibits *S. aureus*-induced skin damage. Overall, these findings highlight that a botanical extract can inhibit *S aureus in vitro* and *in vivo*, supporting the potential use of OAPO to prevent and control *S. aureus* infections in the near future.

Author contributions

LL wrote the original draft of the manuscript. GC and CT provided edits to finalize the submission. All authors contributed to the article and approved the submitted version.

Conflict of interest

The authors declare that the research was conducted in the absence of any commercial or financial relationships that could be construed as a potential conflict of interest.

Publisher's note

frontiers | Frontiers in Microbiology

TYPE Perspective
PUBLISHED 22 July 2022
DOI 10.3389/fmicb.2022.957957

OPEN ACCESS

EDITED BY
Claudia Maria Trombetta,
University of Siena, Italy

REVIEWED BY
Fulvio Marsilio,
University of Teramo, Italy
Serena Marchi,
University of Siena, Italy
Silvia Spoto,
Policlinico Universitario Campus Bio-Medico, Italy

*CORRESPONDENCE
Annamaria Pratelli
annamaria.pratelli@uniba.it

SPECIALTY SECTION
This article was submitted to Infectious Agents and Disease, a section of the journal Frontiers in Microbiology

RECEIVED 31 May 2022
ACCEPTED 06 July 2022
PUBLISHED 22 July 2022

CITATION
Pratelli A, Pellegrini F, Ceci L, Tatò D, Lucente MS, Capozzi L, Camero M and Buonavoglia A (2022) Severe acute respiratory syndrome coronavirus 2 detection by real time polymerase chain reaction using pooling strategy of nasal samples.
Front. Microbiol. 13:957957.
doi: 10.3389/fmicb.2022.957957

Severe acute respiratory syndrome coronavirus 2 detection by real time polymerase chain reaction using pooling strategy of nasal samples

Annamaria Pratelli[1]*, Francesco Pellegrini[1], Luigi Ceci[2], Daniela Tatò[3], Maria Stella Lucente[1], Loredana Capozzi[4], Michele Camero[1] and Alessio Buonavoglia[5]

[1]Department of Veterinary Medicine, University Aldo Moro of Bari, Valenzano, Italy, [2]Clinical Pathology and Microbiology, Hospital Bonomo, Andria, Italy, [3]Clinical Pathology, Hospital Monsignor Dimiccoli, Barletta, Italy, [4]Istituto Zooprofilattico Sperimentale di Puglia e Basilicata, Putignano, Italy, [5]Dental Surgeon, Capurso, Italy

COVID-19 is a life-threatening multisistemic infection caused by *severe acute respiratory syndrome coronavirus 2* (SARS-CoV-2). Infection control relies on timely identification and isolation of infected people who can alberg the virus for up to 14 days, providing important opportunities for undetected transmission. This note describes the application of rRT-PCR test for simpler, faster and less invasive monitoring of SARS-CoV-2 infection using pooling strategy of samples. Seventeen positive patients were provided with sterile dry swabs and asked to self-collected 2 nasal specimens (#NS1 and #NS2). The #NS1 was individually placed in a single tube and the #NS2 was placed in another tube together with 19 NSs collected from 19 negative patients. Both tubes were then tested with conventional molecular rRT-PCR and the strength of pooling nasal testing was compared with the molecular test performed on the single NS of each positive patient. The pooling strategy detected SARS-CoV-2 RNA to a similar extent to the single test, even when Ct value is on average high (Ct 37–38), confirming that test sensibility is not substantially affected even if the pool contains only one low viral load positive sample. Furthermore, the pooling strategy have benefits for SARS-CoV-2 routinary monitoring of groups in regions with a low SARS-CoV-2 prevalence.

KEYWORDS

SARS-CoV-2, real time PCR, nasal swabs, pooling strategy, surveillance

Introduction

Coronavirus disease-2019 (COVID-19) is a life-threatening respiratory and multisystem infection caused by *severe acute respiratory syndrome coronavirus 2* (SARS-CoV-2) and declared pandemic by the World Health organization (WHO) in March, 2020. Virus transmission occurs mainly *via* respiratory droplets released by talking, breathing, coughing, and sneezing, as well as though close contact between people in closed and poorly ventilated environments. Additionally, SARS-CoV-2 can persist in asymptomatic individuals with high titers for up to 14 days, providing important opportunities for silent and undetected transmission (Roque et al., 2021). Therefore, the infection control relies primarily on timely identification and isolation of infected people. In order to limit and circumscribe the pandemic, health authorities around the world urged the development of preventive measures, as virucidal agents (Buonavoglia et al., 2021, 2022) and effective diagnostic tests for rapid and accurate identification of SARS-CoV-2 in the infected patients (Ji et al., 2020), using real-time reverse-transcription polymerase chain reaction (rRT-PCR) on deep nasopharyngeal swabs (NPS) as gold standard test (Azzi et al., 2021). Anyhow, NPS collection is time-consuming, uncomfortable, invasive, can generate stress (chiefly for children), requires trained health care personnel and is associated with a no negligible risk of viral transmission (Azzi et al., 2021). These difficulties were addressed and innovative approaches were proposed for simpler and less invasive sampling and for accelerating the screening of groups of people and large populations (Czumbel et al., 2020; Pratelli et al., 2021). From the very first months of pandemic onset, growing interest was addressed to the use of self-collected sampling as a suitable first-line screening test for SARS-CoV-2 infection (Böger et al., 2020; Mohammadi et al., 2020; Tsang et al., 2021), reducing the risk for healthcare workers involved in sampling, and increasing the number of analyses where supplies of personal protection equipment (PPE) are lacking or difficult to find. In a recent study, Tsang et al. (2021) showed that nasal swab (NS) provides a very good diagnostic performance and that represents a valuable alternative to NPS in the outpatient setting. For the epidemiological monitoring of SARS-CoV-2 infection, especially in "closed" environments (offices, schools, kindergartens, airplanes, etc.), high participation rate and an easy sampling are important concerns to consider when testing asymptomatic population.

The strategy described in the present note represents the application for the diagnosis of SARS-CoV-2 of the pooling test on bovine coronavirus (BCoV) samples reported by Pratelli et al. (2021). The application of an rRT-PCR test for the diagnosis of SARS-CoV-2 using a pooling strategy with 20 NSs, in order to validate the test for systematic mass monitoring of COVID-19 in companies and in schools, is reported.

Materials and methods

Study design and sampling

The survey was carried out in the laboratory of Clinical Pathology and Microbiology of the hospital Bonomo of Andria, Italy, in collaboration with the hospital Monsignor Dimiccoli of Barletta, Italy, and the Department of Veterinary Medicine of the University of Bari, Italy. The trial was approved and authorized from the Interprovincial Ethical Commission, Area 1, of A.O.U Foggia, ASL FG, ASL BAT (Authorization n°: 34/CE/2022 of February 28, 2022). The COVID-19 positive patients, subject to the release of informed consent, were recruited from March 1st, 2022 to April 1st, 2022 based on the positive rRT-PCR performed on envelope (E), nucleocapside (N), and RdRP genes (Blairon et al., 2021). Specifically, 17 patients individually tested positive were retested using pooling strategy. For this purpose, two sterile dry swabs (Nuova Aptaca srl, Canelli, At, Italy) (**Figure 1A**) were provided for each positive patient who was asked to self-collected 2 nasal specimens (#NS1 and #NS2) inserting the swabs in the nasal vestibule for up to 1 cm.

Real-time reverse-transcription polymerase chain reaction

The #NS1 of each positive patient was cut about 5 cm above the cotton swab, individually collected in a single 50 mL sterile conical centrifuge tube and then tested by rRT-PCR. At the same time, the #NS2, after being cut, was collected in a single 50 mL sterile conical centrifuge tube together with 19 NSs collected and cut as described above from 19 patients tested negative with molecular rRT-PCR. Two mL of Dulbecco Minimal Essential Medium (DMEM, Corning, Mediatech, Inc., 9345 Discovery Blvd, Manassa, VA 20109, United States) were added to each conical centrifuge tube containing the pool which included a total of 20 NSs (1 positive NS from each positive patient and 19 negative NSs) (**Figure 1B**), and to each conical centrifuge tube containing the single positive swab. After vortexing the tubes for 1 min, acid nucleic was extracted using STARMag 96X4 Viral DBA/RNA200C Kit, an automatic nucleic acid purification system with the convenient handling of magnetic beads, and rRT-PCR was set-up using the SARS-CoV-2 assay [Allplex^{TM}, Seegene Inc., Taewon Bldg., 91 Ogeum-ro, Songpa-gu, Seoul, Corea Republic) with CFX thermal cycler (Bio-Rad Laboratories S.r.l.Via Cellini, 18/A, 20090 Segrate (MI)—Italy] (Blairon et al., 2021).

Results

The strength of pooling nasal testing was monitored in each pool of 20 NSs and then compared with the molecular

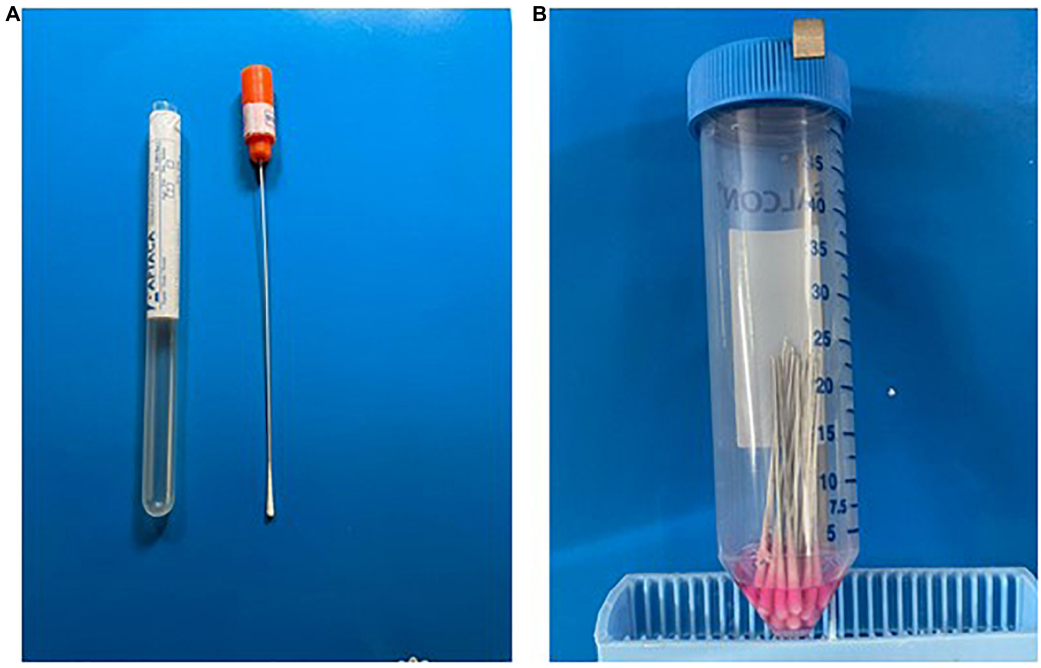

FIGURE 1
Executive steps of sampling and testing. **(A)** Individual test tube. **(B)** Pool of individual swabs in a 50 mL tube containing 2 mL of DMEM.

test performed on the single NS of each positive patient. Interestingly, the pooling strategy was able to detected SARS-CoV-2 RNA to a similar extent to the single sample test, even when Ct value is on average high (Ct 37–38), and therefore also in the presence of a low viral load. This is guaranteed by the high sensitivity of the rRT-PCR which allows to identify even a single positive sample within a pool containing up to 19 negative samples. By performing the test on the 20 pooled samples, the difference between the median Ct value of test performed on the single positive NS and the median Ct value obtained on the 20 samples-pool was 3.11, 3.7, and 4.11 Ct, for E, RdRp and N gene, respectively, thus confirming that pooling strategy is at least as sensitive as testing individual samples (Pratelli et al., 2021). This datum confirms that, even if the pool contains only one low viral load positive sample, the sensibility of the test is not substantially affected.

One sample (10B) revealed a low viral load with Ct 34, 35 and 34 in rRT-PCR on single NS for E, RdRp and N genes, respectively, but when tested as pool resulted negative for E and RdRp genes and positive (Ct 37) for N gene.

Discussion

After more than 2 years the beginning of the SARS-CoV-2 pandemic, epidemiological monitoring and early diagnosis still remain the key factors for the control of the infection. Several antigenic test have been developed, but due to the low sensibility of the assays, rRT-PCR from NPS remains the gold standard for the diagnosis. This sample collection procedure is nevertheless uncomfortable and painful for most people, decreasing the willingness to undergo the test, especially for asymptomatic individuals periodically tested for epidemiological health control (Bergevin et al., 2021).

NSs have been shown to represent a valid alternative sampling method, providing a comparable diagnosis and very good diagnostic performance (Tsang et al., 2021). NSs can be self-collected reducing the health risk of healthcare personnel involved in sampling (preventing any contact with patients) and increasing the number of test that can be carried out especially in regions where PPE supplies are scarce and not very available, and when systematic epidemiological monitoring is required (Ng et al., 2020; Moreno-Contreras et al., 2022). The self-collection for pooled NSs has proven to be a valid and reliable diagnostic method and does not lead to any significant impairment of diagnostic accuracy. The main limits of the study could be the small number of tested patients and, looking forward during the SARS-CoV-2 monitoring in the field, the inadequate sampling by the patient who may not insert the swabs to the proper depth into the nasal vestibules and may not allow sufficient secretions to be adsorbed. Nevertheless, the pooling strategy have practical implications and benefits for SARS-CoV-2 systematic and repeated monitoring.

Similar application has been described (Praharaj et al., 2020; Ayaz et al., 2022). Ayaz et al. (2022) investigated the impact of pool size and mixture level on final Ct values preparing

individual swabs and then take an aliquot to create the pool. The advantage of the strategy described in our study lies in the streamlining and simplification of the laboratory procedure for preparing the pool sample and all the 20 swabs will be processed directly to set up the pool, reducing manual work and execution times. Similarly, Praharaj et al. (2020) developed a comparative analysis of pooled samples but testing for only 5- and 10-sample pools.

Pooling of samples allows to increase the number of samples to test, saving the reagent and consequently reducing the costs, especially in developing regions and with a low prevalence of the virus (Abdalhamid et al., 2020; Moreno-Contreras et al., 2022). Pool testing allows to test up to 20 patients with a molecular test, combining the advantage of testing multiple samples with the sensitivity of the rRT-PCR (Garg et al., 2020; Bish et al., 2021). Subsequently, if the pool tested negative, all samples are considered to be below the detection limit of the assay, and no further investigation should be performed. On the contrary, when the pool is positive, the samples must be tested individually to identify the infected patient(s).

The approach of testing pooled samples is cost-effective and useful to decrease the costs of laboratory analyses, scaling and speeding up the monitoring and the epidemiological activities of local or national health authorities, and/or enabling alternative control measures. This is particularly desirable in low-income countries, where limited economic resources can compromise the activation of epidemiological monitoring surveillance plans. Furthermore, systematic screening of medical and paramedical personnel in hospitals and health facilities, as well as of school and companies' personnel, is a necessity control measure to mitigate and to limit SARS-CoV-2 spreading.

Conclusion

In conclusion, the pooling strategy on self-collection of samples and rRT-PCR on pooled NSs, was not associated with any significant impairment of diagnostic accurancy.

Data availability statement

The raw data supporting the conclusions of this article will be made available by the authors, without undue reservation.

Ethics statement

The study involving human participants was reviewed and approved by the Interprovincial Ethical Commission, Area 1, of A.O.U Foggia, ASL FG, ASL BAT (Authorization n_: 34/CE/2022 of February 28, 2022). The patients/participants provided their written informed consent to participate in this study.

Author contributions

AB was responsible for the concept. AP was responsible for preparing the manuscript. FP and MC were responsible for the literature review. DT, MSL, LCe, and LCa were responsible for the laboratory analysis. FP and AB critically revised the article. All authors reviewed the manuscript prior to submission and contributed to the article and approved the submitted version.

Conflict of interest

The authors declare that the research was conducted in the absence of any commercial or financial relationships that could be construed as a potential conflict of interest.

Publisher's note

All claims expressed in this article are solely those of the authors and do not necessarily represent those of their affiliated organizations, or those of the publisher, the editors and the reviewers. Any product that may be evaluated in this article, or claim that may be made by its manufacturer, is not guaranteed or endorsed by the publisher.

References

Abdalhamid, B., Bilder, C. R., McCutchen, E. L., Hinrichs, S. H., Koepsell, S. A., and Iwen, P. C. (2020). Assessment of specimen pooling to conserve SARS CoV-2 testing resources. *Am. J. Clin. Pathol.* 153, 715–718. doi: 10.1101/2020.04.03.20050195

Ayaz, A., Demir, A. G. O., Ozturk, G., and Kocak, M. (2022). A pooled RT-PCR testing strategy for more efficient COVID-19 pandemic management. *Int. J. Infec. Dis.* 116, 1–6. doi: 10.1016/j.ijid.2021.12.328

Azzi, L., Maurino, V., Baj, A., Dani, M., d'Aiuto, A., Fasano, M., et al. (2021). Diagnostic salivary tests for SARS-CoV-2. *J. Dent. Res.* 100, 115–123. doi: 10.1177/0022034520969670

Bergevin, M. A., Freppel, W., Robert, G., Ambaraghassi, G., Aubry, D., Haeck, O., et al. (2021). Validation of saliva sampling as an alternative to oro-nasopharyngeal swab for detection of SARS-CoV-2 using unextracted rRT-PCR with the Allplex 2019-nCoV assay. *J. Med. Microbiol.* 70:001404. doi: 10.1099/jmm.0.001404

Bish, D. R., Bish, E. K., El-Hajj, H., and Aprahamian, H. (2021). A robust pooled testing approach to expand COVID-19 screening capacity. *PLoS One* 16:e0246285. doi: 10.1371/journal.pone.0246285

Blairon, L., Piteüs, S., Beukinga, I., and Tré-Hardy, M. (2021). Development and implementation of a RT-qPCR extraction-free protocol for the detection of SARS-CoV-2 and impact on the turn-around-time. *J. Med. Virol.* 1, 1–5. doi: 10.1002/jmv.26782

Böger, B., Fachi, M. M., Vilhena, R. O., Cobre, A. F., Tonin, F. S., and Pontarolo, R. (2020). Systematic review with meta-analysis of the accuracy of diagnostic tests for COVID-19. *Am. J. Infect. Control.* 49, 21–29. doi: 10.1016/j.ajic.2020.07.011

Buonavoglia, A., Camero, M., Lanave, G., Catella, C., Trombetta, C. M., Gandolfi, M. G., et al. (2021). Virucidal activity in vitro of mouthwashes against feline coronavirus type II. *Oral Dis.* doi: 10.1111/odi.14067

Buonavoglia, A., Lanave, G., Marchi, S., Lorusso, P., Montomoli, E., Martella, V., et al. (2022). In vitro virucidal activity of mouthwashes on SARS-CoV-2. *Oral Dis.* doi: 10.1111/odi.14205 [Epub ahead of print].

Czumbel, L. M., Kiss, S., Farkas, N., Mandel, I., Hegyi, A., Nagy, A., et al. (2020). Saliva as a candidate for COVID-19 diagnostic testing: a meta-analysis. *Front Med.* 7:465. doi: 10.3389/fmed.2020.00465

Garg, A., Ghoshal, U., Patel, S. S., Singh, D. V., Arya, A. K., Vasanth, S., et al. (2020). Evaluation of seven commercial RT-PCR kits for COVID-19 testing in pooled clinical specimens. *J. Med. Virol.* 93, 2281–2286. doi: 10.1002/jmv.26691

Ji, T., Liu, Z., Wang, G., Guo, X., Akbar Khan, S., Lai, C., et al. (2020). Detection of COVID 19: a review of the current literature and future perspectives. *Biosens. Bioelectron.* 166:112455. doi: 10.1016/j.bios.2020.112455

Mohammadi, A., Esmaeilzadeh, E., Li, Y., Bosch, R. J., and Li, J. (2020). SARS-CoV-2 detection in different respiratory sites: a systematic review and meta-analysis. *EBioMedicine* 59:102903. doi: 10.1016/j.ebiom.2020.102903

Moreno-Contreras, J., Espinoza, M. A., Sandoval-Jaime, C., Cantú-Cuevas, M. A., Madrid-González, D. A., Barón-Olivares, H., et al. (2022). Pooling saliva samples as an excellent option to increase the surveillance for SARS-CoV-2 when re-opening community settings. *PLoS One* 17:e0263114. doi: 10.1371/journal.pone.0263114

Ng, K., Poon, B. H., Kiat Puar, T. H., Shan Quah, J. L., Loh, W. J., Wong, Y. J., et al. (2020). COVID-19 and the risk to health care workers: a case report. *Ann. Intern. Med.* 172, 766–767. doi: 10.7326/L20-0175

Praharaj, J., Jain, A., Singh, M., Balakrishnan, A., Dhodapkar, R., Borkakoty, B., et al. (2020). Pooled testing for COVID-19 diagnosis by real-time RT-PCR: a multi-site comparative evaluation of 5- & 10-sample pooling. *Indian J. Med. Res.* 152, 88–94. doi: 10.4103/ijmr.IJMR_2304_20

Pratelli, A., Lucente, M. S., Mari, V., Cordisco, M., Sposato, A., Capozza, P., et al. (2021). A simple pooling salivary test for SARS-CoV-2 diagnosis: a columbus' egg? *Virus Res.* 305:198575. doi: 10.1016/j.virusres.2021.198575

Roque, M., Proudfoot, K., Mathys, V., Yu, S., Krieger, N., Gernon, T., et al. (2021). A review of nasopharyngeal swab and saliva tests for SARS-CoV-2 infection: disease timelines, relative sensitivities, and test optimization. *J. Surg. Oncol.* 124, 465–475. doi: 10.1002/jso.26561

Tsang, N. N. Y., So, H. C., Ng, K. Y., Cowling, B. J., Leung, G. M., and Ip, D. K. M. (2021). Diagnostic performance of different sampling approaches for SARS-CoV-2 RT-PCR testing: a systematic review and meta-analysis. *Lancet Infect. Dis.* 21, 1233–1245. doi: 10.1016/S1473-3099(21)00146-8

frontiers | Frontiers in Microbiology

TYPE Original Research
PUBLISHED 22 August 2022
DOI 10.3389/fmicb.2022.937970

OPEN ACCESS

EDITED BY
Leon G. Leanse,
Harvard Medical School, United States

REVIEWED BY
Evgeniya V. Nazarova,
Genentech, United States
Liliana Rodrigues,
New University of Lisbon, Portugal

*CORRESPONDENCE
Krishnamohan Atmakuri
atmakrish@thsti.res.in

†These authors have contributed equally to this work

SPECIALTY SECTION
This article was submitted to Infectious Agents and Disease, a section of the journal Frontiers in Microbiology

RECEIVED 06 May 2022
ACCEPTED 12 July 2022
PUBLISHED 22 August 2022

CITATION
Singh N, Sharma N, Singh P, Pandey M, Ilyas M, Sisodiya L, Choudhury T, Gosain TP, Singh R and Atmakuri K (2022) HupB, a nucleoid-associated protein, is critical for survival of *Mycobacterium tuberculosis* under host-mediated stresses and for enhanced tolerance to key first-line antibiotics.
Front. Microbiol. 13:937970.
doi: 10.3389/fmicb.2022.937970

HupB, a nucleoid-associated protein, is critical for survival of *Mycobacterium tuberculosis* under host-mediated stresses and for enhanced tolerance to key first-line antibiotics

Niti Singh[1,2], Nishant Sharma[1], Padam Singh[1†], Manitosh Pandey[1,3†], Mohd Ilyas[1,4], Lovely Sisodiya[1,4], Tejaswini Choudhury[1], Tannu Priya Gosain[1,4], Ramandeep Singh[1] and Krishnamohan Atmakuri[1*]

[1]Infection and Immunology Group, Translational Health Science and Technology Institute, Faridabad, Haryana, India, [2]Manipal University, Manipal, Karnataka, India, [3]Department of Life Sciences, ITM University, Gwalior, Madhya Pradesh, India, [4]School of Life Sciences, Jawaharlal Nehru University, New Delhi, India

To survive and establish its niche, *Mycobacterium tuberculosis* (Mtb) engages in a steady battle against an array of host defenses and a barrage of antibiotics. Here, we demonstrate that Mtb employs HupB, a nucleoid-associated protein (NAP) as its key player to simultaneously battle and survive in these two stress-inducing fronts. Typically, NAPs are key to bacterial survival under a wide array of environmental or host-mediated stresses. Here, we report that for Mtb to survive under different macrophage-induced assaults including acidic pH, nutrient depletion, oxidative and nitrosative stresses, HupB presence is critical. As expected, the *hupB* knockout mutant is highly sensitive to these host-mediated stresses. Furthermore, Mtb aptly modulates HupB protein levels to overcome these stresses. We also report that HupB aids Mtb to gain tolerance to high levels of rifampicin (RIF) and isoniazid (INH) exposure. Loss of *hupB* makes Mtb highly susceptible to even short exposures to reduced amounts of RIF and INH. Overexpressing *hupB* in Mtb or complementing *hupB* in the *hupB* knockout mutant triggers enhanced survival of Mtb under these stresses. We also find that upon loss of *hupB,* Mtb significantly enhances the permeability of its cell wall by modulating the levels of several surface lipids including phthiocerol dimycocerosates (PDIMs), thus possibly influencing overall susceptibility to host-mediated stresses. Loss of *hupB* also downregulates efflux pump expression possibly influencing increased susceptibility to INH and RIF. Finally, we find that therapeutic targeting of HupB with SD1, a known small molecule inhibitor, significantly enhances Mtb susceptibility to INH and THP-1 macrophages and significantly reduces MIC to INH. Thus, our data strongly indicate that HupB is a highly promising therapeutic target especially for potential combinatorial shortened therapy with reduced INH and RIF doses.

KEYWORDS

HupB, Hlp, stress, antibiotics, SD1, *Mycobacterium tuberculosis*, *Mycobacterium smegmatis*

Introduction

Annually, worldwide, tuberculosis (TB) causes ∼10 million fresh individuals to fall sick and kills at least a million individuals (Global tuberculosis report, 2020). Majority of this burden is concentrated in low- and middle-income countries where TB remains endemic. TB-triggered mortality has continued despite diligent BCG vaccination and easy access to first-line anti-TB drugs (Global tuberculosis report, 2020). With rapid emergence of multi- and extremely drug resistant strains of *Mycobacterium tuberculosis* (Mtb) and their increasing contribution to TB burden, second-line anti-TB drugs have also become readily available (Seung et al., 2015; Prasad et al., 2017). However, with treatment duration still lasting for 6–24 months, most patients experience one or more toxicity issues including liver damage, gastritis, vomiting, heartburn, reduced appetite, visual impairment, and rashes (Yee et al., 2003; Forget and Menzies, 2006; Castro et al., 2015; Madhav et al., 2015; Prasad et al., 2019). Consequently, there is widespread poor compliance to anti-TB therapy.

Thus, there is an urgent need to identify novel drug molecules against new pathogen-specific targets that not only exhibit superior efficacy but also significantly shorten treatment regimens, reduce total drug intake, and exhibit minimal to no side effects (Duncan and Barry, 2004; Singh and Mizrahi, 2017; Wellington and Hung, 2018). Since anti-TB therapy is primarily combinatorial, any new identified drug molecule must also be able to work seamlessly with the existing first-line drugs. If such a molecule can show an additive or synergistic effect with the existing first-line drugs and simultaneously reduce the dosage of the other drugs (in combination), it holds a huge promise as a potential novel drug (Duncan and Barry, 2004; Singh and Mizrahi, 2017; Wellington and Hung, 2018; Shetye et al., 2020).

Consequently, several Mtb proteins including nucleoid-associated histone-like proteins (NAPs) are under evaluation as novel therapeutic targets (Pinault et al., 2013; Bhowmick et al., 2014; Peraman et al., 2021). Typically, in bacteria, NAPs are known to orchestrate nucleoid dynamics, operate as global transcription modulators, shield nucleoid under stress conditions, and alter cellular responses to stress (Hołówka and Zakrzewska-Czerwińska, 2020). They are small positively charged transcriptional gene regulators that modulate DNA-dependent processes to influence local and/or global gene expression landscapes (Dorman and Deighan, 2003; Dillon and Dorman, 2010; Priyadarshini et al., 2013; Kriel et al., 2018; Datta et al., 2019). Mycobacterial NAPs are no exception. Mtb encodes at least six different NAPs, *viz.*, EspR, HupB (also referred to as MtbHU/HU), Lsr2, mIHF, MDP2, and NapM (Kriel et al., 2018). Lsr2 and EspR are DNA-bridging proteins, with the former influencing cell wall biosynthesis, oxidative stress, and antibiotic resistance (Chen et al., 2008; Kriel et al., 2018) and the latter regulating secretion of virulent proteins by ESX-1 through two 2-component regulatory systems, viz., PhoP-PhoR and MprA-MprB (Cao et al., 2015; Anil Kumar et al., 2016). In contrast, MDP2, mIHF, and NapM directly bind curved DNA, promote non-curved DNA compactions, and influence Mtb growth *in vitro* (Kriel et al., 2018).

HupB is an Mtb-encoded HU-like protein of *E. coli* and a prominent member of Mtb-encoded NAPs (Kriel et al., 2018; Datta et al., 2019). Not surprisingly, HupB promotes nucleoid compaction by associating with ds DNA (Bhowmick et al., 2014; Gupta et al., 2014; Hołówka et al., 2017). It is also implicated in several important biological functions including (i) immune-modulation (Prabhakar et al., 1998), (ii) adhesion to alveolar macrophages (Pandey et al., 2014a; Kalra et al., 2018; Yaseen et al., 2018), (iii) assembly of mycolic acid layer (Katsube et al., 2007), (iv) acquisition of iron (Pandey et al., 2014a), and (v) biofilm formation (Yaseen et al., 2018). Given its multiple roles, it is not surprising that it has emerged as a key player in influencing Mtb growth *in vitro* and in alveolar macrophages (Sassetti et al., 2003; Pandey et al., 2014a). Consequently, it has been explored as a novel therapeutic target (Bhowmick et al., 2014; Peraman et al., 2021).

HupB, a ∼22 kDa protein, harbors N- and C-terminal domains. While the N-terminal (1-108 amino acids, AAs) DNA-binding domain (Bhowmick et al., 2014; Gupta et al., 2014; Ghosh et al., 2016) holds significant homology to other bacterial histone-like proteins (Kumar et al., 2010; Pandey et al., 2014a), the C-terminal (108-214 AAs) tetrapeptide motif (^{159}KATKSPAK^{166}) containing-domain is identical to eukaryotic histone H1/H5 proteins (Prabhakar et al., 1998; Gupta et al., 2014). Although the N-terminal domain directly interacts with DNA, the C-terminal domain is proposed to influence DNA sequence-specific binding (Kumar et al., 2010). Thus, employing both domains, HupB binds AT-rich sequences prominently localized to promoter regions (Bhowmick et al., 2014; Pandey et al., 2014b; Datta et al., 2019). Given this ability, HupB is considered to influence global gene expression by acting as a transcriptional regulator (Bhowmick et al., 2014; Pandey et al., 2014b; Kriel et al., 2018; Datta et al., 2019). Despite its proposed role, its influence on global gene expression is subjected to control by post-translational modifications (such as phosphorylation and acetylation) of its N-terminal domain (Gupta et al., 2014; Ghosh et al., 2016; Sakatos et al., 2018).

Interestingly, an ortholog of HupB, *viz.*, Hlp (80% AA identity), that is encoded by an avirulent environmental mycobacterium, *M. smegmatis* (Msm), plays a significant role in Msm's adaptation to several environmental stresses. Thus, an *hlp* knockout mutant is more sensitive to UV, cold shock, and exposure to isoniazid (INH) (Shires and Steyn, 2001; Katsube et al., 2007; Mukherjee et al., 2009; Whiteford et al., 2011). Furthermore, *hlp* expression is significantly increased during the abovementioned stresses and under anaerobic-induced dormancy indicating Hlp's direct role in aiding Msm to negotiate

and overcome different stresses (Lee et al., 1998; Shires and Steyn, 2001; Anuchin et al., 2010).

Coincidentally, Mtb also exhibits significantly increased expression of *hupB* upon exposure to INH and during non-replicating persistence (Betts et al., 2002; Reddy et al., 2009; Zhu et al., 2013). Given the above observations and HupB's proposed role as a transcriptional regulator (Bhowmick et al., 2014; Pandey et al., 2014b; Kriel et al., 2018; Datta et al., 2019), we hypothesized that HupB also plays an important role in adapting Mtb to host- and antibiotic-mediated stresses, and that its loss or inactivation makes Mtb highly sensitive to such stresses. Our macrophage infection and *in vitro* culture studies show that while the *hupB* knockout mutant (hereafter referred to as KO) is highly sensitive to these stresses, Mtb (H37Rv; hereafter referred to as WT) robustly thrives. Promisingly, the KO mutant succumbs to even low doses of INH and RIF. In contrast, *hupB* over expression enhanced Mtb tolerance to INH. Comparative surface lipid profiling shows reduced accumulation to loss of several important polar and apolar lipids in the KO mutant that leads to its increased permeability to SDS. Importantly, we show that targeting HupB sensitizes WT to enhance killing by INH and reduces MIC to INH. Thus, our study for the first time demonstrates that not only targeting HupB significantly enhances Mtb's susceptibility to host-mediated stresses and INH- and RIF-mediated killing but also that such a killing is rapid and requires reduced amounts of INH and RIF. In summary, we show that Mtb's HupB is a compelling therapeutic target especially for short-term combinatorial treatment with INH and RIF.

Materials and methods

Bacterial strains and their growth conditions

The mycobacterial strain, *viz.*, *Mycobacterium tuberculosis* H37Rv (WT) (Supplementary Table 1) and its derivatives were grown *in vitro* as indicated in Sharma et al. (2019). Briefly, they were cultured at 37°C in Middlebrook 7H9 broth (BD, United States) or Middlebrook 7H11 agar (BD) supplemented with (i) OADC (BD; 1× as final, 10× OADC – as stock; (ii) 0.2–0.5% of glycerol (for broth, 0.2%; for agar, 0.5%), and (iii) 0.05% Tween 80 (Merck, United States). *Mycobacterium smegmatis* mc^2155 (Msm) (Supplementary Table 1) was grown *in vitro* at 37°C in the abovementioned media except that 1× ADC replaced 1× OADC (Garces et al., 2010). *Escherichia coli* (*E. coli*) strains, *viz.*, DH5α, HB101 (used for cloning; Supplementary Table 1; Thermo Fisher Scientific, United States), and BL21-DE3 with pLysS (used for *hupB* overexpression and antibody generation) (Supplementary Table 1) were grown in Luria-Bertani (LB) broth/agar (HiMedia, India) according to Sezonov et al. (2007). The final concentrations of antibiotics used (either for maintaining plasmids and/or supporting growth) were as follows: for mycobacteria: hygromycin 50 μg/ml (Thermo Fisher Scientific), cycloheximide 50 μg/ml (Thermo Fisher Scientific), and kanamycin 25 μg/ml (Merck) and for *E. coli*: chloramphenicol 25 μg/ml (Merck), kanamycin, 100 μg/ml (Merck), and hygromycin 150 μg/ml (Merck).

Cloning

To clone *hupB* into pET28a (pNA1; Supplementray Table 2), using the genomic DNA of Mtb as the template, a primer pair, KAP403F and KAP404R (Supplementary Table 3), and a Phusion Taq polymerase (Thermo Fisher Scientific), we PCR-amplified *hupB* and digested the eluted (HiMedia) amplicon with NdeI (NEB, United States) and BamHI (NEB). The digested and purified amplicon was ligated [using T4 DNA ligase (NEB)] to similarly digested pET28a to obtain 6X-His*hupB*. The episomal expression vector pVV16 (Yaseen et al., 2018) containing *hupB* (pNA4; Supplementary Table 2) was from our lab collection. To clone *hlp*, using the genomic DNA of Msm as the template, a primer pair, KAP634F and KAP635R, (Supplementary Table 3), and a Phusion Taq polymerase (Thermo Fisher Scientific), we PCR-amplified *hlp* and digested the eluted (HiMedia) amplicon with EcoRI (NEB) and HindIII (NEB). The digested and purified amplicon was ligated [using T4 DNA ligase (NEB)] to similarly digested pVV16 to obtain pVV16+*hlp* (pNA5; Supplementary Table 2). The molecular construction of pNA2 and 3 is provided in the subsection "KO generation and its complementation" (refer below).

Antibody generation and western analyses

BL21 DE3 (pLysS) *E. coli* strain harboring 6X-His: *hupB* (pNA1; Supplementary Table 2) was induced with 0.5 mM isopropyl β-D-1-thiogalactopyranoside (Merck) at 37°C for 4 h. The induced cultures were pelleted down at 4°C and 14,000 rpm. The washed pellet (1X PBS, pH 7.4) was boiled in 1× Laemmli buffer for 15 min at 95°C and electrophoresed on 15% SDS-PAGE gels and evaluated for overexpression by coomassie staining and anti-His antibody (Ab). Since, both HisPur cobalt and Ni-NTA beads non-specifically retained several contaminating *E. coli* proteins, we followed the protocol as reported in Atmakuri et al. (2003) for generation of polyclonal Ab specific to HupB. Briefly, we cut the overexpressed band out, eluted the proteins within, and generated polyclonal Ab to the eluted mix in rabbits (outsourced to TheraIndx Lifesciences, India). We verified the specificity of the generated Ab by Western blot analysis (Mahmood and Yang, 2012) of whole cell

protein lysates of Msm and Mtb using pre-bleed sera of the rabbits as negative control. We further purified the obtained antisera using the method described in Atmakuri et al. (2003). We immediately neutralized the purified Ab eluate with few drops of 1 M Tris, pH 7.5 (tested for pH on pH paper, HiMedia), and stored it as aliquots with 0.1% bovine serum albumin (BSA; Bio Basic, Canada) and 0.02% sodium azide (Merck) for future use. Total proteins in different samples were quantitated using a BCA (bicinchoninic acid) kit (Thermo Fisher Scientific). HupB-specific protein bands were identified by Western blot analysis using purified polyclonal anti-HupB Ab. Western blots were developed using SuperSignal^{TM} West Femto Maximum Sensitivity Substrate (Thermo Fisher Scientific) and HupB-specific signals monitored using a ChemiDoc^{TM} MP Imaging system (Bio-Rad, United States). Image Lab version 6.0.1 (Biorad) was used for semi-quantitation of the HupB-specific bands. The purified anti-HupB Ab could also detect Hlp-specific bands (panel C-ii of Supplementary Figure 3), as HupB and Hlp are orthologs with a significant amino acid identity (∼80%).

For assessing HupB protein levels (by Western blot analyses) across different phases of growth, Mtb grown in either rich (7H9 media containing 10% OADC and 0.05% Tween-80; Garces et al., 2010) or minimal media Sauton's broth, (Parish and Stoker, 2001) were pelleted down at 4,000 rpm and 4°C for 15 min and washed with cold 1 × PBS, pH 7.4. The pellets were then resuspended in a 400 μl bead beating buffer (0.1 M Trizma (pH 6.8) with 1 mM EDTA; Merck) with 1× protease inhibitor cocktail (Thermo Fisher Scientific). The suspension was lysed with bead beating (Biospec Products, United States) for 8 cycles (each 45 s) with 2-min incubation between the cycles on ice. The obtained lysed suspension was spun down at 14,000 rpm for 10 min at 4°C. In 75 μl of total lysate, 25 μl of 4× Laemmli's buffer (Green and Sambrook, 2012) was added, and the mix was boiled at 95°C for 15 min. The boiled lysate was spun down for 5 min at room temperature (RT) at 14,000 rpm, and total proteins were estimated. Equal amount of proteins were resolved on 15% SDS-PAGE for western analyses with anti-GroEL2 (BEI Resources, United States) and anti-HupB (this study) antibodies. The same gel was cut into two halves; the top half was developed for evaluating GroEL2 protein levels, and the bottom half was developed for monitoring HupB protein levels.

KO generation and its complementation

We employed a temperature-sensitive mycobacteriophage-based gene knockout strategy (Bardarov et al., 2002) to generate KO. To clone the immediate flanking regions to *hupB* (i.e., 798 bp upstream and 800 bp downstream) using the genomic DNA of Mtb as the template, primer pairs (KAP475F and KAP476R upstream, and KAP477F and KAP478R downstream; Supplementary Table 3), and a Phusion Taq polymerase, we PCR-amplified each of the flanking regions and digested the eluted (HiMedia) amplicons with HindIII and NheI (for upstream) and XbaI and BspHI (for downstream, NEB), respectively. The digested and purified "upstream" amplicon was first ligated (using T4 DNA ligase) to similarly digested cosmid pYUB584 to obtain pYUB584: *hupB* upstream (pNA2; Supplementary Table 2). Then, the digested and purified "downstream" amplicon was ligated (using T4 DNA ligase) to similarly digested pNA2 to obtain pNA3 (Supplementary Table 2). Clone pNA3 was verified by restriction digestion as well as by sequencing (both upstream and downstream flanks). pNA3 was then digested with PacI, gel eluted, and ligated overnight (O/N) (with T4 DNA ligase at 16°C) with similarly digested phage λDNA. The ligation mixture was then transformed into the *E. coli* strain HB101 (Supplementary Table 1), and positive clones were selected on hygromycin-containing LB agar plates (pNA6; Supplementary Table 2). The DNA representing pNA6 was extracted using a plasmid DNA extraction kit (MDI). Subsequent steps of packaging, transformation, transduction, and phage propagation were as described in Bardarov et al. (2002). We ensured that the phage titers were ∼10^8-10^9 PFU/ml. After checking the sensitivity of phages obtained at 37°C, they were transduced into WT mycobacteria (grown to ∼1 OD_{600}, washed in MP buffer (contains 50 mM Tris Cl (pH 7.4), 150 mM NaCl, 10 mM $MgSO_4$, 2 mM $CaCl_2$) and resuspended in ∼1 ml of rich media. The transduced culture was incubated O/N without shaking at 37°C. Then, the mix was recovered in ∼5 ml of the rich media and incubated O/N at 37°C with continuous shaking (150 rpm). The culture was finally plated on 7H11 (supplemented with 50 μg/ml hygromycin) plates with 10% OADC and 0.05% Tween-80 and incubated at 37°C. Colonies that appeared after 4–6 weeks were screened for KO by PCR.

Putative KO candidates were confirmed by Western blot analysis using a purified anti-HupB antibody. The KO was further confirmed by Sanger sequencing of junction flanks, remaining portions of *hupB* ends, and the inserted hygromycin-resistant gene cassette. The KO was then complemented with either *hupB* (pNA4; Supplementary Table 2) or *hlp* (pNA5; Supplementary Table 2), and the complementation was verified by Western blot analysis with the purified anti-HupB antibody.

Mtb and *E. coli* transformation

WT and KO Mtb strains were transformed as per standard protocol (Parish and Stoker, 2001). Briefly, using Gene Pulser Xcell (BioRad) and required plasmid DNA (∼350 ng), freshly made electrocompetent cells were transformed as per Sharma et al. (2019). All *E. coli* transformations were as per standard protocol (Sambrook and Russell, 2006) that involved use of $CaCl_2$ competent cells with 60 s heat shock at 42°C.

RNA isolation and real-time PCR

The RNA from Mtb strains was isolated as described in Sharma et al. (2019). Approximately 2 × 10^9 WT and KO mycobacterial cells were used for RNA extraction. The RNA was isolated from the WT and KO pellets with a DNA, RNA, and protein purification kit (Machery-Nagel NucleoSpin^{TM}; Germany) as per the manufacturer's protocol. Three μg of the eluted RNA were treated with 1 μl of Turbo DNase enzyme (Turbo DNA-free Kit; Thermo Fischer Scientific, United States) to avoid contaminating the genomic DNA. Two μg of the DNase-treated RNA was used as template to generate cDNA as per PrimeScript 1st strand cDNA synthesis kit (Takara, Japan). One μl of the generated cDNA for each sample was taken for quantitative real-time PCR (qRT-PCR) using 5× HOT FIREPol Evagreen qPCR Mix Plus (SYBR Green; Solis Biodyne, Estonia) on the Stratagene mx3005p system (Agilent Technologies, United States). The primer pairs used are indicated in Supplementary Table 3. *sigA* transcript levels (Ct value) in different strains were used as internal controls for normalization and accurate estimation of Ct values of all genes under study.

Simulating host-induced and antibiotic stresses for western blot analysis

Freshly grown mycobacterial cultures (∼ 1 OD_{600} in 10 ml rich media) were washed once with fresh sterile 10 ml rich media and sub-cultured to 0.05 OD_{600} (by taking the required aliquot) in 50 ml fresh rich media. When OD_{600} reached ∼0.2 −0.3, cells were washed twice in fresh rich media (control) or in media used for inducing stress. Then, pellets were resuspended in 50 ml of appropriate media used for stress. Sublethal concentrations of antibiotics and molecules were employed to induce stress. For oxidative stress, 5 mM H_2O_2 (Merck, United States) was added, and stress was imposed for 72 h. For nitrosative stress, 1 mM sodium nitrite (Merck, United States) (pH 5.2, rich media) was added, and stress was imposed for 72 h. For pH stresses, the rich medium was adjusted to required pH (6.4, 5.6 and 4.2, with concentrated HCl; Merck), and stress was imposed for 72 h. For nutritional depletion, bacteria were conditioned for two generations in Sauton's medium (Garces et al., 2010) and then grown from 0.05 OD_{600} to different phases of growth.

Antibiotic-mediated stress imposition was achieved with 2.91 μM of INH (Merck), 6 nM of RIF (Merck), and 4.9 μM of ethambutol (EMB; Merck) in 50 ml of 0.4 OD_{600} culture (subcultured from ∼0.4 to 0.6 OD_{600} culture). Five days post treatment, cells were washed twice with cold 1× PBS (pH 7.4), and bacteria were pelleted down for 15 min at 4,000 rpm and 4°C. Proteins (for Western blot analyses) and RNA (for real-time PCRs) were extracted from the pellets (described earlier).

AlamarBlue assay for MIC determination

We followed the protocol of Collins and Franzblau (1997) with slight modifications. Briefly, freshly grown mycobacterial cultures (∼ 1 OD_{600} in 10 ml rich medium) were washed once with fresh sterile 10 ml rich medium and subcultured to 0.05 OD_{600} in 10 ml fresh rich medium. When OD_{600} reached 0.4–0.6, the cells were washed once with the fresh rich medium at 4,000 rpm and RT for 15 min and then used for estimation of MIC. Approximately 3.75 to 4 × 10^4 colony-forming units (CFUs) were used for the assays. Two-fold dilutions of different drug concentrations (INH:0.02 to 23.3 μM; RIF:0.75–768 nM; EMB:0.15–156.63 μM) were added in triplicates to different wells with appropriate controls (positive-culture only; negative-medium only, and drug only). The final volume in each well was made up to 200 μl with the rich medium and gently mixed 3–4 times with a 200-μl pipette. After 5 days of incubation at 37°C (without shaking), 22 μl of 10× alamarBlue (HiMedia) was added, and the contents were mixed again before incubation (without shaking) for additional 2 days. Color change from blue (metabolically inactive/dead) to pink (metabolically active/growing) was photographed and recorded. To prevent loss of medium due to evaporation in experimental wells, all the peripheral wells were filled with 200 μl of sterile rich medium.

Colony morphology and growth curves studies

WT, KO, KO+*hupB*, and KO+*hlp* (Supplementary Table 1) were initially grown in the rich medium (10 ml at 37°C and 150 rpm) to ∼1 OD_{600}, and then pelleted down (at 4,000 rpm and RT for 10 min), and the pellets washed in 10 ml of the fresh sterile rich medium, For colony morphology, primary cultures were subcultured to 0.05 OD_{600}, allowed to grow to 0.2–0.3 OD_{600}, and then equal numbers of cells (∼ 1.6 × 10^5CFUs/ml) were spotted on Middlebrook 7H11 agar supplemented with 1× OADC, 0.5% glycerol, and 50 μg/ml cycloheximide. After 45 days of incubation at 37°C, the colony morphology of each was recorded. To monitor *in vitro* growth (axenic cultures in broth) in the rich medium, primary cultures in biological triplicates (as grown above) were subcultured to 0.05 OD_{600}, and growth was monitored across different growth phases (lag to stationary).

Assessment of susceptibility of KO to host-induced and antibiotic stresses

Freshly grown mycobacterial cultures (∼0.8 OD_{600} in 10 ml rich medium) were washed once with 10 ml fresh sterile rich medium and subcultured to 0.05 OD_{600} in 50 ml fresh rich medium. When OD_{600} reached ∼0.2–0.3, cells were washed

twice in the fresh rich medium (control) or in the medium used for inducing stress. The cell pellets were resuspended in appropriate stress medium. A 5-ml culture at 0.25 OD_{600} was used for stress induction. For oxidative stress, 10 mM H_2O_2 was added, and stress was imposed for 72 h. For nitrosative stress, 5 mM sodium nitrite (pH 5.2, rich medium) was added, and stress was imposed for 72 h. For pH stress, the rich medium was adjusted to required pH (6.4, 5.6, and 4.2; with concentrated HCl), and stress was imposed for 7 and 14 days. Growth response to each stress was recorded in CFUs.

The antibiotic-mediated stress was as per Singh et al. (2013). Briefly, different mycobacterial strains (0.1 OD_{600}) at 5 ml were exposed to different concentrations of INH, RIF, and EMB, and growth was recorded in CFUs on days 7 and 14. For targeting HupB with stilbene (SD1), we employed 100 μM SD1 (as obtained from our MIC study, Supplementary Table 4), in 5 ml culture and recorded growth of bacteria in CFUs on 2nd, 6th and 12th days.

Membrane permeability to sodium dodecyl sulfate

Membrane permeability was assessed as described in Garces et al. (2010). Primary cultures (as grown above) of different mycobacterial strains, *viz.*, WT, KO, and KO+*hupB*, were subcultured to 0.05 OD_{600} in 50 ml rich medium. When OD_{600} reached 0.2–0.3, cells were washed twice in the fresh rich medium (control) or in the medium used for inducing stress. Membrane permeability was assessed by exposing 5 ml of 0.25 OD_{600} cultures (in biological triplicates) to 0.05% SDS (Merck) for 72 h, and CFUs were recorded by plating cultures 24, 48, and 72 h post exposure.

Lipid extraction and analyses

Mycobacterial lipids were extracted as previously described by Chauhan et al. (2013), with slight modifications. Briefly, 100 ml of freshly grown (∼ 1 OD_{600}, as described above) mycobacterial cultures, *viz.*, WT, KO, and KO+*hupB*, were pelleted down at 4,000 rpm and RT for 15 min and washed twice in fresh sterile 1× PBS (pH 7.4), and equal weight of pellets (∼14 mg) was heat-killed by exposure to 95°C for 1 h. Apolar lipids were extracted by resuspending the heat-killed pellets in 2 ml of 0.3% sodium chloride (w/v) solution prepared in methanol. To this, 1 ml of petroleum ether was added. The total suspension was thoroughly mixed by gentle shaking O/N on a rotor at RT. The suspension was then spun down for 10 min at RT and 4,000 rpm. The upper layer consisting of apolar lipids was collected in a separate vial. One ml of petroleum ether was added to the lower layer, vortexed, and mixed end-over-end for 15 min. The cell suspension was re-centrifuged to recollect the upper layer. The upper layers comprising apolar lipids were pooled and dried by incubation for 24 h at 37°C.

To the bottom layer, we added 2.3 ml of chloroform: methanol: 0.3% sodium chloride (at 90: 100: 30, v/v/v). The cell suspension was gently rocked O/N (at RT) and then spun down at 2,500 rpm for 10 min. Polar lipids, present in the supernatant fraction, were collected, and the pellet was further treated twice with 750 μl of chloroform: methanol:0.3% sodium chloride (50: 100: 40, v/v/v) to obtain all polar lipids. The supernatants from the three extractions were pooled and further extracted with 1.3 ml of chloroform and 1.3 ml of 0.3% sodium chloride. The lower layer comprising polar lipids was collected into a fresh glass tube and incubated at room temperature until it became dry.

Required amounts of polar and apolar lipids were suspended in chloroform: methanol (2:1, v/v), spotted on TLC plates (Silica gel on TLC Al foil; Fluka, United States), and resolved for visualization of different lipids.

Apolar lipids: equal quantity (for WT and KO+*hupB*) or thrice the quantity (for KO) of phthiocerol dimycocerosate (PDIM) and triacylglycerol (TAG) fractions was separated by 1-dimensional TLC (in petroleum ether:diethyl ether (85: 15), and plates were charred (80°C for 5–10 min on hot plate) and detected by 10% phosphomolybdic acid spray. Similarly, equal quantity (for WT and KO+*hupB*) or thrice the quantity (for KO) of mycolic acid (FAMEs, fatty acid methyl esters, and MAMEs, mycolic acid methyl esters) fraction was separated by 1-dimensional TLC [using solvent hexane: ethyl acetate (95:5)], and plates were charred and detected by 10% phosphomolybdic acid (in ethanol) spray (Chauhan et al., 2013; Sambandan et al., 2013).

Polar lipids: an equal quantity (for WT and KO+*hupB*) or three times the quantity (for KO) of polar lipids was separated by 2-dimensional TLC (size: 10 × 20 cm). First, they were resolved using chloroform:methanol:water (60:25:4) and then later chloroform:acetic acid:methanol:water (40:25:3:6). The plates were then charred (80°C for 5–10 min on hot plate) and detected by 10% phosphomolybdic acid spray (Chauhan et al., 2013).

Killing Mtb *in vitro* with SD1 in combination with INH

WT cultures (in biological triplicates) were inoculated in 5 ml rich medium at 0.1 OD_{600}. Twenty-four hours into growth, SD1 (Chembridge, United States) was added at 100 μM. Twenty-four hours later, (i.e., 48 h from the start of the experiment), different concentrations of INH were added to the cultures. The effect of the combinatorial exposure was measured in CFUs by plating aliquots on days 0, 2, 6, and 12. Appropriate

controls included untreated and treated alone with either INH or SD1.

In vitro intracellular macrophage infection and killing assay

Infection assays with macrophages (THP-1) were broadly conducted according to Sharma et al. (2019). Briefly, required volumes of WT, KO, and KO+*hupB* cultures were washed in a filter-sterilized RPMI medium, clumps were removed by filtering through 5-μm sterile membrane filters (MDI), OD_{600} was monitored and then used for infecting ~2 × 10^5 PMA (Merck)-differentiated THP-1 macrophages at 1:10 MOI. After 4 h of infection, extracellular bacteria were killed with Amikacin (200 μg/ml), and macrophages were lysed at different time points including day 0. The lysates obtained were plated on 7H11 supplemented with 1× (10%) OADC, 0.5% glycerol, and 50 μg/ml cycloheximide.

MIC_{99} assay

The MIC_{99} of SD1 against WT was determined by broth microdilution (Supplementary Table 4; Arora et al., 2020). For this, two-fold serial dilutions of SD1 were prepared on 96-well clear "U" bottom plates followed by addition of ~50 μl culture of 1:1,000 times diluted early logarithmic WT culture (OD_{600} ~0.2). The plates were incubated without shaking at 37°C for 14 days. The lowest concentration of SD1 at which no round pellet formation was visually (using magnifying glass) observed was considered as the MIC_{99} value. The assay plates included controls, *viz.*, medium only and INH alone.

In vitro checkerboard analysis for INH and SD1 drug combination study

An *in vitro* drug combination of INH and SD1 was generated by two drug checkerboard assays on 96-well clear "U" bottom plates (Supplementary Table 5; broth microdilution method; Arora et al., 2020). SD1 was diluted horizontally, and the first line TB drug (INH) was diluted vertically to make various drug combinations. Furthermore, the early logarithmic culture (~0.2 OD_{600}) of WT was diluted 1:1,000 times, and ~50 μl was added to the above plates followed by incubation at 37°C for 14 days. Fractional inhibitory concentration (FIC) and fractional inhibitory concentration index (FICI) were calculated for various concentrations of the drug combinations as in Arora et al. (2021).

Results

Given the various properties of HupB and/or its homolog Hlp (Prabhakar et al., 1998; Katsube et al., 2007; Kumar et al., 2010; Bhowmick et al., 2014; Gupta et al., 2014; Pandey et al., 2014a; Ghosh et al., 2016; Hołówka et al., 2017; Kalra et al., 2018; Yaseen et al., 2018; Datta et al., 2019), its expression *per se* being modulated under low iron conditions (Pandey et al., 2014b), non-replicating persistence (Lee et al., 1998; Shires and Steyn, 2001; Betts et al., 2002; Anuchin et al., 2010), and upon exposure of Mtb to INH (Reddy et al., 2009; Whiteford et al., 2011; Hadizadeh Tasbiti et al., 2016; Sakatos et al., 2018; Arora et al., 2021; Hadizadeh Tasbiti et al., 2021), we hypothesized that to survive and respond to different host- and antibiotic-mediated stresses, Mtb employs HupB as a key player.

HupB protein levels significantly alter in response to Mtb exposure to different host-mediated and antibiotic-induced stresses imposed *in vitro*

Prior to testing our hypothesis, using the WT, we first determined the basal levels of the HupB protein (and as a control we monitored GroEL2 protein levels) in different phases (i.e., lag, early log, mid to late log, and stationary) of Mtb growth *in vitro*, in both rich and nutrient-depleted/minimal (Sauton's, pH 7.4) media (Figures 1A,B; Supplementary Figure 1A). Upon resolving an equal amount of whole cell lysate proteins on denaturing polyacrylamide gels (Supplementary Figure 1B), we observed that, compared to the lag (also used here as reference/control) and early logarithmic (log) phases (Figures 1A,B, respectively), HupB protein levels significantly increased by 2–4 folds in the mid to late log and stationary phases of growth (Figures 1A,B, respectively). Furthermore, in comparison to the rich medium wherein HupB protein levels peaked in the mid to late log phases but dropped by a fold during the stationary phase of growth (Figure 1A), in the nutrient-depleted/minimal medium, HupB protein levels peaked all the way from the lag to the stationary phase of growth (Figure 1B). As expected, under these conditions, GroEL2 levels remained significantly unaltered (Figures 1A,B).

Then, to test our hypothesis, we exposed the WT *in vitro* to different host-mediated *viz.*, nutrient depletion (Garces et al., 2010), acidic pH (Singh et al., 2013), oxidative stress and nitrosative stress (Voskuil et al., 2011), and antibiotics-mediated stresses (Singh et al., 2013), and monitored their HupB protein levels by Western blot analyses [Figures 1C–E; (loading controls-panel (i) of Supplementary Figures 2A–C)]. To thrive and establish its niche in alveolar macrophages, Mtb co-opts phagosomes (Pethe et al., 2004; MacGurn and Cox, 2007; Ehrt and Schnappinger, 2009; Huynh et al.,

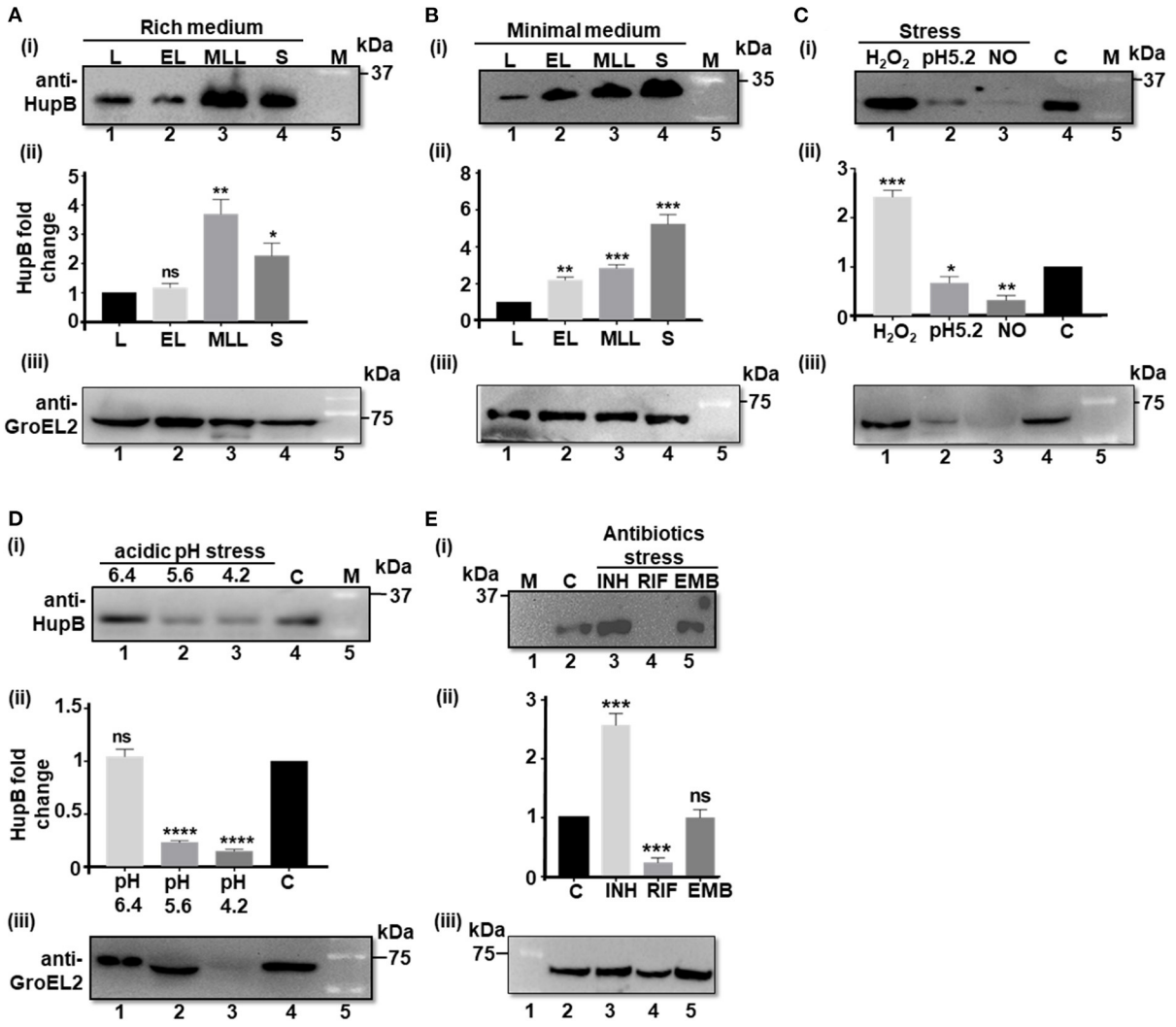

FIGURE 1
HupB protein levels significantly alter in response to Mtb exposure to different host-mediated stresses imposed *in vitro*. **(A)** WT (H37Rv) grown in different phases in rich (7H9 + 1× OADC +0.05% Tween-80), and **(B)** nutrient-depleted/minimal media (Sauton's) or **(C–E)** grown under different stress conditions (details are shown in Materials and methods[#]) was pelleted down, washed, and lysed by bead beating. Equal quantity of lysate proteins (~ 30 μg; also refer to Supplementary Figures 1, 2) was boiled for 15 min in 1× Laemmli sample buffer and resolved (in 15% SDS-PAGE). Western blot analyses were performed with a purified polyclonal anti-HupB antibody [(i) of **(A–E)**] and a polyclonal anti-GroEL2 antibody [(iii) of **(A–E)**]. The intensity of HupB bands was semi-quantified with a densitometer scan (GelDoc, BioRad) and plotted as HupB fold change [Y-axis; (ii) of **(A–E)**]. **(A,B)** L, lag phase; EL, early Log phase; MLL, mid to late log phase; S, stationary phase. **(C)** H_2O_2, oxidative stress imposed for 3 days (d) with 5 mM hydrogen peroxide; NO, nitrosative stress imposed for 3 days with 1 mM sodium nitrite at pH 5.2 (rich medium). **(D)** pH stress (pH 6.4, 5.6, and 4.2) imposed for 3 days in the rich medium. **(E)** INH, isoniazid (2.91 μM); RIF, rifampicin (6 nM); EMB, ethambutol (9.79 μM). All antibiotic exposures were for 5 days. kDa, kilo Daltons; C, control (no treatment, bacteria grown in rich medium); M, reference protein marker [for **(B)** (i) - Genedirex protein marker (Cat # PM007-0500) and for (i) of **(A,C–E)**, BioRad protein marker (Cat # 1610373), respectively]; numericals immediately underneath Western blots i.e., (i) and (iii) of **(A–E)** indicate lanes. (ii) of **(A–E)** represents HupB protein level fold change (Y-axis) determined from three independent (biological triplicates) Western blots (only one shown here); control, bacteria grown in rich medium, plotted as fold change value "1." Significance evaluated by Student *t*-test (comparative analyses with control). *$p < 0.05$, **$p < 0.01$, ***$p < 0.005$, and ****$p < 0.001$; ns non-significant. All the experiments were performed at least three independent times. The semi-quantitations of the protein bands [as in (ii) of **(A–E)** are thus an average of semi-quantitation performed on images from all the three independent experiments (biological triplicates)]. The best representative blots are shown in this Figure. [#]For protein analyses, Mtb had to be subjected to sub-lethal doses such that the stress is imposed but bacteria do not die.

2011). It overcomes oxidative and nitrosative stresses and variation in phagosomal pH (from 6.4 to 4.2) during phagosomal maturation (Pethe et al., 2004; MacGurn and Cox, 2007; Ehrt and Schnappinger, 2009; Huynh et al., 2011; Voskuil et al., 2011; Vergne et al., 2015; Zulauf et al., 2018).

We first ensured that the imparted stress conditions significantly induced the expression of a universal stress protein, Rv2005c [over "no stress" as control (Hingley-Wilson et al., 2010), panel (ii) of Supplementary Figure 2] and altered growth (OD_{600}) as expected (panel (iii) of Supplementary Figure 2). Then, we compared the HupB protein levels across different stresses (again by resolving equal amount of total Mtb proteins-panel (i) of Supplementary Figures 2A–C) to "no stress (at pH 7.4/control)" condition used as reference/control (Figures 1C–E). Under different host-mediated stresses, HupB protein levels significantly altered (Figures 1C,D). Under oxidative stress *in vitro*, HupB protein levels significantly increased by approximately two folds (Figure 1C), while under nitrosative conditions, its levels significantly decreased (∼5 folds; Figure 1C). HupB levels also significantly lowered (∼2–5 folds) at pH 5.6 (Figure 1D) and 4.2 (Figures 1C,D). However, HupB levels remained unaltered when pH was reduced from 7.4 to 6.4 (Figure 1D). Imparting nitrosative stress with sodium nitrite requires reducing medium pH to 5.2. Under these conditions, HupB levels reduced by ∼0.5 to 1 fold (Figure 1C). Again, as expected, although GroEL2 protein levels under most stresses remained significantly unaltered, under acidic stress conditions (pH 5.2 and 4.2), its levels were significantly low (Figures 1C,D).

Interestingly, upon exposing the WT to first-line antibiotic INH, we observed that HupB protein levels significantly increased by ∼1.5 to 2 folds (Figure 1E). On the contrary, its levels significantly reduced (by 3–4 folds) in the presence of RIF (Figure 1E). However, upon exposure to EMB, despite showing a significant increase in the expression of Rv2005c (Supplementary Figure 2), Mtb did not alter HupB levels (Figure 1E). Again, GroEL2 protein levels remained largely unaltered except for a marginal decrease in the presence of RIF (Figure 1E).

Loss of *hupB* significantly restricts Mtb growth *in vitro*

Given that HupB protein levels significantly modulated under different host-induced stresses (Figure 1), we examined how Mtb would respond to the same stresses: (i) in complete absence of *hupB* and (ii) when HupB is pharmaceutically inactivated.

Employing a mycobacteriophage-based homologous recombination approach, we generated a *hupB* KO mutant (Supplementary Figure 3). We replaced *hupB* with a hygromycin-resistant gene marker (Supplementary Figure 3A) and confirmed the KO by PCR (panel (i) of Supplementary Figure 3B), Western blot analysis (panels (ii) and (iii) of Supplementary Figure 3B), and sequencing (panels (iv) to (vii) of Supplementary Figure 3B). We also successfully complemented the KO with not only *hupB* but also with *hlp* (Supplementary Figure 3C). Then, by inoculating equal numbers (CFUs/ml) of KO, KO+*hupB*, and KO+*hlp*, we compared their growth *in vitro* over a defined period in both liquid (broth) and solid (agar) rich media. Loss of *hupB* severely restricts KO mutant's growth in both the liquid (Figure 2A) and solid (Figure 2B) rich media. Especially in the solid rich medium, even after 45 d, the KO grew extremely slow when compared to the WT (diameter of colony: ∼0.3–0.4 cm for KO vs. 1.5–1.6 cm for WT; Figure 2B). Interestingly, only complementation with *hupB* but not *hlp* restored the KO from its growth-restricted phenotype (both in solid and liquid rich media) to the comparative growth phenotype observed with the WT (Figure 2). Consequently, for all our subsequent experiments, we only used KO+*hupB* as the KO-complemented mycobacterial strain.

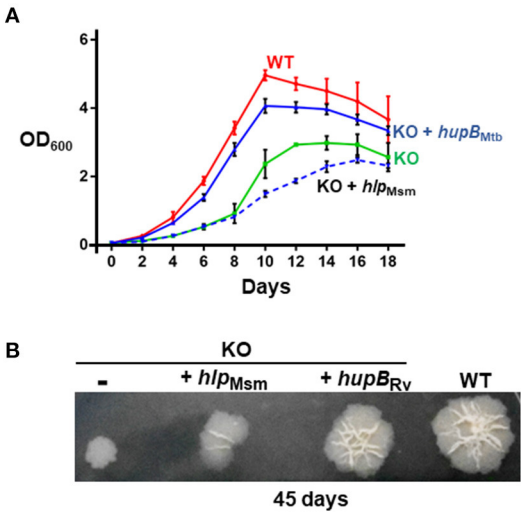

FIGURE 2
Loss of *hupB* significantly restricts Mtb growth *in vitro*. WT (red), KO (green), KO+*hupB* (blue), and KO+*hlp* (blue-dashed line) were grown *in vitro* in the rich medium, in **(A)** broth (liquid) and on **(B)** agar (solid). **(A)** Growth was initiated at 0.05 OD_{600} in the rich medium and monitored as OD_{600} (Y-axis) for 18 days (X-axis). OD_{600} was recorded in technical duplicates and averaged. Three biological triplicate cultures were monitored for growth. Thus, the OD_{600} plotted (Y-axis) is an average (plus standard deviation) of three OD_{600} values. **(B)** Five μL of 0.05 OD_{600} cultures (approximately equal number of bacterial cells) were spotted on rich medium agar plates, and colony morphology was observed after 45 days. Approximately equal CFUs were spotted (WT 1.65×10^5 CFUs/ml, KO 1.66×10^5 CFUs/ml, KO+*hupB* 1.56×10^5 CFUs/ml, and KO+*hlp* 1.6×10^5 CFUs/ml. The "-" in the 1st spot of **(B)** indicates KO with plain vector.

Loss of *hupB* makes Mtb highly susceptible *in vitro* to host-simulated stress conditions

Since loss of *hupB* severely restricted the growth of the KO even in the rich solid medium (Figure 2), we hypothesized that the KO will be much more sensitive to growth when exposed to the host- and antibiotic-mediated stresses that trigger the modulation of HupB protein levels in the WT (Figure 1). To evaluate the influence the host-mediated stresses may have on KO growth, we subjected equal numbers (CFUs/ml) of KO and KO+*hupB* mycobacteria to different host-simulated stresses, again for a defined length of time, and compared their growth (in CFUs) to that observed with similar number of WT bacteria.

As expected and reported earlier (Figure 2), even in the rich medium (at pH 7.4), when monitored at the 7 and 14 d time points, compared to the WT, the KO grew significantly slow (Supplementary Figure 4A). In contrast, under identical conditions, at both time points (7 and 14 d), the KO+*hupB* strain exhibited comparable growth to the WT, indicating successful complementation (Supplementary Figure 4A).

Upon imposing mild acidic stress, i.e., by reducing pH from 7.4 to 6.4, the growth pattern of the KO remained similar (Figure 3A) to its own exhibited at pH

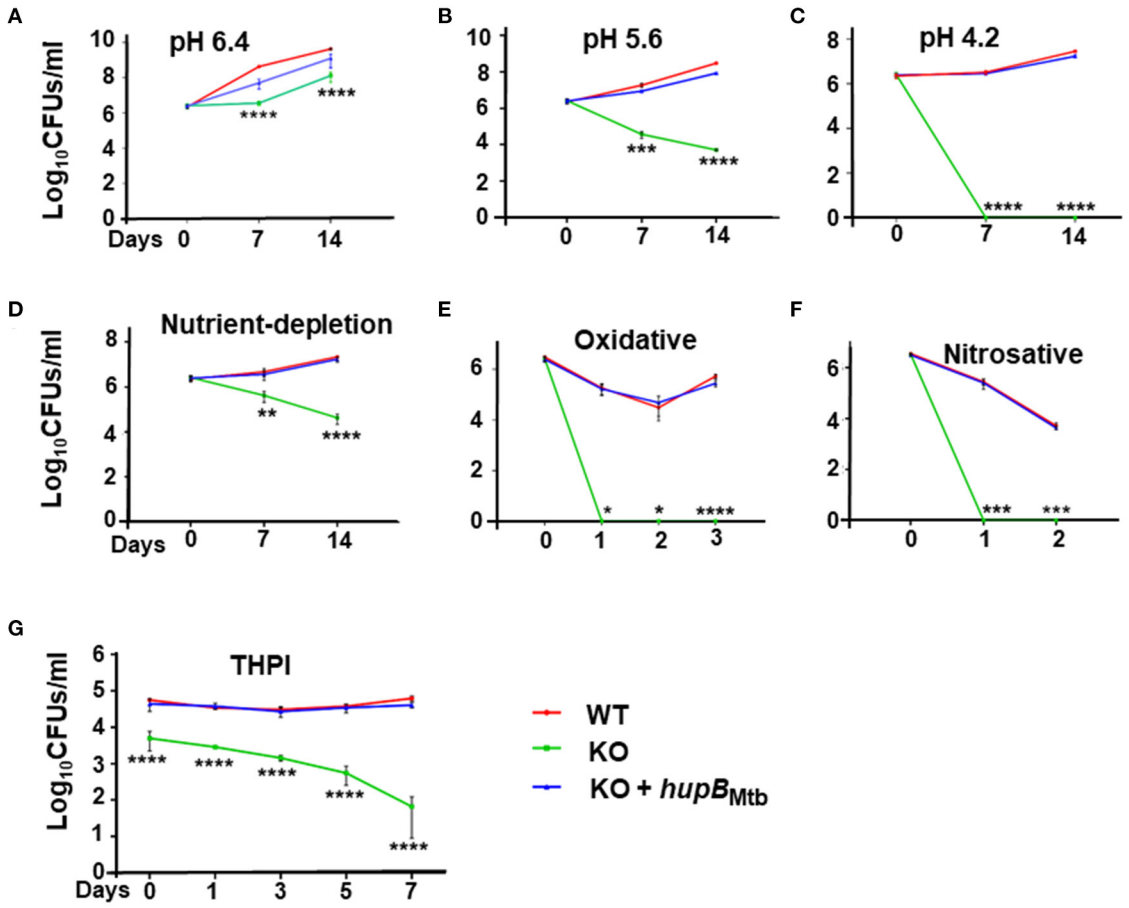

FIGURE 3
Loss of *hupB* makes Mtb highly sensitive to host-simulated stress conditions. WT (red), KO (green), and KO+*hupB* (blue) were grown in the rich medium to ~0.8 OD_{600}, washed, and subcultured at 0.05 OD_{600}. When absorbance reached 0.2–0.3 OD_{600}, they were washed and normalized to 0.25 OD_{600}. Five-ml cultures of each strain were subjected to various forms of host-simulated stress. **(A–C)** pH of the rich medium (pH 7.4) was reduced to pH as denoted; **(D)** medium was changed to 1X TBST (2.5 mM Tris, 4.2 mM NaCl, and 0.05% Tween 80); **(E)** oxidative stress was induced with 10 mM H_2O_2; **(F)** nitrosative stress was induced with 5 mM nitric oxide; **(G)** equal number (CFUs/ml) of the WT, KO, and KO+*hupB* cultures were washed in RPMI and used for infecting PMA (phorbol 12-myristate-13-acetate)-differentiated THP-1 macrophages at 1:10 MOI. After 4 h of infection, extracellular bacteria were killed with amikacin (200 μg/ml), THP-1 macrophages lysed with 0.1% Triton-X-100 at different time points (days on X-axis). The lysates obtained were plated on 7H11 + OADC + cycloheximide (50 μg/ml), CFUs were enumerated, and standard deviation values were calculated and then plotted as Log_{10} CFUs/ml (Y-axis). Student *t*-test was performed for comparative analyses, and significance was evaluated. *$p < 0.05$, ** $p < 0.01$, *** $p < 0.005$, and **** $p < 0.001$. The data are a representation of biological triplicates and technical duplicates.

7.4 (Supplementary Figure 4A). As expected, so did the growth of KO+*hupB* (Figure 3A and Supplementary Figure 4A). However, when we further reduced the pH to 5.6 at both the 7- and 14-day time points, compared to the WT, the KO became more sensitive, and its numbers significantly reduced (by ∼2 log; Figure 3B). Interestingly, upon further acidification of the medium to pH 4.2, the KO became extremely sensitive, and it failed to survive even for 7 d (∼6 log reduction in numbers; Figure 3C). As expected, the KO also struggled to grow in the nutrient-depleted medium (Figure 3D). By day 14 its numbers (CFUs/ml) significantly reduced (∼2 log), indicating again its sensitivity to growing *in vitro* in a nutrient-depleted condition (Figure 3D).

When we subjected the WT, KO, and KO+*hupB* separately to oxidative (Figure 3E) and nitrosative (Figure 3F) stresses, compared to the WT, the KO turned out to be extremely sensitive and failed to survive even for a day (Figures 3E,F). As expected, under all these stresses, similar to the WT, the KO+*hupB* strain continued to proliferate (Figures 3A–F), again indicating successful complementation of KO with *hupB* and the importance of HupB for growth during these stresses. As expected, the aliquots of cells (of these three strains), when used as "no stress controls" for both oxidative (Figure 3E) and nitrosative stresses (Figure 3F), grew similar (Supplementary Figures 4B,C) to their growth observed at pH 7.4 (Supplementary Figure 4A).

Given our observations on KO sensitivity to host-mediated stresses (Figures 3A–F) and since these stresses are imposed by macrophages upon Mtb during infection and survival (Vergne et al., 2015; Zulauf et al., 2018), we also compared the ability of WT, KO, and KO+*hupB* to grow *in vitro* in THP-1 macrophages. Despite using an equal number (CFUs/ml) of bacterial cells for infection, KO numbers reduced immediately post-infection (Figure 3G). As the days progressed, the KO numbers continued to significantly decrease. By day 7, almost 3–3.5 log equivalents of KO bacteria had succumbed to macrophage assault (Figure 3G). In contrast, as expected, even by day 7, similar to WT, KO+*hupB* bacterial cells continued to survive post infection in THP-1. Interestingly, despite using an equal number of KO bacteria for infection, we consistently observed a reduced number (∼0.5–1 log) of them infecting THP-1 (Figure 3G).

Loss of *hupB* makes Mtb highly susceptible *in vitro* to reduced amount of INH and RIF but not EMB

Given that Mtb also experiences stress when exposed to antibiotics (panel (ii) of Supplementary Figure 2C) (Singh et al., 2013; Tiwari et al., 2015), we evaluated the sensitivity of the KO and KO+*hupB* to first-line anti-TB drugs, *viz.*, INH, RIF and EMB. Toward that, employing an equal number of KO and KO+*hupB*, we subjected them at varied lengths of time to different concentrations (around their minimum inhibitory concentrations, MICs) of INH, RIF, and EMB, and compared their growth *in vitro* (in CFUs) to that observed with a similar number of WT bacteria (Figure 4). We evaluated the sensitivity of the WT, KO and KO+*hupB* to INH at $1/5^{th}$, $1/12.5^{th}$, and $1/25^{th}$ fold MIC and at 4, 40, and 400 times its MIC [Figure 4A; represented as "X"; MIC for INH is 2.91 μM; MIC determined with alamarBlue Assay on the WT (Supplementary Figure 5); selection of days of treatment and fold MIC were based on preliminary data obtained (Supplementary Figure 6)]. Interestingly, although none of the three strains survived beyond 7 days, when compared to the WT and KO+*hupB*, the KO turned extremely sensitive to INH (Figure 4A). The KO is sensitive to even $1/5^{th}$ of the MIC (i.e., 0.58 μM), while the WT and KO+*hupB* became completely sensitive only at 400 times of the MIC (i.e., ∼1.16 mM).

We then evaluated the sensitivity of the WT, KO, and KO+*hupB* to RIF at 40 and 400 times the MIC [MIC for RIF is 6 nM; MIC determined with alamarBlue Assay on WT; (Supplementary Figure 7A); selection of days of treatment and fold MIC were based on preliminary data obtained (Supplementary Figure 7B)]. Interestingly, while the KO did not survive beyond 7 days at 40 times the MIC (i.e., 0.24 μM), the WT and KO+*hupB* not only required 400 times the MIC (i.e., 2.4 μM) but they also needed an extended period (∼14 days) of drug exposure to be killed (Figure 4B).

We finally evaluated the sensitivity of the WT, KO and KO+*hupB* to EMB at 10 and 100 times the MIC (MIC of EMB is 9.79 μM, Supplementary Figure 8A). Despite repeated attempts on different days of exposure, *viz.*, 5 (Supplementary Figures 8B,C), 7, and 14 d (Supplementary Figures 8D,E), the KO failed to exhibit significantly higher sensitivity to EMB than the WT and KO+*hupB* (Supplementary Figure 8).

Overexpression of *hupB* in Mtb significantly enhances MIC *in vitro* to INH and marginally to RIF

Since (i) Mtb's exposure to INH enhances HupB protein levels (Figure 1) and (ii) loss of *hupB* significantly increases Mtb's susceptibility to reduced amount of INH (Figure 4A), we wondered if the MIC to INH might shift in response to *hupB* overexpression. To test this, as well as to evaluate if MIC might also shift for RIF and EMB, we overexpressed *hupB* in Mtb (Supplementary Figure 9), exposed the strain for 5 days to a range of concentrations of INH, and then monitored with an alamarBlue assay for any shift in MIC (Supplementary Figure 9A). Interestingly, compared to the WT,

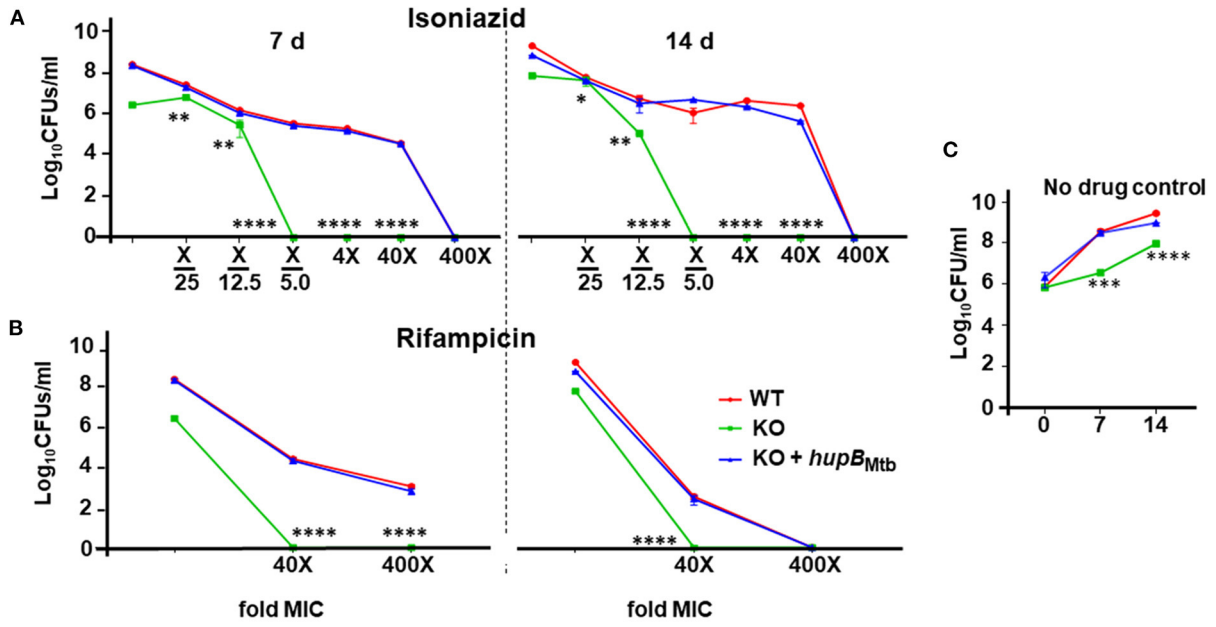

FIGURE 4
Loss of *hupB* makes Mtb highly susceptible *in vitro* to reduced amount of INH and RIF. WT (red), KO (green), and KO+*hupB* (blue) were separately grown in the rich medium to ~0.8 OD_{600}, washed, and subcultured at 0.05 OD_{600}. When absorbance reached 0.4–0.6 OD_{600}, they were washed and then normalized to 0.1 OD_{600}. Five-ml cultures were imparted stress with **(A)** isoniazid and **(B)** rifampicin for 7 and 14 days (separated by a broken black straight line) with varying concentrations (X-axis, denoted as "fold MIC" (minimum inhibitory concentration; MIC denoted as X) and by dilution of surviving bacteria plated on 7H11 + OADC + cycloheximide (50 μg/ml) and enumerated as Log_{10}CFUs/ml (Y-axis). MIC for isoniazid and rifampicin is 2.91 μM and 6 nM, respectively. Three biological triplicates were set up, CFUs were enumerated by technical duplicates, numbers were averaged, and SD values calculated were curve-plotted. Student *t*-test was performed for comparative analyses, and significance was evaluated. *$p < 0.05$, ** $p < 0.01$, *** $p < 0.005$, and **** $p < 0.001$. The data are a representation of biological triplicates and technical duplicates. **(C)** Growth on days 7 and 14 of the three mycobacterial strains [used in **(A)** and **(B)**] without antibiotics (no drug control).

the MIC to INH was increased by ~3 folds (2.91 to 11.6 μM; (Table 1, Supplementary Figure 9A) when HupB protein levels were increased by ~2–3 folds in the WT that overexpressed *hupB* (Supplementary Figure 9B). Surprisingly, although loss of *hupB* makes Mtb more susceptible to low amounts of RIF (Figure 4B), despite several attempts, compared to the WT, we consistently found only a marginal enhancement of MIC to RIF (~ a fold, from 6 to 12 nM) in the Mtb strain overexpressing *hupB* (Supplementary Figure 10). As expected, we did not observe any shift in the MIC to EMB in the *hupB*-overexpressing Mtb strain (Supplementary Figure 11).

Therapeutic targeting of HupB enhances Mtb's susceptibility *in vitro* to reduced amount of INH

Since (i) loss of *hupB* makes Mtb highly susceptible *in vitro* to reduced amount of INH (Figure 4) and (ii) increase in HupB levels of Mtb shifts MIC higher to INH (Table 1, Supplementary Figure 9), we hypothesized that therapeutic targeting of HupB *in vitro* with a reported small molecule inhibitor, *viz.*, SD1 (a stilbene derivative), will also increase Mtb's susceptibility to reduced amounts of INH. Employing the broth micro-dilution method (Arora et al., 2020) and using two-fold increments (0.39–200 μM) of SD1, we first determined its MIC on WT to be 100 μM (Supplementary Table 4). To then evaluate if the SD1 and INH combination kills WT faster, employing the micro-dilution method *in vitro*, we evaluated different concentrations of SD1 (0.39–200 μM) and INH (0.01–08 μM, Supplementary Table 5) by checkerboard assay. We observed that as a combination, SD1 and INH marginally shifted the fractional inhibitory concentration index (FICI; Odds, 2003) to 0.75 (Figure 5A) and were able to improve the efficacy of INH by 4-fold (FIC 0.25) as compared to its independent activity (Figure 5A).

Despite not being synergistic (synergism requires FICI to be ≤ 0.5; Odds, 2003), because the efficacy of INH was improved by 4-fold (FIC 0.25, Figure 5A), we evaluated their combination on actively shaken axenic cultures of the WT (Figure 5B) and in THP-1 macrophages infected with the WT (Figure 5C). Interestingly, only in the presence of SD1 (100 μM), the WT was more susceptible to even a low amount of INH (Figure 5B). When compared to untreated (plot labeled as "- drug" in Figure 5B), INH, even at 1.16 μM (plot labeled as "+X/2.5

TABLE 1 Overexpression of *hupB* in Mtb enhances minimum inhibitory concentration (MIC) *in vitro* to INH.

Mycobacterial strain	INH (μM)										
WT	0.02	0.05	0.09	0.18	0.36	0.73	1.46	2.91	5.82	11.6	23.3
WT overexpressing *hupB*	0.02	0.05	0.09	0.18	0.36	0.73	1.46	2.91	5.82	11.6	23.3

WT with vector (plasmid for episomal-based expression) alone (pVV16) (middle row) or with pVV16+hupB (bottom row) was grown in rich medium to ~0.4–0.6 OD_{600}, washed, and diluted to 0.0015 OD_{600}. Approximately ~3.75 × 10^4 CFUs of both strains were then exposed to 2-fold increments of INH (μM; middle and bottom rows) for 5 days. Required volume of alamarBlue (to final 1×) was added and incubated at 37°C in an incubator for 48 h, color change was recorded, and MIC was determined. Red ovals, MIC (under our conditions). Concentrations below MIC exhibited pink color (Supplementary Figure 9A; indicative of growth and metabolic activity). Concentrations above and including MIC remained blue in color even after 48 h of incubation with alamarBlue (Supplementary Figure 9A; indicative of death and no metabolic activity).

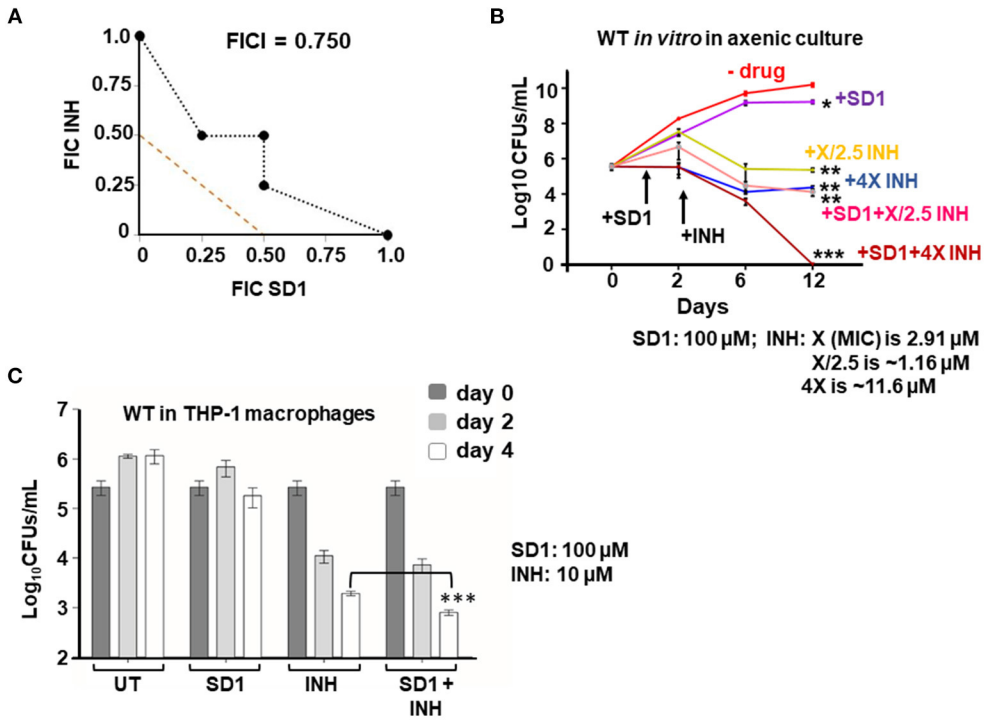

FIGURE 5
Therapeutic targeting of HupB enhances Mtb's susceptibility *in vitro* to reduced amount of INH. **(A)** Isobolograph reflecting the *in vitro* drug combination of SD1 and INH. Two-drug checkerboard was setup on 96-well "U" bottom plates (broth microdilution method; details in Materials and methods) with two-fold serial dilutions of different concentrations of SD1 (0.39–200 μM) cross-diluted with different concentrations of INH (0.01–0.8 μM). Early logarithmic phase (~0.2 OD_{600}) culture of WT was diluted 1,000-fold, and approximately 10^3 was added to and incubated at 37°C for 10–14 days. FIC (fractional inhibitory concentration) and FICI (fractional inhibitory concentration index) values for their combination were calculated and plotted. **(B)** Evaluation of the combination of SD1 and INH on WT growth *in vitro* and its survival. WT was grown to 0.2–0.3 OD_{600}, washed, and cultured to 0.1 OD_{600}. Approximately 5-ml culture of the WT was subjected to treatment with indicated concentrations of INH alone or in combination with SD1 (details in Materials and methods). Growth/survival (log_{10}CFUs/ml; Y-axis) was monitored for over 12 days (X-axis) and plotted. **(C)** Evaluation of the combination of SD1 and INH on WT growth in THP-1 macrophages. THP-1 macrophages were infected with the WT at an MOI of 1:10, treated with INH alone or in combination with SD1 (at indicated concentrations), and then monitored for bacterial load after 2 and 4 days. Bacteria were collected by lysing THP-1 macrophages with 0.1% Triton-X-100. Their numbers in CFUs were enumerated 3 weeks after plating. The enumerated CFUs were averaged, SD value was calculated and then plotted (log_{10} CFUs/ml; Y-axis). Student *t*-test was performed for comparative analyses, and significance was evaluated. *$p < 0.05$, ** $p < 0.01$, and *** $p < 0.005$. The data are a representation of biological triplicates and technical duplicates.

INH" in Figure 5B; X is MIC 2.91 μM), could efficiently reduce WT bacterial numbers from 10^{10} to only 10^6 (~4-log killing). However, to further kill the WT, just a log more, i.e., from 10^6 to 10^5, a 10-fold higher concentration of INH (i.e., 11.6 μM; plot labeled as "+4X INH" in Figure 5B) was necessary. However, surprisingly, such a 5-log killing could be easily achieved with only 1.16 μM INH when bacteria were exposed to INH in combination with SD1 (plot labeled as "+SD1+X/2.5 INH" of Figure 5B). Impressively, an additional 5-log killing (no live bacteria were observed) could be achieved with 11.6 μM of INH

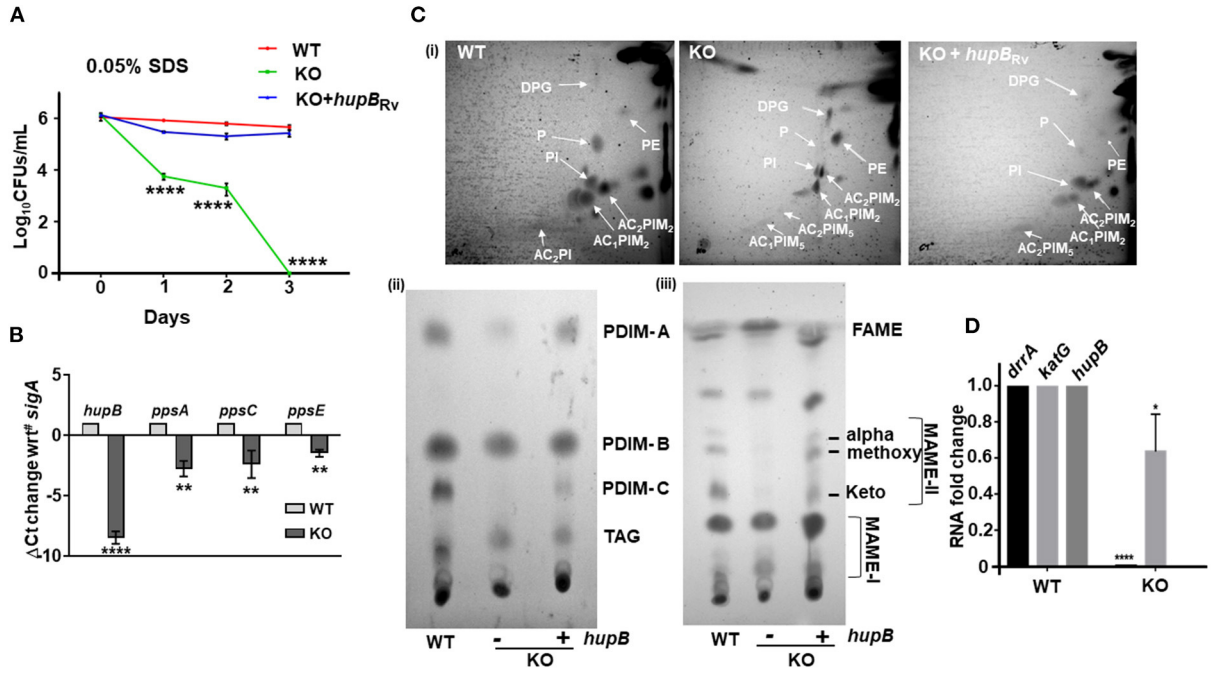

FIGURE 6
Loss of *hupB* in Mtb alters membrane permeability through reduced expression of polyketide synthases and altered levels of polar and apolar lipids. **(A)** Enhanced permeability of membrane and susceptibility of KO to 0.05% SDS. WT (red), KO (green), and KO+*hupB* (blue) were grown in the rich medium to 0.6–0.8 OD_{600}, washed, and subcultured to 0.05 OD_{600}. When absorbance reached 0.2–0.3 OD_{600}, cells were washed and normalized to 0.25 OD_{600}. Approximately 15 ml of cultures of each strain were subjected to stress. Membrane permeability was assessed by exposing bacterial strains (biological triplicates) for 72 h (time on X-axis) to 0.05% SDS. Cultures were plated on appropriate medium, CFUs were enumerated and averaged, and SD values were calculated and then plotted as $\log_{10}$ CFUs/ml scale on the Y-axis. Student *t*-test was performed for comparative analyses, and significance was evaluated. **** $p < 0.001$. The data are a representation of biological triplicates and technical duplicates for SDS stress, while in the case of lipid, it is perform in biological triplicates. **(B)** Comparative gene expression analyses of type I polyketide synthases. WT and KO were grown to 0.8 OD_{600} *in vitro*, washed, subcultured to 0.05 OD_{600}, and grown to ~1OD_{600}, RNA was isolated (from 10-ml cultures), RT-PCR was performed, and ΔCt value of *sigA* was plotted. **(C)** KO exhibits altered levels of polar and apolar lipids. WT, KO, and KO+*hupB* were grown to 1 OD_{600} (100-ml cultures), and total lipids were extracted (details in Materials and methods). [**(C)**-i]: Equal quantity (for WT and KO+*hupB*) or three times the quantity (for KO) of polar lipid fractions from the three strains were separated by 2-dimensional TLC [in chloroform:methanol:water (60:25:4) in the 1st direction and chloroform:acetic acid:methanol:water (40:25:3:6) for the 2nd direction], and then plates were charred (using hot plate) and detected by 10% phosphomolybdic acid spray. White arrows point to specific lipids. DPG, diphosphatidyl glycerol; PI, phosphatidylinositol, PIMs, phosphatidylinositol mannosides, P, phospholipid. [**(C)**-ii]: Equal quantity (for WT and KO+*hupB*) or three times the quantity (for KO) of apolar lipid (PDIM, phthiocerol dimycocerosate; TAG, triacylglycerol) fractions were separated by 1-dimensional TLC [in petroleum ether:diethyl ether (85: 15)], and plates were charred and detected by 10% phosphomolybdic acid spray. [**(C)**-iii] Equal quantity (for WT and KO+*hupB*) or three times the quantity (for KO) of mycolic acid (FAME-fatty acid methyl esters; MAMEs I and II, family of mycolic acid methyl esters) fractions were separated by 1-dimensional TLC [using solvent hexane: ethyl acetate (95:5)], and plates were charred and detected by 10% phosphomolybdic acid (in ethanol) spray (Fontán et al., 2009). **(D)** Comparative gene expression analyses of an efflux pump (*drrA*) and *katG* (catalase peroxidase-peroxynitritase). WT and KO were grown to 0.8 OD_{600} *in vitro*, washed, subcultured to 0.05 OD_{600}, and grown to ~1 OD_{600}, RNA was isolated (from 10-ml cultures), RT-PCR was performed, and RNA fold change was plotted. *$p < 0.05$, ** $p < 0.01$. The data are a representation of biological triplicates and technical duplicates.

only when combined with SD1 (see plot of +SD1+4X INH of Figure 6B).

We also evaluated the SD1 and INH combination on THP-1 macrophages infected with WT bacteria. By day 4, the individual efficacy of INH (~110-fold reduction in intracellular Mtb) was significantly improved to ~240-fold reduction in intracellular Mtb only when INH was used in combination with SD1 (Figure 6C). Importantly, SD1 did not exhibit any cytotoxic effect on THP-1 even at 8 folds its MIC (i.e., at 800 μM, Supplementary Figure 12).

Loss of *hupB* in Mtb alters membrane permeability through reduced expression of polyketide synthases and altered levels of polar and apolar lipids

Interestingly, Hlp, the ortholog of HupB, also influences cell wall assembly in Msm (Katsube et al., 2007). Since loss of *hupB* makes Mtb (i) struggle with its growth *in vitro* (Figure 2), (ii) turn hypersensitive to several host-induced stresses (Figure 3), and (iii) become highly susceptible to reduced amounts of INH and RIF (Figure 4, Supplementary Figures 6, 7), we speculated

that the phenotypes due to loss of *hupB* may be driven by altered surface permeability triggered by loss or reduction of surface lipids. To test this, we first treated an equal number (CFUs/ml) of the WT, KO, and KO+*hupB* with 0.05% SDS, a standard detergent routinely used to test Mtb's membrane integrity (Fontán et al., 2009; Garces et al., 2010) and monitored their growth (in CFUs/ml) over a defined length of time. As expected, WT numbers were barely altered even after 3 days of exposure to SDS (Figure 6A). In contrast, the KO was highly sensitive to the detergent exposure (Figure 6A). Within 1 day, 50% of KO bacteria died. By day 3, none of them survived. As expected, the KO restored its tolerance to SDS only upon complementation with *hupB* (Figure 6A).

The mycolic acid layer is a formidable barrier (Dover et al., 2004; Gebhardt et al., 2007) that protects Mtb from detergent-mediated damage and cell death. Several polyketide synthases including *ppsA*, *ppsC*, and *ppsE* play a key role in its biosynthesis, especially PDIMs (Goude and Parish, 2008; Bisson et al., 2012; Rens et al., 2021). Given the sensitivity of KO to even 0.05% SDS (Figure 6A), we next compared its *ppsA*, *ppsC* and *ppsE* transcript levels to those WT (Figure 6B). As expected, compared to the WT, the expression of all the three enzymes in the KO were significantly downregulated (Figure 6B). Given this observation, to evaluate if this downregulation of polyketide synthases in the KO influenced the levels/synthesis of different mycobacterial lipids, we performed detailed TLC lipid analyses (Chauhan et al., 2013; Sambandan et al., 2013) and compared the levels of different polar and apolar lipids of the KO and KO+*hupB* to that of the WT (Figure 6C). Interestingly, among the polar lipids, compared to the WT, the phospholipids (Ps) and diacylated-phosphatidyl-myo-inositol mannosides (AC_2PIM_5) of the KO were significantly reduced, while phosphatidylethanolamine (PE) was significantly enhanced (panel (i) of Figure 6C). As expected, in KO+*hupB*, most of the modulated lipids were restored and comparable to those of the WT (panel (i) of Figure 6C). Among the apolar lipids, PDIM-A and C (panel (ii) of Figure 6C) and α, methoxy and keto MAMEs (panel (iii) of Figure 6C) were significantly reduced in the KO. As expected, in KO+*hupB*, we observed a restoration of most lipids to WT levels (panels (i, ii, and iii) of Figure 6C). It is important to note that for superior visualization and comparative analyses of detectable levels of apolar lipids of the KO, we had to spot thrice the quantity of the one used for spotting the WT and KO+*hupB* (panels (ii and iii) of Figure 6C).

Since loss of *hupB* led to downregulated expression of type I polyketide synthases (Figure 6B), we wondered if *drrA* (Rv2936), an efflux pump present just adjacent to *ppsE*, is also downregulated. It is well-established that while *ppsA*-E is involved in the synthesis of several lipids including PDIMs (Trivedi et al., 2005; Goude and Parish, 2008; Bisson et al., 2012; Rens et al., 2021), *drrA*-C is involved in generation of an ABC transporter that also transports PDIMs to the required location on the surface of pathogenic mycobacteria (Remm et al., 2022). Interestingly, *drrA* levels were also significantly downregulated in the KO but not in the WT (Figure 6D). Finally, since the KO is susceptible to low amounts of INH, we tested if *katG*, the catalase peroxidase (Rv1908c) enzyme that converts INH to its active form (Ando et al., 2011), is upregulated. Surprisingly, we found that *katG* expression was marginally downregulated and not upregulated (Figure 6D).

Discussion

Globally, directly observed treatment, short-course (DOTS) therapy has saved the lives of millions of patients with TB (Out, 2013; Mandal et al., 2017). Despite that, since the anti-TB drug cocktail induces several adverse effects, 1/3 to 1/2 of all patients with TB fail to diligently complete their recommended treatment regimen (Cazabon et al., 2017; Kaul et al., 2019). Such poor compliance has led to rapid emergence of drug-resistant mycobacteria and extended durations of treatment especially with second-line antibiotics that induce more severe adverse effects (Madhav et al., 2015; Kaul et al., 2019). Some of the side effects often generate a sequel and last lifelong. Consequently, this has warranted discovery of novel drug targets and anti-TB drugs that not only exhibit superior killing of infecting mycobacteria and reduced side effects but also help to reduce the daily dose intake of the existing drugs (Bhat et al., 2018; Shetye et al., 2020). We predict that our *in vitro* results with HupB, a prominent Mtb-encoded NAP, are broadly aligned to this effort.

Since NAPs help bacteria cope with stress, they are known to significantly accumulate *in vitro* during the mid to late log and stationary phases of growth (Bhat et al., 2018; Hołówka and Zakrzewska-Czerwińska, 2020). For example, IHF, MDP1, and Lsr2 accumulate in the stationary phase of growth (Ali Azam et al., 1999; Matsumoto et al., 2000; Kołodziej et al., 2021). Interestingly, we also find HupB accumulating in the mid to late log and stationary phases of Mtb growth (Figures 1A,B), indicating its possible role during stress. Global transcriptome datasets from different labs indicate that upon exposure to stress such as first-line drugs, especially INH, *hupB* expression levels are significantly increased (Reddy et al., 2009; Whiteford et al., 2011; Hadizadeh Tasbiti et al., 2016; Sakatos et al., 2018; Arora et al., 2021). A similar enhanced expression of *hupB* occurs in response to non-replicating persistence (Lee et al., 1998; Betts et al., 2002) and low-iron conditions (Pandey et al., 2014a). Interestingly, such increased expression also occurs in Msm with *hupB*'s ortholog *hlp* when Msm is exposed to different environmental stress conditions including anaerobic-induced dormancy (Lee et al., 1998; Shires and Steyn, 2001; Anuchin et al., 2010). Our semi-quantitative Western blot analyses of HupB protein levels during host-mediated and antibiotic-induced stresses align with these reports and demonstrate that HupB levels are indeed modulated in response to the stresses

tested (Figure 1). Upon exposure to H_2O_2 and INH, HupB protein levels significantly increased (Figures 1C,E) and upon exposure to RIF, nitrosative, acidic, and nutrient stresses, HupB protein levels decreased (Figures 1C,D).

When compared to significant modulations of HupB protein levels during different phases of growth (Figures 1A,B) and stresses (Figures 1C–E), GroEL2 protein levels largely remained unaltered except that they significantly decreased during acidic stress (Figures 1C,D) and marginally decreased in the presence of RIF (Figure 1E). Given that RIF suppresses DNA-dependent RNA polymerase activity (Zhang et al., 2019), we did anticipate reduced accumulation of GroEL2 in Mtb in its presence (Figure 1E). The expression of *groEL2* is modulated when Mtb is present in macrophages (Monahan et al., 2001; Lin et al., 2016; Salina et al., 2019) and perhaps acidic stress is the main driver (Figures 1C,D). We infer that the reduced GroEL2 levels under nitrosative stress is primarily due to altered medium pH (from 7.4 to 5.2, Figure 1C).

Since HupB (i) aligns with several typical NAP properties; (ii) accumulates in late phases of growth *in vitro*, (iii) gets modulated during different stresses; and (iv) is an ortholog to Hlp whose KO is more sensitive to UV, cold shock, and exposure to INH (Shires and Steyn, 2001; Katsube et al., 2007; Mukherjee et al., 2009; Whiteford et al., 2011), we hypothesized that HupB also plays a definitive role in Mtb's response to host-mediated and antibiotic-induced stresses. This would imply that a *hupB* KO would exhibit increased sensitivity and susceptibility to these stresses.

Previously, a transposon insertion mutant of *hupB* was shown to restrict Mtb growth *in vitro* (Sassetti et al., 2003). As expected, our KO also exhibits a severely restricted growth phenotype *in vitro* (Figure 2). Growth retardation was more severe on the agar plates (Figure 2B) than in the axenic broth cultures (Figure 2A). The marked influence of HupB on *in vitro* growth, especially in low-iron conditions, has also been reported earlier (Pandey et al., 2014a). Furthermore, the KO also fails to survive in THP-1 (Figure 3G) and murine (Pandey et al., 2014a) macrophages, indicating HupB's role in Mtb growth in macrophages. Consistent with Pandey et al. (2014a), we also observed fewer KO bacteria able to infect and enter into THP-1 macrophages (Figure 3G). It is well-established that macrophages, besides generating acidic, nitrosative, and oxidative assaults, restrict Mtb growth by sequestering iron away from Mtb (Neyrolles et al., 2015; Sritharan, 2016; Upadhyay et al., 2018). It was earlier reported that the availability of siderophores is severely restricted in KO because, in WT, HupB binds to *hupB* boxes present upstream of mbt genes (Pandey et al., 2014a). Our comparative lipid profiling of the WT and KO (Figure 6C) indicates that perhaps the altered levels/almost loss of several polar and apolar lipids including PIMs, PDIMs, and mycolic acid esters in the KO influences its cell wall assembly and its architecture such that it significantly contributes to KO susceptibility to macrophage assaults and its inability to establish infection. Interestingly, the HupB ortholog Hlp also influences cell wall assembly in Msm (Katsube et al., 2007).

It is well-established that lipid composition and availability of lipids including PIMs and PDIMs significantly determine infection and virulence (Domenech and Reed, 2009). Since our KO contains reduced amounts of PDIM-A and –C, we evaluated the expression of three key type I polyketide synthases. Enzymes *ppsA* and *ppsC* are primarily involved in biosynthesis of the phthiocerol backbone of PDIM, while *ppsE* adds a methylmalonyl-CoA to phthiocerol (Trivedi et al., 2005; Bisson et al., 2012). Interestingly, when compared to the WT, the expression of all the three polyketide synthases in the KO was significantly reduced (Figure 6B). We predict that this altered lipid profile in the KO also largely influences its susceptibility to acidic (Figures 3A–C), oxidative (Figure 3E), nitrosative (Figure 3F), and nutrient depletion (Figure 3D). Reduced quantity of PDIMs and PIMs has been shown to increase cell wall permeability to detergents (Camacho et al., 2001), perhaps explaining why our KO exhibits altered cell wall permeability and enhanced susceptibility to 0.05% SDS (Figure 6A).

Since reduced levels of *ppsA*, C, and E expression led to reduced levels of PDIMs, we also checked the expression of the gene *drrA* that is located adjacent to *ppsE*. The gene *drrA* encodes for a nucleotide-binding domain of a type II ABC transporter, DrrABC (Remm et al., 2022), that transports PDIMs across the inner membrane for PDIM localization to Mtb's surface (Braibant et al., 2000; Remm et al., 2022). Gene *drrA* expression is very high in INH and RIF-resistant MDR and XDR Mtb isolates (Li et al., 2015; Coll et al., 2018; Khosravi et al., 2019), indicating its possible role as a drug efflux pump in increasing Mtb tolerance to INH, RIF, and other antibiotics (Remm et al., 2022). Our KO, when compared to the WT, shows barely any expression of *drrA* (Figure 6D) and, as expected, is highly susceptible to both INH and RIF (Figure 4, Supplementary Figures 6A, 7B). Upon exposure to different concentrations (i.e., folds MIC) of INH, although both the KO and the WT died within 7 days, the KO was highly susceptible to INH (Figure 4A). When compared to the WT, it requires a ∼2,000-fold less amount of INH (Figure 4A). Further analyses indicates that the KO is not only susceptible to $1/5^{th}$ the MIC for INH (Figure 4A), but that it is also susceptible to this amount within 5 days (Supplementary Figure 6).

Interestingly, when compared to the logarithmic growth phase, the expression of the catalase gene *katG* during the stationary phase of growth is less; thus, Mtb cells that exhibit a lower amount of KatG become more tolerant to INH (Ando et al., 2011; Niki et al., 2012). Since lower quantity of INH kills KO but not WT bacteria (Figure 4A), we predicted that this phenotype may be due to *drrA* down regulation. Since *drrA* expression indeed goes down (Figure 6D), we then wondered if, in KO, *katG* expression also gets modulated or remains similar to that observed in WT. It is well-established that

sensitivity to INH differences exists among the Mtb complex, *Mycobacterium marinum*, and non-tuberculous mycobacteria (NTM) primarily because of genetic variants of *katG*, and they determine the amount of INH required to kill different mycobacteria (Reingewertz et al., 2020). It turns out that the KO, when compared to the WT, exhibits a slightly reduced expression of *katG* (∼20–40%, Figure 6D), and that seems to not influence KO's enhanced susceptibility to INH (Figure 4A).

The KO also exhibits enhanced susceptibility to RIF (Figure 4B). Upon exposure to different concentrations (i.e., folds MIC) of RIF, not only all KO bacteria died within 5 days (Supplementary Figure 7), they also required only a 10-fold lower amount of RIF than that required to kill all WT bacteria (Figure 4B). Importantly, to be killed, the WT requires higher amounts of RIF with longer duration of exposure (Figure 4B), thus indicating that enhanced levels of *hupB* make Mtb more tolerant to both RIF and INH. We also observed that overexpressing *hupB* enhanced WT's MIC to INH by 4-fold (Table 1, Supplementary Figure 9A) and to RIF by approximately a fold (Supplementary Figures 7, 10). Interestingly, *rpoB* mutants also modify Mtb into RIF-resistant bacteria, and these exhibit enhanced levels of PDIM and higher expression of *ppsA*-E (Bisson et al., 2012). In contrast, the *hupB* KO mutant not only accumulates significantly reduced amounts of PDIM-A and PDIM-C (Figure 6C) but also exhibits lower expression of *ppsA*, C, E (Figure 6B) and *drrA* (Figure 6D) and becomes more susceptible to lower concentration of RIF (Figure 4B). Despite the KO showing reduced levels of apolar lipids such as PDIMs and MAMEs (panels (ii) and (iii) of Figure 6C, respectively), surprisingly, the KO did not exhibit any enhanced sensitivity to the hydrophilic drug EMB (Supplementary Figure 8).

Our data (Figures 3, 4 and Table 1), albeit *in vitro*, clearly demonstrate that while the lack of *hupB* makes Mtb more susceptible to stresses and antibiotics, the presence and enhanced accumulation of HupB makes Mtb cope with them. Specifically, since lack of *hupB* makes Mtb susceptible to significantly low quantity of INH, when we inhibited WT HupB with a stilbene inhibitor, *viz*., SD1, and then tested the sensitivity of the SD1-treated WT strain to INH, excitingly, the combination of SD1 and INH, despite not being synergistic (Figure 5A), increased the efficacy of SD1 by 2-fold and INH by 4-fold (Figure 5A, Supplementary Table 5) and rapidly killed the axenically cultured bacteria with just 4× MIC of INH (Figure 5B) as compared to the 400× MIC of INH required for the WT (Figure 4A). As expected, we could also significantly kill more THP-1 macrophage-infecting WT bacteria upon combinatorial treatment with SD1 and INH as compared to SD1 and INH alone (Figure 5C), again indicating that targeting HupB helps significantly reduce the dose of INH necessary to kill Mtb.

Although one desires and strives hard to discover an alternate, superior, and novel therapeutic target that supplants the current anti-TB therapeutic molecules, we predict that achieving such a goal is extremely challenging. As an alternate and potentially achievable target that may better support the United Nations (UN) Sustainable Development Goals and is aligned with the UN combinatorial therapy recommendations, we speculate that HupB-targeting together with INH and RIF holds a great promise. While we have just begun our efforts to pre-clinically recapitulate our *in vitro* observations with HupB, in principle, we emphasize that HupB is a very promising combinatorial target when used together with RIF and INH. Given the high MIC for SD1 (Supplementary Table 4), we clearly echo that an alternate to SD1 is absolutely essential to take this target to the next level of promising ones. One promising candidate is the small molecule "3d" developed very recently (Peraman et al., 2021). We are also currently screening a library of small molecules for an alternate to SD1 and "3d".

In summary, our detailed *in vitro* studies with *hupB* and its significant role in helping Mtb cope with stress suggest a model wherein targeting Mtb's HupB with a small molecule inhibitor helps to significantly reduce the expression of type-I polyketide synthases. This, in turn, significantly reduces the levels of several lipids including virulent PDIMs. This promotes increased permeability of the pathogen membrane and enhanced susceptibility to host-mediated stresses (in macrophages) and antibiotic-induced stresses (during treatment). The simultaneous reduction in the expression of PDIMs synthesizing enzymes and *drrA* (and perhaps *drrB* and C because together they form one transporter and are genetically organized as an operon) perhaps prevents any efflux/expulsion of administered INH and RIF, thus significantly reducing their MICs and duration of therapeutic treatment.

Data availability statement

The original contributions presented in the study are included in the article/Supplementary material, further inquiries can be directed to the corresponding author/s.

Author contributions

KA: conceptualization, methodology, resources, supervision, project administration, funding acquisition, data analysis, writing review and editing, and final revision. RS: methodology, resources, and supervision. NSi, NSh, PS, MP, MI, LS, TC, and TG: investigation and data generation. KA, RS, NSi, and PS: formal analysis. KA, NSi, PS, MP, and MI: writing original draft preparation. All authors have read and agreed to the published version of the manuscript.

Funding

This research was primarily funded by the Translational Health Science and Technology Institute's internal grant to KA supported through the Department of Biotechnology, India. KA is a recipient of a Ramalingaswami fellowship from the Department of Biotechnology, India. The Department of Biotechnology, India, funded NSi through a graduate program fellowship. RS acknowledges the funding received from the Department of Biotechnology, India (grant ID BT/PR30215/MED/29/1343/2018). RS is also a recipient of a Ramalingaswami fellowship and National Bioscience Award from the Department of Biotechnology, India, and is a senior fellow of Wellcome Trust-DBT India Alliance (IA/S19/2/504646), India. PS sincerely acknowledges the Science and Engineering Research Board, Government of India for his national post-doctoral fellowship.

Acknowledgments

KA sincerely acknowledges Sarah M. Fortune of Harvard University, United States, for sharing the WT and MSm mycobacterial strains. KA thanks Amit Pandey for the reagent support for lipid extractions. KA thanks the support and help from the purchase, finance, and administrative staff of THSTI. KA and NSi sincerely acknowledge Garima Arora and RS for the phage packing to generate the KO. KA acknowledges the BSL-3 facility of THSTI, India and ICGEB, India. NSi acknowledges the Department of Biotechnology, Government of India for the research fellowship. KA thanks Surjeet Yadav for his laboratory maintenance-related efforts.

Conflict of interest

The authors declare that the research was conducted in the absence of any commercial or financial relationships that could be construed as a potential conflict of interest.

Publisher's note

All claims expressed in this article are solely those of the authors and do not necessarily represent those of their affiliated organizations, or those of the publisher, the editors and the reviewers. Any product that may be evaluated in this article, or claim that may be made by its manufacturer, is not guaranteed or endorsed by the publisher.

Supplementary material

The Supplementary Material for this article can be found online at: https://www.frontiersin.org/articles/10.3389/fmicb.2022.937970/full#supplementary-material

References

Ali Azam, T., Iwata, A., Nishimura, A., Ueda, S., and Ishihama, A. (1999). Growth phase-dependent variation in protein composition of the *Escherichia coli* nucleoid. *J. Bacteriol.* 181, 6361–6370. doi: 10.1128/JB.181.20.6361-6370.1999

Ando, H., Kitao, T., Miyoshi-Akiyama, T., Kato, S., Mori, T., and Kirikae, T. (2011). Downregulation of *katG* expression is associated with isoniazid resistance in *Mycobacterium tuberculosis*. *Mol. Microbiol.* 79, 1615–1628. doi: 10.1111/j.1365-2958.2011.07547.x

Anil Kumar, V., Goyal, R., Bansal, R., Singh, N., Sevalkar, R. R., Kumar, A., et al. (2016). EspR-dependent ESAT-6 protein secretion of *Mycobacterium tuberculosis* requires the presence of virulence regulator PhoP*. *J. Biol. Chem.* 291, 19018–19030. doi: 10.1074/jbc.M116.746289

Anuchin, A. M., Goncharenko, A. V., Demina, G. R., Mulyukin, A. L., Ostrovsky, D. N., and Kaprelyants, A. S. (2010). The role of histone-like protein, Hlp, in *Mycobacterium smegmatis* dormancy. *FEMS Microbiol. Lett.* 308, 101–107. doi: 10.1111/j.1574-6968.2010.01988.x

Arora, G., Bothra, A., Prosser, G., Arora, K., and Sajid, A. (2021). Role of post-translational modifications in the acquisition of drug resistance in *Mycobacterium tuberculosis*. *FEBS J.* 288, 3375–3393. doi: 10.1111/febs.15582

Arora, G., Gagandeep, Behura, A., Gosain, T. P., Shaliwal, R. P., and Kidwai, S., et al. (2020). NSC 18725, a pyrazole derivative inhibits growth of intracellular *Mycobacterium tuberculosis* by induction of autophagy. *Front. Microbiol.* 10, 3051. doi: 10.3389/fmicb.2019.03051

Atmakuri, K., Ding, Z., and Christie, P. J. (2003). VirE2, a type IV secretion substrate, interacts with the VirD4 transfer protein at cell poles of *Agrobacterium tumefaciens*. *Mol. Microbiol.* 49, 1699–1713. doi: 10.1046/j.1365-2958.2003.03669.x

Bardarov, S., Bardarov, S., Pavelka, M. S., Sambandamurthy, V., Larsen, M., Tufariello, J., et al. (2002). Specialized transduction: an efficient method for generating marked and unmarked targeted gene disruptions in *Mycobacterium tuberculosis*, *M. bovis* BCG and *M. smegmatis*. *Microbiology* 148, 3007–3017. doi: 10.1099/00221287-148-10-3007

Betts, J. C., Lukey, P. T., Robb, L. C., McAdam, R. A., and Duncan, K. (2002). Evaluation of a nutrient starvation model of *Mycobacterium tuberculosis* persistence by gene and protein expression profiling. *Mol. Microbiol* 43, 717–731. doi: 10.1046/j.1365-2958.2002.02779.x

Bhat, Z. S., Rather, M. A., Maqbool, M., and Ahmad, Z. (2018). Drug targets exploited in *Mycobacterium tuberculosis*: pitfalls and promises on the horizon. *Biomed. Pharmacother.* 103, 1733–1747. doi: 10.1016/j.biopha.2018.04.176

Bhowmick, T., Ghosh, S., Dixit, K., Ganesan, V., Ramagopal, U. A., Dey, D., et al. (2014). Targeting *Mycobacterium tuberculosis* nucleoid-associated protein HU with structure-based inhibitors. *Nat. Commun* 5, 4124. doi: 10.1038/ncomms5124

Bisson, G. P., Mehaffy, C., Broeckling, C., Prenni, J., Rifat, D., Lun, D. S., et al. (2012). Upregulation of the phthiocerol dimycocerosate biosynthetic pathway by rifampin-resistant, rpoB mutant *Mycobacterium tuberculosis*. *J. Bacteriol.* 194, 6441–6452. doi: 10.1128/JB.01013-12

Braibant, M., Gilot, P., and Content, J. (2000). The ATP binding cassette (ABC) transport systems of *Mycobacterium tuberculosis*. *FEMS Microbiol. Rev.* 24, 449–467. doi: 10.1111/j.1574-6976.2000.tb00550.x

Camacho, L. R., Constant, P., Raynaud, C., Laneelle, M. A., Triccas, J. A., Gicquel, B., et al. (2001). Analysis of the phthiocerol dimycocerosate locus of *Mycobacterium tuberculosis*. Evidence that this lipid is involved in the cell wall permeability barrier. *J. Biol. Chem.* 276, 19845–19854. doi: 10.1074/jbc.M100662200

Cao, G., Howard, S. T., Zhang, P., Wang, X., Chen, X.-L., Samten, B., et al. (2015). EspR, a regulator of the ESX-1 secretion system in *Mycobacterium tuberculosis*, is directly regulated by the two-component systems MprAB and PhoPR. *Microbiology* 161, 477–489. doi: 10.1099/mic.0.000023

Castro, A. T. E., Mendes, M., Freitas, S., and Roxo, P. C. (2015). Incidence and risk factors of major toxicity associated to first-line antituberculosis drugs for latent and active tuberculosis during a period of 10 years. *Rev. Port. Pneumol (2006)* 21, 144–150. doi: 10.1016/j.rppnen.2014.08.004

Cazabon, D., Alsdurf, H., Satyanarayana, S., Nathavitharana, R., Subbaraman, R., Daftary, A., et al. (2017). Quality of tuberculosis care in high burden countries: the urgent need to address gaps in the care cascade. *Int. J. Infect. Dis.* 56, 111–116. doi: 10.1016/j.ijid.2016.10.016

Chauhan, P., Reddy, P. V., Singh, R., Jaisinghani, N., Gandotra, S., and Tyagi, A. K. (2013). Secretory phosphatases deficient mutant of *Mycobacterium tuberculosis* imparts protection at the primary site of infection in guinea pigs. *PLoS ONE* 8, e77930. doi: 10.1371/journal.pone.0077930

Chen, J. M., Ren, H., Shaw, J. E., Wang, Y. J., Li, M., Leung, A. S., et al. (2008). Lsr2 of *Mycobacterium tuberculosis* is a DNA-bridging protein. *Nucleic Acids Res.* 36, 2123–2135. doi: 10.1093/nar/gkm1162

Coll, F., Phelan, J., Hill-Cawthorne, G. A., Nair, M. B., Mallard, K., Ali, S., et al. (2018). Genome-wide analysis of multi- and extensively drug-resistant *Mycobacterium tuberculosis*. *Nat. Genet.* 50, 307–316. doi: 10.1038/s41588-017-0029-0

Collins, L., and Franzblau, S. G. (1997). Microplate alamar blue assay versus BACTEC 460 system for high-throughput screening of compounds against *Mycobacterium tuberculosis* and *Mycobacterium avium*. *Antimicrob. Agents Chemother.* 41, 1004–1009. doi: 10.1128/AAC.41.5.1004

Datta, C., Jha, R. K., Ahmed, W., Ganguly, S., Ghosh, S., and Nagaraja, V. (2019). Physical and functional interaction between nucleoid-associated proteins HU and Lsr2 of *Mycobacterium tuberculosis*: altered DNA binding and gene regulation. *Mol. Microbiol.* 111, 981–994. doi: 10.1111/mmi.14202

Dillon, S. C., and Dorman, C. J. (2010). Bacterial nucleoid-associated proteins, nucleoid structure and gene expression. *Nat. Rev. Microbiol.* 8, 185–195. doi: 10.1038/nrmicro2261

Domenech, P., and Reed, M. B. (2009). Rapid and spontaneous loss of phthiocerol dimycocerosate (PDIM) from *Mycobacterium tuberculosis* grown *in vitro*: implications for virulence studies. *Microbiology* 155, 3532–3543. doi: 10.1099/mic.0.029199-0

Dorman, C. J., and Deighan, P. (2003). Regulation of gene expression by histone-like proteins in bacteria. *Curr. Opin. Genet. Dev.* 13, 179–184. doi: 10.1016/S0959-437X(03)00025-X

Dover, L. G., Cerdeño-Tárraga, A. M., Pallen, M. J., Parkhill, J., and Besra, G. S. (2004). Comparative cell wall core biosynthesis in the mycolated pathogens, *Mycobacterium tuberculosis* and *Corynebacterium diphtheriae*. *FEMS Microbiol. Rev.* 28, 225–250. doi: 10.1016/j.femsre.2003.10.001

Duncan, K., and Barry, C. E. (2004). Prospects for new antitubercular drugs. *Curr. Opin. Microbiol.* 7, 460–465. doi: 10.1016/j.mib.2004.08.011

Ehrt, S., and Schnappinger, D. (2009). Mycobacterial survival strategies in the phagosome: defence against host stresses. *Cell Microbiol.* 11, 1170–1178. doi: 10.1111/j.1462-5822.2009.01335.x

Fontán, P. A., Voskuil, M. I., Gomez, M., Tan, D., Pardini, M., Manganelli, R., et al. (2009). The *Mycobacterium tuberculosis* sigma factor σB is required for full response to cell envelope stress and hypoxia *in vitro*, but it is dispensable for *in vivo* growth. *J. Bacteriol.* 191, 5628–5633. doi: 10.1128/JB.00510-09

Forget, E. J., and Menzies, D. (2006). Adverse reactions to first-line antituberculosis drugs. *Expert Opin. Drug Saf.* 5, 231–249. doi: 10.1517/14740338.5.2.231

Garces, A., Atmakuri, K., Chase, M. R., Woodworth, J. S., Krastins, B., Rothchild, A. C., et al. (2010). EspA acts as a critical mediator of ESX1-dependent virulence in *Mycobacterium tuberculosis* by affecting bacterial cell wall integrity. *PLoS Pathog* 6, e1000957. doi: 10.1371/journal.ppat.1000957

Gebhardt, H., Meniche, X., Tropis, M., Krämer, R., Daffé, M., and Morbach, S. (2007). The key role of the mycolic acid content in the functionality of the cell wall permeability barrier in Corynebacterineae. *Microbiology* 153, 1424–1434. doi: 10.1099/mic.0.2006/003541-0

Ghosh, S., Padmanabhan, B., Anand, C., and Nagaraja, V. (2016). Lysine acetylation of the *Mycobacterium tuberculosis* HU protein modulates its DNA binding and genome organization. *Mol. Microbiol.* 100, 577–588. doi: 10.1111/mmi.13339

Global tuberculosis report (2020). Available online at: https://www.who.int/publications-detail-redirect/9789240013131 (accessed October 14, 2020).

Goude, R., and Parish, T. (2008). The genetics of cell wall biosynthesis in *Mycobacterium tuberculosis*. *Future Microbiol.* 3, 299–313. doi: 10.2217/17460913.3.3.299

Green, M. R., and Sambrook, J. (2012). *Molecular Cloning: A Laboratory Manual*. 4th ed. Cold Spring Harbor, N.Y: Cold Spring Harbor Laboratory Press.

Gupta, M., Sajid, A., Sharma, K., Ghosh, S., Arora, G., Singh, R., et al. (2014). HupB, a nucleoid-associated protein of *Mycobacterium tuberculosis*, is modified by serine/threonine protein kinases *in vivo*. *J. Bacteriol.* 196, 2646–2657. doi: 10.1128/JB.01625-14

Hadizadeh Tasbiti, A., Yari, S., Davar Siadat, S., Karimipoor, M., Badmasti, F., Masoumi, M., et al. (2021). Comparing mRNA expression and protein abundance in MDR Mycobacterium tuberculosis: Novel protein candidates, Rv0443, Rv0379 and Rv0147 as TB potential diagnostic or therapeutic targets. *Biotechnol Rep (Amst).* 30:e00641. doi: 10.1016/j.btre.2021.e00641

Hadizadeh Tasbiti, A. R., Yari, S., Ghanei, M., Siadat, S. D., Niknami, S., and Bahrmand, A. (2016). Differential protein expression in *Mycobacterium tuberculosis* susceptible and multidrug resistant isolates. *Vaccine Res.* 3, 26–30. doi: 10.18869/acadpub.vacres.2.5.118

Hingley-Wilson, S. M., Lougheed, K. E. A., Ferguson, K., Leiva, S., and Williams, H. D. (2010). Individual *Mycobacterium tuberculosis* universal stress protein homologues are dispensable *in vitro*. *Tuberculosis* 90, 236–244. doi: 10.1016/j.tube.2010.03.013

Hołówka, J., Trojanowski, D., Ginda, K., Wojtaś, B., Gielniewski, B., Jakimowicz, D., et al. (2017). HupB is a bacterial nucleoid-associated protein with an indispensable eukaryotic-like tail. *mBio*. 8. doi: 10.1128/mBio.01272-17

Hołówka, J., and Zakrzewska-Czerwińska, J. (2020). Nucleoid associated proteins: the small organizers that help to cope with stress. *Front. Microbiol.* 11:590. doi: 10.3389/fmicb.2020.00590

Huynh, K. K., Joshi, S. A., and Brown, E. J. (2011). A delicate dance: host response to mycobacteria. *Curr. Opin. Immunol.* 23, 464–472. doi: 10.1016/j.coi.2011.06.002

Kalra, P., Mishra, S. K., Kaur, S., Kumar, A., Prasad, H. K., Sharma, T. K., et al. (2018). G-quadruplex-forming DNA aptamers inhibit the DNA-binding function of HupB and *Mycobacterium tuberculosis* entry into host cells. *Mol. Ther. Nucleic Acids* 13, 99–109. doi: 10.1016/j.omtn.2018.08.011

Katsube, T., Matsumoto, S., Takatsuka, M., Okuyama, M., Ozeki, Y., Naito, M., et al. (2007). Control of cell wall assembly by a histone-like protein in mycobacteria. *J. Bacteriol.* 189, 8241–8249. doi: 10.1128/JB.00550-07

Kaul, G., Kapoor, E., Dasgupta, A., and Chopra, S. (2019). Management of multidrug-resistant tuberculosis in the 21st century. *Drugs Today* 55, 215–224. doi: 10.1358/dot.2019.55.3.2927587

Khosravi, A. D., Sirous, M., Absalan, Z., Tabandeh, M. R., and Savari, M. (2019). Comparison Of *drrA* and *drrB* efflux pump genes expression in drug-susceptible and -resistant *Mycobacterium tuberculosis* strains isolated from tuberculosis patients in Iran. *Infect Drug Resist.* 12, 3437–3444. doi: 10.2147/IDR.S221823

Kołodziej, M., Trojanowski, D., Bury, K., Hołówka, J., Matysik, W., Kakolewska, H., et al. (2021). Lsr2, a nucleoid-associated protein influencing mycobacterial cell cycle. *Sci. Rep.* 11, 2910. doi: 10.1038/s41598-021-82295-0

Kriel, N. L., Gallant, J., van Wyk, N., van Helden, P., Sampson, S. L., Warren, R. M., et al. (2018). Mycobacterial nucleoid associated proteins: an added dimension in gene regulation. *Tuberculosis* 108, 169–177. doi: 10.1016/j.tube.2017.12.004

Kumar, S., Sardesai, A. A., Basu, D., Muniyappa, K., and Hasnain, S. E. (2010). DNA clasping by mycobacterial HU: the C-terminal region of HupB mediates increased specificity of DNA binding. *PLoS ONE* 5, e12551. doi: 10.1371/journal.pone.0012551

Lee, B. H., Murugasu-Oei, B., and Dick, T. (1998). Upregulation of a histone-like protein in dormant *Mycobacterium smegmatis*. *Mol. Gen. Genet.* 260, 475–479. doi: 10.1007/s004380050919

Li, G., Zhang, J., Guo, Q., Jiang, Y., Wei, J., Zhao, L., et al. (2015). Efflux pump gene expression in multidrug-resistant *Mycobacterium tuberculosis* clinical isolates. *PLoS ONE* 10, e0119013. doi: 10.1371/journal.pone.0119013

Lin, W., de Sessions, P. F., Teoh, G. H. K., Mohamed, A. N. N., Zhu, Y. O., Koh, V. H. Q., et al. (2016). Transcriptional profiling of *Mycobacterium tuberculosis* exposed to *in vitro* lysosomal stress. *Infect. Immun.* 84, 2505–2523. doi: 10.1128/IAI.00072-16

MacGurn, J. A., and Cox, J. S. (2007). A genetic screen for *Mycobacterium tuberculosis* mutants defective for phagosome maturation arrest identifies components of the ESX-1 secretion system. *Infect. Immun.* 75, 2668–2678. doi: 10.1128/IAI.01872-06

Madhav, B., Iyer, A., and Jayalakshmi, T. K. (2015). Side effect profile of 2nd line drugs in multi drug resistant (MDR) and extensively drug resistant (XDR) tuberculosis. *Eur. Respir. J.* 46:PA2708. doi: 10.1183/13993003.congress-2015.PA2708

Mahmood, T., and Yang, P. C. (2012). Western blot: technique, theory, and trouble shooting. *N. Am. J. Med. Sci*. 4, 429–434. doi: 10.4103/1947-2714.100998

Mandal, S., Chadha, V. K., Laxminarayan, R., and Arinaminpathy, N. (2017). Counting the lives saved by DOTS in India: a model-based approach. *BMC Med.* 15, 47. doi: 10.1186/s12916-017-0809-5

Matsumoto, S., Furugen, M., Yukitake, H., and Yamada, T. (2000). The gene encoding mycobacterial DNA-binding protein I (MDPI) transformed rapidly growing bacteria to slowly growing bacteria. *FEMS Microbiol. Lett*. 182, 297–301. doi: 10.1111/j.1574-6968.2000.tb08911.x

Monahan, M. I., Betts, J., Banerjee, K. D., and Butcher, D. P. (2001). Differential expression of mycobacterial proteins following phagocytosis by macrophages. *Microbiology* 147, 459–471 doi: 10.1099/00221287-147-2-459

Mukherjee, A., DiMario, P. J., and Grove, A. (2009). *Mycobacterium smegmatis* histone-like protein Hlp is nucleoid associated. *FEMS Microbiol. Lett*. 291, 232–240. doi: 10.1111/j.1574-6968.2008.01458.x

Neyrolles, O., Wolschendorf, F., Mitra, A., and Niederweis, M. (2015). Mycobacteria, metals, and the macrophage. *Immunol. Rev*. 264, 249–263. doi: 10.1111/imr.12265

Niki, M., Niki, M., Tateishi, Y., Ozeki, Y., Kirikae, T., Lewin, A., et al. (2012). A novel mechanism of growth phase-dependent tolerance to isoniazid in mycobacteria. *J. Biol. Chem*. 287, 27743–27752. doi: 10.1074/jbc.M111.333385

Odds, F. C. (2003). Synergy, antagonism, and what the chequerboard puts between them. *J. Antimicrob. Chemother*. 52, 1. doi: 10.1093/jac/dkg301

Out, A. A. (2013). Is the directly observed therapy short course (DOTS) an effective strategy for tuberculosis control in a developing country? *Asian Pac. J. Trop. Dis*. 3, 227–231. doi: 10.1016/S2222-1808(13)60045-6

Pandey, S. D., Choudhury, M., and Sritharan, M. (2014b). Transcriptional regulation of *Mycobacterium tuberculosis* hupB gene expression. *Microbiology* 160, 1637–1647. doi: 10.1099/mic.0.079640-0

Pandey, S. D., Choudhury, M., Yousuf, S., Wheeler, P. R., Gordon, S. V., Ranjan, A., et al. (2014a). Iron-regulated protein HupB of *Mycobacterium tuberculosis* positively regulates siderophore biosynthesis and is essential for growth in macrophages. *J. Bacteriol*. 196, 1853–1865. doi: 10.1128/JB.01483-13

Parish, T., and Stoker, N. G. (2001). *Mycobacterium tuberculosis Protocols*. London: Springer Science and Business Media.

Peraman, R., Meka, G., Chilamakuru, N. B., Kutagulla, V. K., Malla, S., Ashby, C. R., et al. (2021). Novel stilbene scaffolds efficiently target *Mycobacterium tuberculosis* nucleoid-associated protein, HU. *New J. Chem*. 45, 10683–10692. doi: 10.1039/D0NJ05947A

Pethe, K., Swenson, D. L., Alonso, S., Anderson, J., Wang, C., and Russell, D. G. (2004). Isolation of *Mycobacterium tuberculosis* mutants defective in the arrest of phagosome maturation. *Proc. Natl. Acad. Sci. U. S. A*. 101, 13642–13647. doi: 10.1073/pnas.0401657101

Pinault, L., Han, J.-S., Kang, C.-M., Franco, J., and Ronning, D. R. (2013). Zafirlukast Inhibits Complexation of Lsr2 with DNA and Growth of *Mycobacterium tuberculosis*. *Antimicrob. Agents Chemother*. 57, 2134–2140. doi: 10.1128/AAC.02407-12

Prabhakar, S., Annapurna, P. S., Jain, N. K., Dey, A. B., Tyagi, J. S., and Prasad, H. K. (1998). Identification of an immunogenic histone-like protein (HLPMt) of *Mycobacterium tuberculosis*. *Tuber Lung Dis*. 79, 43–53. doi: 10.1054/tuld.1998.0004

Prasad, R., Singh, A., Balasubramanian, V., and Gupta, N. (2017). Extensively drug-resistant tuberculosis in India: current evidence on diagnosis and management. *Indian J. Med. Res*. 145, 271–293. doi: 10.4103/ijmr.IJMR_177_16

Prasad, R., Singh, A., and Gupta, N. (2019). Adverse drug reactions in tuberculosis and management. *Indian J. Tuberc*. 66, 520–532. doi: 10.1016/j.ijtb.2019.11.005

Priyadarshini, R., Cugini, C., Arndt, A., Chen, T., Tjokro, N. O., Goodman, S. D., et al. (2013). The nucleoid-associated protein HUβ affects global gene expression in *Porphyromonas gingivalis*. *Microbiology* 159, 219–229. doi: 10.1099/mic.0.061002-0

Reddy, T. B. K., Riley, R., Wymore, F., Montgomery, P., DeCaprio, D., Engels, R., et al. (2009). TB database: an integrated platform for tuberculosis research. *Nucleic. Acids Res*. 37, D499–508. doi: 10.1093/nar/gkn652

Reingewertz, T. H., Meyer, T., McIntosh, F., Sullivan, J., Meir, M., Chang, Y.-F., et al. (2020). Differential sensitivity of mycobacteria to isoniazid is related to differences in *KatG*-mediated enzymatic activation of the drug. *Antimicrob Agents Chemother*. 64, e01899–e01819. doi: 10.1128/AAC.01899-19

Remm, S., Earp, J. C., Dick, T., Dartois, V., and Seeger, M. A. (2022). Critical discussion on drug efflux in *Mycobacterium tuberculosis*. *FEMS Microbiol. Rev*. 46, fuab050. doi: 10.1093/femsre/fuab050

Rens, C., Chao, J. D., Sexton, D. L., Tocheva, E. I., and Av-Gay, Y. (2021). Roles for phthiocerol dimycocerosate lipids in *Mycobacterium tuberculosis* pathogenesis. *Microbiology (Reading)*. 167:001042. doi: 10.1099/mic.0.001042

Sakatos, A., Babunovic, G. H., Chase, M. R., Dills, A., Leszyk, J., Rosebrock, T., et al. (2018). Posttranslational modification of a histone-like protein regulates phenotypic resistance to isoniazid in mycobacteria. *Sci. Adv*. 4, eaao1478. doi: 10.1126/sciadv.aao1478

Salina, E. G., Grigorov, A., Skvortsova, Y., Majorov, K., Bychenko, O., Ostrik, A., et al. (2019). MTS1338, a small *Mycobacterium tuberculosis* RNA, regulates transcriptional shifts consistent with bacterial adaptation for entering into dormancy and survival within host macrophages. *Front. Cell. Infect. Microbiol*. 9:405. doi: 10.3389/fcimb.2019.00405

Sambandan, D., Dao, D. N., Weinrick, B. C., Vilcheze, C., Gurcha, S. S., Ojha, A., et al. (2013). Keto-mycolic acid-dependent pellicle formation confers tolerance to drug-sensitive *Mycobacterium tuberculosis*. *mBio*4, e00222–e00213 doi: 10.1128/mBio.00222-13

Sambrook, J., and Russell, D. W. (2006). Preparation and transformation of competent *E. coli* using calcium chloride. *CSH Protoc*. 2006:pdb.prot3932. doi: 10.1101/pdb.prot3932

Sassetti, C. M., Boyd, D. H., and Rubin, E. J. (2003). Genes required for mycobacterial growth defined by high density mutagenesis. *Mol. Microbiol*. 48, 77–84. doi: 10.1046/j.1365-2958.2003.03425.x

Seung, K. J., Keshavjee, S., and Rich, M. L. (2015). Multidrug-resistant tuberculosis and extensively drug-resistant tuberculosis. *Cold Spring Harb. Perspect. Med*. 5, a017863. doi: 10.1101/cshperspect.a017863

Sezonov, G., Joseleau-Petit, D., and D'Ari, R. (2007). *Escherichia coli* physiology in luria-bertani broth. *J. Bacteriol*. 189, 8746–8749. doi: 10.1128/JB.01368-07

Sharma, N., Aggarwal, S., Kumar, S., Sharma, R., Choudhury, K., Singh, N., et al. (2019). Comparative analysis of homologous aminopeptidase PepN from pathogenic and non-pathogenic mycobacteria reveals divergent traits. *PLoS ONE* 14, e0215123. doi: 10.1371/journal.pone.0215123

Shetye, G. S., Franzblau, S. G., and Cho, S. (2020). New tuberculosis drug targets, their inhibitors, and potential therapeutic impact. *Transl. Res*. 220, 68–97. doi: 10.1016/j.trsl.2020.03.007

Shires, K., and Steyn, L. (2001). The cold-shock stress response in *Mycobacterium smegmatis* induces the expression of a histone-like protein. *Mol. Microbiol*. 39, 994–1009. doi: 10.1046/j.1365-2958.2001.02291.x

Singh, R., Singh, M., Arora, G., Kumar, S., Tiwari, P., and Kidwai, S. (2013). Polyphosphate deficiency in *Mycobacterium tuberculosis* is associated with enhanced drug susceptibility and impaired growth in guinea pigs. *J. Bacteriol*. 95, 2839–2851. doi: 10.1128/JB.00038-13

Singh, V., and Mizrahi, V. (2017). Identification and validation of novel drug targets in *Mycobacterium tuberculosis*. *Drug Discovery Today* 22, 503–509. doi: 10.1016/j.drudis.2016.09.010

Sritharan, M. (2016). Iron homeostasis in *Mycobacterium tuberculosis*: mechanistic insights into siderophore-mediated iron uptake. *J. Bacteriol*. 198, 2399–2409. doi: 10.1128/JB.00359-16

Tiwari, P., Arora, G., Singh, M., Kidwai, S., Narayan, O. P., and Singh, R. (2015). MazF ribonucleases promote *Mycobacterium tuberculosis* drug tolerance and virulence in guinea pigs. *Nat. Commun*. 6, 6059. doi: 10.1038/ncomms7059

Trivedi, O. A., Arora, P., Vats, A., Ansari, M. Z., Tickoo, R., and Sridharan, V., et al. (2005). Dissecting the mechanism and assembly of a complex virulence mycobacterial lipid. *Molecular Cell* 17, 631–643. doi: 10.1016/j.molcel.2005.009

Upadhyay, S., Mittal, E., and Philips, J. A. (2018). Tuberculosis and the art of macrophage manipulation. *Pathog. Dis*. 76:fty037. doi: 10.1093/femspd/fty037

Vergne, I., Gilleron, M., and Nigou, J. (2015). Manipulation of the endocytic pathway and phagocyte functions by *Mycobacterium tuberculosis* lipoarabinomannan. *Front. Cell. Infect. Microbiol*. 4, 187. doi: 10.3389/fcimb.2014.00187

Voskuil, M. I., Bartek, I. L., Visconti, K., and Schoolnik, G. K. (2011). The response of *Mycobacterium tuberculosis* to reactive oxygen and nitrogen species. *Front. Microbiol*. 2, 105. doi: 10.3389/fmicb.2011.00105

Wellington, S., and Hung, D. T. (2018). The expanding diversity of *Mycobacterium tuberculosis* drug targets. *ACS Infect. Dis*. 4, 696–714. doi: 10.1021/acsinfecdis.7b00255

Whiteford, D. C., Klingelhoets, J. J., Bambenek, M. H., and Dahl, J. L. (2011). Deletion of the histone-like protein (Hlp) from *Mycobacterium smegmatis* results in increased sensitivity to UV exposure, freezing and isoniazid. *Microbiology* 157, 327–335. doi: 10.1099/mic.0.045518-0

Yaseen, I., Choudhury, M., Sritharan, M., and Khosla, S. (2018). Histone methyltransferase SUV39H1 participates in host defense by methylating mycobacterial histone-like protein HupB. *EMBO J.* 37, 183–200. doi: 10.15252/embj.201796918

Yee, D., Valiquette, C., Pelletier, M., Parisien, I., Rocher, I., and Menzies, D. (2003). Incidence of serious side effects from first-line antituberculosis drugs among patients treated for active tuberculosis. *Am. J. Respir. Crit. Care Med*. 167, 1472–1477. doi: 10.1164/rccm.200206-626OC

Zhang, Q., An, X., Liu, H., Wang, S., Xiao, T., and Liu, H. (2019). Uncovering the resistance mechanism of *Mycobacterium tuberculosis* to rifampicin due to RNA polymerase H451D/Y/R mutations from computational perspective. *Front. Chem.* 7, 819. doi: 10.3389/fchem.2019.00819

Zhu, C., Zhao, Y., Huang, X., Pang, Y., Zhao, Y., Zhuang, Y., et al. (2013). Quantitative proteomic analysis of streptomycin resistant and sensitive clinical isolates of *Mycobacterium tuberculosis*. *Wei Sheng Wu Xue Bao* 53, 154–163.

Zulauf, K. E., Sullivan, J. T., and Braunstein, M. (2018). The SecA2 pathway of *Mycobacterium tuberculosis* exports effectors that work in concert to arrest phagosome and autophagosome maturation. *PLoS Pathog.* 14, e1007011. doi: 10.1371/journal.ppat.1007011

frontiers | Frontiers in Microbiology

TYPE Opinion
PUBLISHED 03 October 2022
DOI 10.3389/fmicb.2022.1020198

OPEN ACCESS

EDITED BY
George William Carnell,
University of Cambridge,
United Kingdom

REVIEWED BY
Jaime Martinez,
University of Miami Health System,
United States
Jatin Ashar,
Mumbai Eye Care, India
Alice Matoba,
Baylor College of Medicine,
United States

*CORRESPONDENCE
Jodhbir S. Mehta
jodmehta@gmail.com

SPECIALTY SECTION
This article was submitted to Infectious Agents and Disease, a section of the journal Frontiers in Microbiology

RECEIVED 16 August 2022
ACCEPTED 20 September 2022
PUBLISHED 03 October 2022

CITATION
Ting DSJ, Chodosh J and Mehta JS (2022) Achieving diagnostic excellence for infectious keratitis: A future roadmap.
Front. Microbiol. 13:1020198.
doi: 10.3389/fmicb.2022.1020198

Achieving diagnostic excellence for infectious keratitis: A future roadmap

Darren S. J. Ting[1,2], James Chodosh[3] and Jodhbir S. Mehta[4,5]*

[1]Academic Ophthalmology, School of Medicine, University of Nottingham, Nottingham, United Kingdom, [2]Department of Ophthalmology, Queen's Medical Centre, Nottingham, United Kingdom, [3]Department of Ophthalmology, Massachusetts Eye and Ear and Harvard Medical School, Boston, MA, United States, [4]Department of Cornea & Refractive Surgery, Singapore National Eye Centre, Singapore, Singapore, [5]Singapore Eye Research Institute, Singapore, Singapore

KEYWORDS

corneal ulcer, corneal infection, microbial keratitis, infectious keratitis, artificial intelligence, next generating sequencing, digital technologies, diagnosis

Introduction

Infectious keratitis (IK), also known as corneal infection, is the 5th leading cause of vision impairment and blindness globally (Flaxman et al., 2017). Once recognized as a "silent epidemic," the incidence of IK is now estimated at 2.5–799 per 100,000 population-year, with a significantly higher incidence noted in low- and middle-income countries (LMICs) (Ting et al., 2021a). It has so far resulted in ∼5 million cases of blindness and/or significant vision impairment and is estimated to account for 1.5–2.0 million cases of monocular blindness per year. A recent systematic review estimated that fungal keratitis alone affects >1 million people annually, particularly in Africa and Asia, particularly China, India and Nepal (Brown et al., 2021). In addition, approximately $175 million dollars are being spent on IK annually within the healthcare systems of the United States. In view of the significant burden on the global population, healthcare system and economy, a recent international consortium has proposed the addition of IK to the list of neglected tropical diseases (NTDs), with an aim to draw global concerted and sustained efforts in tackling this important disease (Ung et al., 2019).

IK is a painful and potentially sight-threatening condition that often requires intensive medical and/or surgical interventions (Khor et al., 2018; Ting et al., 2021b). Complications such as corneal melt, perforation, endophthalmitis and complete loss of the eye may sometimes ensue despite intensive treatment (Khor et al., 2018; Cabrera-Aguas et al., 2021; Ting et al., 2021b,c). A timely and accurate diagnosis is often the key to a successful clinical outcome, though this is not always possible in clinical practice due to various barriers (Table 1). In this Opinion article, we discuss the current diagnostic modalities for IK and their limitations and highlight the potential solutions that can be offered by the recent advancement in digital innovations and clinical metagenomic next generation sequencing (NGS).

Current diagnostic approach and limitations

IK is primarily diagnosed on clinical grounds with support of microbiological findings. It is characterized by corneal ulceration, inflammation and/or infiltrate (an abscess manifesting as a white corneal opacity). A wide range of pathogens, including bacteria, fungi, parasites, and viruses, are capable of causing IK. However, the clinical features are often poorly differentiated, especially in patients with late presentation (common in LMIC populations), and may be complicated by the presence of polymicrobial infections (occurring in 2–15%) (Ting et al., 2019a, 2021a; Khoo et al., 2020). Several studies have highlighted the inability of corneal experts to accurately determine the underlying cause of IK (based on clinical photographs) in >50% cases, highlighting the diagnostic challenges based on clinical presentation alone (Redd et al., 2022a).

Corneal sampling for microbiological investigations such as microscopy, culture and sensitivity testing is the current "gold standard" in clinical practice to help determine the underlying causative pathogens and guide the choice of antimicrobial treatment. Nonetheless, due to a considerably low bioburden in IK (as compared to systemic infections), the culture yield is hindered by invariably low sensitivity (30–50%) and slow turnaround time for positive results (e.g., the incubation time may take up to 2 weeks for certain pathogens). A negative culture result can lead to significant therapeutic challenges, particularly in cases with poor initial treatment response to broad-spectrum antimicrobial therapy, as clinicians are often pressured to subject the affected patients to polypharmacy (i.e., concurrent use of different antimicrobials) to ensure the maximal coverage of possible causative organisms (a "blanket approach"). This can in turn lead to undesirable dose-dependent ocular toxicity, impede corneal healing and exacerbate corneal ulceration/melt, culminating in corneal opacity and blindness.

The limitations of the current diagnostic approaches are varied in different settings and may be more specific or relevant to certain populations/countries. For instance, in LMICs, the lack of access to healthcare services and the lower level of patient education can result in late presentation of the disease. This can lead to poorly differentiated clinical features, less accurate diagnosis, and most importantly, worse clinical outcomes. In addition, the relative lack of resources in such settings (e.g., microbiological services and facilities) limits the clinician's capacity to make the clinical diagnosis. On the other hand, patients residing in high-income countries (HICs) have better access to healthcare systems, and in these settings, improving the likelihood of a microbiologic diagnosis would be beneficial. Understanding the diagnostic limitations specific to certain regions or populations will enable a more efficient and effective implementation of future innovations for improving the diagnosis and treatment of IK.

Potential solutions for improving diagnostic performance

Digital innovations

In recent years, the simultaneous advancement in deep learning (DL)-based artificial intelligence (AI) techniques, computer processing power, internet-of-things, and big data analytics have unlocked the potential of digital health. Within ophthalmology, AI-assisted models have facilitated image-based automated medical diagnosis for a range of ocular diseases and assisted in clinical triage and decision making, thereby enhancing the workflow efficiency in healthcare services in both high-income countries (HICs) and LMICs (Li et al., 2020, 2021; Rampat et al., 2021; Tiwari et al., 2022). Recently, Li et al. (2020) demonstrated the potential of using a DL-based algorithm with densely annotated slit-lamp photographs to accurately diagnose and distinguish various ocular diseases, including IK, conjunctivitis, pterygium, and cataract, and to provide automated treatment recommendation. The AI model was further tested prospectively in a real-world setting and demonstrated high accuracy (>90%) in making the correct treatment recommendation, with good end-user satisfaction (including both patients and doctors).

In addition, DL-based models have demonstrated good accuracy in differentiating the underlying cause of IK, particularly between bacterial and fungal keratitis (Hung et al., 2021; Redd et al., 2022b), which is a common diagnostic dilemma in clinical practice. Redd et al. (2022b) recently evaluated five convolutional neural networks using images of culture-proven IK obtained from handheld cameras and reported a higher diagnostic accuracy of the CNN-based DL models when compared to cornea experts (area under the ROC = 0.84 vs. 0.76). Another study has also shown the ability of a CNN-based DL model in accurately distinguishing between corneal scars and IK (Tiwari et al., 2022), which serves as a useful and inexpensive system to aid the triage, assessment, initiation and cessation of antimicrobial therapy for IK in regions with limited access to eye care.

Clinical metagenomic next generation sequencing

Polymerase chain reaction (PCR)-based molecular diagnostics have proven to be a useful diagnostic tool for various infectious diseases, including IK (Yang and Rothman, 2004). The advent of next generation sequencing (NGS), a

TABLE 1 Current diagnostic challenges of infectious keratitis (IK) and future potential solutions enabled by digital innovations and clinical metagenomic next generation sequencing (NGS).

Current challenges	Underlying reasons	Potential solutions
Delayed diagnosis	• Limited access to healthcare systems, particularly in LMICs. • Lack of clinical expertise and resources. • Poor awareness/education of the condition among the patients. • Use of traditional eye medicine delaying the presentation to healthcare professionals.	• Teleophthalmology enables real-time, synchronous, remote assessment by the clinicians, enabling a timely diagnosis. • AI-assisted tools may allow for timely and automated diagnosis with limited input from clinical experts.
Undifferentiated clinical phenotypes	• IK, either due to bacterial, fungal, parasitic and/or viral, usually presents as corneal infiltrate(s)/abscess (appearing as a white corneal opacity).	• AI-assisted tools may help distinguish the underlying causes of IK (e.g., bacterial keratitis vs. fungal keratitis).
Low culture yield	• Prior use of topical antimicrobial treatment before the diagnosis. • Low bioburden with limited infectious sample compared to systemic infection. • Poor techniques in corneal sampling and/or microbiological processing.	• NGS provides higher sensitivity and specificity results than conventional microbiological culture techniques. This is particularly useful for disease such as IK with low infectious bioburden. • Close collaboration between the ophthalmologists and the microbiologists to refine the sampling-to-processing pathway.
Long turnaround time for culture results	• The incubation period is usually 1–2 days for bacteria (or longer for some atypical bacteria) and 5–14 days for fungi.	• NGS can provide the results within 24 h (particularly with short-read, targeted amplicon sequencing). This is especially valuable for cases that are affected by atypical bacteria or fungi.
Polymicrobial infection	• The ocular surface (including cornea) is exposed to a multitude of organisms and potential risk factors (e.g., trauma, CL, etc.).	• NGS can sequence all types of infection in parallel. • NGS can also facilitate the examination of antimicrobial resistance and virulence genes (usually achieved by long-read, whole genome sequencing).

LMICs, Low- and middle-income countries; AI, Artificial intelligence; CL, Contact lens.

technology that allows for rapid, massive parallel sequencing of DNA and RNA, has significantly increased the efficiency and quality of sequencing, with significantly reduced costs (Goodwin et al., 2016). It can be performed using either two approaches, namely short-read sequencing (or targeted-amplicon sequencing; TAS) or long-read sequencing (or whole-genome sequencing; WGS), depending on clinical needs. TAS allows for a more rapid sequencing with quicker yield of results, but at the expense of reduced comprehensiveness than WGS, which provides a higher resolution of genomic examination, facilitating the study of antimicrobial resistance and virulence genes, disease transmission and potential outbreaks.

So far, NGS has demonstrated promise in augmenting clinical microbiology and public health laboratory practice (Gwinn et al., 2019), and its applicability is now gradually gaining traction in the field of IK (Ung et al., 2020). Owing to its high sensitivity and specificity, studies have shown that NGS is able to yield positive results in culture-negative IK cases (where the infectious bioburden is usually low or the infection is caused by atypical organisms or fungi), with a quick turnaround time (Seitzman et al., 2019a,b). It can sequence all types of organisms, including bacteria, fungi, viruses, and parasites, an advantage that is particularly valuable for IK where polymicrobial infection is relatively common. It was also able to identify new pathogens that were previously unknown to

be associated with ocular infections. Seitzman et al. (2019b) reported the use of metagenomic NGS in aiding the diagnosis of a case of *Capnocytophaga spp.*-related keratitis, where all the traditional microbiological techniques (including Gram stain, potassium hydroxide stain, and culture), corneal biopsy, and *in vivo* confocal microscopy were unrevealing. During the first 2 months of treatment (prior to the correct diagnosis), the patient progressively worsened despite being on various antibiotic and antifungal treatments. Fortunately, the initiation of the appropriate therapy (topical clindamycin 5%) successfully eradicated the infection and inflammation within 6 weeks, highlighting the clinical value of metagenomic NGS in IK. Moreover, the sensitivity of NGS is not affected by the prior use of antimicrobials, which is a common impediment to culture yield (a common issue that is observed in HICs due to widespread use of antibiotics).

Discussion

The diagnostic modalities for IK have remained largely similar for the past few decades, with conventional microbiological technique being the most prevailing method. Digital innovations such as AI (particularly DL) and telemedicine have demonstrated their potential clinical utility in improving the rapidity, efficiency and accuracy for diagnosing IK in the recent years, though the deployment of such technology in this field still remains in its infancy. Other than diagnosing and distinguishing IK from other ocular surface diseases, potential AI research areas for IK may further include the prediction of culture positivity, clinical outcomes and complications of IK, including need for surgical interventions, based on the initial clinical presentations and photos. These digital innovations can provide a much-needed solution in LMICs where IK is most prevalent and healthcare services are constrained by physical, financial, workforce, societal, environmental and policy limitations (Mills, 2014). An ideal model of care would be an AI-assisted teleophthalmology or mHealth-based platform which allows the non-ophthalmologists (e.g., trained technicians) or affected patients to capture and upload the corneal photos remotely using either slit-lamp photography (in dedicated community facilities) or mobile device, respectively, followed by cloud-based, AI-assisted automated analysis and clinical decision making (Ting et al., 2019b).

Although NGS has demonstrated significant promise in improving the diagnosis of various types of infection, the routine use of NGS in clinical practice is hindered by its high cost (i.e., around $150–200 for each NGS per patient), though parallel sequencing of multiple samples and pathogens may improve laboratory efficiency and reduce cost. In addition, NGS can result in non-selective amplifications of the RNA / DNA of the causative organisms and normal ocular surface commensals, which will require special bioinformatic consideration and analysis (hence the need for additional resources, facilities and expertise). Another issue that has been highlighted is that NGS may produce inconsistent results to the conventional culture methods, which may complicate the clinical findings and decision making in IK (An et al., 2022).

Broad-spectrum antimicrobial therapy is currently the mainstay of treatment for IK, and studies have shown that the majority of IK pathogens are usually susceptible to the commonly used antibiotics (Ting et al., 2021d). In view of the above-highlighted limitations of NGS at its current state, we suggest that the use of NGS is best reserved for selective cases of IK where the initial treatment response was unsatisfactory and in regions where antimicrobial resistant ocular pathogens are more prevalent (e.g., the USA, China and India) (Ting et al., 2021a).

In conclusion, timely and accurate diagnosis of IK is critical in achieving a good outcome, though many barriers still exist. It is envisaged that the continual evolution of digital innovations and NGS will likely transform the diagnostic landscape of IK in the coming years. Further considerations and effort are required to improve the infrastructure, accessibility, costs and cost-effectiveness of these technologies to facilitate their implementations, particularly in LMICs.

Author contributions

DT and JM: study design and conceptualization. DT: literature review and manuscript drafting. JC and JM: critical revision of the manuscript. DT, JC, and JM: final approval of the manuscript. All authors contributed to the article and approved the submitted version.

Funding

DT acknowledges support from the Medical Research Council/Fight for Sight (FFS) Clinical Research Fellowship (MR/T001674/1).

Conflict of interest

The authors declare that the research was conducted in the absence of any commercial or financial relationships that could be construed as a potential conflict of interest.

Publisher's note

References

An, N., Wang, C., Dou, X., Liu, X., Wu, J., and Cheng, Y. (2022). Comparison of 16S rDNA amplicon sequencing with the culture method for diagnosing causative pathogens in bacterial corneal infections. *transl. Vis. Sci. Technol.* 11, 29. doi: 10.1167/tvst.11.2.29

Brown, L., Leck, A. K., Gichangi, M., Burton, M. J., and Denning, D. W. (2021). The global incidence and diagnosis of fungal keratitis. *Lancet Infect. Dis.* 21, e49–e57. doi: 10.1016/S1473-3099(20)30448-5

Cabrera-Aguas, M., Khoo, P., and Watson, S. L. (2021). Presumed microbial keratitis cases resulting in evisceration and enucleation in Sydney, Australia. *Ocul. Immunol. Inflamm.* 1–7. doi: 10.1080/09273948.2021.1998546. [Epub ahead of print].

Flaxman, S. R., Bourne, R. R. A., Resnikoff, S., Ackland, P., Braithwaite, T., Cicinelli, M. V., et al. (2017). Global causes of blindness and distance vision impairment 1990-2020: a systematic review and meta-analysis. *Lancet Glob. Health*.5, e1221–e34. doi: 10.1016/S2214-109X(17)30393-5

Goodwin, S., McPherson, J. D., and McCombie, W. R. (2016). Coming of age: ten years of next-generation sequencing technologies. *Nat. Rev. Genet.* 17, 333–351. doi: 10.1038/nrg.2016.49

Gwinn, M., MacCannell, D., and Armstrong, G. L. (2019). Next-generation sequencing of infectious pathogens. *JAMA*. 321, 893–894. doi: 10.1001/jama.2018.21669

Hung, N., Shih, A. K., Lin, C., Kuo, M. T., Hwang, Y. S., Wu, W. C., et al. (2021). Using Slit-lamp images for deep learning-based identification of bacterial and fungal keratitis: model development and validation with different convolutional neural networks. *Diagnostics (Basel)* 11, 1246. doi: 10.3390/diagnostics11071246

Khoo, P., Cabrera-Aguas, M. P., Nguyen, V., Lahra, M. M., and Watson, S. L. (2020). Microbial keratitis in Sydney, Australia: risk factors, patient outcomes, and seasonal variation. *Graefes Arch. Clin. Exp. Ophthalmol.* 258, 1745–1755. doi: 10.1007/s00417-020-04681-0

Khor, W. B., Prajna, V. N., Garg, P., Mehta, J. S., Xie, L., Liu, Z., et al. (2018). The Asia cornea society infectious keratitis study: a prospective multicenter study of infectious keratitis in Asia. *Am. J. Ophthalmol.* 195, 161–170. doi: 10.1016/j.ajo.2018.07.040

Li, J. O., Liu, H., Ting, D. S. J., Jeon, S., Chan, R. V. P., Kim, J. E., et al. (2021). Digital technology, tele-medicine and artificial intelligence in ophthalmology: a global perspective. *Prog. Retin. Eye Res.* 82, 100900. doi: 10.1016/j.preteyeres.2020.100900

Li, W., Yang, Y., Zhang, K., Long, E., He, L., Zhang, L., et al. (2020). Dense anatomical annotation of slit-lamp images improves the performance of deep learning for the diagnosis of ophthalmic disorders. *Nat. Biomed. Eng.* 4, 767–777. doi: 10.1038/s41551-020-0577-y

Mills, A. (2014). Health care systems in low- and middle-income countries. *N. Engl. J. Med.* 370, 552–557. doi: 10.1056/NEJMra1110897

Rampat, R., Deshmukh, R., Chen, X., Ting, D. S. W., Said, D. G., Dua, H. S., et al. (2021). Artificial intelligence in cornea, refractive surgery, and cataract: basic principles, clinical applications, and future directions. *Asia Pac. J. Ophthalmol.* 10, 268–281. doi: 10.1097/APO.0000000000000394

Redd, T. K., Prajna, N. V., Srinivasan, M., Lalitha, P., Krishnan, T., Rajaraman, R., et al. (2022a). Expert performance in visual differentiation of bacterial and fungal keratitis. *Ophthalmology*. 129, 227–230. doi: 10.1016/j.ophtha.2021.09.019

Redd, T. K., Prajna, N. V., Srinivasan, M., Lalitha, P., Krishnan, T., Rajaraman, R., et al. (2022b). Image-based differentiation of bacterial and fungal keratitis using deep convolutional neural networks. *Ophthalmol. Sci.* 2, 100119. doi: 10.1016/j.xops.2022.100119

Seitzman, G. D., Hinterwirth, A., Zhong, L., Cummings, S., Chen, C., Driver, T. H., et al. (2019a). Metagenomic deep sequencing for the diagnosis of corneal and external disease infections. *Ophthalmology* 126, 1724–1726. doi: 10.1016/j.ophtha.2019.06.013

Seitzman, G. D., Thulasi, P., Hinterwirth, A., Chen, C., Shantha, J., and Doan, T. (2019b). Capnocytophaga keratitis: clinical presentation and use of metagenomic deep sequencing for diagnosis. *Cornea* 38, 246–248. doi: 10.1097/ICO.0000000000001790

Ting, D. S. J., Ang, M., Mehta, J. S., and Ting, D. S. W. (2019b). Artificial intelligence-assisted telemedicine platform for cataract screening and management: a potential model of care for global eye health. *Br. J. Ophthalmol.* 103, 1537–1538. doi: 10.1136/bjophthalmol-2019-315025

Ting, D. S. J., Bignardi, G., Koerner, R., Irion, L. D., Johnson, E., Morgan, S. J., et al. (2019a). Polymicrobial keratitis with cryptococcus curvatus, candida parapsilosis, and stenotrophomonas maltophilia after penetrating keratoplasty: a rare case report with literature review. *Eye Contact Lens.* 45, e5–e10. doi: 10.1097/ICL.0000000000000517

Ting, D. S. J., Cairns, J., Gopal, B. P., Ho, C. S., Krstic, L., Elsahn, A., et al. (2021b). Risk factors, clinical outcomes, and prognostic factors of bacterial keratitis: the nottingham infectious keratitis study. *Front. Med.* 8, 715118. doi: 10.3389/fmed.2021.715118

Ting, D. S. J., Galal, M., Kulkarni, B., Elalfy, M. S., Lake, D., Hamada, S., et al. (2021c). Clinical characteristics and outcomes of fungal keratitis in the United Kingdom 2011-2020: a 10-year study. *J. Fungi* 7, 966. doi: 10.20944/preprints202110.0104.v1

Ting, D. S. J., Ho, C. S., Cairns, J., Elsahn, A., Al-Aqaba, M., Boswell, T., et al. (2021d). 12-year analysis of incidence, microbiological profiles and in vitro antimicrobial susceptibility of infectious keratitis: the Nottingham Infectious Keratitis Study. *Br. J. Ophthalmol.* 105, 328–333. doi: 10.1136/bjophthalmol-2020-316128

Ting, D. S. J., Ho, C. S., Deshmukh, R., Said, D. G., and Dua, H. S. (2021a). Infectious keratitis: an update on epidemiology, causative microorganisms, risk factors, and antimicrobial resistance. *Eye* 35, 1084–1101. doi: 10.1038/s41433-020-01339-3

Tiwari, M., Piech, C., Baitemirova, M., Prajna, N. V., Srinivasan, M., Lalitha, P., et al. (2022). Differentiation of active corneal infections from healed scars using deep learning. *Ophthalmology* 129, 139–146. doi: 10.1016/j.ophtha.2021.07.033

Ung, L., Acharya, N. R., Agarwal, T., Alfonso, E. C., Bagga, B., Bispo, P. J., et al. (2019). Infectious corneal ulceration: a proposal for neglected tropical disease status. *Bull. World Health Organ.* 97, 854–856. doi: 10.2471/BLT.19.232660

Ung, L., Bispo, P. J. M., Doan, T., Van Gelder, R. N., Gilmore, M. S., Lietman, T., et al. (2020). Clinical metagenomics for infectious corneal ulcers: Rags to riches? *Ocul. Surf.* 18, 1–12. doi: 10.1016/j.jtos.2019.10.007

Yang, S., and Rothman, R. E. (2004). PCR-based diagnostics for infectious diseases: uses, limitations, and future applications in acute-care settings. *Lancet Infect. Dis.* 4, 337–348. doi: 10.1016/S1473-3099(04)01044-8

frontiers | Frontiers in Microbiology

TYPE Review
PUBLISHED 14 November 2022
DOI 10.3389/fmicb.2022.1042362

OPEN ACCESS

EDITED BY
Claudia Maria Trombetta,
University of Siena,
Italy

REVIEWED BY
Dana Marshall,
Meharry Medical College,
United States
Carmen Judith Serrano,
Mexican Social Security Institute (IMSS),
Mexico

*CORRESPONDENCE
Frank Schmidt
frs4001@qatar-med.cornell.edu

SPECIALTY SECTION
This article was submitted to Infectious Agents and Disease, a section of the journal Frontiers in Microbiology

RECEIVED 12 September 2022
ACCEPTED 26 October 2022
PUBLISHED 14 November 2022

CITATION
Sohail MU, Mashood F, Oberbach A, Chennakkandathil S and Schmidt F (2022) The role of pathogens in diabetes pathogenesis and the potential of immunoproteomics as a diagnostic and prognostic tool.
Front. Microbiol. 13:1042362.
doi: 10.3389/fmicb.2022.1042362

The role of pathogens in diabetes pathogenesis and the potential of immunoproteomics as a diagnostic and prognostic tool

Muhammad Umar Sohail[1], Fathima Mashood[1], Andreas Oberbach[2], Sareena Chennakkandathil[1] and Frank Schmidt[1]*

[1]Proteomics Core, Weill Cornell Medicine, Doha, Qatar, [2]Experimental Cardiac Surgery LMU Munich, Department of Cardiac Surgery, Ludwig Maximillian University of Munich, Munich, Germany

Diabetes mellitus (DM) is a group of metabolic diseases marked by hyperglycemia, which increases the risk of systemic infections. DM patients are at greater risk of hospitalization and mortality from bacterial, viral, and fungal infections. Poor glycemic control can result in skin, blood, bone, urinary, gastrointestinal, and respiratory tract infections and recurrent infections. Therefore, the evidence that infections play a critical role in DM progression and the hazard ratio for a person with DM dying from any infection is higher. Early diagnosis and better glycemic control can help prevent infections and improve treatment outcomes. Perhaps, half (49.7%) of the people living with DM are undiagnosed, resulting in a higher frequency of infections induced by the hyperglycemic milieu that favors immune dysfunction. Novel diagnostic and therapeutic markers for glycemic control and infection prevention are desirable. High-throughput blood-based immunoassays that screen infections and hyperglycemia are required to guide timely interventions and efficiently monitor treatment responses. The present review aims to collect information on the most common infections associated with DM, their origin, pathogenesis, and the potential of immunoproteomics assays in the early diagnosis of the infections. While infections are common in DM, their role in glycemic control and disease pathogenesis is poorly described. Nevertheless, more research is required to identify novel diagnostic and prognostic markers to understand DM pathogenesis and management of infections. Precise monitoring of diabetic infections by immunoproteomics may provide novel insights into disease pathogenesis and healthy prognosis.

KEYWORDS

diabetes, infections, *Staphylococcus aureus*, early diagnosis, immunoproteomics, biomarkers

Introduction

Diabetes Mellitus (DM) is a complex metabolic disorder characterized by abnormal immune-inflammatory processes that increase vulnerability to severe infections. About 463 million people have DM worldwide, and future projections predict that this figure will grow to 700 million by 2045 (Saeedi et al., 2019). More than 90% of diabetic patients have diabetes mellitus type 2 (DM2), which leads to severe micro-and macro-vascular diseases and places a massive burden on the healthcare system (Chatterjee et al., 2017). People with unmanaged hyperglycemia are at greater risk of experiencing severe medical complications, resulting in lower quality of life, higher medical costs, and mortality (Baena-Díez et al., 2016). Persistent hyperglycemia induces generalized vascular damage, resulting in hypertension, retinopathy, nephropathy, and neuropathy (Chatterjee et al., 2017).

Industrialization, a sedentary lifestyle, smoking, and calorie-rich foods are established risk factors for developing DM2 (Kolb and Martin, 2017). Although these only partially explain the pathophysiology of the disease, chronic infections with environmental or opportunistic pathogens are the other significant contributors to the disease pathogenesis (Tayebi et al., 2021). Pathogens, particularly enteroviruses, *Chlamydia pneumoniae*, herpes simplex virus (HSV), and *Helicobacter pylori*, enhance the risk of cardiovascular events and have the strongest relationship with insulin resistance (Fernández-Real et al., 2006; Nabipour et al., 2006). Blood, skin, urine, and respiratory tract infections are common in diabetic patients that may cause irreversible organ loss or death (Abu-Ashour et al., 2017). According to a meta-analysis of 97 prospective studies involving 820,900 patients, DM-associated infections were one of the leading causes of death (Rao Kondapally Seshasai et al., 2011). Critchley et al. (2018) reported that impaired glycemic control [elevated levels of glycated hemoglobin (HbA1c)] has a positive association with severe infections compared with healthy controls or DM patients with optimal HbA1c. The infection promotes inflammatory markers such as interleukin (IL)-6 and C-reactive protein (CRP) and prevents insulin secretion or interaction with receptors. Furthermore, pathogen's secretory proteins, such as lipopolysaccharides (LPS), activate toll-like receptors and autoimmune reactions that eventually lead to abnormal energy harvest, obesity, and insulin resistance (Manco et al., 2010). Fernández-Real et al. (2006) observed that higher antibody titers against *C. pneumoniae*, enteroviruses, and HSV are associated with insulin resistance in DM2 patients. Schneider and von Herrath (2014) found that viral infections may act as a longitudinal factor during the induction of autoimmune antibodies against pancreatic β-cells and progression to DM type 1 (DM1). Similarly, other studies also report that infections accelerate the initiation and progression of autoantibodies synthesis at an early stage of the disease and lead to clinical DM1 (Dotta et al., 2007; Morse and Horwitz, 2021). Likewise, DM2 is also associated with infections, including *Staphylococcus aureus*, *Escherichia coli*, *Klebsiella pneumoniae*, *Acinetobacter baumannii*, SARS-CoV-2, HBV, HCV, HHV8, HSV1, and H1N1 virus (Gan, 2013; Leung and Liu, 2019; Lontchi-Yimagou et al., 2021; Carrillo-Larco et al., 2022). Infections with antibiotic-resistant pathogens, such as *S. aureus* and *A. baumannii*, are common in DM2 patients, resulting in poor glycemic control and prognosis (Al-Sultan, 2014; Yan et al., 2022). Leung and Liu (2019) observed a higher mortality rate in DM2 patients infected with carbapenem-resistant *A. baumannii* complex bacteremia.

Early diagnosis and treatment of infections are critical to prevent or postpone secondary DM complications. Kumar et al. (2006) suggested that every hour of delay in antibiotic therapy raises the death risk by 7.6% in patients with sepsis and septic shocks. However, early clinical diagnosis and appropriate antibiotic selection can be difficult when multiple microorganisms are involved. Some of the most common laboratory methods for infection diagnosis include classic microbial culturing, molecular biology techniques, such as targeted PCR or nonspecific high throughput sequencing, and immunoassay. The former two procedures are either very time-consuming or fail to provide a definitive diagnosis and therefore lack clinical relevance in DM management, mainly because many DM-associated infections are polymicrobial (Hitam et al., 2019). Although early diagnosis is vital, classic culturing techniques may take 24 to 72 hto grow the specimen and test drug sensitivity. PCR is a very sensitive and reliable diagnostic tool. However, the clinical application is restricted because of false-positive results and the low throughput of the assay for simultaneous identification of multiple species, drug resistance, and virulence factors (Yang and Rothman, 2004). On the other hand, sequencing requires a large amount of resources and lacks precision (Wajid et al., 2016). MALDI-Biotyping has further improved the diagnosis of pathogens but still cannot distinguish subspecies (Kostrzewa et al., 2019).

Immunoproteomics is a powerful tool to identify immunoreactive molecules and develop candidate vaccines against pathogens. Immunoproteomics combines proteomics for the detection of immunoreactive antigens expressed during infections (Dennehy and McClean, 2012). High throughput immunoproteomics arrays offer a rapid, sensitive, and specific diagnosis of pathogens and their drug resistance profiles, which are otherwise difficult to culture or are multi-species infections. A viral proteome array comprising 646 viral antigens was developed by Bian et al. (2016) to examine the relationship between viral infections and the early onset of DM1. The study observed a trend toward early Epstein–Barr virus (EBV) infection among DM1 patients, suggesting a potential role of EBV in DM1 development. A similar strategy against most common viral, bacterial, and fungal pathogens shall be implemented utilizing comprehensive serum antigen profiles of DM2 patients to predict novel diagnostic and prognostic markers.

Common sites of infection and prevalent pathogens

The most common sites of infection and their common inhabitant pathogens are discussed in the following sections. However, we highlight that *S. aureus,* a nosocomial infection, is the most common pathogen associated with significant morbidity and mortality in diabetic patients (Smit et al., 2016). The pathogen has a considerable economic and clinical burden, significantly increasing hospital costs associated with methicillin-resistant *S. aureus* (MRSA) infections. Klekotka et al. (2018) reviewed that *S. aureus* is one of the most isolated pathogens in diabetic patients, causing meningitis, sepsis, bacteremia, skin infections, and nasal carriage. Considering *S. aureus* clinical significance, the pathogen will be discussed thoroughly in the DM infection pathogenesis and immunoproteomics sections.

Skin and soft tissue infections

Skin and soft tissues are the most common infection sites in DM patients, including diabetic foot infections (DFIs) and surgical site infections. In diabetic patients, DFIs account for up to 20% of hospital admissions and 17.4% of hospital-related deaths (Saseedharan et al., 2018; Rastogi et al., 2020). Although DFIs occur on the outer skin layer, bacterial infections can spread the wound to subcutaneous tissues, including fascia, muscles, tendons, bones, and joints. Oh et al. (2018) reported that in DM2 patients, the SSTIs are most frequently caused by *S. aureus*, with a prevalence rate of 50% in DFI. Saseedharan et al. (2018) reported that in DFI patients, *S. aureus* was the most frequently (26.9%) isolated pathogen, followed by *P. aeruginosa* (20.9%). Similarly, Taylor and Napolitano (2004) detected *S. aureus* in 35% of postoperative infections (61% of them being surgical site infections) among patients undergoing vascular surgery (40% of whom were DM patients). In DM1 patients, *S. aureus* mostly colonizes the nose and skin (Smith and O'connor, 1966). The bacterium expresses a range of virulence factors, including surface and secreted protein or vesicle. Chronic *S. aureus* superantigens may induce endotoxemia, resulting in systemic inflammation, impaired glucose tolerance, and accelerated DM pathogenesis (Vu et al., 2015). Dunyach-Remy et al. (2016) reviewed global prevalence of Gram-positive cocci (GP), *S. aureus*, and MRSA in DFIs, stating that toxinogenic strains of *S. aureus* (secreting exfoliatin, EDIN, PVL or TSST proteins) are often present in infections with a more severe grade and systemic impact. *S. aureus* has been observed to co-exist in many cases with *A. baumannii*, which is also associated with a higher incidence (24.4%) of major amputation in patients with DFI (Cardoso et al., 2017; Ryu et al., 2017).

Staphylococcus aureus grows and secretes virulent factors in glucose-rich diabetic conditions, where insulin deficiency prevents or delays immune response (Thurlow et al., 2020). *Staphylococcus aureus* has expanded its glycolytic capacity by acquiring several additional glucose transporters. Carbohydrate transporters in *S. aureus* allow efficient uptake of carbohydrates and support anaerobic growth in inflamed tissues. Eleven carbohydrate transporters have been identified in *S. aureus*, while four of them (glcA, glcB, glcC, and glcU) are strictly responsible for glucose transportation (Vitko et al., 2016). Vitko et al. (2016) observed that in a murine model of wound infection, the inactivation of carbohydrate transporter might reduce glucose uptake and attenuate *S. aureus* growth. Other metabolites, such as fructose, glucose-6-phosphate, and mannose also induced higher expression of *S. aureus* toxins (leukocidins) in DM, indicating a physiologically relevant role of these molecules in DM (Seo et al., 2021). In diabetic skin infections, a lack of nutritional immunity promotes *S. aureus* virulence, including α-hemolysin and a myriad of secreted proteases. Many of these proteins are also expressed in DFI in DM patients, notably the autolysin proteins (Amd), glucosaminidase (Gmd), and the iron-regulated surface determinant proteins (IsdA, IsdB, and IsdH). Therefore, antibody responses against bacterial proteins could predict infection outcomes in patients with *S. aureus* induced SSTIs.

Respiratory tract infections

Diabetic patients are also more susceptible to various respiratory infections, including *Streptococcus pneumonia, Mycobacterium tuberculosis, S. aureus, Candida albicans*, and influenza virus (Klekotka et al., 2015). Hine et al. (2017) observed a higher prevalence of respiratory infections (23.5%), followed by SSTIs (14.6%) and urogenital tract (10.4%) infections in a large primary care cohort study conducted in the United Kingdom. Hyperglycemia in diabetic patients admitted to an intensive care unit increased the pulmonary bacterial load of *Pseudomonas* spp. (26–32%) *S. aureus* (14–16%) *Klebsiella* spp. (13–14%), *E. coli* (12–13%), and *Enterobacter* spp. (8–12%) (Gill et al., 2016). In The Environmental Determinants of Diabetes in the Young (TEDDY) study, respiratory infections were also positively associated with the onset of β-islet autoimmunity and increased risk of DM1 development (Lönnrot et al., 2017). The nasal cavity is an ecological niche for *S. aureus* carriage (persistent or intermittent) in 20 to 50% of healthy people with a high probability of severe and recurrent infections, particularly in diabetic patients (Wertheim et al., 2005). Furthermore, *S. aureus* carriage rate in adult diabetic patients receiving insulin is 34.0–53.4% compared with the healthy controls (10.7–34.2%) (Sollid et al., 2014). Toxic shock syndrome toxin-1 (TSST-1) and staphylococcal enterotoxin are the most common *S. aureus* superantigens found in the nasal cavity (Klekotka et al., 2018). Schmidt et al. (2017) identified more than 600 *S. aureus* proteins in nasal polyps, 115 of which had a strong IgA-and IgG-specific immunoglobulin response.

Many other respiratory pathogens are also associated with DM. The prevalence of pulmonary tuberculosis is 4–5 times higher in diabetic patients than in healthy subjects (Noubiap et al., 2019). Likewise, Badawi and Ryoo (2016) reported a high

prevalence rate (54.4%) of Middle East respiratory syndrome coronavirus (MERS-CoV) and H1N1 influenza infection (14.6%) in DM patients. More recent outbreaks of coronavirus disease (COVID-19) also revealed that the disease severity and mortality rates are higher in DM patients (Cyprian et al., 2021). A meta-analysis of 35 studies revealed that DM-related mortality was relatively high (22.14%) in COVID-19 patients (Gupta et al., 2021). Furthermore, DM2 is a known risk factor for severe acute respiratory distress and prolonged viral shedding in critically ill COVID-19 patients (Buetti et al., 2020). Increased susceptibility to pulmonary infections in DM result from reduced activation of lymphocytes, macrophages, and natural killer (NK) cells and reduced immunoglobulins production against antigenic proteins (Lönnrot et al., 2017).

Urogenital tract infections

DM patients are more likely to get urinary tract infections caused by frequent urination and high glucose levels that provide a suitable growing environment for the pathogens (Woldemariam et al., 2019). High urine glucose concentration provides a good source of nutrients for pathogens to colonize, replicate, and make a UTIs base. Several immune and neuroendocrine defects in DM patients, including reduced T-cell activation, impaired neutrophil function, and low levels of thromboxane B2, prostaglandin E, and leukotriene B4 may lead to a higher UTIs risk (Nabaigwa et al., 2018). *E. coli*, *Klebsiella* spp., *S. aureus*, and *C. albicans* are the most isolated pathogens from UTIs in DM patients (Zubair et al., 2019). Recently, Woldemariam et al. (2019) observed a higher prevalence rate of infections among diabetic patients, where *E. coli* (23.2%), *Coagulase negative Staphylococci* (12.5%), *Enterococcus* spp. (10.7%), *C. albicans* (17.9%) and Non-*albicans Candida* spp. (16.1%) were the most frequently isolated pathogens. Similarly, Nabaigwa et al. (2018) reported that in DM patients, UTIs were positively associated with hyperglycemia with no pathogen detection in the urine of the patients with low fasting blood glucose.

UTIs in diabetic patients are frequently caused by compromised polymorphonuclear leukocyte function, including impaired chemotaxis and phagocytosis (Daryabor et al., 2020). Flagellae of *E. coli* attach to urinary tract epithelium through toll-like receptor 5 and ascend the urinary tract against urine flow (Avalos Vizcarra et al., 2016). Furthermore, adhesin type 1 fimbriae are critical for invading the bladder and evading extracellular antibiotics (Avalos Vizcarra et al., 2016). *E. coli* proteins, such as YbcL, are responsible for delayed immune response in the urinary bladder that helps bacteria multiply easily in the urine and invade the bladder epithelium, a prerequisite for bacterial infection and pathogenesis (Lau et al., 2012). *E. coli* haemolysins act either directly as cytotoxic agents or indirectly by causing inflammation and haematuria (Ambite et al., 2021). Many *E. coli* toxins, such as adhesins, iron acquisition factors, polysaccharide capsules, lipopolysaccharides, and invasins are associated with UTIs and can also spread to the blood and cause systemic infection (Ambite et al., 2021). Floyd et al. (2015) analyzed biofilms of uropathogenic *E. coli*, proposing a novel role of proteomics in uncovering host-pathogen interactions for early diagnosis and treatment of UTIs.

Blood sepsis

Sepsis and septic shock can arise from an infection anywhere in the body, such as UTIs, pneumonia, or skin wound. Sepsis can be caused by a bloodstream infection leading to fever, septic shock, and a fatal decrease in blood pressure. Diabetic patients have a 4.4 times greater risk of bloodstream infection than non-diabetic patients and are more vulnerable to sepsis of uncertain cause (Stoeckle et al., 2008). Diabetic patients are more likely than non-diabetic to be colonized by MRSA (Stacey et al., 2019). A 25-yearlong study using the National Hospital Discharge Survey US discovered that sepsis occurred in 12.5 million of 930 million acute-care hospitalizations, with DM present in 17% of the sepsis cases (Esper et al., 2009). Moreover, post-sepsis complications and rising mortality are more common in diabetic patients (Frydrych et al., 2017).

Stoeckle et al. (2008) observed that sepsis was more common in diabetic patients than non-diabetic patients, and UTIs were the most common route of sepsis. In general, *E. coli* was the most common etiological agent of sepsis in both diabetic and non-diabetic patients. However, *K. pneumoniae* was a more common pathogen in diabetic patients alone. Patra et al. (2017) studied microbial etiology of bacteremia, reporting a high prevalence of *E. coli* (19.7%), *S. aureus* (15%) *Streptococcus* sp. (10.2%), *Staphylococcus sp.* (9.4%), *Enterococcus sp.* (7.84%), and *Klebsiella* (5.5%) in DM2 patients. The infection rate was far higher in uncontrolled DM2 than in controlled DM2. Thaiss et al. (2018) reported a strong association between HbA1c and serum levels of pathogen recognition receptor (PRR) ligands. Bacteria with increased glucose import capacity, such as *S. aureus*, have a better glycolytic flux during infection, enhancing pathogen survival and pathogenicity rate (Vitko et al., 2016). Similarly, *Streptomyces achromogenes* and *P. aeruginosa* infections can also produce irreversible damage to pancreatic β-cells (Schuetz et al., 2011). Chronic bacteremia and prolonged sequestration of viable microorganisms in the liver, lung, kidney, and spleen results in lower IFN-γ and interleukin (IL)-12 cytokine due to fewer antigen–responsive T lymphocytes in diabetic mice (Yamashiro et al., 2005).

Gastrointestinal (GI) infections

DM increases the risk of enteric infections and intestinal barrier dysfunction, elevating systemic infection risk. The GI tract hosts a complex microbial community, including archaea, bacteria, fungi, protozoans, and viruses, that dynamically

influence immune, endocrine, and metabolic homeostasis (Sohail et al., 2019b). Gao et al. (2022) reported that in obese people, bacterial DNA-containing extracellular vesicles (mEVs) could easily cross the gut barrier and deliver microbial DNA into β cells, causing cell injury and impaired insulin secretion by activating cGAS-STING pathway. Several studies have reported changes in the gut microbiome and phage community composition (phageome) in DM2 patients (Sohail et al., 2017, 2019b; Chen et al., 2020). Yao et al. (2018) conducted a meta-analysis of fourteen studies involving 1,841,653 participants and observed that DM significantly increased the risk of enteric infections. Individualized glycemic control, as measured by HbA1c, correlates with systemic transport of gut microbiome secretions (Thaiss et al., 2018). In rodents, infection with systemic *Salmonella* analog, *Citrobacter rodentium*, has been shown to cause hyperglycemia (Thaiss et al., 2018). Chen et al. (2020) observed an increase in the intestinal phage population, particularly *Enterobacteriaceae*, that correlated with a significant increase in systemic LPS concentration in DM2 patients. Furthermore, the authors suggested a consortium of eight phages that could distinguish DM2 patients from healthy controls (ROC-AUC > 0.99).

Several enteric virus infections are also associated with DM pathogenesis. Viral infections are the instigator of gut dysbiosis and disruption of intestinal homeostasis that lead to subclinical enteropathy before DM1 onset (Morse and Horwitz, 2021). Fabiani et al. (2018) found that infection with the hepatitis C virus was associated with an elevated risk of DM2 and vice versa DM2 raised the risk of liver cirrhosis in HCV patients. Changes in enteric virome are linked with several local and systemic disorders, including inflammatory bowel disease, colorectal cancer, obesity, and DM (Oikarinen et al., 2011). Enteroviruses infiltrate gut epithelium for systemic transmission and replication in the immune system, gradually infecting and making pancreatic islet cells vulnerable to autoimmune attack in DM1. Particularly, Oikarinen et al. (2011) observed that infections with enteroviruses triggered systemic inflammation, T-cell infiltration, overexpression of HLA-DR, transglutaminase 2–targeted IgA deposits, and β-cell damage. A bidirectional association between COVID-19 and DM has recently been suggested, with catastrophic consequences in diabetic patients suffering from GIT-form of COVID-19 infection (Cyprian et al., 2021).

Periodontal disease

Periodontal diseases are common in DM patients and are one of the primary risk factors of DM. Periodontitis is a common complication of DM, which is also associated with other DM complications and exacerbated by uncontrolled hyperglycemia (Nguyen et al., 2020). Similarly, periodontitis is also associated with gestational DM (Abariga and Whitcomb, 2016). Nguyen et al. (2020) conducted a systematic review of the literature to see whether there was a correlation between periodontitis and DM complications. They found that diabetic patients with periodontitis were more likely to develop retinopathy, neuropathy, nephropathy, and cardiovascular complications. Several oral pathogens, including *Aggregatibacter actinomycetemcomitans*, *P. gingivalis*, *Tannerella forsythia*, and *T. denticola*, are associated with hyperglycemia and contribute to periodontal disease development and gingivitis (Feng et al., 2014; Sohail et al., 2019a; Graves et al., 2020). Awan (2020) observed a higher prevalence of *S. aureus* in the dental cavities of diabetic patients compared with the controls. Al-Obaida et al. (2020) observed higher abundances of periodontal pathogens, *A. actinomycetemcomitans* and *Capnocytophaga ochracea*, in the dental cavities of diabetic patients. Bacteria or their products such as LPS from the sub-gingival plaque are thought to trigger the release of pro-inflammatory cytokines (interleukin-1β, interleukin-6, and interleukin-8, and tumor necrosis factor-alpha) that enter the systemic circulation and interfere with insulin signaling, causing insulin antagonism and pancreatic β-cell destruction (Moller, 2000; Chokwiriyachit et al., 2013).

Pathophysiology of diabetes infection

DM and infections are linked bidirectional, with infections impairing glycemic control and hyperglycemia promoting bacterial growth. Improved glycemic control prevents infection and improves treatment outcomes (Martinez et al., 2017; Ciancio et al., 2018). Pathogens can elicit strong immune responses, effectively activating immune regulatory mechanisms and causing autoimmune reactions that cause β-cell damage or insulin receptor deactivation (Fallahi et al., 2013; Seyyed Mousavi et al., 2017). In diabetic patients, both humoral and cellular immune responses are compromised, resulting in impaired cytokine production and the activation of phagocytic cells. Chronic hyperglycemia continuously stimulates polymorphonuclear lymphocytes and baseline cytokine levels, causing cellular and humoral responses insufficient for pathogens (Dryden et al., 2015). Hyperglycemia impairs neutrophils, significantly reducing their chemotactic migration, phagocytosis, and bactericidal functions (Jafar et al., 2016). Poor glycemic control in DM2 patients also suppresses the immune activity of monocytes and monocyte-derived macrophages (MDM) (Valtierra-Alvarado et al., 2020). Valtierra-Alvarado et al. (2021) observed lower activation markers in MDM from T2D patients in response to an *in vitro M. tuberculosis* infection. Therefore, diabetic patients, especially those with peripheral vascular disease, have immunosuppression, diabetic neuropathy, and impaired blood circulation, making them vulnerable to infections (Berbudi et al., 2020).

Infection-induced IFN-γ downregulates insulin receptor expression resulting in compensatory hyperinsulinemia to keep euglycemia (Šestan et al., 2018). The liver regulates blood glucose levels by glycogenolysis, gluconeogenesis, and glycogenesis. However, in diabetic patients, viral infections jeopardize euglycemia by disrupting glucose homeostasis. Šestan et al. (2018)

observed that viral infections activate the inflammasomes, which generate the pro-diabetic cytokine IL-1β that disturbs glucose homeostasis in the liver. Furthermore, viral infections trigger hepatic insulin resistance, accelerating DM pathogenesis. However, not all diabetic patients experience the same risks; improved glycemic regulation is related to lower infection incidence, as shown in many postoperative DM treatment reports (Cancienne et al., 2018a,b). Similarly, in patients with COVID-19 and pre-existing T2D, well-controlled glycemia was related to significantly lower mortality and better disease prognosis (Zhu et al., 2020).

Although hyperglycemia is generally believed as an immune-compromised condition that attracts infections, some research suggests that pathogens may initiate primary tissue insult to exacerbate DM pathogenesis. Since the host's genetic background plays a relatively minor role in inducing a self-immune reaction, epidemiological and molecular data point to infectious agents as the primary environmental factor that trigger autoimmune disorders (Vu et al., 2015). Adenovirus, cytomegalovirus, enteroviruses, mumps, and rubella are among the viruses linked to the pathogenesis of DM1 (Op de Beeck and Eizirik, 2016). *S. aureus*, one of the most common opportunistic pathogens, has also been linked to the onset of insulin resistance by blocking insulin receptors (Weidenmaier, 2018). Perhaps these infections are a catalyst for initiating a complex chain of immune-inflammatory processes that lead to chronic hyperglycemia (Peleg et al., 2007).

Several DM1 candidate genes, such as PTPN2, MDA5, and TYK2, also control antiviral responses in both β-cells and the immune system, triggering autoimmune destruction of the cell (Op de Beeck and Eizirik, 2016). Sequence homology between a pathogen-derived peptide and a self-peptide can cause an immune response against self-tissue, activating the release of autoantigens and bystander T-cell activation, resulting in inflammation and cell death (Cusick et al., 2012). The most compelling proof of infection-induced insulin-deficient hyperglycemia and enterovirus infection comes from cases of fulminant DM1, a typical type of DM1 in Japan (Tanaka et al., 2013). Similarly, insulin resistance may occur possibly through *S. aureus* membrane-bound enzyme lipoteichoic acid synthase (LtaS), which inhibits insulin binding to insulin receptors and prevents GLUT4 from being transported (Figure 1; Weidenmaier, 2018). Perhaps these pathogens or their products may not induce DM on their own. Instead, patients are frequently diagnosed with DM during or after an infection, indicating a connection between the two. Furthermore, a greater affinity among diabetic patients for acquiring infections suggests that DM falls in the first order before infection. This indicates that these pathogens or their peptides do not function as the primary trigger but act as confounding factors in impaired insulin production or sensitivity, ultimately exacerbating the disease outcomes.

Role of virulence factors/proteins in diabetes pathophysiology

Virulence of pathogens and host immune factors may determine the pathogenesis and fatality of DM infection. Pathogen-related factors, such as secretory or surface-attached peptides, play a significant role in adhesion, motility, and invasion while evading host immune responses. Each pathogen can secrete various virulence factors depending on the host environment and infection site. To simplify the role of virulence factors in DM pathophysiology, we focus on *S. aureus* as one of the most common opportunistic pathogens that has a high capacity to cause infections in obese and diabetic patients.

Liew et al. (2015) noted that *S. aureus* infections develop heterogeneous and broadly diverse virulence factors and host immune responses based on their site of infection. Furthermore, in diabetic patients, *S. aureus* needs fewer virulence factors (hemolytic and cytotoxic) to establish severe infection. Particularly, *S. aureus* has increased glucose import capabilities, which aid the bacteria in optimizing glycolytic flux during infection and pathogenesis (Vitko et al., 2016). Even less-virulent *S. aureus* strains survive in higher numbers, producing superantigens and inducing infection in the murine footpad injection model (Tuchscherr et al., 2018). In hyperglycemic environment catabolite control protein A (CcpA) may affect *S. aureus* infectivity, growth, glucose metabolism, and transcription of selected virulence determinants, including the agr locus, altering the transcription patterns of hla, α-hemolysin, and spa (Seidl et al., 2006; Bischoff et al., 2017).

Staphylococcus aureus secretes various virulence factors, including lipases, adhesins, and pore-forming toxins (Tuchscherr et al., 2018). Their volumes can increase after the pathogen internalization (Surmann et al., 2018). The secreted toxins, such as increasing adhesins and pore-forming toxins, detour host immunity by enhancing cell attachment or lysis (Thammavongsa et al., 2015).

Toxic shock syndrome toxin-1 (TSST-1), another popular superantigen from *S. aureus*, plays a critical role in DM pathogenesis. Vu et al. (2013) observed that rabbits exposed to *S. aureus* superantigen TSST-1 had impaired glucose tolerance, elevated endotoxin levels, and systemic inflammation. Macrophages and T-lymphocytes are stimulated by TSST-1 to produce inflammatory cytokines. TSST-1 induces a massive release of cytokines that specifically attach to T-lymphocytes' variable domains, resulting in hyperimmune response clinically characterized as fever, endotoxic shock, rash, and progressive multi-organ failure (Silversides et al., 2010). This nonspecific interaction stimulates less than 20% of the total population of T lymphocytes in diabetic patients, culminating in a severe cytokine storm (Que and Moreillon, 2015).

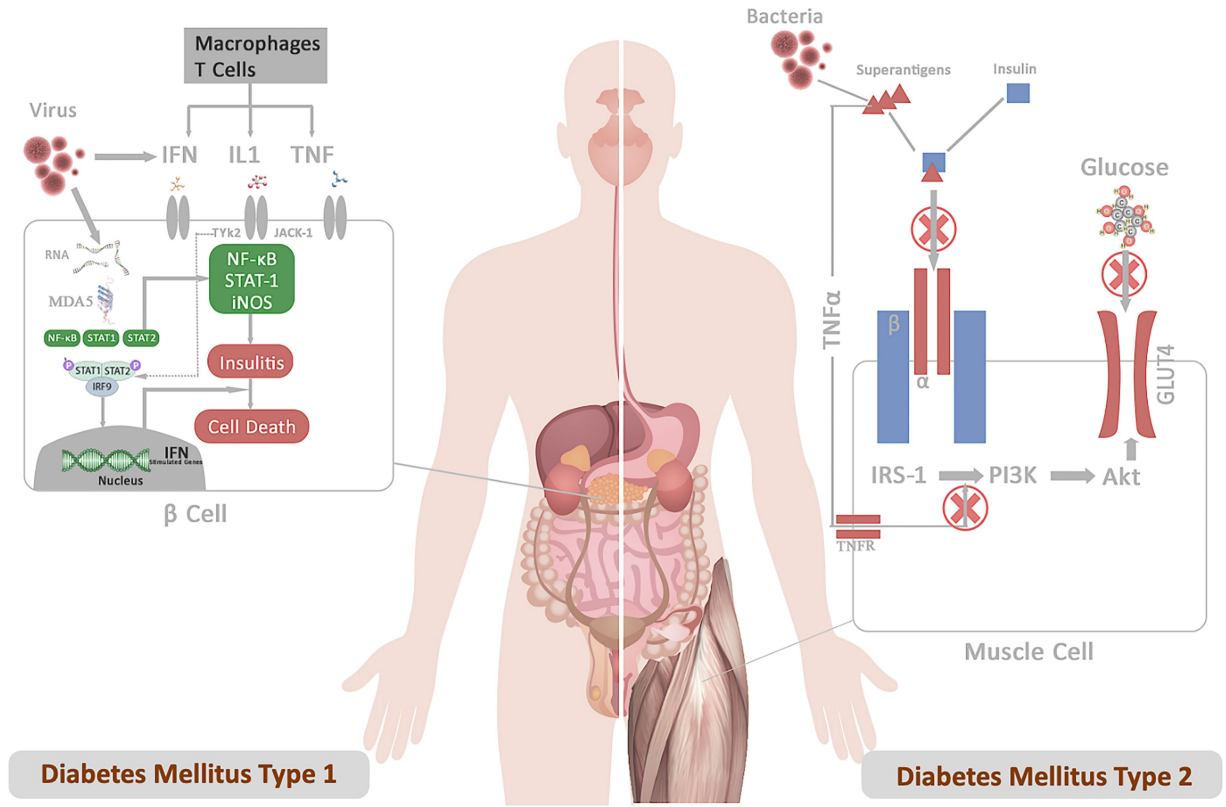

FIGURE 1
Represents the mechanistic of diabetes infection emphasizing the role of infection in DM1 and DM2 pathogenesis. **(A)** DM1: Following the infection, viral particles release viral RNA in the host cells, which is recognized by the cytoplasmic receptor MDA5. The binding of MDA5 to the RNA activates the transcription factors NF-κB and STATs pathway. The binding of IFN, IL, and TNF to their receptors results in the activation of the JAKs and TYK2 pathway, triggering activation of STAT-1–STAT-2–IFN-regulatory factor 9 complex. These complexes translocate to the nucleus and bind IFN-stimulated response elements in DNA to initiate the transcription of genes involved in host defense. Production of type I interferons contributes to insulitis and cell death. **(B)** DM2: Superantigens secreted from bacterial pathogens (*S. aureus*) (a) prevent insulin binding to the IR and abrogate signal transduction (b) LPS-stimulated inflammatory cytokine block PI3 kinase-Akt pathway. These signals inhibit downstream IR signaling events involved in promoting glucose conversion, reducing recruitment of the glucose transporter GLUT4 to the cell membrane, and impairs glucose uptake.

Immunoproteomics as novel diagnostic and prognostic tool

Proteomics

Proteomics and immunoproteomics studies of human body fluids and infection-specific antibodies offer complementary knowledge and hold the potential for developing novel biomarkers for DM infection (Larman et al., 2013; Yu et al., 2022). Proteomics in general has advanced linearly over the last few decades, with two-dimensional polyacrylamide gel electrophoresis (2D-PAGE) and Western blot being the mainstay of comparative proteomics studies. Protein research is crucial for better knowledge of disease pathogenesis and therapeutic response. DM is a polygenic disease with significant contribution from genetic, environmental, and behavioral factors, making it suitable for proteomics research. Most genome-wide association studies (GWAS) of DM identified only a small number of genetic variants contributing to DM risk (Mahajan et al., 2018). A more comprehensive biological readout of these factors can be obtained by proteomics, which analyzes downstream products of gene transcription. Recent technical developments have made it possible to profile circulating proteins quickly and on a much broader scale; a few of these are briefly discussed here.

Proteomics based on 2DE is a powerful tool for simultaneously separating and fractionating thousands of proteins. The technique has significantly evolved to identify and quantify proteins with mass spectrometry or immunological tools. 2DE is used for whole proteome analysis, protein purification and characterization, cell differentiation, drug discovery, disease biomarkers, and bacterial pathogenesis studies (Magdeldin et al., 2014). The technique provides direct visual confirmation of post-translational modifications, which cannot be predicted from the genomic sequence. Proteins of interest can be identified using peptide mass fingerprinting (PMF; Thiede et al., 2005) or antibody probes (Backert et al., 2000). For PMF, the protein of interest is isolated from the gel and digested using Trypsin to produce 8–10 amino acid-long peptides. These peptides can be analyzed with

MALDI-TOF mass spectrometer (MS), a fast, sensitive, high throughput, and accurate procedure. Molloy et al. (2001) used 2DE-PMF to identify the outer membrane proteins of *E. coli, S. typhimurium*, and *K. pneumoniae* that are otherwise difficult to identify. Similarly, Kundu et al. (2020) performed 2DE-PMF of PBMCs from comorbid DM-tuberculosis patients, identifying 18 protein spots with differential expression. MALDI-TOF based PMF revealed that these overexpressed proteins are involved in cell structure, cell cycle, signaling, and intermediary metabolism. Kalita et al. (2020) reviewed the application of 2DE-PMF in DM-associated organs and tissues, such as the pancreas (Ahmed et al., 2005), liver, skeletal muscle (Højlund et al., 2008), and adipose tissue secretome (Alvarez-Llamas et al., 2007). Liew et al. (2015) compared host immune response and *S. aureus* exoproteome in SSTI, bacteremia, and healthy carriage using 2-DGE, 2D-immunoblotting, and MS/MS (MS2). Using different proteomics techniques, the authors discovered a diverse exoproteome profile that varied significantly across infection sites. Differential expression of the Isd protein and host cytokine/chemokine response pattern were particularly important in understanding *S. aureus* infection. Luo et al. (2012) combined 2DE, Western blot, and MALDI-TOF MS to discover immunoreactive proteins for *A. baumannii* for vaccine development. Rational proteomics analysis discovered higher anti-OmpA antibody titers in *in vivo* testing of the OmpA antigen in diabetic mice, protecting the mice from intravenous infection with *A. baumannii* (Luo et al., 2012).

While it is true that gel-based techniques were the foundation of the early proteomic research in DM, they frequently have poor sensitivity in finding low-abundant proteins and are time-consuming (Kalita et al., 2020). Parallel advances in sample preparation methods, MS technology, and data analysis have prompted a shift toward gel-free techniques that profile thousands of proteins in a relatively shorter time and with small sample volumes. With higher sensitivity and resolution power, MS uses chromatography for molecules ionization and separation by mass to measure proteins. Chromatography improves the quantitative accuracy and throughput of MS, particularly for analytes with low abundance (Pocsfalvi et al., 2016). There are two types of chromatographic techniques: gas chromatography (GC) and liquid chromatography (LC), each with its own set of specifications and pros and cons. In GC, for example, nonpolar, low-molecular mass, and volatile analytes are vaporized into a mobile gas phase and passed through a liquid layer. LC, on the other hand, is ideally equipped for polar, high-molecular mass, heat-labile molecules. The analytes are dissolved in a liquid mobile phase and passed through a column filled with beads coated with various compounds that serve as the stationary phase.

The precision and sensitivity of the MS can be increased by the depletion of high-abundance plasma proteins and affinity binding techniques. Physical separation of the proteins by liquid chromatography or gel electrophoresis and trypsin digestion prior to MS and follow-up with immunoassays can further improve the diagnostic limits of proteomics (Chen and Gerszten, 2020). Data acquisition techniques in MS also affect the throughput of the analysis. Data dependent acquisition (DDA) MS acquires MS2 data so that the user can define specific precursor ions based on abundance or other criteria. Unlike DDA, data independent acquisition (DIA) acquires MS1 and MS2 data without bias for all precursor ions within isolation windows for full mass ranges without prior knowledge of precursors (Ludwig et al., 2018). Malipatil et al. (2019) quantified insulin growth factor, vitamin D binding proteins, and HbA1C using DIA-MS to predict the effect of diet and exercise on weight loss and insulin sensitivity. Salivary proteomics of diabetic patients identified TXNDC17, ZG16B, and FAM3D as novel biomarkers of hyperglycemia and oral disease in DM2 patients with poor glycemic control (Jia et al., 2021). An MS-DIA based proteomic analysis of infected root canals of DM2 patients identified fortythree overexpressed proteins, the majority of which were related to immune-inflammatory response (Loureiro et al., 2022). Withatanung et al. (2019) performed proteomics of *Burkholderia pseudomallei* infected Neutrophils isolated from DM2 patients observing elevated levels of pro-inflammatory cytokines IL-1β, IL-6, IL-17, and TNFα as well as enhanced apoptosis. Likewise, Gagnaire et al. (2012) used MALDI-TOF MS to detect *S. aureus* delta-toxin in DFI and chronic lung infections. Acar et al. (2022) applied a subtractive proteomics approach to study immunodominant *A. baumannii* exoproteome/surfactome for candidate vaccine discovery. The researchers used IgGs to capture *A. baumannii* proteins and identified them using LC–MS/MS analysis, observing 34 unique proteins and several notable vaccine candidates, including A0A0R4J8QA3, B0V9Z6, B0V885, B0V4F6, B0VD00, B0VAB5, B0V8H0, B0VE52, B0VC68.

Analytical protein arrays or multiplexing have a wide range of applications, including cell signaling pathways and protein interactions analysis, which could aid in the discovery of novel autoantigens for DM diagnosis, prevention, and treatment (Chang et al., 2015). Among many other proteomics platforms, proximity extension assay (PEA) technology based Olink and SOMAScan have attained widespread application in clinical testing and discovering new biomarkers (Liu et al., 2022; Sánchez-Maldonado et al., 2022). SOMAScan is a highly sensitive proteomic multiplexing platform based on affinity capture and low off-rate modified aptamers (SOMAmers). Elhadad et al. (2020) observed over 1,000 proteins in DM2 patients, revealing 24 replicated proteins, of which 8 are novel. Aminoacylase-1, GHR, insulin-like growth factor-binding protein 2, cathepsin Z, and rennin were associated with the incidence and prevalence of DM2. Aminoacylase-1 was associated with both prevalent and incident DM2. SOMAScan of respiratory mucosa analyzed over 1,000 secreted proteins, identifying 162 differentially expressed proteins, including IL-6 and CXCL10, as highly expressed proteins in human influenza infection patients (Marion et al., 2016). SOMAScan was used to diagnose *M. tuberculosis* infection by measuring bacterial antigens (85A, 85B, 85C, CFP2, CFP10, DnaK, GroEL2, GroES, KAD, RplL, and Tpx), with only 85B and CFP10 revealing a significant difference (Russell et al., 2017).

Olink uses oligonucleotide antibody pairs containing unique DNA sequences to identify up to 3072 proteins in a sample. Proximity extension through oligonucleotide hybridization creates unique DNA reporter sequences that improve multiplexing and limit antibody cross-reactivity. Brown et al. (2022) investigated the inflammatory response of polymicrobial wound biofilm in an *in vitro* DM foot infection model using Olink proteomics, discovering elevated levels of CDCP1, CXCL1, IL-20, IL-8, MMP-1, TGF-alpha, and VEGFA. Petrera et al. (2021) compared the proteomics of DM, cardiovascular disease, and lung disease patients using DD-MS, DIA-MS, and Olink, measuring 300 proteins using MS techniques and 728 proteins using Olink. The study observed 35 overlapping proteins, highlighting the limitations and benefits of both techniques as well as demonstrating their complementary strengths. Furthermore, the proteins discovered in untargeted MS can be used as targets for immunoproteomics approaches.

Immunoproteomics

Immunoproteomics draws on proteomics to systematic study the adaptive immune system, measuring antigenic peptides and antibodies directed against them. Immunoproteomics refers to a rapidly expanding collection of techniques (Figure 2) for identifying and quantifying antigen proteins and *in silico* methods to understand disease pathogenesis, prognosis, and vaccine development (Fulton et al., 2019). Affinity-based assays that use antibodies coupled to a reporter (florescence, luminescence, radioactivity, or enzymatic activity) remain the gold standard for disease diagnosis. These assays are routinely used to diagnose and classify DM based upon conventional biomarkers, such as HbA1c, fructosamine, adiponectin, glycated albumin, and leptin (Dorcely et al., 2017; Chen and Gerszten, 2020). Enzyme linked immunosorbent assay (ELISA), radioimmune assay (RIA), and Chemiluminescence immunoassay (CLIA) are the most common techniques in immunoproteomics. Perhaps, these assays lack multiplexity, as they can only measure one analyte per reaction and cannot provide an unbiased measurement of all proteins present in the reaction. Recent developments in affinity-based assays have increased the efficiency and spectrum of protein quantification. Multiplexing antigens or antibodies in samples has significantly increased the number of proteins measured in one reaction.

Gel-based immune assays pioneer multiplexing by combining Western blotting for the detection of antigenic proteins and mass spectrometry-based identification. Using Western blotting and transcriptomics improves our understanding of the pathophysiology of infection-induced delayed healing of DM wounds (Ramirez et al., 2018). Chip-based proteome arrays have greatly improved the throughput of proteome-wide antibody screening. Particularly, natively folded, full-length, and completely functional proteins expressed using the KREX technology are used in high-density immunome arrays, including autoimmune, mutant, and epitope screening assays (Poulsen et al., 2020). The groundbreaking technology is widely used to discover novel biomarkers in cancer, autoimmune disorders, and infection biology research (Sumera et al., 2020; Schmidt et al., 2022).

Immunocapture MS, multiple affinity protein profiling (MAPPing), and nucleic acid programmable protein array (NAPPA) are a few of the other novel antigen expression arrays that are recently developed for high throughput host immune response screening and autoimmune analysis (Bian et al., 2016, 2017; Fulton et al., 2019). NAPPA uses cell-free expression systems to directly translate cDNA-encoded bait (target) proteins on glass slides. Anti-tag antibodies co-spotted with cDNA precisely capture *de novo* synthesized proteins. Co-expression of bait and inquiry proteins is captured using the *in vitro* transcription/translation (IVTT) system, allowing efficient and reproducible analysis of protein interactions (Montor et al., 2009; Yu et al., 2015). The query protein is IVTT co-expressed with the bait protein in protein interaction assays to study autoimmune responses, protein–protein interactions, and vaccine development (Arévalo-Pinzón et al., 2018). Using NAPPA, Yu et al. (2015) discovered 10,000 interaction networks of human proteins with *Legionella pneumophila* antigen proteins (SidM and LidA). NAPPA immunoproteomic analysis of *H. pylori* revealed IgG humoral immune response, characterized by a panel of anti-Ggt, -HslU, -NapA, and-CagA antibodies to differentiate gastric cancer patients from healthy control (Song et al., 2021). Similarly, Bian et al. (2016) studied antiviral antibodies in new-onset DM1 using NAPPA protein–protein interactions immunoproteomic profiling arrays, discovering higher antibody responses against EBV in DM1 patients.

Similarly, microsphere suspension array technology (e.g., Luminex FLEXMAP 3D®), which allows for multiplex analysis of up to 500 analytes, is also gaining popularity in immunoproteomics and infection studies. The technology offers flexible options for optimization and multiplexing by binding pathogen antigens with the microspheres to study antibody responses, as previously reported for EBV, papillomavirus, and *M. tuberculosis* (Altuglu et al., 2007; Clifford et al., 2007; Khan et al., 2008). Jiménez-Munguía et al. (2017) studied humoral immune responses against *Pneumococcal pneumonia* to develop a diagnostic array for antigens against infectious pneumonia. *S. aureus* immunoproteomics is performed using suspension array technology (e.g., Luminex® FLEXMAP 3D) to quantify up to 64 antigens across a broad dynamic spectrum (Stentzel et al., 2015). The array was used to examine *S. aureus* IgG profiles in sepsis and non-sepsis patients, revealing a protective signature of eight proteins for the bacteria (Stentzel et al., 2015). Another similar study discovered a panel of eight *S. aureus* proteins that can help early diagnosis of septicemia and could potentially develop *S. aureus* vaccine (Michalik et al., 2020). The authors found that the IgG marker panel against MsrB, FadB, EsxA, Pbp2, FadB, SspB, and SodA proteins could accurately discriminate early *S. aureus* infection (ROC-UAC 0.98). However, these studies did not observe differences in antibody responses through both studies had diabetic and non-diabetic patients infected with

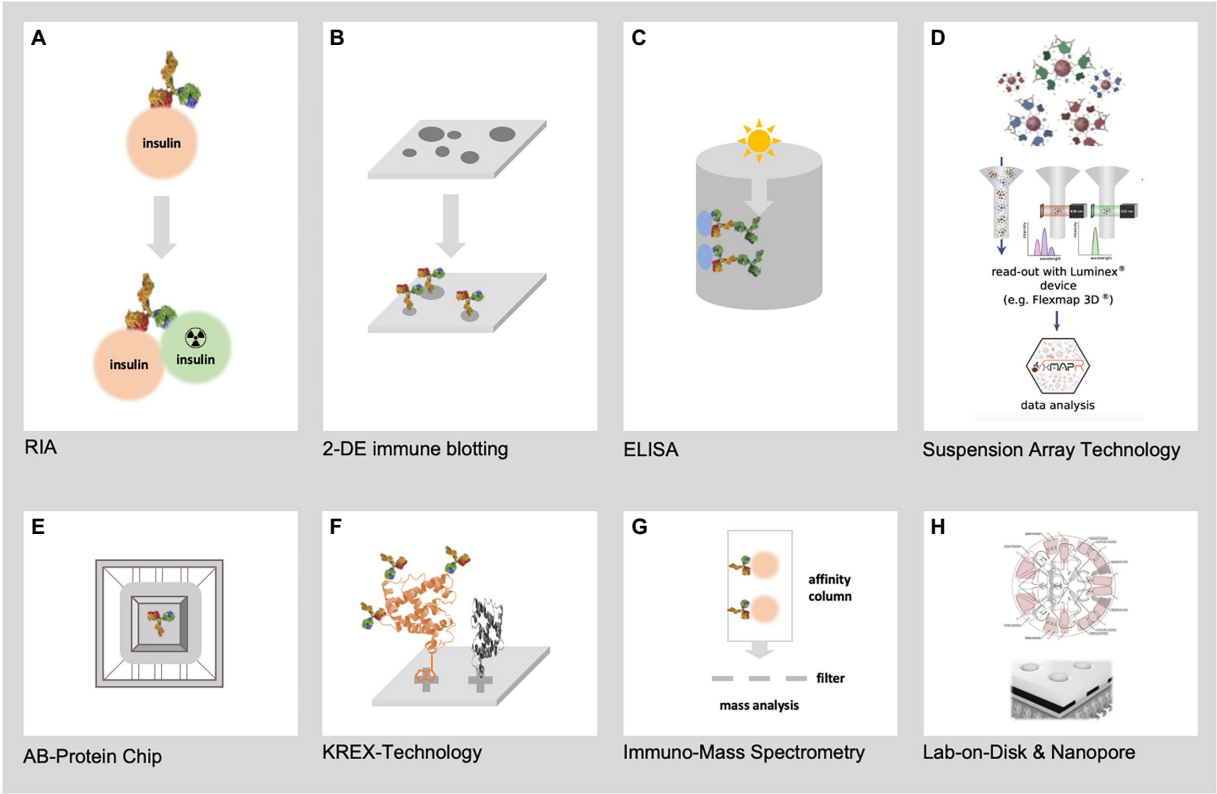

FIGURE 2
Represents the most relevant techniques for immunoproteomics. **(A)** First immunoproteomics approach (RIA) to detect AB against insulin **(B)** 2-DE immune blotting combining 2-DE electrophoresis of hundreds of native pathogen proteoforms and Western blotting **(C)** Classical ELISA technology using single recombinant proteins **(D)** SAT technology such as FLEXMAP 3D for up to 500 different recombinant proteins **(E)** AB-Protein chips for the detection of thousands of AB against recombinant proteins **(F)** KREX technology for the detection of AB against thousands of correctly folded recombinant proteins **(G)** Mass spectrometry based immunoproteomics using native pathogen proteins **(H)** New lab-on-chip and Nanopore technologies will allow the miniaturization of immunoproteomics in high dimension from recombinant and native pathogen proteins.

S. aureus (Stentzel et al., 2015; Michalik et al., 2020). In contrast, a general population study of 996 individuals that tested specific IgG and IgA responses to 79 *S. aureus* antigens found that IgG binding to 66 antigens decreased with increasing BMI and serum glucose concentrations (Meyer et al., 2021). The study observed that smoking, BMI and blood glucose levels moderately influenced the *S. aureus* IgG response (Meyer et al., 2021). Antibody response against naturally occurring 202 glycans, including aminoglysides, glycolipids, ganglio-series, O-linked glycans, and blood group A and B antigens, were observed using FLEXMAP, reporting an association with pathogenesis and progression to DM1 (Tran et al., 2022). Particularly, antibodies against gentamicin and its related structures, G418 and sisomicin, were associated with islet autoimmunity.

To clinically validate the *S. aureus* 4-Antigen (SA4Ag) Vaccine (clinical trial no. NCT02388165), Luminex immunoassays are being used to study humoral immune response against *S. aureus* CP5, CP8, rmClfA, and rMntC proteins (Begier et al., 2017). Furthermore, SA4Ag vaccine efficacy in obese, diabetic, and metabolic syndrome patients was tested using Luminex immunoassays (Scully et al., 2017). Although no significant difference in antibody responses against SA4Ag proteins was observed among different study cohorts, the researchers predicted that an effective *S. aureus* vaccine could enhance neutrophil-mediated bacterial killing and prevent lethal complications in these comorbid populations (Scully et al., 2017). Farnsworth et al. (2015) investigated the humoral immune response to *S. aureus* infections in mice with DM2 and DM1. Total IgG and total IgM levels were determined using whole *S. aureus* extract and selected *S. aureus* intracellular, attachment, and functional proteins (Amd, ClfA, ClfB, FnbA Gmd, IsdA, IsdB, and IsdH). Compared with the controls, infection severity was much worse in both mouse models of diabetes, with DM2 mice generally having lower anti-*S. aureus* IgG response and higher IgM response.

Oh et al. (2018) used Luminex multiplex immunoassay to measure anti-*S. aureus* IgG levels in the serum of DFI patients. The study showed strong prognostic and diagnostic potential of IgG antibodies against *S. aureus* IsdA, IsdH, Amd, Gmd, and Hla antigens in DFI with more than 0.85 ROC-AUC for anti-IsdA and anti-IsdH antibodies. The findings suggest that early detection of *S. aureus* exoproteins using multiplex immune assays improves disease prognosis and holds promise for vaccine development.

Conclusion

Available literature reveals that the prevalence and severity of microbial infections is higher in diabetic patients. The molecular interactions between infection and host immunity are very complex. Effective preventive strategies, such as vaccination or early detection of diabetic infections, are critical for reducing DM complications and fatalities. The current review discusses the most common DM infections and their prognostic role in DM pathogenesis. *Staphylococcus aureus* is the most contagious and lethal pathogen in SSTIs and septicemia. Both proteomics and immunoproteomics complement each other and have the potential to discover new biomarkers. The lack of reliable infection markers suggests that the diagnostic scope of immunoproteomics, which uses both infection and host marker molecules, should be expanded. Immunoproteomics holds promise for early infection diagnosis, emphasizes the protective function of the adaptive immune system, and promotes further research in producing a clinically successful *S. aureus* vaccine. The above-mentioned latest proteomics and immunoproteomics techniques represent a new milestone in sensitivity, selectivity, and automation analytics. As we can now screen large cohorts for antibodies to pathogens and autoimmune antibodies, a new chapter is being opened in studying the role of antibodies in various diseases. Immunoproteomics techniques can plausibly identify new targets for vaccines and can also be used to conclude mimicry of pathogenic proteins, which has been poorly studied and was not possible on a large scale. However, recent immunoproteomics study of antigenic mimicry of viral and bacterial antigens, as investigated for autoantibody response against blood coagulation proteins (Root-Bernstein et al., 2022), heralds a new era in metabolic disease research. Therefore, the authors believe antibody screening should be a standard part of the future infection-and diabetes-related cohort screening.

Author contributions

All authors listed have made a substantial, direct, and intellectual contribution to the work and approved it for publication.

Funding

This work was supported by the Biomedical Research Program at Weill Cornell Medicine in Qatar, a program funded by the Qatar Foundation. This publication was made possible by NPRP-Standard (NPRP-S) 12th Cycle grant # NPRP12S-0318-190392 from the Qatar National Research Fund (a member of Qatar Foundation). The findings herein reflect the work and are solely the responsibility of the authors.

Conflict of interest

The authors declare that the research was conducted in the absence of any commercial or financial relationships that could be construed as a potential conflict of interest.

Publisher's note

References

Abariga, S. A., and Whitcomb, B. W. (2016). Periodontitis and gestational diabetes mellitus: a systematic review and meta-analysis of observational studies. *BMC Pregnancy Childbirth* 16:344. doi: 10.1186/s12884-016-1145-z

Abu-Ashour, W., Twells, L., Valcour, J., Randell, A., Donnan, J., Howse, P., et al. (2017). The association between diabetes mellitus and incident infections: a systematic review and meta-analysis of observational studies. *BMJ Open Diabetes Res. Care* 5:e000336

Acar, M. B., Ayaz-Güner, Ş., Güner, H., Dinç, G., Kılıç, A. U., Doğanay, M., et al. (2022). A subtractive proteomics approach for the identification of immunodominant *Acinetobacter baumannii* vaccine candidate proteins. *bioRxiv*. doi: 10.1101/2022.06.26.497689

Ahmed, M., Forsberg, J., and Bergsten, P. (2005). Protein profiling of human pancreatic islets by two-dimensional gel electrophoresis and mass spectrometry. *J. Proteome Res.* 4, 931–940. doi: 10.1021/pr050024a

Al-Obaida, M. I., Al-Nakhli, A. K. M., Arif, I. A., Faden, A., Al-Otaibi, S., Al-Eid, B., et al. (2020). Molecular identification and diversity analysis of dental bacteria in diabetic and non-diabetic females from Saudi Arabia. *Saudi J. Biol. Sci.* 27, 358–362. doi: 10.1016/j.sjbs.2019.10.005

Al-Sultan, A. A. (2014). Diabetic patients are threatened by "superbugs" *Acinetobacter baumannii* in Saudi Arabia hospitals. *Int. J. Infect. Dis.* 21:351. doi: 10.1016/j.ijid.2014.03.1144

Altuglu, I., Bozkurt, H., Samlioglu, P., and Zeytinoglu, A. (2007). Evaluation of three different assays for the assessment of Epstein Barr virus immunological status. *New Microbiol.* 30, 393–398. PMID: 18080674

Alvarez-Llamas, G., Szalowska, E., De Vries, M. P., Weening, D., Landman, K., Hoek, A., et al. (2007). Characterization of the human visceral adipose tissue Secretome*. *Mol. Cell. Proteomics* 6, 589–600. doi: 10.1074/mcp.M600265-MCP200

Ambite, I., Butler, D., Wan, M. L. Y., Rosenblad, T., Tran, T. H., Chao, S. M., et al. (2021). Molecular determinants of disease severity in urinary tract infection. *Nat. Rev. Urol.* 18, 468–486. doi: 10.1038/s41585-021-00477-x

Arévalo-Pinzón, G., González-González, M., Suárez, C. F., Curtidor, H., Carabias-Sánchez, J., Muro, A., et al. (2018). Self-assembling functional programmable protein array for studying protein–protein interactions in malaria parasites. *Malar. J.* 17:270. doi: 10.1186/s12936-018-2414-2

Avalos Vizcarra, I., Hosseini, V., Kollmannsberger, P., Meier, S., Weber, S. S., Arnoldini, M., et al. (2016). How type 1 fimbriae help Escherichia coli to evade extracellular antibiotics. *Sci. Rep.* 6:18109. doi: 10.1038/srep18109

Awan, S. (2020). Isolation and PCR based identification of *staphylococcus Aureus* from Oral cavity of diabetic patients in Quetta City. *Pak-Euro J. Med. Life Sci.* 3, 156–167. doi: 10.31580/pjmls.v2i4.1712

Backert, S., Ziska, E., Brinkmann, V., Zimny-Arndt, U., Fauconnier, A., Jungblut, P. R., et al. (2000). Translocation of the helicobacter pylori CagA protein in gastric epithelial cells by a type IV secretion apparatus. *Cell. Microbiol.* 2, 155–164. doi: 10.1046/j.1462-5822.2000.00043.x

Badawi, A., and Ryoo, S. G. (2016). Prevalence of diabetes in the 2009 influenza A (H1N1) and the Middle East respiratory syndrome coronavirus: A systematic review and meta-analysis. *J. Public Health Res.* 5:jphr.2016.733. doi: 10.4081/jphr.2016.733

Baena-Díez, J. M., Peñafiel, J., Subirana, I., Ramos, R., Elosua, R., Marín-Ibañez, A., et al. (2016). Risk of cause-specific death in individuals with diabetes: A competing risks analysis. *Diabetes Care* 39, 1987–1995. doi: 10.2337/dc16-0614

Begier, E., Seiden, D. J., Patton, M., Zito, E., Severs, J., Cooper, D., et al. (2017). SA4Ag, a 4-antigen *Staphylococcus aureus* vaccine, rapidly induces high levels of bacteria-killing antibodies. *Vaccine* 35, 1132–1139. doi: 10.1016/j.vaccine.2017.01.024

Berbudi, A., Rahmadika, N., Tjahjadi, A. I., and Ruslami, R. (2020). Type 2 diabetes and its impact on the immune system. *Curr. Diabetes Rev.* 16, 442–449. doi: 10.2174/1573399815666191024085838

Bian, X., Wallstrom, G., Davis, A., Wang, J., Park, J., Throop, A., et al. (2016). Immunoproteomic profiling of antiviral antibodies in new-onset type 1 diabetes using protein arrays. *Diabetes* 65, 285–296. doi: 10.2337/db15-0179

Bian, X., Wasserfall, C., Wallstrom, G., Wang, J., Wang, H., Barker, K., et al. (2017). Tracking the antibody immunome in type 1 diabetes using protein arrays. *J. Proteome Res.* 16, 195–203. doi: 10.1021/acs.jproteome.6b00354

Bischoff, M., Wonnenberg, B., Nippe, N., Nyffenegger-Jann, N. J., Voss, M., Beisswenger, C., et al. (2017). CcpA affects infectivity of *Staphylococcus aureus* in a hyperglycemic environment. *Front. Cell. Infect. Microbiol.* 7:172. doi: 10.3389/fcimb.2017.00172

Brown, J. L., Townsend, E., Short, R. D., Williams, C., Woodall, C., Nile, C. J., et al. (2022). Assessing the inflammatory response to in vitro polymicrobial wound biofilms in a skin epidermis model. *npj Biofilms Microbiomes* 8:19. doi: 10.1038/s41522-022-00286-z

Buetti, N., Trimboli, P., Mazzuchelli, T., Lo Priore, E., Balmelli, C., Trkola, A., et al. (2020). Diabetes mellitus is a risk factor for prolonged SARS-CoV-2 viral shedding in lower respiratory tract samples of critically ill patients. *Endocrine* 70, 454–460. doi: 10.1007/s12020-020-02465-4

Cancienne, J. M., Brockmeier, S. F., and Werner, B. C. (2018a). Association of perioperative glycemic control with deep postoperative infection after shoulder arthroplasty in patients with diabetes. *JAAOS* 26, e238–e245. doi: 10.5435/JAAOS-D-16-00784

Cancienne, J. M., Miller, M. D., Browne, J. A., and Werner, B. C. (2018b). Not all patients with diabetes have the same risks: perioperative glycemic control is associated with postoperative infection following knee arthroscopy. *Arthroscopy* 34, 1561–1569. doi: 10.1016/j.arthro.2017.11.034

Cardoso, N. A., Cisneiros, L. L., Machado, C. J., Cenedezi, J. M., Procópio, R. J., and Navarro, T. P. (2017). Bacterial genus is a risk factor for major amputation in patients with diabetic foot. *Rev. Col. Bras. Cir.* 44, 147–153. doi: 10.1590/0100-69912017002007

Carrillo-Larco, R. M., Anza-Ramírez, C., Saal-Zapata, G., Villarreal-Zegarra, D., Zafra-Tanaka, J. H., Ugarte-Gil, C., et al. (2022). Type 2 diabetes mellitus and antibiotic-resistant infections: a systematic review and meta-analysis. *J. Epidemiol. Community Health* 76, 75–84. doi: 10.1136/jech-2020-216029

Chang, D. C., Piaggi, P., Hanson, R. L., Knowler, W. C., Bucci, J., Thio, G., et al. (2015). Use of a high-density protein microarray to identify autoantibodies in subjects with type 2 diabetes mellitus and an HLA background associated with reduced insulin secretion. *PLoS One* 10:e0143551. doi: 10.1371/journal.pone.0143551

Chatterjee, S., Khunti, K., and Davies, M. J. (2017). Type 2 diabetes. *Lancet* 389, 2239–2251. doi: 10.1016/S0140-6736(17)30058-2

Chen, Z. Z., and Gerszten, R. E. (2020). Metabolomics and proteomics in type 2 diabetes. *Circ. Res.* 126, 1613–1627. doi: 10.1161/CIRCRESAHA.120.315898

Chen, Q., Ma, X., Li, C., Shen, Y., Zhu, W., Zhang, Y., et al. (2020). Enteric Phageome alterations in patients with type 2 diabetes. *Front. Cell. Infect. Microbiol.* 10:575084. doi: 10.3389/fcimb.2020.575084

Chokwiriyachit, A., Dasanayake, A. P., Suwannarong, W., Hormdee, D., Sumanonta, G., Prasertchareonsuk, W., et al. (2013). Periodontitis and gestational diabetes mellitus in non-smoking females. *J. Periodontol.* 84, 857–862. doi: 10.1902/jop.2012.120344

Ciancio, A., Bosio, R., Bo, S., Pellegrini, M., Sacco, M., Vogliotti, E., et al. (2018). Significant improvement of glycemic control in diabetic patients with HCV infection responding to direct-acting antiviral agents. *J. Med. Virol.* 90, 320–327. doi: 10.1002/jmv.24954

Clifford, G. M., Shin, H.-R., Oh, J.-K., Waterboer, T., Ju, Y.-H., Vaccarella, S., et al. (2007). Serologic response to oncogenic human papillomavirus types in male and female university students in Busan, South Korea. *Cancer Epidemiol. Biomark. Prev.* 16, 1874–1879. doi: 10.1158/1055-9965.EPI-07-0349

Critchley, J. A., Carey, I. M., Harris, T., Dewilde, S., Hosking, F. J., and Cook, D. G. (2018). Glycemic control and risk of infections among people with type 1 or type 2 diabetes in a large primary care cohort study. *Diabetes Care* 41, 2127–2135. doi: 10.2337/dc18-0287

Cusick, M. F., Libbey, J. E., and Fujinami, R. S. (2012). Molecular mimicry as a mechanism of autoimmune disease. *Clin. Rev. Allergy Immunol.* 42, 102–111. doi: 10.1007/s12016-011-8294-7

Cyprian, F., Sohail, M. U., Abdelhafez, I., Salman, S., Attique, Z., Kamareddine, L., et al. (2021). SARS-CoV-2-immune-microbiome interaction: lessons from respiratory viral infections. *Int. J. Infect. Dis.* 105, 540–550. doi: 10.1016/j.ijid.2021.02.071

Daryabor, G., Atashzar, M. R., Kabelitz, D., Meri, S., and Kalantar, K. (2020). The effects of type 2 diabetes mellitus on organ metabolism and the immune system. *Front. Immunol.* 11:1582. doi: 10.3389/fimmu.2020.01582

Dennehy, R., and Mcclean, S. (2012). Immunoproteomics: the key to discovery of new vaccine antigens against bacterial respiratory infections. *Curr. Protein Pept. Sci.* 13, 807–815. doi: 10.2174/138920312804871184

Dorcely, B., Katz, K., Jagannathan, R., Chiang, S. S., Oluwadare, B., Goldberg, I. J., et al. (2017). Novel biomarkers for prediabetes, diabetes, and associated complications. *Diabetes Metab. Syndr. Obes.* 10, 345–361. doi: 10.2147/DMSO.S100074

Dotta, F., Censini, S., Van Halteren, A. G., Marselli, L., Masini, M., Dionisi, S., et al. (2007). Coxsackie B4 virus infection of beta cells and natural killer cell insulitis in recent-onset type 1 diabetic patients. *Proc. Natl. Acad. Sci. U. S. A.* 104, 5115–5120. doi: 10.1073/pnas.0700442104

Dryden, M., Baguneid, M., Eckmann, C., Corman, S., Stephens, J., Solem, C., et al. (2015). Pathophysiology and burden of infection in patients with diabetes mellitus and peripheral vascular disease: focus on skin and soft-tissue infections. *Clin. Microbiol. Infect.* 21, S27–S32. doi: 10.1016/j.cmi.2015.03.024

Dunyach-Remy, C., Ngba Essebe, C., Sotto, A., and Lavigne, J.-P. (2016). *Staphylococcus aureus* toxins and diabetic foot ulcers: role in pathogenesis and interest in diagnosis. *Toxins* 8:209. doi: 10.3390/toxins8070209

Elhadad, M. A., Jonasson, C., Huth, C., Wilson, R., Gieger, C., Matias, P., et al. (2020). Deciphering the plasma proteome of type 2 diabetes. *Diabetes* 69, 2766–2778. doi: 10.2337/db20-0296

Esper, A. M., Moss, M., and Martin, G. S. (2009). The effect of diabetes mellitus on organ dysfunction with sepsis: an epidemiological study. *Crit. Care* 13:R18. doi: 10.1186/cc7717

Fabiani, S., Fallahi, P., Ferrari, S. M., Miccoli, M., and Antonelli, A. (2018). Hepatitis C virus infection and development of type 2 diabetes mellitus: systematic review and meta-analysis of the literature. *Rev. Endocr. Metab. Disord.* 19, 405–420. doi: 10.1007/s11154-017-9440-1

Fallahi, P., Ferrari, S. M., Colaci, M., Ruffilli, I., Vita, R., Azzi, A., et al. (2013). Hepatitis C virus infection and type 2 diabetes. *Clin. Ter.* 164, e393–e404. doi: 10.7417/CT.2013.1620

Farnsworth, C. W., Shehatou, C. T., Maynard, R., Nishitani, K., Kates, S. L., Zuscik, M. J., et al. (2015). A Humoral immune defect distinguishes the response to *Staphylococcus aureus* infections in mice with obesity and type 2 diabetes from that in mice with type 1 diabetes. *Infect. Immun.* 83, 2264–2274. doi: 10.1128/IAI.03074-14

Feng, X., Zhang, L., Xu, L., Meng, H., Lu, R., Chen, Z., et al. (2014). Detection of eight periodontal microorganisms and distribution of Porphyromonas gingivalis fimA genotypes in Chinese patients with aggressive periodontitis. *J. Periodontol.* 85, 150–159. doi: 10.1902/jop.2013.120677

Fernández-Real, J. M., López-Bermejo, A., Vendrell, J., Ferri, M. J., Recasens, M., and Ricart, W. (2006). Burden of infection and insulin resistance in healthy middle-aged men. *Diabetes Care* 29, 1058–1064. doi: 10.2337/dc05-2068

Floyd, K. A., Meyer, A. E., Nelson, G., and Hadjifrangiskou, M. (2015). The yin-yang driving urinary tract infection and how proteomics can enhance research, diagnostics, and treatment. *Proteomics Clin. Appl.* 9, 990–1002. doi: 10.1002/prca.201500018

Frydrych, L. M., Fattahi, F., He, K., Ward, P. A., and Delano, M. J. (2017). Diabetes and sepsis: risk, recurrence, and ruination. *Front. Endocrinol.* 8:271. doi: 10.3389/fendo.2017.00271

Fulton, K. M., Baltat, I., and Twine, S. M. (2019). "Immunoproteomics methods and techniques" in *Immunoproteomics: methods and protocols*. eds. K. M. Fulton and S. M. Twine (New York, NY: springer New York), 25–58.

Gagnaire, J., Dauwalder, O., Boisset, S., Khau, D., Freydière, A. M., Ader, F., et al. (2012). Detection of *Staphylococcus aureus* delta-toxin production by whole-cell MALDI-TOF mass spectrometry. *PLoS One* 7:e40660. doi: 10.1371/journal.pone.0040660

Gan, Y.-H. (2013). Host susceptibility factors to bacterial infections in type 2 diabetes. *PLoS Pathog.* 9:e1003794. doi: 10.1371/journal.ppat.1003794

Gao, H., Luo, Z., Ji, Y., Tang, K., Jin, Z., Ly, C., et al. (2022). Accumulation of microbial DNAs promotes to islet inflammation and β cell abnormalities in obesity in mice. *Nat. Commun.* 13:565. doi: 10.1038/s41467-022-28239-2

Gill, S. K., Hui, K., Farne, H., Garnett, J. P., Baines, D. L., Moore, L. S., et al. (2016). Increased airway glucose increases airway bacterial load in hyperglycaemia. *Sci. Rep.* 6:27636. doi: 10.1038/srep27636

Graves, D. T., Ding, Z., and Yang, Y. (2020). The impact of diabetes on periodontal diseases. *Periodontology* 82, 214–224. doi: 10.1111/prd.12318

Gupta, P., Gupta, M., Katoch, N., Garg, K., and Garg, B. (2021). A systematic review and meta-analysis of diabetes associated mortality in patients with COVID-19. *Int. J. Endocrinol. Metab.* 19:e113220. doi: 10.5812/ijem.113220

Hine, J. L., De Lusignan, S., Burleigh, D., Pathirannehelage, S., Mcgovern, A., Gatenby, P., et al. (2017). Association between glycaemic control and common infections in people with type 2 diabetes: a cohort study. *Diabet. Med.* 34, 551–557. doi: 10.1111/dme.13205

Hitam, S. A. S., Hassan, S. A., and Maning, N. (2019). The significant association between polymicrobial diabetic foot infection and its severity and outcomes. *Malays. J. Med. Sci.* 26, 107–114. doi: 10.21315/mjms2019.26.1.10

Højlund, K., Yi, Z., Hwang, H., Bowen, B., Lefort, N., Flynn, C. R., et al. (2008). Characterization of the human skeletal muscle proteome by one-dimensional gel electrophoresis and HPLC-ESI-MS/MS. *Mol. Cell. Proteomics* 7, 257–267. doi: 10.1074/mcp.M700304-MCP200

Jafar, N., Edriss, H., and Nugent, K. (2016). The effect of Short-term hyperglycemia on the innate immune system. *Am. J. Med. Sci.* 351, 201–211. doi: 10.1016/j.amjms.2015.11.011

Jia, S. Y., Zhang, Y. L., Sun, X. Y., Yuan, C., and Zheng, S. G. (2021). Impact of the glycemic level on the salivary proteome of middle-aged and elderly people with type 2 diabetes mellitus: an observational study. *Front. Mol. Biosci.* 8:790091. doi: 10.3389/fmolb.2021.790091

Jiménez-Munguía, I., Van Wamel, W. J. B., Rodríguez-Ortega, M. J., and Obando, I. (2017). Detection of natural antibodies and serological diagnosis of pneumococcal pneumonia using a bead-based high-throughput assay. *Methods Mol. Biol.* 1643, 169–177. doi: 10.1007/978-1-4939-7180-0_13

Kalita, B., Bano, S., Vavachan, V. M., Taunk, K., Seshadri, V., and Rapole, S. (2020). Application of mass spectrometry based proteomics to understand diabetes: A special focus on interactomics. *Biochim. Biophys. Acta* 1868:140469. doi: 10.1016/j.bbapap.2020.140469

Khan, I. H., Ravindran, R., Yee, J., Ziman, M., Lewinsohn, D. M., Gennaro, M. L., et al. (2008). Profiling antibodies to mycobacterium tuberculosis by multiplex microbead suspension arrays for serodiagnosis of tuberculosis. *Clin. Vaccine Immunol.* 15, 433–438. doi: 10.1128/CVI.00354-07

Klekotka, R. B., Mizgała, E., and Król, W. (2015). The etiology of lower respiratory tract infections in people with diabetes. *Pneumonol. Alergol. Pol.* 83, 401–408. doi: 10.5603/PiAP.2015.0065

Klekotka, R. B., Mizgała-Izworska, E., Drzastwa, W., and Mazur, B. (2018). The role of in the clinical diagnosis of diabetic patients. *Postępy Mikrobiol. Advancem. Microbiol.* 57, 166–178. doi: 10.21307/PM-2018.57.2.166

Kolb, H., and Martin, S. (2017). Environmental/lifestyle factors in the pathogenesis and prevention of type 2 diabetes. *BMC Med.* 15:131. doi: 10.1186/s12916-017-0901-x

Kostrzewa, M., Nagy, E., Schröttner, P., and Pranada, A. B. (2019). How MALDI-TOF mass spectrometry can aid the diagnosis of hard-to-identify pathogenic bacteria - the rare and the unknown. *Expert. Rev. Mol. Diagn.* 19, 667–682. doi: 10.1080/14737159.2019.1643238

Kumar, A., Roberts, D., Wood, K. E., Light, B., Parrillo, J. E., Sharma, S., et al. (2006). Duration of hypotension before initiation of effective antimicrobial therapy is the critical determinant of survival in human septic shock. *Crit. Care Med.* 34, 1589–1596. doi: 10.1097/01.CCM.0000217961.75225.E9

Kundu, J., Bakshi, S., Joshi, H., Bhadada, S. K., Verma, I., and Sharma, S. (2020). Proteomic profiling of peripheral blood mononuclear cells isolated from patients with tuberculosis and diabetes copathogenesis - A pilot study. *PLoS One* 15:e0233326. doi: 10.1371/journal.pone.0233326

Larman, H. B., Laserson, U., Querol, L., Verhaeghen, K., Solimini, N. L., Xu, G. J., et al. (2013). PhIP-Seq characterization of autoantibodies from patients with multiple sclerosis, type 1 diabetes and rheumatoid arthritis. *J. Autoimmun.* 43, 1–9. doi: 10.1016/j.jaut.2013.01.013

Lau, M. E., Loughman, J. A., and Hunstad, D. A. (2012). YbcL of uropathogenic Escherichia coli suppresses transepithelial neutrophil migration. *Infect. Immun.* 80, 4123–4132. doi: 10.1128/IAI.00801-12

Leung, C. H., and Liu, C. P. (2019). Diabetic status and the relationship of blood glucose to mortality in adults with carbapenem-resistant Acinetobacter baumannii complex bacteremia. *J. Microbiol. Immunol. Infect.* 52, 654–662. doi: 10.1016/j.jmii.2018.06.005

Liew, Y. K., Awang Hamat, R., Van Belkum, A., Chong, P. P., and Neela, V. (2015). Comparative exoproteomics and host inflammatory response in *Staphylococcus aureus* skin and soft tissue infections, bacteremia, and subclinical colonization. *Clin. Vaccine Immunol.* 22, 593–603. doi: 10.1128/CVI.00493-14

Liu, S., Xu, Y., Jiang, X., Tan, H., and Ying, B. (2022). Translation of aptamers toward clinical diagnosis and commercialization. *Biosens. Bioelectron.* 208:114168. doi: 10.1016/j.bios.2022.114168

Lönnrot, M., Lynch, K. F., Elding Larsson, H., Lernmark, Å., Rewers, M. J., Törn, C., et al. (2017). Respiratory infections are temporally associated with initiation of type 1 diabetes autoimmunity: the TEDDY study. *Diabetologia* 60, 1931–1940. doi: 10.1007/s00125-017-4365-5

Lontchi-Yimagou, E., Feutseu, C., Kenmoe, S., Djomkam Zune, A. L., Kinyuy Ekali, S. F., Nguewa, J. L., et al. (2021). Non-autoimmune diabetes mellitus and the risk of virus infections: a systematic review and meta-analysis of case-control and cohort studies. *Sci. Rep.* 11:8968. doi: 10.1038/s41598-021-88598-6

Loureiro, C., MAR, B., Pessan, J. P., TMO, V., Pelá, V. T., APF, R., et al. (2022). Proteomic analysis of infected root canals with apical periodontitis in patients with type 2 diabetes mellitus: A cross-sectional study. *Int. Endod. J.* 55, 910–922. doi: 10.1111/iej.13794

Ludwig, C., Gillet, L., Rosenberger, G., Amon, S., Collins, B. C., and Aebersold, R. (2018). Data-independent acquisition-based SWATH-MS for quantitative proteomics: a tutorial. *Mol. Syst. Biol.* 14:e8126. doi: 10.15252/msb.20178126

Luo, G., Lin, L., Ibrahim, A. S., Baquir, B., Pantapalangkoor, P., Bonomo, R. A., et al. (2012). Active and passive immunization protects against lethal, extreme drug resistant-*Acinetobacter baumannii* infection. *PLoS One* 7:e29446. doi: 10.1371/journal.pone.0029446

Magdeldin, S., Enany, S., Yoshida, Y., Xu, B., Zhang, Y., Zureena, Z., et al. (2014). Basics and recent advances of two dimensional-polyacrylamide gel electrophoresis. *Clin. Proteomics* 11:16. doi: 10.1186/1559-0275-11-16

Mahajan, A., Taliun, D., Thurner, M., Robertson, N. R., Torres, J. M., Rayner, N. W., et al. (2018). Fine-mapping type 2 diabetes loci to single-variant resolution using high-density imputation and islet-specific epigenome maps. *Nat. Genet.* 50, 1505–1513. doi: 10.1038/s41588-018-0241-6

Malipatil, N., Fachim, H. A., Siddals, K., Geary, B., Wark, G., Porter, N., et al. (2019). Data independent acquisition mass spectrometry can identify circulating proteins that predict future weight loss with a diet and exercise programme. *J. Clin. Med.* 8:141. doi: 10.3390/jcm8020141

Manco, M., Putignani, L., and Bottazzo, G. F. (2010). Gut microbiota, lipopolysaccharides, and innate immunity in the pathogenesis of obesity and cardiovascular risk. *Endocr. Rev.* 31, 817–844. doi: 10.1210/er.2009-0030

Marion, T., Elbahesh, H., Thomas, P. G., Devincenzo, J. P., Webby, R., and Schughart, K. (2016). Respiratory mucosal proteome quantification in human influenza infections. *PLoS One* 11:e0153674. doi: 10.1371/journal.pone.0153674

Martinez, L., Zhu, L., Castellanos, M. E., Liu, Q., Chen, C., Hallowell, B. D., et al. (2017). Glycemic control and the prevalence of tuberculosis infection: A population-based observational study. *Clin. Infect. Dis.* 65, 2060–2068. doi: 10.1093/cid/cix632

Meyer, T. C., Michalik, S., Holtfreter, S., Weiss, S., Friedrich, N., Völzke, H., et al. (2021). A comprehensive view on the human antibody repertoire against *Staphylococcus aureus* antigens in the general population. *Front. Immunol.* 12:651619. doi: 10.3389/fimmu.2021.651619

Michalik, S., Sundaramoorthy, N., Murr, A., Depke, M., Völker, U., Bröker, B. M., et al. (2020). Early-stage *Staphylococcus aureus* bloodstream infection causes changes in the concentrations of lipoproteins and acute-phase proteins and is associated with low antibody titers against bacterial virulence factors. *mSystems* 5, e00632–e00619. doi: 10.1128/mSystems.00632-19

Moller, D. E. (2000). Potential role of TNF-alpha in the pathogenesis of insulin resistance and type 2 diabetes. *Trends Endocrinol. Metab.* 11, 212–217. doi: 10.1016/S1043-2760(00)00272-1

Molloy, M. P., Phadke, N. D., Maddock, J. R., and Andrews, P. C. (2001). Two-dimensional electrophoresis and peptide mass fingerprinting of bacterial outer membrane proteins. *Electrophoresis* 22, 1686–1696. doi: 10.1002/1522-2683(200105)22:9<1686::AID-ELPS1686>3.0.CO;2-L

Montor, W. R., Huang, J., Hu, Y., Hainsworth, E., Lynch, S., Kronish, J.-W., et al. (2009). Genome-wide study of *Pseudomonas aeruginosa* outer membrane protein immunogenicity using self-assembling protein microarrays. *Infect. Immun.* 77, 4877–4886. doi: 10.1128/IAI.00698-09

Morse, Z. J., and Horwitz, M. S. (2021). Virus infection is an instigator of intestinal dysbiosis leading to type 1 diabetes. *Front. Immunol.* 12:751337. doi: 10.3389/fimmu.2021.751337

Nabaigwa, B. I., Mwambi, B., Okiria, J., and Oyet, C. (2018). Common uropathogens among diabetic patients with urinary tract infection at Jinja regional referral hospital, Uganda. *Afr. J. Lab. Med.* 7:621. doi: 10.4102/ajlm.v7i1.621

Nabipour, I., Vahdat, K., Jafari, S. M., Pazoki, R., and Sanjdideh, Z. (2006). The association of metabolic syndrome and chlamydia pneumoniae, helicobacter pylori, cytomegalovirus, and herpes simplex virus type 1: the Persian Gulf healthy heart study. *Cardiovasc. Diabetol.* 5:25. doi: 10.1186/1475-2840-5-25

Nguyen, A. T. M., Akhter, R., Garde, S., Scott, C., Twigg, S. M., Colagiuri, S., et al. (2020). The association of periodontal disease with the complications of diabetes mellitus. A systematic review. *Diabetes Res. Clin. Pract.* 165:108244. doi: 10.1016/j.diabres.2020.108244

Noubiap, J. J., Nansseu, J. R., Nyaga, U. F., Nkeck, J. R., Endomba, F. T., Kaze, A. D., et al. (2019). Global prevalence of diabetes in active tuberculosis: a systematic review

and meta-analysis of data from 2·3 million patients with tuberculosis. *Lancet Glob. Health* 7, e448–e460. doi: 10.1016/S2214-109X(18)30487-X

Oh, I., Muthukrishnan, G., Ninomiya, M. J., Brodell, J. D. Jr., Smith, B. L., Lee, C. C., et al. (2018). Tracking anti-*Staphylococcus aureus* antibodies produced in vivo and ex vivo during foot salvage therapy for diabetic foot infections reveals prognostic insights and evidence of diversified Humoral immunity. *Infect. Immun.* 86:e00629-18. doi: 10.1128/IAI.00629-18

Oikarinen, S., Martiskainen, M., Tauriainen, S., Huhtala, H., Ilonen, J., Veijola, R., et al. (2011). Enterovirus RNA in blood is linked to the development of type 1 diabetes. *Diabetes* 60, 276–279. doi: 10.2337/db10-0186

Op De Beeck, A., and Eizirik, D. L. (2016). Viral infections in type 1 diabetes mellitus--why the β cells? *Nat. Rev. Endocrinol.* 12, 263–273. doi: 10.1038/nrendo.2016.30

Patra, E., Meher, D., Suar, M., Panigrahi, J., and Mishra, S. (2017). Microbial etiology of bacteremia in controlled and uncontrolled type-2Diabetes in eastern part of India. *J. Diabet. Metab.* 8, 1–8. doi: 10.4172/2155-6156.1000744

Peleg, A. Y., Weerarathna, T., Mccarthy, J. S., and Davis, T. M. E. (2007). Common infections in diabetes: pathogenesis, management and relationship to glycaemic control. *Diabetes Metab. Res. Rev.* 23, 3–13. doi: 10.1002/dmrr.682

Petrera, A., Von Toerne, C., Behler, J., Huth, C., Thorand, B., Hilgendorff, A., et al. (2021). Multiplatform approach for plasma proteomics: complementarity of Olink proximity extension assay technology to mass spectrometry-based protein profiling. *J. Proteome Res.* 20, 751–762. doi: 10.1021/acs.jproteome.0c00641

Pocsfalvi, G., Stanly, C., Fiume, I., and Vékey, K. (2016). Chromatography and its hyphenation to mass spectrometry for extracellular vesicle analysis. *J. Chromatogr. A* 1439, 26–41. doi: 10.1016/j.chroma.2016.01.017

Poulsen, T. B. G., Karamehmedovic, A., Aboo, C., Jørgensen, M. M., Yu, X., Fang, X., et al. (2020). Protein array-based companion diagnostics in precision medicine. *Expert. Rev. Mol. Diagn.* 20, 1183–1198. doi: 10.1080/14737159.2020.1857734

Que, Y.-A., and Moreillon, P. (2015). "196 - *Staphylococcus aureus* (including staphylococcal toxic shock syndrome)," in *Mandell, Douglas, and Bennett's principles and practice of infectious diseases*. eds. J. E. Bennett, R. Dolin and M. J. Blaser. *8th Edn.* (Philadelphia: W.B. Saunders)

Ramirez, H. A., Pastar, I., Jozic, I., Stojadinovic, O., Stone, R. C., Ojeh, N., et al. (2018). *Staphylococcus aureus* triggers induction of miR-15B-5P to diminish DNA repair and deregulate inflammatory response in diabetic foot ulcers. *J. Investig. Dermatol.* 138, 1187–1196. doi: 10.1016/j.jid.2017.11.038

Rao Kondapally Seshasai, S., Kaptoge, S., Thompson, A., Di Angelantonio, E., Gao, P., Sarwar, N., et al. (2011). Diabetes mellitus, fasting glucose, and risk of cause-specific death. *N. Engl. J. Med.* 364, 829–841. doi: 10.1056/NEJMoa1008862

Rastogi, A., Goyal, G., Kesavan, R., Bal, A., Kumar, H., Mangalanadanam, K., et al. (2020). Long term outcomes after incident diabetic foot ulcer: multicenter large cohort prospective study (EDI-FOCUS investigators) epidemiology of diabetic foot complications study: epidemiology of diabetic foot complications study. *Diabetes Res. Clin. Pract.* 162:108113. doi: 10.1016/j.diabres.2020.108113

Root-Bernstein, R., Huber, J., and Ziehl, A. (2022). Complementary sets of autoantibodies induced by SARS-CoV-2, adenovirus and bacterial antigens cross-react with human blood protein antigens in COVID-19 coagulopathies. *Int. J. Mol. Sci.* 23:11500. doi: 10.3390/ijms231911500

Russell, T. M., Green, L. S., Rice, T., Kruh-Garcia, N. A., Dobos, K., De Groote, M. D., et al. (2017). Potential of high-affinity, slow off-rate modified Aptamer reagents for mycobacterium tuberculosis proteins as tools for infection models and diagnostic applications. *J. Clin. Microbiol.* 55, 3072–3088. doi: 10.1128/JCM.00469-17

Ryu, S. Y., Baek, W. K., and Kim, H. A. (2017). Association of biofilm production with colonization among clinical isolates of *Acinetobacter baumannii*. *Korean J. Intern. Med.* 32, 345–351. doi: 10.3904/kjim.2015.287

Saeedi, P., Petersohn, I., Salpea, P., Malanda, B., Karuranga, S., Unwin, N., et al. (2019). Global and regional diabetes prevalence estimates for 2019 and projections for 2030 and 2045: results from the international diabetes federation diabetes atlas, 9(th) edition. *Diabetes Res. Clin. Pract.* 157:107843. doi: 10.1016/j.diabres.2019.107843

Sánchez-Maldonado, J. M., Collado, R., Cabrera-Serrano, A. J., Ter Horst, R., Gálvez-Montosa, F., Robles-Fernández, I., et al. (2022). Type 2 diabetes-related variants influence the risk of developing prostate cancer: A population-based case-control study and meta-analysis. *Cancers* 14:2376. doi: 10.3390/cancers14102376

Saseedharan, S., Sahu, M., Chaddha, R., Pathrose, E., Bal, A., Bhalekar, P., et al. (2018). Epidemiology of diabetic foot infections in a reference tertiary hospital in India. *Braz. J. Microbiol.* 49, 401–406. doi: 10.1016/j.bjm.2017.09.003

Schmidt, F., Abdesselem, H. B., Suhre, K., Sohail, M. U., Al-Nesf, M., Bensmail, I., et al. (2022). Auto-Immunoproteomics analysis of COVID-19 ICU patients revealed increased levels of autoantibodies related to male reproductive system. *bioRxiv* 2022.2002.2009.479669

Schmidt, F., Meyer, T., Sundaramoorthy, N., Michalik, S., Surmann, K., Depke, M., et al. (2017). Characterization of human and *Staphylococcus aureus* proteins in respiratory mucosa by in vivo-and immunoproteomics. *J. Proteome* 155, 31–39. doi: 10.1016/j.jprot.2017.01.008

Schneider, D. A., and Von Herrath, M. G. (2014). Potential viral pathogenic mechanism in human type 1 diabetes. *Diabetologia* 57, 2009–2018. doi: 10.1007/s00125-014-3340-7

Schuetz, P., Castro, P., and Shapiro, N. I. (2011). Diabetes and sepsis: preclinical findings and clinical relevance. *Diabetes Care* 34, 771–778. doi: 10.2337/dc10-1185

Scully, I. L., Mcneil, L. K., Pathirana, S., Singer, C. L., Liu, Y., Mullen, S., et al. (2017). Neutrophil killing of *Staphylococcus aureus* in diabetes, obesity and metabolic syndrome: a prospective cellular surveillance study. *Diabetol. Metab. Syndr.* 9:76. doi: 10.1186/s13098-017-0276-3

Seidl, K., Stucki, M., Ruegg, M., Goerke, C., Wolz, C., Harris, L., et al. (2006). *Staphylococcus aureus* CcpA affects virulence determinant production and antibiotic resistance. *Antimicrob. Agents Chemother.* 50, 1183–1194. doi: 10.1128/AAC.50.4.1183-1194.2006

Seo, K. S., Park, N., Rutter, J. K., Park, Y., Baker, C. L., Thornton, J. A., et al. (2021). Role of Glucose-6-phosphate in metabolic adaptation of *Staphylococcus aureus* in diabetes. *Microbiol Spectr* 9:e0085721. doi: 10.1128/Spectrum.00857-21

Šestan, M., Marinović, S., Kavazović, I., Cekinović, Đ., Wueest, S., Turk Wensveen, T., et al. (2018). Virus-induced interferon-γ causes insulin resistance in skeletal muscle and derails glycemic control in obesity. *Immunity* 49, 164–177.e6. doi: 10.1016/j.immuni.2018.05.005

Seyyed Mousavi, M. N., Mehramuz, B., Sadeghi, J., Alizadeh, N., Oskouee, M. A., and Kafil, H. S. (2017). The pathogenesis of *Staphylococcus aureus* in autoimmune diseases. *Microb. Pathog.* 111, 503–507. doi: 10.1016/j.micpath.2017.09.028

Silversides, J. A., Lappin, E., and Ferguson, A. J. (2010). Staphylococcal toxic shock syndrome: mechanisms and management. *Curr. Infect. Dis. Rep.* 12, 392–400. doi: 10.1007/s11908-010-0119-y

Smit, J., Søgaard, M., Schønheyder, H. C., Nielsen, H., Frøslev, T., and Thomsen, R. W. (2016). Diabetes and risk of community-acquired *Staphylococcus aureus* bacteremia: a population-based case-control study. *Eur. J. Endocrinol.* 174, 631–639. doi: 10.1530/EJE-16-0023

Smith, J. A., and O'connor, J. J. (1966). Nasal carriage of *Staphylococcus aureus* in diabetes mellitus. *Lancet* 2, 776–777. doi: 10.1016/S0140-6736(66)90367-9

Sohail, M. U., Elrayess, M. A., Al Thani, A. A., Al-Asmakh, M., and Yassine, H. M. (2019a). Profiling the Oral microbiome and plasma biochemistry of obese hyperglycemic subjects in Qatar. *Microorganisms* 7:645. doi: 10.3390/microorganisms7120645

Sohail, M. U., Shabbir, M. Z., Steiner, J. M., Ahmad, S., Kamran, Z., Anwar, H., et al. (2017). Molecular analysis of the gut microbiome of diabetic rats supplemented with prebiotic, probiotic, and synbiotic foods. *Int. J. Diabet. Develop. Countries* 37, 419–425. doi: 10.1007/s13410-016-0502-9

Sohail, M. U., Yassine, H. M., Sohail, A., and Al Thani, A. A. (2019b). Impact of physical exercise on gut microbiome, inflammation, and the pathobiology of metabolic disorders. *Rev. Diabet. Stud.* 15, 35–48. doi: 10.1900/RDS.2019.15.35

Sollid, J. U., Furberg, A. S., Hanssen, A. M., and Johannessen, M. (2014). *Staphylococcus aureus*: determinants of human carriage. *Infect. Genet. Evol.* 21, 531–541. doi: 10.1016/j.meegid.2013.03.020

Song, L., Song, M., Rabkin, C. S., Williams, S., Chung, Y., Van Duine, J., et al. (2021). Helicobacter pylori Immunoproteomic profiles in gastric cancer. *J. Proteome Res.* 20, 409–419. doi: 10.1021/acs.jproteome.0c00466

Stacey, H. J., Clements, C. S., Welburn, S. C., and Jones, J. D. (2019). The prevalence of methicillin-resistant *Staphylococcus aureus* among diabetic patients: a meta-analysis. *Acta Diabetol.* 56, 907–921. doi: 10.1007/s00592-019-01301-0

Stentzel, S., Sundaramoorthy, N., Michalik, S., Nordengrün, M., Schulz, S., Kolata, J., et al. (2015). Specific serum IgG at diagnosis of *Staphylococcus aureus* bloodstream invasion is correlated with disease progression. *J. Proteome* 128, 1–7. doi: 10.1016/j.jprot.2015.06.018

Stoeckle, M., Kaech, C., Trampuz, A., and Zimmerli, W. (2008). The role of diabetes mellitus in patients with bloodstream infections. *Swiss Med. Wkly.* 138, 512–519.

Sumera, A., Anuar, N. D., Radhakrishnan, A. K., Ibrahim, H., Rutt, N. H., Ismail, N. H., et al. (2020). A novel method to identify autoantibodies against putative target proteins in serum from beta-thalassemia major: A pilot study. *Biomedicine* 8:97. doi: 10.3390/biomedicines8050097

Surmann, K., Depke, M., Dhople, V. M., Pané-Farré, J., Hildebrandt, P., Gumz, J., et al. (2018). Analysis of *Staphylococcus aureus* proteins secreted inside infected human epithelial cells. *Int. J. Med. Microbiol.* 308, 664–674. doi: 10.1016/j.ijmm.2018.06.002

Tanaka, S., Aida, K., Nishida, Y., and Kobayashi, T. (2013). Pathophysiological mechanisms involving aggressive islet cell destruction in fulminant type 1 diabetes. *Endocr. J.* 60, 837–845. doi: 10.1507/endocrj.EJ13-0222

Tayebi, Z., Fazeli, M., Hashemi, A., Abdi, S., Dadashi, M., Nasiri, M. J., et al. (2021). Molecular characterization of invasive *Staphylococcus aureus* strains isolated from patients with diabetes in Iran: USA300 emerges as the major type. *Infect. Genet. Evol.* 87:104679. doi: 10.1016/j.meegid.2020.104679

Taylor, M. D., and Napolitano, L. M. (2004). Methicillin-resistant *Staphylococcus aureus* infections in vascular surgery: increasing prevalence. *Surg. Infect.* 5, 180–187. doi: 10.1089/sur.2004.5.180

Thaiss, C. A., Levy, M., Grosheva, I., Zheng, D., Soffer, E., Blacher, E., et al. (2018). Hyperglycemia drives intestinal barrier dysfunction and risk for enteric infection. *Science* 359, 1376–1383. doi: 10.1126/science.aar3318

Thammavongsa, V., Kim, H. K., Missiakas, D., and Schneewind, O. (2015). Staphylococcal manipulation of host immune responses. *Nat. Rev. Microbiol.* 13, 529–543. doi: 10.1038/nrmicro3521

Thiede, B., Höhenwarter, W., Krah, A., Mattow, J., Schmid, M., Schmidt, F., et al. (2005). Peptide mass fingerprinting. *Methods* 35, 237–247. doi: 10.1016/j.ymeth.2004.08.015

Thurlow, L. R., Stephens, A. C., Hurley, K. E., and Richardson, A. R. (2020). Lack of nutritional immunity in diabetic skin infections promotes *Staphylococcus aureus* virulence. *Sci. Adv.* 6:eabc5569. doi: 10.1126/sciadv.abc5569

Tran, P., Dong, F., Kin, E., Richardson, K., Tran, L., Waugh, K., et al. (2022). The anti-carbohydrate antibody repertoire in type 1 diabetes. *Res. Sq.* 1–32. [Preprint]. doi: 10.21203/rs.3.rs-1490184/v1

Tuchscherr, L., Korpos, È., Van De Vyver, H., Findeisen, C., Kherkheulidze, S., Siegmund, A., et al. (2018). *Staphylococcus aureus* requires less virulence to establish an infection in diabetic hosts. *Int. J. Med. Microbiol.* 308, 761–769. doi: 10.1016/j.ijmm.2018.05.004

Valtierra-Alvarado, M. A., Castañeda Delgado, J. E., Ramírez-Talavera, S. I., Lugo-Villarino, G., Dueñas-Arteaga, F., Lugo-Sánchez, A., et al. (2020). Type 2 diabetes mellitus metabolic control correlates with the phenotype of human monocytes and monocyte-derived macrophages. *J. Diabetes Complicat.* 34:107708. doi: 10.1016/j.jdiacomp.2020.107708

Valtierra-Alvarado, M. A., Lugo-Villarino, G., Dueñas-Arteaga, F., González-Contreras, B. E., Lugo-Sánchez, A., Castañeda-Delgado, J. E., et al. (2021). Impact of type 2 diabetes on the capacity of human macrophages infected with mycobacterium tuberculosis to modulate monocyte differentiation through a bystander effect. *Immunol. Cell Biol.* 99, 1026–1039. doi: 10.1111/imcb.12497

Vitko, N. P., Grosser, M. R., Khatri, D., Lance, T. R., and Richardson, A. R. (2016). Expanded glucose import capability affords *Staphylococcus aureus* optimized glycolytic flux during infection. *MBio* 7:7. doi: 10.1128/mBio.00296-16

Vu, B. G., Gourronc, F. A., Bernlohr, D. A., Schlievert, P. M., and Klingelhutz, A. J. (2013). Staphylococcal Superantigens stimulate immortalized human adipocytes to produce chemokines. *PLoS One* 8:e77988. doi: 10.1371/journal.pone.0077988

Vu, B. G., Stach, C. S., Kulhankova, K., Salgado-Pabón, W., Klingelhutz, A. J., and Schlievert, P. M. (2015). Chronic superantigen exposure induces systemic inflammation, elevated bloodstream endotoxin, and abnormal glucose tolerance in rabbits: possible role in diabetes. *MBio* 6:e02554. doi: 10.1128/mBio.02554-14

Wajid, B., Sohail, M. U., Ekti, A. R., and Serpedin, E. (2016). The A, C, G, and T of genome assembly. *Biomed. Res. Int.* 2016, 1–10. doi: 10.1155/2016/6329217

Weidenmaier, C. (2018). *Staphylococcus aureus* blocks insulin function. *Nat. Microbiol.* 3, 533–534. doi: 10.1038/s41564-018-0153-3

Wertheim, H. F., Melles, D. C., Vos, M. C., Van Leeuwen, W., Van Belkum, A., Verbrugh, H. A., et al. (2005). The role of nasal carriage in *Staphylococcus aureus* infections. *Lancet Infect. Dis.* 5, 751–762. doi: 10.1016/S1473-3099(05)70295-4

Withatanung, P., Kurian, D., Tangjittipokin, W., Plengvidhya, N., Titball, R. W., Korbsrisate, S., et al. (2019). Quantitative proteomics reveals differences in the response of neutrophils isolated from healthy or diabetic subjects to infection with capsule-variant *Burkholderia thailandensis*. *J. Proteome Res.* 18, 2848–2858. doi: 10.1021/acs.jproteome.9b00166

Woldemariam, H. K., Geleta, D. A., Tulu, K. D., Aber, N. A., Legese, M. H., Fenta, G. M., et al. (2019). Common uropathogens and their antibiotic susceptibility pattern among diabetic patients. *BMC Infect. Dis.* 19:43. doi: 10.1186/s12879-018-3669-5

Yamashiro, S., Kawakami, K., Uezu, K., Kinjo, T., Miyagi, K., Nakamura, K., et al. (2005). Lower expression of Th1-related cytokines and inducible nitric oxide synthase in mice with streptozotocin-induced diabetes mellitus infected with mycobacterium tuberculosis. *Clin. Exp. Immunol.* 139, 57–64. doi: 10.1111/j.1365-2249.2005.02677.x

Yan, X., Song, J.-F., Zhang, L., and Li, X. (2022). Analysis of risk factors for multidrug-resistant organisms in diabetic foot infection. *BMC Endocr. Disord.* 22:46. doi: 10.1186/s12902-022-00957-0

Yang, S., and Rothman, R. E. (2004). PCR-based diagnostics for infectious diseases: uses, limitations, and future applications in acute-care settings. *Lancet Infect. Dis.* 4, 337–348. doi: 10.1016/S1473-3099(04)01044-8

Yao, M.-J., Li, J.-Y., Li, J.-Z., Wu, T.-F., Xu, J.-H., Huang, C.-Z., et al. (2018). Diabetes mellitus increases the risk of enteric infections: A meta-analysis. *Int. J. Clin. Exp. Med.* 11, 5457–5468.

Yu, X., Decker, K. B., Barker, K., Neunuebel, M. R., Saul, J., Graves, M., et al. (2015). Host-pathogen interaction profiling using self-assembling human protein arrays. *J. Proteome Res.* 14, 1920–1936. doi: 10.1021/pr5013015

Yu, X. T., Wang, F., Ding, J. T., Cai, B., Xing, J. J., Guo, G. H., et al. (2022). Tandem mass tag-based serum proteomic profiling revealed diabetic foot ulcer pathogenesis and potential therapeutic targets. *Bioengineered* 13, 3171–3182. doi: 10.1080/21655979.2022.2027173

Zhu, L., She, Z.-G., Cheng, X., Qin, J.-J., Zhang, X.-J., Cai, J., et al. (2020). Association of Blood Glucose Control and Outcomes in patients with COVID-19 and pre-existing type 2 diabetes. *Cell Metab.* 31, 1068–1077.e3. doi: 10.1016/j.cmet.2020.04.021

Zubair, K. U., Shah, A. H., Fawwad, A., Sabir, R., and Butt, A. (2019). Frequency of urinary tract infection and antibiotic sensitivity of uropathogens in patients with diabetes. *Pak. J. Med. Sci.* 35, 1664–1668. doi: 10.12669/pjms.35.6.115

frontiers | Frontiers in Microbiology

TYPE Original Research
PUBLISHED 15 November 2022
DOI 10.3389/fmicb.2022.1042916

OPEN ACCESS

EDITED BY
George William Carnell,
University of Cambridge,
United Kingdom

REVIEWED BY
Sushant Bhat,
The Pirbright Institute, United Kingdom
Ting-Hsuan Chen,
National Tsing Hua University, Taiwan

*CORRESPONDENCE
Mizhou Hui
huimizhou@163.com
Junwei Li
junwli@yeah.net

SPECIALTY SECTION
This article was submitted to Infectious Agents and Disease, a section of the journal Frontiers in Microbiology

RECEIVED 17 September 2022
ACCEPTED 26 October 2022
PUBLISHED 15 November 2022

CITATION
Ren W, Pei S, Jiang W, Zhao M, Jiang L, Liu H, Yi Y, Hui M and Li J (2022) A replication-deficient H9N2 influenza virus carrying H5 hemagglutinin conferred protection against H9N2 and H5N1 influenza viruses in mice. *Front. Microbiol.* 13:1042916. doi: 10.3389/fmicb.2022.1042916

A replication-deficient H9N2 influenza virus carrying H5 hemagglutinin conferred protection against H9N2 and H5N1 influenza viruses in mice

Weigang Ren[1], Shuli Pei[2], Wenming Jiang[3], Meixia Zhao[4], Le Jiang[4], Honggang Liu[4], Yongxiang Yi[5,6], Mizhou Hui[1]* and Junwei Li[5,6]*

[1]School of Life Science, Northeast Agricultural University, Harbin, China, [2]Henan Vocational College of Agriculture, Zhongmu, China, [3]Laboratory of Surveillance for Avian Diseases, China Animal Health and Epidemiology Center, Qingdao, China, [4]College of Veterinary Medicine, Qingdao Agricultural University, Qingdao, China, [5]Department of Infectious Diseases, The Second Hospital of Nanjing, Nanjing University of Chinese Medicine, Nanjing, China, [6]The Clinical Infectious Disease Center of Nanjing, Nanjing, China

H5N1 and H9N2 influenza viruses have been reported to cause human infections and are believed to have pandemic potential. The vaccine is an effective tool to prevent influenza virus infection. However, inactivated influenza vaccines sometimes result in low antigenicity as result leads to generating of incomplete immune protection in the form of low cellular and humoral immunity. While the low temperature adapted, traditional live attenuated influenza vaccine (LAIV) is associated with the potential risk to revert to a virulent phenotype, there appears an essential need for an alternative potent methodology to design and develop influenza vaccines with substantial safety and efficacy which may confer solid protection against H9N2 or H5N1 influenza virus infections. In the present study, a replication-deficient recombinant influenza virus, WM01ma-HA(H5), expressing hemagglutinin (HA) of both H9N2 and H5N1 subtypes was developed. The chimeric gene segment expressing HA(H5), was designed using the sequence of an open reading frame (ORF) of HA adopted from A/wild duck/Hunan/021/2005(H5N1)(HN021ma) which was flanked by the NA packaging signals of mouse-adapted strain A/Mink/Shandong/WM01/2014(H9N2)(WM01ma). Due to the absence of ORF of structural protein NA, the replication of this engineered H9N2 influenza viruses WM01ma-HA(H5) was hampered *in vitro* and *in vivo* but was well competent in MDCK cells stably expressing the NA protein of WM01ma. Intranasal vaccination of mice with WM01ma-HA(H5) stimulated robust immune response without any clinical signs and conferred complete protection from infection by H5N1 or H9N2 subtype influenza viruses.

KEYWORDS

replication-deficient virus vaccine, recombination, influenza A virus, H9N2, H5N1

Introduction

Avian influenza viruses (AIV) target a wide variety of hosts including birds, swine, humans, and several other mammals (Proenca-Modena et al., 2007; Yoon and Webby, 2014). Few years back, H9N2 and H5N1 influenza viruses were the most prevalent subtypes in several provinces of China (Stallknecht and Shane, 1988; Olsen et al., 2006; Tong et al., 2013). Currently, different epidemiological studies indicate that H9N2 AIV(s) is present in various regions of the globe as this strain is being isolated from several animal species including duck, swine, quail, pigeon, and pheasant (Sun and Liu, 2015; Xu et al., 2015). The H5N1 subtype is a highly pathogenic avian influenza (HPAI) virus which is often considered to have pandemic potential owing to its high transmissibility and immune escape (Skeik and Jabr, 2008; Young et al., 2016). Presently, the H5N1 HPAI virus is reported to have been detected in more than 60 countries and its existence blows to the economy and industry linked with poultry (Eagles et al., 2009; Swayne, 2012; Saito et al., 2015). Some research studies suggest that H9N2 AIV(s) may have contributed to the genetic and geographic diversity of H5N1 virus(s) (Monne et al., 2013; Munir et al., 2013). In addition, it is well-studied that the H9N2 virus is competent enough to contribute internal genes to emerging influenza viruses, such as H7N9 and H10N3. This property of sharing the genetic potential facilitates the development of influenza virus vaccine candidates to prevent the possible emerging influenza virus through the reassortment of gene segment exchange (Liu et al., 2013; Wang et al., 2021).

In the current scenario, H9N2 and H5N1 influenza viruses pose a significant threat not only to the poultry industry but also to general public health, owing to the spillover from avian to mammalian species (Peiris et al., 1999; Butt et al., 2005; Ali et al., 2019). Plethora of cases have been reported that people were infected with H9N2 or H5N1 viruses due to direct contact with infected animals (Guan et al., 1999, 2000; Lin et al., 2000; Chen et al., 2009; Guan and Smith, 2013). A comprehensive surveillance study results showed H9N2 seropositivity in a huge number of poultry farm workers because of occupational exposure in China (Li et al., 2007). It is, therefore, obvious that H9 and H5 AIV subtypes pose a potential threat to human public health and place a dire need for designing a methodology to block their spread (Li et al., 2004; Butt et al., 2005; Zhao et al., 2013).

In the initial step of replication of the influenza virus, HA takes lead in performing functions, such as receptor-binding and membrane fusion. Hemagglutinin (HA) is also the predominant inducer of neutralizing antibody production to block virus infection. Apart from the recent technical and technological advancement, it appears that vaccinating poultry birds with inactivated influenza vaccine is still the key strategy to control AIV(s) infections; however, there are certain limitations lying with this strategy as the partial humoral and cellular immune response indicates that inactivated influenza vaccines fail to trigger a vigorous immune response, hence, creating a room for advanced research into a more potent vaccine development is necessary. Live attenuated influenza vaccines (LAIVs) are reported to provide strong long-lasting cell-mediated and potent humoral immunity, nevertheless, the biological safety of LAIV is a major concern for researchers and poultry farmers. The fear of virulence reversal and viral shedding by the LAIV is a key hurdle for the farmers and poultry business community to take risks for a better understanding of vaccine functions (Guo et al., 2014; Li et al., 2014; Zhou et al., 2016).

Research studies with LAIV showed that it conferred heterosubtypic immunity in animal models. Unfortunately, clinical trials have provided evidence that a licensed temperature-sensitive influenza vaccine, FluMist, shed virus postvaccination in children and adults (Straight et al., 2006; Kreijtz et al., 2007; Block et al., 2008; Hammitt et al., 2009). Keeping in view all the above-mentioned facts that there appears a dire need to design and develop novel approaches, are in order to invent safe and potent vaccines that can or may assure and elicit effective, cross-reactive, and confer long-lasting immunity.

The influenza virus genome includes eight segmented RNAs, which facilitate the reassortment and exchange of RNA segments. For the occurrence of an efficient replication, all the eight viral RNA (vRNA) segments must get incorporated into progeny virions. Segment-specific RNA packaging sequences which play a crucial role in successful packaging have been identified on each segment of influenza virus (Fujii et al., 2003; Hutchinson et al., 2010). The 3' and 5' ends of noncoding regions (NCRs) and the 183- and 157-nt of the coding region at the 3' and 5' terminals of the NA vRNA are essential to efficiently encapsulate vRNAs into progeny virions (Fujii et al., 2003). These packaging signals have been used to generate bivalent vaccines, genome-modified LAIVs, and replication-deficient recombinant influenza viruses (Gao et al., 2010; Masic et al., 2013).

In this study, a replication-deficient recombinant H9N2 influenza virus bearing H5 HA coding sequence was generated. Due to the lack of structural protein NA, the recombinant influenza virus is non-replicative both *in vitro* and *in vivo*; however, replicates well on an MDCK cell line stably expressing NA protein. Vaccination with this replication-deficient recombinant H9N2 influenza virus elicited a robust immune response which provided the host with standard protection against both H9N2 and H5N1 subtype viruses, highlighting its potential to serve as a safe bivalent vaccine candidate.

Results

Generation of MDCK stably expressing the NA protein of WM01ma

In the current study, a helper cell line was established to facilitate the package of chimeric recombinant influenza virus virions. Following the standard procedure, the ORF of the NA

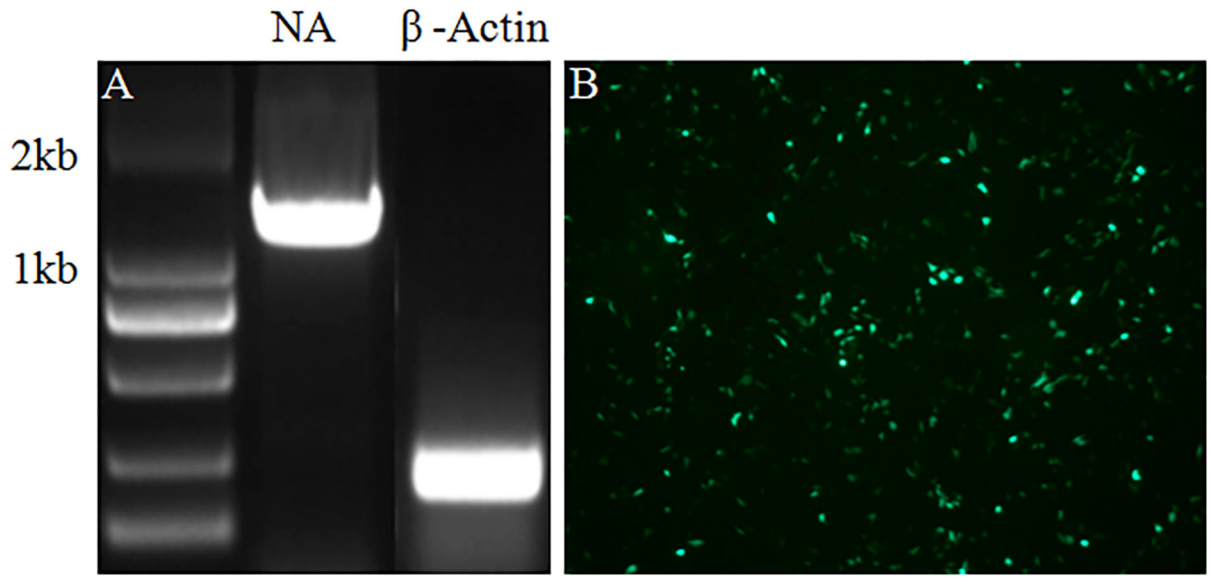

FIGURE 1
RT-PCR and IFA were performed to verify the integration and expression of the NA in MDCK cells stably expressing NA protein. **(A)** The NA gene was amplified by RT-PCR with mRNA of β-Actin as internal control. **(B)** Expression of the NA protein was tested by IFA.

gene was inserted into a G418 selection plasmid, and MDCK cells were transfected with a plasmid carrying the neomycin-resistance gene. Then, the transfected MDCK cells were selected in a medium with 600 μg/ml G418 by the virtue of serial passages. To verify the successful integration of the NA gene into the genome of MDCK cells and its expression, RNA of the MDCK cells showing stable expression of the NA protein was extracted and the NA ORF gene segment was amplified by reverse transcription-polymerase chain reaction (RT-PCR). As indicated in Figure 1A, the NA gene segment was amplified by RT-PCR. The result in Figure 1B indicated that the NA protein was expressed in MDCK cells stably expressing the NA protein tested by immunofluorescence assay (IFA). All-inclusive results showed that MDCK cells stably expressing the NA protein were generated by transfection and serial selection with G418.

Generation of recombinant H9N2 influenza viruses carrying H5 subtype HA

Previous studies indicated a live-attenuated swine influenza vaccine (LASIV) candidate harboring two different HAs of H1 and H3 subtypes was generated by utilizing modified packaging signals of the NA gene segment (Masic et al., 2013; Landreth et al., 2021). Referring to the standard method, a replication-deficient recombinant influenza virus was rescued by using the genetic information of A/wild duck/HN/021/2005(H5N1)(HN021ma) (Li et al., 2009) and A/Mink/SD/WM01/2014(H9N2) (WM01ma) (Ren et al., 2020). Initially, a chimeric influenza HA(H5) gene segment was designed and synthesized flanked with the NA(H9) packaging signals at the 3' and 5' ends (202 nucleotides and 195 nucleotides, respectively) (Figure 2A). In the next step, the chimeric DNA sequence was cloned into pHW2000 (Hoffmann et al., 2000). The translation initial codon and stop codon in the packaging signals of the NA(H9) gene segment were mutated to facilitate the HA(H5) to get translated adequately. Subsequently, the designated plasmid pHW-NAps-HA-NAps along with other seven plasmids (pHW-PB2, pHW-PB1, pHW-PA, pHW-HA, pHW-NP, pHW-M, and pHW-NS) coding gene segments of WM01ma (H9N2) influenza virus were co-transfected into 293T cells and MDCK cells which were stably expressing the H9N2 NA protein. In the final step, the recombinant swap virus was successfully rescued and named WM01ma-HA(H5) virus (Figures 2B,C).

Characterization of the H9N2 influenza virus carrying H5 subtype HA

In the current study, the morphology of the WM01ma H9N2 influenza virus and the rescued WM01ma-HA(H5) was tested by using transmission electron microscopy (TEM). The results indicate that virion particles exhibit homogeneous morphologies of spheres with an average particle size of ~100 nm (Figures 3A,B). The plaque assay was also performed on MDCK cells and MDCK cells stably expressed the H9N2 NA protein. From the results, it is clear that WM01ma-HA (H5)

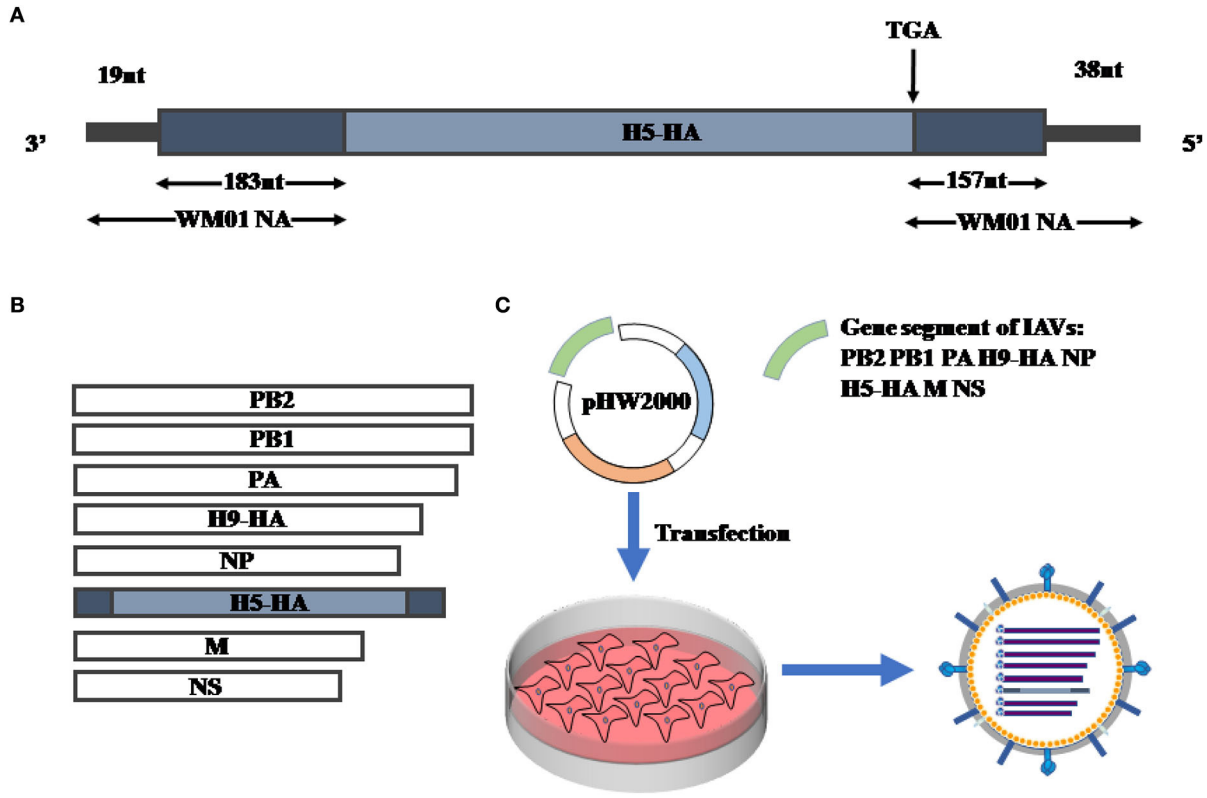

FIGURE 2
Generation of replication-deficient recombinant WM01ma-HA (H5). **(A)** Schematic representation of chimeric HA gene segment. The open reading frame (ORF) of HA (HN01ma, H5N1) is flanked by the NA segment-specific packaging sequences derived from WM01ma (H9N2). **(B)** The eight segments for WM01ma-HA (H5) recombinant viruses. **(C)** Rescue of recombinant WM01ma-HA (H5) influenza virus by the reverse genetic system.

replicated well on MDCK cells stably expressing the H9N2 NA protein but not in normal MDCK cells (Figures 3C,D).

In order to verify that both H9 and H5 HAs are expressed on WM01ma-HA(H5) virus particles, gene segments of H9 and H5 HA were amplified by RT-PCR, and HA proteins were tested by Western blotting. The result evidenced the presence of H9 and H5 HA segments as they were detected in WM01ma-HA(H5) influenza virus (Figure 4A), and H9 and H5 HAs were concurrently presented in WM01ma-HA(H5) (Figure 4B). It was desired to know the discrepancy in the replication abilities of the WM01ma and WM01ma-HA(H5) viruses. A viral replication test was conducted in MDCK cells stably expressing the H9N2 NA protein. The results indicate that the WM01ma-HA(H5) virus exhibited reduced replication kinetics compared with that of the parental virus WM01ma with no significant difference (Figure 5). At 48-h postinfection, WM01ma and recombinant WM01ma-HA(H5) influenza virus attained the highest replication rate.

Safety of the recombinant WM01ma-HA(H5) virus in mice

To confirm the safety of the WM01ma-HA(H5) influenza virus in mice, three groups comprising of 8-week-old female BABL/c mice were inoculated intranasally with 10^3, 10^4, 10^5 × PFU WM01ma-HA(H5) influenza virus, respectively, and one group was set as control. Mice of each group were monitored daily for 15 consecutive days for weight and illness (Figure 6A). As can be observed from the data, the weight of mice evenly increased over time and it indicated there was no adverse effect caused by inoculation with the WM01ma-HA(H5) influenza virus in all groups. The result suggested that the WM01ma-HA(H5) virus produced no harmful effect and stood safe *via* intranasal administration. Histopathological examination suggested that WM01ma-HA(H5) did not cause any pathological changes in lungs of mice (Supplementary Figure S2).

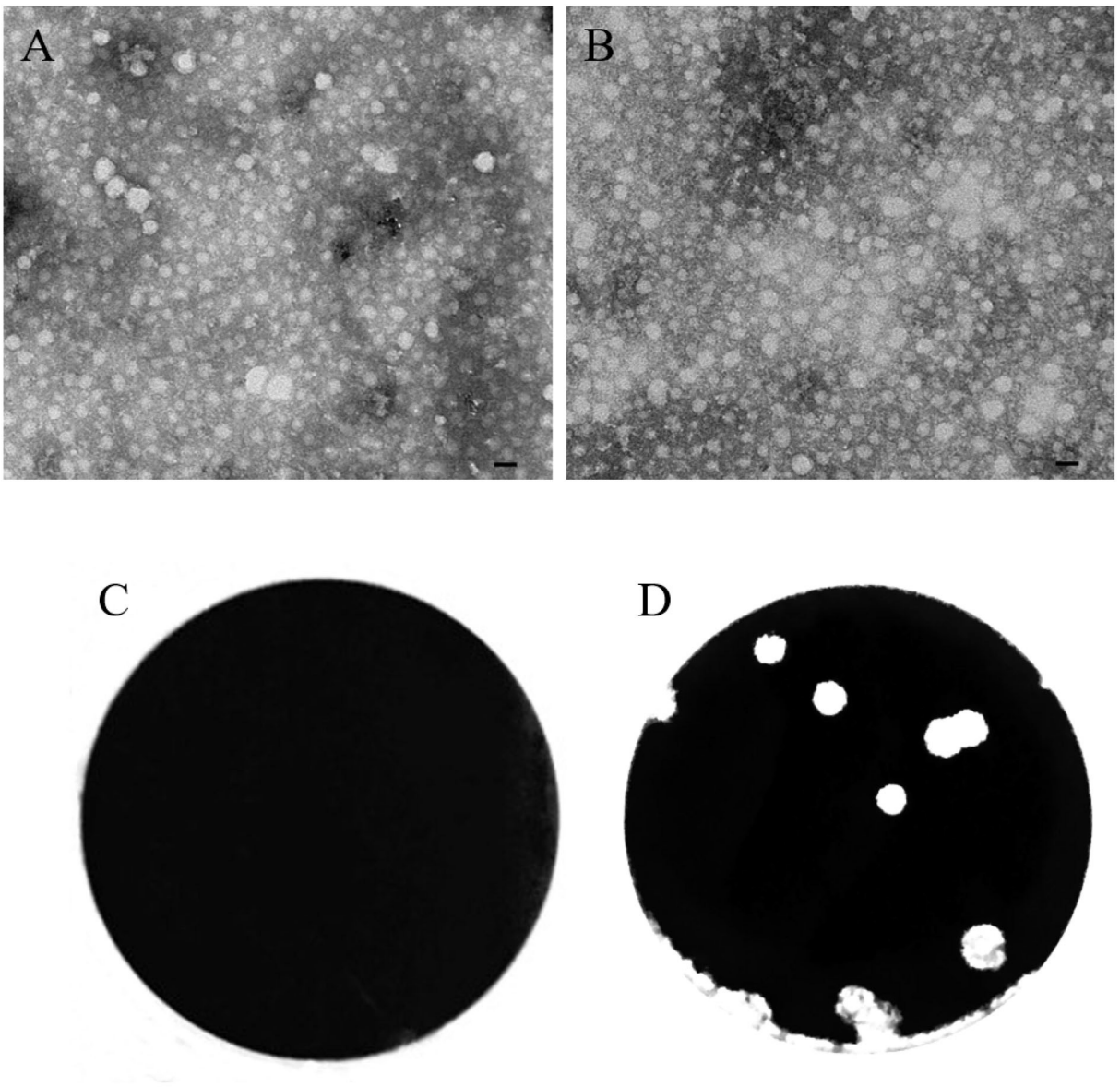

FIGURE 3
Characterization of the recombinant WM01ma-HA (H5) influenza virus. Comparison of the morphologies of WM01ma **(A)** and the recombinant WM01ma-HA (H5) influenza virus **(B)** by scanning electron microscopy (scale bar 100 nm), plaque formed by the recombinant WM01ma-HA (H5) influenza virus on wild-type MDCK cells **(C)** and MDCK cells stably expressing the NA protein **(D)**.

WM01ma-HA(H5) influenza virus induced potent immune response and protection against H9N2 and H5N1 viruses in mice

To test the humoral immune response indicated by HAI titer by the replication-deficient WM01ma-HA(H5) influenza viruses, previously immunized mice were given a booster dose on day 15 with the identical dose of WM01ma-HA(H5) influenza viruses. Mice serum samples were collected on day 29 to determine the titers of HA antibodies against homologous H5N1 (HN021ma) (Figure 6B) and H9N2 (WM01ma) (Figure 6C) viruses. To further validate the humoral immune response contributes to the protection against homologous H5N1 and H9N2 influenza virus infection, antibody microneutralization assays were performed using MDCK cells. The results demonstrated that inoculation with WM01ma-HA(H5) elicits neutralizing serum antibody titers against H5N1(HN021ma) and H9N2 (WM01ma) influenza virus (Supplementary Figure S3). It showed immunization with WM01ma-HA(H5) influenza viruses induced high

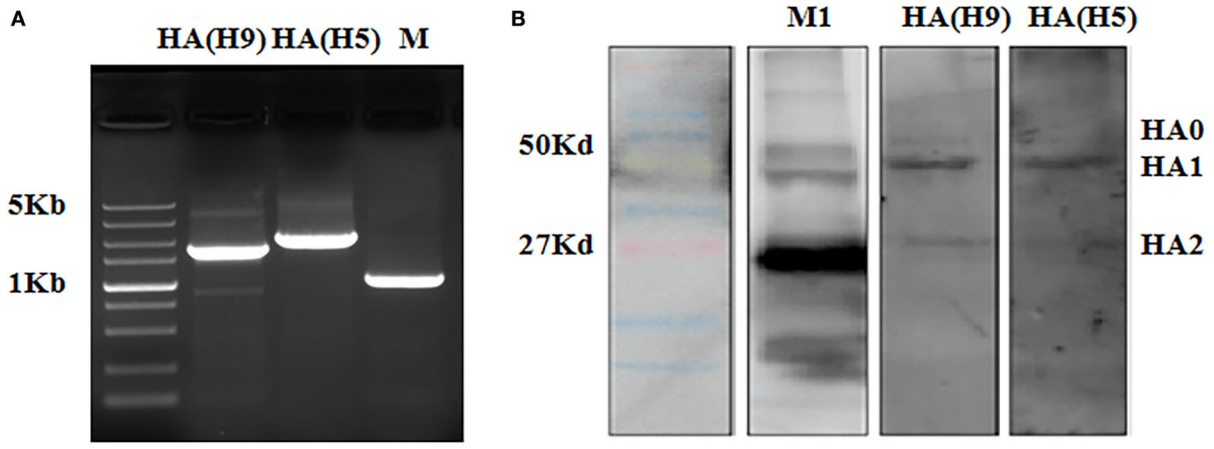

FIGURE 4
HAs of H9 and H5 were verified in the recombinant WM01ma-HA (H5) influenza virus by RT-PCR **(A)** and western blotting **(B)**.

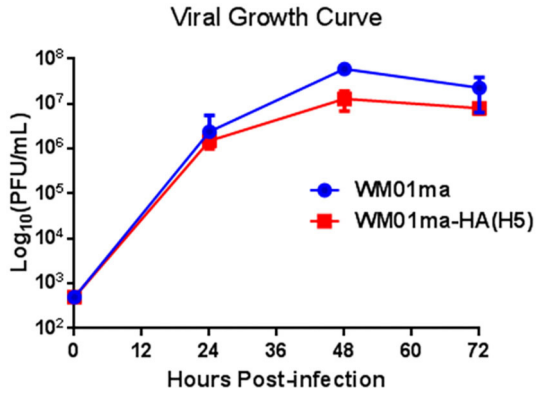

FIGURE 5
Growth curve of the recombinant WM01ma-HA (H5) influenza virus on MDCK cells stably expressing NA protein. The viral titers in each time point were calculated in triplicate. The values represent the means ± standard deviations (SD).

levels of HA antibodies against H9N2 and H5N1 avian influenza viruses.

To determine the associated host immune activation and inflammation during the mouse vaccination with replication-deficient WM01ma-HA(H5) influenza viruses, four groups of 8-week-old female BABL/c mice were inoculated intranasally with PBS or 10^3, 10^4, 10^5 × PFU WM01ma-HA(H5) influenza virus, respectively. Mice serum samples were collected on day 3 for analysis by ELISA assay to determine the cytokine levels. High levels of proinflammatory cytokine were detected in mice inoculated with the WM01ma-HA(H5) influenza virus compared with the PBS control group ($p \leq 0.0001$) (Figure 7A).

Furthermore, we evaluated the antigen-specific IFN-γ and IL-5 secreting cells induced by WM01ma-HA(H5) vaccination. The mouse splenocytes were harvested after the prime (day 15) and the booster (day 29) vaccination from the PBS control group, 10^3, 10^4, 10^5 × PFU WM01ma-HA(H5) vaccinated mice. The amount of secreting cells was measured by both the IFN-γ and IL-5 ELISpot assay. The IFN-γ levels remained low compared with the PBS control group after the first inoculation with WM01ma-HA(H5). However, the booster vaccination with WM01ma-HA(H5) induced a significantly higher number of the IFN-γ secreting cells compared with the mock-vaccinated PBS control group (Figure 7B). Concomitantly, the levels of IL-5 were still significantly increased compared with the PBS group, although not as high as IFN-γ (Figure 7C).

BABL/c mice of each group were inoculated intranasally with different doses of WM01ma-HA(H5) virus and challenged with 10 × MLD_{50} wild-type H9 or H5 subtype virus, respectively. After the mice were challenged, the vaccinated mice groups survived 100% and no weight losses were observed (Figure 8). However, animals of the positive control group challenged with the H9N2 influenza virus were all sacrificed in humanity at day 10 postinfection, and mice in the positive control group challenged with the H5N1 influenza virus died by day 6 because the weight loss is >25%.

Four mice from each group were humanely sacrificed on 4 days postinfection (d.p.i) and the lungs were collected for virus isolation and titration. High virus titers could be detected in all unvaccinated mice (PBS mock-vaccinated) challenged with either WM01ma or HN021ma. No infectious virus could be detected in the lungs of WM01ma, HN021ma, or WM01ma-HA(H5) virus vaccinated mice (Figures 9A,B). It is consistent with survival and weight data. These results suggest that replication-deficient WM01ma-HA(H5) vaccination provides robust protection against the H9 or H5 subtype influenza virus with as low as 100 × PFU immunization.

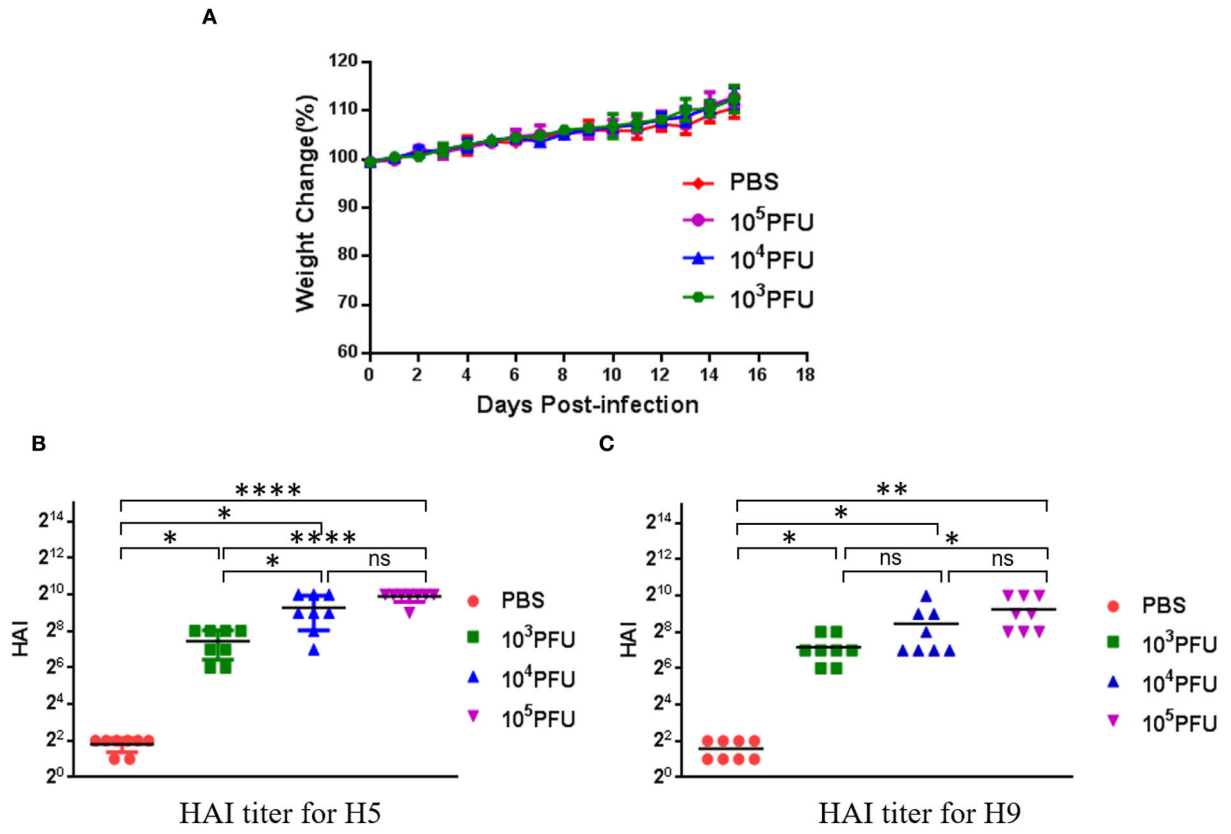

FIGURE 6
Evaluation of safety of the recombinant WM01ma-HA (H5) influenza virus as indicated by weight changes of experimental mice **(A)** and HAI titers against the HN021ma influenza virus **(B)** and the WM01ma influenza virus **(C)**. Each symbol represents an individual mouse, and the horizontal lines indicate mean values. The differences between the two groups were analyzed by a one-way ANOVA with Tukey's multiple-comparison test. ns indicates not significant. ($p > 0.05$), *($p \leq 0.05$), **($p \leq 0.01$), ****($p \leq 0.0001$).

Discussion

The development of an effective vaccine against the avian influenza virus has been a core issue for many researchers in recent years. The scientific community anticipates another influenza pandemic will be devastating. Progress has been made in designing and developing a safe vaccine. However, the chances of viral strain mutation and emergence of the zoonotic, more virulent subtype cannot be excluded. It is very enlightening that no report till now surfaced highlighting human-to-human infection by H9N2 and H5Nx influenza viruses. Nevertheless, the influenza virus subtypes such as H9N2 and H5N1 flush from avian to human worsen the situation. In order to prevent and control the influenza virus led pandemic particularly when it acquires the capability for human-to-human transmission, an urgency appears to design and develop an effective vaccine that may confer solid immunity. In this study, a chimeric H9N2 replication-defective influenza virus was generated by reverse-genetic technology expressing both H9 and H5 HA in the genetic background of the mouse-adapted H9N2 IAV. This chimeric influenza virus is unproductive *in vitro* and *in vivo* unless functional NA is trans-complemented in a permissive cell line. The safety, immunogenicity, and protective efficacy of this replication-deficient recombinant WM01ma-HA(H5) influenza virus were studied and evaluated in mice. The results showed that this engineered virus was safe *in vivo* and capable of inducing a potent immune response against H9 and H5 IAVs.

Several studies reported the development of a trivalent or bivalent vaccine to prevent the infection caused by H9N2 and H5N1 influenza viruses, but these vaccines had certain limitations. Inactivated influenza viral vaccines developed as the result of these studies were applied in several clinical trials and data showed poor performance with salient feature low immunogenicity (Kandeil et al., 2016; Kim et al., 2017; Gomaa et al., 2019). Therefore, the above study was designed to find a way forward.

The research found that the 5' and 3' packaging signals of each vRNA segment of the influenza virus are crucial to assemble a progeny virion with newly synthesized vRNA

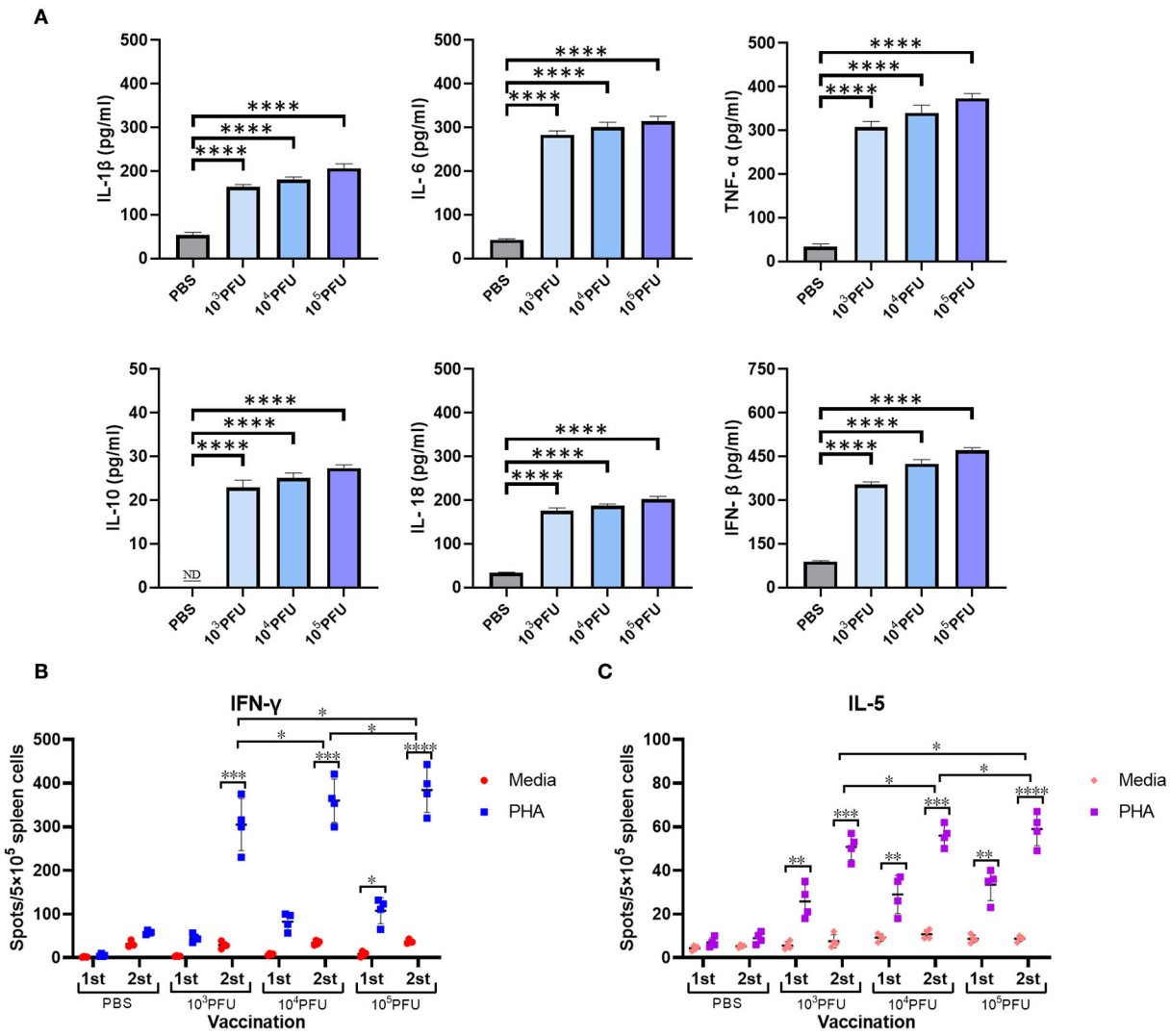

FIGURE 7
Cytokine secretion in intranasally vaccinated mice. Mice serum was collected at 3 days postinfection for analysis by ELISA to determine cytokine levels **(A)**. The number of antigen-specific splenocytes secreting IFN-γ **(B)** or IL-5 **(C)** was determined by ELISpot. ND, nondetected. Each sample was tested in triplicate. The values represent the means ± standard deviations (SD). The dots represent the individual mice. ns indicates not significant. ($p > 0.05$), *($p \leq 0.05$), **($p \leq 0.01$), ***($p \leq 0.001$),****($p \leq 0.0001$).

segments. Previously, one group reported an approach for the generation of a reassortant chimeric replication-defective influenza virus which grew well *in vitro* through the addition of bacterial sialidase and provided protection against H5N1 and H7N9 infection in mice (Tian et al., 2021). Based on this information, it is workable to generate a genome-modified LAIV. Current inactivated influenza vaccines are suboptimal without inducing broad cross-protective activity (Houser and Subbarao, 2015). One of the key advantages of LAIVs over inactivated split or subunit influenza vaccines is their ability to induce both humoral and cellular immunity. Commercial LAIV (FluMist) is based on the cold-adaptation character which allows it to replicate at lower temperatures in the upper respiratory tract. However, replication is attenuated at the higher temperature in the lungs. Live attenuated influenza vaccines (LAIVs) have been shown to induce a significant amount of mucosal IgA but modest levels of serum IgG (Coelingh et al., 2014). The extraordinary potentiality of LAIVs to induce potent mucosal immunity is crucial for limiting virus transmission, especially when applied in response to a pandemic or a severe epidemic. However, this cold-adapted LAIV virus replicates efficiently in the upper respiratory tract of seronegative young children or those who have not been exposed to the previous infection with influenza viruses and shed at a comparatively high titer for a long period of time. Therefore, an improved more effective version of LAIV without suspected

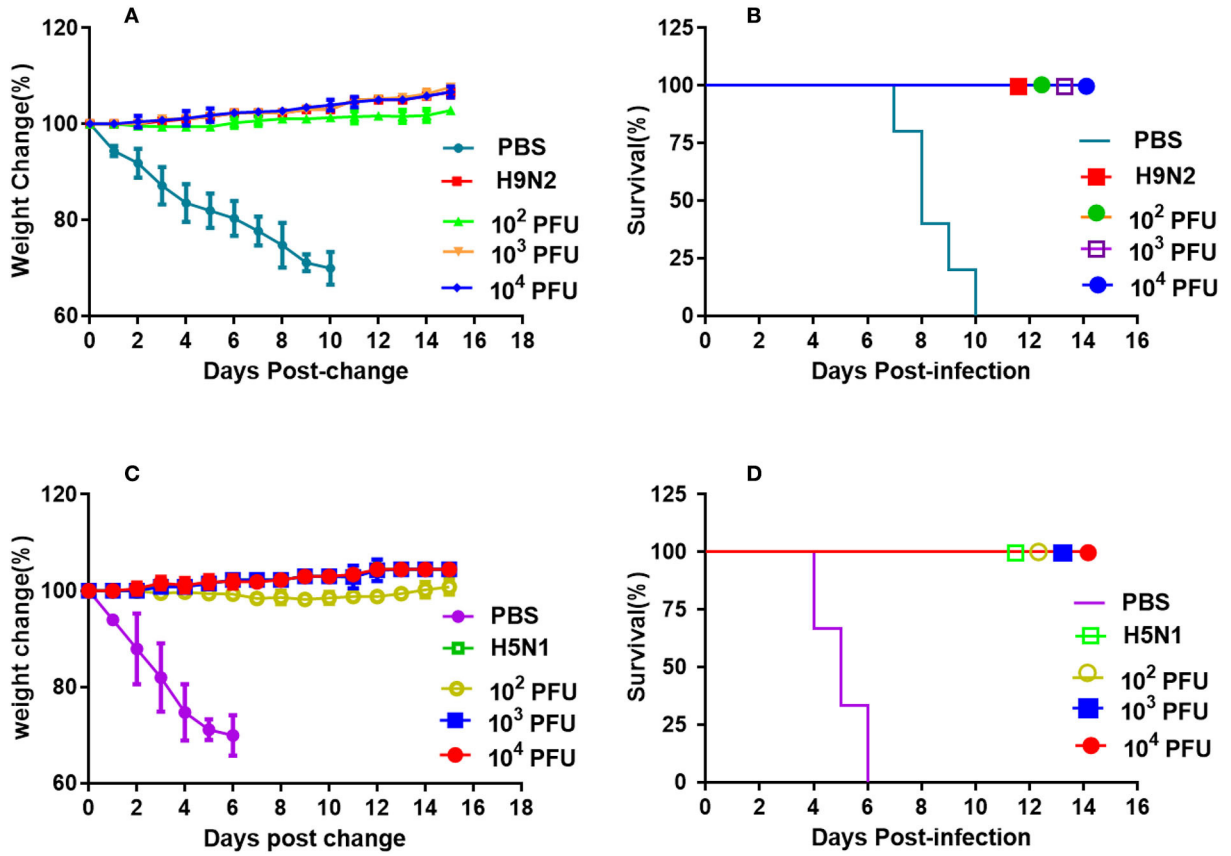

FIGURE 8
Vaccination with the recombinant WM01ma-HA (H5) virus conferred protection against HN021ma and WM01ma. **(A)** weight changes and **(B)** survival rates of mice vaccinated with the recombinant WM01ma-HA (H5) influenza virus and challenged with H9N2 (WM01ma) virus, **(C)** weight changes and **(D)** survival rates of mice vaccinated with the recombinant WM01ma-HA (H5) influenza virus and challenged with H5N1 (HN01ma) virus.

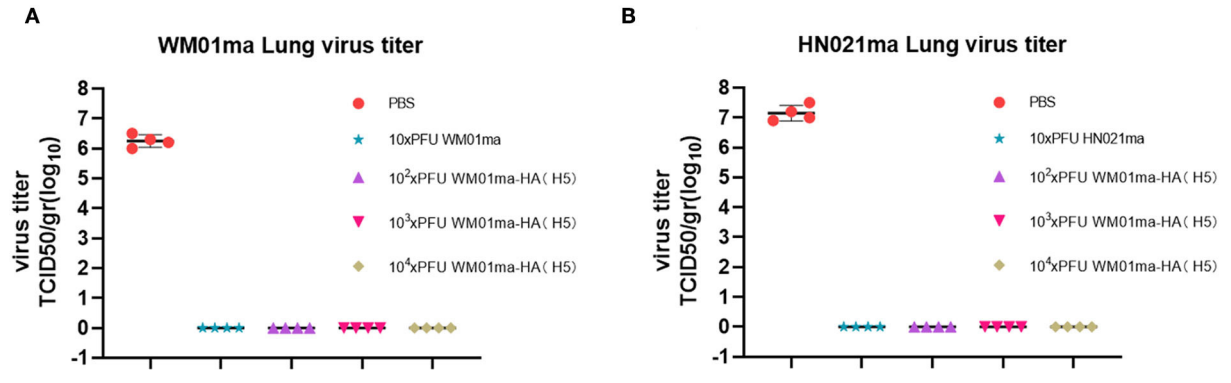

FIGURE 9
The viral titration in the lung tissues of WM01ma **(A)** or HN021ma **(B)** challenged mice at 4 d.p.i. Each experiment was performed in quadruplicate. The dots correspond to the values obtained from the individual mouse values and are represented as the means ± SD.

viral shedding and with extra potent properties inducing a full spectrum of protective immunity in the elderly population is necessary.

We successfully rescued a recombinant virus bearing a chimeric NA-HA(H5) segment in MDCK cells stably expressing the NA protein. The incorporation of the chimeric gene segment

into the virion was confirmed by RT-PCR (Figure 4A) and the expression of the H9 and H5 HA was further confirmed by Western blotting (Figure 4B). *In vitro* study revealed that the safety of the vaccine is based on exogenous NA, as evidenced by the fact that the engineered virus was able to replicate and form visible plaques only in MDCK cells stably expressing the NA protein (Figures 3C,D). The replacement of the NA ORF with the H5 HA ORF resulted in the loss of the natural influenza virus neuraminidase enzymatic activity and reduced the replication potential of the chimeric recombinant virus WM01ma-(H5). One of the main functions of the NA is to help the viral particle to infect the host cell, without the NA activity, progeny virions will be stranded on the cellular membrane, unable to cleave sialic acids, and initiate a new replication cycle. The viral kinetics of the WM01ma-HA(H5) was slightly lower than that of the parental virus WM01ma but without significant differences (Figure 5). These results suggested that the virus could be a promising vaccine candidate with high-yield properties and might be applicable for future influenza vaccine development.

The pathogenicity of the replication-deficient virus WM01ma-(H5) was evaluated in mice. Clinical signs and histopathology results indicated that the replication-deficient virus WM01ma-(H5) was safe *via* intranasal administration (Figure 6A; Supplementary Figure S2). Furthermore, intranasal inoculation with the chimeric virions was able to induce neutralizing antibodies in serum against both the homologous WM01ma (H9N2) virus and HN021ma (H5N1) virus (Figures 6B,C; Supplementary Figure S3), suggesting that the presence of neutralizing antibodies is required to provide immunity against virus infection.

The continuous emergence of human infection with avian influenza A virus poses a persistent threat to human public health, therefore, we generated this replication-defective virus encoding two different subtypes of HA and desired it would alleviate public health stress by potential pandemic caused by H9N2 influenza virus as a vaccine candidate. In this study, a replication-defective influenza virus was generated, which is with certain unproductiveness unless functional NA is trans-complemented in the permissive cell line. This initial study evidences the biological safety and improved immune functionality of LAIVs both *in vitro* and in mice. In the following study, viral shedding and immune response after immunizations will be examined in mice and ferrets. Hopefully, it will serve as an effective vaccine candidate for the possible pandemic caused by the H9N2 or H5N1 influenza virus in humans.

Materials and methods

Cells and viruses

Madin–Darby canine kidney (MDCK) cells were maintained in Eagle's minimal essential medium (MEM) containing 10% fetal bovine serum (FBS; Biological Industries) and 1% Penicillin–Streptomycin Solution (PS; Biological Industries). Mouse-adapted A/Mink/Shandong/WM01/2014(H9N2)(WM01ma) and mouse-adapted A/wild duck/Hunan/021/2005 (H5N1)(HN021ma) were propagated at 37°C in the allantoic cavities of 9-day-old specific-pathogen-free (SPF) embryonated chicken eggs.

Construction of the expression plasmid pd2-NA

The plasmid pd2EGFP-N1 and NA (WM01ma) coding DNA segments were enzymatically dissolved with restriction enzyme NheI and NotI, respectively, then the purified NA segment was inserted into the pd2EGFP-N1 vector. The linked product was transformed into *E.coli* DH5α competent cells and the target clones carrying designated plasmid pd2-NA were screened on the solid LB plates containing 50 μg/ml Kanamycin for 14 h at 37°C. The target plasmid pd2-NA was extracted and stored for further use.

Establishment and verification of the MDCK stably expressing NA protein

3 × 105 MDCK cells were seeded in 35-mm dishes with MEM medium containing 10% fetal bovine serum (FBS) and 1% Penicillin–Streptomycin Solution (PS). On the following day, MDCK cells were electroporated with the pd2-NA following the protocol of the Nucleofector Kit for MDCK cells (Lonza, Cologne, Germany) (Wen et al., 2015). Briefly, MDCK cells were resuspended in a 0.1 ml solution I, and 5 μg plasmid pd2-NA was added into Solution I and mixed with MDCK cells. Then, the cell-plasmid mixture was transferred to an electroporation cuvette and treated on the Amaxa Nucleofector II machine (Lonza, Cologne, Germany) by using the A24 program. After being electroporated, cells were transferred to 6-well plates containing DMEM with 10% FBS. At 48-h post transmission, the cell monolayer was trypsinized, diluted 1:100, and seeded into 24-well plates containing DMEM with 5% FBS and the final concentration was 600 μg/ml G418. The medium was replaced every 3 days and cultured for 2 weeks. Surviving cell colonies were transferred to a 25 mm^2 flask and continued to be cultured in the presence of G418. Finally, cells were scaled up and cultured for at least 10 passages to generate MDCK cells stably expressing the NA protein.

To verify the stable expression of the NA gene in MDCK-NA stable cells, RT-PCR and immunofluorescence assay (IFA) were performed. RNA of 5 × 10^6 MDCK-NA cells was extracted with RNAiso Plus Reagent (Takara, Dalian, China) and was reverse transcribed with a PrimeScript^{TM}II 1st Strand DNA

Synthesis Kit (Takara, Dalian, China). The PCR product was separated on 1% agarose gel and data in the form of snaps were taken on Gel Doc Efficient Zeitgeist (Bio-Rad, Hercules, CA). The MDCK cells expressing the H9N2 NA protein were seeded in a 6-well plate fixed in 4% paraformaldehyde for 1 h, then permeabilized in PBS with 0.1% Triton X-100 for 30 min, and the cell samples were blocked in PBS containing 1% BSA for 1 h at room temperature. In the next step, the MDCK cells were incubated with H9N2 NA antibody at 4°C overnight. After three washes with PBST, the transfected MDCK cells were incubated with a secondary antibody (Goat anti-mouse IgG FITC antibody, BI). Finally, MDCK cells were observed and images were taken under a fluorescence microscope (ZEISS, AxioVert.A1).

Construction of pHW-NAps-HA-NAps

The designated sequence NAps-HA-NAps contains the ORF of H5N1 HA flanked by the NA (H9N2) segment-specific packing signals at the 3' and 5' ends (202 nucleotides and 195 nucleotides, respectively) and was synthesized by GenScript. The translation initial codon and stop codon in the packaging signals of the NA (H9N2) gene segment were altered, then, the NAps-HA-NAps gene was amplified by PCR and cloned to vector pHW2000 (Hoffmann et al., 2001).

Rescue of recombinant WM01ma-HA(H5) influenza virus

The recombinant virus was rescued with a standard reverse genetics method using the eight bidirectional plasmids system (Hoffmann et al., 2000). 3.5×10^5 293T cells and 3.5×10^5 MDCK cells stably expressing NA protein were co-seeded in each well of a 6-well plate cultured in MEM medium supplemented with 10% FBS and 1% PS. On the following day, the medium was replaced by Opti-MEM (Gibco). The cells were co-transfected with eight plasmids including pHW-PB2, pHW-PB1, pHW-PA, pHW-HA, pHW-NP, pHW-M, pHW-NS, and pHW-NAps-HA-NAps mixing with Lipofectamine 2000 (Invitrogen). At 6-h post-transfection, the medium was replaced with 2 ml of fresh Opti-MEM. At 12-h post-transfection, TPCK-trypsin was added at the final concentration of 1 μg/ml into the medium. Supernatants containing WM01ma-HA(H5) influenza virus were harvested for 72 h after transfection. Then, the virus was propagated on MDCK cells stably expressing the NA protein for further use.

Transmission electron microscopy

Recombinant WM01ma-HA(H5) virus was ultracentrifuged at 36,000 rotations per minute (rpm) for 2 h in a 20% glucose gradient. The pellet was then re-suspended in 30 μl PBS. The samples were adsorbed onto freshly glow discharged carbon-stabilized Parlodion-coated 400-mesh copper grids. The grids were then rinsed with buffer containing 20 mM Tris (pH 7.4) and 120 mM KCl, negatively stained with 1% phosphotungstic acid (pH 7.2), and then dried by blotting onto filter paper. Virions were visualized on a Hitachi H7600 transmission electron microscope (Hitachi High Technologies, USA, Schaumburg, IL) operating at 80 kV and digitally captured with a charge-coupled device (CCD) camera at 5-megapixel resolution (Core facility of Qingdao Agricultural University).

Western blot

Recombinant WM01ma-HA(H5) virus was ultracentrifuged at 36,000 rpm for 2 h in a 20% glucose gradient. The pellet was re-suspended in 30 μl RIPA buffer and given an overnight incubation on ice. Lysed virus samples were loaded and separated on 10% SDS-PAGE, then transferred onto nitrocellulose membrane using a semi-dry trans-blot apparatus (Bio-Rad, Hercules, CA). The membranes were blocked in PBS with 1% Tween (PBST) and 5% non-fat milk for 1 h with anti-M1 monoclonal antibody (Abcam, catalog# ab25919), anti-HA(H9), or anti-HA(H5) multiclonal antibody (prepared and reserved in our lab) at 4°C overnight. After washing with PBST, the membranes were incubated with horseradish peroxidase (HRP)-conjugated goat anti-mouse IgG antibody (Abcam) at room temperature for 1 h. After being washed, the membranes were developed with chemiluminescent HRP substrate before imaging. Finally, the membranes were scanned in FUSION FX7(VILBER, French).

Growth kinetics

Madin–Darby canine kidney (MDCK) cells stably expressing the NA protein were seeded in wells of 6-well plate. The confluent cell monolayer was infected with viruses in the multiplicity of infection (MOI) of 0.001. After 1 h of adsorption, the viral supernatant was removed, and the cells were washed two times with phosphate-buffered saline (PBS) and incubated in MEM containing 1 μg/ml TPCK-treated trypsin at 37°C. Supernatants were collected at indicated time points, and titers were determined by standard plaque assay in triplicate.

Safety test, hemagglutination inhibition, and microneutralization assay in mice

Six–eight-week-old BALB/c mice were divided randomly into four groups with eight mice in each group. The virus was

serially diluted in DPBS, and 50 μl was intranasally inoculated into mice anesthetized by isoflurane. After being challenged, mice were monitored for 15 days for clinical symptoms, weight loss, and death. At 15-day postinfection, the same doses were boosted. At 29-day postinfection, blood samples were collected for the HAI test.

Mouse sera were treated with a receptor-destroying enzyme to inactivate non-specific inhibitors (Denka Seiken Co. LTD.). Briefly, serum samples were 2-fold serially diluted in PBS in a 25 μl volume in 96-well V-shape microtiter plate, then an equal volume of 4-uint virus in 25 μl was added into each well. The plate was incubated at 37°C for 30 min. Subsequently, 25 μl of 0.8% (v/v) chicken red blood cell suspension was added to each well. The HAI titer was determined by the reciprocal dilution of the last well that contained non-agglutinated chicken red blood cells.

Neutralization antibody titers in inoculated mouse sera, reactive with HN021ma (H5N1) and WM01ma (H9N2) influenza viruses were detected in triplicate using a microneutralization assay, as described previously (Grund et al., 2011).

For histopathologic examination, mice were anesthetized with isoflurane and inoculation intranasally with PBS or 10^5 × PFU WM01ma-HA(H5). Four days after inoculation, treated animals were sacrificed and the lungs were collected and fixed in 10% buffered formalin, processed, and stained with hematoxylin and eosin (H&E).

Cytokine levels assay

For this study, 6–8-week-old BALB/c mice were divided randomly into four groups with eight mice in each group. The virus was serially diluted in DPBS, and 50 μl was intranasally inoculated into mice anesthetized by isoflurane. At 15-day postinfection, the same doses were boosted. At 3-day postinfection, serum samples were collected for cytokine levels test. Meanwhile, the mouse spleens were harvested after the prime (day 15) and the booster (day 29) vaccination, and IFN-γ and IL-5 secreting cells were measured by the ELISpot assay.

Cytokine levels of IL-1β, IL-6, TNF-α, IL-10, IL-18, and IFN-β in the peripheral blood for each mouse were determined by enzyme-linked immunosorbent assay (ELISA) kits according to the manufacturer's instructions (Invitrogen, USA; R&D Systems, Minneapolis, USA). The plates were read at 450 nm in the PowerWaveXS2 (BioTek, Instruments, India).

MultiScreen Filter Plates (Millipore, cat# MAIPS4510) were coated with either purified rat anti-mouse IFN-γ monoclonal antibody (BD Bioscience, cat# 551216) or purified rat anti-mouse IL-5 monoclonal antibody (BD Bioscience, cat# 554393) in coating buffer at a concentration of 5 μg/ml at 4°C overnight. Splenocyte cells were isolated from mice. After being washed, 5×10^5 cells were seeded in each well, followed by stimulation with 10 μg/ml of either PHA or media at 37°C in 5% CO2 overnight. After stimulation of cells were washed five times with PBS containing 0.05% Tween 20 (PBST) and incubated with biotin-conjugated rat anti-mouse IFN-γ antibody or IL-5 antibody (2.0 μg/ml) at room temperature for 2 h. The plates were washed and incubated with horseradish peroxidase (HRP) conjugated streptavidin (BD Bioscience, cat# 555214) at room temperature for 1.5 h, washed with PBS, and then HRP substrate was added. Subsequently, the plates were kept at room temperature for 10 min in the dark, and the substrate was removed. After being washed with double-distilled water, the plates were dried overnight. Finally, spots were counted under the ELISpot reader (AID, Germany).

Animal challenge experiments

Six–eight-week-old female BABL/c mice were assigned to five groups and 12 mice were assigned to each group. Mice in group 1 were set as positive control inoculated with PBS. Mice in group 2 as negative control were intranasally inoculated with 10 × PFU WM01ma, and groups 3–5 were intranasally inoculated with 10^2, 10^3, 10^4 × PFU recombinant WM01ma-HA(H5) virus, respectively. On day 15 post-immunization, mice were infected with 10 × MLD_{50} WM01ma and monitored for 15 consecutive days for weight and clinical symptoms. Another set experiment was performed, the negative control was intranasally inoculated with 10 × PFU HN021ma, and mice were infected with 10 × MLD_{50} HN021ma on post-immunization day 15.

Four mice from each group were humanely sacrificed on 4 days postinfection (d.p.i) and their lung tissues were collected, weighed, and homogenized in 1 ml of cold PBS under sterile conditions, centrifuged at 12,000 rpm for 10 min at 4°C. Virus titers in the homogenized supernatant were measured by the 50% tissue culture infectious dose ($TCID_{50}$) assay on MDCK cells. Madin–Darby canine kidney (MDCK) cells were seeded in 96-well plates at a density of 1.0×10^4 cells/well and incubated at 37°C overnight. The homogenized supernatants were diluted 10 × fold serially. The MDCK cells were inoculated with a 100 μl diluted supernatant sample. After 3 days of incubation at 37°C, the $TCID_{50}$ was determined using the Reed and Muench method.

Statistical analysis

Comparisons between groups were performed by using a nonparametric one-way ANOVA with Tukey's multiple comparison test and Fisher's exact test, and survival rates were analyzed using the log-rank test. The analyses were performed using GraphPad Prism version 6.0 for Windows (GraphPad Software). *P*-values < 0.05 were considered to be significant.

Data availability statement

The original contributions presented in the study are included in the article/Supplementary material, further inquiries can be directed to the corresponding author/s.

Ethics statement

The animal study was reviewed and approved by the Institutional Animal Care and Use Committee at Qingdao Agricultural University (approval reference number # 20190020).

Author contributions

WR, SP, and MZ conducted all experiments. LJ and HL collected samples. WJ and JL wrote the manuscript. YY and MH revised the manuscript. All authors have read and agreed to the published version of the manuscript.

Funding

This study was supported by the National Natural Science Foundation of China (General Program, 32072837), Nanjing Important Science and Technology Specific Projects (2021-11005), Key Research and Development Program of the Department of Health of Jiangsu (ZDB2020036), and Key R&D Program of Jiangsu Province (Social Development) (BE2021603).

Conflict of interest

The authors declare that the research was conducted in the absence of any commercial or financial relationships that could be construed as a potential conflict of interest.

Publisher's note

All claims expressed in this article are solely those of the authors and do not necessarily represent those of their affiliated organizations, or those of the publisher, the editors and the reviewers. Any product that may be evaluated in this article, or claim that may be made by its manufacturer, is not guaranteed or endorsed by the publisher.

Supplementary material

The Supplementary Material for this article can be found online at: https://www.frontiersin.org/articles/10.3389/fmicb.2022.1042916/full#supplementary-material

References

Ali, M., Yaqub, T., Mukhtar, N., Imran, M., Ghafoor, A., Shahid, M. F., et al. (2019). Avian Influenza A(H9N2) Virus in Poultry Worker, Pakistan, 2015. *Emerg. Infect. Dis.* 25, 136–139. doi: 10.3201/eid2501.180618

Block, S. L., Yogev, R., Hayden, F. G., Ambrose, C. S., Zeng, W., and Walker, R. E. (2008). Shedding and immunogenicity of live attenuated influenza vaccine virus in subjects 5-49 years of age. *Vaccine* 26, 4940–4946. doi: 10.1016/j.vaccine.2008.07.013

Butt, K. M., Smith, G. J., Chen, H., Zhang, L. J., Leung, Y. H., Xu, K. M., et al. (2005). Human infection with an avian H9N2 influenza A virus in Hong Kong in 2003. *J Clin Microbiol.* 43, 5760–5767. doi: 10.1128/JCM.43.11.5760-5767.2005

Chen, J., Fang, F., Yang, Z., Liu, X., Zhang, H., Zhang, Z., et al. (2009). Characterization of highly pathogenic H5N1 avian influenza viruses isolated from poultry markets in central China. *Virus Res.* 146, 19–28. doi: 10.1016/j.virusres.2009.08.010

Coelingh, K. L., Luke, C. J., Jin, H., and Talaat, K. R. (2014). Development of live attenuated influenza vaccines against pandemic influenza strains. *Exp. Rev. Vacc.* 13, 855–871. doi: 10.1586/14760584.2014.922417

Eagles, D., Siregar, E. S., Dung, D. H., Weaver, J., Wong, F., and Daniels, P. (2009). H5N1 highly pathogenic avian influenza in Southeast Asia. *Rev. Sci. Tech.* 28, 341–348. doi: 10.20506/rst.28.1.1864

Fujii, Y., Goto, H., Watanabe, T., Yoshida, T., and Kawaoka, Y. (2003). Selective incorporation of influenza virus RNA segments into virions. *Proc. Natl. Acad. Sci. U. S. A.* 100, 2002–2007. doi: 10.1073/pnas.0437772100

Gao, Q., Lowen, A. C., Wang, T. T., and Palese, P. (2010). A nine-segment influenza a virus carrying subtype H1 and H3 hemagglutinins. *J. Virol.* 84, 8062–8071. doi: 10.1128/JVI.00722-10

Gomaa, M. R., Khalil, A. A., Kandeil, A., Sabir, J. S. M., Kayed, A., Moatasim, Y., et al. (2019). Development of an effective contemporary trivalent avian influenza vaccine against circulating H5N1, H5N8, and H9N2 in Egypt. *Poult. Sci.* 98, 6289–6295. doi: 10.3382/ps/pez385

Grund, S., Adams, O., Wählisch, S., and Schweiger, B. (2011). Comparison of hemagglutination inhibition assay, an ELISA-base micro-neutralization assay and colorimetric microneutralization assay to detect antibody responses to vaccination against influenza A H1N1 2009 virus. *J. Virol. Methods* 171, 369–373. doi: 10.1016/j.jviromet.2010.11.024

Guan, Y., Shortridge, K. F., Krauss, S., Chin, P. S., Dyrting, K. C., Ellis, T. M., et al. (2000). H9N2 influenza viruses possessing H5N1-like internal genomes continue to circulate in poultry in southeastern China. *J. Virol.* 74, 9372–9380. doi: 10.1128/JVI.74.20.9372-9380.2000

Guan, Y., Shortridge, K. F., Krauss, S., and Webster, R. G. (1999). Molecular characterization of H9N2 influenza viruses: were they the donors of the "internal" genes of H5N1 viruses in Hong Kong? *Proc. Natl. Acad. Sci. U. S. A.* 96, 9363–9367. doi: 10.1073/pnas.96.16.9363

Guan, Y., and Smith, G. J. (2013). The emergence and diversification of panzootic H5N1 influenza viruses. *Virus Res.* 178, 35–43. doi: 10.1016/j.virusres.2013.05.012

Guo, H., Baker, S. F., Martinez-Sobrido, L., and Topham, D. J. (2014). Induction of CD8 T cell heterologous protection by a single dose of single-cycle infectious influenza virus. *J. Virol.* 88, 12006–12016. doi: 10.1128/JVI.01847-14

Hammitt, L. L., Bartlett, J. P., Li, S., Rahkola, J., Lang, N., Janoff, E. N., et al. (2009). Kinetics of viral shedding and immune responses in adults following administration of cold-adapted influenza vaccine. *Vaccine* 27, 7359–7366. doi: 10.1016/j.vaccine.2009.09.041

Hoffmann, E., Neumann, G., Kawaoka, Y., Hobom, G., and Webster, R. G. (2000). A DNA transfection system for generation of influenza A virus from eight plasmids. *Proc. Natl. Acad. Sci. U. S. A.* 97, 6108–6113. doi: 10.1073/pnas.100133697

Hoffmann, E., Stech, J., Guan, Y., Webster, R. G., and Perez, D. R. (2001). Universal primer set for the full-length amplification of all influenza A viruses. *Arch. Virol.* 146, 2275–2289. doi: 10.1007/s007050170002

Houser, K., and Subbarao, K. (2015). Influenza vaccines: challenges and solutions. *Cell Host Microbe* 17, 295–300. doi: 10.1016/j.chom.2015.02.012

Hutchinson, E. C., Von Kirchbach, J. C., Gog, J. R., and Digard, P. (2010). Genome packaging in influenza A virus. *J. Gen. Virol.* 91, 313–328. doi: 10.1099/vir.0.017608-0

Kandeil, A., Moatasim, Y., Gomaa, M. R., Shehata, M. M., El-Shesheny, R., Barakat, A., et al. (2016). Generation of a reassortant avian influenza virus H5N2 vaccine strain capable of protecting chickens against infection with Egyptian H5N1 and H9N2 viruses. *Vaccine* 34, 218–224. doi: 10.1016/j.vaccine.2015.11.037

Kim, S. M., Kim, Y. I., Park, S. J., Kim, E. H., Kwon, H. I., Si, Y. J., et al. (2017). Vaccine efficacy of inactivated, chimeric hemagglutinin H9/H5N2 avian influenza virus and its suitability for the marker vaccine strategy. *J. Virol.* 91, 1963–1916 doi: 10.1128/JVI.01693-16

Kreijtz, J. H., Bodewes, R., Van Amerongen, G., Kuiken, T., Fouchier, R. A., and Osterhaus, A. D. (2007). Primary influenza A virus infection induces cross-protective immunity against a lethal infection with a heterosubtypic virus strain in mice. *Vaccine* 25, 612–620. doi: 10.1016/j.vaccine.2006.08.036

Landreth, S., Detmer, S., Gerdts, V., and Zhou, Y. (2021). A bivalent live attenuated influenza virus vaccine protects against H1N2 and H3N2 viral infection in swine. *Vet. Microbiol.* 253, 108968–108962. doi: 10.1016/j.vetmic.2020.108968

Li, J., Arevalo, M. T., Chen, Y., Chen, S., and Zeng, M. (2014). T-cell-mediated cross-strain protective immunity elicited by prime-boost vaccination with a live attenuated influenza vaccine. *Int. J. Infect. Dis.* 27, 37–43. doi: 10.1016/j.ijid.2014.05.016

Li, J., Ishaq, M., Prudence, M., Xi, X., Hu, T., Liu, Q., et al. (2009). Single mutation at the amino acid position 627 of PB2 that leads to increased virulence of an H5N1 avian influenza virus during adaptation in mice can be compensated by multiple mutations at other sites of PB2. *Virus Res.* 144, 123–129. doi: 10.1016/j.virusres.2009.04.008

Li, K. S., Guan, Y., Wang, J., Smith, G. J., Xu, K. M., Duan, L., et al. (2004). Genesis of a highly pathogenic and potentially pandemic H5N1 influenza virus in eastern Asia. *Nature* 430, 209–213. doi: 10.1038/nature02746

Li, X., Tian, B., Zhou, J., Chen, Y., Li, X., Zhu, W., et al. (2007). A comprehensive retrospective study of the seroprevalence of H9N2 avian influenza viruses in occupationally exposed populations in China. *PLoS ONE.* 12:e0178328. doi: 10.1371/journal.pone.0178328

Lin, Y. P., Shaw, M., Gregory, V., Cameron, K., Lim, W., Klimov, A., et al. (2000). Avian-to-human transmission of H9N2 subtype influenza A viruses: relationship between H9N2 and H5N1 human isolates. *Proc. Natl. Acad. Sci. U. S. A.* 97, 9654–9658. doi: 10.1073/pnas.160270697

Liu, D., Shi, W., Shi, Y., Wang, D., Xiao, H., Li, W., et al. (2013). Origin and diversity of novel avian influenza A H7N9 viruses causing human infection: phylogenetic, structural, and coalescent analyses. *Lancet* 381, 1926–1932. doi: 10.1016/S0140-6736(13)60938-1

Masic, A., Pyo, H. M., Babiuk, S., and Zhou, Y. (2013). An eight-segment swine influenza virus harboring H1 and H3 hemagglutinins is attenuated and protective against H1N1 and H3N2 subtypes in pigs. *J. Virol.* 87, 10114–10125. doi: 10.1128/JVI.01348-13

Monne, I., Yamage, M., Dauphin, G., Claes, F., Ahmed, G., Giasuddin, M., et al. (2013). Reassortant avian influenza A(H5N1) viruses with H9N2-PB1 gene in poultry, Bangladesh. *Emerg. Infect. Dis.* 19, 1630–1634. doi: 10.3201/eid1910.130534

Munir, M., Zohari, S., Iqbal, M., Abbas, M., Perez, D. R., and Berg, M. (2013). The non-structural (NS) gene segment of H9N2 influenza virus isolated from backyard poultry in Pakistan reveals strong genetic and functional similarities to the NS gene of highly pathogenic H5N1. *Virulence* 4, 612–623. doi: 10.4161/viru.26055

Olsen, B., Munster, V. J., Wallensten, A., Waldenstrom, J., Osterhaus, A. D., and Fouchier, R. A. (2006). Global patterns of influenza a virus in wild birds. *Science* 312, 384–388. doi: 10.1126/science.1122438

Peiris, M., Yuen, K. Y., Leung, C. W., Chan, K. H., Ip, P. L., Lai, R. W., et al. (1999). Human infection with influenza H9N2. *Lancet* 354, 916–917. doi: 10.1016/S0140-6736(99)03311-5

Proenca-Modena, J. L., Macedo, I. S., and Arruda, E. (2007). H5N1 avian influenza virus: an overview. *Braz. J. Infect. Dis.* 11, 125–133. doi: 10.1590/S1413-86702007000100027

Ren, W., Zhang, C. H., Li, G., Liu, G., Shan, H., and Li, J. (2020). Two genetically similar H9N2 influenza viruses isolated from different species show similar virulence in minks but different virulence in mice. *Acta Virol.* 64, 67–77. doi: 10.4149/av_2020_109

Saito, T., Tanikawa, T., Uchida, Y., Takemae, N., Kanehira, K., and Tsunekuni, R. (2015). Intracontinental and intercontinental dissemination of Asian H5 highly pathogenic avian influenza virus (clade 2.3.4.4) in the winter of 2014-2015. *Rev. Med. Virol.* 25, 388–405. doi: 10.1002/rmv.1857

Skeik, N., and Jabr, F. I. (2008). Influenza viruses and the evolution of avian influenza virus H5N1. *Int. J. Infect. Dis.* 12, 233–238. doi: 10.1016/j.ijid.2007.07.002

Stallknecht, D. E., and Shane, S. M. (1988). Host range of avian influenza virus in free-living birds. *Vet. Res. Commun.* 12, 125–141. doi: 10.1007/BF00362792

Straight, T. M., Ottolini, M. G., Prince, G. A., and Eichelberger, M. C. (2006). Evidence of a cross-protective immune response to influenza A in the cotton rat model. *Vaccine* 24, 6264–6271. doi: 10.1016/j.vaccine.2006.05.092

Sun, Y., and Liu, J. (2015). H9N2 influenza virus in China: a cause of concern. *Protein Cell.* 6,18–25. doi: 10.1007/s13238-014-0111-7

Swayne, D. E. (2012). Impact of vaccines and vaccination on global control of avian influenza. *Avian Dis.* 56, 818–828. doi: 10.1637/10183-041012-Review.1

Tian, X., Landreth, S., Lu, Y., Pandey, K., and Zhou, Y. (2021). A replication-defective influenza virus harboring H5 and H7 hemagglutinins provides protection against H5N1 and H7N9 infection in mice. *J. Virol.* 95, e02154–e02120. doi: 10.1128/JVI.02154-20

Tong, S., Zhu, X., Li, Y., Shi, M., Zhang, J., Bourgeois, M., et al. (2013). New world bats harbor diverse influenza A viruses. *PLoS Pathog.* 9, e1003657. doi: 10.1371/journal.ppat.1003657

Wang, Y., Niu, S., Zhang, B., Yang, C., and Zhou, Z. (2021). The whole genome analysis for the first human infection with H10N3 influenza virus in China. *J. Infect.* 21, 318–312. doi: 10.1016/j.jinf.2021.06.021

Wen, Z., Wu, C., Chen, W., Zeng, X., Shi, J., Ge, J., et al. (2015). Establishment of MDCK stable cell lines expressing TMPRSS2 and MSPL and their applications in propagating influenza vaccine viruses in absence of exogenous trypsin. *Biotechnol. Res. Int.* 2015, 402628–402634. doi: 10.1155/2015/402628

Xu, T., Wang, C., Zhang, R., Xu, M., Liu, B., Wei, D., et al. (2015). Carnosine markedly ameliorates H9N2 swine influenza virus-induced acute lung injury. *J. Gen. Virol.* 96, 2939–2950. doi: 10.1099/jgv.0.000238

Yoon, S. W., and Webby, R. J. (2014). Webster RG. Evolution and ecology of influenza A viruses. *Curr. Top Microbiol. Immunol.* 385, 359–375. doi: 10.1007/82_2014_396

Young, S. G., Carrel, M., Malanson, G. P., Ali, M. A., and Kayali, G. (2016). Predicting avian influenza co-infection with H5N1 and H9N2 in Northern Egypt. *Int. J. Environ. Res. Public Health.* 13, 866–902. doi: 10.3390/ijerph13090886

Zhao, K., Gu, M., Zhong, L., Duan, Z., Zhang, Y., Zhu, Y., et al. (2013). Characterization of three H5N5 and one H5N8 highly pathogenic avian influenza viruses in China. *Vet. Microbiol.* 163, 351–357. doi: 10.1016/j.vetmic.2012.12.025

Zhou, B., Meliopoulos, V. A., Wang, W., Lin, X., Stucker, K. M., Halpin, R. A., et al. (2016). Reversion of cold-adapted live attenuated influenza vaccine into a pathogenic virus. *J. Virol.* 90, 8454–8463. doi: 10.1128/JVI.00163-16

frontiers | Frontiers in Microbiology

TYPE Original Research
PUBLISHED 17 November 2022
DOI 10.3389/fmicb.2022.1055536

OPEN ACCESS

EDITED BY
George William Carnell,
University of Cambridge,
United Kingdom

REVIEWED BY
Iti Saraav,
Washington University in St. Louis,
United States
Elizabeth Ann L. Enninga,
Mayo Clinic,
United States

*CORRESPONDENCE
Natália Salomão
natgsalomao@gmail.com

†Deceased

SPECIALTY SECTION
This article was submitted to Infectious Agents and Disease, a section of the journal Frontiers in Microbiology

RECEIVED 28 September 2022
ACCEPTED 28 October 2022
PUBLISHED 17 November 2022

CITATION
Salomão N, Rabelo K, Avvad-Portari E, Basílio-de-Oliveira C, Basílio-de-Oliveira R, Ferreira F, Ferreira L, de Souza TM, Nunes P, Lima M, Sales AP, Fernandes R, de Souza LJ, Dias L, Brasil P, dos Santos F and Paes M (2022) Histopathological and immunological characteristics of placentas infected with chikungunya virus. *Front. Microbiol.* 13:1055536. doi: 10.3389/fmicb.2022.1055536

Histopathological and immunological characteristics of placentas infected with chikungunya virus

Natália Salomão[1,2]*, Kíssila Rabelo[3], Elyzabeth Avvad-Portari[4], Carlos Basílio-de-Oliveira[5], Rodrigo Basílio-de-Oliveira[5], Fátima Ferreira[6], Luiz Ferreira[7], Thiara Manuele de Souza[2], Priscila Nunes[2], Monique Lima[8], Anna Paula Sales[9], Regina Fernandes[10,11], Luiz José de Souza[9,10], Laura Dias[12], Patrícia Brasil[13], Flavia dos Santos[2] and Marciano Paes[1†]

[1]Laboratório Interdisciplinar de Pesquisas Médicas, Instituto Oswaldo Cruz, Fundação Oswaldo Cruz, Rio de Janeiro, Brazil, [2]Laboratório de Imunologia Viral, Instituto Oswaldo Cruz, Fundação Oswaldo Cruz, Rio de Janeiro, Brazil, [3]Laboratório de Ultraestrutura e Biologia Tecidual, Universidade do Estado do Rio de Janeiro, Rio de Janeiro, Brazil, [4]Departamento de Anatomia Patológica, Instituto da Mulher e da Criança Fernandes Figueira, Fundação Oswaldo Cruz, Rio de Janeiro, Brazil, [5]Departamento de Anatomia Patológica, Universidade Federal do Estado do Rio de Janeiro, Rio de Janeiro, Brazil, [6]Departamento de Neonatologia, Universidade Federal do Estado do Rio de Janeiro, Rio de Janeiro, Brazil, [7]Departamento de Anatomia Patológica, Instituto Nacional de Infectologia Evandro Chagas, Fundação Oswaldo Cruz, Rio de Janeiro, Brazil, [8]Laboratório Estratégico de Diagnóstico Molecular, Instituto Butantan, São Paulo, Brazil, [9]Centro de Referência de Doenças Imuno-infecciosas (CRDI), Campos dos Goytacazes, Rio de Janeiro, Brazil, [10]Faculdade de Medicina de Campos, Campos dos Goytacazes, Rio de Janeiro, Brazil, [11]Laboratório de Biotecnologia, Universidade Estadual do Norte Fluminense, Campos dos Goytacazes, Rio de Janeiro, Brazil, [12]Hospital Geral Dr. Beda, CEPLIN – Uti Neonatal Nicola Albano, Campos dos Goytacazes, Rio de Janeiro, Brazil, [13]Laboratório de Doenças Febris Agudas, Instituto Nacional de Infectologia Evandro Chagas, Fiocruz, Rio de Janeiro, Brazil

Although vertical transmission of CHIKV has been reported, little is known about the role of placenta in the transmission of this virus and the effects of infection on the maternal-fetal interface. In this work we investigated five placentas from pregnant women who became infected during the gestational period. Four formalin-fixed paraffin-embedded samples of placenta (cases 1–4) were positive for CHIKV by RT-PCR. One (case 5) had no positive test of placenta, but had positive RT-PCR for CHIKV in the serum of the mother and the baby, confirming vertical transmission. The placentas were analyzed regarding histopathological and immunological aspects. The main histopathological changes were: deciduitis, villous edema, deposits, villous necrosis, dystrophic calcification, thrombosis and stem vessel obliteration. In infected placentas we noted increase of cells ($CD8^+$ and $CD163^+$) and pro- (IFN-γ and TNF-α) and anti-inflammatory (TGF-β and IL-10) cytokines compared to control placentas. Moreover, CHIKV antigen was detected in decidual cell, trophoblastic cells, stroma villi, Hofbauer cells, and endothelial cells. In conclusion, CHIKV infection seems to disrupt placental homeostasis leading to histopathological alterations in addition to increase in cellularity and cytokines overproduction, evidencing an altered and harmful environment to the pregnant woman and fetus.

KEYWORDS

placenta, chikungunya, histopathology, immunohistochemistry, cytokines

Introduction

Chikungunya virus (CHIKV) is an arbovirus of the *Togaviridae* family and *Alphavirus* genus (Schuffenecker et al., 2006), which was first isolated in 1953 in Tanzania. It is endemic in Africa and Asia (Lumsden, 1955); however in 2014, it was introduced in the Americas, causing major epidemics (Escobar et al., 2016). CHIKV is a positive-strand RNA virus, enveloped, and spherical with a 60–70 nm-diameter (Higashi et al., 1967; Simizu et al., 1984; Powers et al., 2001). Its name is derived from a Makonde word meaning "the one which bends up" due to the posture some infected individuals assume as a result of arthralgia (Mavalankar et al., 2008). Other common symptoms are fever, rash, headache and myalgia (Silva and Dermody, 2017).

The principal mode of CHIKV transmission is by the bite of infected *Aedes* mosquitoes. However, although rare, CHIKV vertical transmission has already been reported, with the first evidence in June 2005, during an outbreak on La Reunion Island (Robillard et al., 2006). As consequence, symptomatic neonates may develop classic chikungunya similar to adults, which resolves spontaneously within 2 weeks (Ramful et al., 2007). Nevertheless, complicated or severe forms of chikungunya, such as hemorrhagic, cardiac, and neurologic manifestations have also been reported in neonates (Gérardin et al., 2008; Senanayake et al., 2009), requiring admission to intensive care units, intubation, and mechanical ventilation (Ramful et al., 2007). The rate of infected newborn was up to 49%, in mothers with intrapartum viremia (within 2 days of delivery; Ramful et al., 2007), thus, the intrapartum period seems to be the most critical one for transmission to the neonate. Most authors suggest transplacental transmission shortly before delivery is the most likely mode of transmission *via* mother-to-child through microtransfusions when the mother is experiencing CHIKV viremia (Ramful et al., 2007). Early maternal-fetal transmission of CHIKV has also been reported. Spontaneous abortion was observed in three cases of CHIKV infection before 16 weeks of gestation, and the viral genome was detected in amniotic fluid, chorionic villi, and in the fetal brain (Lenglet et al., 2006; Touret et al., 2006). There have also been reports of spontaneous abortion associated with CHIKV infection in which the virus was detected and placental samples exhibited malformations (Salomão et al., 2021). The presence of CHIKV has been reported in the placenta (Prata-Barbosa et al., 2018), newborn cerebrospinal fluid, amniotic fluids (Grivard et al., 2007), serum (Shenoy and Pradeep, 2012; Lyra et al., 2016), and urine (Lyra et al., 2016) along with Chikungunya IgM antibody in cerebrospinal fluid.

Here, we aimed to analyze placentas of five women who had confirmed Chikungunya during pregnancy, focusing on histopathology, investigation of viral antigens, as well as cells and cytokines that may have contributed to placental alterations.

Materials and methods

Ethical procedures

The study was approved by the Ethics Committee of the Oswaldo Cruz Foundation (CAEE: 92728218.5.0000.5248). All the mothers provided written informed consent and authorized publication of the results.

Case descriptions

The pregnant women (PW) became infected between 2018 and 2019 during Chikungunya epidemics in the cities of Rio de Janeiro and Campos dos Goytacazes. In 2019, incidence was 374.05 cases per 100,000 inhabitants in Rio de Janeiro (Superintendência de Vigilância em Saúde, 2018; CGVS, 2019). In 2018, incidence was 918.9 cases per 100,000 in Campos dos Goytacazes and rose to 942.5 cases per 100,000 in the first 6 months of 2019 (Secretaria de estado de saúde do Rio de Janeiro, 2019). The cases are described below:

- Case 1: A 40-year-old patient at 36 weeks of gestation (3rd trimester). She attended the Regional Center for Infectious Diseases (CRDI) of the Plantadores de Cana Hospital (Campos dos Goytacazes) in May 2018, reporting symptoms such as headache, severe arthralgia and exanthema. Three days after the onset of symptoms, she was hospitalized with oligohydramnios. Serological tests were performed during 3rd trimester. The placenta was collected at the time of onset (10 days after symptoms) for investigation of CHIKV infection. Newborn serum was nonreactive IgG and IgM on day 10 (result provided by hospital).
- Case 2: 26-year-old patient, 7 weeks pregnant (1st trimester). In July 2018, she attended the Regional Center for Infectious Diseases (CRDI) at the Plantadores de Cana Hospital (Campos dos Goytacazes) reporting that he had started symptoms such as arthralgia, rash, fever and nausea for 4 days. At the time of consultation, she was afebrile, anicteric and acyanotic, with blood pressure of 120 × 80 mmHg. Serum was collected for serology tests (1st sample was collected on July 17, 2018—IgM reactive; 2nd sample was collected 10 days later—IgG reactive; both during 1st trimester). The placenta was collected at delivery (40 weeks). The newborn was asymptomatic newborn, and not tested.

- Case 3: Patient aged 19 years. She attended the Gafrée and Guinle University Hospital (HUGG), Rio de Janeiro, at 12 weeks of gestation, reporting symptoms such as arthralgia, rash and fever, when the serum was positive for CHIKV (PCR and serology—IgM). At 20 weeks, she was admitted to the ICU with urinary sepsis. The placenta was collected later at delivery at 40 weeks' gestation. There is no information about the serum of the newborn.
- Case 4: A 37-year-old patient compared to the Regional Center for Infectious Diseases (CRDI) at the Plantadores de Cana Hospital (Campos dos Goytacazes). She had symptoms at the time of delivery, in September 2018, when the placenta was collected (38 weeks). The newborn had non-reactive anti-CHIKV IgG and IgM on the first day of life (result provided by hospital).
- Case 5: A 28-year-old patient in the third trimester of pregnancy. Attended the Hospital Dr. Beda (Campos dos Goytacazes) in June 2019 for delivery (38 weeks and 4 days), in which serum was collected for serological tests (IgM reactive; IgG non-reactive). She reported symptoms such as severe arthralgia, rash, fever and headache 2 days before delivery.

Sample collection

Blood samples from the pregnant women were collected upon onset of symptoms. Placenta samples were collected and fixed in formalin (10%) upon delivery. Samples were collected at the Plantadores de Cana Hospital, Gaffrée and Guinle University Hospital, and the Doctor Beda General Hospital. Samples of term placentas from healthy donors served as controls.

Serological diagnosis of chikungunya

Serological diagnosis was performed on serum samples from PW (controls and cases) using commercial kits, according to the manufacturer's protocol. Anti-CHIKV IgM and IgG antibodies were detected using Anti-CHIKV IgM and IgG ELISA kits, respectively (Euroimmun, Lubeck, Germany).

Viral RNA extraction and RT-qPCR for chikungunya virus in placental samples

RNA was extracted from formalin-fixed paraffin-embedded (FFPE) placental samples (collected at term—from the 37th week of pregnancy—during the delivery) using the PureLink™ FFPE RNA Isolation Kit (Invitrogen, Carlsbad California, USA) following the manufacturer's instructions and stored at-70°C. RT-qPCR of CHIKV RNA was performed as described elsewhere (Lanciotti et al., 2007) using the ABI Prism® 7,500 Sequence Detection System (Applied Biosystems, Foster City, California, USA).

Histopathological analysis

Placental samples fixed in formalin (10%) were sectioned, dehydrated in ethanol, clarified in xylene-impregnated paraffin, and embedded in paraffin resin. Tissue was then sectioned into 5 µm slides and incubated for 90 min at 60°C to melt the paraffin. Slides were then deparaffinized in xylene and rehydrated with decreasing concentrations of ethanol (100 to 70%). The slides were subsequently stained with hematoxylin and eosin and visualized by light microscopy (Olympus BX 53F, Japan). Digital images of main histological features were obtained using Image-Pro Plus software version 4.5.

Immunohistochemistry procedure

The paraffin-embedded tissues (4 µm thick) were incubated for 90 min at 60°C, deparaffinized in xylene, and rehydrated with ethanol. Antigen retrieval was performed by heating the tissue in the presence of citrate buffer (pH 6.0). Tissues sections were then incubated with 3% hydrogen peroxide in methanol for 10 min to block endogenous peroxidase and then rinsed in Tris–HCl (pH 7.4). Slides were then rinsed in Protein Blocker solution (ScyTek, Logan, Utah, USA) for 10 min to reduce non-specific binding. Samples were incubated with the following primary antibodies: polyclonal anti-CHIKV mouse hyperimmune ascites fluids diluted 1:700; and monoclonal anti-human against: CD8 (DAKO Cytomation, USA, diluted 1:100); CD163 (Abcam, United Kingdom, 1:200); IFN-γ (R&D Systems, USA, diluted 1:30); TNF-α (Abbiotec, USA, diluted 1:200); TGF-β (Santa Cruz, USA, diluted 1:300) and IL-10 (R&D Systems, USA, diluted 1:100) and at 4°C overnight. Subsequent incubations were performed with the Two-Step Polymer Immunohistoprobe Plus (Redwood, California, USA): Amplifier for Mouse & Rabbit IgG for 15 min and HRP Polymer Detector at room temperature for 15 min. Samples were exposed to diaminobenzidine (ScyTek, Logan, Utah, United States), and Mayer's hematoxylin (Dako, Palo Alto, California, USA) was used to counterstain. Sections were analyzed with an Olympus BX 53 microscope and images were acquired using a coupled Olympus DP72 camera.

Quantification analysis

To quantify positive cells, images from 20 random fields for each specific primary antibody (3 negative controls and 5 positive CHIKV cases) were acquired at 1,000× magnification, in an Olympus BX 53F microscope, using the software Image Pro version 7. The number of positive cells was quantified (manually counted) in each of the 20 fields, and the mean per placenta was calculated. Representative images are provided on the boards. Three placenta controls (negative for CHIKV) collected between the 28th and 40th week of pregnancy were included.

Statistical analysis

Data were analyzed with GraphPad Prism software v 6.0 (GraphPad Software, San Diego, California, USA). Cases and controls were compared using a Mann–Whitney test with a significance level of 0.05.

Results

Serological and molecular tests

Case 1 presented anti-CHIKV IgM and IgG antibodies; whereas cases 2 and 3 presented only anti-CHIKV IgG or anti-CHIKV IgM, respectively. It was not possible to perform the serology of case 4 as the serum sample was not available. Moreover, CHIKV RNA was detected by RT-qPCR in cases l, 2, 3 and 4 in FFPE placenta samples; and in the serum of case 5. All experiments were performed in duplicate (Ct1 and Ct 2). Serum samples of control pregnant women were tested for serology during the 3rd trimester, as well as cases 1 and 5. Cases 2 and 3 were tested during the 1st trimester. Chikungunya RT-qPCR was performed in FFPE placenta samples of 3rd trimester, which were collected at the delivery (Table 1).

Histopathological analysis

In case 1, deciduitis (inflammatory infiltrates in the decidua), and edema in the chorionic villi (Figure 1B) were found; as well as areas of necrosis, fibrin deposits and villous edema in case 2 (Figure 1C). Moderate inflammatory infiltrates were observed in the decidua in case 3 (Figure 1D). Stem vessel with subocclusive (Figure 1E) and occlusive (Figure 1G) and thrombosis were seen in case 4, as well as in case 5 (Figure 1H). Intervillositis was observed in case 5 (Figure 1I). In case 5, a group of avascular villi with stromal fibrosis and karyorrhexis was noted (Figure 1F). As expected, the control placenta tissue did not exhibit alterations (Figure 1A).

TABLE 1 Serological and molecular tests.

Samples	Chikungunya serology		Chikungunya RT-qPCR
	IgM	IgG	Result
Control 1	No	No	Negative
Control 2	No	No	Negative
Control 3	No	No	Negative
Case 1	Yes	Yes	Positive
Case 2	No	Yes	Positive
Case 3	Yes	No	Positive
Case 4	Serology was not performed	Serology was not performed	Positive
Case 5	Yes	No	Positive
Case 5[a]	Yes	No	Positive

Serology was performed using the serum of pregnant women, and the molecular tests were performed using FFPE placenta collected at the delivery. Serum samples: Controls, cases 1 and 5 were tested for serology during the 3rd trimester; cases 2 and 3 were tested during the 1st trimester. Chikungunya RT-qPCR was performed in FFPE placenta samples of 3rd trimester. [a]Newborn's serum.

Chikungunya antigen detection in placental tissues

Using the immunohistochemistry (IHC) technique, it was possible to detect the CHIKV viral antigen in case 1, in decidual cells (Figure 2B), endothelium of fetal cells, stroma villi (Figure 2C) and trophoblastic cells (Figure 2D). In addition, the antigen was present in endothelial cells of case 2 (Figure 2E), in Hofbauer cells of case 3 (Figure 2F) and in trophoblastic cells of cases 4 (Figure 2G) and 5 (Figure 2H). As expected, no viral antigen was detected in the control placental tissue (Figure 2A).

Cellularity in CHIKV-infected placenta

In order to find whether cellularity of the CHIKV-infected placenta was altered, the presence of $CD8^+$ and $CD163^+$ cells were investigated. In control placenta, there was low expression of these markers (Figures 3A,D) compared to infected placenta (Figures 3B,E). There were significant differences between cases and controls in CD8 expression (Figure 3C) and CD163 expression (Figure 3F).

Cytokine expression in CHIKV-infected placentas

Cytokine expression in the tissue was assessed to investigate the immune response profile to CHIKV infection. To this end, pro-inflammatory (IFN-γ and TNF-α) and anti-inflammatory (TGF-β and IL-10) cytokines were analyzed. IFN-γ was expressed by inflammatory cells in the intervillous space (Figure 4B), fetal cells inside fetal capillaries in chorionic villi (Figure 4C), and trophoblastic cells (Figure 4D). IFN-γ had low or no expression in controls (Figure 4A). TNF-α was expressed in trophoblastic cells in the control placenta (Figure 4F), and in Hofbauer cells in infected placenta (Figure 4G). TGF-β was found in trophoblast cells (Figure 4I), Hofbauer cells and endothelial cells (Figure 4J); and IL-10 in inflammatory cells in the intervillous space (Figure 4M) and trophoblast cells (Figure 4N). IL-10 had low or no expression in controls (Figure 4L). Quantification was performed to compare control and CHIKV-infected placenta expression. Cytokines expression evidenced statistical difference between the two groups (controls and cases): IFN-γ (Figure 4E), TNF-α (Figure 4H), TGF-β (Figure 4K), and IL-10 (Figure 4O).

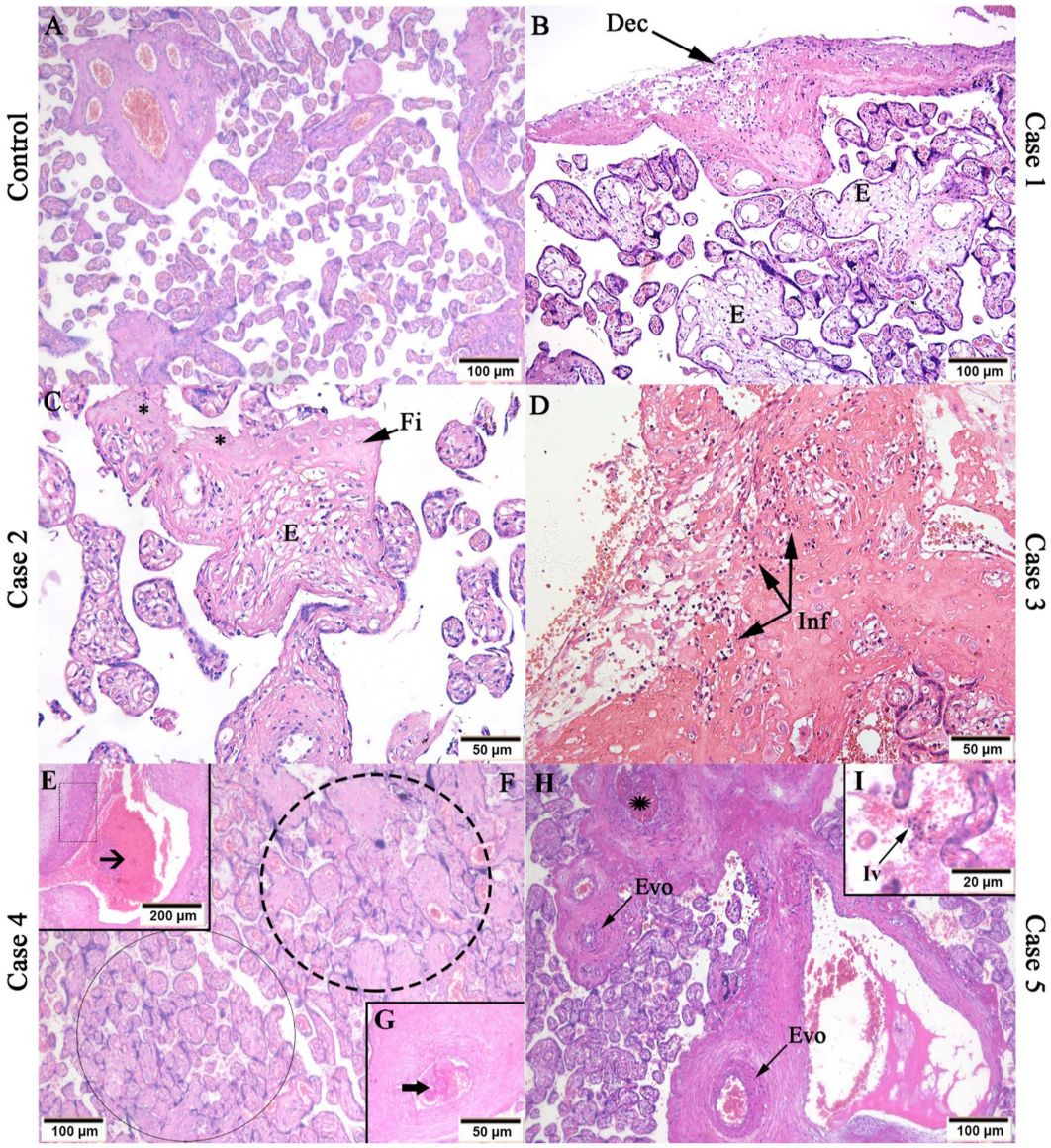

FIGURE 1
Histopathological analysis of CHIKV infected placenta tissues. **(A)** Control placenta tissue with regular aspects; **(B)** Deciduitis (Dec) and villous edema **(E)** in case 1; **(C)** Fibrin deposits (Fi), edema (E) and necrosis (*) in case 2; **(D)** Inflammatory infiltrate (Inf) in case 3; **(E)** Stem vessel vascular intramural fibrinoid deposition (dotted rectangle) and subocclusive thrombosis (black arrow); **(F)** avascular villi with stromal fibrosis (black circle) and villous stromal-vascular karyorrhexis (dotted circle); **(G)** Stem vessel with occlusive thrombosis (black thick arrow) in case 4; **(F)** Stem vessel obliteration/fibromuscular sclerosis (Evo) and thrombosis (black star); intervillositis (Iv) in case 5. Magnification: 5× **(E)**, 10× **(A,B,F,H)**, 20× **(C,D,G)**, 40× **(I)**.

Discussion

The exact mechanism of CHIKV transmission to the fetus and the possible role of the placenta in this process remain unknown. Herein we analyzed placental tissues from five cases of CHIKV infection during the 1st, 2nd and 3rd trimesters. FFPE placental tissues were positive for CHIKV by real time RT-PCR in cases 1, 2, 3, and 4. In case 5, real time RT-PCR was performed only on the serum (mother and newborn) with positives results, evidencing the presence of CHIKV genome.

The serology was performed to analyze the presence of anti-CHIKV antibodies. Usually, IgM antibody is detected during the acute phase (≤7 days post symptom onset) of CHIKV infection, indicating recent infection; however could persist up to 3 months (Andrew et al., 2022). IgG antibodies are used to indicate late infection, since these antibodies are detected mainly in samples of convalescent phase (>7 days post symptom onset; Andrew et al., 2022). For example, the serum of case 2 was collected at delivery and evidenced the presence of IgG antibodies only, displaying a late infection, during the first trimester of gestation.

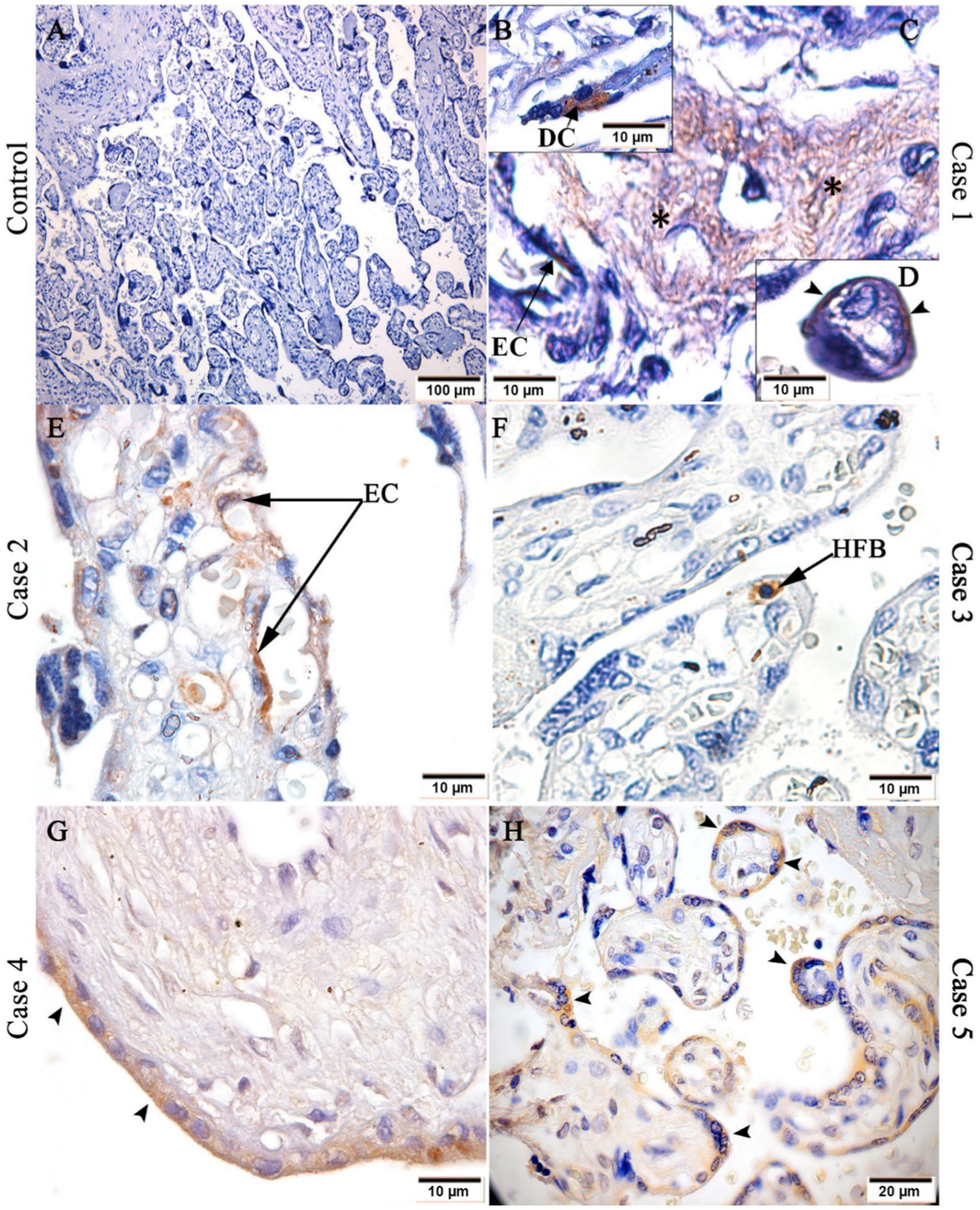

FIGURE 2
Detection of CHIKV antigen in placental tissue. **(A)** Control placenta with no CHIKV antigen detection; CHIKV antigen detection in: **(B)** decidual cell, **(C)** endothelial cell and stroma (black asterisks) of chorionic villi and **(D)** trophoblastic cells of case 1, **(E)** endothelial cells (EC) of case 2; **(F)** Hofbauer cell (HFB) of case 3; **(G)** trophoblastic cells of case 4; and **(H)** trophoblastic cells of case 5. Magnification: 10× **(A)**, 40× **(H)**, 100× **(B–G)**.

Regarding histopathological alterations, we found features of fetal vascular malperfusion: such as (1) stem vessel obliteration, with intramural fibrinoid deposition and also fibromuscular sclerosis, defined as thickening of the vessel wall, that results in partial or complete obliteration of the vascular lumen (Khong et al., 2016); and (2) occlusive thrombosis, a blood clot in the fetal villi vessel which blocks the blood passage, impairing exchanges between mother and fetus (Kraus, 2013). These changes were also reported in placental samples in cases of maternal hypertension and diabetes mellitus (Aldahmash et al., 2021), SARS-CoV-2 (Rebutini et al., 2021), dengue virus (DENV) (Fernandes Ribeiro et al., 2017) and other congenital infections (Stanek et al., 2011; Heider, 2017; Roberts and Torous, 2022).

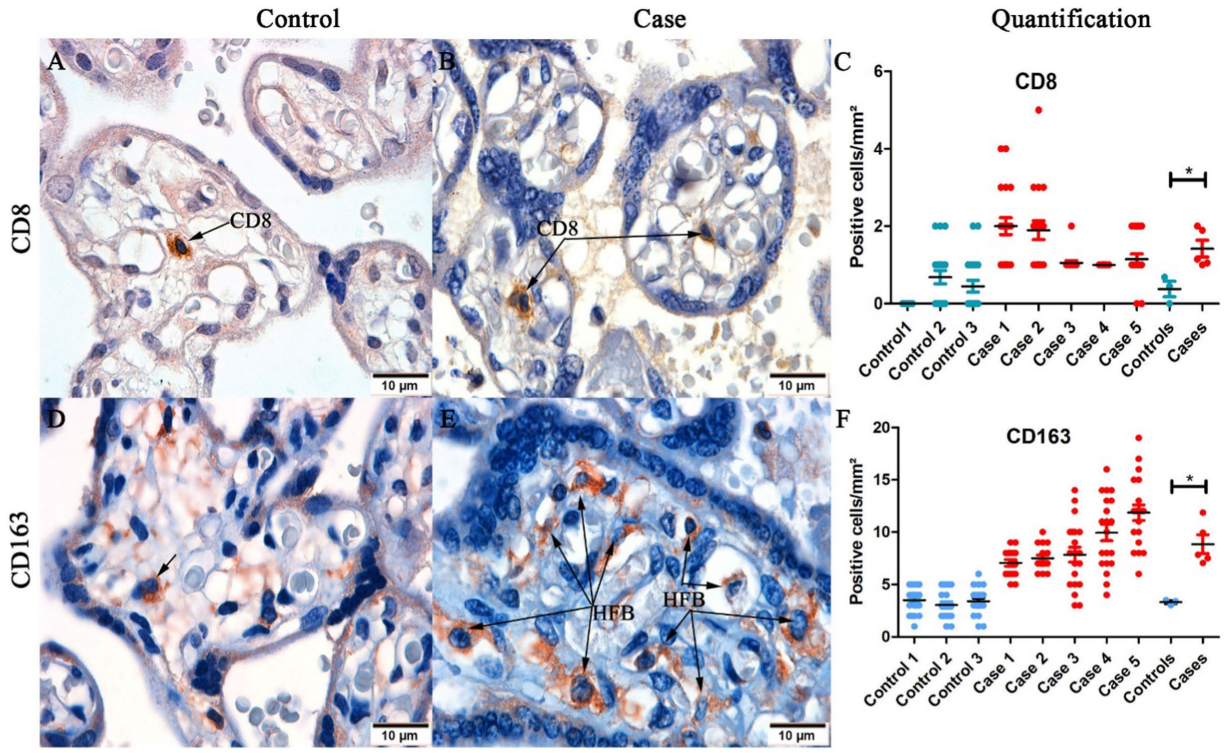

FIGURE 3
Representative images of detection of CD8⁺ and CD163⁺ cells in placental tissue. **(A)** Control placenta with low detection of CD8⁺ T cells; **(B)** Infected placenta with high detection of CD8+ T cells; **(C)** Quantification of CD8+ T cells in control and infected placentas; **(D)** Control placenta with low detection of CD163⁺ cells; **(E)** Infected placenta with high detection of CD163⁺ cells **(F)** Quantification and statistical analysis of CD163⁺ cells between control and infected placentas. (*p<0.05). Data are represented as mean±SDM. Magnification: 100× **(A–D)**.

We also noted villous edema and fibrinoid deposition, which were already described by Sandoval (Sandoval, 2016), and in other arboviruses infections such as DENV (Nunes et al., 2016, 2019; Fernandes Ribeiro et al., 2017) and zika virus (ZIKV; Rabelo et al., 2018, 2020). Villous edema is a pathological change related to hypoxia (Fernandes Ribeiro et al., 2017). Hypoxia in early pregnancy can alter trophoblastic differentiation and placental establishment; and in late gestational hypoxia includes changes in mitochondrial functions, endoplasmic reticulum stress, hormone production, nutrition and secretion of angiogenic factors; which depends on the extent of hypoxia (Colson et al., 2021). The increase of perivillous fibrin seems to occur in cases of trophoblastic necrosis (Chen and Roberts, 2018), which was observed in case 2. Depending on the extent of the fibrin deposition, obstruction of maternal flow may be observed, causing fetal consequences (Chen and Roberts, 2018). Mononuclear inflammatory cell infiltration in the decidua (deciduitis) and in the intervillous space (intervillositis) are chronic inflammatory lesions and have also observed as in other viral infections, such as ZIKV (Chimelli et al., 2017; Zanluca et al., 2018), DENV (Fernandes Ribeiro et al., 2017) and SARS-CoV-2 (Vivanti et al., 2020; Leal et al., 2021; Marton et al., 2021). In addition, placental exhibited dystrophic calcification, a deposition of calcium phosphate crystals in damaged areas, with necrotic portions or decreased circulation. This type of observation was noted also in ZIKV-infected placenta (Azevedo et al., 2018; Rabelo et al., 2020).

The use of the IHC technique facilitated immunolocalization of CHIKV antigen in decidual cells, Hofbauer cells, endothelial cells, stroma of chorionic villi, trophoblast cells and in cells of the intervillous space. Here, we have representative images of CHIKV⁺ cells in each case; however, we cannot relate the period of infection to the cell type positive for the virus; furthermore, the sample size is small to define it. These target cells are also positive in other arboviruses infections, such as DENV (Nunes et al., 2016; Fernandes Ribeiro et al., 2017) and ZIKV (Rabelo et al., 2017, 2020).

CD8⁺ cell expression was increased in infected placentas compared to controls, particularly in cases 1 and 2, consistent with the inflammatory infiltrate areas observed in histopathological findings. The recruitment of CD8+ T cells to tissue typically occurs due to pathogenic infection and contributes to IFN-γ and TNF-α production (Halle et al., 2017). Increase of these cells were reported also in cases of pregnancies complicated by pre-eclampsia, fetal growth restriction and small-for-gestational age (Lager et al., 2020).

CD163, which served as a macrophage activation marker, and Hofbauer cells (fetal-placental macrophages) were

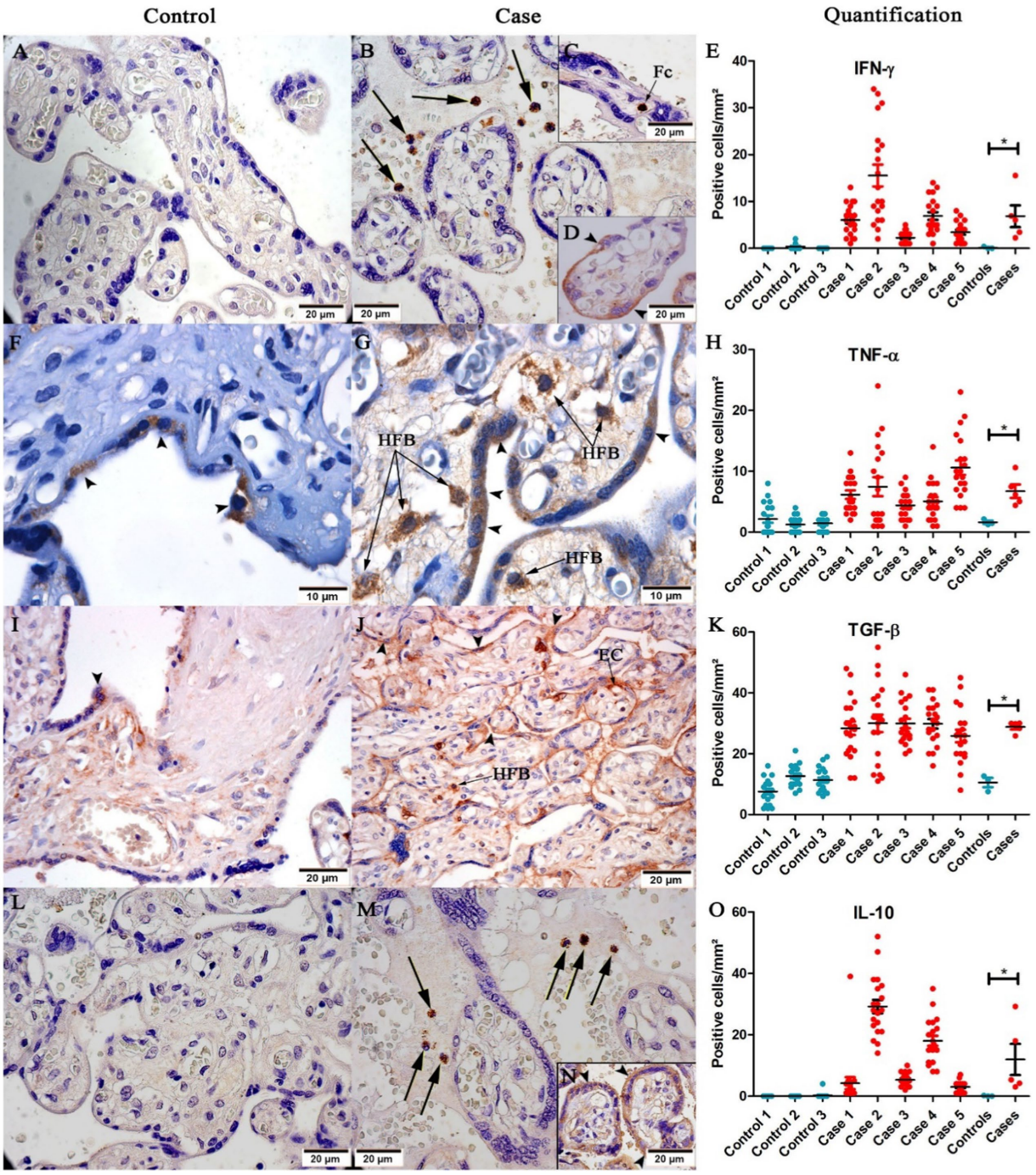

FIGURE 4
Representative images of cytokine detection in placental tissue. **(A)** No IFN-γ expression in control placenta; **(B)** IFN-γ expression in inflammatory cells (black arrows), **(C)** fetal cells (Fc), **(D)** and trophoblast cells (➤) in placental case; **(F)** Low TNF-α expression in trophoblast cells (➤) of the control placenta; **(G)** TNF-α expression in Hofbauer cells (HFB) in placental case; **(I)** Low expression of TGF-β in trophoblast cells (➤) in the control placenta; **(J)** TGF-β expression in trophoblast cells (➤), endothelial cells (EC) and Hofbauer cells (HFB); **(L)** No expression of IL-10 in placental case; **(M)** IL-10 expression in inflammatory cells (black arrows), and **(N)** trophoblast cells (➤). Quantification of **(E)** IFN-γ; **(H)** TNF-α; **(K)** TGF-β; and **(O)** IL-10 expression. (*p<0.05). Data are represented as mean±SDM. Magnification: 40× **(A,B,C,D,I,J,L,M,N)**, 100× **(F,G)**.

increased in infected placental tissues compared to the control. Hyperplasia of Hofbauer cells was also reported in ZIKV-infected placenta (Schwartz, 2017; De Noronha et al., 2018; Rabelo et al., 2020), gestational diabetes mellitus (Barke et al., 2018) and glucocorticoid administration (Tang et al., 2013). Hyperplasia of Hofbauer cells is a pathologic condition reported in ascending infections, TORCH infections, and villitis of unknown etiology (Schwartz, 2017). It contributes to the

immunopathogenesis of the disease, since it plays a role in the production of inflammatory mediators; in addition to being a site of viral replication. In ZIKV studies, authors suggest that these cells could play a role in the dissemination of ZIKV to the fetus, as they are mobile and occur in perivascular locations (Simoni et al., 2017). Similarly, we found that CHIKV was able to infect Hofbauer cells, so it could be a pathway through which the virus reaches the fetus; however, this mechanism needs further investigation.

As well as histopathological changes, the infiltration of $CD8^+$ T cells, fetal macrophages (Hofbauer cells) and several inflammatory cells into the chorionic villi may happen at any stage of pregnancy; which will culminate in complicated gestation or bad outcomes depending on the extension.

In addition to cellularity, cytokine profiles were analyzed through the immunohistochemistry. IFN-γ and TNF-α are pro-inflammatory cytokines, expression of which was increased in infected placentas compared to controls, and was expressed mainly by trophoblast cells, Hofbauer cells and inflammatory cells (in intervillous space and inside fetal capillaries); contributing to a pro-inflammatory environment. High expression of TNF-α in these cell types was also reported in DENV (Nunes et al., 2019) and ZIKV (Rabelo et al., 2020) infections.

In addition to the increase of pro-inflammatory cytokines, we also found increase of anti-inflammatory cytokines; perhaps as an attempt to contain the local inflammatory process without threatening the pregnancy. Anti-inflammatory cytokines such as IL-10 and transforming growth factor (TGF-β) are typically increased primarily in the second trimester, and decrease during the first and third trimesters (Brännn et al., 2019; Meyyazhagan et al., 2022). For the two cytokines we noted statistical difference between controls and cases. This increase has also been reported in cases of pre-eclampsia (Lyall et al., 2001) and molar lesions (Xuan et al., 2007); which could result in inhibition of trophoblast cell migration and invasion (Yang et al., 2021). High IL-10 expression was also reported in ZIKV-infected HTR8 (Luo et al., 2018). Such an increase was also observed in placental cytotrophoblast in Cytomegalovirus infection, associated with reduced matrix metalloproteinase 9 activity, which contributes to impaired cytotrophoblast remodeling of the uterine vasculature and consequently restricted fetal growth (Yamamoto-Tabata et al., 2004). Moreover, TGF-β and IL-10 are associated with tissue repair, healing and angiogenesis (Schliefsteiner et al., 2020).

CHIKV vertical transmission is known to occur, although is a rare event. Here, in all placentas we found histopathological and immunological changes, in addition to CHIKV antigen detection. However, vertical transmission was confirmed in only one case. Our findings highlight the importance of avoiding infections during pregnancy – in this case, Chikungunya – since modifications of the placenta can interfere with the functioning of this organ, and culminate in unfavorable outcomes for the pregnant women and fetus.

Data availability statement

The original contributions presented in the study are included in the article, further inquiries can be directed to the corresponding author.

Ethics statement

The studies involving human participants were reviewed and approved by Ethics Committee of the Oswaldo Cruz Foundation. The patients/participants provided their written informed consent to participate in this study.

Author contributions

MP and NS: conceptualization. NS, KR, TMS, ML, and PN: methodology. MP, NS, LF, and EA-P: formal analysis. PB and MP: investigation. MP, Fd-S, CB-d-O, and RB-d-O: resources. FF, LJ-d-S, RF, APS, and LD: data curation. NS: writing—original draft preparation. KR, Fd-S, PB, and EA-P: writing—review and editing. EA-P, Fd-S, and MP: supervision. MP and Fd-S: project administration. MP, Fd-S, and PB: funding acquisition. All authors contributed to the article and approved the submitted version.

Funding

This research was funded by Fundação Carlos Chagas Filho de Amparo à Pesquisa do Estado do Rio de Janeiro, grants numbers: E-26/210.400/2019 (MP), E-26/202.003/2016 (Fd-S), E-26/202.659/2019 (Fd-S), E-26/211.569/2019 (Fd-S), E-26/211.565/2019 (PB), E-26/202.862/2018 (PB) and by Conselho Nacional de Desenvolvimento Científico e Tecnológico (CNPq), grant numbers: 302462/2018–0 (Fd-S) and 307282/2017-1 (PB); and DECIT/25000.072811/2016-19 (PB).

Acknowledgments

At the time of submission, Dr. Marciano Paes passed away, a victim of COVID-19 and this study is dedicated to his memory. We thank Histotechnology Platform of the Oswaldo Cruz Institute (FIOCRUZ) for providing the paraffin sections and Livia Martins (Arbovirus Section) for the polyclonal anti-CHIKV mouse hyperimmune ascites fluids.

Conflict of interest

The authors declare that the research was conducted in the absence of any commercial or financial relationships that could be construed as a potential conflict of interest.

Publisher's note

References

Aldahmash, W. M., Alwasel, S. H., and Aljerian, K. (2021). Gestational diabetes mellitus induces placental vasculopathies. *Environ. Sci. Pollut. Res.* 29, 19860–19868. doi: 10.1007/S11356-021-17267-Y

Andrew, A., Navien, T. N., Yeoh, T. S., Citartan, M., Mangantig, E., Sum, M. S. H., et al. (2022). Diagnostic accuracy of serological tests for the diagnosis of chikungunya virus infection: a systematic review and meta-analysis. *PLoS Negl. Trop. Dis.* 16:e0010152. doi: 10.1371/JOURNAL.PNTD.0010152

Azevedo, R. S. S., Araujo, M. T., Oliveira, C. S., Filho, A. J. M., Nunes, B. T. D., Henriques, D. F., et al. (2018). Zika virus epidemic in Brazil. II. Post-mortem analyses of neonates with microcephaly, stillbirths, and miscarriage. *J. Clin. Med.* 7:496. doi: 10.3390/JCM7120496

Barke, T. L., Goldstein, J. A., Sundermann, A. C., Reddy, A. P., Linder, J. E., Correa, H., et al. (2018). "Gestational diabetes mellitus is associated with increased CD163 expression and iron storage in the placenta," in *Am. J. Reprod. Immunol.*, vol. 80, e13020.

Bränn, E., Edvinsson, Å., Rostedt Punga, A., Sundström-Poromaa, I., and Skalkidou, A. (2019). Inflammatory and anti-inflammatory markers in plasma: from late pregnancy to early postpartum. *Sci. Rep.* 9, 1863–1810. doi: 10.1038/s41598-018-38304-w

CGVS, C. G. de A. E. de V. em S (2019) 'Área Programática, Regiões Administrativas e Bairros'. Available at: http://www.rio.rj.gov.br/dlstatic/10112/10829614/4293007/Chik2019mes.pdf (Accessed May 11, 2022).

Chen, A., and Roberts, D. J. (2018). Placental pathologic lesions with a significant recurrence risk – what not to miss! *APMIS* 126, 589–601. doi: 10.1111/APM.12796

Chimelli, L., Melo, A. S. O., Avvad-Portari, E., Wiley, C. A., Camacho, A. H. S., Lopes, V. S., et al. (2017). The spectrum of neuropathological changes associated with congenital Zika virus infection. *Acta Neuropathol.* 133, 983–989. doi: 10.1007/s00401-017-1699-5

Colson, A., Sonveaux, P., Debiève, F., and Sferruzzi-Perri, A. N. (2021). Adaptations of the human placenta to hypoxia: opportunities for interventions in fetal growth restriction. *Hum. Reprod. Update* 27, 531–569. doi: 10.1093/HUMUPD/DMAA053

de Noronha, L., Zanluca, C., Burger, M., Suzukawa, A. A., Azevedo, M., Rebutini, P. Z., et al. (2018). Zika virus infection at different pregnancy stages: Anatomopathological findings, target cells and viral persistence in placental tissues. *Front. Microbiol.* 9:2266. doi: 10.3389/FMICB.2018.02266/BIBTEX

Escobar, L. E., Qiao, H., and Peterson, A. T. (2016). Forecasting chikungunya spread in the Americas via data-driven empirical approaches. *Parasit. Vectors* 9, 1–12. doi: 10.1186/S13071-016-1403-Y/FIGURES/6

Fernandes Ribeiro, C., Lopes, V. G. S., Brasil, P., Pires, A. R. C., Rohloff, R., and Nogueira, R. M. R. (2017). '*Dengue infection in pregnancy and its impact on the placenta*'. *Int J Infect Dis*. 55, 109–112.

Gérardin, P., Barau, G., Michault, A., Bintner, M., Randrianaivo, H., Choker, G., et al. (2008). Multidisciplinary prospective study of mother-to-child chikungunya virus infections on the island of La Réunion. *PLoS Med.* 5:e60. doi: 10.1371/journal.pmed.0050060

Grivard, P., le Roux, K., Laurent, P., Fianu, A., Perrau, J., Gigan, J., et al. (2007). Molecular and serological diagnosis of chikungunya virus infection. *Pathol. Biol.* 55, 490–494. doi: 10.1016/j.patbio.2007.07.002

Halle, S., Halle, O., and Förster, R. (2017). Mechanisms and dynamics of T cell-mediated cytotoxicity in vivo. *Trends Immunol.* 38, 432–443. doi: 10.1016/J.IT.2017.04.002

Heider, A. (2017). Fetal Vascular Malperfusion. *Arch. Pathol. Lab. Med.* 141, 1484–1489. doi: 10.5858/ARPA.2017-0212-RA

Higashi, N., Matsumoto, A., Tabata, K., and Nagatomo, Y. (1967). Electron microscope study of development of chikungunya virus in green monkey kidney stable (VERO) cells. *Virology* 33, 55–69. doi: 10.1016/0042-6822(67)90093-1

Khong, T. Y., Mooney, E. E., Ariel, I., Balmus, N. C. M., Boyd, T. K., Brundler, M. A., et al. (2016). Sampling and definitions of placental lesions: Amsterdam placental workshop group consensus statement. *Arch. Pathol. Lab. Med.* 140, 698–713. doi: 10.5858/ARPA.2015-0225-CC

Kraus, F. T. (2013). Fetal thrombotic vasculopathy: perinatal stroke, growth restriction, and other sequelae. *Surg. Pathol. Clin.* 6, 87–100. doi: 10.1016/J.PATH.2012.10.001

Lager, S., Sovio, U., Eddershaw, E., Linden, M. W., Yazar, C., Cook, E., et al. (2020). Abnormal placental CD8+ T-cell infiltration is a feature of fetal growth restriction and pre-eclampsia. *J. Physiol.* 598, 5555–5571. doi: 10.1113/JP279532

Lanciotti, R. S., Kosoy, O. L., Laven, J. J., Panella, A. J., Velez, J. O., Lambert, A. J., et al. (2007). Chikungunya virus in US travelers returning from India, 2006. *Emerg. Infect. Dis.* 13, 764–767. doi: 10.3201/eid1305.070015

Leal, C. R. V., Maciel, R. A. M., and Corrêa Júnior, M. D. (2021). SARS-CoV-2 infection and placental pathology Infecção por SARS-CoV-2 e patologia placentária. *Rev. Bras. Ginecol. Obstet.* 43, 474–479. doi: 10.1055/S-0041-1730291

Lenglet, Y., Barau, G., Robillard, P. Y., Randrianaivo, H., Michault, A., Bouveret, A., et al. (2006). Chikungunya infection in pregnancy: evidence for intrauterine infection in pregnant women and vertical transmission in the parturient. Survey of the Reunion Island outbreak. *J. Gynecol. Obstet. Biol. Reprod. (Paris)* 35, 578–583. doi: 10.1016/S0368-2315(06)76447-X

Lumsden, W. H. R. (1955). An epidemic of virus disease in Southern Province, Tanganyika territory, in 1952–1953 II. General description and epidemiology'. *Transact. R. Soc. Trop. Med. Hyg.* 49, 33–57. doi: 10.1016/0035-9203(55)90081-X

Luo, H., Winkelmann, E. R., Fernandez-Salas, I., Li, L., Mayer, S. V., Danis-Lozano, R., et al. (2018). Zika, dengue and yellow fever viruses induce differential anti-viralimmune responses in human monocytic and first trimester trophoblastcells. *Antivir. Res.* 151, 55–62. doi: 10.1016/J.ANTIVIRAL.2018.01.003

Lyall, F., Simpson, H., Nicola Bulmer, J., Barber, A., and Courtenay Robson, S. (2001). Transforming growth factor-β expression in human placenta and placental bed in third trimester Normal pregnancy, preeclampsia, and fetal growth restriction. *Am. J. Pathol.* 159, 1827–1838. doi: 10.1016/S0002-9440(10)63029-5

Lyra, P., Campos, G., Bandeira, I., Sardi, S., Costa, L., Santos, F., et al. (2016). Congenital chikungunya virus infection after an outbreak in Salvador, Bahia, Brazil. *AJP Rep.* 06, e299–e300. doi: 10.1055/S-0036-1587323

Marton, T., Hargitai, B., Hunter, K., Pugh, M., and Murray, P. (2021). Massive Perivillous fibrin deposition and chronic histiocytic Intervillositis a complication of SARS-CoV-2 infection. *Pediatr. Dev. Pathol.* 24, 450–454. doi: 10.1177/10935266211020723

Mavalankar, D., Shastri, P., Bandyopadhyay, T., Parmar, J., and Ramani, K. V. (2008). Increased mortality rate associated with chikungunya epidemic, Ahmedabad, India. *Emerg. Infect. Dis.* 14, 412–415. doi: 10.3201/eid1403.070720

Meyyazhagan, A., Kuchi Bhotla, H., Pappuswamy, M., Tsibizova, V., al Qasem, M., and di Renzo, G. C. (2022). Cytokine see-saw across pregnancy, its related complexities and consequences. *Int. J. Gynecol. Obstet.* doi: 10.1002/IJGO.14333

Nunes, P., Nogueira, R., Coelho, J., Rodrigues, F., Salomão, N., José, C., et al. (2019). A stillborn multiple organs' investigation from a maternal denv-4 infection: histopathological and inflammatory mediators characterization. *Viruses* 11:319. doi: 10.3390/v11040319

Nunes, P. C. G., Paes, M. V., de Oliveira, C. A. B., Soares, A. C. G., de Filippis, A. M. B., Lima, M. R. Q., et al. (2016). Detection of dengue NS1 and NS3 proteins in placenta and umbilical cord in fetal and maternal death. *J. Med. Virol.* 88, 1448–1452. doi: 10.1002/jmv.24479

Powers, A. M., Brault, A. C., Shirako, Y., Strauss, E. G., Kang, W. L., Strauss, J. H., et al. (2001). Evolutionary relationships and systematics of the alphaviruses. *J. Virol.* 75, 10118–10131. doi: 10.1128/jvi.75.21.10118-10131.2001

Prata-Barbosa, A., Cleto-Yamane, T. L., Robaina, J. R., Guastavino, A. B., de Magalhães-Barbosa, M. C., Brindeiro, R. M., et al. (2018). Co-infection with Zika and chikungunya viruses associated with fetal death—a case report. *Int. J. Infect. Dis.* 72, 25–27. doi: 10.1016/j.ijid.2018.04.4320

Rabelo, K., de Souza Campos Fernandes, R. C., Souza, L. J., Louvain de Souza, T., Santos, F. B., Guerra Nunes, P. C., et al. (2017). Placental histopathology and clinical presentation of severe congenital Zika syndrome in a human immunodeficiency virus-exposed uninfected infant. *Front. Immunol.* 8:1704. doi: 10.3389/fimmu.2017.01704

Rabelo, K., de Souza, L. J., Salomão, N. G., Machado, L. N., Pereira, P. G., Portari, E. A., et al. (2020). Zika induces human placental damage and inflammation. *Front. Immunol.* 11:2146. doi: 10.3389/FIMMU.2020.02146/BIBTEX

Rabelo, K., Souza, L. J., Salomão, N. G., Oliveira, E. R. A., Sentinelli, L. P., Lacerda, M. S., et al. (2018). Placental inflammation and fetal injury in a rare Zika case associated with Guillain-Barré syndrome and abortion. *Front. Microbiol.* 9:1018. doi: 10.3389/fmicb.2018.01018

Ramful, D., Carbonnier, M., Pasquet, M., Bouhmani, B., Ghazouani, J., Noormahomed, T., et al. (2007). Mother-to-child transmission of chikungunya virus infection. *Pediatr. Infect. Dis. J.* 26, 811–815. doi: 10.1097/INF.0b013e3180616d4f

Rebutini, P. Z., Zanchettin, A. C., Stonoga, E. T. S., Prá, D. M. M., de Oliveira, A. L. P., Dezidério, F. S., et al. (2021). Association between COVID-19 pregnant women symptoms severity and placental morphologic features. *Front. Immunol.* 12:685919. doi: 10.3389/FIMMU.2021.685919

Roberts, D. J., and Torous, V. (2022). 'Placental pathology', reproductive and developmental. *3rd Edn. Toxicology*, 1399–1420. doi: 10.1016/B978-0-323-89773-0.00069-2

Robillard, P. Y., Boumahni, B., Gérardin, P., Michault, A., Fourmaintraux, A., Schuffenecker, I., et al. (2006). Transmission verticale materno-fœtale du virus chikungunya: Dix cas observés sur l'île de la Réunion chez 84 femmes enceintes. *Presse Med.* 35, 785–788. doi: 10.1016/S0755-4982(06)74690-5

Salomão, N., Brendolin, M., Rabelo, K., Wakimoto, M., de Filippis, A. M., dos Santos, F., et al. (2021). Spontaneous abortion and chikungunya infection: pathological findings. *Viruses* 13:554. doi: 10.3390/v13040554

Sandoval, O. (2016). *The Placenta in a Case of Pregnant Woman Infected by Chikungunya Virus*.

Schliefsteiner, C., Ibesich, S., and Wadsack, C. (2020). Placental Hofbauer cell polarization resists inflammatory cues in vitro. *Int. J. Mol. Sci.* 21:736. doi: 10.3390/IJMS21030736

Schuffenecker, I., Iteman, I., Michault, A., Murri, S., Frangeul, L., Vaney, M. C., et al. (2006). Genome microevolution of chikungunya viruses causing the Indian Ocean outbreak. *PLoS Med.* 3:e263. doi: 10.1371/journal.pmed.0030263

Schwartz, D. A. (2017). Viral infection, proliferation, and hyperplasia of Hofbauer cells and absence of inflammation characterize the placental pathology of fetuses with congenital Zika virus infection. *Arch. Gynecol. Obstet.* 295, 1361–1368. doi: 10.1007/S00404-017-4361-5

Secretaria de estado de saúde do Rio de Janeiro (2019) 'BOLETIM EPIDEMIOLÓGICO ARBOVIROSES Nº 002/2019 CENÁRIO'. Available at: http://www.riocomsaude.rj.gov.br/Publico/MostrarArquivo.aspx?C=F%2BJ77ZiVqng%3D (Accessed May 11, 2022).

Senanayake, M. P., Senanayake, S. M., Vidanage, K. K., Gunasena, S., and Lamabadusuriya, S. P. (2009). Vertical transmission in chikungunya infection. *Ceylon Med. J.* 54:47. doi: 10.4038/cmj.v54i2.865

Shenoy, S., and Pradeep, G. C. M. (2012). Neurodevelopmental outcome of neonates with vertically transmitted chikungunya fever with encephalopathy. *Indian Pediatr.* 49, 238–240.

Silva, L. A., and Dermody, T. S. (2017). Chikungunya virus: epidemiology, replication, disease mechanisms, and prospective intervention strategies. *J. Clin. Invest.* 127, 737–749. doi: 10.1172/JCI84417

Simizu, B., Yamamoto, K., Hashimoto, K., and Ogata, T. (1984). Structural proteins of chikungunya virus. *J. Virol.* 51, 254–258. doi: 10.1128/jvi.51.1.254-258.1984

Simoni, M. K., Jurado, K. A., Abrahams, V. M, Fikrig, E., and Guller, S. (2017). Zika Virus infection of Hofbauer cells. *Am. J. Reprod. Immunol.* 77. doi: 10.1111/AJI.12613

Stanek, J., Sheridan, R. M., le, L. D., and Crombleholme, T. M. (2011). Placental fetal thrombotic vasculopathy in severe congenital anomalies prompting EXIT procedure. *Placenta* 32, 373–379. doi: 10.1016/J.PLACENTA.2011.02.002

Superintendência de Vigilância em Saúde (2018) Área Programática, Regiões Administrativas e Bairros. Available at: http://www.rio.rj.gov.br/dlstatic/10112/10829527/4267213/Chikmes 2018.pdf (Accessed May 11, 2022).

Tang, Z., Niven-Fairchild, T., Tadesse, S., Norwitz, E. R., Buhimschi, C. S., Buhimschi, I. A., et al. (2013). Glucocorticoids enhance CD163 expression in placental Hofbauer cells. *Endocrinology* 154, 471–482. doi: 10.1210/EN.2012-1575

Touret, Y., Randrianaivo, H., Michault, A., Schuffenecker, I., Kauffmann, E., Lenglet, Y., et al. (2006). Early maternal-fetal transmission of the chikungunya virus. *Presse Med.* 35, 1656–1658. doi: 10.1016/s0755-4982(06)74874-6

Vivanti, A. J., Vauloup-Fellous, C., Prevot, S., Zupan, V., Suffee, C., do Cao, J., et al. (2020). Transplacental transmission of SARS-CoV-2 infection. *Nat Commun.* 11:3572. doi: 10.1038/S41467-020-17436-6

Xuan, Y. H., Choi, Y. L., Shin, Y. K., Ahn, G. H., Kim, K. H., Kim, W. J., et al. (2007). Expression of TGF-beta signaling proteins in normal placenta and gestational trophoblastic disease. *Histol. Histopathol.* 22, 227–234. doi: 10.14670/HH-22.227

Yamamoto-Tabata, T., McDonagh, S., Chang, H. T., Fisher, S., and Pereira, L. (2004). Human cytomegalovirus Interleukin-10 downregulates metalloproteinase activity and impairs endothelial cell migration and placental Cytotrophoblast invasiveness in vitro. *J. Virol.* 78, 2831–2840. doi: 10.1128/JVI.78.6.2831-2840.2004

Yang, D., Dai, F., Yuan, M., Zheng, Y., Liu, S., Deng, Z., et al. (2021). Role of transforming growth factor-β1 in regulating fetal-maternal immune tolerance in Normal and pathological pregnancy. *Front. Immunol.* 12:3525. doi: 10.3389/FIMMU.2021.689181/BIBTEX

Zanluca, C., de Noronha, L., and Duarte dos Santos, C. N. (2018). Maternal-fetal transmission of the zika virus: an intriguing interplay. *Tissue Barriers* 6:e1402143. doi: 10.1080/21688370.2017.1402143

frontiers | Frontiers in Microbiology

TYPE Original Research
PUBLISHED 24 November 2022
DOI 10.3389/fmicb.2022.1052917

OPEN ACCESS

EDITED BY
George William Carnell,
University of Cambridge,
United Kingdom

REVIEWED BY
Iti Saraav,
Washington University in St. Louis,
United States
Laura Schnackenberg,
National Center for Toxicological Research (FDA), United States

*CORRESPONDENCE
Changlong Bi
bichlong@mail.sysu.edu.cn
Chao Wu
wuchao99261@163.com
Aixia Zhai
zhaiaix@mail.sysu.edu.cn;
aixiazhai@126.com

†These authors have contributed equally to this work and share first authorship

SPECIALTY SECTION
This article was submitted to Infectious Agents and Disease, a section of the journal Frontiers in Microbiology

RECEIVED 26 September 2022
ACCEPTED 07 November 2022
PUBLISHED 24 November 2022

CITATION
Yu X, Chen Y, Cui L, Yang K, Wang X, Lei L, Zhang Y, Kong X, Lao W, Li Z, Liu Y, Li Y, Bi C, Wu C and Zhai A (2022) CXCL8, CXCL9, CXCL10, and CXCL11 as biomarkers of liver injury caused by chronic hepatitis B. *Front. Microbiol.* 13:1052917. doi: 10.3389/fmicb.2022.1052917

CXCL8, CXCL9, CXCL10, and CXCL11 as biomarkers of liver injury caused by chronic hepatitis B

Xin Yu[1†], Ying Chen[1†], Lele Cui[2†], Kaming Yang[3], Xumeng Wang[1,4], Linyuan Lei[1], Yanping Zhang[1], Xinyi Kong[1], Wanwen Lao[3], Zhenlin Li[3], Yang Liu[1], Yuetong Li[3], Changlong Bi[3]*, Chao Wu[1]*and Aixia Zhai[1]*

[1]Department of Laboratory Medicine, The Eighth Affiliated Hospital, Sun Yat-sen University, Shenzhen, China, [2]Department of Immunology, School of Basic Medical Sciences, Capital Medical University, Beijing, China, [3]Department of Endocrinology, The Eighth Affiliated Hospital, Sun Yat-sen University, Shenzhen, China, [4]Department of Microbiology, Harbin Medical University, Harbin, China

Background: Chronic hepatitis B (CHB) remains a significant global health problem, leading to recurrent inflammation and liver-damaging diseases such as fibrosis, cirrhosis, and hepatocellular carcinoma (HCC). Currently, although diagnostic markers for CHB are well established, the indicators for predicting liver injury caused by hepatitis B virus (HBV) infection still need to be further explored. Thus, the identification of credible infectious indicators is urgently needed to facilitate timely clinical intervention and avoid the progression of disease malignancy.

Methods: The Gene Expression Omnibus (GEO) database GSE83148 data set was used to explore the hub genes for HBV infection. The quantitative real-time polymerase chain reaction (qPCR) was used to identify the impact of HBV infection on the expression of hub gene at the cell level. At the same time, serum samples and clinical information were collected from healthy, HBV-free and CHB patients. The enzyme-linked immunosorbent assay (ELISA) was used to verify the results of cell experiments and Pearson correlation analysis was used to clarify hub genes correlation with HBV infection indicators and liver injury-related indicators. Finally, the Gene Expression Profiling Interactive Analysis (GEPIA) database was used to analyze the differences in the expression of hub gene in liver injury diseases.

Results: Chemokine (C-X-C motif) ligand (CXCL)8, CXCL9, CXCL10, and CXCL11 were identified as hub genes in HBV infection. After HBV infection, the expression of the four chemokines was significantly increased and the concentrations secreted into serum were also increased. Moreover, the four chemokines were significantly correlated with HBV infection-related indicators and liver injury-related indicators, which were positively correlated with alanine aminotransferase (ALT), aspartate aminotransferase (AST) and hepatitis B e antigen (HBeAg), and negatively correlated with AST/ALT ratio and hepatitis B core antibody (HBcAb). In addition, the expression of CXCL9, CXCL10, and CXCL11 in HCC tissues was significantly higher than in normal tissues.

Conclusion: Using a combination of bioinformatics, cell experiments, and clinical correlation analysis, this study showed that CXCL8, CXCL9, CXCL10, and CXCL11 can be used as serum biomarkers to forecast liver injury caused by HBV infection.

KEYWORDS

hepatitis B virus, CXCL8, CXCL9, CXCL10, CXCL11

Introduction

Hepatitis B virus (HBV) is the most critical factor in acute and chronic hepatitis infection (Yang et al., 2017). Currently, 350 million people worldwide suffer from chronic hepatitis B (CHB), about 120 million of whom are Chinese (Yuen et al., 2018; Gao et al., 2019). CHB, a canonical inflammatory disease, has been identified as the primary cause for the progression of liver-related diseases, which can result in death. After HBV infection, cytokines of the liver microenvironment change, as exemplified by inflammatory cytokine aggregation (Zhong et al., 2021). The expression of chemokines increases, generating a concentration gradient signal that helps in recruiting inflammatory cells such as neutrophils and T lymphocytes to the inflammation parts, triggering an inflammatory reaction. On the one hand, these inflammatory cells assist organisms in eliminating viruses. On the other hand, they constantly destroy liver parenchyma. Consequently, HBV infection lasts over a long period and finally triggers liver damage disease (Kolaczkowska and Kubes, 2013; Mehrfeld et al., 2018; Peng et al., 2020; Zhong et al., 2021).

The World Health Organization (WHO) reported that, in 2019, HBV resulted in an estimated 820,000 deaths, mostly from cirrhosis and hepatocellular carcinoma (HCC; World Health Organization (WHO) Hepatitis B factsheet, 2018). At present, the most effective therapeutic strategy for HCC is hepatectomy, but only a small fraction of patients can be operated on because they were diagnosed with advanced liver cancer (Sugawara and Hibi, 2021). As a result, valid biomarkers are urgently needed in clinical practice to predict CHB-induced liver injury to facilitate timely clinical intervention, preventing the progression of disease malignancy. Therefore, we began with differentially expressed genes in the liver microenvironment to explore biomarkers secreted into the blood that could be used to predict liver damage after HBV infection. Microarray analysis is frequently applied to research the pathogenesis of cancer, but more and more studies concentrate on infectious diseases. Therefore, we downloaded gene chips *via* a Gene Expression Omnibus (GEO) data set to analyze and predict the correlation of four chemokines, expressions with CHB in the liver tissue microenvironment, including chemokine (C-X-C motif) ligand (CXCL)8, CXCL9, CXCL10, and CXCL11. Then, these four chemokines were examined in clinical blood samples to determine whether they could be used as predictors of liver injury caused by HBV infection.

Materials and methods

Patients

The Research Ethics Board of the Eighth Affiliated Hospital of Sun Yat-sen University approved this study. Written informed consent was obtained from all patients involved. 93 patients at the Eighth Affiliated Hospital of Sun Yat-sen University from February 2020 to April 2021 provided the serum samples used in this research. In this study, 28 healthy patients, 45 patients with CHB and 20 patients without HBV infection and alanine aminotransferase (ALT) levels comparable to CHB patients were enrolled. The latter served as the disease control group and was named as the HBV-free group. Following the Chinese Society of Liver Diseases and the Chinese Society of Infectious Diseases standards, the criteria for inclusion in the CHB group were positive serum hepatitis B surface antigen (HBsAg) and continuous or repeated elevation of serum alanine aminotransferase for more than 6 months. The HBV DNA, HBsAg, ALT and aspartate aminotransferase (AST) data of the patients were obtained from the laboratory report. HBV DNA was detected by ABIQ5 PCR instrument using quantitative real-time polymerase chain reaction (qPCR). HBsAg was detected by Roche cobas e601 automatic immunoassay system using electrochemiluminescence method with a detection limit of 0.05 IU/ml. ALT and AST were quantified by lactate dehydrogenase method and malate dehydrogenase method, respectively, with the detection limit of 40 U/ml by Beckman AU5800 automatic biochemical analyzer. In addition, the clinical diagnosis was consistent with the "Guidelines for the Prevention and Treatment of Chronic Hepatitis B 2019" excluding the influences of pregnancy, hepatitis C virus (HCV), human immunodeficiency virus (HIV), and other diseases.

Microarray data

The microarray data for GSE83148 were downloaded from the GEO database[1] based on the GPL570 [HG-U133_Plus_2] Affymetrix Human Genome U133 Plus 2.0 Array. A total of 128 liver tissues, including 122 HBV infected samples and 6 healthy samples, were used in this study.

1 http://www.ncbi.nlm.nih.gov/geo/

Data processing and differential expression analysis

For the GSE83148 dataset, the original array data was downloaded by the R packages named *GEOquery* and *tinyarray*. Data collating was conducted *via* stringr, an R package. The IDs of genes were converted with the R packages called *AnnoProbe* and *hgu133plus2.db*. Then the differential expression analysis was carried out using an R package named DESeq2 to identify differentially expressed genes (DEGs) between HBV and normal samples and using R package *dplyr* to process the data derived from the above analysis. We used a series of indexes for DEG screening, including a |log2FC| >1 and a *p* value cutoff <0.05. We used the R packages called *ggplot2* and *tinyarray* to create a volcano map and clustering heatmap of DEGs.

We used the Gene Expression Profiling Interactive Analysis (GEPIA) database[2] to compare the expression of CXCL8, CXCL9, CXCL10, and CXCL11 in normal tissues and HCC tissues by setting the threshold of *p* value to 0.05 and the threshold of |log2FC| to 0.5. The data of GEPIA were obtained from The Cancer Genome Atlas (TCGA[3]) and Genotype-Tissue Expression (GTEx[4]) databases, in which HCC tissue data were obtained from TCGA database, and normal tissue data were obtained from TCGA and GTEx database.

Go and KEGG pathway analyses

Genome Ontology (GO) analysis is usually used to investigate the annotation of genes and proteins as a bioinformatics tool. Kyoto Encyclopedia of Genes and Genomes (KEGG) is a database used to systematically analyze gene functions, genomic link information, and integrate protein interaction network information. The R packages named *clusterProfiler*, *org.Hs.eg.db*, *GOplot*, *stringr* and *tinyarray* were applied to implement GO enrichment analysis and KEGG annotations. A *p* value cutoff <0.05 was identified as a significant difference.

PPI network analysis and module analysis

The Search Tool for the Retrieval of Interacting Genes (STRING)[5] database is a resource to evaluate protein–protein interaction (PPI) network information. Nodes represented genes, and nodes were connected by lines, representing gene relationships in the PPI network. PPI network production was performed with the above top50 DEGs of clustering heatmap. Genes with more than five nodes between them and other genes are defined as the hub genes, which perform essential biological functions in HBV. Cytoscape and cytoHubba were used to analyze the hub genes and map the molecular interaction networks.

Cell culture

A liver cancer cell line (HepG2) derived from a 15-year-old Caucasian boy is often used to study liver-related diseases. HepG2.215 cells are derived from HepG2 cells and are transfected with four 5′-3′ tandem copies of the HBV genome, usually used as cell models of hepatitis B virus infection (Sells et al., 1987). HepG2 cells and HepG2.215 cells were cultured in DMEM medium, supplemented with 10% FBS and 1% penicillin–streptomycin, and incubated at 37°C in a 5% CO_2 environment.

qPCR

According to the manufacturer's instructions, total RNA was extracted from cells using Trizol reagent (Invitrogen, Carlsbad, CA, United States). One microgram of total RNA from each sample was used to generate cDNAs with the PrimeScript™ RT Master Mix (#RR036A; Takara Bio Inc., Shiga, Japan). The resultant cDNA was amplified by TB Green® Premix Ex Taq™ II (#RR820A; Takara Bio Inc., Shiga, Japan). The primer sequence is shown in Table 1. The program was as follows: holding stage 95°C 30 s; cycling stages 95°C for 5 s, 60°C for 30 s, and 60°C for 30 s, repeated for 50 cycles; and melting stages 95°C for 15 s, 69°C for 60 s, and 95°C for 15 s. The levels of mRNA were normalized relative to GAPDH. The expression of genes was analyzed by using the $2^{-\triangle\triangle CT}$ method.

ELISA

The levels of CXCL8, CXCL9, CXCL10, and CXCL11 expression in human serum samples were detected using CXCL8, CXCL9, CXCL10, and CXCL11 enzyme-linked immunosorbent assay (ELISA) kits (CXCL8, YH-10139; CXCL9, YH-10060; CXCL10, 10,080; CXCL11, 10,061, YIHE biological, Shanghai, China), according to the manufacturer's instructions. Absorbance at 450 nm in each well measured the intensity of the developed color. Standard curves for the assay system were obtained from dilutions of the standards of the ELISA kit. The concentrations of CXCL8, CXCL9, CXCL10, and CXCL11 were then obtained by extrapolation from the standard curve.

Statistical analysis

Statistical analysis was carried out using SPSS 25 software. Pearson's correlation coefficient was used to evaluate the correlations among the expressions of four chemokines and the levels of ALT

2 http://gepia2.cancer-pku.cn/#analysis
3 https://tcga-data.nci.nih.gov/tcga/
4 https://www.gtexportal.org/
5 https://cn.string-db.org

TABLE 1 qPCR primer sequences.

Name	Forward primer	Reverse primer
GAPDH	F:GGACCTGACCTGCCGTCTAG	R:GTAGCCCAGGATGCCCTTGA
CXCL8	F:AACTTTCAGAGACAGCAGAGCACAC	R:CACACAGTGAGATGGTTCCTTCCG
CXCL9	F:CAGCACCAACCAAGGGACTATC	R:CACATCTGCTGAATCTGGGTTTAG
CXCL10	F:CTGCCATTCTGATTTGCTGCC	R:AATGCTGATGCAGGTACAGCG
CXCL11	F:GGCAGATATTGAGAAAGCCTCCA	R:GCCTTGCTTGCTTCGATTTGG

and AST. All statistical data were analyzed and visualized with GraphPad Prism 6.0 software (GraphPad Software, La Jolla, CA). The qPCR validation of all samples was tested by a paired *t* test, and a p value < 0.05 was considered statistically significant. All continuous variables were expressed as the means ± SD. Analysis of variance (ANOVA) was used for statistical comparison among groups. All cell experiments were performed in triplicate.

Results

Identification of hub genes related to HBV infection

In the GEO database, we compared the genes expression between the HBV infected samples and normal control samples, 444 DEGs were successfully identified, including 338 upregulated and 106 downregulated genes. We according to the genetic |log2FC| and take the top50 genes for heatmap display (Figure 1A). Figure 1B show the volcano plot of DEGs. To further investigate the biological function of DEGs, GO analysis was performed. The results showed that DEGs were enriched in leukocyte migration, lymphocyte migration, response to chemokine (Figure 1C). Furthermore, KEGG analysis showed that DEGs were concentrated in 10 signaling pathways, including cytokine-cytokine receptor interaction, chemokine signaling pathway, viral protein interaction with cytokines and cytokine receptors (Figure 1D). Based on the STRING database, we performed the PPI network of the top50 DEGs (Figure 1E) and combined it with the KEGG results. CytoHubba was used to map the hub gene network (Figure 1F). Ultimately, we identified four HBV infection-related hub genes: CXCL8, CXCL9, CXCL10, and CXCL11, which were all upregulated.

HBV infection upregulated the expressions of CXCL8, CXCL9, CXCL10, and CXCL11

To validate the relationship between HBV infection and hub genes, we analyzed the mRNA expression of hub genes in HepG2 cells and HepG2.215 cells by qPCR. As shown in Figure 2A, the mRNA levels of CXCL8, CXCL9, CXCL10, and CXCL11 were upregulated in HepG2.215 cells which containing HBV genome compared to HepG2 cells. We also re-verified the above results in the HepG2 cells with transient HBV genome (Figure 2B). On this basis, we conclude that the expression of chemokines CXCL8, CXCL9, CXCL10, and CXCL11 was markedly upregulated after HBV infection.

Serum levels of CXCL8, CXCL9, CXCL10, and CXCL11 in CHB patients were increased

To further clarify the correlation between these four chemokines in serum samples and HBV infection, ELISA experiments were conducted. We tested the concentrations of the four chemokines in the serum samples from 28 healthy patients, 45 CHB patients and 20 HBV-free patients (Figure 3). Compared with the Healthy group and the HBV-free group, the serum levels of CXCL8, CXCL9, CXCL10, and CXCL11 in patients with the CHB group were significantly higher. Combined with cell experiments, we speculated that the changes of the four chemokines may be detected by blood samples to speculate the occurrence of HBV infection-related liver injury, so as to meet the requirements of simple, efficient and accurate detection in clinical practice.

CXCL8, CXCL9, CXCL10, and CXCL11 were positively correlated with HBV infection and ALT

We sorted out the clinical data of Healthy patients, CHB patients and HBV-free patients. ALT is a common marker of hepatocyte injury and inflammation. As show in Table 2, ALT levels between the Healthy group and the CHB group were significantly different, while the difference between the HBV-free group and the CHB group was not statistically significant. We analyzed the clinical association between these four factors and ALT and AST using the Pearson correlation analysis. As shown in Figure 4; Table 3, CXCL8, CXCL9, CXCL10, and CXCL11 showed positive correlation with ALT, AST, hepatitis B e antigen (HBeAg), and negatively correlated with AST/ALT ratio, hepatitis B core antibody (HBcAb). In addition, the results indicated that both CXCL8 and CXCL10 were positively correlated with total bilirubin (TBIL) and indirect Bilirubin (IBIL; Table 3). These results

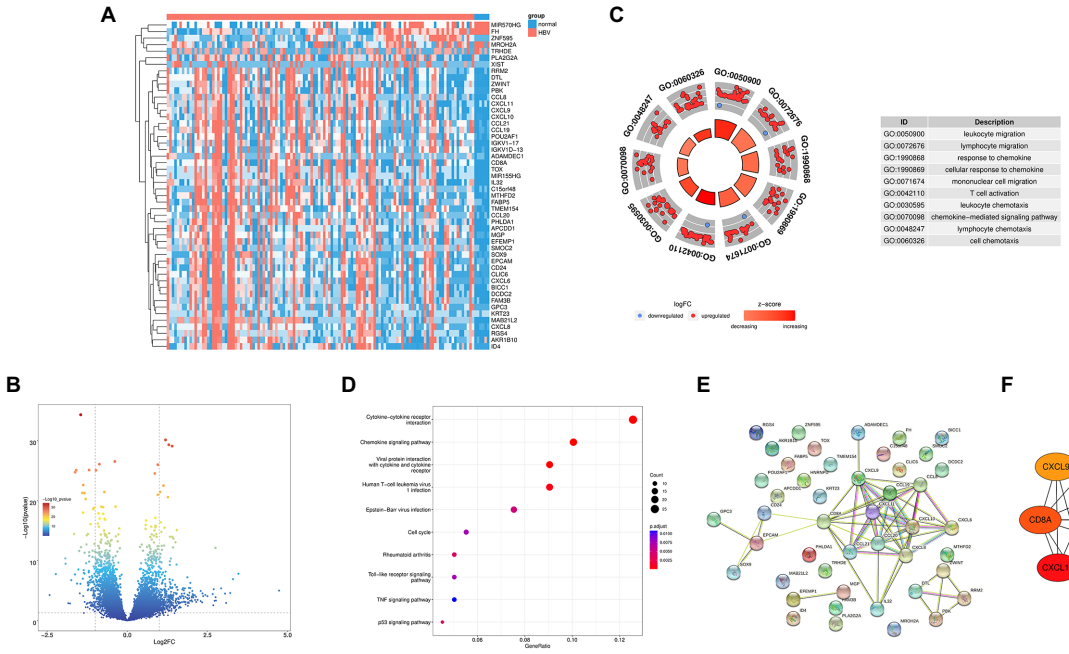

FIGURE 1
Identification of the Hub genes in HBV infection. **(A)** Heat map of top50 differential genes, with blue representing downregulated genes and pink representing upregulated genes; **(B)** Volcanic plot of differentially expressed genes. **(C)** GO analysis diagrams of differential gene; **(D)** KEGG analysis diagrams of differential genes; **(E)** PPI network for top50 differential genes. **(F)** Interaction network for hub genes.

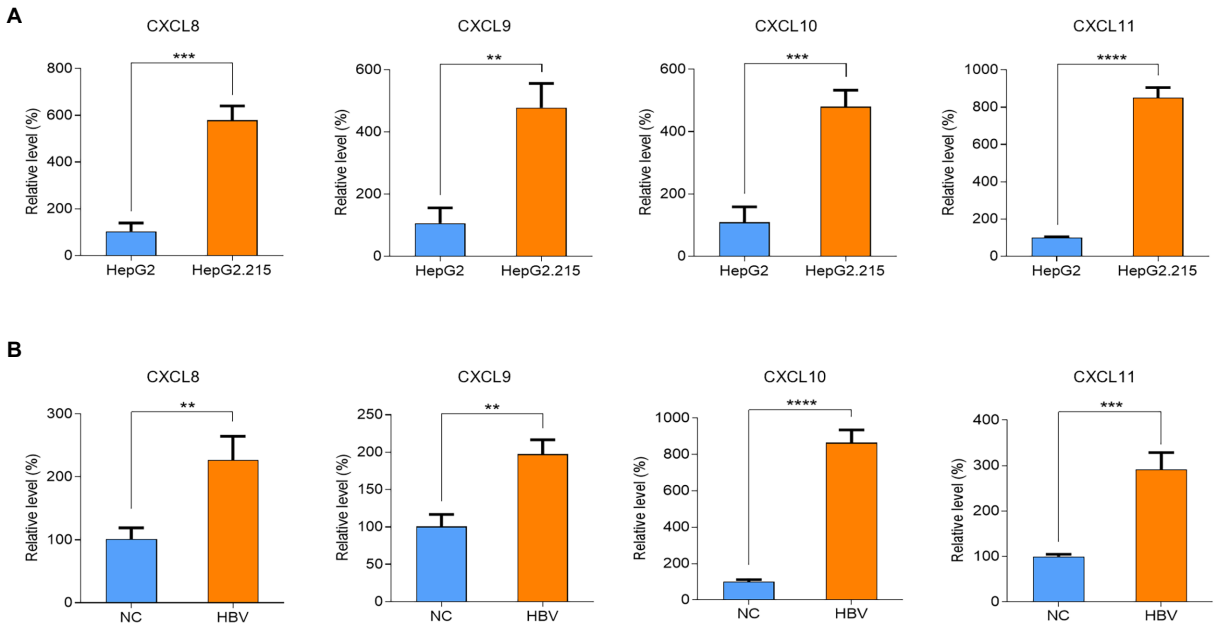

FIGURE 2
Differences of CXCL8, CXCL9, CXCL10 and CXCL11 mRNA levels after HBV infection. **(A)** Validation of CXCL8, CXCL9, CXCL10 and CXCL11 mRNA levels. **(B)** Validation of CXCL8, CXCL9, CXCL10 and CXCL11 mRNA levels after transfection with HBV plasmid. NC refers to HBV control plasmid, HBV refers for HBV 1.3-mer WT replicon plasmid. ** $p<0.01$, *** $p<0.001$, **** $p<0.0001$.

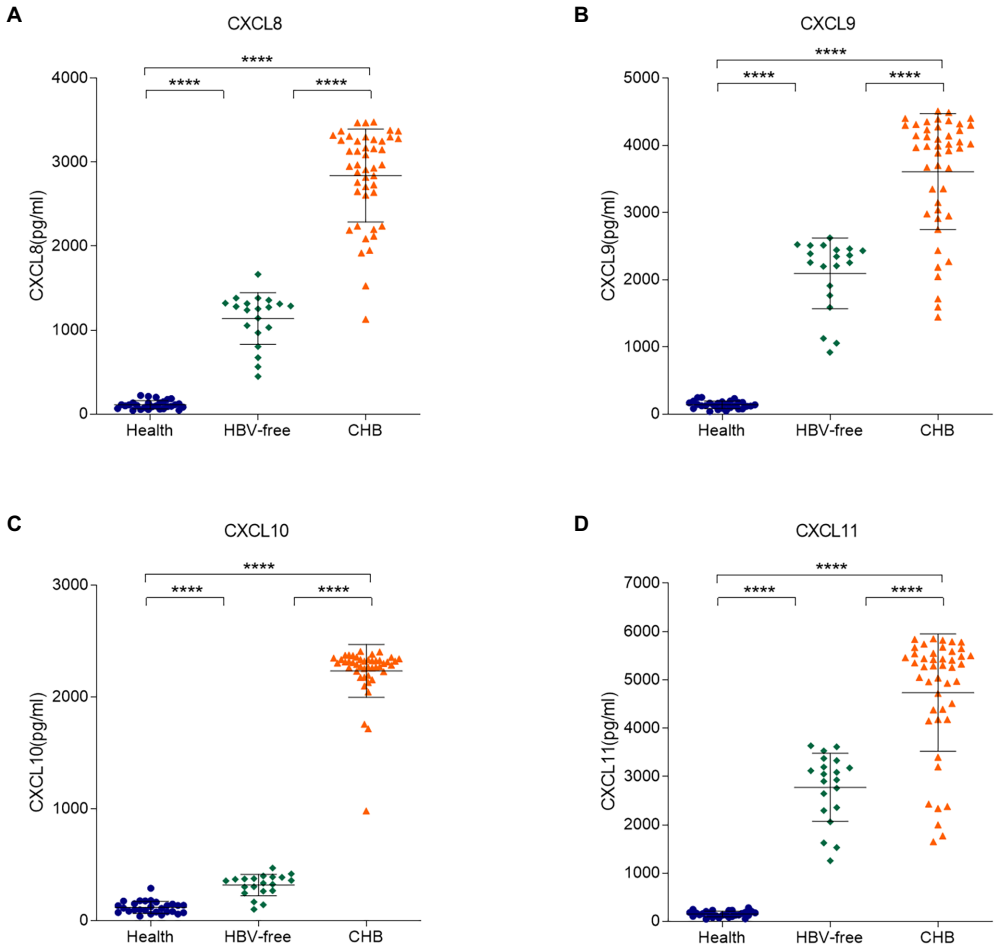

FIGURE 3
Differences in serum levels of CXCL8, CXCL9, CXCL10, and CXCL11 between the HBV-infected, HBV-free and the Healthy groups. The serum levels of **(A)** CXCL8, **(B)** CXCL9, **(C)** CXCL10, and **(D)** CXCL11 in the Healthy group, the HBV-free group and the HBV-infected group were detected by ELISA. The detection limit of CXCL8, CXCL9, CXCL10, and CXCL11 is 12.5–9,000pg./ml, 17.8–12,000pg./ml, 28–3,200pg./ml and 31–16,000pg./ml, respectively. **** $p<0.0001$.

suggested that the changes of CXCL8, CXCL9, CXCL10, and CXCL11 are significantly positive association with HBV infection and indicators related to traditional liver injury related indicators, indicating that these four factors can be used as potential specific predictors of liver injury caused by HBV infection.

The expression of CXCL9, CXCL10, and CXCL11 was elevated in HCC

HBV infection can cause inflammation, and if the patient is not treated effectively, repeated inflammation can lead to further liver damage, progressing to HCC. Therefore, based on GEPIA database, we analyzed the expressions of CXCL8, CXCL9, CXCL10, and CXCL11 in normal tissues and HCC tissues. As shown in Figure 5, CXCL9, CXCL10 and CXCL11 were markedly upregulated in HCC tissues compared with normal tissues, and the differences were statistically significant. In conclusion, CXCL9, CXCL10, and CXCL11 may play a warning role in the early stage of liver injury, so as to prevent the further aggravation of injury and the development of HCC.

Discussion

In recent years, distorted cytokine expression has been found in acute and chronic hepatitis B patients (Ribeiro et al., 2022). Our study found that CXCL8 was disregulated in HBV infection. In addition, the chemokines CXCL9, CXCL10, and CXCL11 were also predicted to play an important role in HBV infection. Chemokines are necessary for leukocyte migration during inflammation, and are closely related to the localization of leukocytes in lymphatic follicles and specific organs and tissues (Vanheule et al., 2015). Chemokines are mainly induced by inflammatory cytokines, growth factors, and pathogenic

TABLE 2 Comparison of differences between the Healthy group, the HBV-free group and the CHB group.

Indexes	Healthy group ($n = 28$)	HBV-free group($n = 20$)	CHB group ($n = 45$)	Healthy vs. CHB *t* value	Healthy vs. CHB *p* value	HBV-free vs. CHB *t* value	HBV-free vs. CHB *p* value
Age	39.36 ± 1.4500	43.25 ± 2.8040	35.73 ± 1.4930	1.638	0.1059	2.581	0.0122
TBIL	13.23 ± 0.6905	11.32 ± 0.9489	15.78 ± 1.1730	1.612	0.1113	2.381	0.0203
DBIL	2.38 ± 0.1391	2.31 ± 0.2913	2.73 ± 0.1860	1.349	0.1815	1.245	0.2179
IBIL	10.85 ± 0.5816	8.80 ± 0.7396	13.05 ± 1.0030	1.629	0.1077	2.676	0.0095
TP	71.40 ± 0.7522	69.99 ± 1.7410	71.31 ± 0.6065	0.0951	0.9245	0.8957	0.3738
ALB	42.31 ± 0.3893	42.12 ± 0.9505	42.52 ± 0.3661	0.3694	0.7129	0.4829	0.6308
γ-GT	37.07 ± 6.5700	32.28 ± 3.7140	29.70 ± 3.4390	1.089	0.2799	0.4497	0.6545
ALT	20.01 ± 2.3380	31.51 ± 2.6540	33.57 ± 4.7790	2.137	0.036	0.2779	0.782
AST	20.36 ± 1.1490	25.08 ± 1.0280	26.33 ± 1.6710	2.585	0.0118	0.4801	0.6328
AST/ALT	1.21 ± 0.0766	0.85 ± 0.0459	1.05 ± 0.0762	1.421	0.1598	1.656	0.1027
GLB	29.09 ± 0.6338	27.80 ± 0.9000	28.79 ± 0.4340	0.4011	0.6896	1.119	0.2673
A/G	1.48 ± 0.0355	1.53 ± 0.0491	1.49 ± 0.0247	0.384	0.7021	0.8495	0.3988
HBeAg	0.12 ± 0.0017	0.10 ± 0.0021	179.90 ± 63.8200	2.216	0.0299	1.87	0.0661
HBeAb	1.21 ± 0.0966	1.25 ± 0.1408	0.89 ± 0.2505	0.9641	0.3383	0.9153	0.3635
HBcAb	1.51 ± 0.2016	1.29 ± 0.2546	0.05 ± 0.0364	8.849	<0.0001	7.042	<0.0001
CXCL8	112.80 ± 9.5560	227.8 ± 13.7800	2,842 ± 82.5600	25.94	<0.0001	20.96	<0.0001
CXCL9	140.40 ± 10.6700	2096 ± 117.7000	3,609 ± 128.6000	21.2	<0.0001	7.252	<0.0001
CXCL10	118.70 ± 10.1700	317.9 ± 21.4100	2,234 ± 35.2300	46.5	<0.0001	34.88	<0.0001
CXCL11	153.10 ± 11.5500	2,774 ± 157.8000	4,735 ± 181.4000	19.86	<0.0001	6.709	<0.0001

Comparisons were made using *t*-test analysis.

TBIL, total bilirubin; DBIL, direct bilirubin; IBIL, indirect bilirubin; TP, total protein; ALB, albumin, γ-GT γ-glutamyl transpeptidase; ALT, alanine aminotransferase; AST, aspartate transaminase; AST/ALT, ratio of aspartate aminotransferase to alanine aminotransferase; GLB, globulin, A/G ratio of albumin to globulin; HBeAg, hepatitis B e antigen; HBeAb, hepatitis B e antibody; HBcAb, hepatitis B core antibody.

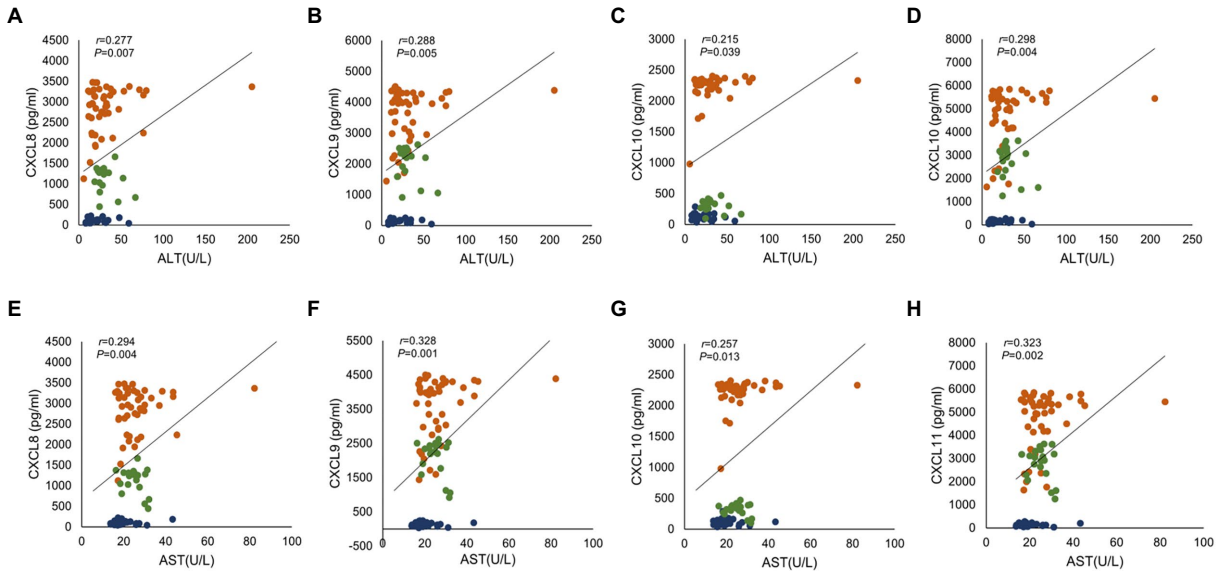

FIGURE 4
The correlation analysis between serum chemokines and ALT and AST. Association of four chemokines with ALT and AST in 28 healthy subjects, 45 CHB patients and 20 HBV-free patients. Correlation with ALT: **(A)** CXCL8, **(B)** CXCL9, **(C)** CXCL10 and **(D)** CXCL11; Correlation with AST: **(E)** CXCL8, **(F)** CXCL9, **(G)** CXCL10 and **(H)** CXCL11. Orange indicates CHB group, green indicates HBV-free group and blue indicates Healthy group. Comparisons were made using Pearson correlation analysis.

TABLE 3 Correlation analysis of serum chemokines expression levels with biochemical indexes and HBV infection related indexes.

	CXCL8		CXCL9		CXCL10		CXCL11	
	r	*p*	*r*	*p*	*r*	*p*	*r*	*p*
AST/ALT	**−0.211**	0.042	**−0.219**	0.035	−0.101	0.333	**−0.246**	0.018
TBIL	**0.238**	0.022	0.158	0.13	**0.274**	0.008	0.189	0.07
DBIL	0.19	0.068	0.139	0.185	0.194	0.062	0.168	0.107
IBIL	**0.242**	0.019	0.156	0.134	**0.287**	0.005	0.185	0.076
HBeAg	**0.288**	0.005	**0.249**	0.016	**0.306**	0.003	**0.205**	0.048
HBcAb	**−0.575**	<0.0001	**−0.521**	<0.0001	**−0.638**	<0.0001	**−0.512**	<0.0001

Association of four chemokines with biochemical indexes and HBV infection related indexes in 28 healthy subjects, 45 CHB patients and 20 HBV-free patients. Comparisons were made using Pearson correlation analysis.

ALT, alanine aminotransferase; AST, aspartate transaminase, AST/ALT, ratio of aspartate aminotransferase to alanine aminotransferase; TBIL, total bilirubin; DBIL, direct bilirubin; IBIL indirect bilirubin; HBeAg, hepatitis B e antigen; HBcAb, hepatitis B core antibody.

Bold values indicate that the group of comparisons is statistically significant.

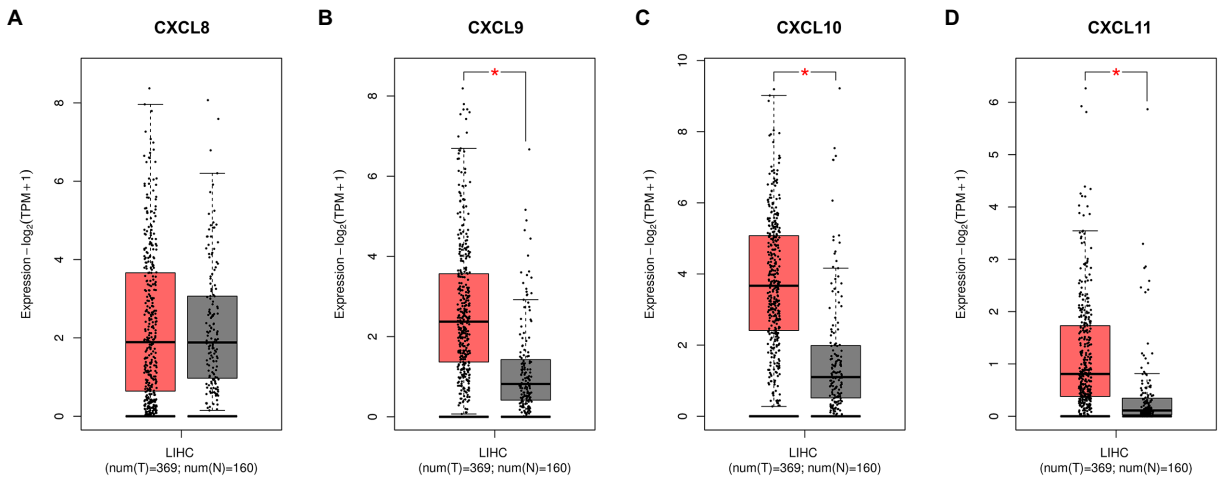

FIGURE 5
The differences of serum chemokines between normal tissues and HCC tissues. Differences in **(A)** CXCL8, **(B)** CXCL9, **(C)** CXCL10, and **(D)** CXCL11 levels between normal tissues and HCC tissues, based on GEPIA database. HCC tissue is shown in red and normal tissue is shown in gray. Expression-$\log_2$ (TPM+1) indicates the expression level of corresponding genes in HCC tissues and normal tissues. Asterisk (*) in red indicates $p<0.05$.

microorganisms (Reid-Yu et al., 2015), which can be divided into four subtypes: C, CC, CXC, and CX3C, according to the position of the NH2 terminal cysteine (Hughes and Nibbs, 2018). CXCL8, CXCL9, CXCL10, and CXCL11 are members of the CXC family. They are the inflammatory chemokines that participate in cell migration and the inflammatory response.

CXCL8, also known as interleukin 8 (IL-8) and neutrophil activator (NAF), is a multifunctional proinflammatory chemokine that activates neutrophils and sends recruitment signals through concentration gradients to recruit activated neutrophils to inflammatory sites (Xu et al., 2016; Asokan and Bandapalli, 2021). Many studies have shown that high levels of CXCL8 can be detected in the serum of HBV-infected patients (Pollicino et al., 2013). HBV can directly target the CXCL8 promoter and regulate the expression of CXCL8 through epigenetic modifications, but the protein of hepatitis B virus X (HBx) encoded by HBV can promote the increase of CXCL8 expression through the MEK–ERK signal pathway (Pollicino et al., 2013; Zhang et al., 2021). We used an HBV stable and transient cell model to detect the relationship between HBV and CXCL8 expression. The results showed that CXCL8 expression was significantly upregulated in the presence of the HBV genome. We further analyzed CXCL8 expression in serum samples from CHB patients, and found that the levels of CXCL8 released into the serum was significantly higher in CHB patients than in Healthy group. To investigate the possibility of CXCL8 as a predictor of liver-damaging diseases caused by HBV infection, we conducted a correlation analysis between CXCL8 and liver injury related indexes (ALT, AST), which showed a positive correlation. All these results confirmed that CXCL8 could be used to predict liver-damaging diseases caused by HBV infection.

Our results showed that there was no difference in CXCL8 expression between normal tissues and HCC tissues, but we confirmed that HBV infection may increase the expression of CXCL8 in both cell experiments and clinical blood samples. In addition, studies have shown that CXCL8 is related to the

occurrence and development of HCC (Xu et al., 2021). HBV-induced CXCL8/CXCR1/TGF-β signaling cascade can mediate HCC vascular invasion and local microenvironment immune escape to induce intrahepatic metastasis of HCC (Zhang et al., 2021). CXCL8 can also promote up-regulation of integrin β3 and enhance the invasion ability of HCC cells through the PI3K/AKt pathway (Sun et al., 2019). In conclusion, CXCL8 may plays an important role in the occurrence and development of liver injury diseases caused by HBV infection.

It has been reported that CXCL9, CXCL10, and CXCL11 all play an important role in HBV infection and exert signaling functions through C-X-C motif chemokine receptor 3 (CXCR3) receptors (Yoshio et al., 2018). Studies have shown that these three chemokines correlate significantly with serum alanine aminotransferase (Lian et al., 2014). Their main function is chemotactic, recruiting immune cells to sites of inflammation for repair and enhancing the T-cell response to viral infection (Macura et al., 2016; Vanheule et al., 2017; Marcovecchio et al., 2021). Several studies have shown that CXCL9, CXCL10, and CXCL11 are associated with HBV infection. For example, HBx binds to its promoter by activating NF-κB, which induces CXCL9 transcription and promotes leukocyte migration to the HBV-infected liver (Xia et al., 2009). CXCL10 was found to be the strongest signal marker that can be used to characterize the stage of chronic HBV infection (Wiegand et al., 2019). The increase in CXCR3-related chemokines (including CXCL9, CXCL10, and CXCL11) may be associated with the migration of tumor necrosis factor-associated apoptosis-inducing ligand CD56 natural killer (NK) cells to the liver (Jiang et al., 2021).

In addition, these three chemokines play a key role in liver-damaging diseases such as hepatocellular carcinoma. Tumor-associated dendritic cells can produce high levels of CXCL9, which promotes tumor progression by increasing programmed death-ligand 1 (PD-L1) expression through the activation of CXCR3-related signals (Marcovecchio et al., 2021). Transwell assays showed that silencing CXCL10 significantly inhibited the migration of MHCC97H cells, suggesting that CXCL10 promotes the invasion and metastasis of HCC cells (Srivastava et al., 2017). Moreover, CXCL11 is highly associated with tumor formation, progression, metastasis, and angiogenesis, as well as with the adverse effects of chemotherapy (Bandapalli et al., 2012). Cancer-associated fibroblasts secrete significantly higher levels of CXCL11 than normal fibroblasts (NFs), and CXCL11 expression is significantly elevated, indicating that CXCL11 can promote HCC cell migration (Liu et al., 2021). It has been shown that CXCL9, CXCL10, and CXCL11 expression increases after HBV infection, which positively correlates with ALT levels (Jiang et al., 2021). In addition, CXCL9, CXCL10, and CXCL11 are related to the migration of TRAIL CD56$^{+bright}$ NK cells that promote liver injury to the liver in chronic hepatitis B-associated cirrhosis (Lian et al., 2014; Okuhara et al., 2014; Yoshio et al., 2018; Jiang et al., 2021).

ALT and AST are probably the most commonly used biomarkers in clinical diagnosis and research involving liver injury, they catalyze the transfer of an amino group from an amino acid to α-ketoglutarate and the reaction products are L-glutamate and either pyruvate or oxaloacetate, respectively (McGill, 2016). AST is mainly present in myocardium, followed by liver. The exclusive production site of ALT is liver, where the content of ALT was the highest (Kolahdoozan et al., 2020). It is generally thought that aminotransferase elevations are due to cell damage with plasma membrane disruption (Kolahdoozan et al., 2020). When liver tissue damage or destruction increases or cell membrane permeability changes, ALT leaks into the circulation, leading to the increase of the expression level of ALT factor in serum (Nguyen et al., 2014). Therefore, ALT and AST, initially considered markers of liver damage, are increasingly being considered indicators of "liver metabolic function." (Sookoian and Pirola, 2012; Sookoian and Pirola, 2015). Kechagias et al. (2008) showed that fast-food-based hyper-alimentation in combination with a sedentary lifestyle resulted in elevated serum ALT levels. Moreover, the authors showed that this elevated transaminase is not associated with the development of hepatic steatosis. This finding reinforces the hypothesis that increased ALT activity is an adaptive response to the metabolic demands of the liver (Sookoian and Pirola, 2012, 2015). Therefore, there is an urgent need to explore new and reliable biomarkers of liver injury. In order to reflect the advantages of CXCL8, CXCL9, CXCL10, and CXCL11 in HBV infection-related liver injury compared with ALT, we set the HBV-free group as the disease control group. The subjects of HBV-free group were chronic hepatitis patients without HBV infection and whose ALT levels were comparable to those of patients in the CHB group, including drug-induced liver injury, autoimmune liver disease, alcoholic liver disease and so on. The results showed that CXCL8, CXCL9, CXCL10, and CXCL11 was slightly increased in the HBV-free group compared with the Healthy controls. It was considered that the possible cause was the presence of a certain degree of liver inflammation in patients in the HBV-free group. Therefore, some inflammatory factors in serum are elevated, which is consistent with the reports in the report (Seki and Schwabe, 2015; Czepielewski et al., 2017). However, in this study, serum levels of CXCL8-11 were significantly higher in CHB patients compared to Healthy controls and HBV-free groups. Therefore, CXCL8, CXCL9, CXCL10, and CXCL11 has obvious advantages in HBV-related liver injury compared with traditional ALT markers, suggesting the importance of these four chemokines as a liver injury associated with HBV infection.

In addition, Du et al. found that the bilirubin level in HBsAg-positive group was higher than that in HBsAg-negative group (Du et al., 2016). Consistent with the findings in this report, we found significant differences in TBIL and IBIL between HBV-free and CHB groups. TBIL and IBIL expression was found to be elevated in liver injury (Yang et al., 2016). Our results showed that TBIL and IBIL expression was significantly higher in the CHB group compared to the HBV-free group. In HBV infection, ALT conveys limited information, which can only indicate the liver injury caused by viral factors. However, the result of HBV infection is not only dependent on viral factors, but also related to host factors, such as the immune response of the body (Ribeiro et al., 2022). CXCL8, CXCL9, CXCL10, and CXCL11 can recruit immune cells to the site of

inflammation to play a role in clearing pathogens. When inflammation persists, these inflammatory cells will aggravate liver parenchymal cell damage. Therefore, the changes in the expression of these four chemokines can not only reveal the liver injury caused by the virus, but also reflect the strength of the immune function of patients, which has a good indication for the direction of the prognosis of inflammation caused by HBV infection and inflammation-related complications.

Importantly, recurrent inflammation caused by CHB can promote hepatocarcinogenesis. The association between tumors and chemokines has been a hot topic in recent studies on the mechanism of inflammatory cancer transformation (Greten and Grivennikov, 2019; Hou et al., 2021). Based on the results, it is hypothesized that the expression of chemokines CXCL8, CXCL9, CXCL10, and CXCL11 increases after HBV infection, and these four chemokines signal the inflammation as the center and build a concentration gradient to promote the migration of neutrophils and immune cells to the inflammation site to clear the damaged liver parenchyma cells. However, when there is long-lasting inflammation, neutrophils and immune cells are continuously recruited, causing damage to the liver parenchyma, eventually leading to serious irreversible hepatocellular carcinogenesis. Previous studies only focused on a single factor. Our results are the first to link these four chemokines to HBV infection, revealing that all four chemokines are elevated in HBV infection and can be used as predictors of liver-damaging diseases caused by HBV infection. As a key member of the innate immune system, NK cells are the main lymphocytes in liver and play an important role in the immunity of liver diseases (Sun et al., 2015). Chemokines CXCL8, CXCL9, CXCL10, and CXCL11 can promote the directed migration of NK cells during inflammation (Robertson, 2002). In addition, previous studies have found that NK cells can produce CXCL8 factor after activation to promote the chemotaxis of T cells (Robertson, 2002). CXCL10 can enhance the cytolytic activity of NK cells by promoting the release of cytotoxic particles (Taub et al., 1995). Therefore, we hypothesized that the elevated expression of these four chemokines in liver injury caused by HBV infection may be related to the recruited NK cells. However, its specific molecular mechanism and the synergistic effect of these four chemokines in HBV infection remains to be explored. Therefore, we will continue to investigate the synergistic effect of the four chemokines in HBV infection and the mechanism of exacerbating the inflammatory response.

In conclusion, chemokines participate in various cellular processes and the regulation of viral infection, leading to inflammatory injury. Therefore, CXCL8, CXCL9, CXCL10, and CXCL11 are expected to become reliable predictors of liver-damaging diseases caused by HBV infection to facilitate timely intervention measures in clinical treatment and avoid further aggravation of liver injury.

Data availability statement

The original contributions presented in the study are included in the article/supplementary material, further inquiries can be directed to the corresponding authors.

Ethics statement

The studies involving human participants were reviewed and approved by the Research Ethics Board of the Eighth Affiliated Hospital of Sun Yat-sen University. The patients/participants provided their written informed consent to participate in this study.

Author contributions

XY, YC, and LC: data analysis and manuscript writing. KY: data analysis. XW, LL, and YZ: data collection and management. XK, WL, ZL, YaL, and YuL: data collection. CB: data collection and grant support. CW: data management. AZ: manuscript writing and editing, grant support. All authors contributed to the article and approved the submitted version.

Funding

This work was supported by the National Natural Science Foundation of China (82072267, 82272271, 82172215, and 81871562), Science and Technology Project of Guangdong Province (2021A1515011396 and 2021A1515012109) and Shenzhen Futian District Public Health Research Project (FTWS2020017 and FTWS2020008).

Acknowledgments

All authors would like to acknowledge the Eighth Affiliated Hospital of Sun Yat-sen University (Shenzhen, China) for providing the patient samples.

Conflict of interest

The authors declare that the research was conducted in the absence of any commercial or financial relationships that could be construed as a potential conflict of interest.

Publisher's note

References

Asokan, S., and Bandapalli, O. R. (2021). CXCL8 signaling in the tumor microenvironment. *Adv. Exp. Med. Biol.* 1302, 25–39. doi: 10.1007/978-3-030-62658-7_3

Bandapalli, O. R., Ehrmann, F., Ehemann, V., Gaida, M., Macher-Goeppinger, S., Wente, M., et al. (2012). Down-regulation of CXCL1 inhibits tumor growth in colorectal liver metastasis. *Cytokine* 57, 46–53. doi: 10.1016/j.cyto.2011.10.019

Czepielewski, R. S., Jaeger, N., Marques, P. E., Antunes, M. M., Rigo, M. M., Alvarenga, D. M., et al. (2017). GRPR antagonist protects from drug-induced liver injury by impairing neutrophil chemotaxis and motility. *Eur. J. Immunol.* 47, 646–657. doi: 10.1002/eji.201646394

Du, M., Zhang, S., Xiao, L., Xu, Y., Liu, P., Tang, Y., et al. (2016). The relationship between serum bilirubin and elevated fibrotic indices among HBV carriers: a cross-sectional study of a Chinese population. *Int. J. Mol. Sci.* 17:2057. doi: 10.3390/ijms17122057

Gao, Q., Zhu, H., Dong, L., Shi, W., Chen, R., Song, Z., et al. (2019). Integrated Proteogenomic characterization of HBV-related hepatocellular carcinoma. *Cells* 179, 561–577.e22. doi: 10.1016/j.cell.2019.08.052

Greten, F. R., and Grivennikov, S. I. (2019). Inflammation and cancer: triggers, mechanisms, and consequences. *Immunity* 51, 27–41. doi: 10.1016/j.immuni.2019.06.025

Hou, J., Karin, M., and Sun, B. (2021). Targeting cancer-promoting inflammation-have anti-inflammatory therapies come of age? *Nat. Rev. Clin. Oncol.* 18, 261–279. doi: 10.1038/s41571-020-00459-9

Hughes, C. E., and Nibbs, R. (2018). A guide to chemokines and their receptors. *FEBS J.* 285, 2944–2971. doi: 10.1111/febs.14466

Jiang, Y., Qin, S., Wei, X., Liu, X., Guan, J., Zhu, H., et al. (2021). Highly activated TRAIL CD56$^{+bright}$ NK cells are associated with the liver damage in HBV-LC patients. *Immunol. Lett.* 232, 9–19. doi: 10.1016/j.imlet.2020.12.008

Kechagias, S., Ernersson, A., Dahlqvist, O., Lundberg, P., Lindström, T., Nystrom, F. H., et al. (2008). Fast-food-based hyper-alimentation can induce rapid and profound elevation of serum alanine aminotransferase in healthy subjects. *Gut* 57, 649–654. doi: 10.1136/gut.2007.131797

Kolaczkowska, E., and Kubes, P. (2013). Neutrophil recruitment and function in health and inflammation. *Nat. Rev. Immunol.* 13, 159–175. doi: 10.1038/nri3399

Kolahdoozan, S., Mirminachi, B., Sepanlou, S. G., Malekzadeh, R., Merat, S., and Poustchi, H. (2020). Upper Normal limits of serum alanine aminotransferase in healthy population: a systematic review. *Middle East J. Digest. Dis.* 12, 194–205. doi: 10.34172/mejdd.2020.182

Lian, J. Q., Yang, X. F., Zhao, R. R., Zhao, Y. Y., Li, Y., Zhang, Y., et al. (2014). Expression profiles of circulating cytokines, chemokines and immune cells in patients with hepatitis B virus infection. *Hepat. Mon.* 14:e18892. doi: 10.5812/hepatmon.18892

Liu, G., Sun, J., Yang, Z. F., Zhou, C., Zhou, P. Y., Guan, R. Y., et al. (2021). Cancer-associated fibroblast-derived CXCL11 modulates hepatocellular carcinoma cell migration and tumor metastasis through the circUBAP2/miR-4756/IFIT1/3 axis. *Cell Death Dis.* 12:260. doi: 10.1038/s41419-021-03545-7

Macura, S. L., Lathrop, M. J., Gui, J., Doncel, G. F., Asin, S. N., and Rollenhagen, C. (2016). Blocking CXCL9 decreases HIV-1 replication and enhances the activity of prophylactic Antiretrovirals in human cervical tissues. *J. Acquir. Immune Defic. Syndr.* 71, 474–482. doi: 10.1097/QAI.0000000000000891

Marcovecchio, P. M., Thomas, G., and Salek-Ardakani, S. (2021). CXCL9-expressing tumor-associated macrophages: new players in the fight against cancer. *J. Immunother. Cancer* 9:e002045. doi: 10.1136/jitc-2020-002045

McGill, M. R. (2016). The past and present of serum aminotransferases and the future of liver injury biomarkers. *EXCLI J.* 15, 817–828. doi: 10.17179/excli2016-800

Mehrfeld, C., Zenner, S., Kornek, M., and Lukacs-Kornek, V. (2018). The contribution of non-professional antigen-presenting cells to immunity and tolerance in the liver. *Front. Immunol.* 9:635. doi: 10.3389/fimmu.2018.00635

Nguyen, L. H., Chao, D., Lim, J. K., Ayoub, W., and Nguyen, M. H. (2014). Histologic changes in liver tissue from patients with chronic hepatitis B and minimal increases in levels of alanine aminotransferase: a meta-analysis and systematic review. *Clin. Gastroenterol. Hepatol.* 12, 1262–1266. doi: 10.1016/j.cgh.2013.11.038

Okuhara, S., Umemura, T., Joshita, S., Shibata, S., Kimura, T., Morita, S., et al. (2014). Serum levels of interleukin-22 and hepatitis B core-related antigen are associated with treatment response to entecavir therapy in chronic hepatitis B. *Hepatol. Res.* 44, E172–E180. doi: 10.1111/hepr.12287

Peng, Z. P., Jiang, Z. Z., Guo, H. F., Zhou, M. M., Huang, Y. F., Ning, W. R., et al. (2020). Glycolytic activation of monocytes regulates the accumulation and function of neutrophils in human hepatocellular carcinoma. *J. Hepatol.* 73, 906–917. doi: 10.1016/j.jhep.2020.05.004

Pollicino, T., Bellinghieri, L., Restuccia, A., Raffa, G., Musolino, C., Alibrandi, A., et al. (2013). Hepatitis B virus (HBV) induces the expression of interleukin-8 that in turn reduces HBV sensitivity to interferon-alpha. *Virology* 444, 317–328. doi: 10.1016/j.virol.2013.06.028

Reid-Yu, S. A., Tuinema, B. R., Small, C. N., Xing, L., and Coombes, B. K. (2015). CXCL9 contributes to antimicrobial protection of the gut during citrobacter rodentium infection independent of chemokine-receptor signaling. *PLoS Pathog.* 11:e1004648. doi: 10.1371/journal.ppat.1004648

Ribeiro, C., Beghini, D. G., Lemos, A. S., Martinelli, K. G., de Mello, V., de Almeida, N., et al. (2022). Cytokines profile in patients with acute and chronic hepatitis B infection. *Microbiol. Immunol.* 66, 31–39. doi: 10.1111/1348-0421.12947

Robertson, M. J. (2002). Role of chemokines in the biology of natural killer cells. *J. Leukoc. Biol.* 71, 173–183. doi: 10.1189/jlb.71.2.173

Seki, E., and Schwabe, R. F. (2015). Hepatic inflammation and fibrosis: functional links and key pathways. *Hepatology* 61, 1066–1079. doi: 10.1002/hep.27332

Sells, M. A., Chen, M. L., and Acs, G. (1987). Production of hepatitis B virus particles in Hep G2 cells transfected with cloned hepatitis B virus DNA. *Proc. Natl. Acad. Sci. U. S. A.* 84, 1005–1009. doi: 10.1073/pnas.84.4.1005

Sookoian, S., and Pirola, C. J. (2012). Alanine and aspartate aminotransferase and glutamine-cycling pathway: their roles in pathogenesis of metabolic syndrome. *World J. Gastroenterol.* 18, 3775–3781. doi: 10.3748/wjg.v18.i29.3775

Sookoian, S., and Pirola, C. J. (2015). Liver enzymes, metabolomics and genome-wide association studies: from systems biology to the personalized medicine. *World J. Gastroenterol.* 21, 711–725. doi: 10.3748/wjg.v21.i3.711

Srivastava, R., Khan, A. A., Chilukuri, S., Syed, S. A., Tran, T. T., Furness, J., et al. (2017). CXCL10/CXCR3-dependent mobilization of herpes simplex virus-specific CD8+ TEM and CD8+ TRM cells within infected tissues allows efficient protection against recurrent herpesvirus infection and disease. *J. Virol.* 91, e00278–e00217. doi: 10.1128/JVI.00278-17

Sugawara, Y., and Hibi, T. (2021). Surgical treatment of hepatocellular carcinoma. *Biosci. Trends* 15, 138–141. doi: 10.5582/bst.2021.01094

Sun, C., Sun, H., Zhang, C., and Tian, Z. (2015). NK cell receptor imbalance and NK cell dysfunction in HBV infection and hepatocellular carcinoma. *Cell. Mol. Immunol.* 12, 292–302. doi: 10.1038/cmi.2014.91

Sun, F., Wang, J., Sun, Q., Li, F., Gao, H., Xu, L., et al. (2019). Interleukin-8 promotes integrin β3 upregulation and cell invasion through PI3K/Akt pathway in hepatocellular carcinoma. *J. Exp. Clin. Cancer Res.* 38:449. doi: 10.1186/s13046-019-1455-x

Taub, D. D., Sayers, T. J., Carter, C. R., and Ortaldo, J. R. (1995). Alpha and beta chemokines induce NK cell migration and enhance NK-mediated cytolysis. *J. Immunol.* 155, 3877–3888.

Vanheule, V., Boff, D., Mortier, A., Janssens, R., Petri, B., Kolaczkowska, E., et al. (2017). CXCL9-derived peptides differentially inhibit neutrophil migration in vivo through interference with glycosaminoglycan interactions. *Front. Immunol.* 8:530. doi: 10.3389/fimmu.2017.00530

Vanheule, V., Janssens, R., Boff, D., Kitic, N., Berghmans, N., Ronsse, I., et al. (2015). The positively charged COOH-terminal glycosaminoglycan-binding CXCL9(74-103) peptide inhibits CXCL8-induced neutrophil extravasation and monosodium urate crystal-induced gout in mice. *J. Biol. Chem.* 290, 21292–21304. doi: 10.1074/jbc.M115.649855

Wiegand, S. B., Beggel, B., Wranke, A., Aliabadi, E., Jaroszewicz, J., Xu, C. J., et al. (2019). Soluble immune markers in the different phases of chronic hepatitis B virus infection. *Sci. Rep.* 9:14118. doi: 10.1038/s41598-019-50729-5

World Health Organization (WHO) Hepatitis B factsheet (2018). https://www.who.int/news-room/fact-sheets/detail/hepatitis-b (Accessed March 31, 2020).

Xia, L. M., Huang, W. J., Wu, J. G., Yang, Y. B., Zhang, Q., Zhou, Z. Z., et al. (2009). HBx protein induces expression of MIG and increases migration of leukocytes through activation of NF-kappaB. *Virology* 385, 335–342. doi: 10.1016/j.virol.2008.11.042

Xu, R., Bao, C., Huang, H., Lin, F., Yuan, Y., Wang, S., et al. (2016). Low expression of CXCR1/2 on neutrophils predicts poor survival in patients with hepatitis B virus-related acute-on-chronic liver failure. *Sci. Rep.* 6:38714. doi: 10.1038/srep38714

Xu, X., Ye, L., Zhang, Q., Shen, H., Li, S., Zhang, X., et al. (2021). Group-2 innate lymphoid cells promote HCC progression through CXCL2-neutrophil-induced immunosuppression. *Hepatology* 74, 2526–2543. doi: 10.1002/hep.31855

Yang, X., Li, H., Sun, H., Fan, H., Hu, Y., Liu, M., et al. (2017). Hepatitis B virus-encoded MicroRNA controls viral replication. *J. Virol.* 91, e01919–e01916. doi: 10.1128/JVI.01919-16

Yang, J., Yu, Y. L., Jin, Y., Zhang, Y., and Zheng, C. Q. (2016). Clinical characteristics of drug-induced liver injury and primary biliary cirrhosis. *World J. Gastroenterol.* 22, 7579–7586. doi: 10.3748/wjg.v22.i33.7579

Yoshio, S., Mano, Y., Doi, H., Shoji, H., Shimagaki, T., Sakamoto, Y., et al. (2018). Cytokine and chemokine signatures associated with hepatitis B surface antigen loss in hepatitis B patients. *JCI Insight.* 3:e122268. doi: 10.1172/jci.insight.122268

Yuen, M. F., Chen, D. S., Dusheiko, G. M., Janssen, H., Lau, D., Locarnini, S. A., et al. (2018). Hepatitis B virus infection. *Nat. Rev. Dis. Primers.* 4:18035. doi: 10.1038/nrdp.2018.35

Zhang, C., Gao, Y., Du, C., Markowitz, G. J., Fu, J., Zhang, Z., et al. (2021). Hepatitis B-induced IL8 promotes hepatocellular carcinoma venous metastasis and intrahepatic Treg accumulation. *Cancer Res.* 81, 2386–2398. doi: 10.1158/0008-5472.CAN-20-3453

Zhong, S., Zhang, T., Tang, L., and Li, Y. (2021). Cytokines and chemokines in HBV infection. *Front. Mol. Biosci.* 8:805625. doi: 10.3389/fmolb.2021.805625

frontiers | Frontiers in Microbiology

TYPE Original Research
PUBLISHED 25 November 2022
DOI 10.3389/fmicb.2022.1035941

OPEN ACCESS

EDITED BY
Claudia Maria Trombetta,
University of Siena,
Italy

REVIEWED BY
Iti Saraav,
Washington University in St. Louis,
United States
Alexander Larcombe,
University of Western Australia, Australia

*CORRESPONDENCE
Zongyuan Hong
zyhong@wnmc.edu.cn
Shuzhi Zhong
zhongshuzhi2006@163.com

†These authors have contributed equally to this work

SPECIALTY SECTION
This article was submitted to Infectious Agents and Disease, a section of the journal Frontiers in Microbiology

RECEIVED 03 September 2022
ACCEPTED 27 October 2022
PUBLISHED 25 November 2022

CITATION
Xu P, Yang Z, Du S, Hong Z and Zhong S (2022) Intestinal microbiota analysis and network pharmacology reveal the mechanism by which Lianhua Qingwen capsule improves the immune function of mice infected with influenza A virus. *Front. Microbiol.* 13:1035941. doi: 10.3389/fmicb.2022.1035941

Intestinal microbiota analysis and network pharmacology reveal the mechanism by which Lianhua Qingwen capsule improves the immune function of mice infected with influenza A virus

Ping Xu[1,2†], Zhu Yang[1†], Shuangqiu Du[1†], Zongyuan Hong[1*] and Shuzhi Zhong[1*]

[1]Wannan Medical College, Wuhu, China, [2]Nanjing University of Chinese Medicine, Nanjing, China

Objective: Lianhua Qingwen capsule (LHQW) can attenuate lung injury caused by influenza virus infection. However, it is unclear whether the intestinal microbiota plays a role in LHQW activity in ameliorating viral infectious pneumonia. This study aimed to investigate the role of intestinal microbiota in LHQW activity in ameliorating viral infectious pneumonia and its possible mechanisms.

Research design and methods: A mouse model of influenza A viral pneumonia was established by intranasal administration in BALB/c mice. Detection of influenza virus in the lungs, pathological examination of the lungs and small intestine, and biochemical detection of inflammatory indices were performed. The effects of LHQW on intestinal microbiota were evaluated by 16S rRNA gene sequencing. The key components and targets of LHQW were screened *via* network pharmacology and verified through molecular docking, molecular dynamics simulation, and free binding energy calculations.

Results: Body weight decreased, inflammatory factor levels were disturbed, and the lung and intestinal mucosal barriers were significantly injured in the infected group. The alpha diversity of the intestinal microbiota decreased, and the abundance of *Bacteroidetes, Muribaculaceae*_unclassified, and *Streptococcus* decreased significantly. LHQW treatment reduced the viral load in the lungs, rescued body weight and survival, alleviated lung and intestinal mucosal barrier injury, reversed the reduction in the intestinal microbiota alpha diversity, and significantly increased the abundance of *Bacteroidetes* and *Muribaculaceae*. Network pharmacological analysis showed that six active herbal medicinal compounds from LHQW could regulate the intestinal microbiota and inhibit the immune-inflammatory response through the Toll-like receptor (TLR) and nuclear factor-κB (NF-κB) signalling pathways in the lungs.

Conclusion: These results suggest that LHQW is effective for treating influenza A virus infectious pneumonia, and the mechanism is associated with the regulation of the TLR4/NF-κB signalling pathway in the lungs by restoring intestinal microbiota and repairing the intestinal wall.

KEYWORDS

influenza A virus, intestinal microbiota, network pharmacology, TLR4/NF-κB signalling pathway, Lianhua Qingwen capsule

Introduction

In the past two decades, there have been several respiratory virus pandemics, which seriously threaten human health and negatively impact on the national economy and social life worldwide. Influenza viruses circulating in humans are mainly of two subtypes: type A (HA), H1N1, and H3N2. Human seasonal influenza virus A can generate new strains *via* antigenic drift. The new strain overcomes existing immunity in humans, leading to a new influenza epidemic (Caton et al., 1982; Treanor, 2004; Boni, 2008). Another significant way of influenza virus evolution leading to pandemics is the antigenic shift, in which the viral genome is rearranged to produce new subtypes with significant antigenic changes (Webster et al., 1982; Zhang et al., 2017). If the new influenza virus spreads efficiently from person to person, it could lead to a global pandemic. Four classes of antiviral drugs are currently approved worldwide for the treatment of influenza: amamantane derivatives, neuraminidase inhibitors, membrane fusion inhibitors, and RNA-dependent RNA polymerase inhibitors (Li et al., 2022). Due to mutations and rearrangements in the influenza virus genome, the antiviral effect of these drugs is also decreasing (Paules and Subbarao, 2017); therefore, it is necessary to explore new therapeutic strategies.

Lianhua Qingwen capsule (LHQW), a traditional Chinese medicine compound, has complex components and various effects (Liang et al., 2020; Huang et al., 2021; Zhou et al., 2021). The LHQW was first used clinically in 2003. Since then, it has been used to treat atypical pneumonia, severe acute respiratory syndrome coronavirus (SARS-CoV), Middle East respiratory syndrome coronavirus (MERS-CoV), influenza A H1N1 virus, influenza A H3N2 virus, and influenza H7N9 virus infections (Xing and Liu, 2021). In 2020, the LHQW capsule was recommended for COVID-19 treatment in China (Ni et al., 2020; Wu et al., 2020; Zhuang et al., 2020; Li et al., 2021; Hu et al., 2022). Literature and clinical evidence have indicated that LHQW, which ameliorates symptoms of influenza, regulates the expression of cytokines after viral infection, alleviates lung injury, and has protective effects against COVID-19 (Liang et al., 2020; Huang et al., 2021; Shen and Yin, 2021; Hu et al., 2022). LHQW, combined with routine treatment, can be used as synergistic therapy to significantly improve symptoms and reduce the mortality rate of critically ill patients (Wu et al., 2021; Yang et al., 2021). Animal experiments have also confirmed that LHQW can reduce the viral load in the lungs of mice with viral pneumonia, reduce the expression of inflammatory factors in the lungs, and improve lung injury (Xia et al., 2020; Su et al., 2022). It is well known that viral clearance in the lung depends mainly on lymphocytes and macrophages (Bedi et al., 2022; Cammann et al., 2022; Harris and Borg, 2022; McGee et al., 2022; Verma et al., 2022; Wei et al., 2022; Zhang H. et al., 2022; Zhang M. et al., 2022); however, the present findings do not clarify how LHQW reduces the viral load in the lung and improves lung injury with viral pneumonia.

According to TCM theory, the lung and large intestine interact in terms of physiological, pathophysiological, and immune functions. Both belong to the mucosal immune system, although the intestine and respiratory tract are two separate organs. The latest research has indicated that changes in intestinal microbial composition and function are correlated with the development of lung diseases ("intestine–lung axis") (Bulanda and Wypych, 2022; Chen et al., 2022; Melo-Gonzalez et al., 2022; Shi et al., 2022; Wang L. et al., 2022; Wang Z. et al., 2022). Moreover, available data indicate that intestinal microbes are strongly correlated with clinical symptoms and inflammatory indices of severe acute respiratory syndrome coronavirus 2 (SARS-CoV-2) infection (Wang H. et al., 2021; Gutierrez-Castrellon et al., 2022; Sencio et al., 2022; Xavier-Santos et al., 2022). However, the composition and characteristics of the intestinal microbiota altered by LHQW treatment for influenza A virus infection and the relationship between microbiota changes and the antiviral effects of drugs need to be further explored.

This study aimed to investigate the role of intestinal microbiota in LHQW activity in ameliorating viral infectious pneumonia and its possible mechanisms. In this study, 16S rRNA was used to analyze the characteristics of the intestinal microbiota. Computer-aided design technology was used to integrate disease, drug-related genes, and proteins for comprehensive analysis to explore the relationship between microbes and respiratory diseases mediated by LHQW through the "intestine-lung axis" and the potential molecular mechanism of the major active components and targets of LHQW.

Materials and methods

Animal experiment

Reagents and materials

A total of 90 SPF BALB/c mice aged between 6 and 8 weeks (half males and half females) were used in this study. Mice were purchased from Qinglongshan Animal Farm, Jiangning District, Nanjing. The same pathogen-free room was used to accommodate all the mice at 18–25°C and 50–60% humidity. All animal experimental procedures strictly followed the protocol approved by the Ethics Committee of Wannan Medical College (YJS-2020-10-006).

Anti-TLR4 rabbit pAb (A11226, ABclonal Technology Co., Ltd., China), anti-NF-κB p65 rabbit mAb (D14E12, Cell Signaling Technology, United States), anti-phospho-NF-κB p65 (Ser536) anti-rabbit mAb (93H1, Cell Signaling Technology, USA), anti-MyD88 rabbit mAb (D80F5, Cell Signaling Technology, USA), anti-occludin rabbit anti-mouse (ab216327, Abcam, United Kingdom), and anti-ZO1 rabbit anti-mouse (ab216880, Abcam, UK) were used as primary antibodies. The secondary antibody was horseradish enzyme-labelled anti-rabbit IgG [Zsbio ZB-2301]. TRNzol Universal Total RNA Extraction Reagent (DP424, Beijing), Scientific Revertaid First-Strand cDNA Synthesis Kit (10,071,325, Thermo Fisher, USA), and One-Step Prime Script RT–PCR Kit (Perfect Real Time; RR064A, Takara, Japan) were used. Primers were synthesized by Shanghai Shenggong Bioengineering Technology Co., Ltd. Lianhua Qingwen capsules (Z20040063, Yiling, China) and oseltamivir phosphate capsules (H20065415, China Kewei) were used. A nucleic acid protein tester (Biophotometer D30, Germany), high-speed freezing centrifuge (Beckman 64R, USA), and real-time fluorescence quantitative PCR instrument (ABI7500, USA) were used. An enzyme-linked immunosorbent assay (ELISA) test kit for Lipopolysaccharide (LPS) was purchased from Hangzhou Lianke Biotechnology Co., Ltd.

Grouping and administration

The A/Puerto Rico/8/34 (H1N1; PR8) strain was subcultured in chicken embryos. The titer of the amplified virus was 1:440, and the median lethal dose (LD50) was $10^{-2.1}$/50 μl. After the mice were lightly anesthetized with ether, 50 μl of $10^{-2.1}$ LD50 influenza virus solution was evenly dropped into the nostrils of each mouse to establish the model. The control group(control) received nasal drip of normal saline. Mice were randomly assigned to a control group (18) or an infected group (Buckley and Turner, 2018; Zhang et al., 2021). The mice were fed normally after the nasal drip.

The incidence and death of mice were recorded daily. After nasal drip, the mice were randomly assigned to the virus-infected group (infected), 11 mg d^{-1} (LHQW-M) Lianhua Qingwen capsule, 22 mg d^{-1} (LHQW-H) Lianhua Qingwen capsule high-dose group and 395.90 μg d^{-1} oseltamivir group (OSTW) (Figure 1A). There were 9 female and 9 male mice in each group. The drug group was administered 0.2 ml by gavage at the same time for 7 days, whereas the control and infected groups were given the same amount of distilled water by gavage. The gavage volume of mice is 0.1–0.2 ml/10 g, and what we used is 0.2 ml/20 g. Firstly, opened the Lianhua Qingwen capsule, accurately weighed the powder in the capsule, added it to distilled water, and prepared solutions with different final concentrations. Then, stored the prepared solution in a refrigerator at 4°C, and recovered to room temperature half an hour before each gavage. Food consumption was calculated by weighing the added feed with an electronic balance on the same day and the remaining feed on the next day. The total food intake of the cage mice was the amount of feed added minus the remaining amount (Total food intake of each group of mice).

Sample collection and preparation

Mice were anesthetized with ether. Blood was collected from the orbit of each mouse. The mice were sacrificed by cervical dislocation. The abdominal cavity was opened using surgical scissors, and the intestinal canal was dissected. Furthermore, 6 cm jejunum and ileum segments were taken. RNA was extracted from the first 1/2 segment to detect the expression of the inflammatory factor-related mRNAs. The first two segments were fixed in 10% neutral-buffered formalin. The lung tissues of mice were aseptically extracted and evenly divided into three parts. One-third of the total RNA was extracted to detect the expression of inflammatory factor-related mRNA. The other third was homogenized, and the last third was fixed in 10% neutral buffered formalin.

The lung tissue of the mice was aseptically removed, and the connective tissue was trimmed. The blood on the surface was absorbed with filter paper, and the changes in lung organ index were weighed and recorded using an analytical balance. The formulae used in this study were $A = B/C*100\%$, where A represents the lung organ index, B represents the lung weight (mg), and C represents the body weight (g); and $D = (E - F)/G*100\%$, where D represents the inhibition rate of the lung index (%), E represents the average lung index of the infected group, F represents the average lung index of the administration group, and G represents the average lung index of the infected group (Han et al., 2021; Song et al., 2021; Li-Juan et al., 2022; Wei et al., 2022).

Quantitative real-time reverse transcription-PCR was used to detect the expression of related genes

The homogenate supernatants of the lung and small intestine were collected, and the amounts of virus, Interleukin-6 (IL-6), and tumor necrosis factor-α (TNF-α) in the mouse lung were detected using quantitative real-time reverse transcription PCR (qRT-PCR), as was the expression level of Interleukin-1β (IL-1β) and interleukin-10 (IL-10). After homogenization at 4°C and 12,000 RPM, centrifugation was performed for 15 min, after which the

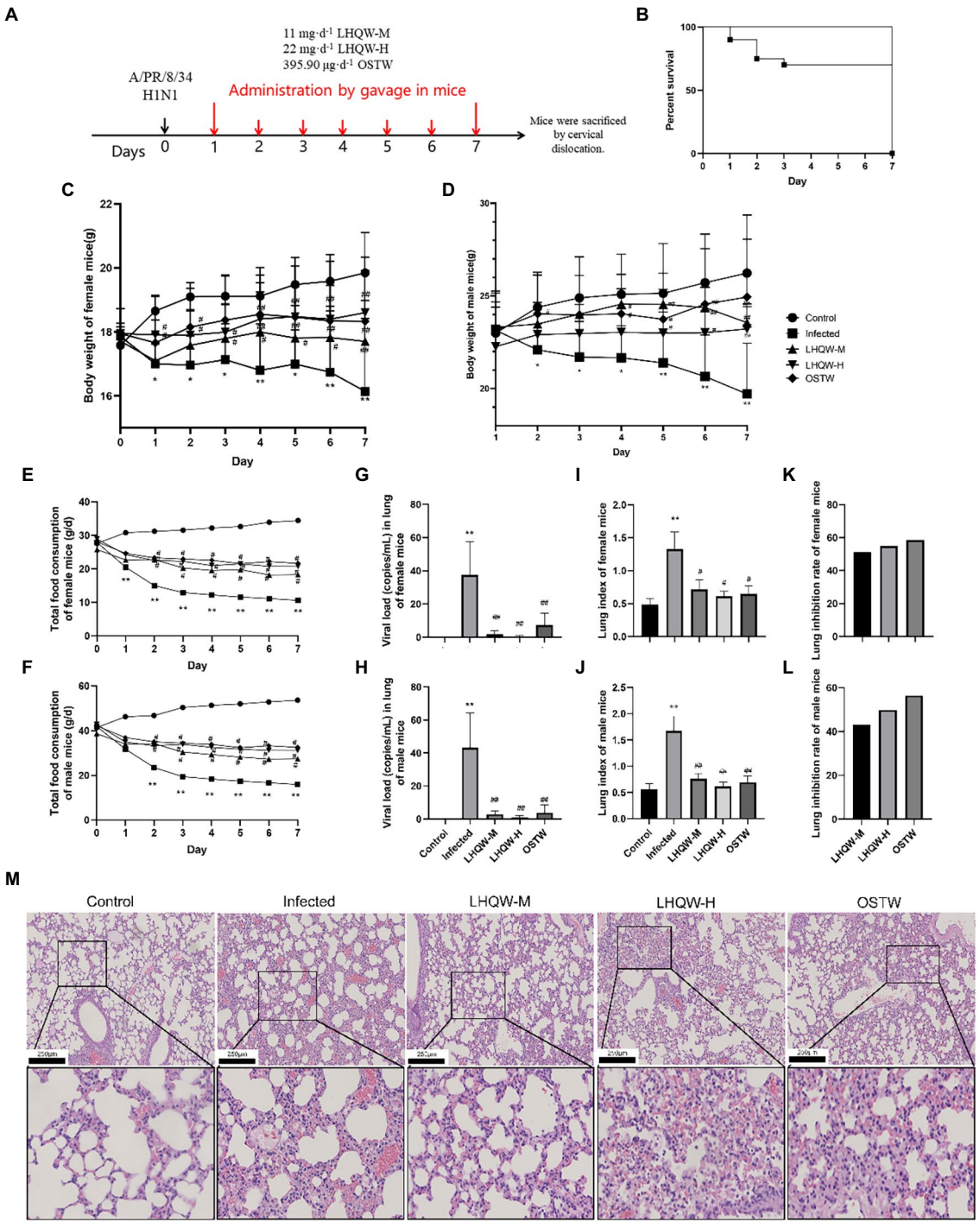

FIGURE 1
LHQW improves lung injury and inflammation. **(A)** Flow diagram; **(B)** Mouse survival curve: The survival rate of mice in other groups except the infected group (72%) were 100%(n=90); **(C)** Weight changes of female mice infected with influenza virus **(G)** (n=45); **(D)** Weight changes of male mice infected with influenza virus (g; n=45); **(E)** Daily changes of total food consumption of female mice in each group (g/d; n=45); **(F)** Daily changes of total food consumption of male mice in each group (g/d; n=45); **(G)** Viral load (copies/mL) in lung tissue of female mice (n=45); **(H)** Viral load (copies/mL) in lung tissue of male mice (n=45); **(I)** Lung index of female mice (n=45); **(J)** Lung index of male mice (n=45); **(K)** Lung inhibition rate of female mice (n=45); **(L)** Lung inhibition rate in male mice (n=45); **(M)** HE staining of mouse lung tissue (200 and 400 times). The mice were randomly assigned to the virus infected group (infected), 11mg·d^{-1} (LHQW-M) Lianhua Qingwen capsule, 22mg·d^{-1} (LHQW-H) Lianhua Qingwen capsule high-dose group and 395.90μg·d^{-1} oseltamivir group (OSTW). Compared with control group, *p<0.05, **p<0.01; Compared with infected group, $^{\#}p$<0.05, $^{\#\#}p$<0.01.

supernatant was collected, isopropanol was added at an equal volume to the supernatant, and the mixture was allowed to stand before centrifugation. The supernatant was discarded, and the precipitate remained.

In addition, 1 ml of 75% ethanol was added to each tube and mixed evenly. The supernatant was then centrifuged, discarded, and dried for 5 min. A total of 60 μl of DEPC-treated water was pipetted repeatedly until it was evenly mixed. The sample was dissolved at room temperature, shaken to properly mix, and centrifuged at a low speed for 10 s. After the system was prepared, 20 μl was centrifuged at a low speed for 10 s, vortexed, properly mixed, and then centrifuged again. The reaction parameters were 95°C for 1 min (preheating), 95°C for 15 s, and 60°C for 30 s (40 cycles), followed by the production of a dissolution curve (95°C for 15 s, 60°C for 1 min, and 95°C for 15 s) using β-actin as an internal reference gene. After the reaction, $2^{-\Delta\Delta Ct}$ and the relative gene expression were calculated using the CT method.

Detection of LPS in serum by ELISA

After 30 min of blood sample agglutination and centrifugation, the serum sample was drawn and stored at −80°C. A concentrated standard sample was used for gradient dilution to prepare a standard curve of the serum sample. All the reagents and samples were maintained at room temperature before testing. After soaking the enzyme standard plate, add the standard, add the standard diluent to the blank well, and add 1 × to the sample well detection buffer 90 and 10 μl of sample. Following the kit instructions, double wavelength detection was performed using a microplate reader to determine the optical density (OD) value at the maximum absorption wavelength of 450 nm and a reference wavelength of 570 nm.

Pathological examination

Paraffin sections of the lung and intestine were stained with H&E and alcian blue. After HE staining, the structure of small intestine wall was observed under light microscope. 10 slices of small intestine were taken from each group of mice. Each slice had 10 visual fields, and digital photography was taken. In each photo, the deepest recess depth (subject to the junction of intestinal gland villi to the base of intestinal gland), the thickest mucosal thickness and muscular layer thickness were measured. The morphology and distribution of goblet cells in the epithelium were observed under light microscope, and the number of goblet cell positive cells distributed in each recess was counted. The expression levels of zonula occludens 1 (ZO-1) and occludin were detected by immunohistochemistry. Pathological sections were randomly photographed at magnifications of 100 × and 200 ×. The OD values of the immunohistochemical images were analyzed using ImageJ software to obtain relative expression.

For immunohistochemistry, the fixed small intestine was removed, embedded in paraffin, cut into 5-μm-thick slices, and H_2O_2 was added and incubated at room temperature for 10 min. After rinsing, 5% bovine serum albumin (BSA) was added and incubated at room temperature for 60 min. Rabbit anti-mouse primary ZO-1 and occludin antibodies were added dropwise without washing before incubation at 4°C overnight. After rinsing, biotinylated sheep anti-rabbit IgG and rabbit anti-goat IgG antibodies were added. The sample was then washed and 3, 3′ diaminobenzidine tetrahydrochloride (DAB) was added at room temperature for 60 min.

For Alcian blue staining, the slices were placed in a drying oven and baked at 66°C for 20–30 min. Three courses of xylene and three courses of ethanol were added successively. Alcian blue staining solution (100 μl) was added dropwise to each slice, which was then dyed in a wet box for 1 h. The staining solution was removed, 100 μl of nuclear solid red staining solution was added to each slice, and sections were washed with water. These samples were passed through three successive passes of ethanol, phenol-xylene, I, and xylene II.

Analysis and characterization of the intestinal microbiota

16S rDNA high-throughput sequencing was performed on the mouse feces collected from each group. The total DNA of bacteria in feces was extracted, and 10 ng of DNA template was used for PCR amplification according to the sequence of the v3–v4 region. The library was constructed using a library building kit, quantified using Qubit and qPCR, and sequenced on a computer. Representative sequences were selected and annotated, and the species were classified using a database.

Western blotting

Fresh small intestinal tissue was collected, and proteins were extracted and quantified. SDS–PAGE, membrane transfer, blocking, and incubation of both primary and secondary antibodies, as well as chemiluminescence and development were carried out. The grayscale of the target protein and internal reference protein was scanned using ImageJ software, and then semiquantitative analysis of the protein content was conducted to obtain NF-κBand p-NF-κB (Phospho NF-κB) levels, as well as the relative expression of Toll-likereceptor4(TLR4) and myeloid differentiation factor 88 (MYD88).

Network pharmacology

Chinese drug compounds were searched in the Traditional Chinese Medicine Systems Pharmacology Database and Analysis Platform (TCMSP) and Traditional Chinese Medicines Integrated

TABLE 1 Statistics of basic information of traditional Chinese Medicine components - com–onents - targets in drug group.

Drug name	Number of components	Number of predicted targets
Radix isatidis	39	575
Mint	10	234
Chinese rhubarb	10	345
Licorice	92	777
Cyrtomium fortunei	7	278
Patchouli	11	307
Rhodiola	26	337
Honeysuckle	23	372
Semen armeniacae amarae	19	398
Forsythia suspensa	23	485
Ephedra	23	348
Gypsum	3	15
Houttuynia cordata	7	278

Database (TCMID). The PubChem database was used to obtain the structures of the described components, which were imported into the Swiss target prediction database. A target with a prediction score greater than 0 was considered the drug target, and the Batman database was used to obtain the components and targets of gypsum. Oral bioavailability (OB) and drug-likeness (DL) were set at ≥ 30% and ≥ 0.18, respectively, in the TCMSP database to screen for effective components in the LHQW drug group. Finally, the components of Rhodiola in the TCMID database and gypsum in the Batman database were searched (Table 1).

A total of 253 potentially active components were obtained, and 1,077 drug targets were screened. The GeneCards database was searched using "influenza virus" as the keyword. The targets were selected with an evaluation score greater than 10, and the disease targets were obtained after the removal of weightings.

Cytoscape 3.7.2 software was used to construct the "drug component target disease" network diagram, and a network analyzer was used to analyze the topology of the network diagram. In addition, a PPI cluster analysis diagram was drawn using Cytoscape software. After running the common target in the R language, gene ontology (GO) analysis identified the molecular function, cell composition, biological process, and Kyoto Encyclopedia of Gene and Genome (KEGG) pathway of the top 20 hits.

Molecular docking

The Schrodinger software was used to construct a ligand molecular database for molecular docking. The crystal structure was downloaded from RCSB PDB. The protein structure was imported into Maestro 11.9 platform, and the protein structure was prepared using Schrodinger. The receptor was pretreated, optimized, and minimized (the OPLS3e force field was applied for constraint minimization).

Molecular dynamics simulation

Desmond version 2020 was used for the MD simulation of proteins and compounds. OPLS3e was selected as the molecular force field for the MD simulation, and the TIP3 water model was used to solvate the system. Energy minimization of the entire system was achieved using the OPLS3e force field (all-atomic force field). A Berendsen coupling algorithm was used to create coupling between the temperature and pressure parameters. In the later preparation of the system, 100 ns were run at a time step of 1.2 femtoseconds, and the track was recorded every 10 ps, recording a total of 1,000 frames. The root-mean-square deviation (RMSD) of backbone atoms was calculated, and graphical analysis was performed to illustrate the nature of the interactions between proteins and ligands. The root-mean-square fluctuation (RMSF) of each residue was calculated to determine the major conformational changes in each residue between the initial and dynamic states.

Calculation of MM-GBSA

The basic principle of the molecular mechanics/Poisson Boltzmann (generalized boron) surface area (MM-GBSA) method is to calculate the difference between the binding free energies of two solvated molecules in the binding and free states or to compare the free energies of different solvated conformations of the same molecule.

$$\Delta G^0_{\text{vacuum}} = \Delta E^0_{\text{MM}} - T\Delta S^0 = \left(\Delta E^0_{\text{int}} + \Delta E^0_{\text{vdw}} + \Delta E^0_{\text{ele}}\right) - T\Delta S^0$$

where ΔE^0_{int} includes the bond, bond angle, and dihedral angle energies, ΔE^0_{vdw} is the non-bond van der Waals energy, ΔE^0_{ele} is the nonbond electrostatic energy, and $T\Delta S^0$ is the entropy contribution, which can be obtained by normal mode analysis.

Statistical processing

All statistical analyses were performed using the SPSS software (version 18.0). Measurement data are expressed as $\bar{\chi} \pm$ s. Multiple groups were compared using one-way ANOVA. The LSD-t test was used to compare data between the groups.

Results

Lianhua Qingwen capsule reduces lung injury

In this study, the degree of lung injury was evaluated using the mouse lung index, lung inhibition rate, and lung histology (HE staining). Compared with the control group mice, H1N1 infected

mice (infected group) showed reduced diet (Figures 1E,F) and weight loss (Figures 1C,D). The infected group had a significantly higher lung index ($p < 0.01$, Figures 1I,J), widened alveolar septum in the lung tissue, increased inflammatory cell infiltration, and partially collapsed alveolar cavities (Figure 1M). Compared with the infected group, LHQW reduced the viral load in the lungs ($p < 0.01$, Figures 1G,H) and alleviated the reduction in body weight ($p < 0.05$, $p < 0.01$, Figures 1C,D). The LHQW group had a significantly decreased lung index, reduced inflammatory cell infiltration in the pulmonary alveoli and mesenchyme, and a significantly reduced degree of pulmonary interstitial swelling ($p < 0.01$, Figures 1I–M). The survival rate of mice was significantly higher in the LHQW group (100%) than that in the infected group (72%) (Figures 1B, $p < 0.01$). Body weight change, total daily food consumption of mice, viral load in mouse lung tissue, lung index, and lung inhibition rate were separately classified and counted for female and male mice. According to the results of statistical calculation, the sex difference is not significant ($p > 0.05$), so no sex classification statistics was carried out in the subsequent experiments.

Lianhua Qingwen capsule improves the intestinal microbe community

There were differences between the three groups, indicating no errors in the experimental group (Figure 2A). The stacked bar chart of the intestinal microbiota classification at the phylum and genus levels showed that the intestinal microbiota composition was significantly different (Figures 2B,D). Compared with those in the control group, the four indices of alpha diversity of the intestinal microbiota in the infected group decreased to varying degrees, of which the Simpson index decreased significantly ($p < 0.05$). At the phylum level, the microbiota abundance (*Bacteroidetes*) decreased significantly, and at the genus level, the microbiota abundance (*Muribaculaceae*_unclassified, *Muribaculum*, *Odoribacter*, *Lachnospiraceae*_ UCG-006, *Prevotellaceae*_UCG-001, *Anaeroplasma, Absiella, Eubacterium_coprostanoligenes*_Group, and *Streptococcus*) decreased significantly. Compared with the infected group intervention, LHQW reversed the red function in the four indices to varying degrees, and the Shannon index increased significantly ($p < 0.05$) (Figure 2F). The microbiota abundance (*Bacteroidetes, Muribaculaceae*_unclassified, *Muribaculum, Lachnospiraceae*_ UCG-006, and *Prevotellaceae*_Ucg-001) was significantly higher in the LHQW group and was close to that of the control group ($p < 0.05$).

Lianhua Qingwen capsule reduces intestinal inflammation and improves intestinal mucosal barrier function

HE staining of the small intestine showed that the crypt depth decreased, the muscle layer thinned, and the colon length was shortened in the infected group compared to that in the control group (Figure 3A). Alcian blue staining showed that the number of small intestinal goblet cells and the amount of mucin secreted decreased in the infected group (Figure 3B). Immunohistochemical staining showed reduced expression of ZO-1 (Figure 3C) and occludin (Figure 3D) in the infected group (tan indicates positive expression; Figure 3C). In the LHQW group, the small intestinal crypt depth increased (Figure 3B), the muscle layer thickened (Figure 3C), and the colon length increased compared with that in the infected group (Figure 3A). Alcian blue staining showed that the number of small intestinal goblet cells and the amount of mucin secreted increased in the LHQW group (Figure 3D). LHQW increased ZO-1 and occludin protein expression in the intestinal epithelium. Furthermore, qRT-PCR results showed that IL-6, IL-1β, and TNF-α levels decreased, whereas IL-10 levels increased in the LHQW group compared with those in the infected group (Figure 3E).

Network pharmacology screening results

Network pharmacological screening detected 1,077 drug targets and 421 disease targets. A total of 115 common drug-disease targets were obtained at the intersection of the targets (Figure 4A). The PPI network results were topologically analyzed (Figure 4B), and genes with a degree value greater than the average score were selected as the core targets (Figure 4C).

GO results showed that the intersection gene set was enriched in 2333 biological process pathways (Figure 4D), 89 cell components (Figure 4E), and 144 processes related to molecular function (Figure 4F). A total of 172 KEGG pathways were identified using R language. The top 20 terms in the KEGG enrichment bar graph (Figure 4G) were Posey's sarcoma-associated herpesvirus infection, hepatitis B, lipids and atherosclerosis, AGE-RAGE signalling pathways in diabetes complications, human cytomegalovirus infection, Chagas disease, influenza A virus, toxoplasmosis, measles, C-type lectin receptor signalling pathway, pancreatic cancer, fluid shear stress and atherosclerosis, PD-L1 expression and PD-1 checkpoint pathway in cancer, Toll-like receptor signalling pathway, coronavirus (COVID-19), human T-cell leukemia virus 1 infection, Jerson Prand infection, HIF-1 signalling pathway, TNF signalling pathway, and chemokine signalling pathway. KEGG enrichment analysis showed that infectious diseases mainly caused hair coloring. These results indicate that the Toll-like receptor signalling pathway may be the core mechanism of LHQW-mediated amelioration of influenza A virus infection.

Efficacy analysis of the combination mode and method

AKT1 (PDB ID: 4gv1) target was used to assess the effectiveness of the docking method. The protein had high crystal structure accuracy, no deletion of key residues, clear active sites, and a clear binding mode between small-molecule

10.3389/fmicb.2022.1035941

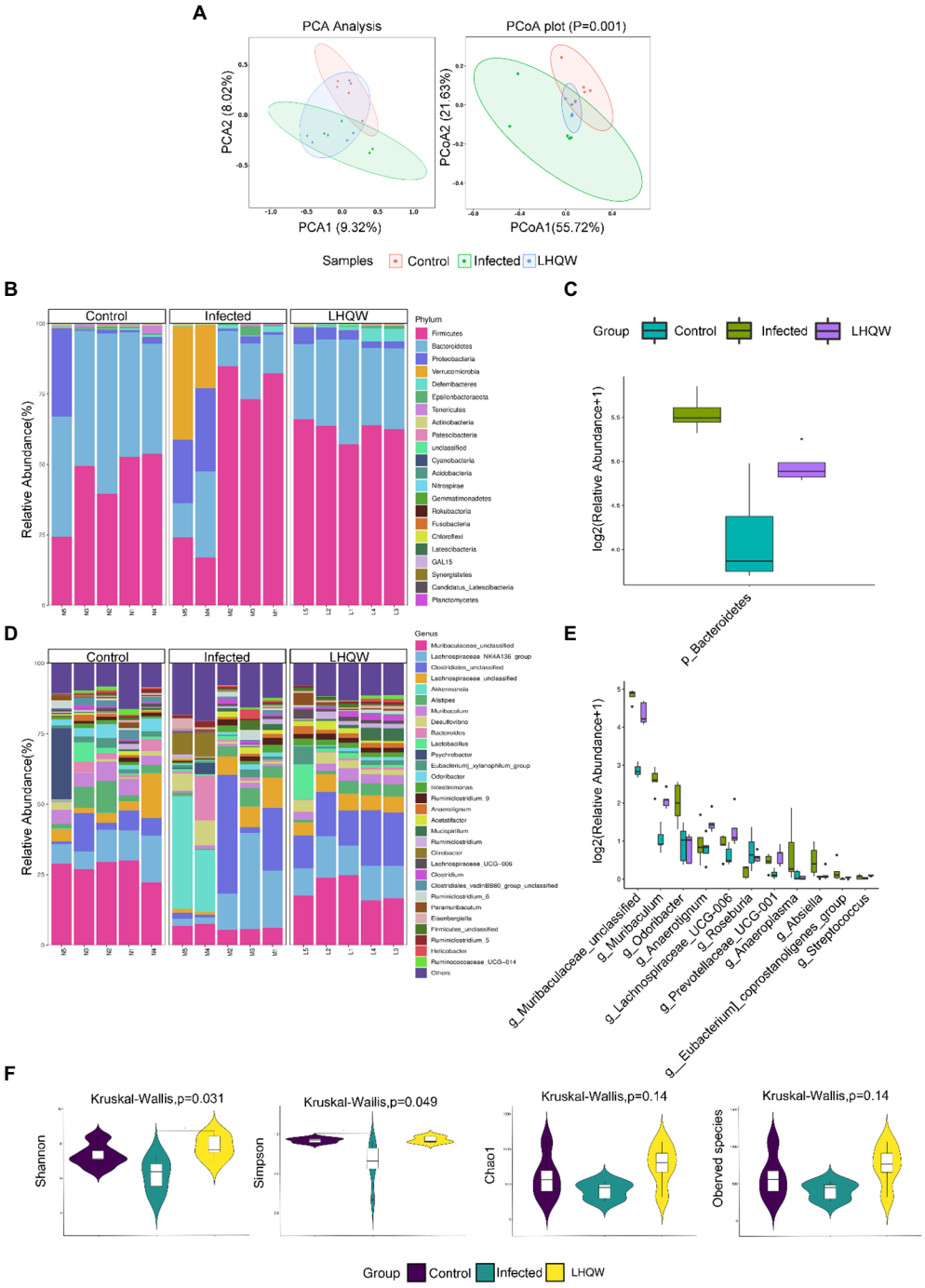

FIGURE 2
LHQW significantly improves the imbalance of intestinal flora induced by H1N1. **(A)** Beta diversity observed using principal component analysis (PCA) and principal coordinates analysis (PCoA). The same group is circled according to the 95% confidencce interval. The closer the distance between the two samples, the more similar the microbial composition structure between the samples and the smaller the difference. The sp©re analyzed at the phylum and genus levels, and those with significant differences were used to draw a box diagram. Using the genus level as an example, the abscissa represents the species with significant difference with a value of p less than 0.05 in the difference analysis, arranged from left to right according to the abundance from high to low. The ordinate represents the relative abundance. The figure shows the relative abundance of each species in each group. The taxonomic distribution of intestinal bacterial composition at the phylum level, including column stacking diagram **(B)** and box line diagram **(C)**; The taxonomic distribution of intestinal bacterial composition at the genus level, including column stacking diagram **(D)** an©ox line diagram **(E)**. **(F)** Alpha diversity indexes, including Chao1, observed species, Shannon, and Simpson indexes. Chao1 and ACE indexes are mainly used to evaluate flora richness. The larger the value, the higher the flora richnes'. Shannon and Simpson's indexes are mainly used to evaluate flora diversity. Higher Shannon index and lower Simpson index indicate higher species diversity of the sample.

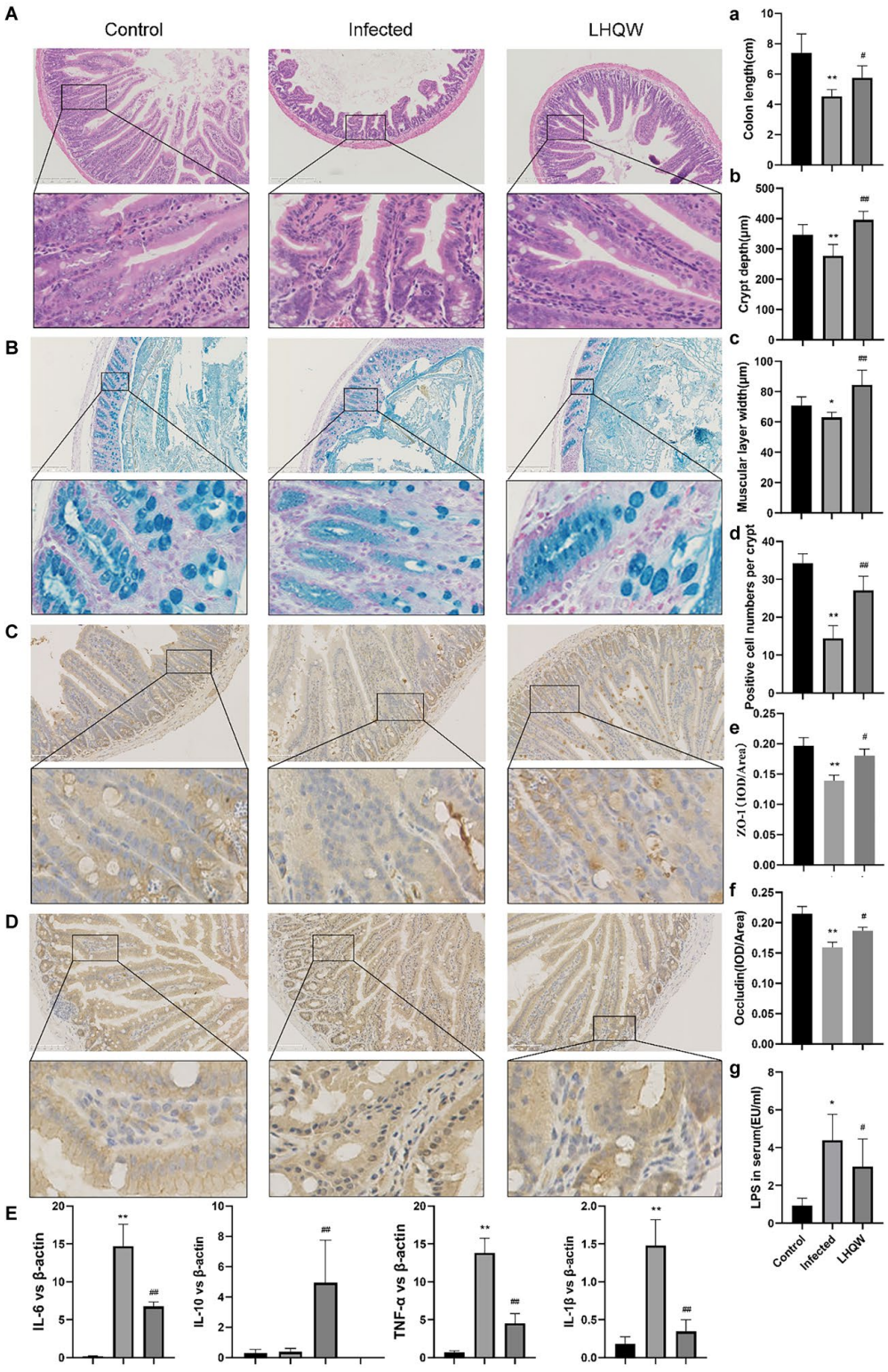

FIGURE 3
LHQW reduces intestinal wall inflammation and improves intestinal mucosal barrier function. **(A)** Small intestinal HE (100 times, 200 times) and **(B)** small intestinal recess depth **(C)** small intestinal muscle layer width according to HE; **(A)** Colon length; **(B,D)** the number of goblet cells; Immunohistochemical staining of intestinal mucosal barrier©otein **(C)** ZO-1 and **(E)** semi-quantitative analysis of Image J, **(D)** immunohistochemical staining of Occludin and **(F)** semi-quantitative analysis of ImageJ. **(G)** The content of LPS in serum of mic©as detected by ELISA. **(E)** the expression of inflammatory cytokines in the small intestinal wall was determined by qRT-PCR (IL-6, IL-1β, IL-10, and TNF-α). Compared with control group, *p<0.05, **p<0.01; Compared with infected group, $^{\#}p$<0.05, $^{\#\#}p$<0.01.

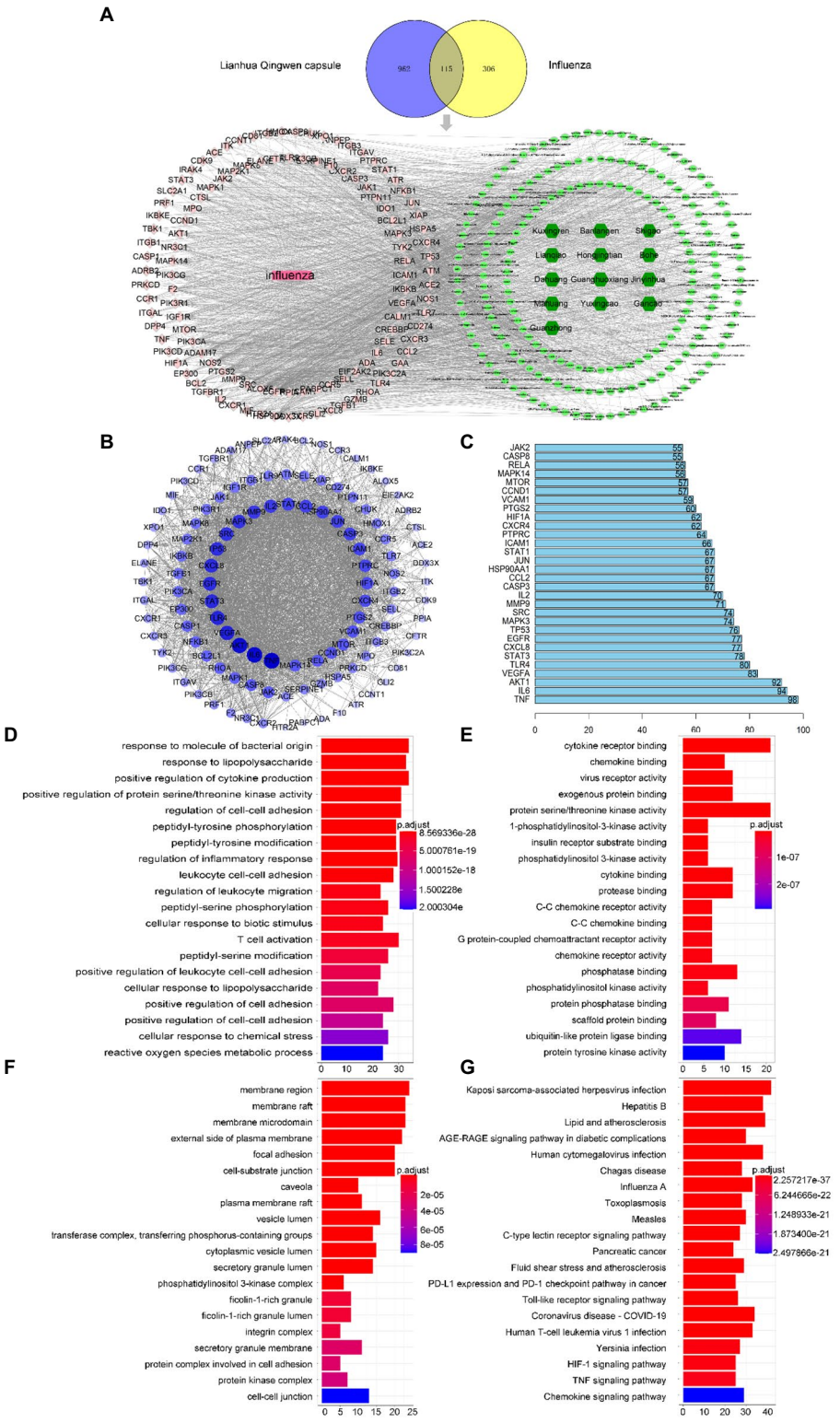

FIGURE 4
Network pharmacology screening results. **(A)** Drug disease comm"n target Wayne diagram and "d"ug component target disease" network diagram. Dark green, light green, pink, and rose red represent drugs, 204 active components in LHQW, 115 common targets, and diseases, respectively. **(B)** PPI network diagram of protein interaction. **(C)** Ranking of core targets based on PPI topology analysis (degree ranks the top 30). GO enrichment analysis of LHQW-treated influenza virus: (©Biological process (BP); **(E)** Cellular component **(CC)**; **(F)** Molecular function (MF). **(G)** The top 20 signaling pathways in the KEGG enrichment analysis.

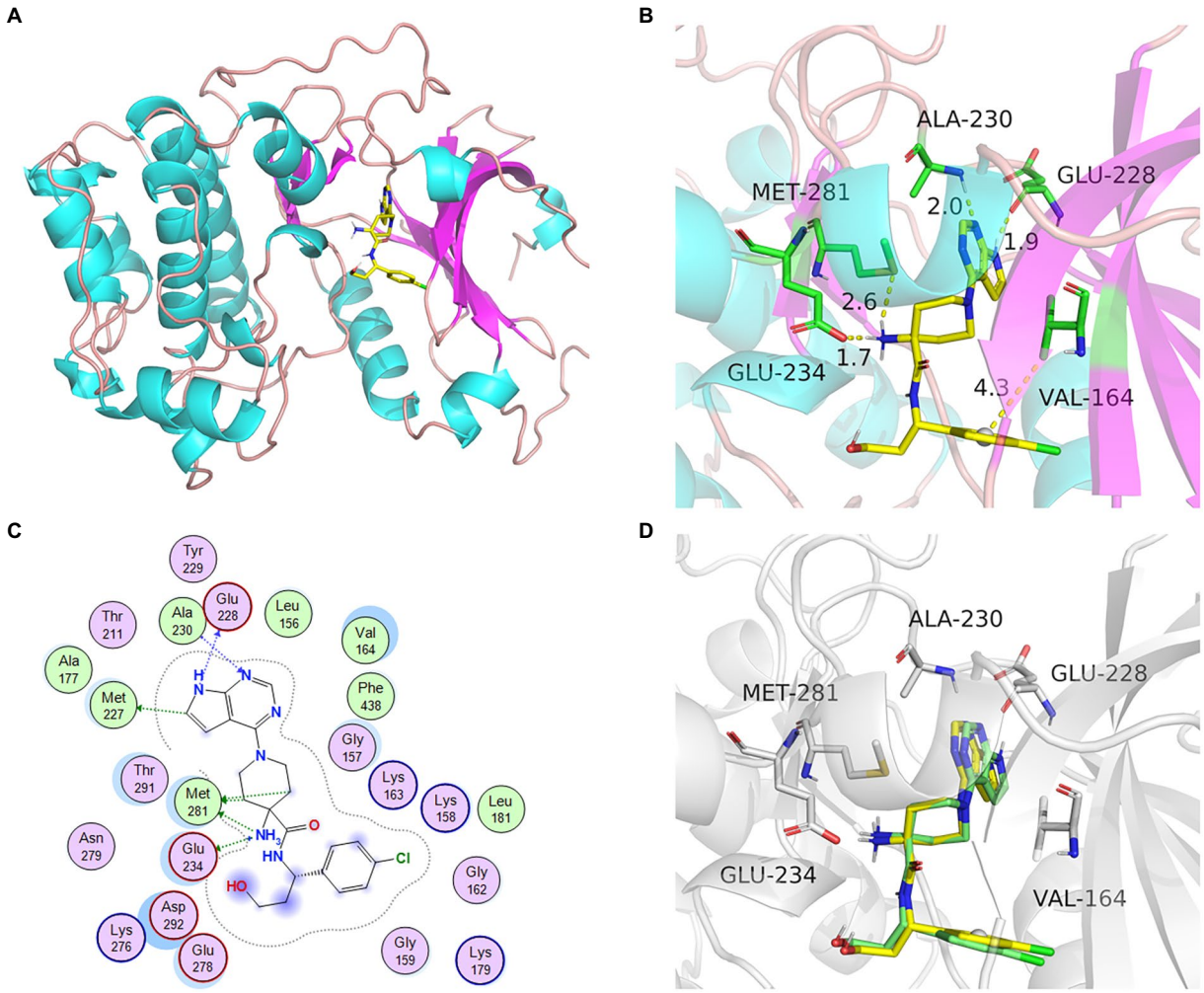

FIGURE 5
The docking model and analysis of AKT1 with natural ligand. **(A)** The overall 3D structure of AKT1 complex. The protein backbone was shown as a tube and colored bright blue and pink. The ligand was shown in stick and colored element. **(B)** A close view of the active site binding with natural ligand. Key residues interacting with ligand were shown as sticks and colored green. **(C)** The 2D protein-ligand interaction diagram of ligand-AKT1 complex. Protein residues were shown as circles and colored based on their properties: green, hydrophobic residue; purple, polar residue. **(D)** The re-docking results of active compounds with target.

ligands and active sites (Figure 5C). Protoligand molecules can form strong π-π conjugate bonds with key residues (Ala-230, Met-281, Glu-234, Val-164, and Glu-228). For instance, small ligand molecules form strong hydrophobic bonds with Val-164, thereby stabilizing small molecules. Small molecules can also form strong hydrogen bonds with amino acids (Ala-230, Met-281, Glu-234, and Glu-228) with hydrogen bond distances of 2.0, 2.6, 1.7, and 1.9 Å, respectively. They form short hydrogen bonds with strong binding ability, thus stabilizing small molecules in the active protein sites. In this study, known protoligand pairs were linked to the AKT1 binding site to determine a suitable docking method for screening potential active compounds. The binding conformation overlapped well with that of the ligands in the previous complex (Figure 5D), indicating that the screening method was suitable and effective.

Virtual screening results

The top 50 compounds were selected based on the energy score obtained from the docking results. 10 compounds were obtained for each gene target by scoring the binding energy and evaluating the key residues of the active sites (Table 2).

Interaction analysis of small protein molecules

The core active components (204) of LHQW were docked with AKT1, STAT3, TLR4, TNF, VEGFA, and IL6 targets. The PyMOL21 software was used to visualize the complexes formed

by docking. For each target, the compound was selected with the best score for protein targeting and docking (ligand063, ligand113, ligand103, ligand073, and ligand121). The binding mode between the compounds and proteins was then used to visualize the amino acid residues between the compounds and protein pockets.

TABLE 2 The docking results for AKT1, STAT3, TLR4, TNF, VEGFA, and IL6 with top 10 compound.

Target	ID	Name	Degree	Docking score (kcal/mol)
TNF	Ligand103	3-[2′-(5′-Hydroxymethyl) furyl]-1(2H)-isoquinolinone-7-O-BETA-D-glucoside	8	−11.248
	Ligand024	Licochalcone a	15	−11.209
	Ligand055	6-Prenylated eriodictyol	12	−11.091
	Ligand076	Rhein	10	−11.054
	Ligand127	(+)-Pinoresinol monomethyl ether-4-D-beta-glucoside_qt	7	−10.992
	Ligand018	Glycyrin	16	−10.898
	Ligand167	Isoglycyrol	11	−10.762
	Ligand068	Euchrenone	11	−10.751
	Ligand014	Glabrene	16	−10.728
	Ligand072	Sigmoidin-B	11	−10.319
VEGFA	Ligand073	l-SPD	11	−8.346
	Ligand169	Anthocyan	4	−7.791
	Ligand068	Euchrenone	11	−7.567
	Ligand142	Quindoline	5	−7.518
	Ligand103	3-[2′-(5′-Hydroxymethyl) furyl]-1(2H)-isoquinolinone-7-O-BETA-D-glucoside	8	−7.365
	Ligand064	DFV	11	−7.252
	Ligand100	Eriodyctiol(flavanone)	9	−7.164
	Ligand083	Eriodictyol	9	−7.138
IL-6	Ligand198	Salidroside	2	−7.086
	Ligand089	8-Prenylated eriodictyol	9	−7.046
	Ligand121	Inflacoumarin A	7	−8.586
	Ligand194	Phenanthrone	2	−7.814
	Ligand114	Machiline	8	−7.758
	Ligand093	Glycyrol	9	−7.624
	Ligand198	salidroside	2	−7.275
	Ligand153	Rutin	5	−7.212
	Ligand110	Licoricone	8	−7.124
	Ligand073	l-SPD	11	−7.082
	Ligand026	Medicarpin	15	−7.047
	Ligand104	Toralactone	8	−7.039
STAT3	Ligand113	Dinethylsecologanoside	8	−7.394
	Ligand066	Sennoside E	11	−8.992
	Ligand185	3-[[(2R,3R,5R,6S)-3,5-Dihydroxy-6-(1H-indol-3-yloxy)-4-oxooxan-2-yl]methoxy]-3-oxopropanoic acid	2	−7.098
	Ligand116	Procyanidin B-5,3′-O-gallate	7	−7.022
	Ligand173	CLR	3	−7.004
	Ligand175	Glabrone	3	−6.864
	Ligand133	Dehydroglyasperins C	6	−6.755
	Ligand164	Dehydroglyasperins C	4	−6.678
	Ligand139	(−)-(3R,8S,9R,9aS,10aS)-9-Ethenyl-8-(beta-D-glucopyranosyloxy)-2,3,9,9a,10,10a-hexahydro-5-oxo-5H,8H-pyrano[4,3-d]oxazolo[3,2-a]pyridine-3-carboxylic acid	6	−6.625
	Ligand005	Sennoside D	20	−6.624

(Continued)

TABLE 2 (Continued)

Target	ID	Name	Degree	Docking score (kcal/mol)
TLR4	Ligand103	3-[2′-(5′-Hydroxymethyl) furyl]-1(2H)-isoquinolinone-7-O-BETA-D-glucoside_qt	8	−7.729
	Ligand177	Licoisoflavone B	3	−7.684
	Ligand039	7,2′,4′-Trihydroxy-5-methoxy-3-arylcoumarin	13	−7.608
	Ligand035	Vestitol	14	−7.59
	Ligand023	Kanzonols W	15	−7.59
	Ligand087	3-(2,4-Dihydroxyphenyl)-8-(1,1-dimethylprop-2-enyl)-7-hydroxy-5-methoxy-coumarin	9	−7.51
	Ligand098	Flavidin	9	−7.499
	Ligand153	Flavidin	5	−7.497
	Ligand051	Naringenin	12	−7.464
	Ligand135	Glyasperin F	6	−7.365
AKT1	Ligand063	Herbacetin	12	−8.529
	Ligand198	Salidroside	2	−8.447
	Ligand043	Phaseolinisoflavan	13	−8.327
	Ligand035	1,3-Dihydroxy-9-methoxy-6-benzofurano[3,2-c]chromenone	5	−8.275
	Ligand023	Kanzonols W	15	−8.275
	Ligand149	Glyzaglabrin	5	−8.206
	Ligand046	Kaempferol	13	−8.115
	Ligand009	Herbacetin	18	−8.115
	ligand177	Licoisoflavone B	3	−8.099
	Ligand191	Semilicoisoflavone B	2	−8.072

Ligand063 has multiple hydrogen bond donors and receptors and thus forms strong hydrogen and hydrophobic bonds with protein active sites (Figure 6A). The hydrogen bond distance was significantly shorter (average of 1.86 Å) than that of the traditional hydrogen bond (3.5 Å). Moreover, the ligand has a strong binding ability and thus anchors small molecules in the protein pockets. Ligand121 contains three benzene rings with strong hydrophobicity and forms strong hydrogen and hydrophobic bonds with the hydrophobic cavity of the protein (Figure 6B). The hydrogen bond distances are 1.6 Å and 1.8 Å. Ligand 113 had a six-membered sugar ring at one end and an oxygen-containing six-membered ring with multiple carboxyl groups at the other end, yielding multiple hydrogen bonds for the receptor (Figure 6C). Ligand103 and ligand073 highly matched the target protein pocket and formed hydrogen, hydrophobic, and other bonds with the protein pocket (Figures 6D-F). These results indicate that ligand063, ligand121, ligand113, and ligand073 are potential active compounds with good binding affinity and matching with AKT1, IL6, STAT3, TLR4, TNF, and VEGFA.

Molecular dynamics simulation analysis

The stability of reactive proteins and small molecules depends on the RMSD. The larger the RMSD, the more unstable is the protein. The stability of small molecules fluctuated at the beginning and tended to stabilize during movement, reflecting the continuous collision between small molecules and active sites in the protein pocket (Figure 7). This result also showed that the small molecules combined well with the protein pocket and reached a dynamic equilibrium. The average RMSD values of the VEGFA-ligand073, TLR4-ligand103, AKT1-ligand063, and IL6-ligand121 complexes were approximately 2, 5, 10, and 40 ns, respectively. The average RMSD value of TNF-ligand103 was < 2.4 Å and had a slight RMSD fluctuation; thus, the small molecule–protein complex could quickly reach a stable state, reflecting the good stability of the complex. The above results also indicated that the small molecule had a high degree of matching with the protein. The average RMSD of the STAT3-ligand113 complex was < 4.0 Å and showed a slight RMSD fluctuation, possibly due to the unstable chain of the protein. Protein and small molecule complexes quickly reached dynamic equilibrium, with a consistent change trend in the RMSDs of the complexes, indicating that small molecules and proteins can form stable complexes, which change with the conformational state of the proteins in the solvent. Ligand063, ligand121, ligand103, ligand073, and ligand063 formed strong hydrogen and hydrophobic bonds with the active site (Figure 7). In addition, ligand121 exhibited a strong electrostatic interaction with the active site. Ligand 113 formed a strong hydrogen bond with the active site, which induced its binding to the protein. These interactions can improve the stability of small molecules in the protein pockets.

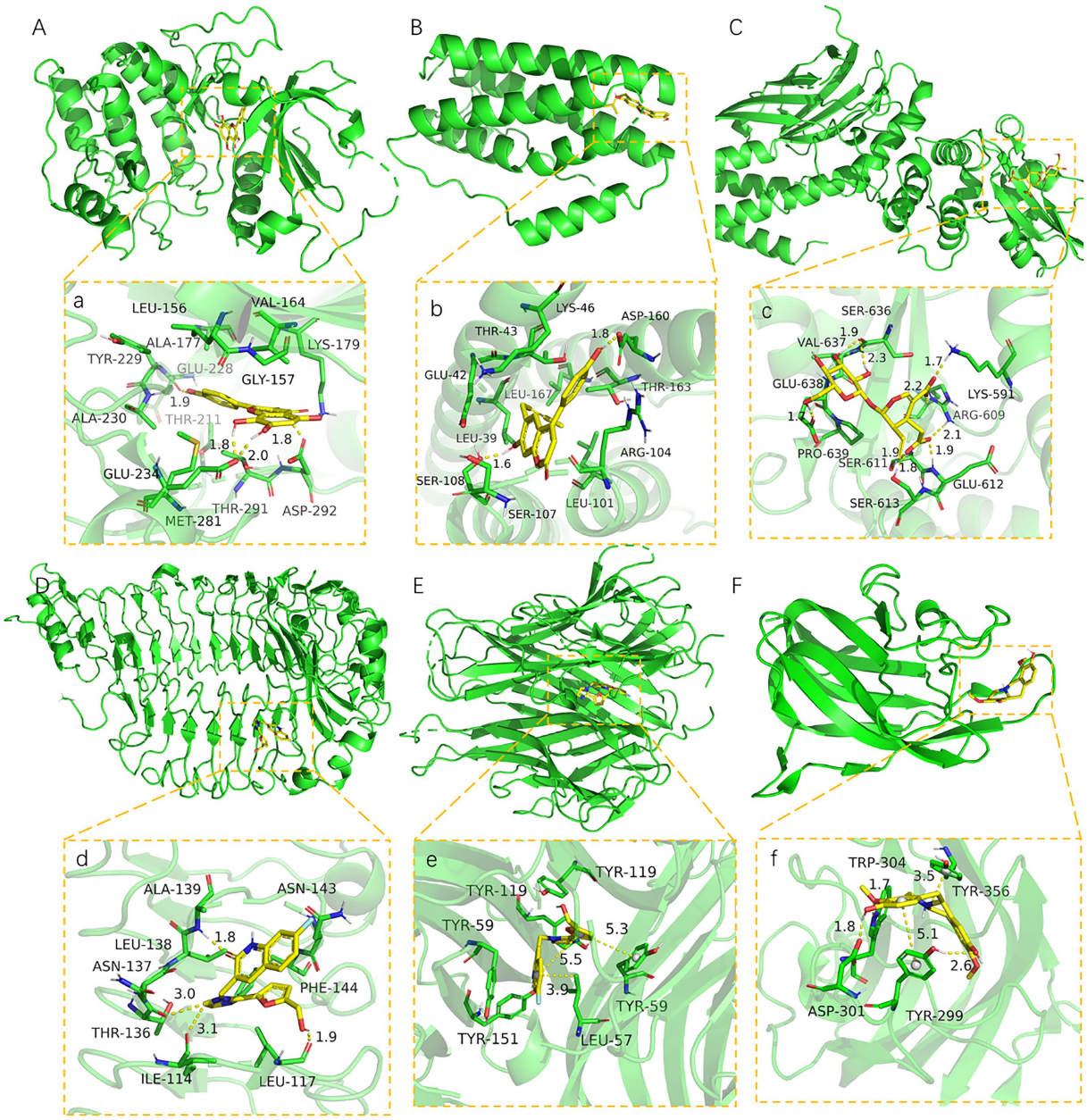

FIGURE 6
The binding site of target with compound **(A-F)**. The 3D structure of AKT1-ligand063, IL6-ligand121, STAT3-ligand113, TLR4-ligand103, TNF-ligand103, VEGFA-ligand073. **(a-f)** A close view of the active site binding with AKT1-ligand063, IL6-ligand121, STAT3-ligand113, TLR4-ligand103, TNF-ligand103, VEGFA-ligand073. Key residues interacting with ligands were shown as sticks and colored green. The protein backbone was shown as a tube and colored bright blue.

Results of the calculation of free binding energy

The calculation of static molecular docking and molecular mechanics generalized Born surface area (MM-GBSA) free binding energy ensures that the complexes of compounds and targets have sufficient energy for biochemical reactions by providing binding posture and binding free energy. The binding free energy calculated using MM-GBSA supported the molecular docking results. Ligand103 had the highest binding ability to TNF (210.26 ± 22.01) and TLR4 (180.53 ± 19.85; Table 3).

Correlation analysis

Network pharmacological screening and molecular docking results showed that the TNF and Toll receptor signalling pathways targeting TNF and TLR4 might be the main pathways involved in

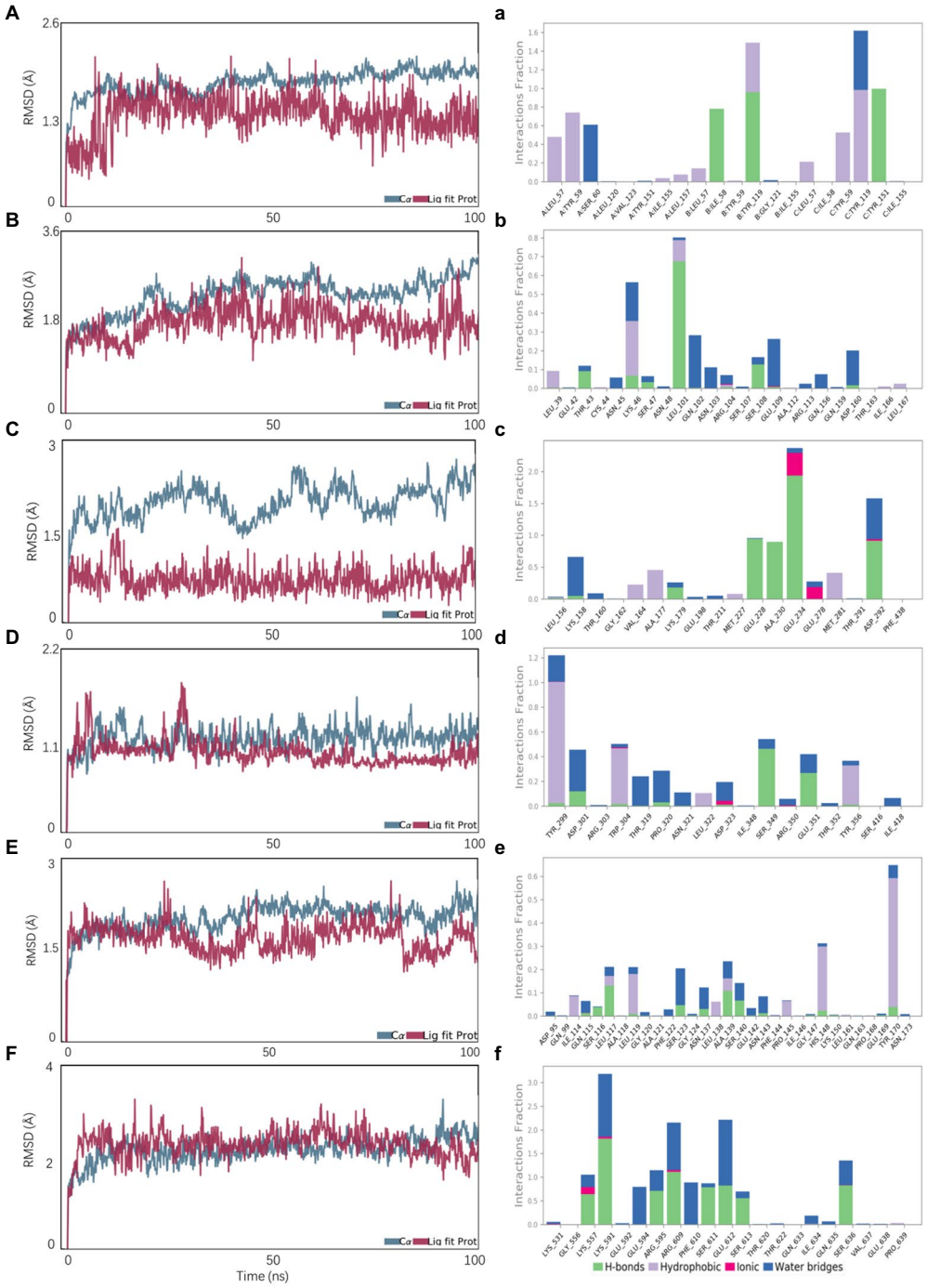

FIGURE 7
Molecular dynamics simulations. **A, B, C, D, E, F** represent the RMSD plot during molecular dynamics simulations of AKT1-ligand063, IL6-ligand121, STAT3-ligand113, TLR4-ligand103, TNF-ligand103, VEGFA-ligand073; **a, b, c, d, e, f** represent the interaction residues of AKT1-ligand063, IL6-ligand121, STAT3-ligand113, TLR4-ligand103, TNF-ligand103, VEGFA-ligand073.

LHQW-mediated amelioration of influenza A virus infection. The 16S rDNA results were combined with the results of molecular biology experiments (qRT–PCR and WB results of lung tissue) to determine the relationship between the amount of virus in the mouse lung and the main target of LHQW in the treatment of influenza A virus and abundance of the intestinal microbiota. The correlation between the abundance of the intestinal microbiota at the phylum and genus levels and the targets screened using computer-aided design technology was also assessed.

At the phylum level, the influenza A virus (Inf A) and TLR4, NF-κB, TNF-α, IL-6, and IL-1β levels were negatively correlated with *Bacteroidetes* abundance. In contrast, these levels were

TABLE 3 MM/GBSA of the best candidate compounds and protein targets for each target.

Chemical compound	Target	Van der Waals force (kJ/mol)	Electrostatic potential energy (kJ/mol)	Polar solvation energy (kJ/mol)	Surface solvation (kJ/mol)	Binding free energy (kJ/mol)
Ligand063	AKT1	−258.71 ± 16.21	−89.23 ± 13.49	220.17 ± 18.22	−25.37 ± 1.46	−178.23 ± 18.29
Ligand121	IL6	−229.17 ± 13.98	−101.37 ± 17.21	232.01 ± 16.31	−30.19 ± 1.01	−156.91 ± 17.35
Ligand113	STAT3	−252.66 ± 18.21	−92.37 ± 15.76	219.32 ± 19.06	−28.37 ± 0.92	−176.22 ± 16.47
Ligand103	TLR4	−210.37 ± 12.90	−99.28 ± 16.01	211.39 ± 17.88	−33.51 ± 1.33	−180.53 ± 19.85
Ligand103	TNF	−199.58 ± 17.26	−70.56 ± 12.99	245.62 ± 15.90	−32.02 ± 1.47	−210.26 ± 22.01
Ligand073	VEGFA	−241.11 ± 11.08	−118.34 ± 13.37	260.79 ± 15.37	−27.63 ± 0.89	−128.83 ± 19.37

positively correlated with *Verrucomicrobia*, *Gemmatimonadetes*, Rokubacteria, and *Chloroflexi*. At the genus level, INF-α, TLR4, NF-κB, TNF-α, IL-6, and IL-1β levels were negatively correlated with Prevotellaceae_UCG-001, *Muribaculum*, and Muribaculaceae_unclassified abundances. In contrast, these levels were positively correlated with *Blautia*, *Klebsiella*, *Parabacteroides*, *Roseburia*, *Bilophila*, *Eisenbergiella*, *Citrobacter*, Akkermansia, and *Clostridiales*_unclassified abundance (Figure 8).

Discussion

Oseltamivir (OSTW), a neuraminidase inhibitor commonly used to treat influenza, is an antiviral drug listed in China. OSTW is a classic antiviral drug with good antiviral effects. However, based on the principle of neuraminidase inhibition, the protective effect of this drug on influenza patients has a time window. Taking it 48 h after onset can significantly shorten the course of the disease and inhibit virus replication. Therefore, we selected OSTW as the positive control drug in this study. BALB/c inbred line mice had the same genetic background. The use of Balb/c mice can reduce the influence of genetic background factors among individual mice on the difference in virus infection sensitivity; therefore, it is easier to study and analyze the dynamic characteristics of viral pathogenicity and replication. BALB/c mice were selected for this study according to the standard operating procedures of the Institute for Viral Disease Control and Prevention (2007).

In this study, we found that the inflammatory factors in the lungs of mice with viral pneumonia were disordered, the lungs were damaged, and the TLR4 pathway was significantly activated (Figure 8B). One of the important factors of the influenza virus leading to human death is the abundant expression of pro-inflammatory cytokines. Some studies have shown that lung damage caused by influenza A virus (IVA) is mainly caused by an excessive inflammatory response rather than direct damage to the alveolar epithelium by the virus (Brandes et al., 2013). Excessive immune response can cause a "cytokine storm" that induce acute lung injury (ALI), and further develop acute respiratory distress syndrome (ARDS), leading to respiratory failure and even death. Therefore, in the treatment of influenza virus infection, it is very important to reduce the inflammatory response caused by IVA in the lung (de Jong et al., 2006; Perrone et al., 2008; Bermejo-Martin et al., 2009; Brandes et al., 2013; Li et al., 2014).

During the course of influenza virus infection, three different types of innate immune pattern recognition receptors (PRRs) recognize viral RNA, namely Toll-like receptors (TLRs), retinotide-induced gene I (RIG-I), and NLRP3. After receptor activation, interferon regulators 3/7 (IRF 3/7) and NF-κB are activated to promote the expression of IFNs and pro-inflammatory factors, respectively (Sun et al., 2010). TLRs are the main PRRs for host virus recognition, and during IVA infection, TLR 3/7 is involved in pathogen-associated molecular pattern (PAMPs) identification from IVA by activating myeloid differentiation factor 88 (MYD88), activating downstream transcription factors NF-κB or IRF7, and promoting the expression of pro-inflammatory cytokines such as IL-lβ, IL-18, and type I IFN, respectively (McKinstry et al., 2009).

TNF-α is considered the major pro-inflammatory cytokine capable of causing "cytokine storm" (Cheung et al., 2002), thereby exacerbating the pathogenicity of influenza viruses in humans. (Peper and Van Campen, 1995) found that inhibition of TNF-α reduced lung inflammation but did not affect the clearance of the influenza virus. IL-6 plays a crucial role in resistance to H1N1 influenza infection by promoting neutrophil survival (Dienz et al., 2012). A large body of evidence has shown that the presence of IL-6 may be a marker of persistent inflammation and a direct participant in a comprehensive immune response (Dienz et al., 2012; Spencer et al., 2019; Yousif et al., 2021), IL-6 levels in patients with acute exacerbation were significantly increased compared with those in the stable stage and were positively correlated with viral infection (Hutchinson et al., 2010). IL-1β may be a key inflammatory factor that leads to acute lung injury and ARDS (Fukuyama and Kawaoka, 2011; Niu et al., 2019). It is produced by monocyte-macrophages and endothelial cells and is a pro-inflammatory cytokine involved in host defense responses, such as the immune response to inflammation. It can activate vascular endothelial cells and inflammatory cells such as T lymphocytes and macrophages, release inflammatory mediators, and promote effector cells of the immune system to enter the infection site (Yazdi and Ghoreschi, 2016).

The results of this study showed that the alpha diversity of the intestinal microbiota, the abundance of *Bacteroidetes, muribaculaceae*_unclassified, and *Streptococcus* decreased significantly (Figure 2), accompanied by disordered intestinal

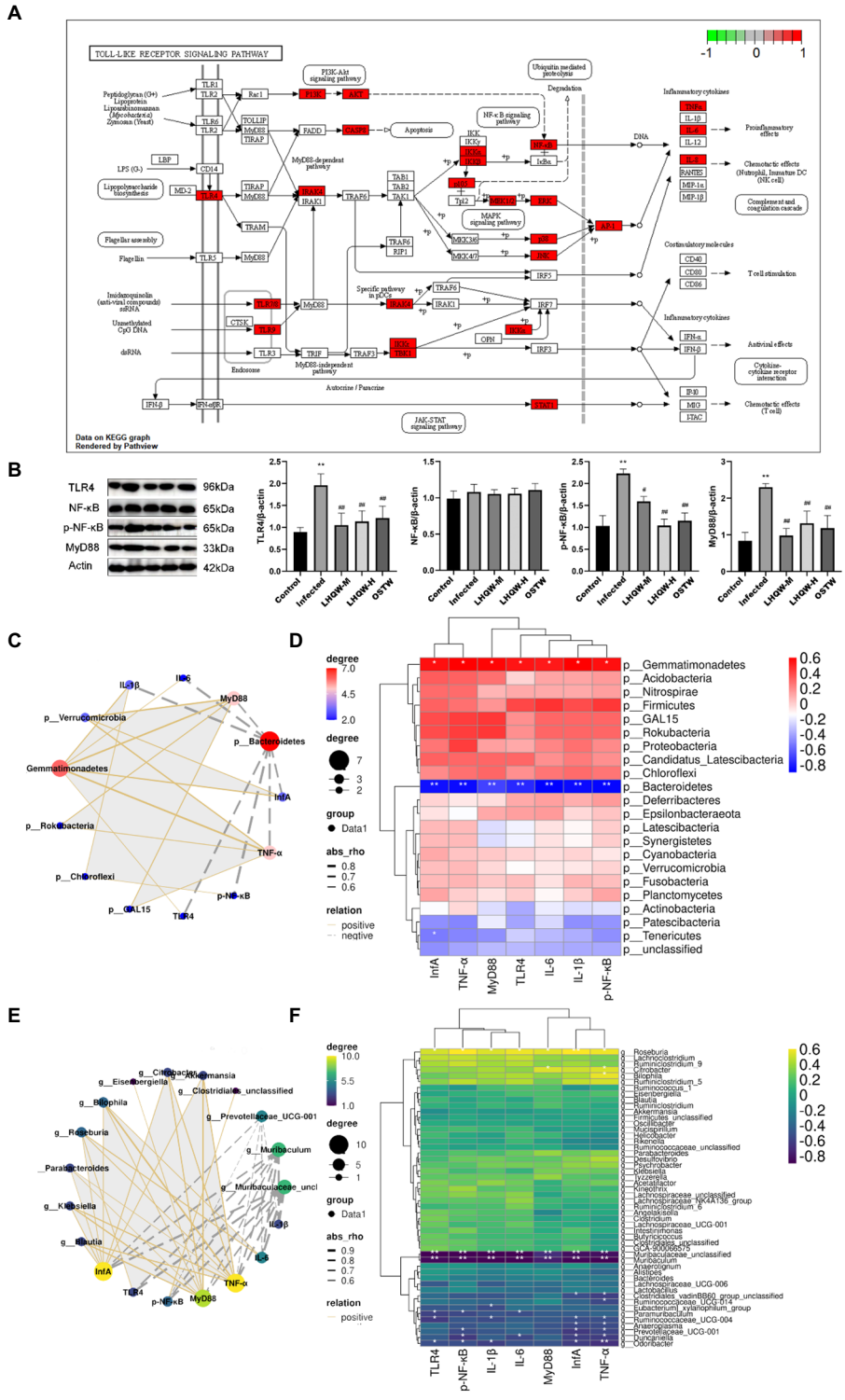

FIGURE 8
Correlation analysis. **(A)** Toll-like receptor signaling pathway; **(B)** TLR4, NF-κB, and p-NF-κB levels in mouse lung tissue. MyD88 protein expression level; Correlation network diagram **(C)** and heat diagram **(D)** at the phylum level; Correlation network diagram **(E)** and heat map **(F)** at the genus level. Compared with control group, *$p<0.05$, **$p<0.01$; Compared with infected group, $^{\#}p<0.05$, $^{\#\#}p<0.01$.

wall inflammatory factors and injured intestinal mucosal barriers (Figure 3). LHQW treatment increased the survival rate, restored the alpha diversity of intestinal microbiota, recovered the *Bacteroidetes* and *muribaculaceae*_unclassified levels, adjusted inflammatory factors of the intestinal walls, and improved the intestinal mucosal barrier (Figure 2).

Intestinal microbiota-derived propionic acid protects against zinc oxide nanoparticle-induced lung injury (Zhang Y. et al., 2022). Baicalin inhibits APEC-induced lung injury by regulating gut microbiota and short-chain fatty acids (SCFA) production (Peng et al., 2021). Mycoplasma gallisepticum baicalin ameliorated-induced inflammatory injury in the chicken lung by regulating the intestinal microbiota and phenylalanine metabolism (Wang J. et al., 2021). The lung and gut microbiota are altered by hyperoxia and contribute to oxygen-induced lung injury in mice (Ashley et al., 2020). Gallacher et al. (2020) found that targeted treatment of the predominant organisms, including those not routinely treated, such as spp., may decrease the development of CLD in preterm-born infants. In summary, these findings suggest that restoration of normal intestinal microbiota can repair lung injury. The lung and intestine have a similar mucosal immune system, which is functionally interconnected. Influenza virus can not only cause lung inflammation but can also be accompanied by gastrointestinal symptoms such as diarrhea and vomiting after infection with influenza H7N9 virus (Gao et al., 2013). In this experiment, we observed numerous inflammatory cell infiltrations in the lungs of mice with pneumonia and significantly increased expression of TNF-α, IL-1β, and IL-6 in the lungs, accompanied by intestinal wall barrier damage, as well as significant changes in the intestinal microbiota (Figures 1C, 2, 3, 8). These phenomena suggest that the pulmonary inflammatory response caused by the virus may lead to cytokines or immune cells entering the intestinal wall through the blood circulation, causing an immune response and resulting in damage to the intestinal wall barrier. Wang et al. (2014) reported that after mice were infected with H1N1 intranasally, the $CCR9^+$ $CD4^+$ T cells in the lungs migrated to the small intestine mediated by CCL25/CCR9 and secreted IFN-γ, changing the composition of the intestinal microbiota and leading to an increase in IL-15 secretion by intestinal epithelial cells, thereby promoting *in situ* differentiation of $CD4^+$ T cells into Th 17 cells, which eventually triggered intestinal inflammation. Other studies found that in BALB/ C mice inoculated intranasally with influenza H1N1 virus, a significant inflammatory response was observed in the large and small intestine, accompanied by intestinal micromicrobiota disorder (Zhang et al., 2015; Li et al., 2018). Another study reported that after influenza virus infection in an animal model, the abundance of intestinal microbiota, such as *Bifidobacterium lactobacillus*, was significantly reduced, *Enterococcus* and *Enterobacteria* increased significantly, and the bacteria associated with the production of short-chain fatty acids (SCFAs) decreased significantly, which plays an important role in intestinal defense against pathogenic bacteria (Wang et al., 2014; Adak and Khan, 2019).

Bacteroidetes, Muribaculaceae, and *Streptococcus* are bacteria that produce SCFCs. The intestine has several lines of defense that protect it against the translocation of microorganisms or microbial products into the bloodstream. This multilayer barrier constitutes the largest interface between the external environment and host (Zhang et al., 2021). The gut-vascular barrier, an additional cellular barrier, is situated below the epithelial barrier and is involved in controlling the translocation of microorganisms into the portal vein (Buckley and Turner, 2018). In addition, gut permeability can be altered by gut microbiota dysbiosis, favoring LPS translocation into systemic circulation, with the development of low-grade endotoxemia. LPS is a component of the membrane of gram-negative bacteria present in the gut that can translocate into the systemic circulation, causing non-septic, low-grade endotoxemia (Violi et al., 2022). Gut dysbiosis is a major determinant of low-grade endotoxemia *via* dysfunction of the intestinal barrier scaffold, which is a prerequisite for LPS translocation into systemic circulation (Johansson et al., 2013; Arbizu et al., 2020). LPS is widely used as an important indicator of intestinal permeability (Li et al., 2021; Liu et al., 2021; Wang Y. et al., 2021; Zhao et al., 2021). Therefore, the detection of LPS in serum by ELISA can be used to evaluate intestinal permeability. In this experiment, the diversity of the intestinal microbiota and the abundance of *Bacteroides*, *Muribaculaceae,* and *Streptococcus* were significantly reduced, resulting in an increase in the abundance of opportunistic bacteria (Figure 2), which then led to intestinal mucosal barrier damage. In this case, enterobacteria metabolites, such as LPS, enter the damaged intestinal wall, aggravate the intestinal wall immune response, and release inflammatory factors, and then amplify the intestinal wall injury, which crosses the injured intestinal wall into the bloodstream and activates the TLR4 signalling pathway in the lungs to aggravate the inflammatory response and injury in the lung, which was also verified in our experiments.

The results of this study showed that LHQW treatment reduced the viral loads and adjusted inflammatory factors in the lungs, alleviated lung injury, and inhibited the activation of the TLR4/NF-κB signalling pathway in viral pneumonia mice (Figures 1C, 8B). Network pharmacological analysis showed that the six active herbal medicine molecules from LHQW could regulate the intestinal microbiota, thereby inhibiting the immune-inflammatory response through the TLR4/NF-κB signalling pathways in the lungs (Table 2). It reveals the relationship between the gut microbiota, intestinal mucosal barrier, and viral pneumonia, and part of the mechanisms of LHQW in the treatment of viral pneumonia. The LHQW capsule, a traditional Chinese medicine compound, has 13 traditional Chinese medicines and many action targets, such as Akt1, P53, Cox-2, and TLR4 (Xia et al., 2020; Su et al., 2022), and has unique advantages in the treatment of influenza virus infection. Formula composition: forsythia suspensa 225 g, honeysuckle 255 g, isatis root 255 g, bitter almond 85 g, menthol 7.5 g, houttuynia cordata 255 g, rhubarb 51 g, patchouli 85 g, Male Fern Rhizome 255 g, Rhodiolae Herba 85 g, Ephedra equisetifolia 85 g, licorice 85 g, gypsum 255 g. Studies have confirmed that the main active ingredients of LHQW are chlorogenic acid, ursolic acid, rutin, luteolin, and quercetin, which exhibit antibacterial activities (Niu et al., 2021; Yang et al., 2021; Zhou et al., 2021).

In this experiment, after treatment with LHQW, the alpha diversity and abundance of probiotics such as *Bacteroidetes, Muribaculaceae,* and *Streptococcus* in the intestinal tract of mice with viral pneumonia were significantly increased, and intestinal mucosal barrier injury was significantly alleviated (Figures 2, 3).

As a result, bacterial metabolites (LPS) entering the intestinal wall are reduced and the resulting immune response and

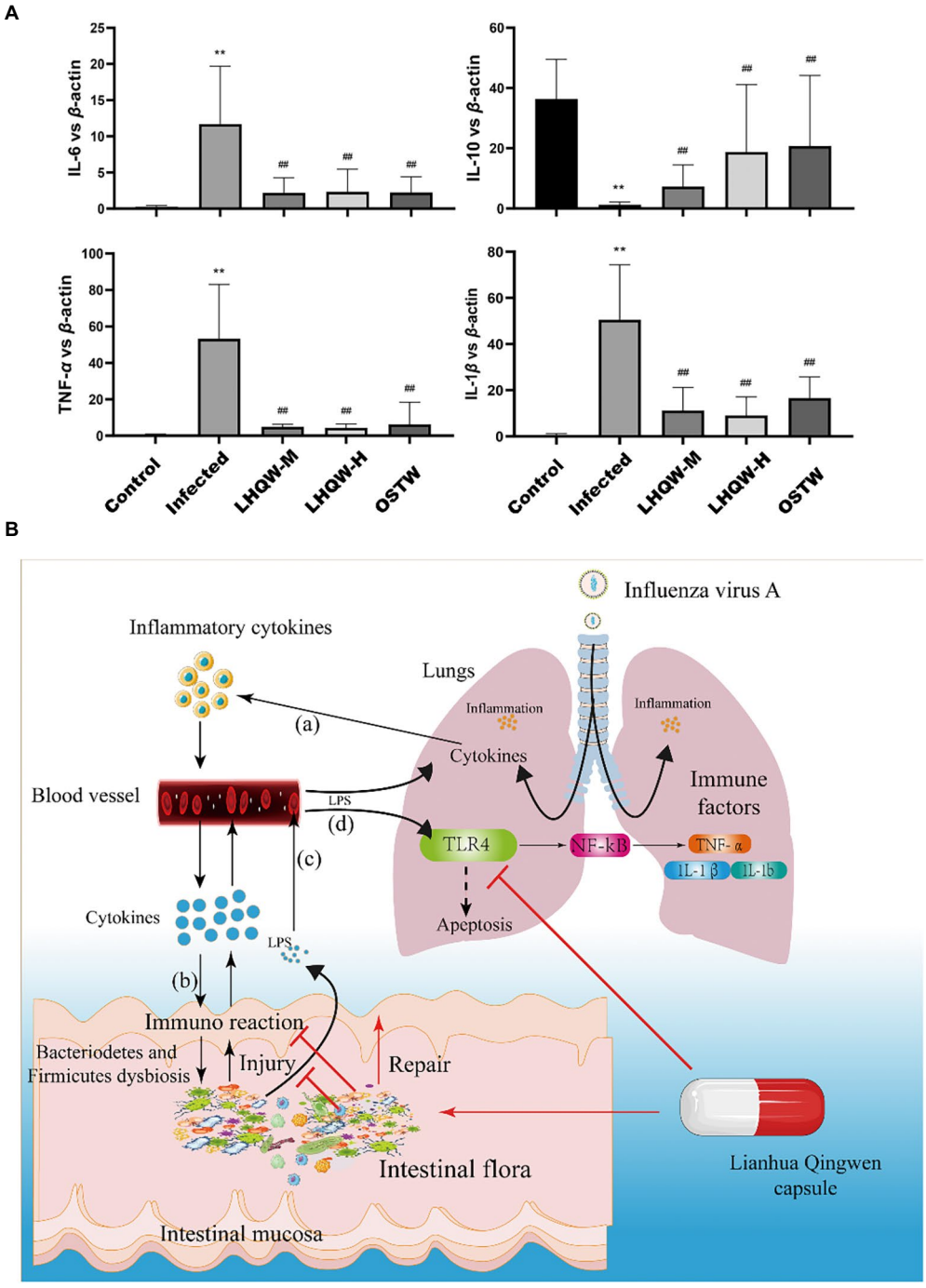

FIGURE 9
(A) qRT-PCR detection of inflammatory factors (IL-6, IL-1β, IL-10, TNF-α) in the mouse lung tissue. Compared with control group, *$p<0.05$, **$p<0.01$; Compared with infected group, $^{\#}p<0.05$, $^{\#\#}p<0.01$. **(B)** The working model of LHQW capsule against influenza A virus infection. (a) The lung infected with influenza A virus induces an immune response in lung, leading to the release of inflammatory cytokines into blood. (b) The inflammatory cytokines from the blood enter the intestinal wall to induce the immune response, resulting in intestinal wall injury. (c) The LPS from the intestine crosses the damaged intestinal mucosal barrier and enters the blood to activate the TLR4-mediated pathway in lung, causing the lung injury (d).

inflammatory factors are also decreased. Meanwhile, LPS crossing the intestinal wall to enter the blood stream and eventually reach the lungs was significantly reduced, thus reducing the activation of the LPS/TLR4/NF-κB signalling pathway (Figures 8A,B), thereby decreasing the expression of inflammatory factors in the lungs. In addition, LPS/TLR4 can also be inhibited (Figure 8A), thus reducing lung injury (Figure 9), which is beneficial for the survival of some immune cells and the clearance of the virus in the lungs.

Conclusion

The present study was designed to determine the effect of intestinal microbiota in the improvement of LHQW activity in viral pneumonia and its possible mechanism. The findings clearly indicate that LHQW is effective for treating influenza A virus infectious pneumonia, and the mechanism is associated with the regulation of the TLR4/NF-κB signalling pathway in the lungs by restoring intestinal microbiota and repairing the intestinal wall. This result provides theoretical support for the effective use of LHQW in the treatment of influenza A virus.

Data availability statement

The data presented in the study are deposited in the NCBI repository, accession number PRJNA889462.

Ethics statement

The animal study was reviewed and approved by all animal experimental procedures strictly followed the protocol approved by the Ethics Committee of Wannan Medical College (YJS-2020-10-006).

Author contributions

PX, ZY, and SD performed the experiments, the data, and wrote the manuscript. ZH and SZ contributed to the study design and overall supervision. All authors have reviewed the manuscript. All authors contributed to the article and approved the submitted version.

Funding

This work was financially supported by the Natural science projects in colleges and universities in Anhui Province (grant number KJ2020ZD56) and the National Natural Science Foundation of China (grant number 81671318). SZ received funding from the Natural science projects in colleges and universities in Anhui Province (grant number KJ2020ZD56). ZH received funding from the National Natural Science Foundation of China (grant number 81671318).

Conflict of interest

The authors declare that the research was conducted in the absence of any commercial or financial relationships that could be construed as a potential conflict of interest.

Publisher's note

All claims expressed in this article are solely those of the authors and do not necessarily represent those of their affiliated organizations, or those of the publisher, the editors and the reviewers. Any product that may be evaluated in this article, or claim that may be made by its manufacturer, is not guaranteed or endorsed by the publisher.

References

Adak, A., and Khan, M. R. (2019). An insight into gut microbiota and its functionalities. *Cell. Mol. Life Sci.* 76, 473–493. doi: 10.1007/s00018-018-2943-4

Arbizu, S., Chew, B., Mertens-Talcott, S. U., and Noratto, G. (2020). Commercial whey products promote intestinal barrier function with glycomacropeptide enhanced activity in downregulating bacterial endotoxin lipopolysaccharides (LPS)-induced inflammation in vitro. *Food Funct.* 11, 5842–5852. doi: 10.1039/D0FO00487A

Ashley, S. L., Sjoding, M. W., Popova, A. P., Cui, T. X., Hoostal, M. J., Schmidt, T. M., et al. (2020). Lung and gut microbiota are altered by hyperoxia and contribute to oxygen-induced lung injury in mice. *Sci. Transl. Med.* 12:eaau9959. doi: 10.1126/scitranslmed.aau9959

Bedi, S., Mudgal, R., Haag, A., and Ono, A. (2022). A Glu-Glu-Tyr sequence in the cytoplasmic tail of the M2 protein renders influenza a virus susceptible to restriction of the Hemagglutinin-M2 association in primary human macrophages. *J. Virol.* 96:e0071622. doi: 10.1128/jvi.00716-22

Bermejo-Martin, J. F., Ortiz de Lejarazu, R., Pumarola, T., Rello, J., Almansa, R., Ramirez, P., et al. (2009). Th1 and Th17 hypercytokinemia as early host response signature in severe pandemic influenza. *Crit. Care* 13:R201. doi: 10.1186/cc8208

Boni, M. F. (2008). Vaccination and antigenic drift in influenza. *Vaccine* 26, C8–C14. doi: 10.1016/j.vaccine.2008.04.011

Brandes, M., Klauschen, F., Kuchen, S., and Germain, R. N. (2013). A systems analysis identifies a feedforward inflammatory circuit leading to lethal influenza infection. *Cells* 154, 197–212. doi: 10.1016/j.cell.2013.06.013

Buckley, A., and Turner, J. R. (2018). Cell biology of tight junction barrier regulation and mucosal disease. *Cold Spring Harb. Perspect. Biol.* 10:a029314. doi: 10.1101/cshperspect.a029314

Bulanda, E., and Wypych, T. P. (2022). Bypassing the gut-lung Axis via microbial metabolites: implications for chronic respiratory diseases. *Front. Microbiol.* 13:857418. doi: 10.3389/fmicb.2022.857418

Cammann, C., Israel, N., Frentzel, S., Jeron, A., Topfstedt, E., Schuler, T., et al. (2022). T cell-specific constitutive active SHP2 enhances T cell memory formation and reduces T cell activation. *Front. Immunol.* 13:958616. doi: 10.3389/fimmu.2022.958616

Caton, A. J., Brownlee, G. G., Yewdell, J. W., and Gerhard, W. (1982). The antigenic structure of the influenza virus a/PR/8/34 hemagglutinin (H1 subtype). *Cells* 31, 417–427. doi: 10.1016/0092-8674(82)90135-0

Chen, T. H., Hsu, M. T., Lee, M. Y., and Chou, C. K. (2022). Gastrointestinal involvement in SARS-CoV-2 infection. *Viruses* 14:1188. doi: 10.3390/v14061188

Cheung, C. Y., Poon, L. L., Lau, A. S., Luk, W., Lau, Y. L., Shortridge, K. F., et al. (2002). Induction of proinflammatory cytokines in human macrophages by influenza a (H5N1) viruses: a mechanism for the unusual severity of human disease? *Lancet* 360, 1831–1837. doi: 10.1016/S0140-6736(02)11772-7

de Jong, M. D., Simmons, C. P., Thanh, T. T., Hien, V. M., Smith, G. J., Chau, T. N., et al. (2006). Fatal outcome of human influenza a (H5N1) is associated with high viral load and hypercytokinemia. *Nat. Med.* 12, 1203–1207. doi: 10.1038/nm1477

Dienz, O., Rud, J. G., Eaton, S. M., Lanthier, P. A., Burg, E., Drew, A., et al. (2012). Essential role of IL-6 in protection against H1N1 influenza virus by promoting

neutrophil survival in the lung. *Mucosal Immunol.* 5, 258–266. doi: 10.1038/mi.2012.2

Fukuyama, S., and Kawaoka, Y. (2011). The pathogenesis of influenza virus infections: the contributions of virus and host factors. *Curr. Opin. Immunol.* 23, 481–486. doi: 10.1016/j.coi.2011.07.016

Gallacher, D., Mitchell, E., Alber, D., Wach, R., Klein, N., Marchesi, J. R., et al. (2020). Dissimilarity of the gut-lung axis and dysbiosis of the lower airways in ventilated preterm infants. *Eur. Respir. J.* 55:1901909. doi: 10.1183/13993003.01909-2019

Gao, H. N., Lu, H. Z., Cao, B., Du, B., Shang, H., Gan, J. H., et al. (2013). Clinical findings in 111 cases of influenza a (H7N9) virus infection. *N. Engl. J. Med.* 368, 2277–2285. doi: 10.1056/NEJMoa1305584

Gutierrez-Castrellon, P., Gandara-Marti, T., Abreu, Y. A. A. T., Nieto-Rufino, C. D., Lopez-Orduna, E., Jimenez-Escobar, I., et al. (2022). Probiotic improves symptomatic and viral clearance in Covid19 outpatients: a randomized, quadruple-blinded, placebo-controlled trial. *Gut Microbes* 14:2018899. doi: 10.1080/19490976.2021.2018899

Han, L., Shi, C., Zeng, X., Cen, L., Mei, X., Fan, J., et al. (2021). A novel bifunctional fusion protein, vunakizumab-IL22, for protection against pulmonary immune injury caused by influenza virus. *Front. Immunol.* 12:727941. doi: 10.3389/fimmu.2021.727941

Harris, J., and Borg, N. A. (2022). The multifaceted roles of NLRP3-modulating proteins in virus infection. *Front. Immunol.* 13:987453. doi: 10.3389/fimmu.2022.987453

Hu, K., Guan, W. J., Bi, Y., Zhang, W., Li, L., Zhang, B., et al. (2022). Efficacy and safety of Lianhua Qingwen capsules, a repurposed Chinese herb, in patients with coronavirus disease 2019: a multicenter, prospective, randomized controlled trial. *Phytomedicine* 85:153242. doi: 10.1016/j.phymed.2021.153800

Huang, K., Zhang, P., Zhang, Z., Youn, J. Y., Wang, C., Zhang, H., et al. (2021). Traditional Chinese medicine (TCM) in the treatment of COVID-19 and other viral infections: efficacies and mechanisms. *Pharmacol. Ther.* 225:107843. doi: 10.1016/j.pharmthera.2021.107843

Hutchinson, A. F., Black, J., Thompson, M. A., Bozinovski, S., Brand, C. A., Smallwood, D. M., et al. (2010). Identifying viral infections in vaccinated chronic obstructive pulmonary disease (COPD) patients using clinical features and inflammatory markers. *Influenza Other Respir. Viruses* 4, 33–39. doi: 10.1111/j.1750-2659.2009.00113.x

Institute for Viral Disease Control and Prevention (2007). Chinese Center for Disease Control and Prevention. Standard operating procedures for the National Influenza Center: revised edition (国家流感中心标准操作规程:修订版)[S].2007, May: 189-199. Availalable at: http://www.cnic.org.cn/chn/down/showdown.php?downid=46

Johansson, M. E., Sjovall, H., and Hansson, G. C. (2013). The gastrointestinal mucus system in health and disease. *Nat. Rev. Gastroenterol. Hepatol.* 10, 352–361. doi: 10.1038/nrgastro.2013.35

Li, D., Feng, Y., Tian, M., Ji, J., Hu, X., and Chen, F. (2021). Gut microbiota-derived inosine from dietary barley leaf supplementation attenuates colitis through PPARgamma signaling activation. *Microbiome* 9:83. doi: 10.1186/s40168-021-01028-7

Li, H., Liu, X., Chen, F., Zuo, K., Wu, C., Yan, Y., et al. (2018). Avian influenza virus subtype H9N2 affects intestinal microbiota, barrier structure injury, and inflammatory intestinal disease in the chicken ileum, viruses. *Viruses* 10:270.

Li, Y., Xiao, P., Liu, N., and Zhang, Z. (2022). Efficacy and safety of Chinese medicine Lianhua Qingwen for treating COVID-19: an updated meta-analysis. *Front. Pharmacol.* 13:888820. doi: 10.3389/fphar.2022.888820

Li, J., Zhang, L., Wu, T., Li, Y., Zhou, X., and Ruan, Z. (2021). Indole-3-propionic acid improved the intestinal barrier by enhancing epithelial barrier and mucus barrier. *J. Agric. Food Chem.* 69, 1487–1495. doi: 10.1021/acs.jafc.0c05205

Li, Q., Zhou, L., Zhou, M., Chen, Z., Li, F., Wu, H., et al. (2014). Epidemiology of human infections with avian influenza a(H7N9) virus in China. *N. Engl. J. Med.* 370, 520–532. doi: 10.1056/NEJMoa1304617

Liang, S. B., Zhang, Y. Y., Shen, C., Liang, C. H., Lai, B. Y., Dai, N., et al. (2020). Chinese herbal medicine used with or without conventional Western therapy for COVID-19: an evidence review of clinical studies. *Front. Pharmacol.* 11:583450. doi: 10.3389/fphar.2020.583450

Li-Juan, L., Kang, S., Zhi-Juan, L., Dan, L., Feng, X., Peng, Y., et al. (2022). *Klebsiella pneumoniae* infection following H9N2 influenza a virus infection contributes to the development of pneumonia in mice. *Vet. Microbiol.* 264:109303. doi: 10.1016/j.vetmic.2021.109303

Liu, Y., Cavallaro, P. M., Kim, B. M., Liu, T., Wang, H., Kuhn, F., et al. (2021). A role for intestinal alkaline phosphatase in preventing liver fibrosis. *Theranostics* 11, 14–26. doi: 10.7150/thno.48468

McGee, M. C., Zhang, T., Magazine, N., Islam, R., Carossino, M., and Huang, W. (2022). PD-1 and ICOS counter-regulate tissue resident regulatory T cell development and IL-10 production during flu. *Front. Immunol.* 13:984476. doi: 10.3389/fimmu.2022.984476

McKinstry, K. K., Strutt, T. M., Buck, A., Curtis, J. D., Dibble, J. P., Huston, G., et al. (2009). IL-10 deficiency unleashes an influenza-specific Th17 response and enhances survival against high-dose challenge. *J. Immunol.* 182, 7353–7363. doi: 10.4049/jimmunol.0900657

Melo-Gonzalez, F., Sepulveda-Alfaro, J., Schultz, B. M., Suazo, I. D., Boone, D. L., Kalergis, A. M., et al. (2022). Distal consequences of mucosal infections in intestinal and lung inflammation. *Front. Immunol.* 13:877533. doi: 10.3389/fimmu.2022.877533

Ni, L., Chen, L., Huang, X., Han, C., Xu, J., Zhang, H., et al. (2020). Combating COVID-19 with integrated traditional Chinese and Western medicine in China. *Acta Pharm. Sin. B* 10, 1149–1162. doi: 10.1016/j.apsb.2020.06.009

Niu, W. H., Wu, F., Cao, W. Y., Wu, Z. G., Chao, Y. C., and Liang, C. (2021). Network pharmacology for the identification of phytochemicals in traditional Chinese medicine for COVID-19 that may regulate interleukin-6. *Biosci. Rep.* 41:BSR20202583. doi: 10.1042/BSR20202583

Niu, J., Wu, S., Chen, M., Xu, K., Guo, Q., Lu, A., et al. (2019). Hyperactivation of the NLRP3 inflammasome protects mice against influenza a virus infection via IL-1beta mediated neutrophil recruitment. *Cytokine* 120, 115–124. doi: 10.1016/j.cyto.2019.04.019

Paules, C., and Subbarao, K. (2017). Influenza. *Lancet* 390, 697–708. doi: 10.1016/S0140-6736(17)30129-0

Peng, L. Y., Shi, H. T., Tan, Y. R., Shen, S. Y., Yi, P. F., Shen, H. Q., et al. (2021). Baicalin inhibits APEC-induced lung injury by regulating gut microbiota and SCFA production. *Food Funct.* 12, 12621–12633. doi: 10.1039/d1fo02407h

Peper, R. L., and Van Campen, H. (1995). Tumor necrosis factor as a mediator of inflammation in influenza a viral pneumonia. *Microb. Pathog.* 19, 175–183. doi: 10.1006/mpat.1995.0056

Perrone, L. A., Plowden, J. K., Garcia-Sastre, A., Katz, J. M., and Tumpey, T. M. (2008). H5N1 and 1918 pandemic influenza virus infection results in early and excessive infiltration of macrophages and neutrophils in the lungs of mice. *PLoS Pathog.* 4:e1000115. doi: 10.1371/journal.ppat.1000115

Sencio, V., Machelart, A., Robil, C., Benech, N., Hoffmann, E., Galbert, C., et al. (2022). Alteration of the gut microbiota following SARS-CoV-2 infection correlates with disease severity in hamsters. *Gut Microbes* 14:2018900. doi: 10.1080/19490976.2021.2018900

Shen, X., and Yin, F. (2021). The mechanisms and clinical application of traditional Chinese medicine Lianhua-Qingwen capsule. *Biomed. Pharmacother.* 142:111998. doi: 10.1016/j.biopha.2021.111998

Shi, C., Zhou, L., Li, H., Shi, X., Zhang, Y., Lu, Y., et al. (2022). Intestinal microbiota metabolizing *Houttuynia cordata* polysaccharides in H1N1 induced pneumonia mice contributed to Th17/Treg rebalance in gut-lung axis. *Int. J. Biol. Macromol.* 221, 288–302. doi: 10.1016/j.ijbiomac.2022.09.015

Song, L., Huang, Y., Liu, G., Li, X., Xiao, Y., Liu, C., et al. (2021). A novel immunobiotics *Bacteroides dorei* ameliorates influenza virus infection in mice. *Front. Immunol.* 12:828887. doi: 10.3389/fimmu.2021.828887

Spencer, S., Kostel Bal, S., Egner, W., Lango Allen, H., Raza, S. I., Ma, C. A., et al. (2019). Loss of the interleukin-6 receptor causes immunodeficiency, atopy, and abnormal inflammatory responses. *J. Exp. Med.* 216, 1986–1998. doi: 10.1084/jem.20190344

Su, H., Wu, G., Zhan, L., Xu, F., Qian, H., Li, Y., et al. (2022). Exploration of the mechanism of Lianhua Qingwen in treating influenza virus pneumonia and new coronavirus pneumonia with the concept of "different diseases with the same treatment" based on network pharmacology. *Evid. Based Complement. Alternat. Med.* 2022:5536266. doi: 10.1155/2022/5536266

Sun, K., Torres, L., and Metzger, D. W. (2010). A detrimental effect of interleukin-10 on protective pulmonary humoral immunity during primary influenza a virus infection. *J. Virol.* 84, 5007–5014. doi: 10.1128/JVI.02408-09

Treanor, J. (2004). Influenza vaccine--outmaneuvering antigenic shift and drift. *N. Engl. J. Med.* 350, 218–220. doi: 10.1056/NEJMp038238

Verma, V., Dileepan, M., Huang, Q., Phan, T., Hu, W. S., Ly, H., et al. (2022). Influenza a virus activates cellular Tropomyosin receptor kinase a (TrkA) signaling to promote viral replication and lung inflammation. *PLoS Pathog.* 18:e1010874. doi: 10.1371/journal.ppat.1010874

Violi, F., Cammisotto, V., Bartimoccia, S., Pignatelli, P., Carnevale, R., and Nocella, C. (2022). Gut-derived low-grade endotoxaemia, atherothrombosis and cardiovascular disease. *Nat. Rev. Cardiol.* 1–14. doi: 10.1038/s41569-022-00737-2 [Epub ahead of print].

Wang, J., Ishfaq, M., and Li, J. (2021). Baicalin ameliorates *Mycoplasma gallisepticum*-induced inflammatory injury in the chicken lung through regulating the intestinal microbiota and phenylalanine metabolism. *Food Funct.* 12, 4092–4104. doi: 10.1039/d1fo00055a

Wang, Z., Li, F., Liu, J., Luo, Y., Guo, H., Yang, Q., et al. (2022). Intestinal microbiota - an unmissable bridge to severe acute pancreatitis-associated acute lung injury. *Front. Immunol.* 13:913178. doi: 10.3389/fimmu.2022.913178

Wang, J., Li, F., Wei, H., Lian, Z. X., Sun, R., and Tian, Z. (2014). Respiratory influenza virus infection induces intestinal immune injury via microbiota-mediated Th17 cell-dependent inflammation. *J. Exp. Med.* 211, 2397–2410. doi: 10.1084/jem.20140625

Wang, L., Pelgrim, C. E., Peralta Marzal, L. N., Korver, S., van Ark, I., Leusink-Muis, T., et al. (2022). Changes in intestinal homeostasis and immunity in a cigarette smoke- and LPS-induced murine model for COPD: the lung-gut axis. *Am. J. Physiol. Lung Cell. Mol. Physiol.* 323, L266–L280. doi: 10.1152/ajplung.00486.2021

Wang, Y., Tian, Y., Zhang, N., Li, X., Wang, X., Wang, W., et al. (2021). *Pediococcus pentosaceus* PP04 improves high-fat diet-induced liver injury by the modulation of gut inflammation and intestinal microbiota in C57BL/6N mice. *Food Funct.* 12, 6851–6862. doi: 10.1039/D1FO00857A

Wang, H., Wang, H., Sun, Y., Ren, Z., Zhu, W., Li, A., et al. (2021). Potential associations between microbiome and COVID-19. *Front. Med. (Lausanne)* 8:785496. doi: 10.3389/fmed.2021.785496

Webster, R. G., Laver, W. G., Air, G. M., and Schild, G. C. (1982). Molecular mechanisms of variation in influenza viruses. *Nature* 296, 115–121. doi: 10.1038/296115a0

Wei, X., Sun, W., Zhu, P., Ou, G., Zhang, S., Li, Y., et al. (2022). Refined polysaccharide from *Dendrobium devonianum* resists H1N1 influenza viral infection in mice by activating immunity through the TLR4/MyD88/NF-kappaB pathway. *Front. Immunol.* 13:999945. doi: 10.3389/fimmu.2022.999945

Wu, L., Chen, Y., Ma, Y., Yang, Z., Yang, N., Deng, W., et al. (2020). Clinical practice guideline on treating influenza in adult patients with Chinese patent medicines. *Pharmacol. Res.* 160:105101. doi: 10.1016/j.phrs.2020.105101

Wu, J., Wang, Q., Yang, L., Li, Z., and Wang, X. (2021). Potency of Lianhua Qingwen granule combined with paramivir sodium chloride injection in treating influenza and level changes of serum inflammatory factors. *Am. J. Transl. Res.* 13, 6790–6795.

Xavier-Santos, D., Padilha, M., Fabiano, G. A., Vinderola, G., Gomes Cruz, A., Sivieri, K., et al. (2022). Evidences and perspectives of the use of probiotics, prebiotics, synbiotics, and postbiotics as adjuvants for prevention and treatment of COVID-19: a bibliometric analysis and systematic review. *Trends Food Sci. Technol.* 120, 174–192. doi: 10.1016/j.tifs.2021.12.033

Xia, Q. D., Xun, Y., Lu, J. L., Lu, Y. C., Yang, Y. Y., Zhou, P., et al. (2020). Network pharmacology and molecular docking analyses on Lianhua Qingwen capsule indicate Akt1 is a potential target to treat and prevent COVID-19. *Cell Prolif.* 53:e12949. doi: 10.1111/cpr.12949

Xing, D., and Liu, Z. (2021). Effectiveness and safety of traditional Chinese medicine in treating COVID-19: clinical evidence from China. *Aging Dis.* 12, 1850–1856. doi: 10.14336/AD.2021.0906

Yang, R., Yang, H., Wei, J., Li, W., Yue, F., Song, Y., et al. (2021). Mechanisms underlying the effects of Lianhua Qingwen on sepsis-induced acute lung injury: a network pharmacology approach. *Front. Pharmacol.* 12:717652. doi: 10.3389/fphar.2021.717652

Yazdi, A. S., and Ghoreschi, K. (2016). The Interleukin-1 family. *Adv. Exp. Med. Biol.* 941, 21–29. doi: 10.1007/978-94-024-0921-5_2

Yousif, A. S., Ronsard, L., Shah, P., Omatsu, T., Sangesland, M., Bracamonte Moreno, T., et al. (2021). The persistence of interleukin-6 is regulated by a blood buffer system derived from dendritic cells. *Immunity* 54:e5. doi: 10.1016/j.immuni.2020.12.001

Zhang, H., Alford, T., Liu, S., Zhou, D., and Wang, J. (2022). Influenza virus causes lung immunopathology through down-regulating PPARgamma activity in macrophages. *Front. Immunol.* 13:958801. doi: 10.3389/fimmu.2022.958801

Zhang, Y., Duan, S., Liu, Y., and Wang, Y. (2021). The combined effect of food additive titanium dioxide and lipopolysaccharide on mouse intestinal barrier function after chronic exposure of titanium dioxide-contained feedstuffs. *Part. Fibre Toxicol.* 18:8. doi: 10.1186/s12989-021-00399-x

Zhang, M., Li, N., He, Y., Shi, T., and Jie, Z. (2022). Pulmonary resident memory T cells in respiratory virus infection and their inspiration on therapeutic strategies. *Front. Immunol.* 13:943331. doi: 10.3389/fimmu.2022.943331

Zhang, S., Wei, T., Tianv, H., Cheng, J., Xiao, J., Wang, M., et al. (2015). Small intestinal injury in mice infected with respiratory influenza a virus: evidence for virus induced gastroenteritis. *Biotechnol. Lett.* 37, 1585–1592. doi: 10.1007/s10529-015-1847-8

Zhang, R., Xu, C., and Duan, Z. (2017). Novel antigenic shift in HA sequences of H1N1 viruses detected by big data analysis. *Infect. Genet. Evol.* 51, 138–142. doi: 10.1016/j.meegid.2017.03.028

Zhang, Q., Yue, S., Wang, W., Chen, Y., Zhao, C., Song, Y., et al. (2021). Potential role of gut microbiota in traditional Chinese medicine against COVID-19. *Am. J. Chin. Med.* 49, 785–803. doi: 10.1142/S0192415X21500373

Zhang, Y., Zhang, L., Mao, L., Fan, J., Jiang, X., Li, N., et al. (2022). Intestinal microbiota-derived propionic acid protects against zinc oxide nanoparticles-induced lung injury. *Am. J. Respir. Cell Mol. Biol.* doi: 10.1165/rcmb.2021-0515OC [Epub ahead of print].

Zhao, L., Xie, Q., Etareri Evivie, S., Liu, D., Dong, J., Ping, L., et al. (2021). *Bifidobacterium dentium* N8 with potential probiotic characteristics prevents LPS-induced intestinal barrier injury by alleviating the inflammatory response and regulating the tight junction in Caco-2 cell monolayers. *Food Funct.* 12, 7171–7184. doi: 10.1039/D1FO01164B

Zhou, Y., Niu, M., Zhang, D., Liu, Z., Wu, Q., Chen, J., et al. (2021). Screening for anti-inflammation quality markers of Lianhua Qingwen capsule based on network pharmacology, UPLC, and biological activity. *Front. Pharmacol.* 12:648439. doi: 10.3389/fphar.2021.648439

Zhuang, W., Fan, Z., Chu, Y., Wang, H., Yang, Y., Wu, L., et al. (2020). Chinese patent medicines in the treatment of coronavirus disease 2019 (COVID-19) in China. *Front. Pharmacol.* 11:1066. doi: 10.3389/fphar.2020.01066

frontiers | Frontiers in Microbiology

TYPE Review
PUBLISHED 29 November 2022
DOI 10.3389/fmicb.2022.1043214

OPEN ACCESS

EDITED BY
George William Carnell,
University of Cambridge,
United Kingdom

REVIEWED BY
Sabino Pacheco,
National Autonomous University of Mexico,
Mexico
Songhai Tian,
Harvard Medical School,
United States
Duolong Zhu,
Baylor College of Medicine, United States

*CORRESPONDENCE
Abbas Yadegar
a.yadegar@sbmu.ac.ir
babak_y1983@yahoo.com

SPECIALTY SECTION
This article was submitted to Infectious Agents and Disease, a section of the journal Frontiers in Microbiology

RECEIVED 14 September 2022
ACCEPTED 13 October 2022
PUBLISHED 29 November 2022

CITATION
Raeisi H, Azimirad M, Asadzadeh Aghdaei H, Yadegar A and Zali MR (2022) Rapid-format recombinant antibody-based methods for the diagnosis of *Clostridioides difficile* infection: Recent advances and perspectives.
Front. Microbiol. 13:1043214.
doi: 10.3389/fmicb.2022.1043214

Rapid-format recombinant antibody-based methods for the diagnosis of *Clostridioides difficile* infection: Recent advances and perspectives

Hamideh Raeisi[1], Masoumeh Azimirad[1], Hamid Asadzadeh Aghdaei[2], Abbas Yadegar[1]* and Mohammad Reza Zali[3]

[1]Foodborne and Waterborne Diseases Research Center, Research Institute for Gastroenterology and Liver Diseases, Shahid Beheshti University of Medical Sciences, Tehran, Iran, [2]Basic and Molecular Epidemiology of Gastrointestinal Disorders Research Center, Research Institute for Gastroenterology and Liver Diseases, Shahid Beheshti University of Medical Sciences, Tehran, Iran, [3]Gastroenterology and Liver Diseases Research Center, Research Institute for Gastroenterology and Liver Diseases, Shahid Beheshti University of Medical Sciences, Tehran, Iran

Clostridioides difficile, the most common cause of nosocomial diarrhea, has been continuously reported as a worldwide problem in healthcare settings. Additionally, the emergence of hypervirulent strains of *C. difficile* has always been a critical concern and led to continuous efforts to develop more accurate diagnostic methods for detection of this recalcitrant pathogen. Currently, the diagnosis of *C. difficile* infection (CDI) is based on clinical manifestations and laboratory tests for detecting the bacterium and/or its toxins, which exhibit varied sensitivity and specificity. In this regard, development of rapid diagnostic techniques based on antibodies has demonstrated promising results in both research and clinical environments. Recently, application of recombinant antibody (rAb) technologies like phage display has provided a faster and more cost-effective approach for antibody production. The application of rAbs for developing ultrasensitive diagnostic tools ranging from immunoassays to immunosensors, has allowed the researchers to introduce new platforms with high sensitivity and specificity. Additionally, DNA encoding antibodies are directly accessible in these approaches, which enables the application of antibody engineering to increase their sensitivity and specificity. Here, we review the latest studies about the antibody-based ultrasensitive diagnostic platforms for detection of *C. difficile* bacteria, with an emphasis on rAb technologies.

KEYWORDS

***Clostridioides difficile*, recombinant antibody, phage display, immunoassays, immunosensors**

Introduction

Clostridioides difficile, an anaerobic Gram-positive spore-forming bacillus, is a medically important pathogen and known as the main cause of diarrhea in humans globally (Burke and Lamont, 2014). *C. difficile* can asymptomatically be present in the gut of healthy individuals (Furuya-Kanamori et al., 2015) or lead to infections with a wide spectrum of clinical disorders, including abdominal pain, diarrhea, pseudomembrane colitis (PMC), or even in some cases death (Burke and Lamont, 2014; Orrell and Melnyk, 2021). Currently, *C. difficile* infection (CDI) is identified as the major cause of nosocomial diseases associated with antibiotic therapy (in particular cephalosporins, clindamycin, metronidazole, and vancomycin) and healthcare-associated diarrhea in adults (Viswanathan et al., 2010; Cornely et al., 2012; Azimirad et al., 2020a, 2022). Additionally, other risk factors are involved in CDI incidence, including immunosuppression, previous hospitalization, age above 65 years, and the use of proton pump inhibitors (Surawicz et al., 2013; Eze et al., 2017; Azimirad et al., 2021). Notably, the spore-forming nature of *C. difficile* can be paired with its ability to rapidly colonize the intestine of patients and arises a critical challenge in infection control and treatment in both the community and healthcare settings (Paredes-Sabja et al., 2014; Castro-Córdova et al., 2021). In the last two decades, the number of CDI patients has been increasing (Depestel and Aronoff, 2013; Azimirad et al., 2020b; Baghani et al., 2020), so that in the USA, *C. difficile* imposes more than 453,000 illnesses per year, leading to 29,600 deaths. These estimates confirm that *C. difficile* is a major continuous burden to public health (Lessa et al., 2015; Kelly et al., 2021). On the other hand, CDI treatment contributed to substantial healthcare cost, and in the USA alone the cost associated with CDI management exceed $4.8 billion annually (Dubberke and Olsen, 2012; Balsells et al., 2016). Additionally, antibiotic therapy for CDI can result in further disruption of the normal gut microbiome and the development of hypervirulent strains of *C. difficile*. Alternatively, 20–30% of the patients with primary infection symptoms experience recurrent disease within 2–6 weeks after the completion of antibiotic treatment (Cornely et al., 2012; Raeisi et al., 2022a), which would be higher after secondary and tertiary CDI and more refractory to treatment regimens (Cornely et al., 2012; Eze et al., 2017). Therefore, rapid and accurate diagnosis of CDI has been a troublesome issue for disease management, implementation of infection control measures, and epidemiological monitoring (Burnham and Carroll, 2013; Peng et al., 2018). Additionally, an early and efficient diagnosis can positively impact the clinical outcome of CDI patients with primary infection and reduce the rate of infection recurrence (Barbut et al., 2014).

In recent years, antibodies, i.e., polyclonal (pAb) and monoclonal antibodies (mAbs), have been extensively applied for diagnostic and therapeutic purposes of various human diseases and cancers (Roovers et al., 2011; Ascoli and Aggeler, 2018; Haji-Hashemi et al., 2018; Raeisi, 2018; Raeisi et al., 2020; Zahavi and Weiner, 2020; Chiari et al., 2021; Hwang et al., 2022). In this regard, antibodies are exploited due to their high affinity and specific binding activity toward target molecules, which highlights their effectiveness as theranostics tools. In recent decades, recombinant antibody (rAb) technologies have widely received much attention as diagnostic tools (Xu et al., 2017; Shali et al., 2018; Fouladi et al., 2019; Raeisi et al., 2019; Alibeiki et al., 2020; Raeisi et al., 2020, 2022b; Berry et al., 2022). The rAb technologies that involve the construction of large libraries of different antibody fragments, such as fragment antigen-binding (Fab), single-chain fragment variable (scFv), minibodies, and nanobodies, can screen antibodies *in vitro* based on their binding properties, thus help develop more cost-effective antibodies with high sensitivity and specificity (Bockstaele et al., 2000; Angela Chiew Wen et al., 2016; Raeisi et al., 2022). This review will focus on currently available procedures for CDI diagnosis and different antibody-based rapid detection methods with an emphasis on rAbs. Additionally, analytical aspects of rAbs as recognition elements to develop ultrasensitive methods will be discussed.

Conventional techniques for *Clostridioides difficile* detection

Some of the major and common *C. difficile* antigens are its surface proteins, including surface-layer proteins (SLPs), cell wall protein 66 (Cwp66) and 84 (CWP84), flagellin FliC, flagellar cap protein FliD, which play key role in attachment to intestinal mucus and have been used as target biomolecules in previous studies (Merrigan et al., 2013; Kandalaft et al., 2015; Shirvan and Aitken, 2016). Additionally, glutamate dehydrogenase (GDH) is a constitutive enzyme produced in large amounts by all toxigenic and non-toxigenic strains of *C. difficile* and can be easily detected in stool samples (Arimoto et al., 2016; Kelly et al., 2021). However,

Abbreviations: AP, Alkaline phosphatase; AAD, Antibiotic-associated diarrhea; CCNA, Cell-culture cytotoxicity neutralization assay; CLIA, Chemiluminescent immunoassay; Cwps, Cell wall protein; *C. difficile*, *Clostridioides difficile*; CDI, *C. difficile* infection; CROPs, Combined repetitive oligopeptide structures; CV, Cyclic voltammetry; EIA, Enzyme immunoassay; ELISA, Enzyme-linked immunosorbent assay; EMA, European Medicines Agency; FliC, Flagellin;; FliD, Flagellin filament cap protein; Fabs, Fragment antigen binding domains; FDA, Food and Drug Administration; GI tract, Gastrointestinal tract; GTD, Glucosyltransferase domain; AuNPs, Gold nanoparticles; LFIAs, Lateral flow immunoassays; LOD, Limit of detection; mAbs, Monoclonal antibodies; NAATs, Nucleic acid amplification tests; PCR, Polymerase chain reaction; pAbs, Polyclonal antibodies; PU, Polyurethane; PMC, Pseudomembranous colitis; QD, Quantum dots; QDNBs, Quantum dot nanobeads; QCM, Quartz crystal microbalance; rAbs, Recombinant antibodies; SARS-CoV-2, Severe acute respiratory syndrome coronavirus 2; SLP, S-layer proteins; scFv, Single-chain fragment variable; sdAb, Single-domain antibodies; SPR, Surface plasmon resonance; TC, Toxigenic culture; VH, Variable regions of heavy domain; VL, Variable regions of light domain; ZIKV, Zika virus.

the introduction of toxin-producing strains of *C. difficile*, as the main cause of antibiotic-associated diarrhea (AAD) in the 1970s, led to the application of several diagnostic methods to detect CDI, most of which relying on the detection of toxin A (TcdA) or B (TcdB) (Kelly et al., 2021). In fact, the main symptoms of CDI are contributed to the secretion of bacterial toxins (Di Bella et al., 2016) that affect the epithelial cells of the gastrointestinal (GI) tract by inactivating Rho/Ras proteins and subsequently lead to loss of epithelial barrier function, cytoskeleton disintegration, condensation of actin, severe inflammation, and eventually cell death (Chen et al., 2015a; Di Bella et al., 2016). These outcomes damage the patient's colonic mucosa and cause severe diarrhea and PMC. Some strains also express an additional toxin, named binary toxin CDT, but its role in the CDI pathogenesis has not been fully understood yet (Chandrasekaran and Lacy, 2017). Notably, the majority of the studies have demonstrated that only toxigenic strains, producing TcdA and/or TcdB, are pathogenic and can cause CDI (Di Bella et al., 2016; Chandrasekaran and Lacy, 2017). Moreover, based on the criteria declared by the European Society of Clinical Microbiology and Infectious Diseases (ESCMID), a CDI case is diagnosed when there are clinical symptoms compatible with CDI (usually diarrhea), stool test positive for TcdA and/or TcdB of *C. difficile* without evidence of another cause of diarrhea, and colonoscopy or histopathological data revealing PMC (van Prehn et al., 2021).

Currently, various methods have been introduced for detecting *C. difficile*, the most important of which being toxigenic culture (TC), cell-culture cytotoxicity neutralization assay (CCNA), enzyme immunoassay (EIA) for TcdA and/or TcdB, GDH detection, polymerase chain reaction (PCR), and stool culturing (Kelly et al., 2021). However, these diagnostic methods have several limitations in terms of speed, sensitivity, specificity, cost and ease-of-use (Gite et al., 2018). Generally, TC and CCNA are considered as reference methods for *C. difficile* identification by detecting toxin A and/or B (Planche and Wilcox, 2011). The application of the TC assay to stool samples leads to the isolation of *C. difficile* strains and determination of their ability to produce toxins. Although this test has shown high sensitivity (95%), it is very cumbersome, expensive, and time-consuming as it takes 3–5 days to be completed (Yücesoy et al., 2002). In addition, TC assays alone may show false-positive results due to the presence of non-toxigenic strains (Alcalá et al., 2008). On other hand, CCNAs have also shown high sensitivity and specificity (90–95%) for detecting toxigenic *C. difficile* strains, but these tests examine the production of toxins *in vitro*, which may not reveal correlations between fecal toxin levels and disease severity. In fact, *in vitro* examination may not reflect the actual *in vivo* toxin levels (Pollock, 2015).

The limitations of using cytotoxicity assays have led to the introduction of alternative techniques, including the application of numerous commercial qualitative EIA tests for detecting toxins A or/and B. These techniques have high specificity (96–98%) compared to toxigenic culture, but low sensitivity (52–75%) (Eastwood et al., 2009; Moon et al., 2016). Therefore, nucleic acid detection techniques that are highly sensitive, should be used as a complementary method (Burnham and Carroll, 2013). However, nucleic acid amplification tests (NAATs) alone are not recommended because these tests can lead to false-positive results as they detect toxin-encoding genes of *C. difficile* regardless of toxin production (Gateau et al., 2018). Recently, detection of pathogen-specific proteins like GDH by EIA or latex particles has been proposed in some studies (Davies et al., 2015; Yoldas et al., 2016). GDH is easily detectable in stool samples and also known as a good screening marker for *C. difficile*. GDH detection methods are of high sensitivity but low specificity as GDH is highly abundant in both toxigenic and non-toxigenic strains, as a result, these methods are incapable to differentiate CDI from asymptomatic colonization or the presence of non-toxigenic strains (Surawicz et al., 2013), thus, additional EIA for detection of toxins A, B, or both is required (Badger et al., 2012; Kelly et al., 2021). A summary of the specificity and sensitivity of various diagnostic tests for CDI compared to toxigenic culture are presented in Table 1.

Presently, there is no agreement on the most appropriate laboratory tests used for CDI diagnosis but much clinical reliance is still on the detection of TcdA and/or TcdB by enzyme-linked immunosorbent assay (ELISA) platforms (Moon et al., 2016; Yoldas et al., 2016; Paitan et al., 2017). However, it is still controversial whether to give priority to detecting bacterial toxins or bacterial infection. Several studies have shown a significant correlation between the level of toxins in the stool and disease severity, as a result, determining the toxin concentrations in the stool can be helpful in disease management and predicting treatment outcomes (Planche et al., 2013; Di Bella et al., 2016; Pollock et al., 2019). Importantly, when the prevalence of *C. difficile* infection is low, no diagnostic test should be used alone because of low positive predictive values. Besides, dissimilarity of the results obtained from different diagnostic tests has made it difficult to consent to a single and reliable standard method, thus, the application of a simple and rapid technique with high sensitivity and specificity for *C. difficile* detection is challenging yet (Burnham et al., 2015; Song et al., 2015). Altogether, the diagnosis of CDI is often confirmed based on the positive results of two or three detection tests (Oldfield et al., 2014), and it is generally recommended to use the three-step algorithm as shown in Figure 1 for accurate CDI diagnosis.

In the past two decades, more rapid methods for detection of toxins of *C. difficile* have been developed and some of them are highly rapid and sensitive but are not yet commercially available (Jarrige et al., 2011; Pollock, 2015; Wilson et al., 2015; Gite et al., 2018). However, providing desirable performance characteristics such as being rapid, easy-to-use, and cost-effective can lead to clinical application of these emerging methods. So far, two commercial clinical biosensor kits have been introduced for CDI diagnosis that can detect the infection in a very short time (Table 2). Additionally, a wide variety of antibody-based diagnostic methods are available for detecting infections of the GI tract. Some of these methods, such as immunofluorescence or ELISA, are laboratory techniques and need trained personnel,

TABLE 1 Summary of diagnostic tests for *Clostridioides defficile* infection.

Test	Substance detected	Sensitivity %	Specificity %	Time required	Limitations	Reference
TC	*C. difficile*	95	80–90	3–5 days	Long turnaround time, trained personnel	Davies et al. (2009), Moon et al. (2016)
CCNA	Toxin	95	90–95	1–3 days	Long turnaround time, trained personnel, technical demands	Huang et al. (2009), Reller et al. (2010)
GDH	*C. difficile*	95–100	88–92	Hours	Low specificity, false-negative results	Eastwood et al. (2009), Cheng et al. (2015), Ramos et al. (2020)
EIA toxin	Toxin	51–80	98–99	Hours	Low sensitivity	Davies et al. (2009), Eastwood et al. (2009)
NAATs	*C. difficile*	92–97	83–100	Hours	Low specificity, costly and technical demands	Davies et al. (2009), Eastwood et al. (2009), Paitan et al. (2017)
GDH and EIA toxin	Toxigenic *C. difficile*	83–100	97–100	Hours	Dependent on toxin results, some variation in reported sensitivity	Kim et al. (2014), Cheng et al. (2015)
NAATs and EIA toxin	Toxigenic *C. difficile*	77–100	91–100	Hours	Some variation in reported sensitivity, technical demands	Huang et al. (2009), Humphries et al. (2013)

TC, toxigenic culture; CCNA, cell-culture cytotoxicity neutralization assay; EIA, enzyme immunoassay; GDH, glutamate dehydrogenase; NAATs, nucleic acid amplification tests.

while others, such as agglutination techniques, membrane EIAs, and lateral flow immunoassays (LFIAs), are very simple and fast (Balsalobre-Arenas and Alarcón-Cavero, 2017). Different formats of antibodies applied in diagnostic tools are discussed below.

Applicable formats of antibody for detection purposes

Antibody-based detection methods, like EIA, ELISA, and LFIAs or immune-chromatographic tests (LFIA/ICT), are mostly designed based on the use of mAbs and pAbs in their platforms. The antibodies were first produced as pAbs and their production is still ongoing for various purposes. Normally, pAbs are made through the vaccination of animals such as rabbits, goats, and sheep, and can be rapidly generated at less expense and not requiring complicated technical skills (Stills, 2012). These molecules are produced by different B cell clones in the body, thus are usually a heterogeneous mixture, which can recognize multiple epitopes of antigen (Figure 2A). This property of pAbs can lead to the risk of low specificity and cross-reactivity with different targets (Ascoli and Aggeler, 2018).

The technique of mAb production, known as hybridoma technology, was invented by Kohler and Milstein in 1975 (Köhler and Milstein, 1975; Figure 2B). Although the hybridoma technology has been successful, it has many shortcomings, e.g., limited number of candidates, time-consuming, inefficiency to generate antibodies toward highly conserved antigens, self-antigens, sensitive antigens, and toxic antigens. A strategy that overcome the disadvantages of hybridoma is techniques based on *in vitro* antibody production, e.g., yeast display, ribosome display, phage display, and mammalian cell display methods (Raeisi et al., 2022a; Valldorf et al., 2022), which among them, phage display and ribosome display are preferred in most laboratories due to their large diversity in the range of 10^{12}–10^{15} variants with high transformation efficiency (Kunamneni et al., 2020; Raeisi et al., 2022a). Here, we discuss the rAb techniques that are currently being studied for diagnosis proposes.

In vitro recombinant antibody technologies

In vitro antibody display technologies, also called recombinant antibody technology, are prepared based on the diverse antibody genes contained in a specified library. The first display technology introduced was phage display, which was presented by Georg P. Smith in 1985 (Willats, 2003). Since these technologies depend on *in vitro* screening rounds, the production of antibodies could be much easier and more cost-effective than *in vivo* conditions (Alfaleh et al., 2020). A unique property of rAbs is the high affinity and specificity of them for detecting target molecules. Alternatively, the main concern in the development of immunoassays has always been the increase in the sensitivity and affinity of antibodies, which can be achieved by the possibility of integration of *in vitro* antibody display technologies with genetic engineering (83). In addition, using *in vitro* expression systems for the production of rAb fragments can finally lead to achieving sufficient amounts of antibodies for diagnostic purposes (Wang et al., 2013; Jensen et al., 2018) and allowing the construct of new different types of rAb fragments, including Fab, scFv, domain antibodies (dAbs), bivalent antibodies, multivalent antibodies,

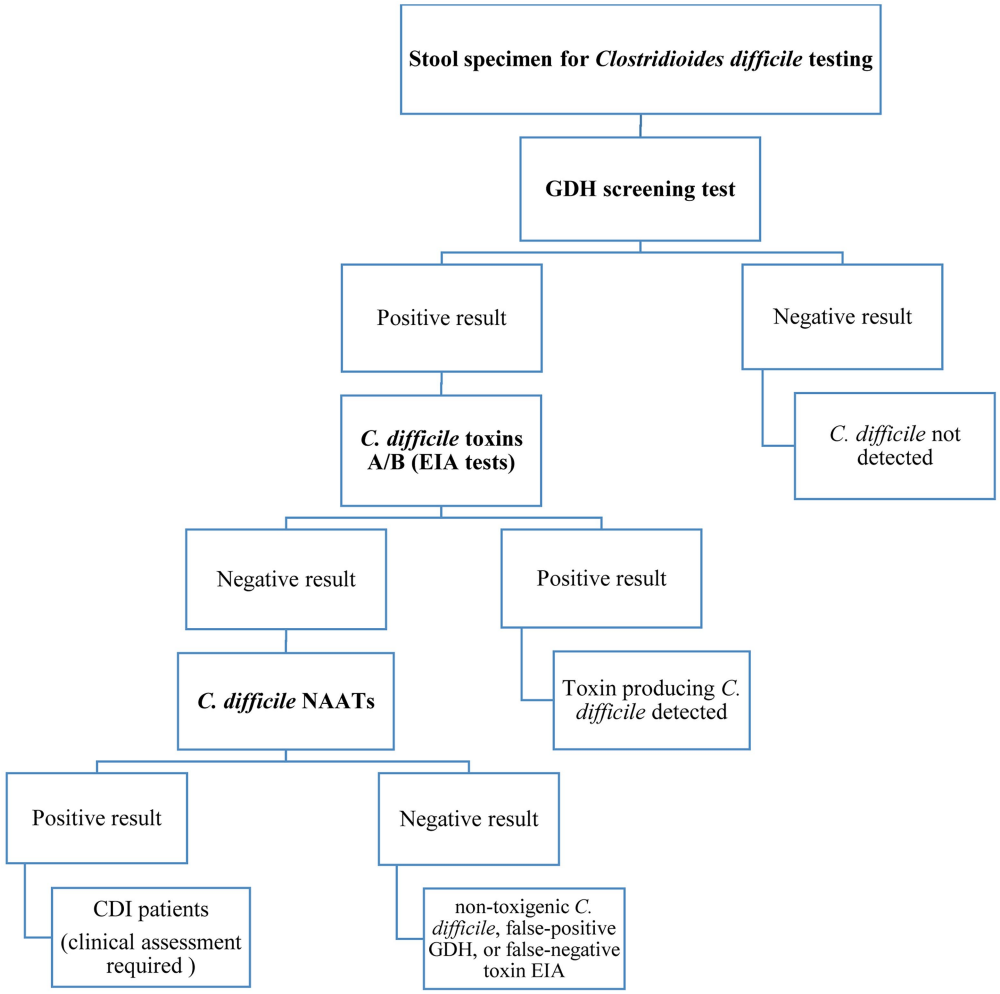

FIGURE 1
Three-step algorithm for diagnosis of *Clostridioides difficile* infection.

TABLE 2 Examples of commercially available clinical biosensors kits for *Clostridioides difficile* infection.

Platform	Target (analyte)	Transducer Platform Biosensor	Detection format	Applicability	LOD	Response time	Reference
Commercially available clinical biosensors	GDH (Clostridioides *K*-SeT)	Membrane-based lateral flow assay	Optical	Stool	0.5 ng/mL	15 min	https://www.corisbio.com/products/Clostridioides-k-set
	Whole cells (DR1107A, Oxoid, Hampshire, UK).	Rapid latex agglutination	Colorimetric latex agglutination	Selective media	N/A	2 min	https://www.thermofisher.com/order/catalog/product/DR1107A#/DR1107A

GDH, glutamate dehydrogenase; N/A, not available.

and bispecific antibodies (Yang et al., 2014; Fan et al., 2015; Høydahl et al., 2016). In terms of production of rAbs, ribosome display and phage display technologies have been introduced as potent *in vitro*, cell-free systems for the screening of large libraries, which can select high-affinity binders against various antigens without compromising the library (Li et al., 2019; Hammerling et al., 2020; Valldorf et al., 2022).

Ribosome display and phage display technologies

Ribosome display technology is known as a powerful tool for the rapid isolation and direct evolution of high-affinity binders, particularly antibodies. This technology generates a stable complex containing antibody–ribosome–mRNA that can link

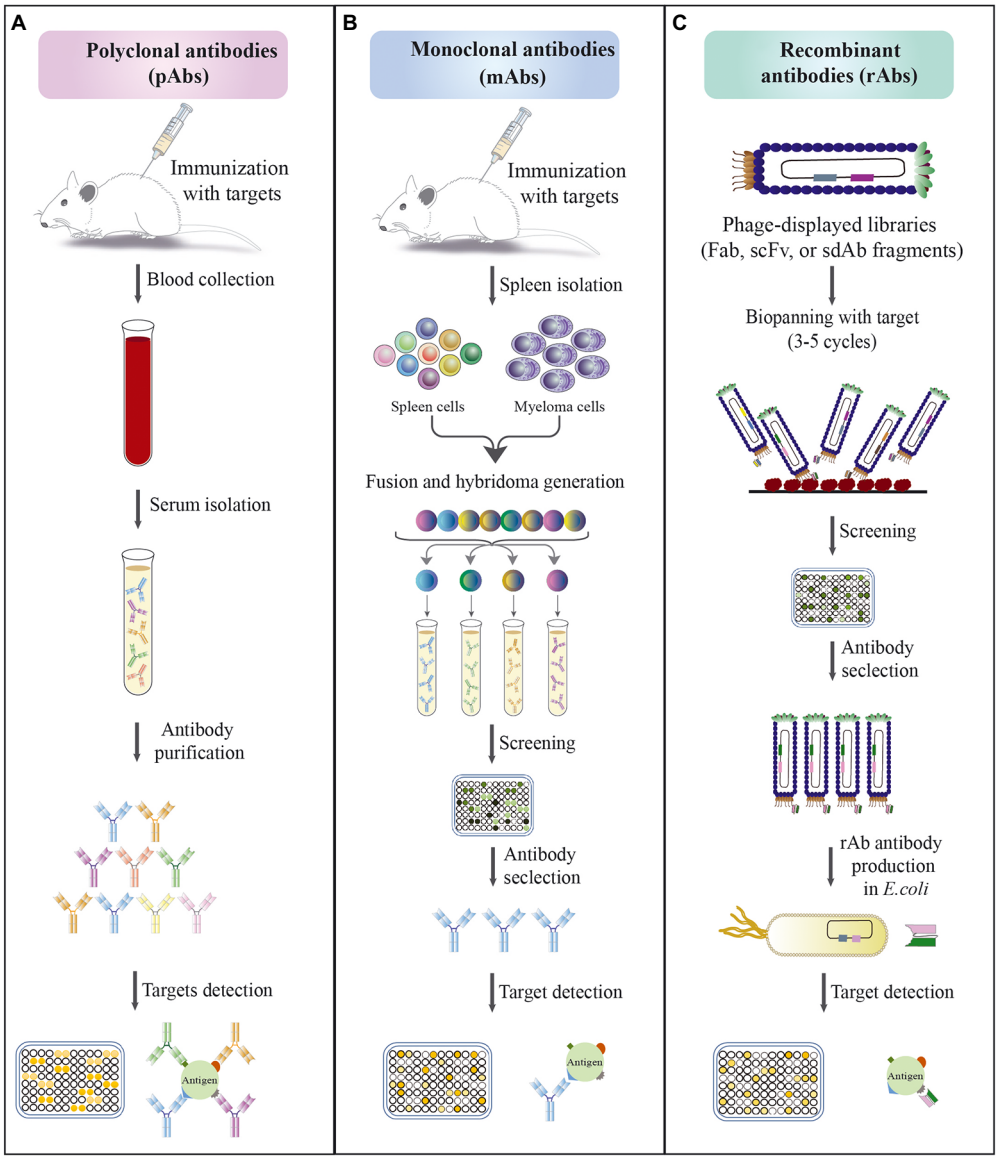

FIGURE 2
Schematic approaches for the development of different types of antibodies. **(A)** Polyclonal antibodies production; the methods' steps include: (1) immunization of animals with an antigen to trigger immune response; (2) blood collection from immunized animals; (3) serum isolation; (4) antibody purification; (5) evaluation of the affinity of antibodies against antigen by immunoassay. **(B)** Monoclonal antibody production by hybridoma technique; the methods' steps include: (1) immunization of animals with an antigen to trigger immune response; (2) isolation of antibody-producing cells from the mouse spleen; (3) fusion of B cells with myeloma cells to produce hybridoma cells; (4) screening and selection of high affinity antibody produced by hybridoma cells; (5) evaluation of the specificity of selected antibodies against antigen by immunoassay. **(C)** Recombinant antibody production by phage display technology; the methods' steps include: (1) amplification of library; (2) exposure of the library to a surface coated with specific antigen; (3) elution of bound phages and their application for a new selection round; (4) screening of positive phage clones by ELISA after 3–5 rounds of biopanning; (5) selection of specific phages and their expression; (6) evaluation of the specificity of selected antibodies against antigen by immunoassay.

individual antibody fragments to their respective mRNA (Kunamneni et al., 2020). Conceptually, the ribosome display technique includes several steps, including library preparation, *in vitro* transcription and translation, screening and selecting a specific mRNA, and reverse transcription-PCR (RT-PCR) for further screening rounds or analysis (Li et al., 2019). Briefly, in this method, the mRNA lacks a termination codon (nonstop mRNA) at the end of the coding sequence, which holds the translating ribosome at the end of mRNA and creates an unreleased nascent polypeptide. This process results in the formation of antibody–ribosome–mRNA complexes, allowing simultaneous isolation of antibody fragments and their corresponding mRNA through an affinity for an immobilized antigen. To isolate high-affinity protein–mRNA complexes, 3–5 rounds of panning are carried out, and selected complexes are subjected to *in situ* RT-PCR to recover the DNA encoding protein sequence (Kunamneni et al., 2020).

Within the past two decades, the production of rAbs, particularly scFvs, has been strikingly accelerated through ribosome display technology. Moreover, this technology has become a popular tool in medicine for basic research, disease diagnostics, and therapy (Park, 2020; Valldorf et al., 2022). However, one of the limitations of this method is the accessible, functional ribosome levels in the reaction for the library, which relates to the library size (Kunamneni et al., 2020). The ribosome display technology has been applied for selecting scFvs with high affinity against different targets such as tumor cells (Huang et al., 2018), Zika virus (ZIKV) (Kunamneni et al., 2018), *Mycobacterium tuberculosis* (Ahangarzadeh et al., 2017), and severe acute respiratory syndrome coronavirus 2 (SARS-CoV-2) (Chen et al., 2021). Moreover, it has been successfully used for scaffold selection, including affibodies (Lagoutte et al., 2019), however, there are no reports about antibody selection through ribosome display for CDI diagnosis or treatment. Overall, this method could be undoubtedly considered to select specific antibodies for new targets for diagnostic or therapeutic purposes in the future.

Additionally, the phage display technique is one of the most widely used technologies for the production of rAbs. In this technology, specific peptides or proteins are displayed on the surface of the filamentous phage particles through fusion between the genes encoding the antibody with the coat protein (pIII or pVIII) of the phage (Figure 2C). Therefore, a foreign phenotype is displayed on the phage surface that it's the genotype is retrievable in the phage (Schirrmann et al., 2011). The phage display technique contains the following steps: cloning of antibody-gene library, packaging of the resulting phagemids into phage particles presenting the respective antibody fragment on its surface, bio-panning to enrich antibodies binding to target structure, amplification of binding antibody phage, screening of individual antibody clones for the desired characteristics, e.g., by ELISA, subcloning of selected antibodies, and expression in format and expression system of choice (Hammers and Stanley, 2014). The most common method of bio-panning is coating antigens on a solid surface with high protein-binding capacity, such as polystyrene tubes (Jensen et al., 2018; Lu et al., 2020). In the next step, the surface coated by antigen is exposed to phage library, then, stringent washing of the surface is performed to remove nonbinding antibody phage. Subsequently, elution of the bound antibody phage is conducted by methods like pH shift or by using trypsin, and then, reamplification is done by infection of *Escherichia coli*. Reamplified phage will be used in the next round of panning. It is expected that after each round of panning, the number of specific binding phages is increased. After 3–5 panning rounds, antigen-specific antibody phage will be checked by several methods such as ELISA, immunoblotting, or flow cytometry (Bazan et al., 2012). This approach is similarly done for the production of both therapeutic and diagnostic antibodies (Schirrmann et al., 2011; Frenzel et al., 2017).

The phage display technique has been widely used for detecting various targets, such as haptens, toxins, foreign and self-antigens (Tullila and Nevanen, 2017; Hussack et al., 2018; Raeisi et al., 2022a). For example, a specific antibody against a tumor marker expressed by breast tumor, named ErBb2 protein, has been selected through naïve antibody library that is useful in immunoassay tools (Bakir et al., 1993). Furthermore, many rAbs derived from page libraries have been examined for diagnosis or therapy of bacterial diseases; the majority of these rAbs have been developed to facilitate disease detection and estimate the presence of contamination in environmental and food samples or levels of sample contamination (Kuhn et al., 2016; Priyanka et al., 2016). These rAbs are usually designed for various purposes, including detection of whole bacterial cells or toxins, blocking receptors, and modulating the host immune system (Kuhn et al., 2016), among them, whole bacterial cells are mostly applied for diagnostics (Byrne et al., 2013). An overview of rAbs derived from phage display libraries against *C. difficile* is presented in Table 3.

Development of rapid detection methods based on recombinant antibodies against *Clostridioides difficile*

In recent decades, the design of rapid diagnostic methods based on pAb or mAb antibodies have been attracted much attention. Accordingly, a wide variety of antibody-based diagnostic methods are available for the diagnosis of GI tract infections, such as immunofluorescence, ELISA, and various immunosensors. Additionally, the rAb technologies are considered as powerful tools to provide next-generation immunoassays (Sang et al., 2015;

TABLE 3 Recombinant antibodies derived from phage display libraries against *Clostridioides difficile*.

Target	Antibody format	Antibody origin	Application	References
TcdB	scFv	Human	ELISA	Deng et al. (2003)
FliC, FliD	scFv	Human	ELISA, WB, *in vitro* assay	Shirvan and Aitken (2016)
SLP	sdAb	Llama	ELISA, WB, *in vitro* assay	Kandalaft et al. (2015)
TcdA	sdAb	Llama	ELISA, WB, *in vitro* neutralization	Hussack et al. (2011)
TcdA, TcdB	sdAb, bispecific	Alpaca	ELISA, *in vitro* assay, *in vivo* protection	Yang et al. (2014)
TcdB	scFv-Fc	Human	*in vitro* neutralization	Chung et al. (2018)
Binary CDT toxin	sdAb, sdAb-Fc	Llama	ELISA, IF	Unger et al. (2015)

TcdA, toxin A; TcdB, toxin B; SLP, surface-layer protein; scFv, single-chain fragment variable; sdAb, single-domain antibodies; Fc, fragment crystallizable region; ELISA, enzyme linked immunosorbent assays; WB, western blot; IF, immuno fluorescence microscopy.

Dinarelli et al., 2016). The advantages of these antibodies, e.g., ease of production in *E. coli* and its reproducibility, have made them much popular than conventional antibodies (Frenzel et al., 2017; Sun et al., 2018). More importantly, this single-chain format of antibodies can be easily fused with other proteins, such as detector enzymes, e.g., alkaline phosphatase (AP), resulting in formation of antibodies with multiple functions which can increase both the reaction rate and the sensitivity of diagnostic assays. In fact, the design of ELISA-based scFv-AP fusion proteins helps simultaneous use of two properties, namely binding specificity of antibody and AP enzyme activity. For instance, application of scFv-AP fusion proteins for different targets such as ractopamine (Dong et al., 2012), aflatoxin (Rangnoi et al., 2011), and glycocholic acid (Cui et al., 2018) have been described.

The following are examples of new diagnostic methods developed for detection of *C. difficile*. Moreover, various other diagnostic platforms based on rAb technology are well discussed.

Enzyme-linked immunosorbent assay

One of the most favorite immunoassay techniques is ELISA. Due to its high performance, low cost, high speed and possibility to test a large number of samples simultaneously, ELISA-based kits became the standard technique for diagnosis of various agents (Mollarasouli et al., 2019). Developing toxin ELISAs as a rapid test that is based on mAbs or pAbs has always attracted much attention. For example, development of double-antibody sandwich (ds) ELISA by using mAb targeting the receptor binding region of TcdB (anti-CDB3) produced by hybridoma technologies was reported by Chen et al. which was regarded as an effective method for reliable diagnosis of CDI by detecting TcdB in diarrhea stools (Chen et al., 2015b).

Additionally, rAbs can be used as an alternative attractive strategy to mAbs and pAbs. Successful application of scFv antibodies in various ELISA platforms is reported in many studies; for instance, the development of ELISA based on phage-displayed scFv antibodies was reported for detecting *B. melitensis* (Hayhurst et al., 2003), IFN-γ antigen (Yang et al., 2018), cowpea chlorotic dwarf virus (Raeisi et al., 2020), citrus tristeza virus (Raeisi et al., 2022b; Chen et al., 2015b), the protein components of type three secretion system of *Xanthomons citri* (Raeisi et al., 2019), *B. thuringiensis* (Dong et al., 2018) and so on. Moreover, several publications have reported the development of diagnostic VHH-based ELISA assays for rapid diagnosis of specific targets. Detection of influenza H5N1 virus (Zhu et al., 2014a), *B. thuringiensis* (Wang et al., 2014), *Listeria monocytogenes* (Tu et al., 2015), and ochratoxin A (Zhang et al., 2019) are few examples of VHHs application in ELISA platforms.

The application of rAbs for the quantitative detection of toxins can also be a reliable approach, which costs less than conventional ELISAs. There are some reports in the literature for successful application of rAbs in detection of toxins. In this regard, scFv antibodies against toxin B of *C. difficile* were reported by Deng et al. (2003). The performance of anti-TcdB scFv fragments was shown by a sandwich ELISA and the results demonstrated that the isolated scFvs had high specificity to detect toxin B and did not have cross-reactivity with toxin B-negative *C. difficile* bacteria. Interestingly, isolated scFv fragment had higher sensitivity than the mAb and could detect a minimum of 10 ng of toxin B/well. In another study, Unger et al. (2015) evaluated the ability of anti-binary toxin sdAb fragments in blocking cytotoxic effect of the binary toxin, and results confirmed the proper function of sdAbs against this toxin; it was concluded that these sdAbs are promising new diagnostic tools for diseases associated with *C. difficile* (Unger et al., 2015).

Chemiluminescent immunoassay

Chemiluminescent immunoassay (CLIA) is an immunoassay technique using luminescent molecule as an indicator of the analytic reaction that composes of combination of chemiluminescence techniques and immunochemical reactions (Cinquanta et al., 2017). This method is similar to other labeled immunoassay such as ELISA, except that CLIA substrates generate light emission in the presence of an enzyme, causing a more sensitive process compared to ELISA. Since CLIA technique has many advantages such as high sensitivity and specificity, rapidity, high stability of reagents, and compatibility with immunology assay protocols, it has been used to measure hormones, tumor markers, autoantibodies, and infectious disease markers (Chen et al., 2012).

Recently, use of magnetic-particle-based chemiluminescent enzyme immunoassay (CLEIA) for detection of *C. difficile* has been reported by Qi et al. (2020a). In this study, a CLEIA was developed using an anti-toxin B mAb-coated magnetic particles and anti-toxin B mAb conjugated to AP enzyme. The proposed CLEIA demonstrated high sensitivity for toxin B detection and showed a linear working range from 0.12 to 150 ng/mL with a limit of detection (LOD) of 0.47 ng/mL, which was similar to those of a commercial ELISA kit. This method could detect antigen in stool samples in less than 30 min, indicating high potential of the proposed method for rapid TcdB detection.

Immunosensors

Antibodies can be used in the design of biosensors for rapid diagnosis purposes. Biosensors are known as devices for rapid detection or determination of the concentration of biological analytes like biomolecules, biological structures or microorganisms (Mehrotra, 2016). A biosensor typically consists of a biorecognition element and a transducer (Figure 3). A biorecognition element must identify a specific analyte and interact with it. The interaction between biorecognition element and analyte changes the biosensor's properties; these changes are converted by the transducer into a measurable signal that is

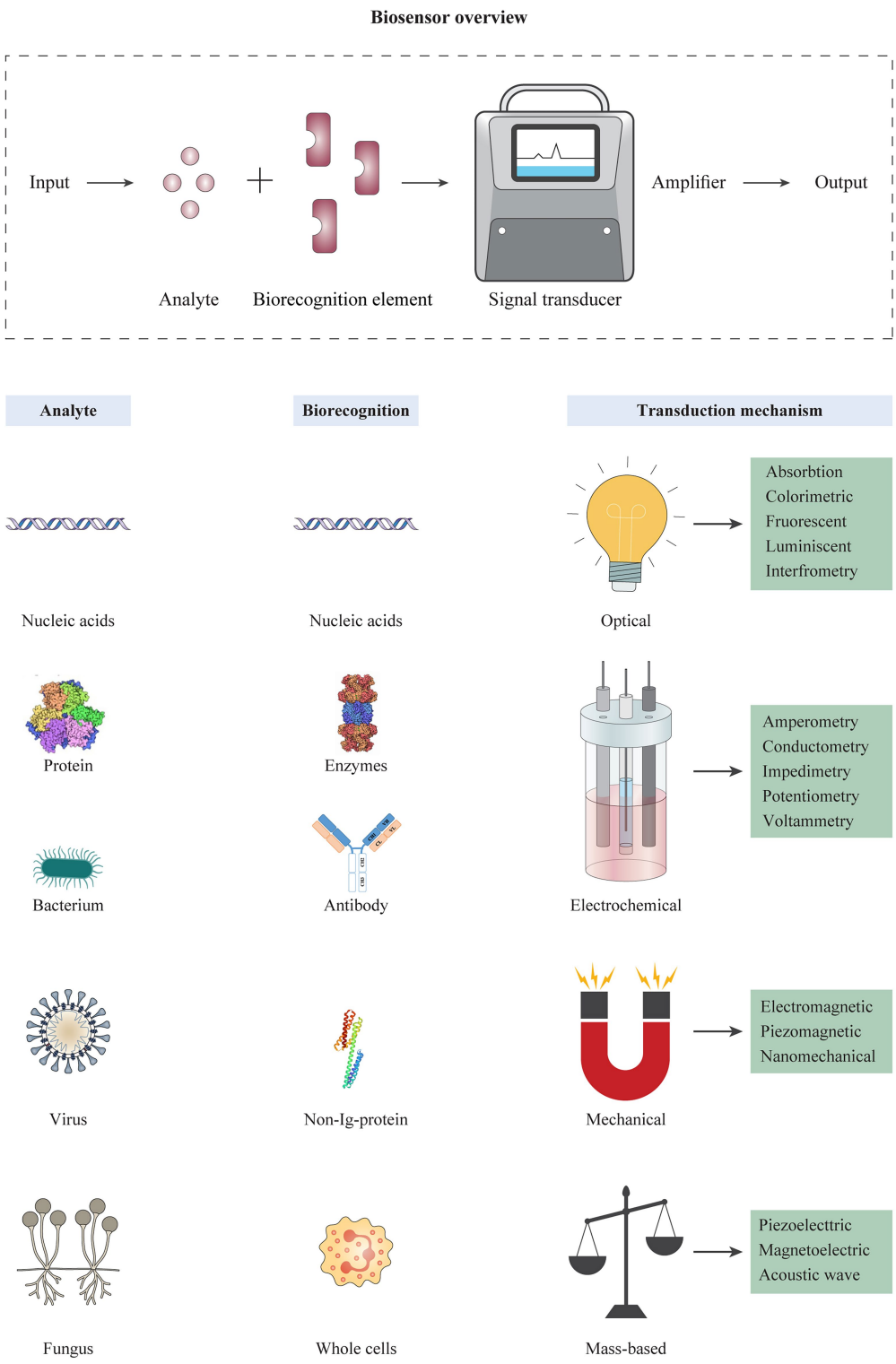

FIGURE 3
Schematic overview of biosensor platforms consisting of different types of analytes, biorecognition elements, and transduction mechanisms. The operation of a biosensor is based on detection of an analyte by a highly specific biorecognition element. Analytes usually include biomolecules such as nucleic acids, proteins, and different cells. The reaction of an analyte with the biorecognition element is transformed into an electrical, optical, or electrochemical signal by a transducer, and converted into displayable data. The different types of biorecognition elements are used in the design of biosensors, including nucleic acids, antibodies, non-long-proteins, and/or synthetic ligands. Biosensors can be categorized based on the transducing mechanism, including optical, electrochemical, mechanical, and mass-based biosensors, which each category contains several platforms.

a form of energy, e.g., optical, thermal, and electrical. Thus, the encounter of sensors with specific pathogens or pathogenic byproducts leads to the production of positive detection signals (Bhalla et al., 2016). Classification of biosensors is based on the type of biorecognition element (e.g., enzyme, antibody, and nucleic acid probe) or the transducing method used (e.g., piezoelectric, optical, and electrochemical; Alhadrami, 2017), and different techniques are classified like nano-or micro-technology platforms accordingly. Importantly, integration of nanotechnology with biosensor systems can augment the analytical efficiency of detection methods and provide more sensitive and accurate diagnosis (Zhu et al., 2014b; Pan et al., 2017; Cho et al., 2020). This technique helps to improve characteristics like sensitivity (e.g., low LODs), assaying time, and analytical procedures. In this regard, gold nanoparticles (AuNPs) are known as one of the most widely used nanomaterials in biomedical research and clinical imaging (Hammami et al., 2021). Biocompatibility, non-toxicity, ease of characterization, and high stability are some of the significant properties of AuNPs that promote their diverse applications (Cabuzu et al., 2015; Hu et al., 2020). So far, there are successful reports for the use of these compounds to detect various viruses and bacterial agents (Mocan et al., 2017; Singh et al., 2017).

Antibody-based sensors or immunosensors, are a popular format of biosensors that change the transducer signal when a specific antigen–antibody reaction is detected (Cho et al., 2020). Various immunosensors have been developed and they have gained much attention in biochemical analyses (Tang and Xia, 2008), clinical diagnoses (Morris, 2013), food quality control (Scognamiglio et al., 2014), and environmental monitoring (Mehrotra, 2016). Therefore, they seem to be excellent candidates for rapid and sensitive diagnosis of diseases and pathogens as far as there are many reports of their use for detection of bacteria such as *E. coli* (Park et al., 2008), *Salmonella enterica* (Cinti et al., 2017), *Salmonella typhimurium* (Fulgione et al., 2018), and *X. citri* (Haji-Hashemi et al., 2018). Immunosensors can be designed on the basis of different types of antibodies (pAbs, mAbs, and rAbs), however, most of the immunosensors are designed based on pAbs and mAbs.

Additionally, fragment antibodies such as sdAbs, scFvs, and Fabs have emerged as suitable alternatives to design biosensors (Ahmad et al., 2012). Although rAbs have several significant advantages over conventional antibodies, they are yet not fully exploited in fabrication of immunosensors. There are some reports for application of rAbs in designing various immunosensors, e.g., optical biosensors (Damborský et al., 2016; Peltomaa et al., 2018), electrochemical detection (Grewal et al., 2013), LFIA (McDonnell et al., 2010; Kim et al., 2020), and piezo-immunosensors (Shen et al., 2007). However, most sensors designed to detect *C. difficile* are based on nucleic acid probes, aptamers or mAbs, examples of which are given in Table 4, there are limited research published on biosensors that are designed based on rAbs. Below, application of different immunosensors for rapid detection of *C. difficile* are discussed.

Electrochemical immunoassays

Among different types of biosensors, electrochemical immunoassays have gained much attention as a bioanalytical method. These diagnostic methods can become a promising approach with high sensitivity and specificity in the future; they have many advantages like ease of signal quantification, low cost, rapidity, high compatibility, high repeatability, high sensitivity, ease of integration, and miniaturization (Kimmel et al., 2012; Cho et al., 2020). Design of a mAb-based electrochemical immunoassay is a successful example of application of electrochemical immunosensor for detecting *C. difficile* (Fang et al., 2013). In particular, Fang and co-workers developed a simple sandwich-assay type electrochemical immunosensor to detect TcdB by using graphene oxide (GO) as a scaffold to improve the surface area to capture a large number of primary antibodies. In this system, horseradish peroxidase (HRP)-labeled secondary TcdB antibody was also introduced on the electrode surface through the unique properties of AuNPs. Coating antibodies with nanoparticles caused a large amount of antibody entering the biosensor system leading to an increase in electrochemical impedance signal, and as a result the sensitivity in diagnosis was increased, so that this system showed a linear working range from 3 pg/mL to 320 ng/mL with a LOD of 0.5 pg/mL under optimal experimental conditions, which was much lower than that of other conventional methods like ELISA. More importantly, high specificity of the produced electrochemical immunosensor for detecting TcdB in stool samples, indicated that application of this immunosensor can be a promising option in clinical diagnosis of CDI.

Application of AuNPs coated by specific antibodies to detect *C. difficile* or its toxins has been also reported by Zhu et al. (2014b). In this work, an electrochemical impedance immunosensor based on AuNPs coated with anti-toxin sdAb antibodies for detecting both TcdA and TcdB was designed (Zhu et al., 2014b). The results showed LODs of 0.61 and 0.60 pg/mL for TcdA and TcdB, respectively, that are indicative of high sensitivity of this method. Evaluation of immunosensor efficiency for detecting toxins in stool samples showed that the designed biosensor can be potentially used in clinical applications. These promising results prove that the use of AuNPs in immunosensors led to an excellent performance with high sensitivity. However, this method requires a relatively complex procedure that is not easily available.

In another study, Cui et al. (2018) developed a label-free electrochemical biosensor for TcdB detection. In this work, sdAb isolated against TcdB was used for preparing polyurethane (PU) electrodes with nanospiked gold electrode-based label-free electrochemical immunosensor. Signal amplification in this method was six times as high as flat PU gold electrode-based immunosensor. Based on these results, the PU nanospiked gold electrode-based immunosensor can be an excellent option for rapid detection of TcdB especially when low cost and simple processing is expected (Cui et al., 2018). Recently, the use of silica

TABLE 4 Examples of rapid detection used for *Clostridioides difficile* infection.

Biorecognition elements	Target (analyte)	Platform	Detection format	Applicability	LOD	Response time	References
Nucleic acid	Spores	Magnetic bead aggregation	LAMP coupled to PiBA	Selective media	N/A	N/A	DuVall et al. (2016)
	Toxins	Magnetic	NMR-based technology	Stool	<180 CFU/mL	45 min	Yang et al. (2017)
	TcdA/B	Magnetic	ELISA sandwich assays	Stool	1.35 μg/mL	N/A	Hong et al. (2015)
	TcdA/B	MEF	Optical	Stool	10 CFU/mL	40 s	Joshi et al. (2014)
	TcdB	PEPS	Electrical impedance (PEPS) (direct detection)	Stool	150 CFU/mL	40 min	Han et al. (2019)
	TcdA/B	FMSM	Optical	Stool	1.12 ng/mL	20 min	Yang et al. (2020)
Aptamer (aptasensor)	TcdA/B, binary toxin	Magnetic Beads/SOMAmer	ELISA sandwich assays	Selective media	1 pg/mL to 300 pg/mL	N/A	Ochsner et al. (2013), Ochsner et al. (2014)
	GDH	Fuorescence emission structure-switching fluorescence signaling aptamer	Optical	Stool	1 pg/mL	60 min	Liu et al. (2018)
	TcdA	Colorimetric	Electrochemical impedance	Stool	1 pg/mL	N/A	Luo et al. (2014)
	TcdB	Colorimetric	Colorimetric assay	Stool	600 and 60 pg/mL	30 min	Liu et al. (2020)
	TcdB	Colorimetric	Colorimetric assay	Stool	5 ng/mL	30 min 60 min	Luo and Liu (2020)
	GDH	Colorimetric	Colorimetric assay	Selective media	10 μg/mL	30 min	Hui et al. (2018)
Enzyme based	Specific protease, PPEP-1	Bioluminescent Sensor	Optical	Stool	10 μg/mL	30 min	Ng et al. (2021)
Antibody	TcdB	Amperometric	Electrochemical	TcdB	0.3 ng/mL	30 min	Xu et al. (2014)
	TcdA/B	Impedance	Electrochemical	Stool	0.6 pg/mL	30 min	Zhu et al. (2014b)
	TcdB	DPV	Electrochemical	Stool	0.7 pg/mL	45 min	Fang et al. (2013)
	GDH	Lateral flow immunoassay	Optical, thermal	Selective media	1.0625 ng/mL 0.1328 ng/mL	N/A	Wang et al. (2016)
	TcdB	Magnetic and fluorescent particles	Automated ELISAs	Stool	45 pg/mL	30 min	Gite et al. (2018)
	Toxins	Single-molecule array technology	Automated ELISAs	Stool	45 pg/mL	N/A	Banz et al. (2018)
	TcdB	Impedance polyurethane (PU) nanospiked gold electrode	Electrochemical (DPV)	Stool	0.5 pg/mL	40 min	Cui et al. (2018)
	TcdA/B	Fluorescence	Optical	Stool	N/A	40 s	Joshi et al. (2014)
	SlpA, TcdB	SERS-based LFA	Optical	Stool	0.01 pg/mL	20 min	Hassanain et al. (2021)
	GDH, TcdB	Split-luciferase assay, luminescent	Optical	Stool	4.5 pg/mL 2 pg/mL	32 min	Adamson et al. (2022)

GDH, glutamate dehydrogenase; TcdA, toxin A; TcdB, toxin B; LAMP, microfluidic loop-mediated isothermal amplification; PiBA, product-inhibited bead aggregation; MEF, metal enhanced fluorescence; MAMEF, microwave accelerated metalenhanced fluorescence; PEPS, piezoelectric plate sensor; FMSM, fluorescent magnetic spore-based microrobot; ELISAs, enzyme-linked immunosorbent assays; PPEP-1, pro-pro endopeptidase 1; DPV, differential pulse voltammetry; SERS-based LFA, surface enhanced Raman scattering-based lateral flow assay; N/A, not available.

10.3389/fmicb.2022.1043214

nanoparticles in designing electrochemical biosensor has led to sensitive and specific detection; this technique was able to sensitively detect bacteria in five minutes by cyclic voltammetry measurements, and interestingly, this device could detect other microorganisms with minor modifications within its features (Mathelie-Guinlet et al., 2019), and can be considered as a potential diagnostic platform in future.

Optical biosensors

In addition to electrochemical immunosensor, optical biosensors are a popular form of detection methods and known as a powerful alternative to conventional analytical techniques, particularly for their small size, high sensitivity, and cost effectiveness (Damborský et al., 2016). Diagnosis made by optical biosensors is based on sensitive detection of photon emission from dyes and molecules excited by light. Hence, fluorescent probes are the most widely used probes in these biosensors that can emit photons after interacting with specific targets such as antigens, antibodies, or genomic material. The fluorescence emission helps to increase the sensitivity, thus, the results obtained by these methods are more reliable than conventional detection methods such as microscopy or enzyme-based detection. These biosensors are widely reported for detecting bacteria, such as *S. typhimurium* (Seo et al., 1999), *E. coli* (Riangrungroj et al., 2019), and *S. enterica* (Quintela et al., 2019).

Generally, optical biosensors have been applied in different platforms. In this regard, the application of MultiPath immunoassay technology that uses non-magnified digital imaging to count molecular targets labeled microscopic fluorescent particles has been reported by Gite et al. (2018). In this work, a novel MultiPath immunoassay technology was developed for highly sensitive detection of *C. difficile* toxin B antigen based on anti-TcdB mAbs, which are conjugated to magnetic and fluorescent particles through a carboxyl linkage (EDC/NHS chemistry; Gite et al., 2018). This technology counts and images target-specific magnetic and fluorescent particles banded together by anti-TcdB in minimally processed stool samples. This technology can efficiently detect CDI due to its advantages including minimal sample preparation, rapid diagnosis, and requiring simple optical equipment. This study demonstrates that the designed immunosensor has an equivalent performance to cytotoxicity assay in terms of sensitivity for toxin B detection, so that the results showed LOD of 45 pg/mL with 97% sensitivity; 98.3% specificity; and 98.2% accuracy for the MultiPath TcdB test, which was similar to cytotoxicity assays and significantly better than on-market EIAs. In addition, this method shows superiority to NAATs because it directly detects the toxins secreted by vegetative *C. difficile* cells even at very low concentrations, while the NAATs detects the toxin in dormant spores which do not cause disease, thus, false positive results can be avoided. Recently, the use of single-molecule array (Simoa) technology was described for ultrasensitive detection of toxins (Song et al., 2015). Simoa technology, also known as digital ELISA, is based on efficient capture, labeling and detection of single protein molecules on paramagnetic beads in arrays of femtoliter-sized wells. This method has a very low LOD, and it is about 1,000-fold more sensitive than conventional ELISA (Rissin et al., 2010). There is no report on the use of specific anti-*C. difficile* rAbs using this technology and only the design of Simoa technology based on mAbs was reported for CDI diagnosis. The development of Simoa technology for detecting TcdA and TcdB by Song et al. (2015) showed that this method can detect all strains producing toxins in the stool specimens with LODs of 0.45 and 1.50 pg/mL for TcdA and TcdB, respectively (Song et al., 2015). In another work, Sandlund et al. (2018) introduced an automated single-molecule counting technology for detecting *C. difficile* toxin A and B (Sandlund et al., 2018) in stool samples with a low LOD of 2.0 pg/mL for TcdA and 0.7 pg/mL for TcdB, which was similar to Simoa technology; however, the dependence of both methods on fluorescent labeling complicates and limits their operations and use.

Lateral flow immunoassays

Recently, researchers have made undeniable efforts to develop assays that do not rely on laboratory equipment. LFIA as one of such examples is a rapid technique which has attracted a lot of attention. Today, LFIA is widely used for various monitoring and diagnostic purposes, particularly for on-site use in veterinary to serve as analytical tests for a range of biochemical analytes, for medical and food safety purposes, home-pregnancy test (Koczuła and Gallotta, n.d.), human immunodeficiency virus (HIV) diagnosis (Nguyen et al., 2009), and SARS-CoV-2 detection (Moshe et al., 2021). The assay is performed on a sheet-shaped matrix, e.g., cellulose, containing freely labeled antibodies with a color or the fluorescent mark. The assay implements where an analyte interacts with a detection reagent and an immobilized capture reagent. Several types of antibodies (mAb, pAb, rAb, HRP-conjugated, AP-conjugated, etc.) are applied in LFIAs. Notably, LFIAs are known as a suitable approach to implement on-site and they are also compatible with already available commercial tests. Due to their customer-friendly and low-cost features, they would be potentially applied in diagnostic platforms in future (Liu et al., 2021). Application of these devices has many advantages as they are fast, easy to use, portable, and they do not require external equipment (Koczula and Gallotta, 2016), leading to the popularity of these biosensors among researchers. Currently, application of LFIA methods for determination of harmful substances in food is being investigated. The use of LFIAs to detect *Enterococcus faecalis*, *Staphylococcus aureus* (Wang et al., 2017a), *L. monocytogenes* (Wang et al., 2017b), *Shigella* (Wang et al., 2016a), and *Leptospirosis* (Nurul Najian et al., 2016) has been successful so far. Combination of LFIA methods with nanoparticles, including AuNPs (Sun et al., 2015; Fu et al., 2017; Jiang et al., 2017), fluorescent-microsphere-derived ICA (F-ICA), and time-resolved Eu/Tb (III) nanoparticles ICA (TRF-ICA) (Tang et al., 2017; Zhang et al., 2017) was

suggested in biomarkers designing. Furthermore, application of nanoparticles such as gold in LFIA tests causes a thermal contrast that leads to increased sensitivity of detection systems. In a recent study, the sensitivity of visual or colorimetric readers was improved up to 8-fold for *C. difficile* (reduced from 1.0625 to 0.1328 ng/mL), thus, thermal contrast readers would receive much attention in future (Wang et al., 2016b).

In addition to lateral-flow assays, latex agglutination techniques (LAT) allow for naked-eye detection. LAT assays are based on the use of latex particles bound to antibodies, so that the antigen-binding sites are exposed and they can bind the target antigen. The binding of antibody to antigen leads to a lattice formation of the latex particles which appears as a visible agglutination. These types of techniques are rapid, easy to perform, inexpensive, fast and they do not require special equipment. The use of particles which change in color when aggregated, e.g., AuNPs, makes the visual detection possible in these techniques. In this context, rapid visual detection of bacteria such as *M. tuberculosis* (Bhaskar et al., 2004) and *E. coli* (Huang et al., 2001) was documented. Integration of this technique with nanoparticles like AuNPs increases the speed of this method in a way that target antigens can be detected in less than 30 min (Koczula and Gallotta, 2016). There is only one report on the use of antibody-latex agglutination test in detection of *C. difficile*, in which positive latex results were confirmed by cytotoxicity assay. Accordingly, this test can be an acceptable diagnostic tool for screening *C. difficile* toxins (Shahrabadi et al., 1984), which can be considered a simple and affordable diagnostic tool for clinical use.

Recently, the results of research on quantum dots (QD) have revealed that they are one of the best candidates for development of novel detection methods (Matea et al., 2017). QDs are very small nanoparticles with strong fluorescence properties that act as semi-conductors. The use of QDs in the tools developed for diagnosis of different diseases has been described (Zhao and Zeng, 2015). These diagnostic methods are semi-quantitative or quantitative and have many advantages such as being simple, fast, and easy, and they require only visual inspection. Additionally, QD technology has advantages over organic chemical fluorescent groups, such as higher quantum yield, wide absorption cross-sections, excellent optical reliability, and adjustable specification of fluorescent transmission (Dubertret et al., 2002).

Use of QDs in *C. difficile* detection has been reported; Qi et al. (2020) developed a LFIA using an anti-TcdB mAb coupled to quantum dot nanobeads (QDNBs). The LOD of QDNBs-LFA in the fecal samples was 0.297 ng/mL that was consistent with those of a commercial ELISA kit. Moreover, concerning sensitivity, QDNBs-LFA showed good correlations with clinical diagnosis. Thus, the performance of QDNBs in this diagnostic system was highly applicable for designing portable and rapid on-the-spot platforms (Qi et al., 2020b). Overall, the use of rAbs can be suggested to increase the efficiency of these biosensors (Sharma et al., 2016; Lara and Perez-Potti, 2018), and should not be ignored in future studies.

Discussion

The current status of CDI diagnosis is still challenging. The available laboratory tests have remained confined and revealed a high frequency of inconsistency in detecting *C. difficile* colonization or diagnosis of suspected CDI patients (McDonald et al., 2018). Additionally, an accurate and early diagnosis of CDI is essential for optimal patient care, timely infection control, pharmacological treatment, and preventing the spread of infection (Gerding et al., 2016; Gateau et al., 2018; Peng et al., 2018). Therefore, the achievement of timely and accurate diagnostic assays with high sensitivity and specificity will play an increasingly pivotal role in more efficient disease management. Today, the development of diagnostic tools based on antibodies has received great attention. Some properties of antibodies, such as their high affinity and specific binding to target molecules, make them reliable therapeutic/diagnostic tools (Ahmad et al., 2012; Sharma et al., 2016). This has led to the introduction of numerous antibody-based diagnostic kits so far, however, obtaining antibodies with specificity, sensitivity, and high affinity has always been a challenge facing researchers (Hammers and Stanley, 2014). Recently, some studies have focused on the application of antibodies for CDI diagnosis; and further research is still being conducted in this area (Fang et al., 2013; Davies et al., 2015; Qi et al., 2020). Most of the research has been done on the production of antibodies using the hybridoma technology, which has been applied successfully in numerous cases, while it has many shortcomings, such as being time-consuming and inefficient in generating antibodies toward highly-conserved antigens, self-antigens, sensitive, and toxic antigens (Parray et al., 2020). In these cases, it is recommended to use alternative methods like non-antibody binding proteins (or protein scaffolds) and *in vitro* antibody display technologies (Alfaleh et al., 2020; Gebauer and Skerra, 2020). In contrast to monoclonal antibodies, protein scaffolds are single polypeptide chain structures without disulfide bridges or post-translational modifications that show high solubility and stability and can allow the selection for affinity, stability, and enzymatic activity (Simeon and Chen, 2018; Gebauer and Skerra, 2020). Additionally, *in vitro* antibody display technologies have many advantages, including the ability to be genetically modified to increase selectivity, specificity, and sensitivity, ease of production in *E. coli*, and reproducibility (Frenzel et al., 2017; Chiu et al., 2019; Raeisi et al., 2022a). Hence, various studies have suggested the use of phage display-derived antibodies for diagnostic purposes (Chamorro and Merkoçi, 2016; Mohd Ali et al., 2021). Innovative developments based on antibodies (e.g. various biosensor platforms) can provide rapid, reliable, and sensitive detection capability, which help the accurate diagnosis of specific targets. Importantly, due to the increase in public health concerns about nosocomial CDI, designing immunosensors can be proposed for rapid detection and disease management (Zhu et al., 2014b). Additionally, the combination of nanotechnology and various biosensor platforms has attracted a lot of attention as an excellent approach for developing fast, highly,

sensitive and specific devices for the diagnosis of bacterial and viral infections (Prasad, 2014; Park et al., 2016), which can improve the quality and precision of disease diagnosis (Castillo et al., 2020; Younis et al., 2020).

Application of rAb fragments (scFv, sdAb, etc.) to develop immunosensors or immunoassays has several distinct advantages, the most important of them is that rAb fragments can be readily produced *in vitro*. In addition, rAbs are easily formatted through genetic engineering or chemical conjugation for coupling antibodies to the sensors used to detect antigens. These advantages in the case of antibodies that have limited *in vivo* production, especially anti-toxins, are more highlighted. Another advantage of rAb antibodies is that in scFv-based label-free immunosensors, for example, piezo-immunosensors, a high-affinity rAb is sufficient to detect the antigen, thus no antigen-specific secondary antibody (i.e., detecting) is required (Shen et al., 2005). In fact, the use of rAb in these biosensors simplifies antigen detection because in some cases, the generation of just one antigen-specific antibody is difficult, let alone two. Furthermore, chemical modification of a sensor's surface under controlled conditions can facilitate correct orientation (e.g., on AuNPs) of rAb fragments at high density, which leads to improved avidity and sensitivity of the assay (Gandhi et al., 2018). In many sensing transducers and imaging technologies, rAb antibodies can be used instead of traditional whole antibodies, including quartz crystal microbalance (QCM), cyclic voltammetry (CV), surface plasmon resonance (SPR), and many other detection techniques (Zeng et al., 2012). These techniques can provide a tool with high sensitivity and specificity to detect antigens in complex samples like feces and blood. Moreover, a QCM based on rAbs can readily sense a change in mass on the sensor's surface, so that antibody concentration on the immunosensor surface can be easily determined to ensure that the same concentration of antibody is used every time and this helps enhance inter-assay reproducibility. This feature is not available for most traditional immunoassays (e.g., ELISAs) (Zeng et al., 2012). Interestingly, reducing the distance between donors and acceptors in optical biosensors increases their efficiency (Damborský et al., 2016), thus the use of small-sized antibodies like rAbs can be considered as a way to increase the efficiency of these biosensors (Sharma et al., 2016; Lara and Perez-Potti, 2018). So far, the application of rAbs in various diagnostic platforms, such as ELISA, LFIA, nanoparticles, and microfluidics, has been reported (Goodchild et al., 2005; Zhang et al., 2012). It seems that due to the desirable properties of rAbs, they can be employed for designing newer diagnostic tools in the future.

Conclusion

Presently, the precise and effective diagnosis of CDI is based on a multistep approach. Thus, the application of rapid and accurate diagnostic tools can be a key step in the management of CDI. Previous studies have demonstrated that rAbs possess high affinity and specificity for the detection of various targets and can be considered as reliable diagnostic tools in CDI management. Moreover, *in vitro* antibody production can be cost-effective compared with the conventional antibodies. This is particularly remarkable for developing novel and rapid detection tests such as biosensors. The effectiveness of rAbs can be enhanced by genetic engineering that would allow designing high performance diagnostic techniques and reducing the assay costs. Therefore, antibody generation by rAb technologies will provide an attractive platform for current and future diagnostic purposes and can be the future trend of research for designing ultrasensitive methods for CDI diagnosis.

Author contributions

HR was involved in literature review, writing of the original draft, and figures illustration. MA was involved in literature review. AY was involved in conceptualization, preparing the draft of the manuscript, reviewing, and editing. HAA and MRZ were involved in revising the manuscript. All authors contributed to the article and approved the submitted version.

Funding

This study was financially supported by a research grant (no. RIGLD 1138, IR.SBMU.RIGLD.REC.1399.051) from the Foodborne and Waterborne Diseases Research Center, Research Institute for Gastroenterology and Liver Diseases, Shahid Beheshti University of Medical Sciences, Tehran, Iran.

Acknowledgments

The authors would like to thank the members of the Foodborne and Waterborne Diseases Research Center at the Research Institute for Gastroenterology and Liver Diseases, Shahid Beheshti University of Medical Sciences, Tehran, Iran.

Conflict of interest

The authors declare that the research was conducted in the absence of any commercial or financial relationships that could be construed as a potential conflict of interest.

Publisher's note

References

Adamson, H., Ajayi, M. O., Gilroy, K. E., McPherson, M. J., Tomlinson, D. C., and Jeuken, L. J. C. (2022). Rapid quantification of C. difficile glutamate dehydrogenase and toxin B (TcdB) with a NanoBiT Split-luciferase assay. *Anal. Chem.* 94, 8156–8163. doi: 10.1021/acs.analchem.1c05206

Ahangarzadeh, S., Bandehpour, M., and Kazemi, B. (2017). Selection of single-chain variable fragments specific for mycobacterium tuberculosis ESAT-6 antigen using ribosome display. *Iran. J. Basic Med. Sci.* 20, 327–333. doi: 10.22038/ijbms.2017.8363

Ahmad, A., Yeap, S. K., Ali, A., Ho, W. Y., Alitheen, N., and Hamid, M. (2012). scFv antibody: principles and clinical application. *Clin. Dev. Immunol.* 2012:980250. doi: 10.1155/2012/980250

Alcalá, L., Sánchez-Cambronero, L., Catalán, M. P., Sánchez-Somolinos, M., Peláez, M. T., Marín, M., et al. (2008). Comparison of three commercial methods for rapid detection of Clostridium difficile toxins a and B from fecal specimens. *J. Clin. Microbiol.* 46, 3833–3835. doi: 10.1128/JCM.01060-08

Alfaleh, M. A., Alsaab, H. O., Mahmoud, A. B., Alkayyal, A. A., Jones, M. L., Mahler, S. M., et al. (2020). Phage display derived monoclonal antibodies: from bench to bedside. *Front. Immunol.* 11, 497–508. doi: 10.3389/fimmu.2020.01986

Alhadrami, H. (2017). Biosensors: classifications, medical applications and future prospective. *Biotechnol. Appl. Biochem.* 65, 497–508. doi: 10.1002/bab.1621

Alibeiki, M., Golchin, M., and Tabatabaei, M. (2020). Development of a double-recombinant antibody sandwich ELISA for quantitative detection of epsilon toxoid concentration in inactivated Clostridium perfringens vaccines. *BMC Vet. Res.* 16:361. doi: 10.1186/s12917-020-02572-4

Angela Chiew Wen, C. N., Choong, Y. S., and Lim, T. (2016). Phage display-derived antibodies: application of recombinant antibodies for diagnostics. *Front. Immunol.* 2016:e0198. doi: 10.3389/fimmu.2020.0198

Arimoto, J., Horita, N., Kato, S., Fuyuki, A., Higurashi, T., Ohkubo, H., et al. (2016). Diagnostic test accuracy of glutamate dehydrogenase for Clostridium difficile: systematic review and meta-analysis. *Sci. Rep.* 6:29754. doi: 10.1038/srep29754

Ascoli, C. A., and Aggeler, B. (2018). Overlooked benefits of using polyclonal antibodies. *BioTechniques* 65, 127–136. doi: 10.2144/btn-2018-0065

Azimirad, M., Jo, Y., Kim, M. S., Jeong, M., Shahrokh, S., Asadzadeh Aghdaei, H., et al. (2022). Alterations and prediction of functional profiles of gut microbiota after fecal microbiota transplantation for Iranian recurrent Clostridioides difficile infection with underlying inflammatory bowel disease: a pilot study. *J. Inflamm. Res.* 15, 105–116. doi: 10.2147/JIR.S338212

Azimirad, M., Krutova, M., Yadegar, A., Shahrokh, S., Olfatifar, M., Aghdaei, H. A., et al. (2020b). Clostridioides difficile ribotypes 001 and 126 were predominant in Tehran healthcare settings from 2004 to 2018: a 14-year-long cross-sectional study. *Emerg. Microb. Infect.* 9, 1432–1443. doi: 10.1080/22221751.2020.1780949

Azimirad, M., Noori, M., Raeisi, H., Yadegar, A., Shahrokh, S., Asadzadeh Aghdaei, H., et al. (2021). How does COVID-19 pandemic impact on incidence of Clostridioides difficile infection and exacerbation of its gastrointestinal symptoms? *Front. Med. (Lausanne).* 8:775063. doi: 10.3389/fmed.2021.775063

Azimirad, M., Yadegar, A., Gholami, F., Shahrokh, S., Asadzadeh Aghdaei, H., Ianiro, G., et al. (2020a). Treatment of recurrent Clostridioides difficile infection using fecal microbiota transplantation in Iranian patients with underlying inflammatory bowel disease. *J. Inflamm. Res.* 13, 563–570. doi: 10.2147/JIR.S265520

Badger, V., Ledeboer, N., Graham, M. B., and Edmiston, J. C. (2012). Clostridium difficile: epidemiology, pathogenesis, management, and prevention of a recalcitrant healthcare-associated pathogen. *JPEN J. Parenter. Enteral Nutr.* 36, 645–662. doi: 10.1177/0148607112446703

Baghani, A., Mesdaghinia, A., Kuijper, E. J., Aliramezani, A., Talebi, M., and Douraghi, M. (2020). High prevalence of Clostridiodes diffiicle PCR ribotypes 001 and 126 in Iran. *Sci. Rep.* 10:4658. doi: 10.1038/s41598-020-61604-z

Bakir, M., Babich, J., Aftab, N., Dean, C., Lambrecht, R., Ott, R., et al. (1993). C-erbB2 protein overexpression in breast cancer as a target for PET using iodine-124-labeled monoclonal antibodies. *J. Nuclear Med.* 33, 2154–2160.

Balsalobre-Arenas, L., and Alarcón-Cavero, T. (2017). Rapid diagnosis of gastrointestinal tract infections due to parasites, viruses, and bacteria. *Enferm. Infecc. Microbiol. Clin.* 35, 367–376. doi: 10.1016/j.eimc.2017.01.002

Balsells, E., Filipescu, T., Kyaw, M. H., Wiuff, C., Campbell, H., and Nair, H. (2016). Infection prevention and control of Clostridium difficile: a global review of guidelines, strategies, and recommendations. *J. Glob. Health* 6:020410. doi: 10.7189/jogh.06.020410

Banz, A., Lantz, A., Riou, B., Foussadier, A., Miller, M. A., Davies, K. A., et al. (2018). Sensitivity of single-molecule Array assays for detection of Clostridium difficile toxins in comparison to conventional laboratory testing algorithms. *J. Clin. Microbiol.* 56. doi: 10.1128/JCM.00452-18

Barbut, F., Surgers, L., Eckert, C., Visseaux, B., Cuingnet, M., Mesquita, C., et al. (2014). Does a rapid diagnosis of Clostridium difficile infection impact on quality of patient management? *Clin. Microbiol. Infect.* 20, 136–144. doi: 10.1111/1469-0691.12221

Bazan, J., Calkosinski, I., and Gamian, A. (2012). Phage display—a powerful technique for immunotherapy. *Hum. Vaccin. Immunother.* 8, 1817–1828. doi: 10.4161/hv.21703

Berry, S. K., Rust, S., Caceres, C., Irving, L., Bartholdson Scott, J., Tabor, D. E., et al. (2022). Phenotypic whole-cell screening identifies a protective carbohydrate epitope on *Klebsiella pneumoniae*. *MAbs* 14:2006123. doi: 10.1080/19420862.2021.2006123

Bhalla, N, Jolly, P, Formisano, N, and Estrela, P. (2016). Introduction to biosensors. *Essays biochem.* 60, 1–8. doi: 10.1042/EBC20150001

Bhaskar, S., Banavaliker, J., and Hanif, M. (2004). Large-scale validation of a latex agglutination test for diagnosis of tuberculosis. *FEMS Immunol. Med. Microbiol.* 39, 235–239.

Bockstaele, F., Holz, J.-B., and Revets, H. (2000). "The development of nanobodies for therapeutic applications," in *Current Opinion in Investigational Drugs*, vol. *2009* (London), 1212–1224.

Burke, K. E., and Lamont, J. T. (2014). Clostridium difficile infection: a worldwide disease. *Gut Liver.* 8, 1–6. doi: 10.5009/gnl.2014.8.1.1

Burnham, C.-A., and Carroll, K. (2013). Diagnosis of Clostridium difficile infection: an ongoing conundrum for clinicians and for clinical laboratories. *Clin. Microbiol. Rev.* 26, 604–630. doi: 10.1128/CMR.00016-13

Burnham, C-A, Dubberke, E, Kociolek, L, Polage, C, and Riley, T. (2015). Clostridium difficile—Diagnostic and Clinical Challenges. *Clin. Chem.* 62, 310–314. doi: 10.1373/clinchem.2015.243717.

Byrne, H., Conroy, P., Whisstock, J., and O'Kennedy, R. (2013). A tale of two specificities: bispecific antibodies for therapeutic and diagnostic applications. *Trends Biotechnol.* 31, 621–632. doi: 10.1016/j.tibtech.2013.08.007.

Cabuzu, D., Cirja, A., Puiu, R., and Grumezescu, A. M. (2015). Biomedical applications of gold nanoparticles. *Curr. Top. Med. Chem.* 15, 1605–1613. doi: 10.2174/1568026615666150414144750

Castillo, L., Vega Baudrit, J., and Lopretti, M. (2020). Biosensors for the detection of bacterial and viral clinical pathogens. *Sensors* 20:6926. doi: 10.3390/s20236926

Castro-Córdova, P., Mora-Uribe, P., Reyes-Ramírez, R., Cofré-Araneda, G., Orozco-Aguilar, J., Brito-Silva, C., et al. (2021). Entry of spores into intestinal epithelial cells contributes to recurrence of Clostridioides difficile infection. *Nat. Commun.* 12:1140. doi: 10.1038/s41467-021-21355-5

Chamorro, A., and Merkoçi, A. (2016). Nanobiosensors in diagnostics. *Nano*:3. doi: 10.1177/1849543516663574

Chandrasekaran, R., and Lacy, D. B. (2017). The role of toxins in Clostridium difficile infection. *FEMS Microbiol. Rev.* 41, 723–750. doi: 10.1093/femsre/fux048

Chen, X., Gentili, M., Hacohen, N., and Regev, A. (2021). A cell-free nanobody engineering platform rapidly generates SARS-CoV-2 neutralizing nanobodies. *Nat. Commun.* 12:5506. doi: 10.1038/s41467-021-25777-z

Chen, W., Jie, W., Chen, Z., Jie, X., and Huang-Xian, J. (2012). Chemiluminescent immunoassay and its applications. *Chin. J. Anal. Chem.* 40, 3–10. doi: 10.1016/S1872-2040(11)60518-5

Chen, W., Liu, W. E., Li, Y. M., Luo, S., and Zhong, Y. M. (2015b). Preparation and preliminary application of monoclonal antibodies to the receptor binding region of Clostridium difficile toxin B. *Mol. Med. Rep.* 12, 7712–7720. doi: 10.3892/mmr.2015.4369

Chen, S., Sun, C., Wang, H., and Wang, J. (2015a). The role of rho GTPases in toxicity of Clostridium difficile toxins. *Toxins (Basel).* 7, 5254–5267. doi: 10.3390/toxins7124874

Cheng, J.-W., Xiao, M., Kudinha, T., Xu, Z.-P., Sun, L.-Y., Hou, X., et al. (2015). The role of glutamate dehydrogenase (GDH) testing assay in the diagnosis of Clostridium difficile infections: a high sensitive screening test and an essential step in the proposed laboratory diagnosis workflow for developing countries like China. *PLoS One* 10:e0144604. doi: 10.1371/journal.pone.0144604

Chiari, E., Weiss, W., Simon, M., Kiessig, S., Pulse, M., Brown, S., et al. (2021). Oral immunotherapy with human secretory IgA improves survival in the hamster model of Clostridioides difficile infection. *J. Infect. Dis.* 224, 1394–1397. doi: 10.1093/infdis/jiab087

Chiu, M., Goulet, D., Teplyakov, A., and Gilliland, G. (2019). Antibody structure and function: the basis for engineering therapeutics. *Antibodies* 8:55. doi: 10.3390/antib8040055

Cho, I.-H., Kim, D., and Park, S. (2020). Electrochemical biosensors: perspective on functional nanomaterials for on-site analysis. Biomaterials. *Research*:24.

Chung, S.-Y., Schöttelndreier, D., Tatge, H., Fuehner, V., Hust, M., Beer, L.-A., et al. (2018). The conserved Cys-2232 in Clostridioides difficile toxin B modulates receptor binding. *Front. Microbiol.* 9:2314. doi: 10.3389/fmicb.2018.02314

Cinquanta, L., Fontana, D. E., and Bizzaro, N. (2017). Chemiluminescent immunoassay technology: what does it change in autoantibody detection? *Autoimmunity High.* 8:9. doi: 10.1007/s13317-017-0097-2

Cinti, S., Volpe, G., Piermarini, S., Delibato, E., and Palleschi, G. (2017). Electrochemical biosensors for rapid detection of foodborne salmonella: a critical overview. *Sensors* 17:1910. doi: 10.3390/s17081910

Cornely, O. A., Miller, M. A., Louie, T. J., Crook, D. W., and Gorbach, S. L. (2012). Treatment of first recurrence of Clostridium difficile infection: fidaxomicin versus vancomycin. *Clin. Infect. Dis.* 55, S154–S161. doi: 10.1093/cid/cis462

Cui, X., Vasylieva, N., Shen, D., Barnych, B., Yang, J., He, Q., et al. (2018). Biotinylated single-chain variable fragment-based enzyme-linked immunosorbent assay for Glycocholic acid. *Analyst* 143, 2057–2065. doi: 10.1039/C7AN02024D

Damborský, P., Švitel, J., and Katrlík, J. (2016). Optical biosensors. Essays in. *Biochemistry* 60, 91–100. doi: 10.1042/EBC20150010

Davies, K., Berry, C., Morris, K. A., Smith, R., Young, S., Davis, T., et al. (2015). Comparison of the Vidas C. difficile GDH automated enzyme-linked fluorescence immunoassay (ELFA) with another commercial enzyme immunoassay (EIA) (Quik Chek-60), two selective media, and a PCR assay for gluD for detection of Clostridium difficile in fecal samples. *J. Clin. Microbiol.* 53, 1931–1934.

Deng, X., Nesbit, L., and Morrow, K. (2003). Recombinant single-chain variable fragment antibodies directed against Clostridium difficile toxin B produced by use of an optimized phage display system. *Clin. Diagn. Lab. Immunol.* 10, 587–595. PMID: 12853390

Depestel, D. D., and Aronoff, D. M. (2013). Epidemiology of Clostridium difficile infection. *J. Pharm. Pract.* 26, 464–475. doi: 10.1177/0897190013499521

Di Bella, S., Ascenzi, P., Siarakas, S., Petrosillo, N., and Di Masi, A. (2016). Clostridium difficile toxins A and B: insights into pathogenic properties and Extraintestinal effects. *Toxins.* 8:134. doi: 10.3390/toxins8050134

Dinarelli, S., Girasole, M., Kasas, S., and Longo, G. (2016). Nanotools and molecular techniques to rapidly identify and fight bacterial infections. *J. Microbiol. Methods* 138, 72–81. doi: 10.1016/j.mimet.2016.01.005

Dong, S., Bo, Z., Zhang, C. Z., Feng, J., and Liu, X. (2018). Screening for single-chain variable fragment antibodies against multiple Cry1 toxins from an immunized mouse phage display antibody library. *Appl. Microbiol. Biotechnol.* 102, 3363–3374. doi: 10.1007/s00253-018-8797-8

Dong, J.-X., Li, Z., Lei, H., Sun, Y.-M., Ducancel, F., Boulain, J.-C., et al. (2012). Development of a single-chain variable fragment-alkaline phosphatase fusion protein and a sensitive direct competitive chemiluminescent enzyme immunoassay for detection of ractopamine in pork. *Anal. Chim. Acta* 736, 85–91. doi: 10.1016/j.aca.2012.05.033

Dubberke, E. R., and Olsen, M. A. (2012). Burden of Clostridium difficile on the healthcare system. *Clin. Infect. Dis.* 55, S88–S92. doi: 10.1093/cid/cis335

Dubertret, B., Skourides, P., Norris, D., Noireaux, V., Brivanlou, A., and Libchaber, A. (2002). *In vivo* imaging of quantum dots encapsulated in phospholipid micelles. *Science (New York, N.Y.)* 298, 1759–1762. doi: 10.1126/science.1077194

DuVall, J. A., Cabaniss, S. T., Angotti, M. L., Moore, J. H., Abhyankar, M., Shukla, N., et al. (2016). Rapid detection of Clostridium difficile via magnetic bead aggregation in cost-effective polyester microdevices with cell phone image analysis. *Analyst* 141, 5637–5645. doi: 10.1039/C6AN00674D

Eastwood, K., Else, P., Charlett, A., and Wilcox, M. (2009). Comparison of nine commercially available Clostridium difficile toxin detection assays, a real-time PCR assay for C. difficile tcdB, and a glutamate dehydrogenase detection assay to cytotoxin testing and cytotoxigenic culture methods. *J. Clin. Microbiol.* 47, 3211–3217. doi: 10.1128/JCM.01082-09

Eze, P., Balsells, E., Kyaw, M. H., and Nair, H. (2017). Risk factors for Clostridium difficile infections - an overview of the evidence base and challenges in data synthesis. *J. Glob. Health* 7:010417. doi: 10.7189/jogh.07.010417

Fan, G., Wang, Z., Hao, M., and Li, J. (2015). Bispecific antibodies and their applications. *J. Hematol. Oncol.* 8:130. doi: 10.1186/s13045-015-0227-0

Fang, Y.-S., Wang, H.-Y., Wang, L.-S., and Wang, J.-F. (2013). Electrochemical immunoassay for procalcitonin antigen detection based on signal amplification strategy of multiple nanocomposites. *Biosens. Bioelectron.* 51, 310–316. doi: 10.1016/j.bios.2013.07.035

Fouladi, M., Sarhadi, S., Tohidkia, M., Fahimi, F., Samadi, N., Sadeghi, J., et al. (2019). Selection of a fully human single domain antibody specific to helicobacter pylori urease. *Appl. Microbiol. Biotechnol.* 103, 3407–3420. doi: 10.1007/s00253-019-09674-6

Frenzel, A., Kügler, J., Helmsing, S., Meier, D., Schirrmann, T., Hust, M., et al. (2017). Designing human antibodies by phage display. *Transfus. Med. Hemother.* 44, 312–318. doi: 10.1159/000479633

Fu, X., Chu, Y., Zhao, K., and Deng, A. (2017). Ultrasensitive detection of the β-adrenergic agonist brombuterol by a SERS-based lateral flow immunochromatographic assay using flower-like gold-silver core-shell nanoparticles. *Microchim. Acta* 184, 1711–1719. doi: 10.1007/s00604-017-2178-3

Fulgione, A., Cimafonte, M., Della Ventura, B., Iannaccone, M., Ambrosino, C., Capuano, F., et al. (2018). QCM-based immunosensor for rapid detection of salmonella typhimurium in food. *Sci. Rep.* 8. doi: 10.1038/s41598-018-34285-y

Furuya-Kanamori, L., Marquess, J., Yakob, L., Riley, T. V., Paterson, D. L., Foster, N. F., et al. (2015). Asymptomatic Clostridium difficile colonization: epidemiology and clinical implications. *BMC Infect. Dis.* 15:516. doi: 10.1186/s12879-015-1258-4

Gandhi, S., Banga, I., Maurya, P. K., and Eremin, S. A. (2018). A gold nanoparticle-single-chain fragment variable antibody as an immunoprobe for rapid detection of morphine by dipstick. *RSC Adv.* 8, 1511–1518. doi: 10.1039/C7RA12810J

Gateau, C., Couturier, J., Coia, J., and Barbut, F. (2018). How to: diagnose infection caused by Clostridium difficile. *Clin. Microbiol. Infect.* 24, 463–468. doi: 10.1016/j.cmi.2017.12.005

Gebauer, M., and Skerra, A. (2020). Engineered protein scaffolds as next-generation therapeutics. *Annu. Rev. Pharmacol. Toxicol.* 60, 391–415. doi: 10.1146/annurev-pharmtox-010818-021118

Gerding, D. N., File, T. M., and McDonald, L. C. (2016). Diagnosis and treatment of Clostridium difficile infection (CDI). *Infect. Dis. Clin. Pract.* 24, 3–10. doi: 10.1097/IPC.0000000000000350

Gite, S., Archambault, D., Cappillino, M., Cunha, D., Dorich, V., Shatova, T., et al. (2018). A rapid, accurate, single molecule counting method detects Clostridium difficile toxin B in stool samples. *Sci. Rep.* 8. doi: 10.1038/s41598-018-26353-0

Goodchild, S., Love, T., Hopkins, N., and Mayers, C. (2005). Engineering antibodies for biosensor technologies. *Adv. Appl. Microbiol.* 58C, 185–226. doi: 10.1016/S0065-2164(05)58006-7

Grewal, Y, Shiddiky, M, Gray, S, Weigel, K, Cangelosi, G, and Trau, M. *Label-free Electrochemical Detection of an Entamoeba histolytica Antigen using Cell-free Yeast-scFv Probes* (Chemical Communications, Cambridge). (2013).

Haji-Hashemi, H., Norouzi, P., Safarnejad, M. R., Larijani, B., Habibi, M. M., Raeisi, H., et al. (2018). Sensitive electrochemical immunosensor for citrus bacterial canker disease detection using fast Fourier transformation square-wave voltammetry method. *J. Electroanal. Chem.* 820, 111–117. doi: 10.1016/j.jelechem.2018.04.062

Hammami, I., Alabdallah, N. M., Jomaa, A. A., and Kamoun, M. (2021). Gold nanoparticles: synthesis properties and applications. *J. King Saud University* 33:101560. doi: 10.1016/j.jksus.2021.101560

Hammerling, M. J., Fritz, B. R., Yoesep, D. J., Kim, D. S., Carlson, E. D., and Jewett, M. C. (2020). *In vitro* ribosome synthesis and evolution through ribosome display. *Nat. Commun.* 11:1108. doi: 10.1038/s41467-020-14705-2

Hammers, C., and Stanley, J. (2014). Antibody phage display: technique and applications. *J. Invest. Dermatol.* 134:e17. doi: 10.1038/jid.2013.521

Han, S., Soylu, M. C., Kirimli, C. E., Wu, W., Sen, B., Joshi, S. G., et al. (2019). Rapid, label-free genetic detection of enteropathogens in stool without genetic isolation or amplification. *Biosens. Bioelectron.* 130, 73–80. doi: 10.1016/j.bios.2019.01.025

Hassanain, W., Spoors, J., Johnson, C., Faulds, K., Keegan, N., et al. (2021). Rapid ultra-sensitive diagnosis of clostridium difficile infection using a SERS-based lateral flow assay. *Analyst* 146, 4495–4505. doi: 10.1039/D1AN00726B

Hayhurst, A., Happe, S., Mabry, R., Koch, Z., Iverson, B., et al. (2003). Isolation and expression of recombinant antibody fragment to the biological warfare pathogen *Brucella melitensis*. *J. Immunol. Methods* 276, 185–196. doi: 10.1016/S0022-1759(03)00100-5

Hong, K. L., Maher, E., Williams, R. M., and Sooter, L. J. (2015). In vitro selection of a single-stranded DNA molecular recognition element against Clostridium difficile toxin B and sensitive detection in human fecal matter. *J Nucleic Acids.* 2015:808495, 1–12. doi: 10.1155/2015/808495

Høydahl, L. S., Nilssen, N. R., Gunnarsen, K. S., Pré, M. F., Iversen, R., Roos, N., et al. (2016). Multivalent pIX phage display selects for distinct and improved antibody properties. *Sci. Rep.* 6:39066. doi: 10.1038/srep39066

Hu, X., Zhang, Y., Ding, T., Liu, J., and Zhao, H. (2020). Multifunctional Gold nanoparticles: a novel nanomaterial for various medical applications and biological activities. *Front. Bioeng. Biotechnol.* 13:8. doi: 10.3389/fbioe.2020.0099

Huang, Y. H., Chang, H.-C., and Chang, T. (2001). Development of a latex agglutination test for rapid identification of Escherichia coli. *Eur. J. Clin. Microbiol. Infect. Dis.* 20, 97–103. doi: 10.1007/PL00011250

Huang, S., Feng, L., An, G., Zhang, X., Zhao, Z., Han, R., et al. (2018). Ribosome display and selection of single-chain variable fragments effectively inhibit growth and progression of microspheres in vitro and in vivo. *Cancer Sci.* 109, 1503–1512. doi: 10.1111/cas.13574

Huang, H., Weintraub, A., Fang, H., and Nord, C. E. (2009). Comparison of a commercial multiplex real-time PCR to the cell cytotoxicity neutralization assay for diagnosis of clostridium difficile infections. *J. Clin. Microbiol.* 47, 3729–3731. doi: 10.1128/JCM.01280-09

Hui, C. Y., Liu, M., Li, Y., and Brennan, J. D. (2018). A paper sensor printed with multifunctional bio/nano materials. *Angew. Chem.* 130, 4639–4643. doi: 10.1002/ange.201712903

Humphries, R. M., Uslan, D. Z., and Rubin, Z. (2013). Performance of Clostridium difficile toxin enzyme immunoassay and nucleic acid amplification tests stratified by patient disease severity. *J. Clin. Microbiol.* 51, 869–873. doi: 10.1128/JCM.02970-12

Hussack, G., Arbabi Ghahroudi, M., Faassen, H., Songer, J., Ng, K., Mackenzie, R., et al. (2011). Neutralization of Clostridium difficile toxin a with single-domain antibodies targeting the cell receptor binding domain. *J. Biol. Chem.* 286, 8961–8976. doi: 10.1074/jbc.M110.198754

Hussack, G., Ryan, S., Faassen, H., Rossotti, M., Mackenzie, C., et al. (2018). Neutralization of Clostridium difficile toxin B with VHH-fc fusions targeting the delivery and CROPs domains. *PLoS One* 13:e0208978. doi: 10.1371/journal.pone.0208978

Hwang, Y.-C., Lu, R.-M., Su, S.-C., Chiang, P.-Y., Ko, S.-H., Ke, F.-Y., et al. (2022). Monoclonal antibodies for COVID-19 therapy and SARS-CoV-2 detection. *J. Biomed. Sci.* 29:1. doi: 10.1186/s12929-021-00784-w

Jarrige, V., Nieuwenhuis, J., Son, J., Martens, M., and Vissers, J. (2011). A fast intraoperative PTH point-of-care assay on the Philips handheld magnotech system. *Deutsche Gesellschaft für Chirurgie.* 396, 337–343. doi: 10.1007/s00423-010-0733-z

Jensen, L., Kilstrup, M., Karatt-Vellatt, A., McCafferty, J., and Laustsen, A. (2018). Basics of antibody phage display technology. *Toxins.* 10:236. doi: 10.3390/toxins10060236

Jiang, X., Li, X., Yang, Z., Eremin, S., and Zhang, X. Y. (2017). Evaluation and optimization of three different immunoassays for rapid detection Zearalenone in fodders. *Food Anal. Methods* 10, 256–262. doi: 10.1007/s12161-016-0576-5

Joshi, L. T., Mali, B. L., Geddes, C. D., and Baillie, L. (2014). Extraction and sensitive detection of toxins a and B from the human pathogen Clostridium difficile in 40 seconds using microwave-accelerated metal-enhanced fluorescence. *PLoS One* 9:e104334. doi: 10.1371/journal.pone.0104334

Kandalaft, H., Hussack, G., Aubry, A., van Faassen, H., Guan, Y., Arbabi-Ghahroudi, M., et al. (2015). Targeting surface-layer proteins with single-domain antibodies: a potential therapeutic approach against Clostridium difficile-associated disease. *Appl. Microbiol. Biotechnol.* 99, 8549–8562. doi: 10.1007/s00253-015-6594-1

Kelly, C. R., Fischer, M., Allegretti, J. R., LaPlante, K., Stewart, D. B., Limketkai, B. N., et al. (2021). ACG clinical guidelines: prevention, diagnosis, and treatment of Clostridioides difficile infections. *Am. J. Gastroenterol.* 116, 1124–1147. doi: 10.14309/ajg.0000000000001278

Kim, H., Kim, W. H., Kim, M., Jeong, S. H., and Lee, K. (2014). Evaluation of a rapid membrane enzyme immunoassay for the simultaneous detection of glutamate dehydrogenase and toxin for the diagnosis of Clostridium difficile infection. *ALM* 34, 235–239. doi: 10.3343/alm.2014.34.3.235

Kim, H.-Y., Lee, J.-H., Kim, M., Park, S., Choi, M., Lee, W., et al. (2020). Development of a SARS-CoV-2-specific biosensor for antigen detection using scFv-fc fusion proteins. *Biosens. Bioelectron.* 175:112868. doi: 10.1016/j.bios.2020.112868

Kimmel, D. W., LeBlanc, G., Meschievitz, M. E., and Cliffel, D. E. (2012). Electrochemical sensors and biosensors. *Anal. Chem.* 84, 685–707. doi: 10.1021/ac202878q

Koczula, K. M., and Gallotta, A. (2016). Lateral flow assays. *Essays Biochem.* 60, 111–120. doi: 10.1042/EBC20150012

Koczuła, K, and Gallotta, A. *Lateral Flow Assays*.

Köhler, G., and Milstein, C. (1975). Continuous cultures of fused cells secreting antibody of predefined specificity. *Nature* 256, 495–497. doi: 10.1038/256495a0

Kuhn, P., Fuehner, V., Unkauf, T., Moreira, G., Frenzel, A., Miethe, S., et al. (2016). Recombinant antibodies for diagnostics and therapy against pathogens and toxins generated by phage display. *Proteomics Clin. Appl.* 10, 922–948. doi: 10.1002/prca.201600002

Kunamneni, A., Ogaugwu, C., Bradfute, S., and Durvasula, R. (2020). Ribosome display technology: applications in disease diagnosis and control. *Antibodies (Basel)* 9. doi: 10.3390/antib9030028

Kunamneni, A., Ye, C., Bradfute, S. B., and Durvasula, R. (2018). Ribosome display for the rapid generation of high-affinity Zika-neutralizing single-chain antibodies. *PLoS One* 13:e0205743. doi: 10.1371/journal.pone.0205743

Lagoutte, P., Lugari, A., Elie, C., Potisopon, S., Donnat, S., Mignon, C., et al. (2019). Combination of ribosome display and next generation sequencing as a powerful method for identification of affibody binders against β-lactamase CTX-M15. *New Biotechnol.* 50, 60–69. doi: 10.1016/j.nbt.2019.01.004

Lara, S., and Perez-Potti, A. (2018). Applications of nanomaterials for Immunosensing. *Biosensors* 8:104. doi: 10.3390/bios8040104

Lessa, F. C., Mu, Y., Bamberg, W. M., Beldavs, Z. G., Dumyati, G. K., Dunn, J. R., et al. (2015). Burden of Clostridium difficile infection in the United States. *N. Engl. J. Med.* 372, 825–834. doi: 10.1056/NEJMoa1408913

Li, R., Kang, G., Hu, M., and Huang, H. (2019). Ribosome display: a potent display technology used for selecting and evolving specific binders with desired properties. *Mol. Biotechnol.* 61, 60–71. doi: 10.1007/s12033-018-0133-0

Liu, M., Wang, J., Chang, Y., Zhang, Q., Chang, D., Hui, C. Y., et al. (2020). In vitro selection of a DNA aptamer targeting degraded protein fragments for biosensing. *Angew. Chem. Int. Ed. Engl.* 59, 7706–7710. doi: 10.1002/anie.202000025

Liu, M., Yin, Q., Brennan, J. D., and Li, Y. (2018). Selection and characterization of DNA aptamers for detection of glutamate dehydrogenase from Clostridium difficile. *Biochimie* 145, 151–157. doi: 10.1016/j.biochi.2017.08.015

Liu, Y., Zhan, L., Qin, Z., Sackrison, J., and Bischof, J. C. (2021). Ultrasensitive and highly specific lateral flow assays for point-of-care diagnosis. *ACS Nano* 15, 3593–3611. doi: 10.1021/acsnano.0c10035

Lu, R.-M., Hwang, Y.-C., Liu, I. J., Lee, C.-C., Tsai, H.-Z., Li, H.-J., et al. (2020). Development of therapeutic antibodies for the treatment of diseases. *J. Biomed. Sci.* 27:1. doi: 10.1186/s12929-019-0592-z

Luo, P., and Liu, Y. (2020). Detection of toxin B of Clostridium difficile based on immunomagnetic separation and aptamer-mediated colorimetric assay. *Lett. Appl. Microbiol.* 71, 596–604. doi: 10.1111/lam.13383

Luo, P., Liu, Y., Xia, Y., Xu, H., and Xie, G. (2014). Aptamer biosensor for sensitive detection of toxin a of Clostridium difficile using gold nanoparticles synthesized by Bacillus stearothermophilus. *Biosens. Bioelectron.* 54, 217–221. doi: 10.1016/j.bios.2013.11.013

Matea, C.-T., Mocan, T., Tabaran, F., Pop, T. A., Mosteanu, O., Puia, I., et al. (2017). Quantum dots in imaging, drug delivery and sensor applications. *Int. J. Nanomedicine* 12, 314–320. doi: 10.1016/j.snb.2019.03.144

Mathelie-Guinlet, M., Cohen-Bouhacina, T., Gammoudi, I., Martin, A., Beven, L., Delville, M. H., et al. (2019). Silica nanoparticles-assisted electrochemical biosensor for the rapid, sensitive and specific detection of *Escherichia coli*. *Sensors Actuat. B Chemical* 12, 5421–5431. doi: 10.2147/IJN.S138624

McDonald, L. C., Gerding, D. N., Johnson, S., Bakken, J. S., Carroll, K. C., Coffin, S. E., et al. (2018). Clinical practice guidelines for Clostridium difficile infection in adults and children: 2017 update by the Infectious Diseases Society of America (IDSA) and Society for Healthcare Epidemiology of America (SHEA). *Clin. Infect. Dis.* 66, e1–e48. doi: 10.1093/cid/cix1085

McDonnell, B., Hearty, S., Finlay, W., and O'Kennedy, R. (2010). A high-affinity recombinant antibody permits rapid and sensitive direct detection of myeloperoxidase. *Anal. Biochem.* 410, 1–6. doi: 10.1016/j.ab.2010.09.039

Mehrotra, P. (2016). Biosensors and their applications – a review. Journal of Oral biology and craniofacial. *Research* 6, 153–159. doi: 10.1016/j.jobcr.2015.12.002

Merrigan, M., Venugopal, A., Roxas, J., Anwar, F., Mallozzi, M., Roxas, B., et al. (2013). Surface-layer protein a (SlpA) is a major contributor to host-cell adherence of Clostridium difficile. *PLoS One* 8:e78404. doi: 10.1371/journal.pone.0078404

Mocan, T., Matea, C., Pop, T. A., Mosteanu, O., Buzoianu, A., Puia, I., et al. (2017). Development of nanoparticle-based optical sensors for pathogenic bacterial detection. *J. Nanobiotechnol.* 15.doi: 10.1186/s12951-017-0260-y

Mohd Ali, M. R., Sum, J. S., Nn, A. B., Choong, Y. S., Amdan, A., Amran, F., et al. (2021). Development of monoclonal antibodies against recombinant LipL21 protein of pathogenic Leptospira through phage display technology. *Int. J. Biol. Macromol.* 168, 289–300. doi: 10.1016/j.ijbiomac.2020.12.062

Mollarasouli, F., Kurbanoglu, S., and Ozkan, S. A. (2019). The role of electrochemical Immunosensors in clinical analysis. *Biosensors* 9:86. doi: 10.3390/bios9030086

Moon, H. W., Kim, H. N., Hur, M., Shim, H. S., Kim, H., and Yun, Y. M. (2016). Comparison of diagnostic algorithms for detecting toxigenic Clostridium difficile in routine practice at a tertiary referral Hospital in Korea. *PLoS One* 11:e0161139. doi: 10.1371/journal.pone.0161139

Morris, M. (2013). Fluorescent biosensors - probing protein kinase function in cancer and drug discovery. *Biochim. Biophys. Acta* 1834, 1387–1395. doi: 10.1016/j.bbapap.2013.01.025

Moshe, M., Daunt, A., Flower, B., Simmons, B., Brown, J. C., Frise, R., et al. (2021). SARS-CoV-2 lateral flow assays for possible use in national covid-19 seroprevalence surveys (react 2): diagnostic accuracy study. *BMJ* 372:n423. doi: 10.1136/bmj.n423

Ng, K. K., Reinert, Z. E., Corver, J., Resurreccion, D., Hensbergen, P. J., and Prescher, J. A. (2021). A bioluminescent sensor for rapid detection of PPEP-1, a Clostridioides difficile biomarker. *Sensors* 21:7485. doi: 10.3390/s21227485

Nguyen, S., Wells, S., Pau, C.-P., Owen, M., Dong, X., LaBorde, R., et al. (2009). Rapid detection of HIV-1 p24 antigen using magnetic immuno-chromatography (MICT). *J. Virol. Methods* 160, 14–21. doi: 10.1016/j.jviromet.2009.04.003

Nurul Najian, A. B., Engku Nur Syafirah, E. A., Ismail, N., Mohamed, M., and Yean, C. Y. (2016). Development of multiplex loop mediated isothermal amplification (m-LAMP) label-based Gold nanoparticles lateral flow dipstick biosensor for detection of pathogenic Leptospira. *Anal. Chim. Acta* 903, 142–148. doi: 10.1016/j.aca.2015.11.015

Ochsner, U. A., Green, L. S., Gold, L., and Janjic, N. (2014). Systematic selection of modified aptamer pairs for diagnostic sandwich assays. *BioTechniques* 56:125-8, 30–32-3. doi: 10.2144/000114134

Ochsner, U. A., Katilius, E., and Janjic, N. (2013). Detection of Clostridium difficile toxins a, B and binary toxin with slow off-rate modified aptamers. *Diagn. Microbiol. Infect. Dis.* 76, 278–285. doi: 10.1016/j.diagmicrobio.2013.03.029

Oldfield, E. C. I. V., Oldfield, E. C., and Johnson, D. A. (2014). Clinical update for the diagnosis and treatment of Clostridium difficile infection. *World J. Gastrointest. Pharmacol. Ther.* 5, 1–26. doi: 10.4292/wjgpt.v5.i1.1

Orrell, K. E., and Melnyk, R. A. (2021). Large Clostridial toxins: mechanisms and roles in disease. *Microbiol. Mol. Biol. Rev.* 85:e0006421. doi: 10.1128/MMBR.00064-21

Paitan, Y., Miller-Roll, T., and Adler, A. (2017). Comparative performance study of six commercial molecular assays for rapid detection of toxigenic Clostridium difficile. *Clin. Microbiol. Infect.* 23, 567–572. doi: 10.1016/j.cmi.2017.02.016

Pan, M., Gu, Y., Yun, Y., Li, M., Jin, X., and Wang, S. (2017). Nanomaterials for electrochemical Immunosensing. *Sensors (Basel).* 17:1041. doi: 10.3390/s17051041

Paredes-Sabja, D., Shen, A., and Sorg, J. A. (2014). Clostridium difficile spore biology: sporulation, germination, and spore structural proteins. *Trends Microbiol.* 22, 406–416. doi: 10.1016/j.tim.2014.04.003

Park, M. (2020). Surface display Technology for Biosensor Applications: a review. *Sensors (Basel).* 20. doi: 10.3390/s20102775

Park, S., Kim, H., Paek, S.-H., Cho, D.-W., and Kim, Y.-K. (2008). Enzyme-linked immuno-strip biosensor to detect Escherichia coli O157: H7. *Ultramicroscopy* 108, 1348–1351. doi: 10.1016/j.ultramic.2008.04.063

Park, C. S., Lee, C., and Kwon, O. S. (2016). Conducting Polymer Based Nanobiosensors. *Polymers* 8:249. doi: 10.3390/polym8070249

Parray, H., Shukla, S., Samal, S., Shrivastava, T., Ahmed, S., Sharma, C., et al. (2020). Hybridoma technology a versatile method for isolation of monoclonal antibodies, its applicability across species, limitations, advancement and future perspectives. *Int. Immunopharmacol.*:85. doi: 10.1016/j.intimp.2020.106639

Peltomaa, R., Glahn-Martínez, B., Benito-Peña, E., and Moreno-Bondi, M. C. (2018). Optical biosensors for label-free detection of small molecules. *Sensors (Basel)* 18:4126. doi: 10.3390/s18124126

Peng, Z., Ling, L., Stratton, C. W., Li, C., Polage, C. R., Wu, B., et al. (2018). Advances in the diagnosis and treatment of Clostridium difficile infections. *Emerg. Microb. Infect.* 7:15. doi: 10.1038/s41426-017-0019-4

Planche, T. D., Davies, K. A., Coen, P. G., Finney, J. M., Monahan, I. M., Morris, K. A., et al. (2013). Differences in outcome according to Clostridium difficile testing method: a prospective multicentre diagnostic validation study of C difficile infection. *Lancet Infect. Dis.* 13, 936–945. doi: 10.1016/S1473-3099(13)70200-7

Planche, T., and Wilcox, M. (2011). Reference assays for Clostridium difficile infection: one or two gold standards? *J. Clin. Pathol.* 64, 1–5. doi: 10.1136/jcp.2010.080135

Pollock, N. (2015). Ultrasensitive detection and quantification of toxins for optimized diagnosis of Clostridium difficile infection. *J. Clin. Microbiol.* 54, 259–264.

Pollock, N. R., Banz, A., Chen, X., Williams, D., Xu, H., Cuddemi, C. A., et al. (2019). Comparison of Clostridioides difficile stool toxin concentrations in adults with symptomatic infection and asymptomatic carriage using an ultrasensitive quantitative immunoassay. *Clin. Infect. Dis.* 68, 78–86. doi: 10.1093/cid/ciy415

Prasad, S. (2014). Nanobiosensors: the future for diagnosis of disease? *Nanobiosens. Dis. Diagn.* 3, 1–10. doi: 10.2147/NDD.S39421

Priyanka, B., Patil, R. K., and Dwarakanath, S. (2016). A review on detection methods used for foodborne pathogens. *Indian J. Med. Res.* 144, 327–338. doi: 10.4103/0971-5916.198677

Qi, H., Sun, Q., Ma, Y., Wu, P., and Wang, J. (2020b). Advantages of lateral flow assays based on fluorescent submicrospheres and quantum dots for Clostridium difficile toxin B detection. *Toxins.* 12. doi: 10.3390/toxins12110722

Qi, H., Wang, Y., Wu, P., Ma, Y., and Wang, J. (2020a). Rapid and fully-automated detection of Clostridium difficile toxin B via magnetic-particle-based chemiluminescent immunoassay. *Am. J. Transl. Res.* 12, 4228–4236. PMID: 32913500

Quintela, I. A., de Los Reyes, B. G., Lin, C.-S., and Wu, V. C. H. (2019). Simultaneous colorimetric detection of a variety of salmonella spp. in food and environmental samples by optical biosensing using oligonucleotide-Gold nanoparticles. *Front. Microbiol.* 10:1138. doi: 10.3389/fmicb.2019.01138

Raeisi, H. (2018). Production of polyclonal phages harbouring antibody fragment genes against *Xanthomonas citri* subsp citri using phage display technology. *Appl. Entomol. Phytopathol.* 85, 265–276.

Raeisi, H., Azimirad, M., Nabavi-Rad, A., Asadzadeh Aghdaei, H., Yadegar, A., and Zali, M. R. (2022a). Application of recombinant antibodies for treatment of Clostridioides difficile infection: current status and future perspective. *Front. Immunol.* 13:972930. doi: 10.3389/fimmu.2022.972930

Raeisi, H., Safarnejad, M. R., Alavi, S. M., Elahinia, S. A., and Farrokhi, N. (2020). Applying the pthA effector protein of Xanthomonas citri subsp. citri for production of specific antibodies and its application for detection of infected plants. *J. Plant Pathol.* 102, 79–87. doi: 10.1007/s42161-019-00385-5

Raeisi, H., Safarnejad, M. R., Alavi, S. M., Farrokhi, N., Elahinia, S. A., Safarpour, H., et al. (2019). Development and molecular analyses of Xanthomonas pthA specific scFv recombinant monoclonal antibodies. *Mdrsjrns.* 8, 417–429.

Raeisi, H., Safarnejad, M. R., and Sadeghkhani, F. (2022b). A new single-chain variable fragment (scFv) antibody provides sensitive and specific detection of citrus tristeza virus. *J. Virol Methods* 300:114412. doi: 10.1016/j.jviromet.2021.114412

Raeisi, H., Safarnejad, M. R., Moeini, P., Safarpour, H., and Sokhansanj, Y. (2020). Isolation of single-chain variable fragment (scFv) antibodies for detection of chickpea chlorotic dwarf virus (CpCDV) by phage display. *Arch. Virol.* 165, 2789–2798. doi: 10.1007/s00705-020-04813-1

Ramos, C. P., Lopes, E. O., Diniz, A. N., Lobato, F. C. F., Vilela, E. G., and Silva, R. O. S. (2020). Evaluation of glutamate dehydrogenase (GDH) and toxin a/B rapid tests for Clostridioides (prev. clostridium) difficile diagnosis in a university hospital in Minas Gerais, Brazil. Braz. *J. Microbiol.* 51, 1139–1143. doi: 10.1007/s42770-020-00288-z

Rangnoi, K., Jaruseranee, N., O'Kennedy, R., Pansri, P., and Yamabhai, M. (2011). One-step detection of aflatoxin-B1 using scFv-alkaline phosphatase-fusion selected from human phage display antibody library. *Mol. Biotechnol.* 49, 240–249. doi: 10.1007/s12033-011-9398-2

Reller, M. E., Alcabasa, R. C., Lema, C. A., and Carroll, K. C. (2010). Comparison of two rapid assays for Clostridium difficile common antigen and a C difficile toxin a/B assay with the cell culture neutralization assay. *Am. J. Clin. Pathol.* 133, 107–109. doi: 10.1309/AJCPO3QWOU8CYGEU

Riangrungroj, P., Bever, C. S., Hammock, B. D., and Polizzi, K. M. (2019). A label-free optical whole-cell Escherichia coli biosensor for the detection of pyrethroid insecticide exposure. *Sci. Rep.* 9:12466. doi: 10.1038/s41598-019-48907-6

Rissin, D., Kan, C., Campbell, T., Howes, S., Fournier, D., Song, L., et al. (2010). Single-molecule enzyme-linked immunosorbent assay detects serum proteins at subfemtomolar concentrations. *Nat. Biotechnol.* 28, 595–599. doi: 10.1038/nbt.1641

Roovers, R., Vosjan, M., Laeremans, T., Khoulati, R., de Bruin, R., Ferguson, K., et al. (2011). A biparatopic anti-EGFR nanobody efficiently inhibits solid tumour growth. *Int. J. Cancer* 129, 2013–2024. doi: 10.1002/ijc.26145

Sandlund, J., Bartolome, A., Almazan, A., Tam, S., Biscocho, S., Abusali, S., et al. (2018). Ultrasensitive detection of C. difficile toxins a and B using automated single molecule counting technology. *J. Clin. Microbiol.*:56. doi: 10.1128/JCM.00908-18

Sang, S., Wang, Y., Feng, Q., Wei, Y., Ji, J., and Zhang, W. (2015). Progress of new label-free techniques for biosensors: a review. *Crit. Rev. Biotechnol.* 36, 1–17. doi: 10.3109/07388551.2014.991270

Schirrmann, T., Meyer, T., Schütte, M., Frenzel, A., and Hust, M. (2011). Phage display for the generation of antibodies for proteome research, diagnostics and therapy. *Molecules (Basel, Switzerland)* 16, 412–426. doi: 10.3390/molecules16010412

Scognamiglio, V., Arduini, F., Palleschi, G., and Rea, G. (2014). Biosensing technology for sustainable food safety. *TrAC Trends Anal. Chem.* 62, 1–10. doi: 10.1016/j.trac.2014.07.007

Seo, K.-H., Brackett, R., Hartman, N., and Campbell, D. (1999). Development of a rapid response biosensor for detection of salmonella typhimurium. *J. Food Prot.* 62, 431–437. doi: 10.4315/0362-028X-62.5.431

Shahrabadi, M. S., Bryan, L. E., Gaffney, D., Coderre, S. E., Gordon, R., and Pai, C. H. (1984). Latex agglutination test for detection of Clostridium difficile toxin in stool samples. *J. Clin. Microbiol.* 20, 339–341. doi: 10.1128/jcm.20.3.339-341.1984

Shali, A., Hasannia, S., Gashtasbi, F., Shahangian, S., and Jalili, S. (2018). Generation and screening of efficient neutralizing single domain antibodies (VHHs) against the critical functional domain of anthrax protective antigen (PA). *Int. J. Biol. Macromol.* 114, 1267–1278. doi: 10.1016/j.ijbiomac.2018.03.034

Sharma, S., Byrne, H., and O'Kennedy, R. (2016). Antibodies and antibody-derived analytical biosensors. *Essays Biochem.* 60, 9–18. doi: 10.1042/EBC20150002

Shen, Z., Stryker, G., Mernaugh, R., Yu, L., Yan, H., and Zeng, X. (2005). Single-Chain Fragment Variable Antibody Piezoimmunosensors. *Anal. Chem.* 77, 797–805. doi: 10.1021/ac048655w

Shen, Z., Yan, H., Parl, F. F., Mernaugh, R. L., and Zeng, X. (2007). Recombinant antibody piezoimmunosensors for the detection of cytochrome P450 1B1. *Anal. Chem.* 79, 1283–1289. doi: 10.1021/ac061211a

Shirvan, A. N., and Aitken, R. (2016). Isolation of recombinant antibodies directed against surface proteins of Clostridium difficile. *Braz. J. Microbiol.* 47, 394–402. doi: 10.1016/j.bjm.2016.01.017

Simeon, R., and Chen, Z. (2018). In vitro-engineered non-antibody protein therapeutics. *Protein Cell* 9, 3–14. doi: 10.1007/s13238-017-0386-6

Singh, R., Hong, S., and Jang, J. (2017). Label-free detection of influenza viruses using a reduced graphene oxide-based electrochemical Immunosensor integrated with a microfluidic platform. *Sci. Rep.* 7:42771. doi: 10.1038/srep42771

Song, L., Zhao, M., Duffy, D. C., Hansen, J., Shields, K., Wungjiranirun, M., et al. (2015). Development and validation of digital enzyme-linked immunosorbent assays for ultrasensitive detection and quantification of Clostridium difficile toxins in stool. *J. Clin. Microbiol.* 53, 3204–3212. doi: 10.1128/JCM.01334-15

Stills, H. F. (2012). "Chapter 11 - polyclonal antibody production." in *The Laboratory Rabbit, Guinea Pig, Hamster, and Other Rodents*. eds. M. A. Suckow, K. A. Stevens and R. P. Wilson (Boston: Academic Press).

Sun, Z., Wang, X., Qi, C., Yun, Y.-H., Tang, Z., and Liu, X. (2018). Nanobody-alkaline phosphatase fusion protein-based enzyme-linked immunosorbent assay for one-step detection of Ochratoxin a in Rice. *Sensors* 18:4044. doi: 10.3390/s18114044

Sun, Y., Xing, G., Yang, J., Wang, F., Deng, R., Zhang, G., et al. (2015). Development of an Immunochromatographic test strip for simultaneous, qualitative and quantitative detection of Ochratoxin a and Zearalenone in cereal. *J. Sci. Food Agric.* 96, 3673–3678. doi: 10.1002/jsfa.7550

Surawicz, C., Brandt, L., Binion, D., Ananthakrishnan, A., Curry, S., Gilligan, P., et al. (2013). Guidelines for diagnosis, treatment, and prevention of Clostridium difficile infections. *Am. J. Gastroenterol.* 108, 478–498. doi: 10.1038/ajg.2013.4

Tang, X., Li, P., Zhang, Q., Zhang, Z., Zhang, W., and Jiang, J. (2017). Time-resolved fluorescence Immunochromatographic assay developed using two Idiotypic Nanobodies for rapid, quantitative, and simultaneous detection of aflatoxin and Zearalenone in maize and its products. *Anal. Chem.* 89, 11520–11528. doi: 10.1021/acs.analchem.7b02794

Tang, D., and Xia, B. (2008). Electrochemical immunosensor and biochemical analysis for carcinoembryonic antigen in clinical diagnosis. *Microchim. Acta* 163, 41–48. doi: 10.1007/s00604-007-0918-5

Tu, Z., Qi, C., Li, Y., Xiong, Y., Xu, Y., Hu, N., et al. (2015). Identification and characterization of species-specific nanobodies for the detection of listeria monocytogenes in milk. *Anal. Biochem.* 493, 1–7. doi: 10.1016/j.ab.2015.09.023

Tullila, A., and Nevanen, T. (2017). Utilization of multi-immunization and multiple selection strategies for isolation of Hapten-specific antibodies from recombinant antibody phage display libraries. *Int. J. Mol. Sci.* 18:1169. doi: 10.3390/ijms18061169

Unger, M., Eichhoff, A., Schumacher, L., Strysio, M., Menzel, S., Schwan, C., et al. (2015). Selection of Nanobodies that block the enzymatic and cytotoxic activities of the binary clostridium difficile toxin CDT. *Sci. Rep.* 5:5. doi: 10.1038/srep07850

Valldorf, B., Hinz, S. C., Russo, G., Pekar, L., Mohr, L., Klemm, J., et al. (2022). Antibody display technologies: selecting the cream of the crop. *Biol. Chem.* 403, 455–477. doi: 10.1515/hsz-2020-0377

van Prehn, J., Reigadas, E., Vogelzang, E. H., Bouza, E., Hristea, A., Guery, B., et al. (2021). European Society of Clinical Microbiology and Infectious Diseases: 2021 update on the treatment guidance document for Clostridioides difficile infection in adults. *Clin. Microbiol. Infect.* 27, S1–S21. doi: 10.1016/j.cmi.2021.09.038

Viswanathan, V. K., Mallozzi, M. J., and Vedantam, G. (2010). Clostridium difficile infection: An overview of the disease and its pathogenesis, epidemiology and interventions. *Gut Microbes* 1, 234–242. doi: 10.4161/gmic.1.4.12706

Wang, X., Coljee, V., and Maynard, J. (2013). Back to the future: recombinant polyclonal antibody therapeutics. *Curr. Opin. Chem. Eng.* 2, 405–415. doi: 10.1016/j.coche.2013.08.005

Wang, P., Guanghui, L., Yan, J., Hu, Y., Zhang, C. Z., Liu, X., et al. (2014). Bactrian camel nanobody-based immunoassay for specific and sensitive detection of Cry1Fa toxin. *Toxicon* 92, 186–192. doi: 10.1016/j.toxicon.2014.10.024

Wang, Y., Li, H., Wang, Y., Li, H., Luo, L., Xu, J., et al. (2017b). Development of multiple cross displacement amplification label-based gold nanoparticles lateral flow biosensor for detection of listeria monocytogenes. *Int. J. Nanomedicine* 12, 473–486. doi: 10.2147/IJN.S123625

Wang, Y., Li, H., Wang, Y., Zhang, L., Xu, J., and Ye, C. (2017a). Loop-mediated isothermal amplification label-based Gold nanoparticles lateral flow biosensor for detection of enterococcus faecalis and Staphylococcus aureus. *Front. Microbiol.* 8. doi: 10.3389/fmicb.2017.00192

Wang, Y., Qin, Z., Boulware, D., Pritt, B., Sloan, L., González, I., et al. (2016b). Thermal contrast amplification reader yielding 8-fold analytical improvement for disease detection with lateral flow assays. *Anal. Chem.* 88, 11774–11782. doi: 10.1021/acs.analchem.6b03406

Wang, Y., Wang, Y., Xu, J., and Ye, C. (2016a). Development of multiple cross displacement amplification label-based Gold nanoparticles lateral flow biosensor for detection of Shigella spp. *Front. Microbiol.* 7 doi: 10.3389/fmicb.2016.01834

Willats, W. (2003). Phage display: practicalities and prospects. *Plant Mol. Biol.* 50, 837–854. doi: 10.1023/a:1021215516430

Wilson, D., Rissin, D., Kan, C., Fournier, D., Piech, T., Campbell, T., et al. (2015). The Simoa HD-1 analyzer: a novel fully automated digital immunoassay analyzer with single-molecule sensitivity and multiplexing. *J. Lab. Automat.* 21, 533–547. doi: 10.1177/2211068215589580

Xu, X., Fang, Y., and Wang, L. (2014). A label-free electrochemical Immunosensor for clostridium difficile toxin B based on one-step immobilization of Thionine in a silica matrix. *Anal. Lett.* 47, 2255–2265. doi: 10.1080/00032719.2014.900623

Xu, C., Zhang, C. Z., Zhong, J., Hu, H., Luo, S., Liu, X., et al. (2017). Construction of an immunized rabbit phage display library for selecting high-activity of against bacillus thuringiensis Cry1F toxin single-chain antibodies. *J. Agric. Food Chem.* 65, 6016–6022. doi: 10.1021/acs.jafc.7b01985

Yang, P., Hash, S., Park, K., Wong, C., Doraisamy, L., Petterson, J., et al. (2017). Application of nuclear magnetic resonance to detect toxigenic Clostridium difficile from stool specimens. *J. Mol. Diagn.* 19, 230–235. doi: 10.1016/j.jmoldx.2016.09.012

Yang, Z., Schmidt, D., Liu, W., Li, S., Shi, L., Sheng, J., et al. (2014). A novel multivalent, single-domain antibody targeting TcdA and TcdB prevents fulminant Clostridium difficile infection in mice. *J. Infect. Dis.* 210, 964–972. doi: 10.1093/infdis/jiu196

Yang, L., Zhang, Y., Wang, Q., and Zhang, L. (2020). An automated microrobotic platform for rapid detection of C. diff toxins. *I.E.E.E. Trans. Biomed. Eng.* 67, 1517–1527. doi: 10.1109/TBME.2019.2939419

Yang, H., Zhong, Y., Wang, J., Zhang, Q., Li, X., Ling, S., et al. (2018). Screening of a ScFv antibody with high affinity for application in human IFN-γ immunoassay. *Front. Microbiol.* 9:261. doi: 10.3389/fmicb.2018.00261

Yoldas, O., Altindis, M., Cufali, D., Asik, G., and Kesli, R. (2016). A diagnostic algorithm for the detection of Clostridium difficile-associated diarrhea. *Balkan Med. J.* 33, 80–86. doi: 10.5152/balkanmedj.2015.15159

Younis, S., Taj, A., Zia, R., Hayat, H., Shaheen, A., Awan, F., et al. (2020). Nanosensors for the detection of viruses. *Nanosens. Smart Cities*, 327–338. doi: 10.1016/B978-0-12-819870-4.00018-9

Yücesoy, M., McCoubrey, J., Brown, R., and Poxton, I. (2002). Detection of toxin production in Clostridium difficile strains by three different methods. *Clin. Microbiol. Infect.* 8, 413–418. doi: 10.1046/j.1469-0691.2002.00440.x

Zahavi, D., and Weiner, L. (2020). Monoclonal antibodies in cancer therapy. *Antibodies (Basel).* 9. doi: 10.3390/antib9030034

Zeng, X., Shen, Z., and Mernaugh, R. (2012). Recombinant antibodies and their use in biosensors. *Anal. Bioanal. Chem.* 402, 3027–3038. doi: 10.1007/s00216-011-5569-z

Zhang, W.-J., Sui, Y.-X., Budha, A., Zheng, J.-B., Sun, X.-J., Hou, Y.-C., et al. (2012). Affinity peptide developed by phage display selection for targeting gastric cancer. *World J. Gastroenterol.* 18, 2053–2060. doi: 10.3748/wjg.v18.i17.2053

Zhang, X., Yu, X., Wen, K., Li, C., Mujtaba, G., Jiang, H., et al. (2017). Multiplex lateral flow immunoassays based on amorphous carbon nanoparticles for detecting three fusarium mycotoxins in maize. *J. Agric. Food Chem.* 65, 8063–8071. doi: 10.1016/j.jmoldx.2016.09.012

Zhang, C., Zhang, Q., Tang, X., Zhang, W., and Li, P. (2019). Development of an anti-Idiotypic VHH antibody and toxin-free enzyme immunoassay for Ochratoxin a in cereals. *Toxins.* 11:280. doi: 10.3390/toxins11050280

Zhao, M.-X., and Zeng, E.-Z. (2015). Application of functional quantum dot nanoparticles as fluorescence probes in cell labeling and tumor diagnostic imaging. *Nanoscale Res. Lett.* 10:171. doi: 10.1186/s11671-015-0873-8

Zhu, M., Gong, X., Hu, Y., Ou, W., and Wan, Y. (2014a). Streptavidin-biotin-based directional double Nanobody sandwich ELISA for clinical rapid and sensitive detection of influenza H5N1. *J. Transl. Med.* 12:352. doi: 10.1186/s12967-014-0352-5

Zhu, Z., Shi, L., Feng, H., and Zhou, H. S. (2014b). Single domain antibody coated gold nanoparticles as enhancer for Clostridium difficile toxin detection by electrochemical impedance immunosensors. *Bioelectrochemistry* 101, 153–158. doi: 10.1016/j.bioelechem.2014.10.003

frontiers | Frontiers in Microbiology

TYPE Original Research
PUBLISHED 19 December 2022
DOI 10.3389/fmicb.2022.1048997

OPEN ACCESS

EDITED BY
George William Carnell,
University of Cambridge,
United Kingdom

REVIEWED BY
Kiran Chawla,
Manipal Academy of Higher Education,
India
Abbas Yadegar,
Shahid Beheshti University of Medical
Sciences, Iran

*CORRESPONDENCE
Lianjun Lin
✉ 06474@pkufh.com
Xinmin Liu
✉ lxm2128@163.com

†These authors have contributed equally to this work and share last authorship

SPECIALTY SECTION
This article was submitted to Infectious Agents and Disease, a section of the journal Frontiers in Microbiology

RECEIVED 20 September 2022
ACCEPTED 01 December 2022
PUBLISHED 19 December 2022

CITATION
Wei S, Wang L, Shi M, Li J, Sun C, Liu Y, Zhang Z, Wu Y, Huang L, Tang F, Lv L, Mu X, Tian W, Lin C, Lu J, Sun B, Dai B, Xiong H, Nie X, Ding W, Ouyang Y, Lin L and Liu X (2022) Rapid, accurate, and novel diagnostic technique for respiratory pathogens: Clinical application of loop-mediated isothermal amplification assay in older patients with pneumonia, a multicenter prospective observational study.
Front. Microbiol. 13:1048997.
doi: 10.3389/fmicb.2022.1048997

Rapid, accurate, and novel diagnostic technique for respiratory pathogens: Clinical application of loop-mediated isothermal amplification assay in older patients with pneumonia, a multicenter prospective observational study

Shanchen Wei[1], Lina Wang[1], Mingwei Shi[1], Jun Li[1], Chunping Sun[1], Yingying Liu[2], Zhi Zhang[2], Yiqun Wu[3], Lei Huang[4], Fei Tang[5], Liping Lv[5], Xiangdong Mu[6], Wei Tian[7], Caiwei Lin[8], Jianrong Lu[9], Baojun Sun[10], Bin Dai[11], Hui Xiong[12], Xiuhong Nie[13], Weimin Ding[14], Yuqing Ouyang[1], Lianjun Lin[1†] and Xinmin Liu[1*†]

[1]Department of Geriatrics, Peking University First Hospital, Beijing, China, [2]Bio Biological Group Co., Ltd, Beijing, China, [3]School of Public Health, Peking University Health Science Center, Beijing, China, [4]Department of Clinical Laboratory , Peking University First Hospital, Beijing, China, [5]Department of Respiratory, Anhui Chest Hospital, Hefei, China, [6]Department of Respiratory, Tsinghua ChangGung Hospital, Beijing, China, [7]Department of Geriatrics, Jishuitan Hospital, Beijing, China, [8]Department of Emergency, Aerospace Center Hospital, Beijing, China, [9]Department of Emergency, Jingmei Group General Hospital, Beijing, China, [10]Department of Respiratory, Chinese People's Liberation Army General Hospital, Beijing, China, [11]Department of Neurosurgery, Shijitan Hospital, Beijing, China, [12]Department of Emergency, Peking University First Hospital, Beijing, China, [13]Department of Respiratory, Xuanwu Hospital, Beijing, China, [14]Department of Respiratory Endoscopy, Beijing Chest Hospital, Beijing, China

Background: Loop-mediated isothermal amplification (LAMP) is a novel nucleic acid amplification method using only one type of enzyme that can amplify DNA with high specificity, efficiency and rapidity under isothermal conditions. Chips for Complicated Infection Detection (CCID) is based on LAMP. This study translate CCID into clinical application and evaluate its diagnostic value for pneumonia.

Methods: Eighty one older patients with pneumonia were prospectively enrolled from January 1 to July 23, 2021, and 57 sputum/airway secretion and 35 bronchoalveolar lavage fluid samples were collected and analyzed by CCID and conventional microbiological tests (CMTs). Samples were collected, transported, monitored, and managed by a multidisciplinary team using a sample management information system.

Results: CCID turnaround time was 50min, and the detection limit was 500 copies/reaction. The percentage of positive samples was significantly higher using CCID than CMTs, especially for *Klebsiella pneumoniae* (odds ratio [OR],

9.0; 95% confidence interval [CI], 1.1–70.5; $p<0.05$), *Enterococcus faecalis* (OR, ∞; $p<0.01$), *Stenotrophomonas maltophilia* (OR, ∞; $p<0.01$), fungi (OR, 26.0; 95% CI, 3.6–190.0; $p<0.01$), and viruses (CCID only; $p<0.01$). In addition, the percentage of positive results was significantly higher using CCID than CMTs in patients who used antibiotics for more than 3days (91.9% vs. 64.9%; $p<0.01$). Analyzing clinical impact, 55 cases (59.8%) benefited from CCID.

Conclusion: CCID allows the rapid and accurate detection of pneumonia in older patients. Moreover, this technique is less affected by previous antibiotic treatment and can improve patient care.

KEYWORDS

loop-mediated isothermal amplification, chip, pneumonia, clinical, application, diagnostic, respiratory, pathogens

Introduction

The incidence of pneumonia is high in the elderly, which is a public health problem due to high mortality (Welte et al., 2012; Millett et al., 2013; Luna et al., 2016). Therefore, an accurate and rapid diagnosis is essential to identify the etiological agent, initiate targeted treatment, and reduce the mortality (Garau et al., 2008). However, conventional microbiological tests (CMTs) used in clinical practice have disadvantages. For instance, the detection rate of pathogens using CMTs is 27·4% (Lidman et al., 2002); among these, sputum culture has a long turnaround time (≥2 days), and the detection rate is 26–30% (Garcia-Vazquez et al., 2004; Signori et al., 2008; Shariatzadeh and Marrie, 2009). Therefore, there is an urgent need to find new diagnostic methods.

In 2019, the American Thoracic Society and the Infectious Diseases Society of America published guidelines and pointed out that rapid, cost-effective, sensitive, and specific diagnostic tests are key to supporting targeted therapies for community-acquired pneumonia and improving prognosis (Metlay et al., 2019). In recent years, the development and implementation of molecular diagnostic methods for pneumonia have improved clinical diagnosis. Nucleic acid amplification is one of the most valuable tools, and in addition to the widely used PCR-based assays (Saiki et al., 1985, 1988), several amplification methods have been invented, including nucleic acid sequence-based amplification (NASBA; Compton, 1991), self-sustained sequence replication (3SR) (Guatelli et al., 1990) and strand displacement amplification (SDA; Walker et al., 1992a,b). Each of these amplification methods has its own shortcomings when applied to the clinic. For example, the requirement of high-precision thermal cyclers in PCR prevents this powerful method from being widely used. NASBA and 3SR, which do not use thermal cycling, have weak points as well: increased backgrounds due to digestion of irrelevant DNA contained in the sample and the necessity to use costly modified nucleotides as substrate. Excitingly, a novel method called loop-mediated isothermal amplification (LAMP) is invented, which employs a type of DNA polymerase and a set of four specially designed primers (Notomi et al., 2000). In LAMP cycling, one inner primer hybridizes to the loop on the product and initiates displacement DNA synthesis, yielding the original stem–loop DNA and a new stem–loop DNA with a stem twice as long. Thus it can amplify DNA with high specificity, efficiency and rapidity under isothermal conditions (Notomi et al., 2000).

Chips for Complicated Infection Detection (CCID), developed by the Bio Biological Group Co., Ltd., uses LAMP-based microfluidic chip platforms (Huang et al., 2011). One such chip detecting eight respiratory bacteria has China Food and Drug Administration's medical device registration (Registration No. 20173401346). Their previous data found that compared with DNA sequencing, the sensitivity and specificity of CCID are over 95 and 99%, respectively (Hou et al., 2018). However, the application value of CCID has not been verified by rigorous clinical studies. To achieve this goal, a prospective multicenter observational study was performed. CCID is transformed into clinical application and assessed the clinical value of diagnosis and treatment by a multidisciplinary team. We want to develop a rapid, accurate, and novel diagnostic technique for respiratory pathogens to improve the management of older patients with pneumonia.

Materials and methods

Participants and ethics

Patients diagnosed with pneumonia were prospectively recruited in 10 hospitals in China— Peking University First Hospital, Jishuitan Hospital, Xuanwu Hospital, Shijitan Hospital, Tsinghua ChangGung Hospital, Jingmei Group General Hospital, Aerospace Center Hospital, Beijing Chest Hospital, Chinese People's Liberation Army General Hospital, and Anhui Chest Hospital from January 1, 2021, to July 23, 2021. According to the 2019 and 2007 Official Clinical Practice Guidelines of the American Thoracic Society and Infectious Diseases Society of America (Mandell et al., 2007; Metlay et al., 2019), pneumonia was defined as (1) cough, expectoration, or worsening symptoms of

existing respiratory diseases with or without purulent sputum, chest pain, dyspnea, and hemoptysis; (2) fever; (3) signs of lung consolidation or rales; (4) peripheral blood leukocytes $>10\times10^9$ or $<4\times10^9$ per liter with or without a shift to the left. The inclusion criteria were patients aged ≥60 years, at least one of the features above, and the presence of patchy infiltrates, consolidation, ground-glass opacities, or interstitial changes with or without pleural effusion on chest imaging. The exclusion criteria were pregnant women, patients unable to give written informed consent, patients unable to produce sputum spontaneously, and patients with tuberculosis, lung tumors, non-infectious interstitial lung diseases, pulmonary edema, atelectasis, pulmonary embolism, pulmonary eosinophil infiltration, or pulmonary vasculitis.

The research ethics committee of our institution approved the study protocol (Number 2021–132). Written informed consent was obtained from all participants.

Data collection and case discussion

Demographic data, clinical manifestations, vital signs, laboratory indicators, CMT and imaging results, and antibiotic data were collected. Chinese infectious disease experts, laboratory personnel, clinicians, and researchers reached consensus on the etiological agent.

Sample collection and CMTs.

Sputum and BALF samples were collected in accordance with clinical guidelines (Hospital infection control branch of Chinese preventive medicine association, 2018; Wang et al., 2019). The quality of sputum samples was verified by sputum smears. The results showed that the count of leukocytes was greater than 25 per low-power field, and the count of epithelial cells was less than 10 per low-power field, or the ratio of leukocytes to epithelial cells was greater than 2.5, indicating that the sputum samples were qualified. Bacterial pneumonia was confirmed by the presence of Gram-positive or Gram-negative bacteria on smears or routine cultures (at least10^4 CFU/ml). Viral pathogens were screened by PCR. Fungi were detected by sputum smear microscopy, culture, or the detection of (1, 3)-β-D-glucan and galactomannan antigens. Pulmonary tuberculosis was confirmed by positive sputum smears for acid-fast bacilli or positive sputum culture for Mycobacterium tuberculosis.

CMTs were performed according to the Guidelines for the Diagnosis and Treatment of Chinese Adult Community-Acquired Pneumonia (2016 Edition) (Qu and Cao, 2016).

Sample preparation and DNA extraction

Sputum and BALF samples were transferred to sterile test tubes and analyzed by CCID and CMTs. For CCID, the volume of sputum needed to be at least 2 ml, and the volume of BALF needs to be at least 3 ml. Samples were pretreated with an equal volume of 4% NaOH, vortexed for 15 min, and centrifuged at 12,000 rpm for 5 min. The supernatant was discarded, and Tris-EDTA buffer solution and glass beads were added to the pellet. The test tubes were centrifuged at 1,000 rpm for 5 min and heated at 95°C for 5 min to release nucleic acids. After centrifugation at 12,000 rpm for 5 min, 25 μl of the supernatant was mixed with 25 μl of the amplification reagent, and the mixture was added to the chip. Assays were performed using the Pathogenic Bacteria Nucleic Acid Detection Kit (CapitalBio Technology, Beijing, China) following the manufacturer's instructions.

Pathogens detection

The schematic and amplification curves for pathogens detection were shown in Figure 1. The disc chip was used in this study, and its structure was shown in Figure 2. The process from sample loading to completion of amplification was shown in the animation (Supplementary material 1). The chip was centrifuged at 3,000 rpm for 30 s, making the mixture drop into the bottom of the reaction wells. Air trapped in the chip was released through air vents of each well, and inlet ports were covered to prevent contamination. Reactions were performed on an RTisochip-A nucleic acid analyzer equipped with a real-time imaging system (Figure 1; CapitalBio Technology, Beijing, China). The amplification conditions consisted of 1 cycle at 37°C for 3 min and 1 cycle at 65°C for 47 min. Data were analyzed using nucleic acid detection software. The CCID panel could detect 47 bacterial species, 22 fungal species, 21 DNA viruses, and 37 antibiotic resistance genes (Supplementary material 2).

Determination of clinical impact

A positive impact was defined as a definitive diagnosis, supporting empirical antibiotic treatment, or change in therapeutic management based on CCID results, leading to a favorable clinical outcome. No impact was defined as valueless results or detecting no pathogens using CCID.

Statistics analysis

Statistical analysis was performed using SPSS version 26.0 and R software version 3.6.1, and data were transferred to Excel spreadsheets. Data were expressed as mean ± standard deviation for normally distributed continuous variables and as median (interquartile range) for non-normally distributed continuous variables. Categorical data were presented as percentages. The difference in the detection rates between CCID and CMTs was analyzed by Pearson chi-square test, Fisher exact test, or McNemar test for discrete variables. A two-tailed $p<0.05$ was considered statistically significant.

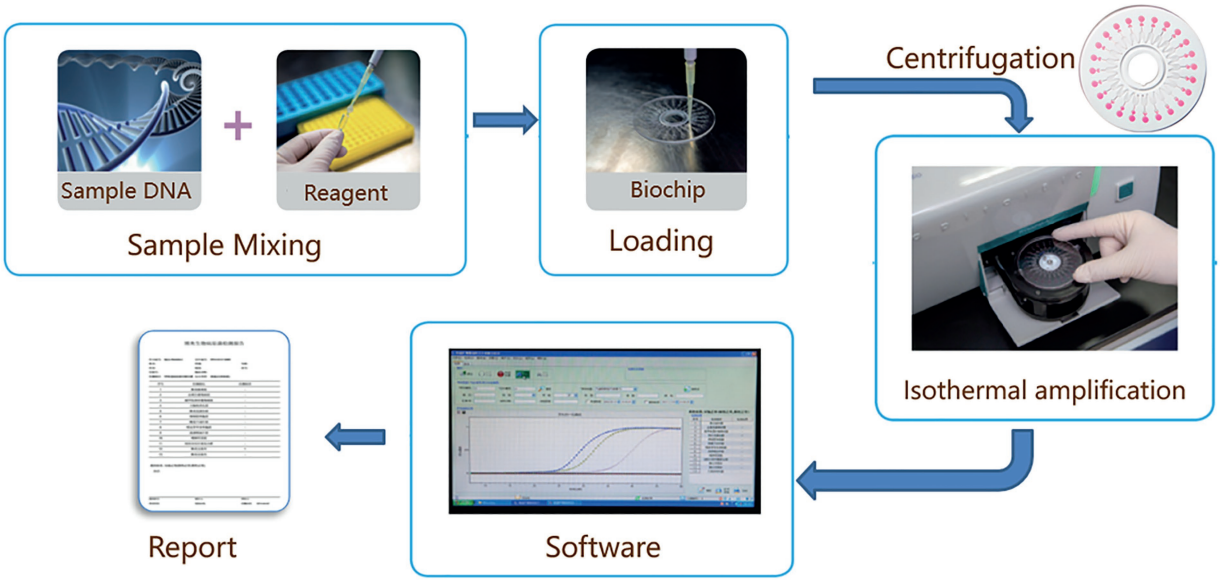

FIGURE 1
Experimental setup using the RTisochip amplification system.

Results

Sample management information system and efficacy of CCID

Sample collection, transport, monitoring, and management were performed by a multidisciplinary team using a sample management information system.[1]. The turnaround time of CCID was 50 min, and the limit of detection was 500 copies per reaction.

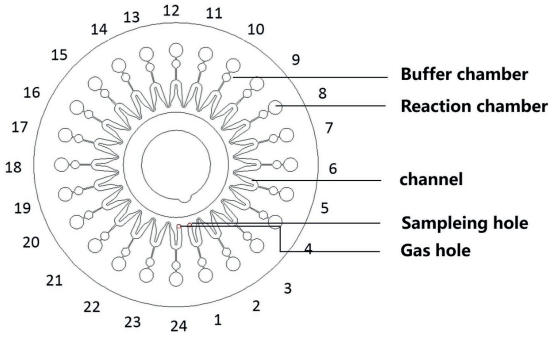

FIGURE 2
Schematic of the microfluidic chip consisting of an array of 24 reaction wells and microchannel for sample inlet, distribution, and reaction.

Baseline statistics

The demographic and clinical characteristics of our cohort are presented in Table 1. The median age was 78 (67.5–85.5) years. Fifty-eight patients were male, and 23 were female. The most common comorbidity was hypertension (43, 53.1%). The main clinical manifestations were cough (58, 71.6%), expectoration (55, 67.9%), fever (44, 54.3%), dyspnea (31, 38.3%), and disturbance of consciousness (18, 22.2%). Eighteen patients (22.2%) had respiratory failure, and 36 (44.4%) had severe pneumonia. As of July 23, 2021, 18 patients (22.2%) had died (Table 1). Ninety-two respiratory samples were collected from 81 patients. Sputum and bronchoalveolar lavage fluid (BALF) from the same person were submitted for examination in nine cases (9.8%), and two (2.2%) patients repeatedly submitted samples for examination during disease progression. Eighty-one samples (54 [66.7%] sputum and 27 [33.3%] BALF specimens) were analyzed by CCID and CMTs; of these, 44 (54.3%) and 37 (45.7%) were obtained from patients treated with antibiotics for ≤3 and > 3 days, respectively. The bacterial species most frequently detected by CCID were *Pseudomonas aeruginosa, Klebsiella pneumoniae, Enterococcus faecalis, Enterococcus faecium, Stenotrophomonas maltophilia*, and *Staphylococcus aureus* (Figure 3A). The most common fungal species was *Candida albicans* (Figure 3B), and the most common viruses were Epstein–Barr virus, herpes simplex virus type 1, cytomegalovirus, and mammalian adenovirus type B (Figure 3C).

1 https://smis.capitalbio.com and https://smis-m.capitalbio.com/

Diagnostic performance

Concordance between CCID and CMTs

Forty-six (56.8%) samples analyzed by CCID and CMTs were double positive, and seven (8·6%) were double negative. Twenty-three (28.4%) specimens were positive using CCID, and five (6·2%) were positive using CMTs. For double positive samples, there was complete concordance in two cases, discordance in nine cases, and partial concordance (diagnostic agreement for at least one pathogen) in 35 cases (Figure 4).

Discordance between CCID and CMTs

Twenty-three (28.4%) samples were positive using CCID but negative using CMTs, of which more than half results (13/23) were regarded as pathogenic microbe by case discussion. The remaining cases were regarded as colonization, contamination, or other causes. In five (6.2%) specimens, pathogens were detected by CMTs but not by CCID (Table 2). Of these, one sample was positive by CCID in the second examination.

Diagnostic comparison

Among 234 identified pathogens, CCID had higher ability to detect *Klebsiella pneumoniae* (odds ratio [OR], 9.0; 95% confidence interval [CI], 1.1–70.5; $p = 0.011$), *Enterococcus faecalis* (OR, ∞; $p = 0.001$), *Stenotrophomonas maltophilia* (OR, ∞; $p = 0.008$), fungi (OR, 26·0; 95% CI, 3·6–190.0; $p < 0.001$), and viruses (CCID only; $p < 0.001$). In addition, the rate of detection of *Pseudomonas aeruginosa*, *Staphylococcus aureus*, and *Acinetobacter baumannii* was marginally higher using CCID than CMTs ($p > 0.05$; Figure 5).

Effect of antibiotic treatment on pathogen detection

In our cohort, 37 (45.7%) patients used antibiotics for more than 3 days at the time of specimen collection. The detection rate was significantly higher using CCID than using CMTs (91.9% vs. 64·9%, $p = 0.005$). In the remaining patients, the detection rate was marginally higher using CCID (79.5% vs. 61.4%, $p > 0.05$) (Figure 6).

Impact on clinical diagnosis and management

The analysis of the impact of CCID on patient care showed that this method had positive or no impact in 55 (59.8%) and 37 (40.2%) cases, respectively (Table 3). In the former group, positive CCID results allowed a definitive diagnosis in 55 patients. In the latter group, CCID did not detect the etiological agent in 16 patients, and the results were attributed to contaminants or other causes in 21 cases (Table 3).

Regarding antibiotic management in patients with a clinical benefit, CCID results supported empirical antibiotic treatment in 51 cases and led to a change in treatment in four cases (Table 3).

TABLE 1 Demographic and clinical characteristics of the 81 patients included in the study at baseline.

Characteristics	No. (%)
Age, median (IQR), *y*	78 (67.5–85.5)
Sex	
Female	23 (28.4)
Male	58 (71.6)
History of underlying disease	
Hypertension	43(53.1)
Cardiac diseases	37 (45.7)
Cerebrovascular diseases	22 (27.2)
Diabetes	19 (235)
Neoplasia	10 (12.3)
COPD	8 (9.9)
Kidney disease	9 (11.1)
Autoimmune disease	6 (7.4)
Liver disease	2 (2 5)
Symptoms	
Cough	58 (71.6)
Expectoration	55 (67.9)
Fever	44 (54.3)
Dyspnea	31 (38.3)
Disorders of consciousness	18 (22.2)
Loss of appetite	16 (19.8)
Chest distress	15 (18.5)
Weak	9 (11.1)
Respiratory failure	18 (22.2)
Severe pneumonia	36 (44.4)
Outcome	
Dead	18 (22.2)
Survive	63 (77.8)

IQR, interquartile range; COPD, chronic obstructive pulmonary disease.

Discussion

Loop-mediated isothermal amplification (LAMP) is a novel nucleic acid amplification method that can amplify DNA with high specificity, efficiency and rapidity under isothermal conditions (Notomi et al., 2000). Compared with several other

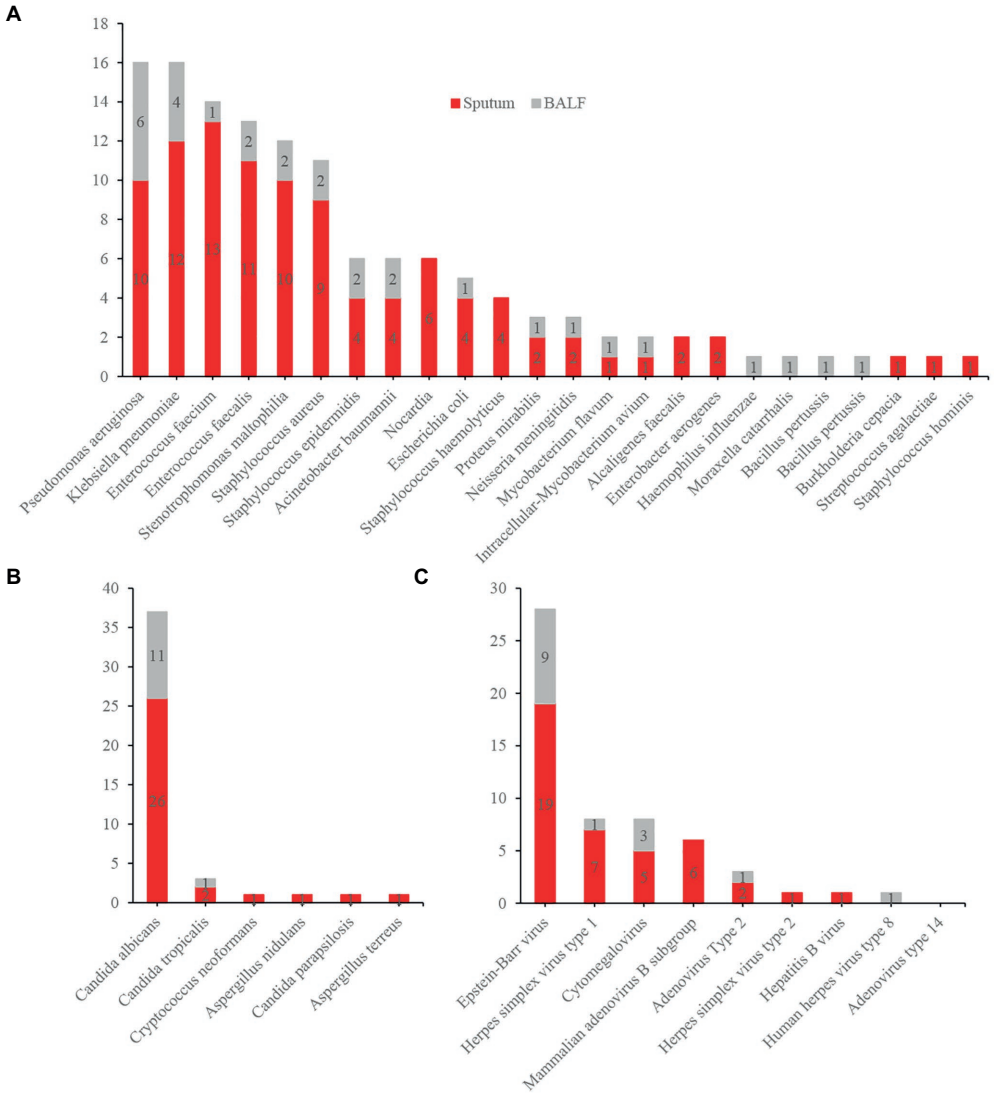

FIGURE 3
Distribution of bacteria **(A)**, fungi **(B)**, and virus **(C)** detected by Chips for Complicated Infection Detection. The most commonly detected bacteria, fungi, and virus are *Pseudomonas aeruginosa*, *Candida albicans*, and Epstein–Barr virus.

methods, such as PCR, NASBA, 3SR and SDA, LAMP is more suitable for clinical application, since their instrumentation is simpler without high-precision thermal cyclers. Other key advantages of LAMP are robustness and the production of pyrophosphate in the presence of the target gene, enabling to detect the reaction products using the naked eye (Zhang et al., 2019). Polymerase inhibitors, presented in clinical samples, do not affect the amplification process, making LAMP suitable for a simple sample-to-answer diagnostic systems with simplified sample preparation (Zhang et al., 2019).

We searched PubMed database for articles with the keywords "LAMP, pneumonia or lower respiratory tract infections." There was no language restriction, and COVID-19 was removed. We found three results (Hou et al., 2018; Scharmann et al., 2020; Wang et al., 2020), all three of which collected respiratory tract specimens and submitted them for LAMP and routine clinical pathogenic testing, but did not confirm and interpret the controversial results from a clinical perspective. The indicators detected by LAMP technology are limited to 2–9 kinds of bacteria, and no attention was paid to the elderly. While our study transformed CCID into clinical application. We found that CCID combined with LAMP has several advantages. First, CCID has a shorter turnaround time of 50 min than other diagnostic methods (Torres et al., 2016; Miao et al., 2018). Second, the percentage of positive samples was significantly higher using CCID than using CMTs. Among 81 samples, the results agreed between CCID and CMTs in 37 samples (two complete matches and 35 partial matches) and did not agree in 44 samples. In the latter cases, the causative agent was identified by consensus in 13 specimens and identified by CCID in one sample after repeating

TABLE 2 Analysis of Inconsistent Results Between CCID and CMTs for Pathogen Detection.

Pathogens Detected Only by CCID (N = 23)					
Sample No.	**Sample types**	**Possible explanation**			
		Pathogenic microbe	**Likely colonization**	**Likely contamination**	**Other causes**
115	sputum	*Nocardia*			Epstein–Barr virus
117	sputum		Mammalian adenovirus B subgroup, herpes simplex virus type 1		*Nocardia*
118	sputum	*Candida albicans*, herpes simplex virus type 1, cytomegalovirus			mammalian adenovirus B subgroup
139	sputum		Epstein–Barr virus		
145	sputum	*Pseudomonas aeruginosa*, *Candida albicans*	*Stenotrophomonas maltophilia*	*Staphylococcus epidermidis*	
262	sputum			*Neisseria meningitidis*, Epstein–Barr virus, cytomegalovirus	*Enterobacter aerogenes*
295	sputum	*Staphylococcus aureus*		Epstein–Barr virus	*Candida albicans*
328	BALF		Epstein–Barr virus		
382	sputum			*Enterococcus faecalis*, *Staphylococcus epidermidis*, adenovirus type 2	
402	sputum			*Candida albicans*, Epstein–Barr virus	
447	sputum	*Pseudomonas aeruginosa*			
482	sputum			*Staphylococcus hominis*	Epstein–Barr virus
489	BALF	*Candida albicans*	Epstein–Barr virus		
529	BALF		*Candida albicans*		
582	sputum	*Candida albicans*			
594	sputum	*Klebsiella pneumoniae*			
683	sputum	*Acinetobacter baumannii*, *Candida albicans*	*Enterococcus faecalis*, *Enterococcus faecium*	Epstein–Barr virus	
691	BALF	*Acinetobacter baumannii*, *Candida tropicalis*	Epstein–Barr virus		*Enterococcus faecium*, *Candida albicans*
695	BALF		Epstein–Barr virus, herpes simplex virus type 1		
697	sputum	*Enterococcus faecium*, *Stenotrophomonas maltophilia*	herpes simplex virus type 1	*Staphylococcus epidermidis*	
807	BALF		*Bacillus pertussis*		
808	BALF	*Pseudomonas aeruginosa*, *Intracellular-Mycobacteria avium*			
836	sputum	*Escherichia coli*	*Cryptococcus neoformans*	Epstein–Barr virus	
Pathogens detected only by CMTs (N = 5)					
Sample No.	**Sample type**	**CMTs result**		**Possible explanation**	
321	sputum	Haemophilus parainfluenzae		Not detected	
366	BALF	*MTB*		Not detected	
377	BALF	*Staphylococcus aureus*, *MTB*		Not detected	
538	sputum	*Pseudomonas aeruginosa*		Repeat CCID test, *Pseudomonas aeruginosa* was detected.	
540	sputum	*Staphylococcus aureus*, *Klebsiella pneumoniae*		Not detected	

CCID, Chips for Complicated Infection Detection; CMTs, Conventional Microbiological Tests; BALF, Bronchoalveolar Lavage Fluid; MTB, Mycobacterium tuberculosis.

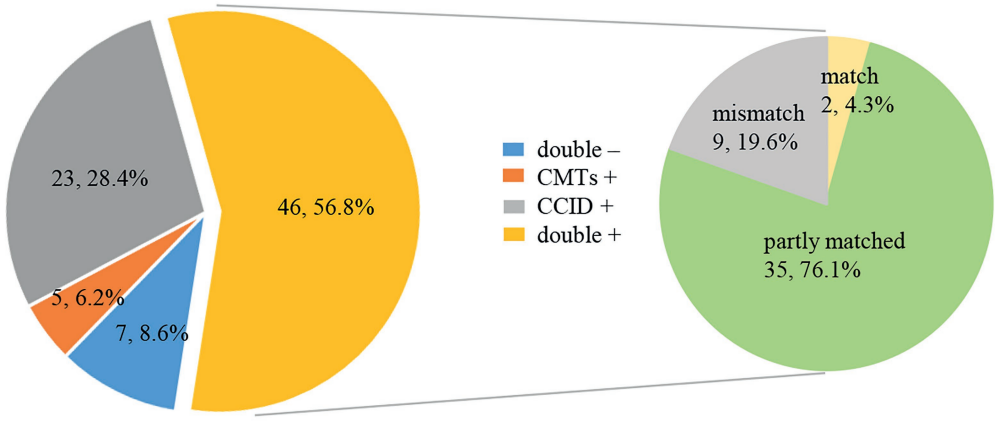

FIGURE 4
Pie chart demonstrating the positivity distribution and concordance between Chips for Complicated Infection Detection (CCID) and conventional microbiological tests (CMTs) for pneumonia in older people (n=81). For the double-positive subset, a high proportion of partial matching (35/46) (at least 1 pathogen identified in the test was confirmed by the other) and complete matching (2/46) is seen, with only 9 conflicts between CCID and CMTs results.

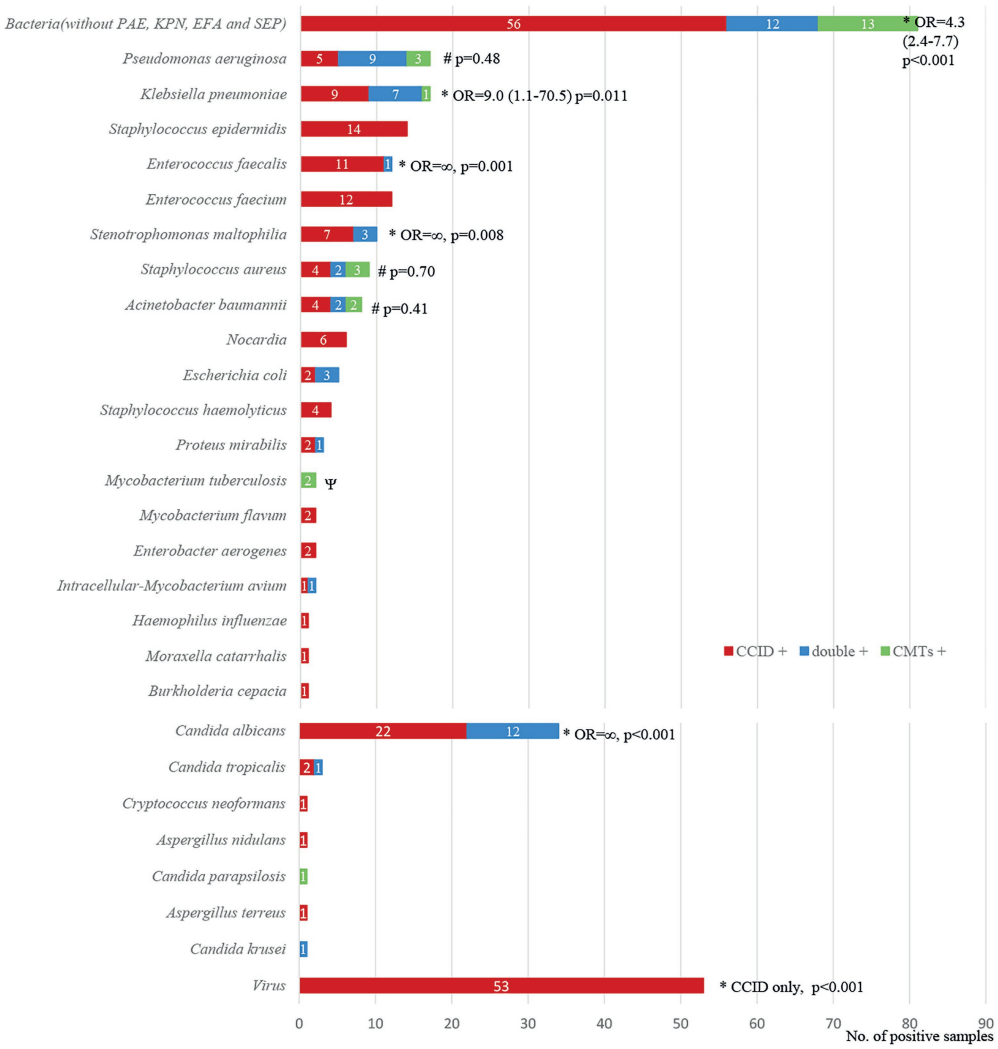

FIGURE 5
Diagnostic concordance between chips for complicated infection detection (CCID) and conventional microbiological tests (CMTs) for different pathogens. *, #The rates of positive results are significantly higher (p<0.05) or marginally higher (p>0.05) using CCID. OR, odds ratio.

TABLE 3 Clinical impact and role of CCID result.

Clinical impact	Role of CCID result	Treatment changes due to CCID
Positive impact ($n = 55$, 59.8%)	Contributed to definitive diagnosis ($n = 55$, 59.8%)	Empirical treatment continued ($n = 51$, 55.4%)
		Treatment adjusted ($n = 4$, 4.4%)
No impact ($n = 37$, 40.2%)	Results deemed valueless ($n = 21$, 22.8%)	No impact
	No pathogen detected ($n = 16$, 17.4%)	

CCID, Chips for Complicated Infection Detection; CMTs, Conventional Microbiological Tests.

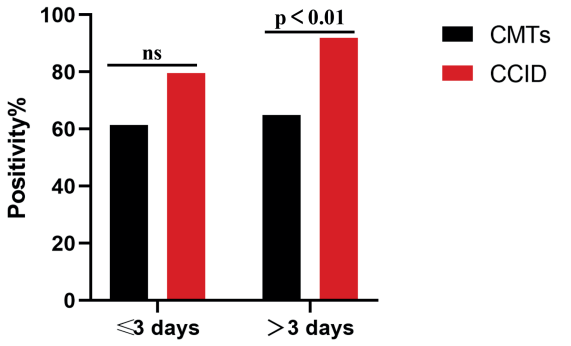

FIGURE 6
Percentage of positive samples in patients with pneumonia treated with antibiotics for ≤3days and>3days. CCID, Chips for Complicated Infection Detection; CMTs, Conventional Microbiological Test; ns, no significance.

the test. Therefore, 51 (63·0%) samples analyzed by CCID had a clinical suggestion, and this rate is higher than that using CMTs (less than 36%; Haessler et al., 2020; Ogawa et al., 2020; Schimmel et al., 2020). Third, CCID had a higher ability to detect *Klebsiella pneumoniae, Enterococcus faecalis, Stenotrophomonas maltophilia*, fungi, and viruses. Fourth, CCID might have a wider scope of application because it was less affected by antibiotic treatment. Fifth, CCID had a clinical benefit in 59·8% of cases, including supporting empirical antibiotic treatment (55·4%) and adjustments in treatment (4·4%). Sixth, CCID is cheaper than other diagnostic methods (Supplementary material 3). A chip can cover 20 indicators and costs only 150–200 RMB.

However, the primers of CCID are specific for the target sequence, precluding the detection of rare subtypes. Moreover, high sensitivity allows identifying more than one pathogen, especially in sputum specimens, and diagnosis should be confirmed by computed tomography and clinical characteristics.

This prospective multicenter observational study standardized operations and procedures for sample collection and transportation and analyzed samples by CCID and CMTs in parallel to eliminate potential confounders. However, this study has limitations. First, the small sample size (92 samples from 10 hospitals) may lead to bias. Second, although standardized procedures were adopted, there is possibility of pollution in the actual operation process. Third, the viruses detected by CCID has not been confirmed. Fourth, CCID included 37 antibiotic resistance markers but disagreed with the results of CMTs.

Larger studies are necessary to resolve the discordant results by performing PCR, especially for the virus results. Regarding the detection of antibiotic resistance, although the discordance between genotype and phenotype is a shortcoming of molecular diagnostic technologies, genes associated with phenotypes can be identified using larger samples to improve clinical diagnosis. Microfluidic platforms can be customized for specific populations to detect a wide range of pathogen types, reduce unnecessary indicators, reduce costs, and improve the clinical utility of CCID. Moreover, pre-amplification for fungi and viruses should be performed to improve diagnostic sensitivity.

Our results showed that CCID was a promising method for accurate diagnosis and development of targeted antibiotic therapies.

Data availability statement

The original contributions presented in the study are included in the article/Supplementary material, further inquiries can be directed to the corresponding authors.

Ethics statement

The studies involving human participants were reviewed and approved by Ethics Committee of Peking University First Hospital. The patients/participants provided their written informed consent to participate in this study.

Author contributions

XL and LL: conceived, designed, and supervised the study. SW, LW, MS, JL, and CS: acquired the data. SW, YW, LH, and YO: analyzed and interpreted the data. SW, FT, LL, XM, WT, CL, JL, BS, BD HX, XN, and WD: conducted the clinical work associated with the study. YL and ZZ: provided the technical support. SW, LL, and XL: verified the underlying data. SW: wrote the draft. LL: revised it. All authors read and approved the final version of the manuscript. The corresponding author

attests that all listed authors meet the authorship criteria and that no others meeting the criteria have been omitted.

Funding

This work was supported by National Key R&D Program of China [2020YFC2005401], Xicheng Financial, Scientific and Technological Project [XCSTS-SD2021-02], and Project funded by Baidu Fund of Peking University [2020BD045].

Acknowledgments

We thank all the patients who participated in this study.

Conflict of interest

YL was employed by CapitalBio Technology Co., Ltd. ZZ was employed by CapitalBio Corporation.

The remaining authors declare that the research was conducted in the absence of any commercial or financial relationships that could be construed as a potential conflict of interest.

Publisher's note

All claims expressed in this article are solely those of the authors and do not necessarily represent those of their affiliated organizations, or those of the publisher, the editors and the reviewers. Any product that may be evaluated in this article, or claim that may be made by its manufacturer, is not guaranteed or endorsed by the publisher.

Supplementary material

The Supplementary material for this article can be found online at: https://www.frontiersin.org/articles/10.3389/fmicb.2022.1048997/full#supplementary-material

References

Compton, J. (1991). Nucleic acid sequence-based amplification. *Nature* 350, 91–92.

Garau, J., Baquero, F., Perez-Trallero, E., Perez, J. L., Martin-Sanchez, A. M., Garcia-Rey, C., et al. (2008). Factors impacting on length of stay and mortality of community-acquired pneumonia. *Clin. Microbiol. Infect.* 14, 322–329. doi: 10.1111/j.1469-0691.2007.01915.x

Garcia-Vazquez, E., Marcos, M. A., Mensa, J., de Roux, A., Puig, J., Font, C., et al. (2004). Assessment of the usefulness of sputum culture for diagnosis of community-acquired pneumonia using the PORT predictive scoring system. *Arch. Intern. Med.* 164, 1807–1811. doi: 10.1001/archinte.164.16.1807

Guatelli, J. C., Whitfield, K. M., Kwoh, D. Y., Barringer, K. J., Richman, D. D., and Gingeras, T. R. (1990). Isothermal, *in vitro* amplification of nucleic acids by a multienzyme reaction modeled after retroviral replication. *Proc. Natl. Acad. Sci. U. S. A.* 87, 1874–1878. doi: 10.1073/pnas.87.5.1874

Haessler, S., Lindenauer, P. K., Zilberberg, M. D., Imrey, P. B., Yu, P. C., Higgins, T., et al. (2020). Blood cultures versus respiratory cultures: 2 different views of pneumonia. *Clin. Infect. Dis.* 71, 1604–1612. doi: 10.1093/cid/ciz1049

Hospital infection control branch of Chinese preventive medicine association (2018). Guidelines for collection and submission of clinical microbiological specimens]. *Chin. J. Nosocomiol.* 28, 3192–3200. doi: 10.11816/ cn.ni.2018-183362

Hou, J., Wu, H., Zeng, X., Rao, H., and Zhao, P. (2018). Clinical evaluation of the loop-mediated isothermal amplification assay for the detection of common lower respiratory pathogens in patients with respiratory symptoms. *Medicine (Baltimore)* 97:e13660. doi: 10.1097/MD.0000000000013660

Huang, G., Wang, C., Ma, L., Yang, X., Yang, X., and Wang, G. (2011). Sensitive sequence-specific molecular identification system comprising an aluminum micro-nanofluidic chip and associated real-time confocal detector. *Anal. Chim. Acta* 695, 1–10. doi: 10.1016/j.aca.2011.03.040

Lidman, C., Burman, L. G., Lagergren, A., and Ortqvist, A. (2002). Limited value of routine microbiological diagnostics in patients hospitalized for community-acquired pneumonia. *Scand. J. Infect. Dis.* 34, 873–879. doi: 10.1080/0036554021000026967

Luna, C. M., Palma, I., Niederman, M. S., Membriani, E., Giovini, V., Wiemken, T. L., et al. (2016). The impact of age and comorbidities on the mortality of patients of different age groups admitted with community-acquired pneumonia. *Ann. Am. Thorac. Soc.* 13, 1519–1526. doi: 10.1513/AnnalsATS.201512-848OC

Mandell, L. A., Wunderink, R. G., Anzueto, A., Bartlett, J. G., Campbell, G. D., Dean, N. C., et al. (2007). Infectious Diseases Society of America/American Thoracic Society consensus guidelines on the management of community-acquired pneumonia in adults. *Clin. Infect. Dis.* 44, S27–S72. doi: 10.1086/511159

Metlay, J. P., Waterer, G. W., Long, A. C., Anzueto, A., Brozek, J., Crothers, K., et al. (2019). Diagnosis and treatment of adults with community-acquired pneumonia. An official clinical practice guideline of the American thoracic society and infectious diseases society of America. *Am. J. Respir. Crit. Care Med.* 200, e45–e67. doi: 10.1164/rccm.201908-1581ST

Miao, Q., Ma, Y., Wang, Q., Pan, J., Zhang, Y., Jin, W., et al. (2018). Microbiological diagnostic performance of metagenomic next-generation sequencing when applied to clinical practice. *Clin. Infect. Dis.* 67, S231–S240. doi: 10.1093/cid/ciy693

Millett, E. R. C., Quint, J. K., Smeeth, L., Daniel, R. M., and Thomas, S. L. (2013). Incidence of community-acquired lower respiratory tract infections and pneumonia among older adults in the United Kingdom: a population-based study. *PLoS One* 8:e75131. doi: 10.1371/journal.pone.0075131

Notomi, T., Okayama, H., Masubuchi, H., Yonekawa, T., Watanabe, K., Amino, N., et al. (2000). Loop-mediated isothermal amplification of DNA. *Nucleic Acids Res.* 28:E63. doi: 10.1093/nar/28.12.e63

Ogawa, H., Kitsios, G. D., Iwata, M., and Terasawa, T. (2020). Sputum gram stain for bacterial pathogen diagnosis in community-acquired pneumonia: a systematic review and Bayesian meta-analysis of diagnostic accuracy and yield. *Clin. Infect. Dis.* 71, 499–513. doi: 10.1093/cid/ciz876

Qu, J. M., and Cao, B. (2016). Guidelines for the diagnosis and treatment of adult community acquired pneumonia in China (2016 edition). *Zhonghua Jie He He Hu Xi Za Zhi* 39, 241–242. doi: 10.3760/cma.j.issn.1001-0939.2016.04.005

Saiki, R. K., Gelfand, D. H., Stoffel, S., Scharf, S. J., Higuchi, R., Horn, G. T., et al. (1988). Primer-directed enzymatic amplification of DNA with a thermostable DNA polymerase. *Science* 239, 487–491. doi: 10.1126/science.2448875

Saiki, R. K., Scharf, S., Faloona, F., Mullis, K. B., Horn, G. T., Erlich, H. A., et al. (1985). Enzymatic amplification of beta-globin genomic sequences and restriction site analysis for diagnosis of sickle cell anemia. *Science* 230, 1350–1354. doi: 10.1126/science.2999980

Scharmann, U., Kirchhoff, L., Schmidt, D., Buer, J., Steinmann, J., and Rath, P. M. (2020). Evaluation of a commercial loop-mediated isothermal amplification (LAMP) assay for rapid detection of pneumocystis jirovecii. *Mycoses* 63, 1107–1114. doi: 10.1111/myc.13152

Schimmel, J. J., Haessler, S., Imrey, P., Lindenauer, P. K., Richter, S. S., Yu, P. C., et al. (2020). Pneumococcal urinary antigen testing in United States hospitals: a missed opportunity for antimicrobial stewardship. *Clin. Infect. Dis.* 71, 1427–1434. doi: 10.1093/cid/ciz983

Shariatzadeh, M. R., and Marrie, T. J. (2009). Does sputum culture affect the management and/or outcome of community-acquired pneumonia? *East Mediterr. Health J.* 15, 792–799.

Signori, L. G., Ferreira, M. W., Vieira, L. C., Muller, K. R., and Mattos, W. L. (2008). Sputum examination in the clinical management of community-acquired pneumonia. *J. Bras. Pneumol.* 34, 152–158. doi: 10.1590/s1806-37132008000300005

Torres, A., Lee, N., Cilloniz, C., Vila, J., and Van der Eerden, M. (2016). Laboratory diagnosis of pneumonia in the molecular age. *Eur. Respir. J.* 48, 1764–1778. doi: 10.1183/13993003.01144-2016

Walker, G. T., Fraiser, M. S., Schram, J. L., Little, M. C., Nadeau, J. G., and Malinowski, D. P. (1992a). Strand displacement amplification--an isothermal, in vitro DNA amplification technique. *Nucleic Acids Res.* 20, 1691–1696. doi: 10.1093/nar/20.7.1691

Walker, G. T., Little, M. C., Nadeau, J. G., and Shank, D. D. (1992b). Isothermal *in vitro* amplification of DNA by a restriction enzyme/DNA polymerase system. *Proc. Natl. Acad. Sci. U. S. A.* 89, 392–396. doi: 0.1073/pnas.89.1.392

Wang, G. F., Huang, J. J., and Zhang, W. (2019). Guidelines for the application of diagnostic flexible bronchoscopy in adults (2019 edition). *Zhonghua Jie He He Hu Xi Za Zhi* 8, 573–590. doi: 10.3760/cma.j.issn.1001-0939.2019.08.005

Wang, Z., Zang, Y., Gao, Y., Han, L., Lin, H., Gao, Y., et al. (2020). Evaluation of bronchoalveolar lavage fluid combined with the loop-mediated isothermal amplification assay in lower respiratory tract infections. *Am. J. Transl. Res.* 12, 4009–4016.

Welte, T., Torres, A., and Nathwani, D. (2012). Clinical and economic burden of community-acquired pneumonia among adults in Europe. *Thorax* 67, 71–79. doi: 10.1136/thx.2009.129502

Zhang, H., Xu, Y., Fohlerova, Z., Chang, H., Iliescu, C., and Neuzil, P. (2019). LAMP-on-a-chip: revising microfluidic platforms for loop-mediated DNA amplification. *Trends Analyt. Chem.* 113, 44–53. doi: 10.1016/j.trac.2019.01.015

frontiers | Frontiers in Microbiology

TYPE Original Research
PUBLISHED 22 December 2022
DOI 10.3389/fmicb.2022.1065159

OPEN ACCESS

EDITED BY
George William Carnell,
University of Cambridge,
United Kingdom

REVIEWED BY
Haiyang Liu,
Zhejiang University, China
Amir Sasan Mozaffari Nejad,
Jiroft University of Medical Sciences, Iran

*CORRESPONDENCE
Hongying Zhang
✉ 290923206@qq.com
Hongcang Gu
✉ gu_hongcang@cmpt.ac.cn

†These authors have contributed equally to this work and share first authorship

SPECIALTY SECTION
This article was submitted to Infectious Agents and Disease, a section of the journal Frontiers in Microbiology

RECEIVED 10 October 2022
ACCEPTED 28 November 2022
PUBLISHED 22 December 2022

CITATION
Zhang H, Wang M, Han X, Wang T, Lei Y, Rao Y, Xu P, Wang Y and Gu H (2022) The application of targeted nanopore sequencing for the identification of pathogens and resistance genes in lower respiratory tract infections.
Front. Microbiol. 13:1065159.
doi: 10.3389/fmicb.2022.1065159

The application of targeted nanopore sequencing for the identification of pathogens and resistance genes in lower respiratory tract infections

Hongying Zhang[1*†], Meng Wang[2†], Ximei Han[1], Ting Wang[1], Yanjuan Lei[3], Yu Rao[1], Peisong Xu[3], Yunfei Wang[3] and Hongcang Gu[4,5*]

[1]Department of Pulmonary Medicine, Fuzhou Pulmonary Hospital of Fujian, Fuzhou, China, [2]Institute of Health Education, Hangzhou Center for Disease Control and Prevention, Hangzhou, China, [3]Department of Medicine, Zhejiang ShengTing Biotech Co., Ltd., Hangzhou, China, [4]Institute of Health and Medical Technology, Hefei Institutes of Physical Science, Chinese Academy of Sciences, Hefei, China, [5]Graduate School, University of Science and Technology of China, Hefei, China

Objectives: Lower respiratory tract infections (LRTIs) are one of the causes of mortality among infectious diseases. Microbial cultures commonly used in clinical practice are time-consuming, have poor sensitivity to unculturable and polymicrobial patterns, and are inadequate to guide timely and accurate antibiotic therapy. We investigated the feasibility of targeted nanopore sequencing (TNPseq) for the identification of pathogen and antimicrobial resistance (AMR) genes across suspected patients with LRTIs. TNPseq is a novel approach, which was improved based on nanopore sequencing for the identification of bacterial and fungal infections of clinical relevance.

Methods: This prospective study recruited 146 patients suspected of having LRTIs and with a median age of 61 years. The potential pathogens in these patients were detected by both TNPseq and the traditional culture workups. We compared the performance between the two methods among 146 LRTIs-related specimens. AMR genes were also detected by TNPseq to prompt the proper utilization of antibiotics.

Results: At least one pathogen was detected in 133 (91.1%) samples by TNPseq, but only 37 (25.3%) samples contained positive isolates among 146 cultured specimens. TNPseq possessed higher sensitivity than the conventional culture method (91.1 vs. 25.3%, $P < 0.001$) in identifying pathogens. It detected more samples with bacterial infections ($P < 0.001$) and mixed infections ($P < 0.001$) compared with the clinical culture tests. The most frequent AMR gene identified by TNPseq was bla_{TEM} ($n = 29$), followed by bla_{SHV} ($n = 4$), bla_{KPC} ($n = 2$), bla_{CTX-M} ($n = 2$), and *mecA* ($n = 2$). Furthermore, TNPseq discovered five possible multi-drug resistance specimens.

Conclusion: TNPseq is efficient to identify pathogens early, thus assisting physicians to conduct timely and precise treatment for patients with suspected LRTIs.

KEYWORDS

pathogen detection, nanopore sequencing, respiratory system, species, resistance genes

Introduction

Lower respiratory tract infections (LRTIs) are one of the most lethal infectious diseases, the majority of which develop into pneumonia, bronchitis, and bronchiolitis, contributing to the increasing number of mortality and morbidity worldwide, particularly among senior citizens in low-income regions (Feldman and Shaddock, 2019; Troeger et al., 2019; Collaborators, 2020). They give rise to 3.5 million deaths and 79 million cases of disabilities annually (Shao et al., 2022). A good deal of pathogens are responsible for infection of the lower respiratory tract such as bacteria, fungi, virus, and atypical pathogens (Man et al., 2017; Chen et al., 2021). More severe diseases can occur in the lungs after an invasion of secondary bacterial pneumonia (Keshavarz et al., 2018).

Traditional culture has long been the gold standard for detecting bacterial or fungal respiratory infections (Gu et al., 2021). However, there are still some pathogens that have not yet been detected. Due to the low-nutrient environment and low bacterial burden of the respiratory tract, most infectious agents are difficult or even virtually impossible to recognize using routine culture (Yatera et al., 2021). In addition, the cultural conditions for these pathogens are rigorous and time-consuming. Immunological methods and polymerase chain reaction (PCR) are also used for laboratory diagnosis of clinical microbes; nonetheless, only a narrowly presupposed group of microorganisms can be detected and identified (Hong et al., 2020). In this case, patients with severe LRTIs were broad-spectrum treated according to the previous experience of physicians. At the same time, antibiotic resistance, caused by the inappropriate use of antimicrobial agents, is likely to cause ineffective treatment, which increases the risk of opportunistic infections, hospital mortality rates, and healthcare costs (Boolchandani et al., 2019). Hence, timely etiological identification is crucial for accurate treatment and early recovery.

Advances in sequencing technology facilitate its application in clinical practice for pathogen identification. Next-generation sequencing (NGS), a culture-independent molecular method, possesses hypothesis-free detection capacity to cover nearly all types of microorganisms (Jun et al., 2021). Nevertheless, the widespread availability of conventional NGS analysis is influenced by host DNA, symbiotic microflora-colonized native positions, and potential contamination by the environment (Gu et al., 2019). Furthermore, its high cost and slow turnaround time concern users. Nanopore sequencing is a new-generation sequencing technology that could alleviate the drawbacks of NGS and PCR (Charalampous et al., 2019; Fu et al., 2022). In recent years, it has emerged to identify pathogenic microbes in infectious and non-infectious diseases (Petersen et al., 2019; Wang et al., 2020). This advance is attributed to its fast turnaround time, long read length, and pathogen enrichment (Deamer et al., 2016; Ciuffreda et al., 2021), which is free from the interference of microflora colonization and host depletion. In addition to pathogen detection, nanopore sequencing can predict antimicrobial resistance (AMR) genes, to speculate the phenotype of resistance (Petersen et al., 2019). However, the characterization of AMR genes with nanopore sequencing is scarce in clinical practice.

In the present study, we compared the clinical effectiveness of targeted nanopore sequencing (TNPseq) with culture, in the pathogenic diagnosis of LRTIs. In addition, the antibiotic resistance genes of pathogens were predicted in patients with LRTIs *via* TNPseq.

Materials and methods

Patient recruitment and specimen collection

Between January and April 2022, 146 patients, including 106 male patients and 40 female patients, were enrolled in the Fuzhou Pulmonary Hospital of Fujian in China for this study. Except for three children, the age range was 16–87 years. These patients were suspected of having LTRIs grounded on clinical symptoms and physical signs, blood biochemistry, imaging features of the chest, and laboratory results. One hundred and forty-six specimens were collected in dedicated sterile tubes after patients had given their written informed consent. All specimens were aseptically divided into two equal parts without dilution. One part was sent to the microbiological laboratory in Fuzhou Pulmonary Hospital for bacterial and fungal culture. The other part, under ice bags or dry ice, was promptly sent to Hangzhou ShengTing Biotech Co. Ltd. (Hangzhou, China) for TNPseq using cold chain logistics.

Clinical microbiology trials

All samples were routinely analyzed according to *The National Clinical Test Regulation of Operation* for the detection of pathogens at clinical microbiology laboratories (Shang et al., 2014). Bronchoalveolar lavage fluid (BALF) was concentrated using centrifugation at 3,000 rpm for 10 min and inoculated onto Columbia blood agar, chocolate agar, and MacConkey agar plates. Then, these plates were incubated at 35 ± 1°C overnight for bacterial culture in an incubator with 5% CO_2 or in anaerobic bags. In order to culture fungi, Sabouraud's dextrose agar was used and incubated at 30°C for 48–72 h. Pathogen identification was performed using a BD Phoenix™ M50 Automated Microbiology System (BD, Inc., USA) and a VITEK® Mass Spectrometry Microbial Identification System (bioMérieux, Inc., France). Viral cultures were not carried out due to limitations of the biosafety facilities.

DNA extraction and amplification

The samples were initially centrifuged, digested with proteinase K and lysozyme, and adequately ground using zirconia grinding beads and standard laboratory practices, according to different specimen sources, to improve the capacity of pathogen detection. The nucleic acid of ground samples was extracted with magnetic beads using the QIAamp DNA Microbiome Kit (Cat. No.51707, Qiagen, Hilden, Germany) and following the manufacturer's protocol. Blank EB buffer was concurrently used as the negative control for the extraction of nucleic acid. The concentration of extracted DNA was detected using an Invitrogen Qubit 4 Fluorometer. Then, PCR amplification was carried out using the universal primers 27F/1492R for bacterial 16S rRNA gene detection and ITS1/4 for fungal IST1/2 gene detection (Chan et al., 2020; Jun et al., 2021). PCR amplification was performed on an ABI 2720 Thermal Cycler (Cat. No. 435659; ABI, California, USA) with conditions as follows: initiation at 95°C × 3 min, 25 cycles of 95°C × 30 s/62°C × 60 s/72°C × 60 s, and a final extension step of 72°C × 3 min. The products of PCR amplification were purified and then quantified using Qubit 4 and agarose gel electrophoresis for subsequent library preparation and nanopore sequencing.

Library preparation and nanopore sequencing

Nanopore barcode PCR was performed with the aforementioned products according to the PCR Barcoding Expansion Pack 1-96 kit (EXP-PBC096). Library pooling was accomplished utilizing ∼50 ng of gDNA with the VAHTS Universal DNA Library Prep Kit (Cat. No. ND607-01, Nanjing Vazyme Biotech, Nanjing, CN). Subsequently, nanopore library preparation was constructed using a ligation sequencing kit (Cat. No. SQK-LSK109, Oxford Nanopore Technologies, Oxford, UK) as per the manufacturer's instructions. Ultimately, ∼100 ng of the pooled library was loaded into a nanopore flow cell (R9.4.1) after chip priming, and sequenced utilizing the GridION platform. MinKNOW version 2.0 was used for outputting base-calling data. Then, barcode demultiplexing was conducted using Porechop (v. 0.2.4).

Identification of pathogen and resistant genetype

Real-time identification of pathogens was performed *via* the 16S workflow and the "What's in my Pot?" (WIMP) workflow, using the EPI2ME platform (version 3.2.2, ONT, Oxford, UK). Furthermore, the EPI2ME platform offered bacterial classification *via* the 16S workflow as well as identification of fungi, bacteria, viruses, or archaea *via* the WIMP workflow. Reads under 200 bp were filtered, and the remaining reads were aligned to all targets and potentially etiological agents using the National Center for Biotechnology Information (NCBI) basic local alignment search tool (BLAST), or reanalyzed using GAIA 2.0 (Chan et al., 2020; Fu et al., 2022). Pathogens were classified at the species level based on the percentage of coverage and identity. Generally, the top 10 microorganisms, ranked by aligned reads and with a relative abundance score of >0.5% were classified as pathogens and subjected to further evaluation. Potential pathogen(s) were reported if the number of reads accounted for ≥1% of microbial reads and if the WIMP alignment score was ≥20 (Charalampous et al., 2018). *Mycobacterium tuberculosis* was considered positive when at least one read was mapped to either the species or genus level (Miao et al., 2018). AMR genes detected by TNPseq were predicted using the Comprehensive Antibiotic Resistance Database (CARD) or the ResFinder database with default alignment settings (≥80% identity over ≥60% of the length of the target gene) (Yonkus et al., 2022).

Statistical analyses

Continuous variables are presented as mean ± standard deviation. Percentages are used to describe individual microbial detection rates in patients. The differences between culture and TNPseq were assessed using the chi-square test *via* IBM SPSS Statistics 24.0 software (IBM Corp, Armonk, NY, USA). Statistical differences were considered significant if the *P*-value was <0.01. Heatmaps and Venn diagrams were plotted on https://www.bioinformatics.com.cn (last accessed on 30 July 2022), an online platform for visualization.

Results

Patient demographics

We enrolled 146 patients with suspected LRTIs. The median age was 61 years, and 106 of the 146 patients were male. Samples were collected, including 122 BALF, seven sputa, eight blood, six puncture fluids, and three transbronchial lung biopsies (Table 1). Of these 146 patients, there were 37 cases of microbial growth from culture trials, including eight mixed infections. In this research, mixed infection was defined as different species infecting the same individual. As for TNPseq, 133 cases were identified at the species level carrying a potential pathogen, and there were 48 cases in which only one species was detected. In addition, AMR genes were detected in 37 patients.

TABLE 1 Cohort characteristics.

Characteristics	Data
Median age (Years)	61
Gender, *n* (%)	
Male	106 (72.6%)
Female	40 (27.4%)
C-reactive protein median (mg/L, IQR)	21.06 (7.17, 68.04)
Procalcitonin median (μg/L, IQR)	0.12 (0.06, 0.79)
Neutrophil count (10^9/L, mean ± SD)	9.53
White blood cell count (10^9/L, mean ± SD)	9.27
Sample type, *n* (%)	
BALF	122 (83.6%)
Sputum	7 (4.8%)
Blood	8 (5.5%)
Puncture fluid	6 (4.1%)
Transbronchial lung biopsy	3 (2.0%)
Culture, *n* (%)	
Negative	109 (74.7%)
Positive	37 (25.3%)
TNPseq, *n* (%)	
Positive	133 (91.1%)
Negative	13 (8.9%)
Only one pathogen, *n* (%)	48 (32.9%)
Antibiotic resistance genes, *n* (%)	36 (24.7%)

BALF, bronchoalveolar lavage fluid.

Comparison of TNPseq with conventional culture

In the present study, the common opportunistic pathogens or microbes harming human health in clinical practice were defined as positive when detected by TNPseq. We identified 133 of 146 (91.1%) samples that provide refuge for pathogens, including 125 bacteria, 34 fungi, 25 viruses, 11 anaerobic bacteria, and 85 mixed infections using TNPseq. The details of mixed infections under different classifications among the aforementioned microbes are shown in Figure 1. A total of 37 of 146 (25.3%) samples harboring 22 bacteria, 18 fungi, and eight mixed infections were detected by routine culture. The sensitivity was significantly increased by 58.9% in TNPseq compared with culture (91.1 vs. 25.3%; $P < 0.001$). A comparison of TNPseq and routine culture of 146 samples is shown in Table 2. Out of these results, TNPseq successfully detected possible etiological agents from 98 of the 109 culture-negative cases (89.9%). In addition, the positive rate of bacteria was higher than that of fungi. The sensitivity of TNPseq was superior to culture in detecting anaerobic bacteria, viruses, and mixed infections. This is imperative for the precision treatment of patients with suspected LRTIs, as polymicrobial infections were not easily perceived using clinical standard workups such as anaerobic culture, viruses were often not detected, or specific classification was lacking during routine clinical culture. The cost of TNPseq was ∼1,000 RMB. The time span from test initiation to the delivery of test results for TNPseq was ∼16–17 h, whereas the time span for the culture test was at least 24–72 h.

As for consistency, 35 out of 37 (94.6%) positive results were detected from the same patients by TNPseq and culture (Figure 1), among 27 (73.0%) cases of which the TNPseq results were entirely consistent for clinical microbiology workups. In other words, microbial strains were present in two samples, but the coincident microbe was absent in TNPseq of the same samples. The results from eight double positive samples analyzed using culture and TNPseq were paradoxical. Ten discrepant cases are listed in Table 3. This incompatibility might be caused by the inadequately lysed fungal cell wall through lysozyme or misidentified EPI2ME.

Microbial population in patients with LRTIs

For identifying the etiological agent of LRTIs, detection at the species level is essential for early diagnosis and precision therapy, particularly for *Streptococcus* and *Mycobacterium* species. However, NGS analysis is frequently not precise enough to identify pathogens at the species level (Haro et al., 2020). We identified 24 species of gram-negative bacteria, 23 species of gram-positive bacteria, 14 species of fungi, and six species of viruses by TNPseq, which has implications for the diagnosis and treatment of patients. The top five gram-negative bacteria were *Pseudomonas aeruginosa* ($n = 13$), *Haemophilus influenzae* ($n = 11$), *Klebsiella pneumoniae* ($n = 11$), *Haemophilus haemolyticus* ($n = 10$), and *Stenotrophomonas maltophilia* ($n = 9$) (Figure 2A). Among 23 detected gram-positive bacteria, *Mycobacterium tuberculosis* ($n = 26$) is superior in number in all specimens, followed by *Streptococcus pneumoniae* ($n = 19$), *Staphylococcus aureus* ($n = 9$), *Mycobacterium intracellulare* ($n = 8$), and *Enterococcus faecium* ($n = 6$) (Figure 2B). Common etiologic microbes of fungal pneumonia were detected, such as *Candida albicans* ($n = 17$), *Aspergillus fumigatus* ($n = 7$), and *Cryptococcus neoformans* ($n = 2$) (Figure 2C). *Human gammaherpesvirus* 4 ($n = 13$), *Human alphaherpesvirus* 1 ($n = 9$), and *Human betaherpesvirus* 5 ($n = 4$) were the top three viral species (Figure 2D). The results of microbial populations in patients with LRTIs, identified *via* TNPseq, conformed to the epidemiology of respiratory infections in China.

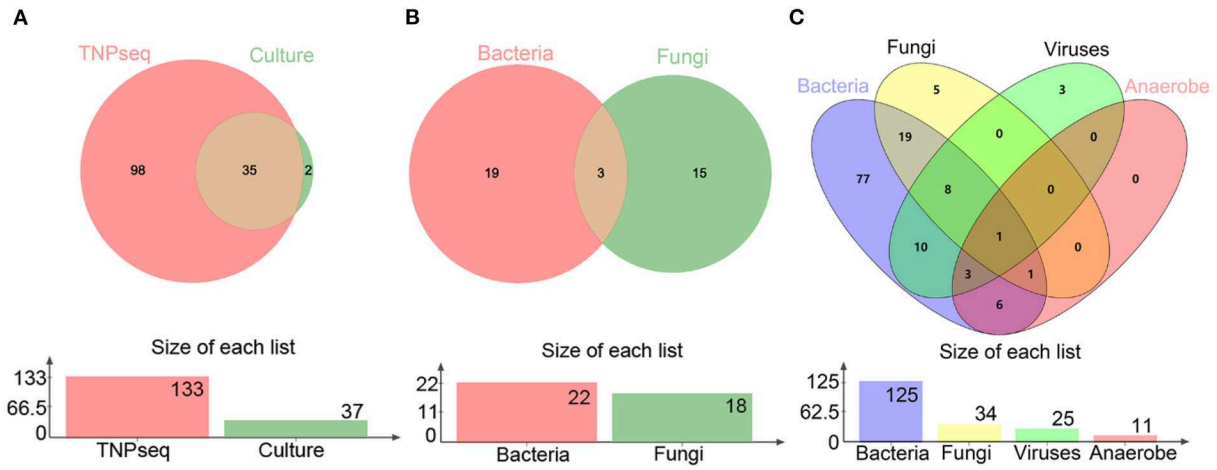

FIGURE 1
Venn diagrams of positive specimens *via* TNPseq and culture. **(A)** The number of sets for positive TNPseq and culture specimens. **(B)** Bacteria and fungi identified by culture. **(C)** Bacteria, fungi, viruses, and anaerobes identified by TNPseq.

TABLE 2 **Effectiveness of routine microbial trails in comparison with targeted nanopore sequencing.**

Pathogen	TNPseq positive	Culture				*P*-value
		Culture positive	TNPseq positive#	Culture negative	TNPseq positive*	
Total	133 (91.1%)	37	35 (94.6%)	109	98 (89.9%)	<0.001
Anaerobe	11 (7.5%)	0	0	146	11 (7.5%)	0.001
Bacteria	125 (84.9%)	22	21 (95.4%)	124	104 (83.8%)	<0.001
Fungi	34 (20.5%)	18	11 (61.1%)	128	23 (17.9%)	<0.001
Viruses	25 (16.4%)	0	0	146	25 (17.1%)	<0.001
Mixed infection	85 (54.1%)	8	8 (100%)	138	77 (55.8%)	<0.001

Mixed infection was defined as different species infecting the same individual. The percentage labeled with # was obtained from TNPseq and culture double positive/double positive + single culture positive; the percentage labeled with * was obtained from TNPseq positive/culture negative.

Antibiotic resistance

Antimicrobial resistance contributes to high mortality and economic costs every year. To assess the antibiotic resistance of patients with LRTIs, we predicted the AMR genes, which can potentially complicate disease treatments and can potentially be transferred to other bacteria with the help of CARD. In the present study, a total of 22 different antimicrobial resistance (AMR) genes were detected among 36 patients (Figure 3). The most prevalent AMR gene in the samples of patients with suspected LRTIs was bla_{TEM}. The other percentages of AMR genes were affiliated with bla_{SHV} ($n = 3$), *mecA* ($n = 2$), $bla_{\mathrm{CTX-M}}$ ($n = 1$), and 23S rRNA ($n = 1$). Moreover, we identified five specimens carrying multidrug resistance (MDR) genes. The results of the antibiotics susceptibility test of patients in this trial are presented in Supplementary Table 1. The presence or absence of a resistance gene is not fully correlated with the resistance phenotype.

Discussion

Culture-dependent methods have severe bottlenecks as guides for the etiologic diagnosis of acute critical infection due to time-consumption, narrow-spectrum detection, and susceptibility to the previous history of antibiotic use. The time required for TNPseq was ∼16–17 h from test initiation to the delivery of test results, which was less than that for Illumina NGS (∼22–24 h) and for the clinical culture test (∼24–72 h). A timely and precise method is essential to balance the clinical curative effect and increased mortality, since empiric therapy is not the best solution in the face of severe pulmonary infection (Glimåker et al., 2015; McGill et al., 2016; Charalampous et al., 2018). TNPseq is a strategy of pivotal importance for the early diagnosis of slow-growing pathogens, for instance, *Mycobacterium* and *Aspergillus,* or for seriously infected patients in urgent need of treatment, with its rapid turnaround time and broad coverage of pathogens (Gu et al., 2021). In the current study, we investigated

10.3389/fmicb.2022.1065159

TABLE 3 Discrepant cases among the TNPseq and culture test.

Case	Gender	Age	Primary diagnosis	Sample	TNPseq (No. of reads)	Culture
21T005333	Male	51	Severe pneumonia	BALF	Negative	*C. albicans*
22T0007678	Male	63	Tuberculosis	BALF	Negative	*E. coli*
22T000494	Male	68	Pneumonia	BALF	*C. argentoratense* (5924)	*C. glabrata*
22T0007653	Male	55	Pneumonia	BALF	*H. haemolyticus* (9), *T. denticola* (556)	*C. glabrata*
22T001387	Male	63	AECOPD	BALF	*H. haemolyticus* (490), *E. rhusiopathiae* (3), *C. albicans* (2), *Human gammaherpesvirus* (42)	*C. albicans, Aspergillus*
22T0016635	Male	37	ABPA	BALF	*H. influenzae* (3)	*Aspergillus*
22T0016719	Male	67	LC, pneumonia	BALF	*H. influenzae* (4)	*Aspergillus*
22T003154	Female	78	COPD	BALF	*P. aeruginosa* (3510), *C. striatum* (1973)	*P. aeruginosa, S. maltophilia*
22T005899	Male	63	Abdominal and pulmonary shadow	BALF	*M. intracellulare* (15), *S. pneumoniae* (34), *A. penicillioides* (7)	*M. avium*
22T0007741	Male	75	COP, pneumonia, secondary pulmonary tuberculosis	Blood	*H. influenzae* (2)	*A. baumannii–A. calcoaceticus complex*

AECOPD, acute exacerbation of chronic obstructive pulmonary disease; ABPA, allergic bronchopulmonary aspergillosis; LC, lung carcinoma; PI, pulmonary infection; COPD, chronic obstructive pulmonary disease; COP, cryptogenic organizing pneumonia; TNPseq, targeted nanopore sequencing.

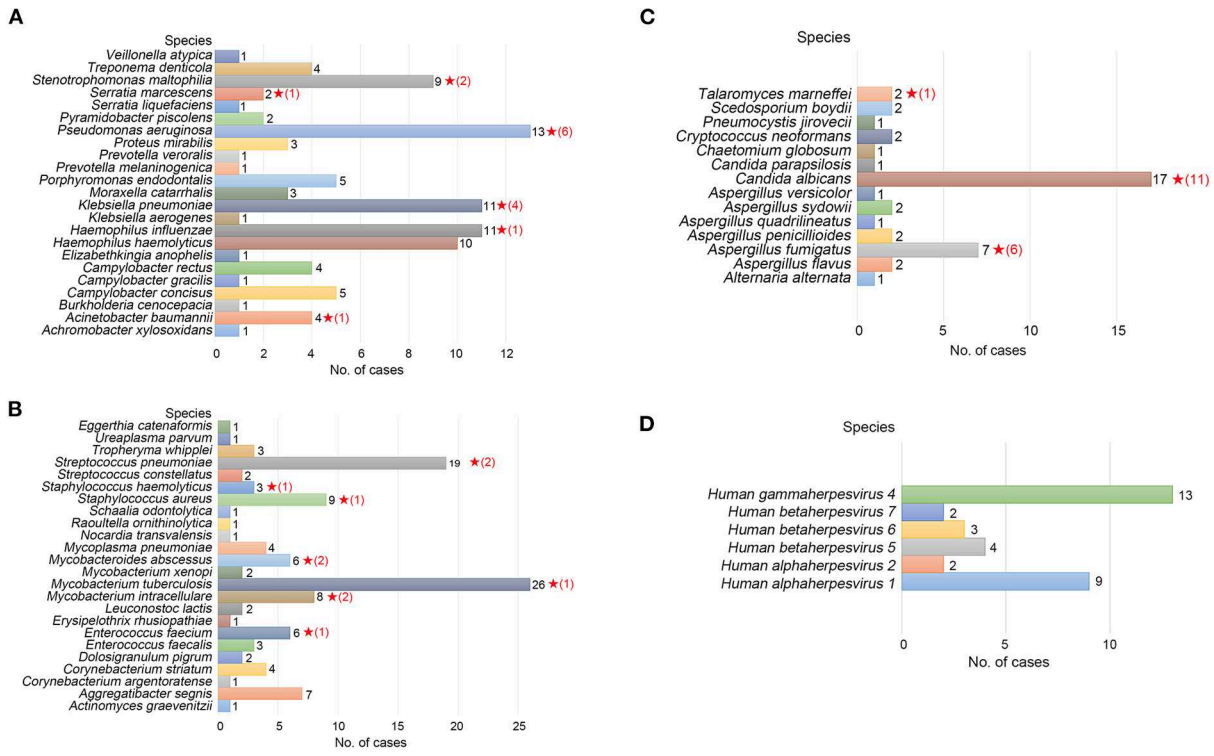

FIGURE 2
Microbial communities of pathogens at the species level of LRTI specimens. **(A)** Gram-negative bacteria. **(B)** Gram-positive bacteria. **(C)** Fungi. **(D)** Viruses. The red, five-pointed star behind the bar represents species isolated in the clinical culture test, and the number in parentheses represents the number of cases.

the effectiveness of TNPseq for the identification of pathogens and AMR genes in 146 patients with a high clinical suspicion of LRTIs.

The sensitivity of TNPseq for the cases of suspected LRTIs was significantly higher than that of typical culture workups in our study. The results were consistent with

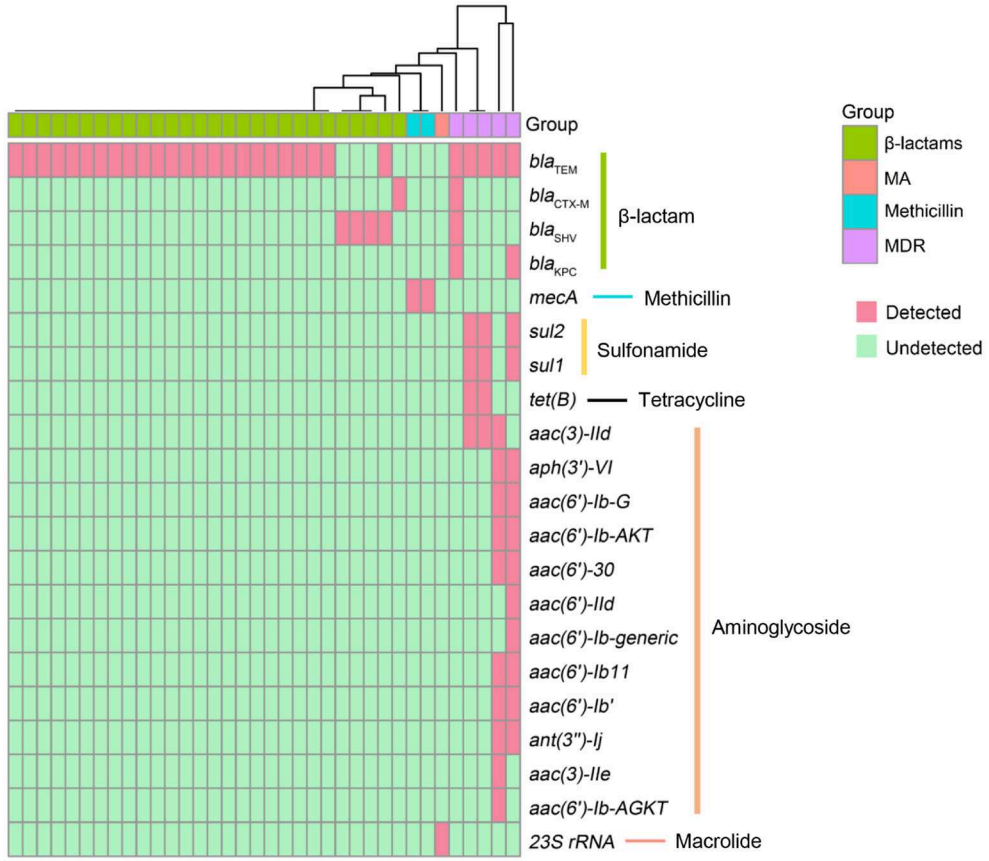

FIGURE 3
Antimicrobial resistance (AMR) genes presented in LRTI specimens. The rows represent AMR genes and the columns represent specimens. MA, macrolide antibiotics; MDR, multidrug resistance.

previous reports (Gu et al., 2021; Hoefnagels et al., 2021; Jun et al., 2021; Fu et al., 2022). As for the samples that were only culture positive, two pathogens of possible single infection detected by culture were missed by TNPseq: *C. albicans* and *Escherichia coli*. The first of the two missed cases was a case with severe pneumonia. Clinical microbial testing showed a diagnosis of a single infection by *C. albicans*. In contrast, TNPseq testing did not detect the common pathogen. The upper respiratory commensals were identified, and included *Streptococcus mitis, Stomatococcus mucilaginosus, and Actinomyces odontolyticus*. The other missed case was that of a patient preliminarily diagnosed with tuberculosis; only *E. coli* was detected by the culture test in the BALF specimen. Similarly, microorganisms such as *Haemophilus parahaemolyticus*, *Streptococcus parasanguinis*, and *Gemella haemolysans* were recognized as microbes colonizing human beings rather than common clinical pathogens. Chan et al. (2020) also reported that the sensitivity for low-abundance microbial specimens was lower in a background of upper respiratory microbiota, and species were likely misidentified by EPI2ME. As for double positive samples *via* culture and TNPseq, *Candida glabrata*, *C. albicans,* and/or *Aspergillus* were detected in five samples *via* culture, but bacteria such as *C. argentoratense*, *H. haemolyticus,* and *T. denticola,* were detected *via* TNPseq. We speculate that the thick fungal cell wall or its low biomass in DNA extraction (Bittinger et al., 2014) contributes to the non-detection of these fungi. *S. maltophilia, M. avium*, and *A. baumannii–A. calcoaceticus complex* were detected *via* culture, while TNPseq failed to recognize them in three double positive cases. Verifying microbial taxon with alternative pipelines is advisable to improve misidentification, and the trade-offs are easy to determine, compared with the high sensitivity. Moreover, TNPseq detected likely pathogens from 98 of 109 culture-negative specimens. Thus, TNPseq is an effective method to identify etiologic microorganisms by comparing routine cultures in clinical microbiology laboratories.

The infection-associated microbiota we detected in lower respiratory tract specimens substantially overlap with the microbial population detected in patients with acute respiratory infections in China during 2009–2019

(Li Z. J. et al., 2021). *S. pneumoniae, M. pneumoniae, P. aeruginosa, K. pneumoniae,* and *H. influenzae* were ranked according to the proportion of positive detection in the adults. In addition, more *Mycobacterium* including *M. intracellulare,* were identified in our research using the specific TNPseq method. TNPseq facilitates the detection of slow-growing pathogens and has solved the difficulties of detecting intracellular bacteria to a certain extent. As for the species level of fungi, *A. fumigatus* is the second most common etiological agent after *C. albicans* in the present study. The early diagnosis of Aspergillosis is mandatory for successful treatment outcomes (Ahmad and Khan, 2020). Furthermore, we have detected a high number of polymicrobial infections using TNPseq. Bacterial–fungal co-infection ($n = 19$) was the most frequent co-infection, and bacterial–viral co-infection ($n = 10$) took second place. It is interesting to note that eight cases of polymicrobial infection with bacteria, fungi, and viruses occurred simultaneously. Independent studies documented similar results, in which bacteria–fungi mixed infection was the most common mode of mixed infection (Leclair and Hogan, 2010; Xie et al., 2021; Nebreda-Mayoral et al., 2022). Bacterial–fungal co-infection, often leads to pulmonary fibrosis and contributes to respiratory failure and even premature death. TNPseq is conducive to the early diagnosis and accurate treatment of pathogens, especially slow-growing pathogens, bacterial–fungal co-infection, and viral co-infection, as well as to improving the prognosis of patients with pneumonia.

Antibiotic resistance due to the misuse and abuse of antibiotics is a global challenge to the therapy of infectious diseases. The transmission and persistence of resistance genes among pathogens have led to attentiveness in public health worldwide (Bhullar et al., 2012; Emond-Rheault et al., 2020; Li R. et al., 2021). In early studies, nanopore sequencing was applied to detect AMR genes in different pathogens. The long reading length of nanopore sequencing is a considerable advantage for reducing omissions of base pairs or small fragments of DNA during the process of assembly, which is crucial for the identification of mutational AMR genes (Koren and Phillippy, 2015; Lemon et al., 2017). The bla_{TEM} gene ($n = 29$) was the most commonly detected among the β-lactamase-encoding genes, followed by bla_{SHV} ($n = 4$), bla_{KPC} ($n = 2$), and $bla_{\mathrm{CTX-M}}$ ($n = 2$). KPC is a multienzyme belonging to class A carbapenemases, which are usually produced by *Enterobacteriaceae*, particularly *K. pneumoniae* and *P. aeruginosa* (Poirel et al., 2010; Liao et al., 2022). In the present study, *K. pneumoniae, H. influenzae,* and *P. mirabilis* were identified in the specimens with the bla_{KPC} gene detected by TNPseq; however, the conventional culture showed no evidence of microbial growth. In addition, bla_{KPC} was the predominant carbapenem resistance gene associated with multidrug-resistant (MDR) pathogens (Haider et al., 2022; Zheng et al., 2022), which is why specimens containing the bla_{KPC} gene clustered in the group of MDR. Among the groups of MDR, aminoglycoside-modifying enzyme (AME)-encoding genes were another example of notable AMR genes. AME-encoding genes are one of the most important resistance genes transferable between gram-negative bacteria, especially in *P. aeruginosa* (Belaynehe et al., 2017). *aac(6′)-II*, *aac (6′)-I*, *ant(2″)-I*, and *aph(3′)* are the most common AME-encoding genes in *P. aeruginosa* (Ahmed, 2018). We detected 12 AME-encoding genes distributed in two cases of culture-negative specimens. Antibacterial drugs had often been used before sample collection, which may have reduced the culture detection rate. At the same time, *P. aeruginosa, H. influenzae,* and *P. mirabilis* were discovered in these two specimens using TNPseq. Similarly, *aph(3')-VI*, *aac(6')-Ib-G*, *aac(6')-IId*, *aac(6')-Ib'*, *aac(6')-Ib11*, *ant(3")-Ij*, *aac(6')-30*, *aac(6')-Ib-AGKT*, *aac(6')-Ib-AKT*, and *aac(3)-IIe* were detected in the specimen in which *P. aeruginosa* was identified. These results implied the crucial role of TNPseq in the identification of pathogens and AMR genes. The application of TNPseq could, to a certain extent, help clinicians make decisions regarding specific antibiotics rather than broad-spectrum antibiotics.

One of the limitations of this study is that only a small number of other sample types, except for BALF, were included in the present research. Future studies of larger sample sizes, including saliva, blood, puncture fluid, and transbronchial lung biopsy, are required to fully explore and compare the performances of TNPseq and conventional culture methods. Moreover, the AMR genes identified by TNPseq did not provide information on susceptibility to antibiotics. It is necessary to further verify the antimicrobial susceptibility test for more patients in the clinical laboratory.

In conclusion, our results underlined the potential value of TNPseq for the rapid identification of etiological agents. From a comprehensive perspective, TNPseq is an effective method for the early identification of pathogens in patients with LRTI. It is vital to treat dangerous acute severe infectious diseases precisely to improve patients' outcomes.

Data availability statement

The datasets presented in this study can be found in online repositories. The names of the repository/repositories and accession number(s) can be found below: https://www.ncbi.nlm.nih.gov/, PRJNA 902511.

Ethics statement

The studies involving human participants were reviewed and approved by Ethics Committee of Fuzhou Tuberculosis Prevention Hospital (number 2022-004-01), Fujian Province. The patients/participants provided their written informed consent to participate in this study.

Author contributions

HZ, MW, YW, and HG conceived, designed, and supervised the study. XH, TW, and YR were responsible for patient recruitment. PX formulated the protocols and performed the experimental implementation process. HZ, MW, YL, and HG analyzed the data and drafted the manuscript. All authors proofread, revised the draft, and agreed to the published version of the manuscript.

Funding

This project was supported by the Science and Technology Bureau of Fuzhou (No. 2020-WS-95). The patrons had no role in the study design, data collection, analysis, decision to publish, or execution of the manuscript.

Acknowledgments

We thank Dr. Bin Wang for his clinical communication and feedback. We also thank Changxiao Xie and Qiankun Li for their bioinformatics support.

Conflict of interest

YL, PX, and YW were employed by Zhejiang ShengTing Biotech Co., Ltd., Hangzhou, China. HG is a co-founder of Zhejiang ShengTing Biotech.

The remaining authors declare that the research was conducted in the absence of any commercial or financial relationships that could be construed as a potential conflict of interest.

Publisher's note

Supplementary material

The Supplementary Material for this article can be found online at: https://www.frontiersin.org/articles/10.3389/fmicb.2022.1065159/full#supplementary-material

References

Ahmad, S., and Khan, Z. (2020). Mixed infection with itraconazole-susceptible and-resistant strains of *Aspergillus fumigatus*: diagnostic and therapeutic implications. *J. Infect. Public Health* 13, 664–666. doi: 10.1016/j.jiph.2020.01.311

Ahmed, O. (2018). Prevalence of aminoglycoside resistance genes in Pseudomonas aeruginosa isolated from a tertiary care hospital in Makkah, KSA. *Clin. Pract.* 15, 391. doi: 10.4172/clinical-practice.1000391

Belaynehe, K. M., Shin, S. W., Hong-Tae, P., and Yoo, H. S. (2017). Occurrence of aminoglycoside-modifying enzymes among isolates of *E. coli* exhibiting high levels of aminoglycoside resistance isolated from Korean cattle farms. *FEMS Microbiol. Lett.* 364, 129. doi: 10.1093/femsle/fnx129

Bhullar, K., Waglechner, N., Pawlowski, A., Koteva, K., Banks, E. D., Johnston, M. D., et al. (2012). Antibiotic resistance is prevalent in an isolated cave microbiome. *PLoS ONE* 7, e34953. doi: 10.1371/journal.pone.0034953

Bittinger, K., Charlson, E. S., Loy, E., Shirley, D. J., Haas, A. R., Laughlin, A., et al. (2014). Improved characterization of medically relevant fungi in the human respiratory tract using next-generation sequencing. *Genome Biol.* 15, 487. doi: 10.1186/s13059-014-0487-y

Boolchandani, M., D'Souza, A. W., and Dantas, G. (2019). Sequencing-based methods and resources to study antimicrobial resistance. *Nat. Rev. Genet.* 20, 356–370. doi: 10.1038/s41576-019-0108-4

Chan, W. S., Au, C. H., Leung, S. M., Ho, D. N., Wong, E. Y. L., To, M. Y., et al. (2020). Potential utility of targeted Nanopore sequencing for improving etiologic diagnosis of bacterial and fungal respiratory infection. *Diagn. Pathol.* 15, 41. doi: 10.1186/s13000-020-00960-w

Charalampous, T., Kay, G. L., Richardson, H., Aydin, A., Baldan, R., Jeanes, C., et al. (2019). Nanopore metagenomics enables rapid clinical diagnosis of bacterial lower respiratory infection. *Nat. Biotechnol.* 37, 783–792. doi: 10.1038/s41587-019-0156-5

Charalampous, T., Richardson, H., Kay, G. L., Baldan, R., Jeanes, C., Rae, D., et al. (2018). Rapid diagnosis of lower respiratory infection using nanopore-based clinical metagenomics. *bioRxiv* 9, 387548. doi: 10.1101/387548

Chen, Y., Feng, W., Ye, K., Guo, L., Xia, H., Guan, Y., et al. (2021). Application of metagenomic next-generation sequencing in the diagnosis of pulmonary infectious pathogens from bronchoalveolar lavage samples. *Front. Cell. Infect. Microbiol.* 11, 541092. doi: 10.3389/fcimb.2021.541092

Ciuffreda, L., Rodríguez-Pérez, H., and Flores, C. (2021). Nanopore sequencing and its application to the study of microbial communities. *Comput. Struct. Biotec.* 19, 1497–1511. doi: 10.1016/j.csbj.2021.02.020

Collaborators, G. D. (2020). Global burden of 369 diseases and injuries in 204 countries and territories, 1990–2019: a systematic analysis for the global burden of disease study 2019. *Lancet* 396, 1204–1222. doi: 10.1016/S0140-6736(20)30925-9

Deamer, D., Akeson, M., and Branton, D. (2016). Three decades of nanopore sequencing. *Nat. Biotechnol.* 34, 518–524. doi: 10.1038/nbt.3423

Emond-Rheault, J. G., Hamel, J., Jeukens, J., Freschi, L., Kukavica-Ibrulj, I., Boyle, B., et al. (2020). The salmonella enterica plasmidome as a reservoir of antibiotic resistance. *Microorganisms* 8, 16. doi: 10.3390/microorganisms8071016

Feldman, C., and Shaddock, E. (2019). Epidemiology of lower respiratory tract infections in adults. *Exp. Rev. Resp. Med.* 13, 63–77. doi: 10.1080/17476348.2019.1555040

Fu, Y., Chen, Q., Xiong, M., Zhao, J., Shen, S., Chen, L., et al. (2022). Clinical performance of nanopore targeted sequencing for diagnosing infectious diseases. *Microbiol. Spectr.* 10, e0027022. doi: 10.1128/spectrum.00270-22

Glimåker, M., Johansson, B., Grindborg, Ö., Bottai, M., Lindquist, L., and Sjölin, J. (2015). Adult bacterial meningitis: earlier treatment and improved outcome following guideline revision promoting prompt lumbar puncture. *Clin. Infect. Dis.* 60, 1162–1169. doi: 10.1093/cid/civ011

Gu, W., Deng, X., Lee, M., Sucu, Y. D., Arevalo, S., Stryke, D., et al. (2021). Rapid pathogen detection by metagenomic next-generation sequencing of infected body fluids. *Nat. Med.* 27, 115–124. doi: 10.1038/s41591-020-1105-z

Gu, W., Miller, S., and Chiu, C. Y. (2019). Clinical metagenomic next-generation sequencing for pathogen detection. *Annu. Rev. Pathol. Mech.* 14, 319–338. doi: 10.1146/annurev-pathmechdis-012418-012751

Haider, M. H., McHugh, T. D., Roulston, K., Arruda, L. B., Sadouki, Z., and Riaz, S. (2022). Detection of carbapenemases bla(OXA48)-bla(KPC)-bla(NDM)-bla(VIM) and extended-spectrum-β-lactamase bla(OXA1)-bla(SHV)-bla(TEM) genes in Gram-negative bacterial isolates from ICU burns patients. *Ann. Clin. Microbiol. Antimicrob.* 21, 18. doi: 10.1186/s12941-022-00510-w

Haro, K., Ogawa, M., Saito, M., Kusuhara, K., and Fukuda, K. (2020). Bacterial composition of nasal discharge in children based on highly accurate 16S rRNA gene sequencing analysis. *Sci. Rep.* 10, 20193. doi: 10.1038/s41598-020-77271-z

Hoefnagels, I., van de Maat, J., van Kampen, J. J. A., van Rossum, A., Obihara, C., Tramper-Stranders, G. A., et al. (2021). The role of the respiratory microbiome and viral presence in lower respiratory tract infection severity in the first 5 years of life. *Microorganisms* 9, 1446. doi: 10.3390/microorganisms9071446

Hong, N. T. T., Nghia, H. D. T., Thanh, T. T., Lan, N. P. H., Ny, N. T. H., Ngoc, N. M., et al. (2020). Cerebrospinal fluid MinION sequencing of 16S rRNA gene for rapid and accurate diagnosis of bacterial meningitis. *J. Infect.* 80, 469–496. doi: 10.1016/j.jinf.2019.12.011

Jun, K. I., Oh, B. L., Kim, N., Shin, J. Y., and Moon, J. (2021). Microbial diagnosis of endophthalmitis using nanopore amplicon sequencing. *Int. J. Med. Microbiol.* 311, 151505. doi: 10.1016/j.ijmm.2021.151505

Keshavarz, M., Tavakoli, A., Nejad, A. S. M., Mokhtari-azad, T., and Rezaei, F. (2018). A review of influenza vaccination among different population groups in Iran. *J. Clin. Diag. Res.* 12, 11647. doi: 10.7860/JCDR/2018/35486.11647

Koren, S., and Phillippy, A. M. (2015). One chromosome, one contig: complete microbial genomes from long-read sequencing and assembly. *Curr. Opin. Microbiol.* 23, 110–120. doi: 10.1016/j.mib.2014.11.014

Leclair, L. W., and Hogan, D. A. (2010). Mixed bacterial-fungal infections in the CF respiratory tract. *Med. Mycol.* 48, S125–132. doi: 10.3109/13693786.2010.521522

Lemon, J. K., Khil, P. P., Frank, K. M., and Dekker, J. P. (2017). Rapid nanopore sequencing of plasmids and resistance gene detection in clinical isolates. *J. Clin. Microbiol.* 55, 3530–3543. doi: 10.1128/JCM.01069-17

Li, R., Du, P., Zhang, P., Li, Y., Yang, X., Wang, Z., et al. (2021). Comprehensive genomic investigation of coevolution of mcr genes in *E. coli* strains *via* nanopore sequencing. *Glob. Chall.* 5, 2000014. doi: 10.1002/gch2.202000014

Li, Z. J., Zhang, H. Y., Ren, L. L., Lu, Q. B., Ren, X., Zhang, C. H., et al. (2021). Etiological and epidemiological features of acute respiratory infections in China. *Nat. Commun.* 12, 5026. doi: 10.1038/s41467-021-25120-6

Liao, Q., Yuan, Y., Zhang, W., Deng, J., Wu, S., Liu, Y., et al. (2022). Detection and characterization of carbapenemases in enterobacterales with a new rapid and simplified carbapenemase detection method called rsCDM. *Front. Microbiol.* 13, 860288. doi: 10.3389/fmicb.2022.860288

Man, W. H., de Steenhuijsen Piters, W. A., and Bogaert, D. (2017). The microbiota of the respiratory tract: gatekeeper to respiratory health. *Nat. Rev. Microbiol.* 15, 259–270. doi: 10.1038/nrmicro.2017.14

McGill, F., Heyderman, R. S., Panagiotou, S., Tunkel, A. R., and Solomon, T. (2016). Acute bacterial meningitis in adults. *Lancet* 388, 3036–3047. doi: 10.1016/S0140-6736(16)30654-7

Miao, Q., Ma, Y., Wang, Q., Pan, J., Zhang, Y., Jin, W., et al. (2018). Microbiological diagnostic performance of metagenomic next-generation sequencing when applied to clinical practice. *Clin. Infect. Dis.* 67, S231–s240. doi: 10.1093/cid/ciy693

Nebreda-Mayoral, T., Miguel-Gómez, M. A., March-Rosselló, G. A., Puente-Fuertes, L., Cantón-Benito, E., Martínez-García, A. M., et al. (2022). Bacterial/fungal infection in hospitalized patients with COVID-19 in a tertiary hospital in the Community of Castilla y León, Spain. *Enferm. Infecc. Microbiol. Clin.* 40, 158–165. doi: 10.1016/j.eimc.2020.11.003

Petersen, L. M., Martin, I. W., Moschetti, W. E., Kershaw, C. M., and Tsongalis, G. J. (2019). Third-generation sequencing in the clinical laboratory: exploring the advantages and challenges of nanopore sequencing. *J. Clin. Microbiol.* 58, 1315. doi: 10.1128/JCM.01315-19

Poirel, L., Nordmann, P., Lagrutta, E., Cleary, T., and Munoz-Price, L. S. (2010). Emergence of KPC-producing *P. aeruginosa* in the United States. *Antimicrob. Agents Chemother.* 54, 3072. doi: 10.1128/AAC.00513-10

Shang, H., Wang, Y., and Shen, Z. (2014). *National Guide to Clinical Laboratory Procedures*. Beijing: People's Medical Publishing House.

Shao, J., Hassouna, A., Wang, Y., Zhang, R., Zhen, L., Li, R., et al. (2022). Next-generation sequencing as an advanced supplementary tool for the diagnosis of pathogens in lower respiratory tract infections: an observational trial in Xi'an, China. *Biomed. Rep.* 16, 14. doi: 10.3892/br.2021.1497

Troeger, C. E., Blacker, B. F., Khalil, I. A., Zimsen, S. R. M., Albertson, S. B., Abate, D., et al. (2019). Mortality, morbidity, and hospitalisations due to influenza lower respiratory tract infections, 2017: an analysis for the global burden of disease study 2017. *Lancet Respir.Med.* 7, 69–89. doi: 10.1016/S2213-2600(18)30496-X

Wang, M., Fu, A., Hu, B., Shen, G., Liu, R., Zhao, W., et al. (2020). Same-day simultaneous diagnosis of bacterial and fungal infections in clinical practice by nanopore targeted sequencing. *medRxiv* 2008, 20057604. doi: 10.1101/2020.04.08.20057604

Xie, G., Zhao, B., Wang, X., Bao, L., Xu, Y., Ren, X., et al. (2021). Exploring the clinical utility of metagenomic next-generation sequencing in the diagnosis of pulmonary infection. *Infect. Dis. Ther.* 10, 1419–1435. doi: 10.1007/s40121-021-00476-w

Yatera, K., Noguchi, S., and Mukae, H. (2021). Perspective on the clone library method for infectious diseases. *Respir. Investig.* 59, 741–747. doi: 10.1016/j.resinv.2021.07.003

Yonkus, J. A., Whittle, E., Alva-Ruiz, R., Abdelrahman, A. M., Horsman, S. E., Suh, G. A., et al. (2022). "Answers in hours": a prospective clinical study using nanopore sequencing for bile duct cultures. *Surgery* 171, 693–702. doi: 10.1016/j.surg.2021.09.037

Zheng, G., Shi, Y., Cao, Y., Qian, L., Lv, H., Zhang, L., et al. (2022). Clinical feature, therapy, antimicrobial resistance gene distribution, and outcome of nosocomial meningitis induced by multidrug-resistant enterobacteriaceae: a longitudinal cohort study from two neurosurgical centers in Northern China. *Front.Cell. Infect. Microbiol.* 12, 839257. doi: 10.3389/fcimb.2022.839257

frontiers | Frontiers in Microbiology

TYPE Original Research
PUBLISHED 11 January 2023
DOI 10.3389/fmicb.2022.1076154

OPEN ACCESS

EDITED BY
Leon G. Leanse,
Harvard Medical School,
United States

REVIEWED BY
Jianfeng Wang,
Jilin University,
China
Piyush Baindara,
University of Missouri,
United States
Dexian Zhang,
Foshan University,
China

*CORRESPONDENCE
Changbo Ou
✉ ouchangbo2004@163.com

†These authors have contributed equally to this work and share first authorship

SPECIALTY SECTION
This article was submitted to Infectious Agents and Disease, a section of the journal Frontiers in Microbiology

RECEIVED 07 November 2022
ACCEPTED 13 December 2022
PUBLISHED 11 January 2023

CITATION
Liu G, Liu A, Yang C, Zhou C, Zhou Q, Li H, Yang H, Mo J, Zhang Z, Li G, Si H and Ou C (2023 *Portulaca oleracea* L. organic acid extract inhibits persistent methicillin-resistant *Staphylococcus aureus in vitro* and *in vivo*. *Front. Microbiol.* 13:1076154. doi: 10.3389/fmicb.2022.1076154

Portulaca oleracea L. organic acid extract inhibits persistent methicillin-resistant *Staphylococcus aureus in vitro* and *in vivo*

Gengsong Liu[1†], Aijing Liu[2†], Cheng Yang[1], Congcong Zhou[1], Qiaoyan Zhou[1], Haizhu Li[1], Hongchun Yang[1], Jiahao Mo[1], Zhidan Zhang[1], Gonghe Li[1,3,4], Hongbin Si[1,3,4] and Changbo Ou[1,3,4*]

[1]College of Animal Science and Technology, Guangxi University, Nanning, China, [2]State Key Laboratory of Veterinary Biotechnology, Harbin Veterinary Research Institute, Chinese Academy of Agricultural Sciences, Harbin, China, [3]Guangxi Zhuang Autonomous Region Engineering Research Center of Veterinary Biologics, Nanning, China, [4]Guangxi Key Laboratory of Animal Reproduction, Breeding and Disease Control, Nanning, China

Staphylococcus aureus continues to be one of the most important pathogens capable of causing a wide range of infections in different sites of the body in humans and livestock. With the emergence of methicillin-resistant strains and the introduction of strict laws on antibiotic usage in animals, antibiotic replacement therapy has become increasingly popular. Previous studies have shown that *Portulaca oleracea* L. extract exerts a certain degree of bacteriostatic effect, although the active ingredients are unknown. In the present study, the antibacterial activity of the organic acid of *P. oleracea* (OAPO) against *S. aureus* was examined using a series of experiments, including the minimum inhibitory concentration, growth curve, and bacteriostasis curve. *In vitro* antibacterial mechanisms were evaluated based on the integrity and permeability of the cell wall and membrane, scanning electron microscopy, and soluble protein content. A mouse skin wound recovery model was used to verify the antibacterial effects of OAPO on *S. aureus in vivo*. The results showed that OAPO not only improved skin wound recovery but also decreased the bacterial load in skin wounds. Moreover, the number of inflammatory cells and cytokines decreased in the OAPO-treated groups. In summary, this study reports a botanical extract that can inhibit *S. aureus in vitro* and *in vivo*, indicating the potential use of OAPO to prevent and control *S. aureus* infection in the near future.

KEYWORDS

***Portulaca oleracea* L., organic acid, *Staphylococcus* aureus, methicillin-resistant, botanical extract, antibacterial activity**

1. Introduction

Staphylococcosis, usually known as *Staphylococcus* infection, is an important zoonotic disease primarily caused by *Staphylococcus aureus*. *S. aureus* is an important clinical pathogen and a common colonizing bacterium found on human skin and mucosal surfaces. It can cause a variety of infections at different sites in humans and animals, ranging from skin and soft tissue infections to serious life-threatening diseases such as osteomyelitis, endocarditis, and necrotizing pneumonia. Moreover, *S. aureus* can pollute food in various ways to produce toxins that cause food poisoning symptoms. Commonly affected foods include milk, raw meat, and frozen food products. In the United States, the number of food poisoning cases caused by *S. aureus* is estimated to be 241,000 per year (Scallan et al., 2011). Many such poisoning events have been reported in China each year (Yan et al., 2012; Lv et al., 2021).

Disinfection and hygienic food/feed management measures are the most important prevention and control strategies for *S. aureus*. *S. aureus*-infected patients and sick animals were first tested for drug sensitivity, and then treated with sensitive drugs. Beta-lactams and glycopeptide antibiotics are used to treat staphylococcosis. However, with the emergence of methicillin-resistant *S. aureus* (MRSA) and the introduction of strict laws on antibiotic usage in animals, an era characterized by the limited use of antibiotics is beginning in China. Many techniques and products replace antibiotics against *Staphylococcus* strains, such as antibacterial peptides, probiotics, prebiotics, enzyme preparations, and traditional Chinese medicine (David and Daum, 2017; Li et al., 2019). Plant extracts are becoming increasingly popular as alternatives to antibiotics, although they cannot completely replace antibiotics. Aqueous extracts of *Galla chinensis* can reduce biofilm formation in methicillin-resistant *S. aureus* and inhibit the invasive ability and pathogenicity of MRSA *in vivo* at a concentration of 31.25 μg/ml (Wu et al., 2019). *Ginkgo biloba* exocarp extracts at concentrations of 4–12 μg/ml were shown to inhibit *S. aureus* and MRSA biofilm formation in a dose-dependent manner and affected biofilm-associated gene expression (Wang et al., 2021). Moreover, herbal extracts and their active constituents can exert synergistic effects in combination with oxacillin or gentamicin against *S. aureus* (Kuok et al., 2017).

Portulaca oleracea L. is listed in the National Drug and Food Homologous Catalogue in China with the functions of clearing heat, removing toxins, cooling blood to stop bleeding, and treating dysentery (Zhou et al., 2015). It is mainly used to treat blood dysentery caused by heat toxins, eczema, inflammatory diseases, and redness of the skin. It is a medicine and food homologous drug with a good safety profile in humans. In recent years, many studies have been conducted on its chemical constituents, pharmacological effects, and molecular mechanisms (Rahimi et al., 2019). Two novel amide glycosides isolated from *P. oleracea* exhibit anticholinesterase and scavenging activities (Liu et al., 2021). *P. oleracea* leaf extract also displays antioxidant and anti-inflammatory activities against LPS-induced acute lung injury in a dose-dependent manner (Rahimi et al., 2019). Moreover, the *P. oleracea* extract show relatively potent anti-asthmatic effects owing to decreased nitric oxide production and increased antioxidant markers (Khazdair et al., 2019). Modern pharmacological studies on *P. oleracea* have demonstrated its gastroprotective and hepatoprotective activities in *in vivo* and *in vitro* models (Farkhondeh and Samarghandian, 2019). However, there have been few studies on antimicrobial activity against *S. aureus*. Two unsaturated fatty acids from *P. oleracea* act synergistically with erythromycin against MRSA *in vitro*, possibly by inhibiting methionine sulfoxide reductase (Fung et al., 2017). The carbon dioxide extraction of *P. oleracea* shows clinical effects against significant microorganisms, such as *Escherichia coli* and *S. aureus* (Tleubayeva et al., 2021). However, the chemical constituents that demonstrate antimicrobial activity against *S. aureus* remain unknown.

This study aimed to investigate the anti-*Staphylococcus* activity of an organic acid extract of *P. oleracea in vitro* and *in vivo*. First, the main chemical constituents of *P. oleracea* extract and the anti-*Staphylococcus* effects of the organic acid extract were evaluated using an *in vitro* model. Finally, organic acid extracts were used to cure skin wounds infected with *S. aureus*.

2. Materials and methods

2.1. Bacterial strain and reagents

Three *S. aureus* strains were used in this study: two field strains (MRSA29 and MRSA85) and one standard strain (ATCC 29213). The 29213 strain was from the First People's Hospital of Nanning, China. MRSA85 and MRSA29 strains were isolated from clinical samples and stored at Guangxi University (Yang et al., 2020). Trimethoprim-sulfamethoxazole (TMP-SMX) was purchased from the TEYI Pharmaceutical Group (Guangdong, China).

2.2. Organic acids of *Portulaca oleracea* preparation

The trunks and leaves of *P. oleracea* were collected from Henan Province (China), and air-dried trunks and leaves were used for organic acid extraction. The obtained *P. oleracea* were identified and stored at the College of Animal Science and Technology, Guangxi University. The organic acid extract was based on a previous study with some modifications (Kim et al., 2016). Briefly, 100 g of dry *P. oleracea* was soaked in a flask with 150 ml petroleum ether overnight and then continuously boiled for 1 h. Finally, the petroleum ether was discarded and dried. The defatted *P. oleracea* was extracted with 95% ethanol at a solid-to-liquid ratio of 1:15 for 1 h at an ultrasonic frequency of 50 kHz. OAPO was obtained by rotary evaporation.

2.3. Analysis of the chemical composition of OAPO

Chemical composition analysis of OAPO was performed using an ultra-high-performance liquid chromatography-mass spectrometer (HPLC-MS; Q-Exactive, Thermo). The main chemical compositions of OAPO were identified by comparing its mass spectra with those in a mass spectral library.

2.4. Antimicrobial activity of OAPO *in vitro*

2.4.1. Determination of minimum inhibitory concentration

The standard broth microdilution method based on the method from Clinical and Laboratory Standards Institute was used to determine the antibacterial effect of OAPO against *S. aureus* with slight modifications (Zhang et al., 2016). The bacterial suspension [final concentration of 7×10^7 colony-forming units (CFU)/ml] was co-cultured with OAPO at a concentration range of 0.05–50 mg/ml in nutrient broth, with shaking for 16 h at 37°C. The minimum concentration of OAPO that inhibited visible bacterial growth was defined as MIC.

2.4.2. *In vitro* antibacterial activity determined by agar diffusion

The agar diffusion method was used to test the antibacterial properties of OAPO, following a previous study with some modifications (Zhang et al., 2021). The nutrient agar plate was evenly coated with 100 μl *S. aureus* suspension and incubated for 5 min. The sterilized Oxford cup (8 mm in diameter) was placed on the surface of the plate, gently pressed and fixed, and 100 μl solution (experimental group: 25 mg/ml OAPO solution; control group: sterile distilled water) was added into the Oxford cup. The experiment was repeated thrice for each group. Bacterial inhibition zones were observed, and the diameter of each inhibition zone (mm) was measured after incubation at 37°C for 18 h. Based on pharmacological methods, the drug was considered medium sensitive against the bacteria when the diameter was between 10 and 15 mm (Zheng et al., 2022).

2.4.3. Growth and bacteriostasis curves

The MRSA85 strain suspension was co-cultured with a one-fold MIC of OAPO at 37°C at 220 rpm. The OD_{600nm} of the bacterial suspension was determined every 2 h. A growth curve of *S. aureus* was constructed based on the OD_{600nm} value of the corresponding bacterial suspension at the indicated time points (Jiang et al., 2019).

The bacteriostasis curve of OAPO was constructed based on the OD_{600nm} value of the corresponding bacterial suspension at the indicated time points (Wicha et al., 2015). Unlike the growth curve, a one-fold MIC of OAPO was added to the bacterial suspension when the OD_{600nm} value was 1.2. Then a suspension was taken for OD_{600nm} value determination at the indicated time points.

2.4.4. Scanning electron microscopy analysis

The MRSA85 suspension at a concentration of 5×10^6 CFU/ml was added to one-fold or two-fold MIC of OAPO and co-cultured in an incubator at 200 rpm and 37°C for 16 h. MRSA85 without OAPO was used as the control group. The bacterial suspension was centrifuged at 4,000 × *g* for 10 min and washed thrice with 0.1 M phosphate buffer solution (PBS, pH = 7.4). The bacterial precipitate was fixed with 2.5% glutaraldehyde and dehydrated with a gradient concentration of ethanol (50–100%). Finally, the samples were sputtered and plated with gold in an ion-plating machine for 2 min and observed using a scanning electron microscope (Hitachi Regulus 8,100, Japan; Hao et al., 2021).

2.4.5. Cell wall damage assay

The effect of OAPO on the cell wall was determined by alkaline phosphatase (AKP) leakage (Hu et al., 2019). The bacterial sample was preprocessed as described in the SEM analysis. The sample was collected at a specific time point and centrifuged at 4,500 × *g* for 10 min. The supernatant was used to determine the AKP content using an AKP kit (JianCheng, Nanjing, China) following the manufacturer's instructions.

2.4.6. DNA leakage content induced by OAPO

The bacterial sample was preprocessed as described in the SEM analysis. The obtained MRSA85 bacterial supernatant was used for DNA content determination using a full-wavelength spectrophotometer for nucleic acid detection (Tiangen, China). This was repeated three times, and the DNA content was calculated as the mean ± standard deviation (Hu et al., 2019).

2.4.7. Soluble protein content influenced by OAPO

The bacterial sample was preprocessed as described in the SEM analysis. The obtained MRSA85 bacterial precipitate was completely dispersed in PBS and subjected to ultrasonication. The soluble protein content in the ultrasonic crushing liquid was determined using a BCA protein determination kit and sodium dodecyl sulfate-polyacrylamide gel electrophoresis (SDS-PAGE; Zhang et al., 2017).

2.5. Experimental animal grouping and treatment

A murine skin wound infection model was used to validate the *in vivo* efficacy of OAPO against *S. aureus*. The animal study protocols were approved by the Animal Management and Ethics Committee of Guangxi University. Seventy-eight male Kunming mice weighing 18–22 g were housed in a controlled environment at 25°C with a 12 h light–dark cycle and free access to food and water. After the mice were adapted to the environment, they were randomly divided into six groups, with 11 to 14 mice in each group according to treatment: non-infected wound control,

infected wound control, infected wound TMP-SMX-treated control, and infected wound OAPO-treated groups.

For dermal wound development, these mice were anesthetized with an intraperitoneal administration of ketamine (25 mg/kg body weight) and xylazine (5 mg/kg body weight) mixture before the surgical procedure (Gupta and Tyagi, 2021). The dorsal surface area of each mouse was shaved and sterilized with 75% ethanol. A full-thickness excision wound of 2 × 2 cm was created. Then the wound was inoculated with 100 µl MRSA85 suspensions at 10^8 CFU/ml, except for the mice in the non-infected wound control group, which were inoculated with 0.9% physiological saline. To ensure that these wounds were successfully infected with MRSA85, the inoculation treatment was repeated 12 h after the first infection. All the mice were orally administered the corresponding drugs. In the OAPO-treated groups, the mice were orally administered 125, 250, and 500 mg/kg body weight. In the TMP-SMX-treated group, the dosages of TMP and SMX were 320 and 1,600 mg/kg of body weight, respectively, and administered orally twice daily (Guo et al., 2013; Miller et al., 2015). The mice in the non-infected and infected wound control groups were treated with the same volume of water. The mice were monitored daily and weighed throughout the study period of 7 days. The wound area was examined daily. All mice were euthanized by CO_2 inhalation on the last day of the study, and skin wound tissues were collected for further analyses. Whole blood was collected in tubes for serum analysis.

2.6. Skin wound closure rate

At the end of the study, each wound was traced by placing a transparent sheet over it. The traced area was placed over a metric grid, and the number of known area squares was counted to calculate the total wound area. The wound closure rate was calculated according to the formula: $(A_0 - A_8)/A_0 \times 100\%$, where A_0 is the wound area on day 0 of wounding, and A_8 is the wound area at the end of the study (Gupta and Tyagi, 2021).

2.7. Quantification of bacterial load in wound

A piece of skin wound tissue was collected, weighed, and homogenized in 1 ml of PBS. Tissue homogenates (100 µl) were serially diluted and inoculated onto brain-heart infusion agar plates. The plates were then incubated under aerobic conditions at 37°C for 24 h. Viable CFUs were counted and plotted as $\log_{10}$ (CFU/g wound tissue; Carneiro et al., 2021).

2.8. Histological analysis

Skin wound tissues from the infected mice were excised for histological analysis. Tissues were fixed in formalin and embedded in paraffin. The embedded tissues were sliced into 4.5 µm-thick sections and stained with hematoxylin/eosin (HE). The slides were examined for cellular infiltration, blood coagulation, and presence of bacterial aggregates under a light microscope (Simonetti et al., 2017).

2.9. Determination of inflammation cytokines by enzyme-linked immunosorbent assay (ELISA)

The levels of the inflammatory cytokines IL-1β, IL-6, and TNF-α in the serum of each mouse were determined at the end of the study using commercial ELISA kits (Nanjing Boyan, China). Serum samples were analyzed according to the manufacturer's instructions. The results are expressed as pg./mL of serum.

2.10. Statistical analysis

The results are expressed as mean ± standard deviation. Statistical evaluations were performed by analysis of variance using GraphPad Prism 5.0 (GraphPad Software Inc., San Diego, CA, United States). Differences were considered statistically significant at $p < 0.05$.

3. Results

3.1. Chemical compositions of the organic acid part of *Portulaca oleracea*

To explore the chemical composition of the organic acid part of *P. oleracea*, HPLC-MS was used to separate and identify the chemical composition of OAPO, and the total ion chromatogram was established, as shown in Figure 1. Moreover, Table 1 shows that the first 25 organic acids in OAPO comprised 5.78% of the total content, including α-eleostearic acid, palmitic acid, L-pyroglutamic acid, linoleic acid, stearidonic acid, azelaic acid, D-pantothenic acid, 6-hydroxypicolinic acid, and phloionolic acid.

3.2. OAPO inhibits *Staphylococcus aureus* replication *in vitro*

The MIC of OAPO was 12.5 mg/ml, as determined by the broth microdilution method. Moreover, the Oxford cup test showed that the diameter of the inhibition zone of OAPO was 13.5 ± 0.5 cm at a concentration of 25 mg/ml, which indicated that OAPO was medium sensitive against MRSA85.

OAPO toxicity against *S. aureus* was determined by measuring staphylococcal growth with a 1-fold MIC of OAPO (Figure 2A). The results showed that the OD_{600nm} measured for OAPO-treated bacteria decreased over the course of the experiment, indicating that OAPO is bactericidal to *S. aureus*. OAPO inhibited the

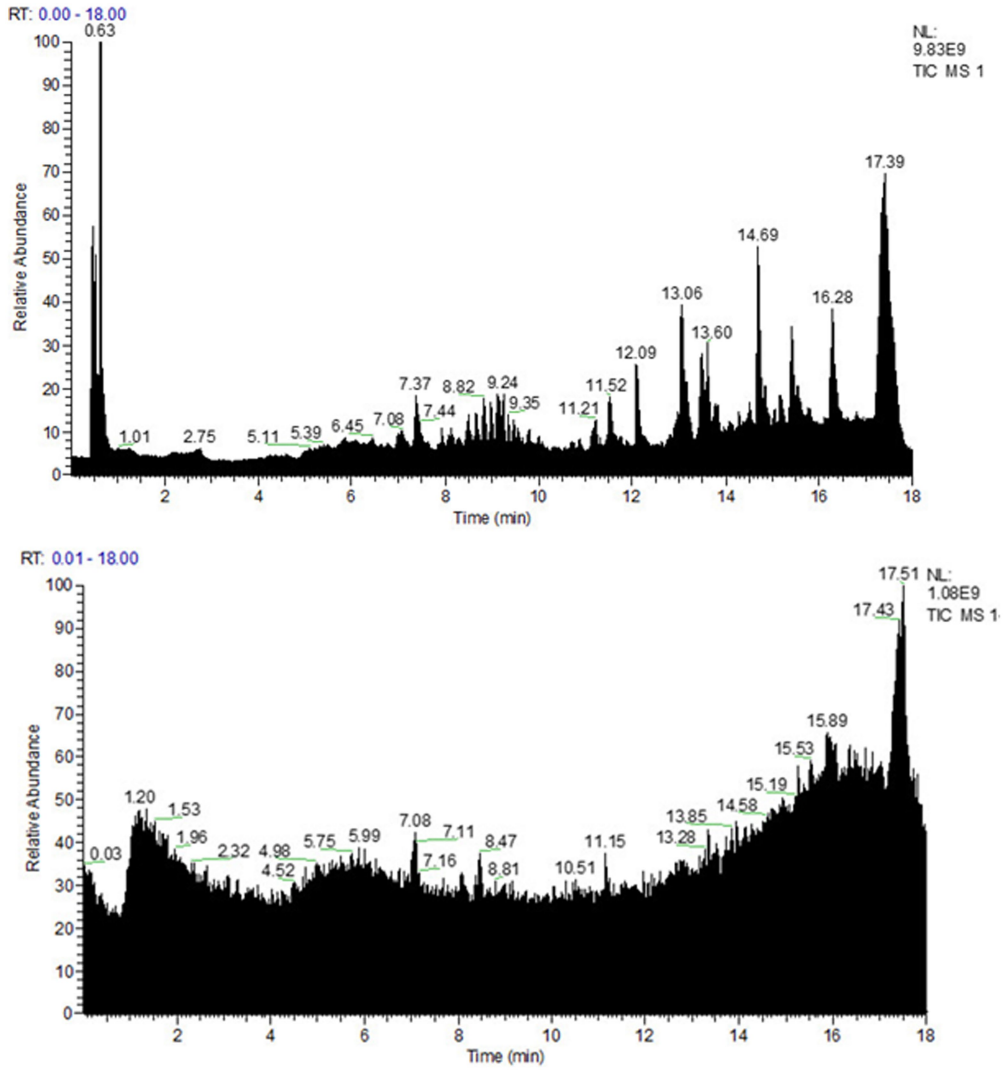

FIGURE 1
Spectra fingerprint of chemical composition analysis of organic acid of *Portulaca oleracea* L. (OAPO) by ultra-high-performance liquid chromatography-mass spectrometer (HPLC-MS). Upper: positive mode (+); Lower: negative mode (–).

growth of *S. aureus* and prolonged the time required to stabilize *S. aureus*. A bacteriostatic curve was constructed to determine whether OAPO was bactericidal or bacteriostatic (Figure 2B). Combined with the one-fold MIC of OAPO, the absorbance value of *S. aureus* steadily declined from the beginning of the experiment.

3.3. Antibacterial mechanism of OAPO against *Staphylococcus aureus*

3.3.1. Destructive effects of OAPO on the integrity of the bacterial cell wall and membrane

The SEM images of the morphological changes induced by OAPO are shown in Figure 3A. In the untreated *S. aureus* control group, almost all bacteria showed a normal and intact morphology with a plump surface; in other words, they were uniform in size and shape. However, OAPO-treated bacteria showed noticeable morphological changes. One-fold MIC of OAPO induced considerable morphological changes with damaged cell walls, shriveled cells, and irregular shapes. In the two-fold MIC-OAPO group, the morphologies were more damaging.

AKP, an enzyme between the cell wall and the cell membrane, is undetectable when the morphology of the bacteria is intact. Owing to increased permeability, the AKP content in the bacterial culture solution was positively correlated with the degree of cell wall destruction. Figure 3B shows the AKP concentration in the bacterial culture solution post-administration of OAPO. OAPO significantly increased the AKP content in the culture solutions of 29,213, MRSA29, and MRSA85 strains ($p < 0.01$) compared to that in the untreated control group. Moreover, the effects of OAPO on AKP content were dose-dependent.

TABLE 1 Top 25 organic acids chemicals in OAPO.

Number	Name	Formula	RT [min]	Content (%)
1	α-Eleostearic acid	C18 H30 O2	13.493	1.26142
2	Palmitic acid	C16 H32 O2	11.501	0.99667
3	L-Pyroglutamic acid	C5 H7 N O3	0.641	0.72849
4	9-Oxo-10(E),12(E)-octadecadienoic acid	C18 H30 O3	13.508	0.49083
5	2′-deoxymugineic acid	C12 H20 N2O7	0.604	0.39817
6	N-Benzoylaspartic acid	C11 H11 N O5	6.118	0.22418
7	D-Pantothenic acid	C9 H17 N O5	4.101	0.19323
8	(12Z)-9,10,11-trihydroxyoctadec-12-enoic acid	C18 H34 O5	11.615	0.16167
9	Stearidonic acid	C18 H28 O2	13.141	0.15746
10	Azelaic acid	C9 H16 O4	9.172	0.13633
11	6-Hydroxypicolinic acid	C6 H5 N O3	0.668	0.10979
12	Phloionolic acid	C18 H36 O5	11.528	0.1057
13	3,8,13,17-tetramethyl-12-vinyl-2,7,18-Porphinetripropionic acid	C35 H36 N4O6	14.828	0.10238
14	(2S)-3-Phenyl-2-({[(3S,4S,5R)-2,3,4-trihydroxy-5-(hydroxymethyl)tetrahydro-2-furanyl]methyl}amino)propanoic acid	C15 H21 N O7	0.63	0.09536
15	10,16-Dihydroxyhexadecanoic acid	C16 H32 O4	11.773	0.0903
16	trans-3-Indoleacrylic acid	C11 H9 N O2	5.09	0.08367
17	4-Guanidinobutyric acid	C5 H11 N3 O2	0.61	0.08359
18	(2R)-2-[(2R,5S)-5-[(2S)-2-hydroxybutyl] oxolan-2-yl]propanoic acid	C11 H20 O4	9.172	0.07039
19	3-[14-Ethyl-13-formyl-21-(methoxycarbonyl)-4,8,18-trimethyl-20-oxo-9-vinyl-3-phorbinyl]propanoic acid	C35 H34 N4O6	14.832	0.06261
20	12-oxo phytodienoic acid	C18 H28 O3	11.737	0.05786
21	3-oxopalmitic acid	C16 H30 O3	13.255	0.05415
22	Ferulic acid	C10 H10 O4	7.85	0.04826
23	4-Isobutylbenzoic acid	C11 H14 O2	7.931	0.03314
24	3-Phenylpropanoic acid	C9 H10 O2	0.633	0.02632
25	2-Oxobutyric acid	C4 H6 O3	0.592	0.00796

The amount of nucleic acid leakage in the bacteria treated with OAPO was also measured to verify the effects of OAPO on the permeability of the bacterial cell membrane. As shown in Figure 3C, the DNA concentration in the bacterial culture solution was not affected 10 h post-treatment with OAPO. However, OAPO significantly increased the DNA concentration 16 h post-administration in all three bacterial strains: 29213, MRSA29, and MRSA85.

3.3.2. Effects of OAPO on soluble protein content

The results of the analysis using the BCA protein concentration determination kit and SDS-PAGE profiles of the bacterial proteins are shown in Figure 4. Compared to the those in the untreated control group at the same culture time, the soluble protein contents of 29,213, MRSA29, and MRSA85 were significantly increased at 10 and 16 h post-OAPO treatment ($p < 0.01$), respectively. As the concentration of OAPO and treatment duration increased, the effect of OAPO on the soluble protein content became more significant.

3.4. OAPO improved *Staphylococcus aureus*-infected skin injury recovery

To explore the effects of OAPO on skin injury induced by *S. aureus* infection, a mouse dermal wound model was used for

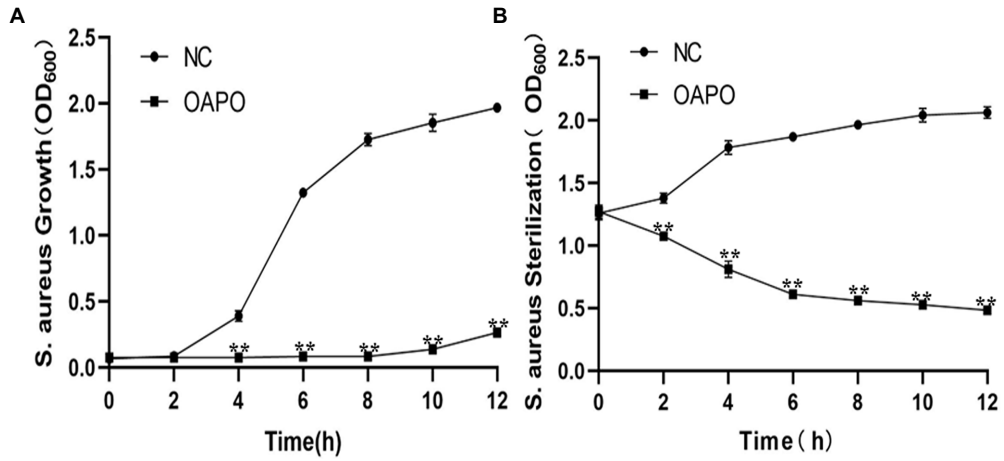

FIGURE 2
Organic acid of *Portulaca oleracea* L. (OAPO) killing of *Staphylococcus aureus* visualized by the growth **(A)** and bacteriostasis curves **(B)**. The OD_{600nm} of *S. aureus* culture suspension at 0, 2, 4, 6, 8, 10, and 12 h post-coculture with or without 1-fold minimum inhibitory concentration (MIC) of OAPO. NC: negative control, *S. aureus* culture without OAPO; OAPO: *S. aureus* culture with 1-fold MIC of OAPO. **indicates $p < 0.01$ when compared with the negative control group (NC, untreated with OAPO).

macroscopic analysis (Figure 5). In the infected control group, slough formation in the wound bed started on day 1 and began to cover the wound thickly on subsequent days. In the non-infected control group, the wound bed started to dry around the edges on day 1, and the wound was almost completely healed at the end of the experiment. In the OAPO- and TMP-SMX-treated infected groups, the wound bed area became smaller than that of the infected control group from days 4 to 7 (Figure 5A). Moreover, the wound healing rate was calculated on day 7, and the results showed that the medium dosage of OAPO significantly increased the wound healing rate compared with that in the infection control group ($p < 0.01$). Interestingly, the wound healing rate of all mice in the medium dosage OAPO group was more than 80% (Figure 5B).

3.5. OAPO decreased bacterial load and inflammation cytokines in the skin wound

The bacterial load in the wound tissue was assessed on day 7 post-wounding and post-infection with *S. aureus*. The bacterial numbers were 5.19×10^4 and 1.71×10^7 CFU/g of tissue in the uninfected and infected control groups, respectively. Moreover, the bacterial load ranged from 1.48 to 9.59×10^6 CFU/g of tissue in the OAPO- or TMP-SMX-treated groups, which was significantly lower than that of the infected control group ($p < 0.01$; Figure 6A).

Micro-anatomical changes were assessed by HE staining on day 7 post-infection. In the infected control group, the wound showed higher inflammatory cell infiltration than in the uninfected control group. Moreover, there was a high prevalence of hemorrhage and red blood cells in the wounds of the infected control group. However, there were few inflammatory and red blood cells in the wounds of the TMP-SMX- and OAPO-treated groups on day 7 post-infection with *S. aureus* (Figure 6B).

Inflammatory responses were also investigated by measuring inflammatory cytokines in mouse serum (Figure 7). IL-1β, IL-6, and TNF-α levels significantly increased in mice in the infected control group. However, a high dose of OAPO decreased the levels of IL-1β and IL-6. Moreover, TNF-α levels were significantly decreased by both OAPO and TMP-SMX ($p < 0.01$).

4. Discussion

Staphylococcus aureus is an important zoonotic pathogen that not only causes local and systemic infections in humans but also induces dermatitis, mastitis, enteritis, and other infections in livestock and poultry (Zhou et al., 2018). The occurrence of methicillin-resistant or multidrug-resistant *S. aureus* strains makes the treatment of staphylococcal diseases more difficult. Moreover, the implementation of strict laws against antibiotic use in animals has complicated the husbandry of *Staphylococcus*-infected animals. However, many new methods could be applied to reduce antibiotic usage and kill *S. aureus*, such as herbal extracts, bacteriophages, acidifiers, and antimicrobial peptides. Aqueous extracts of *P. oleracea* have a slight inhibitory effect on *E. coli* (Okuda et al., 2021). However, the bacteriostatic mechanisms and active ingredients of *P. oleracea* remain unclear. The present study aimed to demonstrate that OAPO is the main active ingredient of *P. oleracea* against *S. aureus* through *in vitro* and *in vivo* experiments.

There have been many studies on the antimicrobial activity of *P. oleracea* against a broad spectrum of bacterial species (Soliman et al., 2017); however, the characteristics of antimicrobial activity

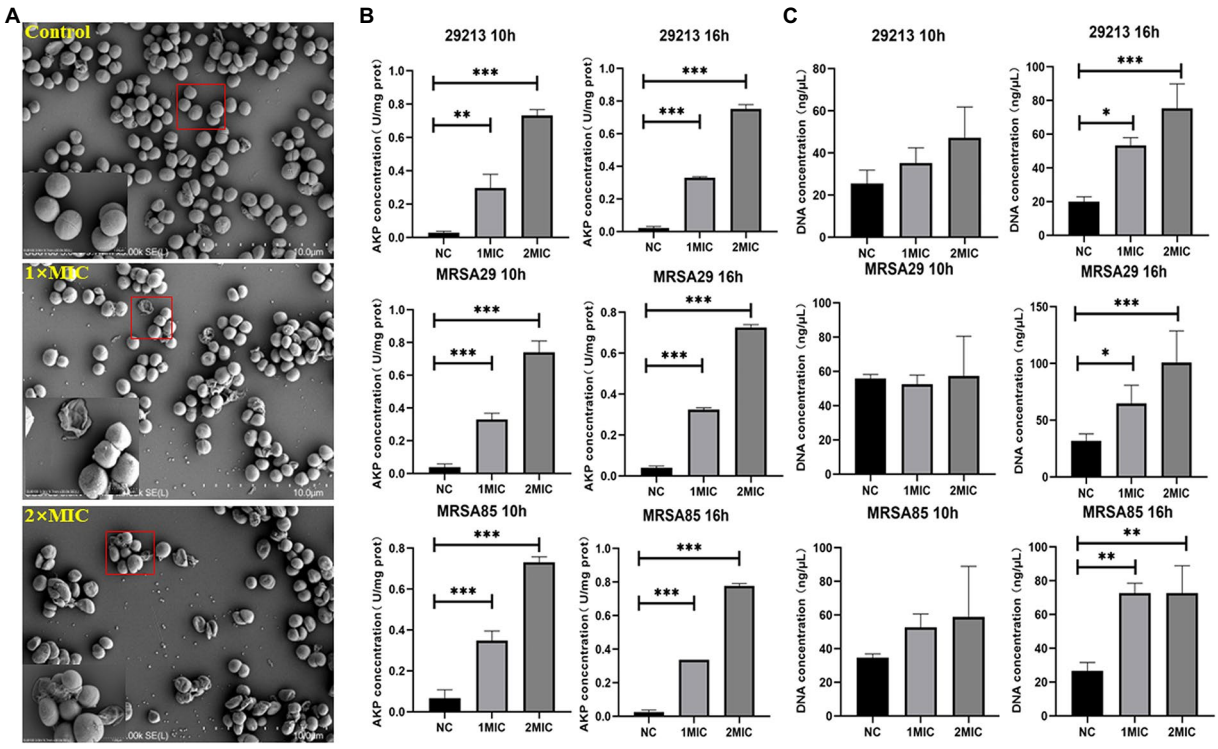

FIGURE 3
Antibacterial effects of organic acid of *Portulaca oleracea* L. (OAPO) on the morphology and integrity of the cell wall and membrane of *Staphylococcus. aureus*. **(A)** The morphology changes of *S. aureus* untreated (Control) or treated with 1× and 2× minimum inhibitory concentration (MIC) of OAPO by scanning electron microscopy (SEM). A red square indicates that this part was magnified by 10 times. **(B)** Effect of OAPO on the cell wall of *S. aureus* (29,213, MRSA29, and MRSA85 strains) at 10 and 16 h post-treatment with one-fold and two-fold MIC of OAPO (or after no treatment). The alkaline phosphatase (AKP) concentration of the bacterial culture solution was determined. **(C)** Effect of OAPO on the integrity of the cell membrane of *S. aureus* (29,213, MRSA29, and MRSA85 strains) at 10 and 16 h post-treatment with one-fold and two-fold MIC of OAPO (or after no treatment). The DNA concentration of the bacterial culture solution was determined. *indicates $p<0.05$, **indicates $p<0.01$, ***indicates $p<0.001$ when compared with the negative control group (NC, untreated with OAPO).

determined by these studies were slightly different from those in ours. Tleubayeva et al. showed that the CO_2 extract of *P. oleracea* had the greatest bactericidal effectiveness against *S. aureus* at 250 μg/ml and against *Escherichia coli*, *Bacillus subtilis*, and *Candida albicans* at 500 μg/ml (Tleubayeva et al., 2021). *Portulaca elatior* leaf lectin also showed strong activity against some phytopathogenic bacteria with a MIC value of 0.185 μg/ml (da Silva et al., 2021). The methanol extracts of *Portulaca quadrifida* at 250 μg/ml and 200 μg/ml showed the most significant antimicrobial activity against all tested gram-positive and gram-negative bacteria (Desta and Cherie, 2018). However, the present study showed that the MIC of OAPO was 12.5 mg/ml, which is inconsistent with the results of the above studies. The sources of herbal medicine and the tested bacterial strains were very different, and these factors might be the main causes of the different MIC results. Moreover, some compounds identified from *P. oleracea* exhibited only weak dose-dependent inhibition against bacterial pathogens, whereas other compounds showed significant antibacterial activity against common enteropathogenic bacteria *in vitro* (Lei et al., 2015; Hu et al., 2021). Interestingly, two unsaturated fatty acids from *P. oleracea* acted synergistically with erythromycin *in vitro* against MRSA, possibly by inhibiting the multidrug efflux pump of the bacteria (Chan et al., 2015; Fung et al., 2017). In summary, the specific substances and/or chemicals that play an antibacterial role in *P. oleracea* are still unclear.

Portulaca oleracea has many constituents, including flavonoids, alkaloids, organic acids, terpenoids, polysaccharides, vitamins, sterols, and other compounds (Zhou et al., 2015). In our preliminary tests, the aqueous extract, flavonoids and polysaccharide extracts did not display antibacterial activity (data not shown), while the organic acids possessed certain *Staphylococcus*-killing properties. Organic acid extracts were prepared according to a previously reported method, with slight modifications (Zhang et al., 2020). HPLC-MS was used to analyze the chemical composition of OAPO, and many organic acids were identified in OAPO, such as α-eleostearic, palmitic, phloionolic, and stearidonic acids. Some organic acids, such as protocatechuic and caffeic acid, were not identified in OAPO by HPLC-MS. There are two important reasons for this: one is that *P. oleracea* contains too little protocatechuic and caffeic acids to be detected, and the other is that the mixture of OAPO affects the measurement accuracy of HPLC-MS. Nevertheless, an organic acid-enriched

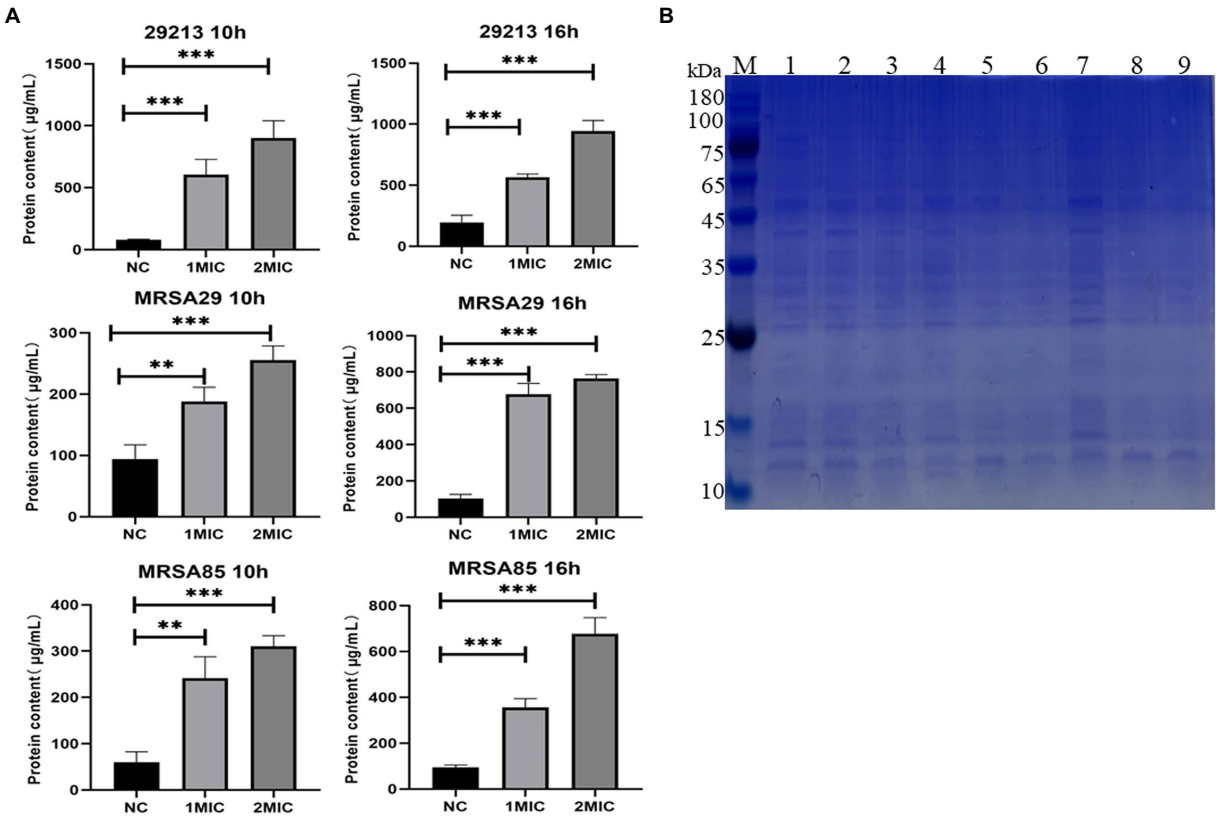

FIGURE 4
Organic acid of *Portulaca oleracea* L. (OAPO) increases the soluble protein content of bacterial culture solution. **(A)** The soluble protein content of *Staphylococcus aureus* (29,213, MRSA29, and MRSA85) at 10 and 16h post-treatment with 1× and 2× minimum inhibitory concentration (MIC) of OAPO was determined by the BCA kit. *indicates $p<0.05$, **indicates $p<0.01$, ***indicates $p<0.001$ when compared with the negative control group (NC, untreated with OAPO). **(B)** Sodium dodecyl sulfate-polyacrylamide gel electrophoresis (SDS-PAGE) of bacterial cells treated with OAPO. M: Marker, Lane 1/4/7: 29213, Lane 2/5/8: MRSA29, Lane 3/6/9: MRSA85; Lane 1/2/3: treated with two-fold MIC of OAPO, Lane 4/5/6: treated with one-fold MIC of OAPO, Lane 7/8/9: untreated with OAPO.

extract was obtained in this study, which proved that OAPO could kill *S. aureus*.

The integrity of the bacterial cell wall and membrane is vital for survival. Many antibiotics can inhibit bacterial growth and induce loss of cell homeostasis by altering or damaging the cell membrane structure (Turgis et al., 2009). Different degrees of OAPO-induced damage were observed in *S. aureus* using SEM, and the lysis effects of OAPO on the cell membrane were dose-dependent, which indicated that this damage in the cell wall and membrane was likely responsible for the observed growth inhibition and bactericidal effects. To further demonstrate the extent of OAPO-induced cell wall damage, the presence of AKP and nucleic acid substances in the supernatant of OAPO-treated *S. aureus* culture medium was used as an indicator of cell wall integrity. AKP is an enzyme located between the bacterial cell wall and cell membrane and, therefore, is undetectable when the bacterial structure is intact. Nevertheless, when the cell wall is damaged, AKP leaks out of the cell owing to an increased permeability (Tang et al., 2017). The present study showed that OAPO was more effective at elevating extracellular AKP levels at higher concentrations, which indicated that OAPO could increase the permeability of the cell wall, and damage to the integrity of the cell wall might be the main cause of AKP release into the supernatant. Moreover, nucleic acids are essential life substances in microorganisms and cannot permeate through the cell membrane during the normal growth of bacteria (Wu et al., 2016). The degree of leakage of nucleic acids from *S. aureus* cells treated with one-fold MIC and two-fold MIC of OAPO was significantly higher than that from untreated *S. aureus*, which suggested that OAPO might induce outer membrane damage in *S. aureus*, causing nucleic acids to leak out from the bacterial cells. Our results are consistent with those regarding the antibacterial activity of lactobionic acid against *S. aureus* by breaking down the structure of the bacterial cell wall and membrane (Cao et al., 2019).

Protein synthesis and energy metabolism are two other factors that affect bacterial survival. Soluble proteins are important osmotic pressure regulators of bacteria, which can improve the water retention capacity of bacteria and ensure their normal life activities (Nguyen et al., 2019). In this study, we determined the prevalence of intracellular biomacromolecules, such as total protein, ATPase, and glucose-6-phosphate dehydrogenase, in *S. aureus* treated with OAPO. The results of SDS-PAGE and BCA

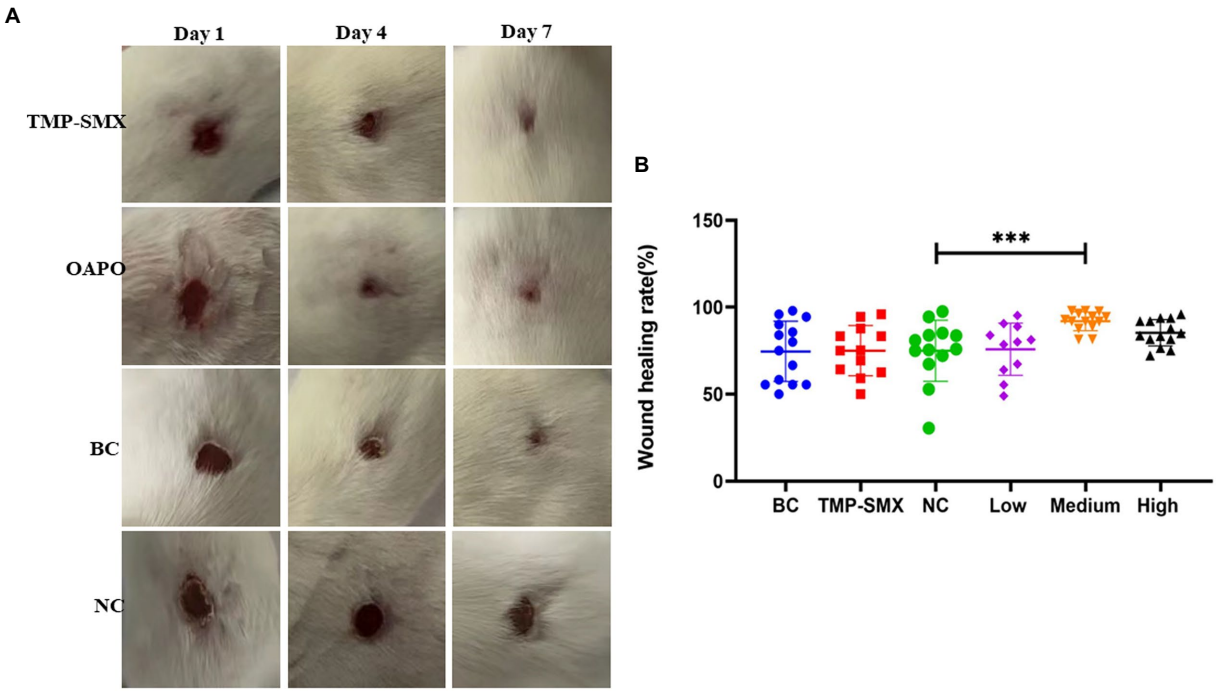

FIGURE 5
Effects of organic acid of *Portulaca oleracea* L. (OAPO) on skin wound recovery. **(A)** Skin wound healing appearance of mice on days 1, 4, and 7 post-inoculation with *Staphylococcus aureus* MRSA85. TMP-SMX: trimethoprim-sulfamethoxazole; OAPO: OAPO medium group; BC: blank group, uninfected, no drug; NC: infected without drug. **(B)** Scatter diagram of the healing rate of mice on day 7 post-inoculation with *S. aureus* MRSA85. ***indicates $p<0.001$ when compared with the negative control group (NC, infected without drug).

assays showed that the soluble protein levels of *S. aureus* were significantly elevated by OAPO, which indicated that interference with protein metabolism might not be the antibacterial mechanism of OAPO. Furthermore, OAPO did not affect intracellular ATPase and glucose-6-phosphate dehydrogenase content (data not shown), thereby indicating that OAPO could not inhibit ATPase activity and could not prevent ion transportation and nutrient absorption (Petrosyan et al., 2015).

To verify that OAPO has the same *S. aureus*-killing effects *in vivo* as it did *in vitro*, an animal model of wound infection with *S. aureus* mimicking clinical conditions was used in our study. The skin is the first line of defense against diseases, and skin wound infection is a useful animal model of *S. aureus* infection, characterized by a series of pathological changes, from local to systemic infection (Edwards and Harding, 2004; Gupta and Tyagi, 2021). Therefore, we used a skin wound infection model induced by *S. aureus* to evaluate the anti-infective effects of OAPO *in vivo*. The results demonstrate three aspects of the antibacterial activity of OAPO. First, OAPO could significantly promote skin wound healing compared with that by TMP-SMX; therefore, the skin histopathology of mice in the OAPO group was close to that of normal skin. It has long been reported that the crude extract of *P. oleracea* accelerates the wound healing process by decreasing the wound surface area and improving tensile strength (Rashed et al., 2003). Moreover, OAPO promotes wound healing better than homogenized plant material, indicating that organic acids might be the main active ingredients for improving wound injury. Second, the bacterial skin load in the OAPO group was significantly lower than that in the self-healing group, especially the bacterial load of the low-dosage group, which was significantly lower than that of the TMP-SMX group. Chan et al. reported that two fatty acids from *P. oleracea* exhibited synergistic effects with erythromycin in combating MRSA (Chan et al., 2015). Other organic acids from *P. oleracea*, such as protocatechuic and palmitic acids, also displayed effective bactericidal activity, which was in accordance with our results (Chao and Yin, 2009; Song et al., 2020). Third, the inflammatory responses induced by *S. aureus* were used to evaluate the anti-inflammatory effects of OAPO. The results demonstrated that OAPO exerted inhibitory effects on inflammatory cytokine expression, which was consistent with the results of previous studies on the anti-inflammatory activity of *P. oleracea* extracts (Rahimi et al., 2019; Moslemi et al., 2021).

5. Conclusion

To conclude, an extract of *Portulaca oleracea* was obtained in this study and it not only inhibits methicillin-resistant *S. aureus* activity *in vitro* but also inhibits *S. aureus*-induced skin damage

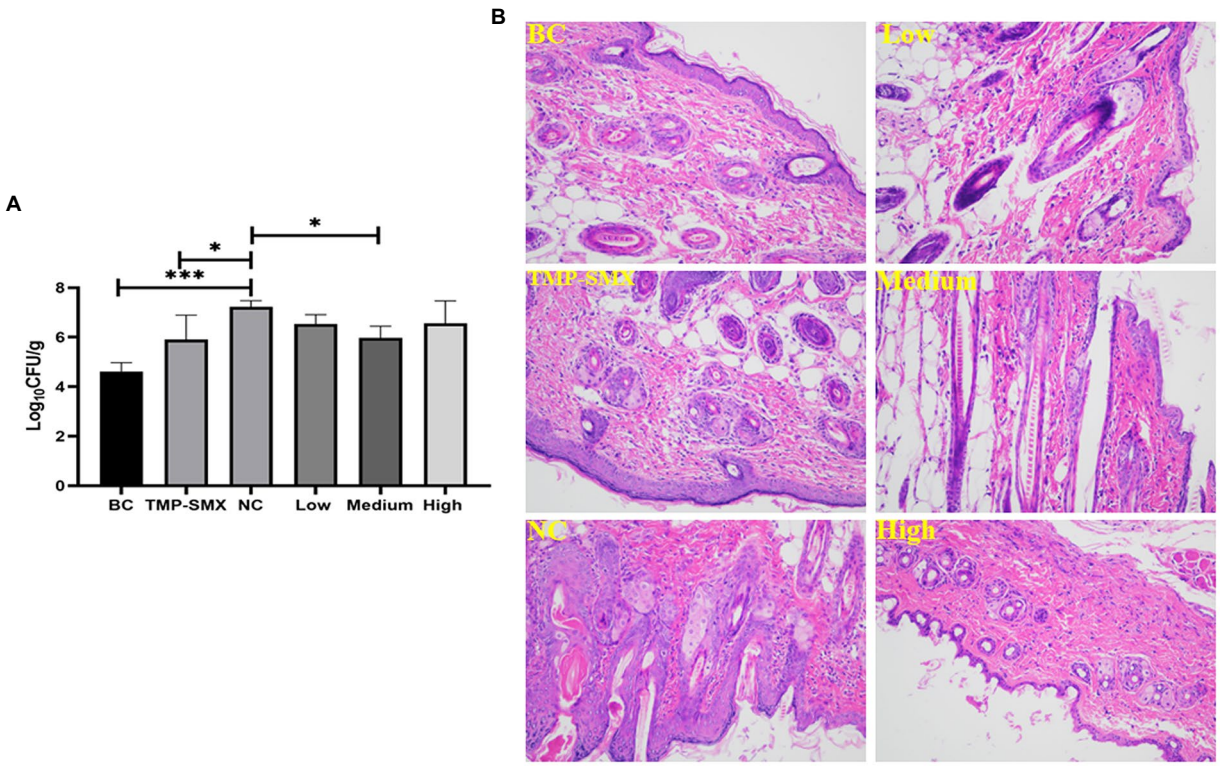

FIGURE 6
Effects of organic acid of *Portulaca oleracea* L. (OAPO) on skin wound bacterial load **(A)** and histopathology changes **(B)** on day 7 post-inoculation with *Staphylococcus aureus* MRSA85. *indicates $p<0.05$, ***indicates $p<0.001$. TMP-SMX: trimethoprim-sulfamethoxazole; BC: blank group, uninfected, no drug; NC: infected without the drug; low, medium and high means groups are given low, medium, and high dosages of OAPO, respectively.

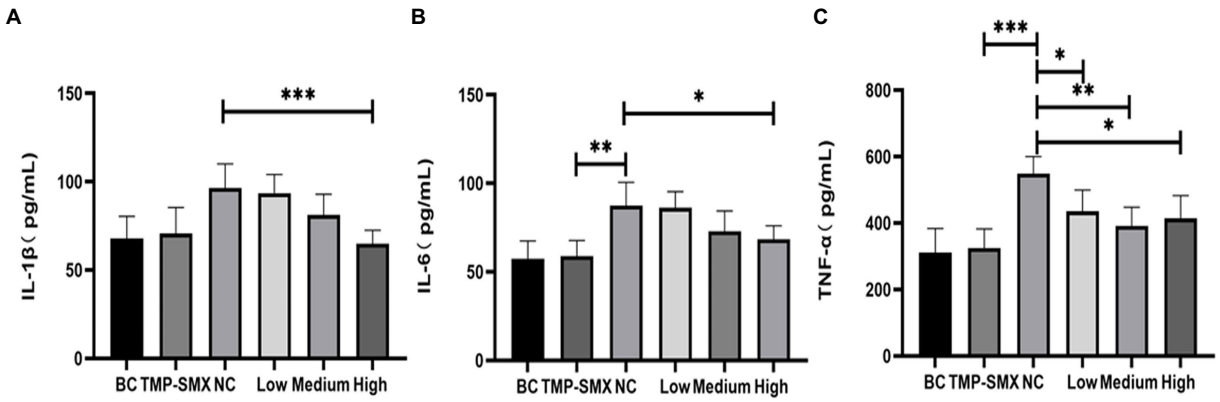

FIGURE 7
Determination of IL-1β **(A)**, IL-6 **(B)**, and TNF-α **(C)** in mice serum by enzyme-linked immunosorbent assay (ELISA). *indicates $p<0.05$, **indicates $p<0.01$, ***indicates $p<0.001$ when compared with the negative control group (NC, untreated with organic acid of *Portulaca oleracea* L. [OAPO]). TMP-SMX: trimethoprim-sulfamethoxazole; BC: blank group, uninfected, no drug; NC: infected without the drug; low, medium, and high means groups were given a low, medium, and high dosage of OAPO, respectively.

in a mouse model. The chemical compositions of the extract contain lots of organic acids, which indicates that OAPO is the main active compositions against MRSA. However, the purity and toxicity of the extracted organic acids was unknown, and which organic acid has stronger antibacterial activity needs to be explored soon.

Data availability statement

The original contributions presented in the study are included in the article/Supplementary material, further inquiries can be directed to the corresponding author.

Ethics statement

The animal study was reviewed and approved by the Animal Management and Ethics Committee of Guangxi University.

Author contributions

GL, HS, and CO conceived and designed this study. GL, AL, CZ, QZ, CY, HL, and HY participated in laboratory work. JM, ZZ, GL, and AL performed the data analysis and the writing of the manuscript. AL and CO participated in revising the manuscript critically. All authors contributed to the article and approved the submitted version.

Funding

This work was supported by scientific research startup funds of Guangxi University. We would like to thank Editage (www.editage.cn) for English language editing, Guangxi Science and Technology Base and Talent Special (2021AC19372) and TCM Industrial Pioneers (GuiNongKeMeng202211).

Acknowledgments

We thank the Wuhan Servicebio biological technology co., LTD (Wuhan, China) for providing scanning electron microscope services, Zhengzhou Biopple biological technology co., LTD (Zhengzhou, China) for making histopathological section.

Conflict of interest

The authors declare that the research was conducted in the absence of any commercial or financial relationships that could be construed as a potential conflict of interest.

Publisher's note

All claims expressed in this article are solely those of the authors and do not necessarily represent those of their affiliated organizations, or those of the publisher, the editors and the reviewers. Any product that may be evaluated in this article, or claim that may be made by its manufacturer, is not guaranteed or endorsed by the publisher.

Supplementary material

The Supplementary material for this article can be found online at: https://www.frontiersin.org/articles/10.3389/fmicb.2022.1076154/full#supplementary-material

References

Cao, J., Fu, H., Gao, L., and Zheng, Y. (2019). Antibacterial activity and mechanism of lactobionic acid against Staphylococcus aureus. *Folia Microbiol. (Praha)* 64, 899–906. doi: 10.1007/s12223-019-00705-3

Carneiro, M. A. M. S., Silva, L. D., Diniz, R. M., Saminez, W. F. D., de Oliveira, P. V., Mendonca, J. S. P., et al. (2021). Immunomodulatory and anti-infective effects of Cratylia mollis lectin (Cramoll) in a model of wound infection induced by Staphylococcus aureus. *Int. Immunopharmacol.* 100:108094. doi: 10.1016/j.intimp.2021.108094

Chan, B. C., Han, X. Q., Lui, S. L., Wong, C. W., Wang, T. B., Cheung, D. W., et al. (2015). Combating against methicillin-resistant Staphylococcus aureus - two fatty acids from purslane (Portulaca oleracea L.) exhibit synergistic effects with erythromycin. *J. Pharm. Pharmacol.* 67, 107–116. doi: 10.1111/jphp.12315

Chao, C. Y., and Yin, M. C. (2009). Antibacterial effects of roselle calyx extracts and protocatechuic acid in ground beef and apple juice. *Foodborne Pathog. Dis.* 6, 201–206. doi: 10.1089/fpd.2008.0187

da Silva, S. P., da Silva, J. D. F., da Costa, C. B. L., da Silva, P. M., de Freitas, A. F. S., da Silva, C. E. S., et al. (2021). Purification, characterization, and assessment of antimicrobial activity and toxicity of Portulaca elatior leaf lectin (PeLL). *Probiotics Antimicrob Proteins.* doi: 10.1007/s12602-021-09837-w

David, M. Z., and Daum, R. S. (2017). Treatment of Staphylococcus aureus infections. *Curr Top Microbiol* 409, 325–383. doi: 10.1007/82_2017_42

Desta, Z. Y., and Cherie, D. A. (2018). Determination of antioxidant and antimicrobial activities of the extracts of aerial parts of Portulaca quadrifida. *Chem. Cent. J.* 12:146. doi: 10.1186/s13065-018-0514-2

Edwards, R., and Harding, K. G. (2004). Bacteria and wound healing. *Curr. Opin. Infect. Dis.* 17, 91–96. doi: 10.1097/00001432-200404000-00004

Farkhondeh, T., and Samarghandian, S. (2019). The therapeutic effects of Portulaca oleracea L. in hepatogastric disorders. *Gastroenterol. Hepatol.* 42, 127–132. doi: 10.1016/j.gastrohep.2018.07.016

Fung, K. P., Han, Q. B., Ip, M., Yang, X. S., Lau, C. B., and Chan, B. C. (2017). Synergists from Portulaca oleracea with macrolides against methicillin-resistant Staphylococcus aureus and related mechanism. *Hong Kong Med. J.* 23, 38–42.

Guo, Y., Ramos, R. I., Cho, J. S., Donegan, N. P., Cheung, A. L., and Miller, L. S. (2013). In vivo bioluminescence imaging to evaluate systemic and topical antibiotics against community-acquired methicillin-resistant Staphylococcus aureus-infected skin wounds in mice. *Antimicrob Agents Ch* 57, 855–863. doi: 10.1128/AAC.01003-12

Gupta, V., and Tyagi, A. (2021). A rat model of polymicrobial infection in full-thickness excision wounds. *J. Tissue Viability* 30, 537–543. doi: 10.1016/j.jtv.2021.06.003

Hao, K. Y., Xu, B. C., Zhang, G. Y., Lv, F. F., Wang, Y. H., Ma, M. X., et al. (2021). Antibacterial activity and mechanism of Litsea cubeba L. essential oil against *Acinetobacter baumannii*. *Nat Prod Commun* 16, 1–7. doi: 10.1177/1934578X21999146

Hu, S., Chai, W. C., Xu, L., Li, S., Jin, C., Zhu, R., et al. (2021). Catecholic alkaloid sulfonates and aromatic nitro compounds from Portulaca oleracea and screening of their anti-inflammatory and anti-microbial activities. *Phytochemistry* 181:112587. doi: 10.1016/j.phytochem.2020.112587

Hu, W., Li, C. Z., Dai, J. M., Cui, H. Y., and Lin, L. (2019). Antibacterial activity and mechanism of Litsea cubeba essential oil against methicillin-resistant Staphylococcus aureus (MRSA). *Ind. Crop. Prod.* 130, 34–41. doi: 10.1016/j.indcrop.2018.12.078

Jiang, L., Yi, T., Shen, Z., Teng, Z., and Wang, J. (2019). Aloe-emodin attenuates Staphylococcus aureus pathogenicity by interfering with the oligomerization of alpha-toxin. *Front. Cell. Infect. Microbiol.* 9:157. doi: 10.3389/fcimb.2019.00157

Khazdair, M. R., Anaeigoudari, A., and Kianmehr, M. (2019). Anti-asthmatic effects of Portulaca Oleracea and its constituents, a review. *J Pharmacopuncture* 22, 122–130. doi: 10.3831/KPI.2019.22.016

Kim, M. S., Bang, J. H., Lee, J., Han, J. S., Kang, H. W., and Jeon, W. K. (2016). Fructus mume ethanol extract prevents inflammation and normalizes the Septohippocampal cholinergic system in a rat model of chronic cerebral Hypoperfusion. *J. Med. Food* 19, 196–204. doi: 10.1089/jmf.2015.3512

Kuok, C. F., Hoi, S. O., Hoi, C. F., Chan, C. H., Fong, I. H., Ngok, C. K., et al. (2017). Synergistic antibacterial effects of herbal extracts and antibiotics on methicillin-resistant Staphylococcus aureus: a computational and experimental study. *Exp. Biol. Med. (Maywood)* 242, 731–743. doi: 10.1177/1535370216689828

Lei, X., Li, J., Liu, B., Zhang, N., and Liu, H. (2015). Separation and identification of four new compounds with antibacterial activity from Portulaca oleracea L. *Molecules* 20, 16375–16387. doi: 10.3390/molecules200916375

Li, T., Wang, P. L., Guo, W. B., Huang, X. M., Tian, X. H., Wu, G. R., et al. (2019). Natural Berberine-based Chinese herb medicine assembled nanostructures with modified antibacterial application. *ACS Nano* 13, 6770–6781. doi: 10.1021/acsnano.9b01346

Liu, X., Wu, H., Tao, X., Ying, X., and Stien, D. (2021). Two amide glycosides from Portulaca oleracea L. and its bioactivities. *Nat. Prod. Res.* 35, 2655–2659. doi: 10.1080/14786419.2019.1660333

Lv, G. P., Jiang, R. P., Zhang, H., Wang, L., Li, L. J., Gao, W. L., et al. (2021). Molecular characteristics of Staphylococcus aureus from food samples and food poisoning outbreaks in Shijiazhuang, China. *Front Microbiol* 12:652276. doi: 10.3389/fmicb.2021.652276

Miller, L. G., Daum, R. S., Creech, C. B., Young, D., Downing, M. D., Eells, S. J., et al. (2015). Clindamycin versus trimethoprim-sulfamethoxazole for uncomplicated skin infections. *New Engl J Med* 372, 1093–1103. doi: 10.1056/NEJMoa1403789

Moslemi, Z., Bahrami, M., Hosseini, E., Mansourian, M., Daneshyar, Z., Eftekhari, M., et al. (2021). Portulaca oleracea methanolic extract attenuate bile duct ligation-induced acute liver injury through hepatoprotective and anti-inflammatory effects. *Heliyon* 7:e07604. doi: 10.1016/j.heliyon.2021.e07604

Nguyen, T., Kim, T., Ta, H. M., Yeo, W. S., Choi, J., Mizar, P., et al. (2019). Targeting mannitol metabolism as an alternative antimicrobial strategy based on the structure-function study of Mannitol-1-phosphate dehydrogenase in Staphylococcus aureus. *MBio* 10:660. doi: 10.1128/mBio.02660-18

Okuda, S., Wajima, T., Yamada, T., Nakaminami, H., Ikoshi, H., and Noguchi, N. (2021). In vitro growth-inhibitory effects of Portulaca oleracea L. formulation on intestinal pathogens. *Access Microbiol* 3:000208. doi: 10.1099/acmi.0.000208

Petrosyan, M., Shcherbakova, Y., Sahakyan, N., Vardanyan, Z., Poladyan, A., Popov, Y., et al. (2015). Alkanna orientalis (L.) Boiss. Plant isolated cultures and antimicrobial activity of their extracts: phenomenon, dependence on different factors and effects on some membrane-associated properties of bacteria. *Plant Cell Tiss Org* 122, 727–738. doi: 10.1007/s11240-015-0806-3

Rahimi, V. B., Rakhshandeh, H., Raucci, F., Buono, B., Shirazinia, R., Kermani, A. S., et al. (2019). Anti-inflammatory and anti-oxidant activity of Portulaca oleracea extract on LPS-induced rat lung injury. *Molecules* 24:139. doi: 10.3390/molecules24010139

Rashed, A. N., Afifi, F. U., and Disi, A. M. (2003). Simple evaluation of the wound healing activity of a crude extract of Portulaca oleracea L. (growing in Jordan) in Mus musculus JVI-1. *J. Ethnopharmacol.* 88, 131–136. doi: 10.1016/S0378-8741(03)00194-6

Scallan, E., Hoekstra, R. M., Angulo, F. J., Tauxe, R. V., Widdowson, M. A., Roy, S. L., et al. (2011). Foodborne illness acquired in the United States--major pathogens. *Emerg. Infect. Dis.* 17, 7–15. doi: 10.3201/eid1701.P11101

Simonetti, O., Lucarini, G., Orlando, F., Pierpaoli, E., Ghiselli, R., Provinciali, M., et al. (2017). Role of Daptomycin on burn wound healing in an animal methicillin-resistant Staphylococcus aureus infection model. *Antimicrob Agents Ch* 61:606. doi: 10.1128/AAC.00606-17

Soliman, S. S. M., Semreen, M. H., El-Keblawy, A. A., Abdullah, A., Uppuluri, P., and Ibrahim, A. S. (2017). Assessment of herbal drugs for promising anti-Candida activity. *BMC Complement. Altern. Med.* 17:257. doi: 10.1186/s12906-017-1760-x

Song, H. S., Choi, T. R., Bhatia, S. K., Lee, S. M., Park, S. L., Lee, H. S., et al. (2020). Combination therapy using low-concentration oxacillin with palmitic acid and Span85 to control clinical methicillin-resistant Staphylococcus aureus. *Antibiotics-Basel* 9:682. doi: 10.3390/antibiotics9100682

Tang, H., Chen, W., Dou, Z. M., Chen, R., Hu, Y., Chen, W., et al. (2017). Antimicrobial effect of black pepper petroleum ether extract for the morphology of listeria monocytogenes and salmonella typhimurium. *J. Food Sci. Technol.* 54, 2067–2076. doi: 10.1007/s13197-017-2644-2

Tleubayeva, M. I., Datkhayev, U. M., Alimzhanova, M., Ishmuratova, M. Y., Korotetskaya, N. V., Abdullabekova, R. M., et al. (2021). Component composition and antimicrobial activity of CO2 extract of Portulaca oleracea, growing in the territory of Kazakhstan. *ScientificWorldJournal* 2021:5434525. doi: 10.1155/2021/5434525

Turgis, M., Han, J., Caillet, S., and Lacroix, M. (2009). Antimicrobial activity of mustard essential oil against Escherichia coli O157:H7 and salmonella typhi. *Food Control* 20, 1073–1079. doi: 10.1016/j.foodcont.2009.02.001

Wang, B., Wei, P. W., Wan, S., Yao, Y., Song, C. R., Song, P. P., et al. (2021). Ginkgo biloba exocarp extracts inhibit S. aureus and MRSA by disrupting biofilms and affecting gene expression. *J. Ethnopharmacol.* 271:113895. doi: 10.1016/j.jep.2021.113895

Wicha, S. G., Kees, M. G., Kuss, J., and Kloft, C. (2015). Pharmacodynamic and response surface analysis of linezolid or vancomycin combined with meropenem against Staphylococcus aureus. *Pharm. Res.* 32, 2410–2418. doi: 10.1007/s11095-015-1632-3

Wu, Y., Bai, J., Zhong, K., Huang, Y., Qi, H., Jiang, Y., et al. (2016). Antibacterial activity and membrane-disruptive mechanism of 3-p-trans-Coumaroyl-2-hydroxyquinic acid, a novel phenolic compound from pine needles of Cedrus deodara, against Staphylococcus aureus. *Molecules* 21:1084. doi: 10.3390/molecules21081084

Wu, S., Liu, Y., Zhang, H., and Lei, L. (2019). The pathogenicity and transcriptome analysis of methicillin-resistant Staphylococcus aureus in response to water extract of Galla chinensis. *Evid. Based Complement. Alternat. Med.* 2019:3276156. doi: 10.1155/2019/3276156

Yan, X. M., Wang, B., Tao, X. X., Hu, Q. H., Cui, Z. G., Zhang, J. Z., et al. (2012). Characterization of Staphylococcus aureus strains associated with food poisoning in Shenzhen, China. *Appl Environ Microb* 78, 6637–6642. doi: 10.1128/AEM.01165-12

Yang, Y., Chen, Y., Zhang, G., Sun, J., Guo, L., Jiang, M., et al. (2020). Transcriptomic analysis of Staphylococcus aureus under the stress condition caused by Litsea cubeba L. essential oil via RNA sequencing. *Front Microbiol* 11:1693. doi: 10.3389/fmicb.2020.01693

Zhang, H., HuangFu, H., Wang, X., Zhao, S., Liu, Y., Lv, H., et al. (2021). Antibacterial activity of lactic acid producing Leuconostoc mesenteroides QZ1178 against pathogenic Gallibacterium anatis. *Front Vet Sci* 8:630294. doi: 10.3389/fvets.2021.630294

Zhang, Y. B., Liu, X. Y., Wang, Y. F., Jiang, P. P., and Quek, S. (2016). Antibacterial activity and mechanism of cinnamon essential oil against Escherichia coli and Staphylococcus aureus. *Food Control* 59, 282–289. doi: 10.1016/j.foodcont.2015.05.032

Zhang, B., Teng, Z. H., Li, X. H., Lu, G. J., Deng, X. M., Niu, X. D., et al. (2017). Chalcone attenuates Staphylococcus aureus virulence by targeting Sortase a and alpha-Hemolysin. *Front. Microbiol.* 8:1715. doi: 10.3389/fmicb.2017.01715

Zhang, J. M., Xu, F. H., Yao, L. L., Wang, L. Y., Wang, M., and Wang, G. (2020). Ethanol extract of Campsis grandiflora flower and its organic acid components have inhibitory effects on autoinducer type 1 quorum sensing. *Molecules* 25:4727. doi: 10.3390/molecules25204727

Zheng, H. F., Liu, Y., Cai, J., Zhang, M., Wen, Y., and Guo, L. (2022). The exploration of anti-Vibrio parahaemolyticus substances from Phellodendri Chinensis cortex as a preservative for shrimp storage. *Front. Microbiol.* 13:4262. doi: 10.3389/fmicb.2022.1004262

Zhou, K. X., Li, C., Chen, D. M., Pan, Y. H., Tao, Y. F., Qu, W., et al. (2018). A review on nanosystems as an effective approach against infections of Staphylococcus aureus. *Int. J. Nanomedicine* 13, 7333–7347. doi: 10.2147/IJN.S169935

Zhou, Y. X., Xin, H. L., Rahman, K., Wang, S. J., Peng, C., and Zhang, H. (2015). Portulaca oleracea L.: a review of phytochemistry and pharmacological effects. *Biomed. Res. Int.* 2015:925631. doi: 10.1155/2015/925631

frontiers | Frontiers in Microbiology

TYPE Original Research
PUBLISHED 25 January 2023
DOI 10.3389/fmicb.2023.1094929

OPEN ACCESS

EDITED BY
Leon G. Leanse,
Harvard Medical School,
United States

REVIEWED BY
Silke Niemann,
University Hospital Münster,
Germany
Adam Graham Stewart,
The University of Queensland, Australia

*CORRESPONDENCE
María Collantes
✉ mcollant@unav.es

†These authors have contributed equally to this work

SPECIALTY SECTION
This article was submitted to Infectious Agents and Disease, a section of the journal Frontiers in Microbiology

RECEIVED 10 November 2022
ACCEPTED 04 January 2023
PUBLISHED 25 January 2023

CITATION
Rua M, Simón JA, Collantes M, Ecay M, Leiva J, Carmona-Torre F, Ramos R, Pareja F, Pulagam KR, Llop J, Del Pozo JL and Peñuelas I (2023) Infection-specific PET imaging with ^{18}F-fluorodeoxysorbitol and 2-[^{18}F]F-ρ-aminobenzoic acid: An extended diagnostic tool for bacterial and fungal diseases.
Front. Microbiol. 14:1094929.
doi: 10.3389/fmicb.2023.1094929

Infection-specific PET imaging with ^{18}F-fluorodeoxysorbitol and 2-[^{18}F]F-ρ-aminobenzoic acid: An extended diagnostic tool for bacterial and fungal diseases

Marta Rua[1,2†], Jon Ander Simón[3†], María Collantes[2,4*], Margarita Ecay[4], José Leiva[1,2], Francisco Carmona-Torre[2,5], Rocío Ramos[3], Félix Pareja[3], Krishna R. Pulagam[6], Jordi Llop[6], José Luis Del Pozo[1,2,5] and Iván Peñuelas[2,3,4]

[1]Clinical Microbiology Laboratory, Clínica Universidad de Navarra, Pamplona, Spain, [2]Instituto de Investigación Sanitaria de Navarra (IdiSNA), Pamplona, Spain, [3]Radiopharmacy Unit, Department of Nuclear Medicine, Clinica Universidad de Navarra, Pamplona, Spain, [4]Translational Molecular Imaging Unit, Department of Nuclear Medicine, Clinica Universidad de Navarra, Pamplona, Spain, [5]Infectious Diseases Division, Clínica Universidad de Navarra, Pamplona, Spain, [6]Basque Research and Technology Alliance (BRTA), CIC BiomaGUNE, San Sebastián, Spain

Introduction: Suspected infectious diseases located in difficult-to-access sites can be challenging due to the need for invasive procedures to isolate the etiological agent. Positron emission tomography (PET) is a non-invasive imaging technology that can help locate the infection site. The most widely used radiotracer for PET imaging (2-deoxy-2[^{18}F] fluoro-D-glucose: [^{18}F]FDG) shows uptake in both infected and sterile inflammation. Therefore, there is a need to develop new radiotracers able to specifically detect microorganisms.

Methods: We tested two specific radiotracers: 2-deoxy-2-[^{18}F]-fluoro-D-sorbitol ([^{18}F]FDS) and 2-[^{18}F]F-ρ-aminobenzoic acid ([^{18}F]FPABA), and also developed a simplified alternative of the latter for automated synthesis. Clinical and reference isolates of bacterial and yeast species (19 different strains in all) were tested *in vitro* and in an experimental mouse model of myositis infection.

Results and discussion: Non-lactose fermenters (*Pseudomonas aeruginosa* and *Stenotrophomonas maltophilia*) were unable to take up [^{18}F]FDG *in vitro*. [^{18}F]FDS PET was able to visualize Enterobacterales myositis infection (i.e., Escherichia coli) and to differentiate between yeasts with differential assimilation of sorbitol (i.e., *Candida albicans* vs. *Candida glabrata*). All bacteria and yeasts tested were detected *in vitro* by [^{18}F]FPABA. Furthermore, [^{18}F]FPABA was able to distinguish between inflammation and infection in the myositis mouse model (*E. coli* and *Staphylococcus aureus*) and could be used as a probe for a wide variety of bacterial and fungal species.

KEYWORDS

FDG (18F-fluorodeoxyglucose)-PET/CT, PABA para-aminobenzoic acid, 18[F]FDS, 18[F] FPABA, mouse model, PET imaging, sorbitol, folate

1. Introduction

Infectious diseases have become a major problem, with an increasing incidence, pandemic scenarios, and the spread of antibiotic resistance (Morens and Fauci, 2020). Diagnosis is usually based on clinical signs and symptoms, laboratory analyses, microbiological tests, and imaging tools. Conventionally, the main laboratory techniques used to identify bacteria and fungi are culture methods, which are accurate but very time consuming and can take several days or even weeks. Furthermore, culture methods sometimes require invasive sampling procedures that can involve risks at the time of collection.

[^{18}F]FDG is a PET radiotracer that is widely used in the diagnosis and follow-up of tumors and degenerative diseases of the central nervous system (Dubois et al., 2014; Rowe and Pomper, 2021; Guedj et al., 2022). Conventional *in vivo* nuclear imaging using radiolabeled monocytes (Chakfé et al., 2020; Erba and Slart, 2020) or positron emission tomography (PET) with 2-deoxy-2[^{18}F]fluoro-D-glucose ([^{18}F]FDG) can provide a rapid diagnosis of difficult-to-diagnose infections (endocarditis, vascular graft infection, and prosthetic joint infection) and at the same time avoid invasive sampling procedures (Kwee et al., 2008; Habib et al., 2015; Mahmood et al., 2019; Haidar and Singh, 2022; Lauri et al., 2022). [^{18}F]FDG is an extensively available radiotracer that can be obtained from a cyclotron center and shipped to the hospital because of the long half-life of ^{18}F (110 min). However, nonspecific uptake at sterile inflammation sites and the inability to differentiate between different microorganisms can however yield ambiguous results (Auletta et al., 2019).

The narrative evidence has expressed the need for PET tracers to be able to selectively detect microorganisms. 2-deoxy-2-[^{18}F]-fluoro-D-sorbitol ([^{18}F]FDS) is a fluorinated probe that specifically detects Enterobacterales (Weinstein et al., 2014; Yao et al., 2016; Ordonez et al., 2021), although infectious diseases caused by Gram-positive bacteria and fungi may be underdiagnosed. [^{18}F]FDS is a fluorine-18 analog of sorbitol that is easy to synthesize from [^{18}F]FDG. The first study conducted with [^{18}F]FDS focused on molecular imaging of brain tumors (Li et al., 2008). However, the active sorbitol transporter (the PTS = phosphoenolpyruvate:glycose phosphotransferase system) and metabolism are specific to certain GN bacilli (i.e., Enterobacterales). Sorbitol is a sugar that requires PTS-mediated uptake into the bacterial cell (Cordaro, 1976). Phosphorylation prevents the [^{18}F]FDS from escaping, and so the probe accumulates within the cell. The PTS is essential for bacterial uptake of [^{18}F]FDS, but not for [^{18}F]FDG (Ordonez et al., 2021). This transporter specificity defines the sorbitol-analog as a class-specific bacterial probe.

In an analysis to find pathogen-specific imaging tracers, para-aminobenzoic acid (PABA) derivatives were identified as potentially suitable tracers for all bacteria (Ordonez et al., 2017). The folate pathway is a key component in DNA and amino acid biosynthesis. Folate biosynthesis is essential in bacteria, yeasts, protozoa, and plants. By contrast, mammalian cells are unable to carry out *de novo* synthesis using this pathway and so need to acquire folate in the diet. PABA is the substrate for an essential enzyme [dihydropteroate synthase (DHPS)] in this process. DHPS catalyzes PABA and a pterin pyrophosphate to produce dihydropteroate (Bermingham and Derrick, 2002). Previous studies have concluded that the fluorinated probe of PABA is an alternative substrate for *Staphylococcus aureus* DHPS that rapidly accumulates in the bacteria (Zhang et al., 2018). Fluorine-18 labeled tracer, 2-[^{18}F]F-ρ-aminobenzoic acid ([^{18}F]FPABA), was used to detect *S. aureus* myositis infection and monitor the efficacy of antibiotic treatment in a rat model of myositis (Zhang et al., 2018). [^{11}C]PABA was tested in human volunteers with no adverse effects (Ordonez et al., 2022), although one of the drawbacks of carbon-11 is the extremely short half-life for radionuclide decay (20.4 min) which would rule out the distribution of [^{11}C]PABA over long periods of time. In addition, metabolism of the carbon-11 moiety could also lead to image distortions, or even require plasma metabolism analysis, an additional challenge for carbon-11-labeled tracers. For these reasons, [^{18}F]FPABA could be a better choice for the development of PET infection radiotracers.

Molecular imaging tracers are mainly developed and tested only for bacterial infections. Fungal infections are rarely considered, although they represent potentially life-threatening opportunistic diseases in certain patients (such as the critically ill and/or immunosuppressed). Invasive fungal infections (IFIs) caused by *Candida* spp. are a leading cause of infection in patients with underlying hematopoietic stem cell transplantation indications, solid organ transplant recipients, and the critically ill (Jenks et al., 2020). Disseminated candidiasis may involve the central nervous system (CNS; Góralska et al., 2018), and [^{18}F]FDG PET imaging reveals high glucose metabolism in the CNS, making diagnosis challenging. In another study, [^{18}F]FDG PET/CT was of added value as a diagnostic tool for IFIs in the management of 74% of patients (Ankrah et al., 2021). Another clinically relevant fungus (*Aspergillus fumigatus*) was evaluated with [^{18}F]FDS without investigators supporting its use (Lai et al., 2022). However, the most recent study on [^{18}F]FDS uptake in *Aspergillus fumigatus in vivo*, in a mouse model, indicated that visualization of infection in the lungs, brain and muscles was possible (Kim et al., 2022). No preclinical studies or experimental animal models have evaluated PABA-labeled radiotracers in yeast or filamentous fungi.

In this study, we tested the *in vitro* uptake of [^{18}F]FPABA, [^{18}F]FDS, and [^{18}F]FDG in multiple species of bacteria and yeast obtained from reference (American Type Culture Collection: ATCC) and clinical isolates (prosthetic infections). We also compared the *in vivo* uptake of these radiotracers in an acute myositis model with representative Gram-positive (GP) and Gram-negative (GN) bacteria. Given that the currently available [^{18}F]FPABA radiotracers are complex and cumbersome, we also aimed to develop a simplified alternative for automated synthesis of this radiotracer that would make it more widely available, using standardized procedures amenable to Good Manufacturing Practices (GMP) compliance. This approach brings innovative, pathogen-specific imaging tracers closer to clinical settings and tests the actual diagnostic use of [^{18}F]FDG by analyzing multiple bacterial species.

2. Materials and methods

2.1. Synthesis of [^{18}F]FDG, [^{18}F]FDS, and [^{18}F]FPABA

Synthesis of [^{18}F]FDG was by standard nucleophilic substitution using an IBA Synthera module (IBA, Louvaine-la-Neuve, Belgium). [^{18}F]FDS was synthesized following previously described methods, with some modifications (Weinstein et al., 2014; Li et al., 2017). Briefly, [^{18}F]FDG was reduced with 2 mg sodium borohydride at 35°C for 30 min with periodic shaking, the reaction was stopped by the addition of 1.4 ml of a sodium acetate/HCl solution (0.9/0.4 M), and the final pH was adjusted to 7 with NaOH. The final product was purified using an Alumina N Light Sep-Pack cartridge and sterile filtered (0.22 μm). Radiochemical purity was >97%, as determined by radio-thin layer chromatography (radio-TLC).

The available synthesis methods of [^{18}F]FPABA (Zhang et al., 2018; Li et al., 2020) are complex and require a precursor that is difficult to

prepare. Consequently, we prepared a new precursor [methyl 4-*N*,*N*-di(Boc)-2-nitro-4-aminobenzoate **(2)**] from a commercially available reagent to enable a one-step nucleophilic substitution synthesis in an automated synthesis module (Figure 1). To a solution of methyl 2-nitro-4-aminobenzoate **(1)** (0.25 g, 34 mmol) and di-tert-butyl dicarbonate (7.4 g, 68 mmol) in methylene chloride (10 ml), cooled with ice water, was added one equivalent of 4-(dimethylamino)pyridine. After stirring for 30 min at room temperature (RT), the mixture was diluted with an additional 50 ml of methylene chloride, washed with brine, and dried over $MgSO_4$. Removal of the solvent gave 370 mg of the crude product, which was purified by silica gel column chromatography using CH_2Cl_2/methanol (95/5) as eluent to yield 290 mg (58%) of **2** as a white solid. For the radiosynthesis, $[^{18}F]F^-$ produced by irradiation of $H_2{}^{18}O$ in a 18/9 cyclotron (IBA, Belgium) was trapped on a QMA cartridge and eluted with 0.5 ml of K_2CO_3/Kryptofix 2.2.2. After azeotropic drying, 2 mg of precursor **2** was added to the reactor in 1 ml *N*, *N*-Dimethylformamide, heated to 150°C for 20 min, hydrolyzed at 110°C for 10 min with 0.5 ml of 5 M NaOH, and then cooled to 40°C and neutralized with 1.5 ml of 1.7 M HCl. The crude product was purified by radio-HPLC using a VP 250/16 Nucleosil 100–7 C18 column, and 90/10 trifluoroacetic acid (TFA) 0.1% in H_2O/MeCN as the mobile phase. $[^{18}F]$FPABA (eluted at 9–10 min) was collected in 40 ml of water, reformulated by trapping on a MCXplus cartridge, and eluted with 2 ml of ethanol/NaOH 1 M (50/50) into a citrate buffer solution to a final volume of 5 ml. All radiosynthesis steps took place in an automated synthesis module (AiO36, Trasis, Belgium), for which a specific program and user interface (Figure 2) were developed.

Radiochemical purity was determined by HPLC on a Mediterranea Sea C18 (150 × 4.6) column with a 0.1% TFA/MeCN gradient at 1 ml/min. $[^{18}F]$FPABA was eluted at 5.7 min, whereas the free $[^{18}F]F^-$ was eluted at 2 min.

2.2. *In vitro* uptake assays

The following bacterial and fungal reference strains (ATCC) were used: *Staphylococcus epidermidis* ATCC 12228 and ATCC 35984, *S. aureus* ATCC 29213 and 25923, *Cutibacterium acnes* ATCC 11827, *Escherichia coli* ATCC 25922, and *Pseudomonas aeruginosa* ATCC 27853 and *Candida albicans* ATCC 10231. Selected clinical isolates from patients with prosthetic material were also included (Supplementary Table S1).

All microorganisms, except *C. acnes*, were cultured the night before on solid agar, followed by 20–24 h of culture in tryptic soy broth (TSB, bioMérieux) at 37°C under constant agitation. *Cutibacterium acnes* was cultured for 48 h on solid agar, then for another 48 h in thioglycolate broth (TG, bioMérieux) under anaerobic conditions. Broth medium was selected to achieve better tracer uptake compared to a solid media. In addition, a prolonged incubation time was set to allow the microorganisms to consume most of the D-glucose.

The next day, the incubation broth was diluted in 4 ml 0.9% NaCl and adjusted with more incubation broth or saline until an optical density of 0.75 McFarland units was reached. Dilution in saline was chosen to reduce the amount of D-glucose in case any traces remained that might be available and compete with the carbohydrate tracers ($[^{18}F]$FDG and $[^{18}F]$FDS). Three replicates (500 µl) of each microorganism were incubated with radiotracers (100 µl, 37 ± 11 MBq/ml) for 2 h under agitation, pelleted by centrifugation, and washed with PBS. Final radioactivity in all pellets was measured using a gamma counter (Hidex Automatic Gamma Counter) calibrated for fluorine-18 and normalized to the initial number of colonies (Bq/10^6 CFU: colony-forming units). Aliquots of *E. coli* ATCC 25922 with the same optical density were used as negative control after inactivation at 90°C for 30 min. Counts per minute were corrected for background and decay. The experiment was repeated three times on each strain in three independent experiments, using triplicate of PBS as background.

The number of viable microorganisms was quantified at the beginning and end of each experiment. CFU per ml (CFU/ml) values were determined by dilutions and plating on trypticase soy agar (TSA) under optimal growth conditions depending on the microorganism. Initial CFUs were measured to normalize to activity (Bq/10^6 CFU) and as a control. The number of colonies in the final pellet was measured to monitor the growth of the microorganisms.

2.3. Mouse myositis infection model

All procedures involving animals were carried out in accordance with the guidelines of the European Communities Council Directive (2010/63/EU) and the Spanish Government (RD 53/2013) and were approved by the Animal Experimentation Ethics Committee of the University of Navarra (Protocol no. 103-17). Four-week-old male and female ICR mice ($n = 42$; males = 16 and females = 26) were purchased from Envigo and socially housed in the animal facilities of the University

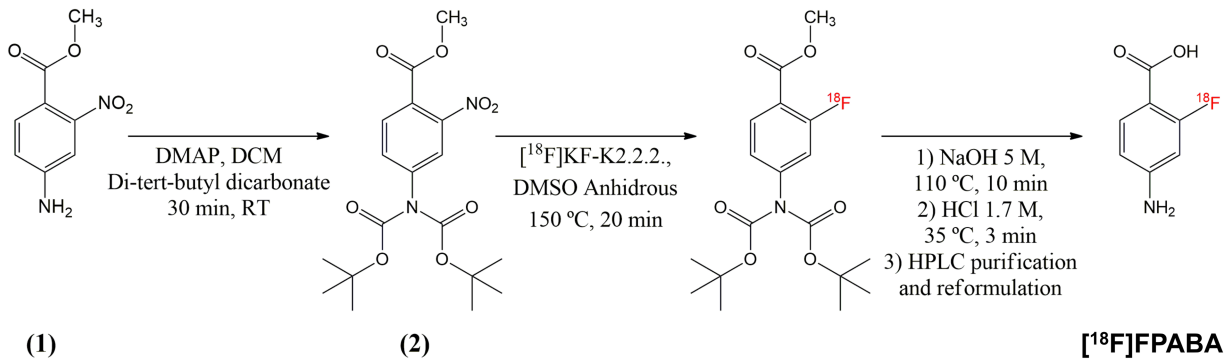

FIGURE 1
Synthesis pathway of $[^{18}F]$FPABA from commercially available methyl 2-nitro-4-aminobenzoate. Compound **(2)** was used as the precursor for the automated radioactive synthesis.

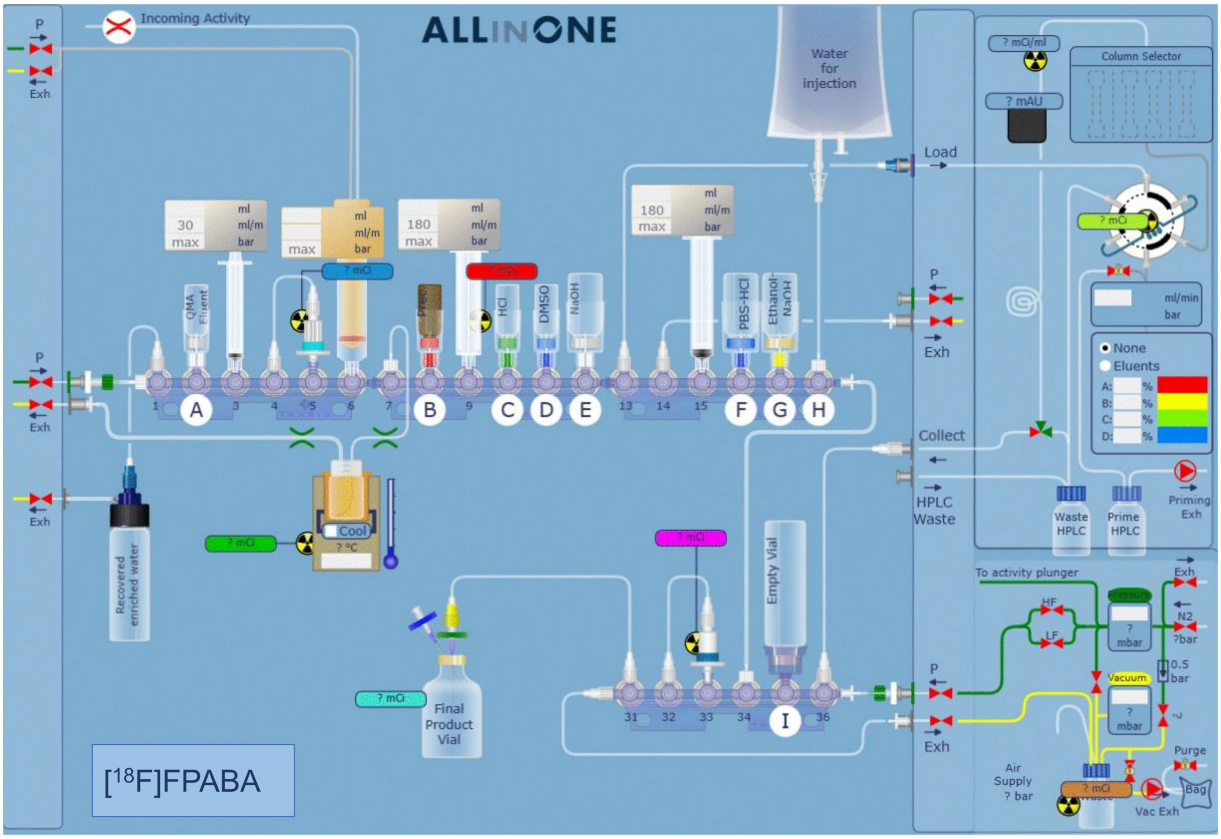

FIGURE 2
Automated synthesis software interface showing the position of the different reagents and systems used for the synthesis. The various steps of the synthesis are described in detail in the methodology section.

of Navarra under controlled conditions (22 ± 2°C, 12-h light/12-h dark cycle; relative humidity 55 ± 10%).

Staphylococcus aureus ATCC 29213 and *E. coli* ATCC 25922 were selected as representative GP and GN bacteria to develop the mouse model of acute myositis.

Fresh bacterial strains were incubated in TSB broth overnight. Inoculated bacteria were diluted and incubated for an extra hour to obtain exponential growth. Bacterial load was adjusted to 7–8 $\log_{10}$ CFU. 50 µl of live bacteria were injected into the right hindlimb of the animals; the same volume of heat-inactivated inoculum (90°C, 30 min) was injected into the left hindlimb to simulate sterile inflammation. The mice were imaged with [^{18}F]FDG, [^{18}F]FDS, or [^{18}F]FPABA 16 to 18 h after the initial infection for comparison.

2.3.1. PET/CT imaging

All PET images were acquired on a dedicated small animal Mosaic tomograph (Philips) and reconstructed, applying dead time, decay, random, and scatter corrections, into a 128 × 128 matrix with voxel size of 1 mm. Computed tomography (CT) scans were also performed in U-SPECT6/E-class (MILabs) imaging equipment to obtain the corresponding anatomical images, using a tube setting of 55 kV and 0.33 mA.

For PET imaging, the mice were fasted overnight with *ad libitum* access to drinking water. On the day of the study, radiotracer was injected intravenously *via* a tail vein ([^{18}F]FDG: 9.2 ± 0.2 MBq; [^{18}F]FDS: 9.3 ± 1.1 MBq; [^{18}F]FPABA: 13.5 ± 5.2 MBq). The mice were kept anesthetized with 2% isoflurane in 100% O_2 gas after administration of the radiotracer. One hour after injection of [^{18}F]FDG or [^{18}F]FPABA (2 h for [^{18}F]FDS), the animals were placed prone on the scanner bed for a 15-min image acquisition. Twenty minutes beforehand, the animals received an intravenous injection of 100 µl furosemide (10 mg/ml) and 1.5 ml of subcutaneous saline solution (0.9%).

All studies were exported and analyzed using PMOD software v 4.105 (PMOD Technologies Ltd., Adliswil, Switzerland) and converted into standardized uptake value (SUV) units using the formula SUV = [tissue activity concentration (Bq/cm^3)/injected dose (Bq)] × body weight (g). The PET images were registered with their corresponding CT scans to localize the uptake signal. A semi-quantitative analysis was performed by manually drawing volumes of interest (VOI) containing signal at the site of infection or inflammation. After obtaining the mean uptake value in each VOI, the ratio of values for infected or inflamed hindlimbs was calculated (SUVr).

2.3.2. *Post-mortem* measurement of radioactivity uptake and microbiological analysis of hindlimbs

After euthanasia, the infected and inflamed limb muscles were harvested and weighed. The ^{18}F radioactivity of each sample was measured with a gamma-counter. ^{18}F uptake in infected and inflamed hindlimbs was presented as percentage of injected dose per gram of tissue (%ID/g).

Colony-forming units were quantified by homogenization in PBS and growth on TSA medium using dilutions, and in BHI broth (brain heart infusion) incubated at 37°C with 10% CO_2 for at least 2 days. The concentration of bacteria was measured as CFU/g of muscle.

2.4. Statistical analysis

For data analysis, the Mann–Whitney U test was used to compare two groups, and the Kruskal Wallis test for multigroup comparison. Multigroup mean comparisons of *in vitro* growth at the beginning and the end of experiments (CFU/g) were analyzed with Sidak's test. Data are shown as mean ± SD.

3. Results

3.1. [^{18}F]FDS synthesis and automated [^{18}F]FPABA synthesis

The [^{18}F]FDS synthesis procedure yielded a high purity product (>97%) over 20 different syntheses. The most suitable TLC chromatography method for analysis was the one used for [^{18}F]FDG following European Pharmacopeia instructions (01/2014:1325). The final product always appeared as a sharp peak at a retention factor (Rf) of 0.15–0.20, while the precursor appeared at over 0.5. We checked that the final pH of the formulation was 7.0 ± 0.5 and adjusted with the corresponding acid or base if necessary.

The precursor, methyl 4-*N*,N-di(Boc)-2-nitro-4-aminobenzoate (used for radiosynthesis of [^{18}F]FPABA), was prepared in a one-step reaction with an average yield of 58%. The implementation of radiosynthesis in the automated system (TRASIS AllinOne 36 module) proved to be reliable, reproducible, and amenable to GMP implementation. Overall, radiosynthesis took less than 80 min (including radio-HPLC purification and reformulation) and [^{18}F]FPABA was produced with a radiochemical yield of 6% (final activities were in the range of 1.3–1.8 GBq in 4 ml) and > 95% radiochemical purity, as assessed by radio-HPLC (Supplementary Figure S2). [^{18}F]FPABA obtained a specific activity of 395.53 ± 189.07 GBq/μmol at the end of synthesis. The injectable solution of [^{18}F]FPABA had a pH of 6, contained 10% ethanol as a stabilizing agent and was stable for at least 8 h as determined by radio-HPLC.

3.2. *In vitro* uptake by reference and clinical strains

All bacteria except *Pseudomonas aeruginosa* and *Stenotrophomonas maltophilia* incorporated [^{18}F]FDG (Figure 3A). [^{18}F]FDG uptake in GP bacteria was higher than in GN bacteria. Among Gram-positives, *Streptococcus agalactiae* obtained the highest uptake. All yeasts tested, *C. albicans* ATCC 10231 and clinical strain (CS 2502) accumulated much more [^{18}F]FDG than bacteria.

Enterobacterales (i.e., *E. coli* and *Enterobacter*) was the only group of bacteria that accumulated [^{18}F]FDS (Figure 3B). The uptake values of [^{18}F]FDS were at least three times lower than those of [^{18}F]FDG, for example, in the reference bacteria *E. coli* ATCC 25922 ([^{18}F]FDG = 605.28 ± 91.91 Bq/10^6 CFU and [^{18}F]FDS = 160.23 ± 71.76 Bq/10^6 CFU).

All bacteria and yeasts accumulated [^{18}F]FPABA (Figure 3C). There were no clear differences between GPs, GNs, yeasts, and the microaerophilic GP, *C. acnes*. The two highest accumulations were obtained in *S. aureus* CS 16557 and *E. coli* ATCC 25922. Comparison of different strains of the same species of *S. aureus* showed large differences (*S. aureus* CS 3082 = 954.29 ± 568.26 Bq/10^6 CFU and *S. aureus* CS MR-methicillin resistant 16557 = 5,192 ± 1334.49 Bq/10^6 CFU). Regardless of their type, the heat-killed bacteria showed virtually no uptake of the radiotracers (Figure 3).

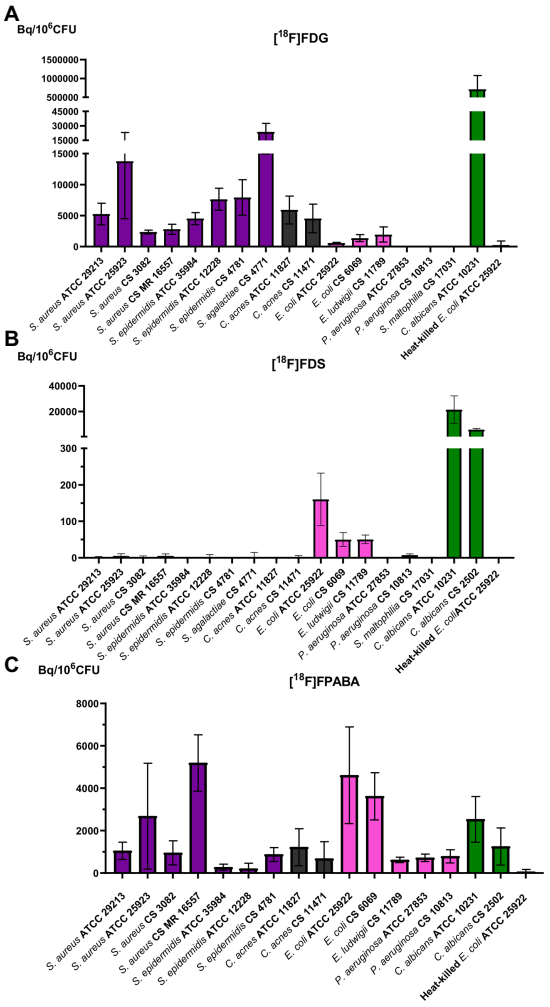

FIGURE 3
Cellular uptake of different probes tested after 2h of accumulation. Purple: Gram-positive bacteria. Gray: *Cutibacterium acnes*. Pink: Gram-negative bacteria. Green: yeasts. CS: clinical strain. **(A)** [^{18}F]FDG; **(B)** [^{18}F]FDS; and **(C)** [^{18}F]FPABA.

Only some yeast species accumulated [^{18}F]FDS. Clinical and reference isolates of *C. albicans* took up the radiotracer, whereas *C. glabrata* did not (Figure 4A). *Candida albicans* showed more accumulation of radiolabeled monosaccharides ([^{18}F]FDG and [^{18}F]FDS) than bacteria. In contrast, [^{18}F]FPABA accumulation was higher in *E. coli* than in fungi (Figure 4B). Interestingly, [^{18}F]FPABA was the only radiotracer that was taken up by *P. aeruginosa* (Figure 4C).

The variation in the initial and final number of viable cells (CFU/ml) is shown in Supplementary Table S3. We found no relevant variation for most of the microorganisms. However, [^{18}F]FDG resulted in a significant decrease in the growth of *C. acnes* ($p \leq 0.0001$). In addition, *C. acnes* ATCC 11827, *P. aeruginosa* and *S. agalactiae* showed a non-statistically significant decrease in growth with [^{18}F]FDG. Incubation with [^{18}F]FDS induced a statistically significant reduction of CFU/mL in *S. agalactiae*, *C. acnes*, and *P. aeruginosa*. Only *E. coli* growth appeared to increase with incubation with [^{18}F]FDS ($p = 0.0229$). [^{18}F]FPABA did not change the number of bacteria or yeast

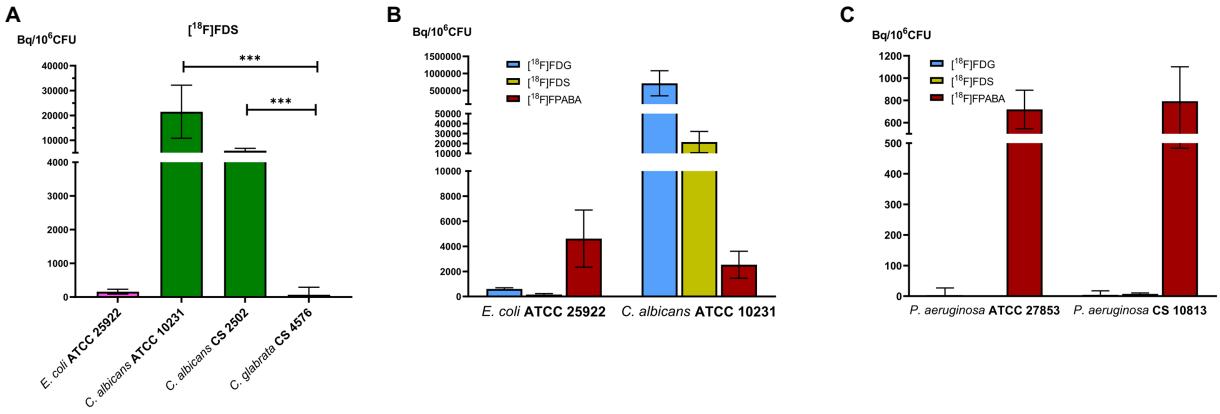

FIGURE 4
Comparison of prokaryotic and eukaryotic cells. *In vitro* experiments with *Pseudomonas aeruginosa*. **(A)** Comparison of [18F]FDS uptake in *Candida* species. ***$p \leq 0.001$; **(B)** Cellular uptake of reference strains of bacteria and yeast by [18F]FDG, [18F]FDS, and [18F]FPABA; **(C)** *P. aeruginosa* uptake between [18F]FDG, [18F]FDS, and [18F]FPABA.

in these experiments, with the sole exception of the clinical strain of *E. coli*.

3.3. *Escherichia coli* myositis

The [18F]FDG, [18F]FDS, and [18F]FPABA PET images detected *E. coli* myositis infection (Figure 5A; Supplementary Figure S4). The SUVr values were similar for [18F]FDG (1.55 ± 0.39), [18F]FDS (2.09 ± 0.84), and [18F]FPABA (1.92 ± 1.19) with no statistically significant differences (Figure 5B).

The *post-mortem* measurements of radioactivity in infected and inflamed tissues, presented as %ID/g, was not significant for [18F]FDS (Figure 5C). By contrast, [18F]FPABA readily discriminated between infection (%ID/g = 0.089 ± 0.078) and inflammation (%ID/g = 0.008 ± 0.002) and showed a statistically significant difference ($p = 0.0079$; Figure 5D).

Mean bacterial load counts at the infection site were similar, approximately 7 $\log_{10}$ across all mice and probe groups (Supplementary Table S5). In addition, strong signals with minimal background were detected at the infection site with bacterial loads of 5.59 $\log_{10}$ CFU/g with [18F]FDG, 5.5 $\log_{10}$ CFU/g with [18F]FDS, and 6.17 $\log_{10}$ CFU/g with [18F]FPABA.

3.4. *Staphylococcus aureus* myositis

[18F]FPABA and [18F]FDG detected *S. aureus* infection in the right limb, as shown in Figure 6A; Supplementary Figure S4. A non-specific [18F]FDG signal was observed in the inflamed muscle. As expected, the [18F]FDS PET images showed no uptake in the inflamed and in the infected muscle. Radiotracer uptake, expressed as SUVr, indicated that [18F]FPABA could distinguish infection from inflammation (SUVr = 3.090 ± 0.807), but with no statistically significant differences when compared with [18F]FDG ($p = 0.1763$; Figure 6B).

Analysis of *post-mortem* biopsies demonstrated a statistically significant difference between infection and inflammation with [18F]FPABA ($p = 0.0079$; Figure 6D).

The means of bacterial load in all experiments are shown in Supplementary Table S5. [18F]FDG PET and [18F]FPABA detected and localized *S. aureus* infection with a minimum bacterial load of 6.31 $\log_{10}$ and 7.15 $\log_{10}$ CFU/g, respectively.

4. Discussion

4.1. Contribution of different PET signals by type of microorganism: [18F]FDG

Our *in vitro* results expanded the number of bacteria studied (Figure 3A) compared to previous studies (Heuker et al., 2017). [18F]FDG uptake was higher in GPs than GNs in our model. *Streptococcus agalactiae* achieved the highest bacterial uptake, as was the case with *Streptococcus pyogenes* in other studies (Heuker et al., 2017). Since we observed almost no uptake in non-lactose fermenting gram-negative bacilli (*P. aeruginosa* and *S. maltophilia*), infections with these bacteria could be difficult to diagnose with [18F]FDG PET (Figure 4C). Some infectious diseases guidelines propose [18F]FDG PET imaging as a criterion for diagnosis (Habib et al., 2015; Haidar and Singh, 2022; Lauri et al., 2022) which may be underestimated if *P. aeruginosa* or *S. maltophilia* is the etiology of infection. These findings should be taken into account when interpreting PET images in biofilm-related infections (endocarditis associated with prosthetic valves or pacemakers). Mature biofilms are formed by stationary (dormant) bacteria that produce a minor inflammatory response. *Pseudomonas aeruginosa* is a well-known biofilm former, especially on medical surfaces, cystic fibrosis patients, or chronic wound infection. The involvement of this bacteria could reduce the negative predictive value of nuclear molecular techniques using [18F]FDG. There is also insufficient evidence on the sensitivity of [18F]FDG in non-lactose fermenters, since only case reports have reported on the use of [18F]FDG-PET as a diagnostic tool in *P. aeruginosa* infections (Kawamura et al., 2021). Although GP bacteria are the main biofilm producers, our data show that [18F]FDG uptake is higher in these microorganisms. This could increase the sensitivity for [18F]FDG imaging in infection related to biofilm-producing GP bacteria.

[18F]FDG accumulation in *Cutibacterium acnes*, which is microaerophilic and typically slow growing, was just 2 h (Figure 3A),

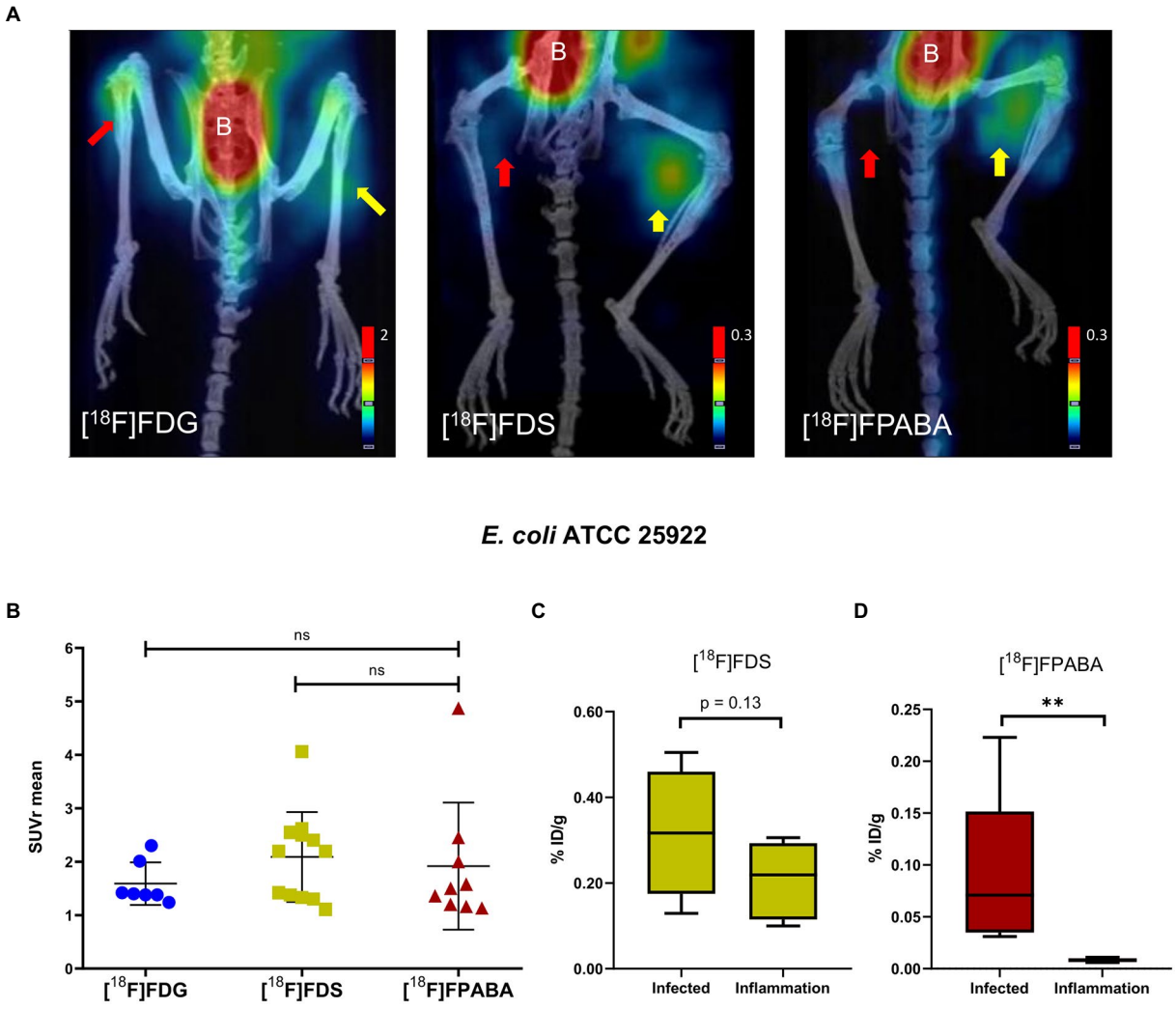

FIGURE 5
Escherichia coli myositis infection and inflammation of the hindlimbs. **(A)** PET/CT image of [18F]FDS (n=12) after 120min, [18F]FDG (n=7), and [18F]FPABA (n=9) after 60min of uptake. The right limb was infected with exponentially growing bacteria (yellow arrow); the left limb was injected with heat-killed bacteria (red arrow). B=bladder. **(B)** Comparison of mean SUVr for uptake of [18F]FDG, [18F]FDS, and [18F]FPABA in infected and inflamed muscle tissue. Represented as mean±SD. ns, not significant ($p > 0.05$). Kruskal-Wallis multiple-comparison test. **(C)** *Ex vivo* comparison of % injected dose of [18F]FDS per gram of infected versus inflamed tissue (%ID/g). **(D)** *Ex vivo* comparison of % injected dose of [18F]FPABA per gram of infected vs. inflamed tissue (%ID/g). $^{**}p \leq 0.01$.

3 h less than the mean growth time known for this bacterium (5.1 h; Hall et al., 1994) The final CFU/ml count in the *in vitro* experiments showed a statistically significant decrease in the clinical strain of *C. acnes* and a non-significant decrease in *C. acnes* ATCC 11827. This could be explained by the fact that uptake of [18F]FDG by these bacteria does not require exponential growth or a suitable environment.

All yeasts tested showed higher uptake of [18F]FDG as compared to bacteria (Figure 3A). [18F]FDG could therefore be a good radiotracer for yeast infections, with the possibility of extending it to filamentous fungi. One study on the *in vitro* uptake of [18F]FDG showed detection of *A. fumigatus*, but unlike our experiments with yeasts, this uptake appeared to be lower than in bacteria (i.e., *E. coli*; Lai et al., 2022).

[18F]FDG uptake was increased in myositis infection, with nonspecific uptake in [18F]FDG-PET imaging of inflamed muscle tissue, notably in heat-killed *E. coli* myositis (Figures 4A, 5A). Toxin production, probably due to *S. aureus* toxins or *E. coli* endotoxins, induces elevated inflammation that generates high levels of glucose transporter expression in infection when compared with inflammation with heat-killed bacteria; this effect corrects SUV ratio values.

4.2. [18F]FDS shows acute *Escherichia coli* myositis infection and can distinguish *Candida* spp.

[18F]FDS was taken up *in vitro* by Enterobacterales species (i.e., *E. coli* and *E. ludwigii*), but not by GPs and non-lactose fermenters (Figure 3B), as described in other studies (Weinstein et al., 2014; Ordonez et al., 2017). *Escherichia coli* has a generation time of 84 min using D-sorbitol (Lengeler, 1975), which allowed these isolates to grow in our experiments by metabolizing [18F]FDS as sorbitol-6-phosphate would, generating fructose-6-phosphate in the process. Only *E. coli* ATCC 25922 showed a statistically significant increase in numbers using [18F]FDS (Supplementary Table S3). Future studies will be necessary therefore to confirm whether this bacterium shows growth with fluorinated sorbitol.

We also demonstrated uptake in yeasts such as *Candida albicans* (Figure 4A). The higher [18F]FDG uptake (3-fold) compared to [18F]FDS may be related to the fact that sorbitol is not the preferred carbon source in Enterobacterales and *C. albicans* (Figure 4B). In recent experiments,

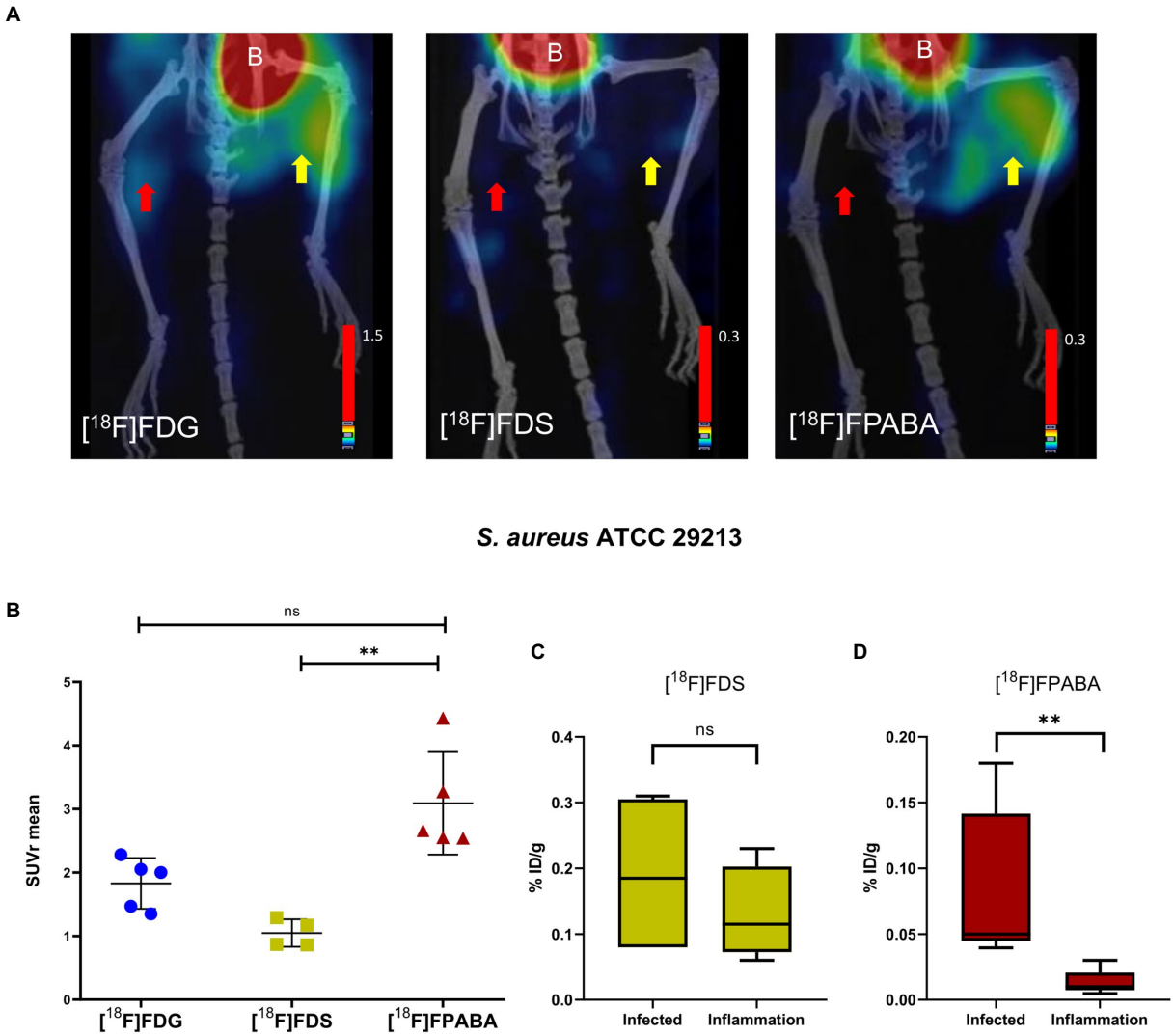

FIGURE 6
Staphylococcus aureus myositis infection and inflammation of hindlimbs. **(A)** PET/CT imaging with [^{18}F]FDS (n=4) after 120min, [^{18}F]FDG (n=5), and [^{18}F]FPABA (n=4) after 60min of acquisition. The right limb was infected with exponentially growing bacteria (yellow arrow); the left limb was injected with heat-killed bacteria (red arrow). B=bladder. **(B)** Comparison of mean SUVr for uptake of [^{18}F]FDG, [^{18}F]FDS, and [^{18}F]FPABA in infected and inflamed muscle tissue. Represented as mean±SD. ns, not significant ($p > 0.05$), *$p \leq 0.05$, **$p \leq 0.01$. Kruskal-Wallis multiple-comparison test. **(C)** *Ex vivo* data of % injected dose of [^{18}F]FDS per gram of infected and inflamed tissue (%ID/g). **(D)** *Ex vivo* data of % injected dose of [^{18}F]FPABA per gram of infected and inflamed tissue (%ID/g). **$p \leq 0.01$.

E. coli and *A. fumigatus* had a higher uptake (approximately 10-fold) with [^{18}F]FDG than with [^{18}F]FDS (Lai et al., 2022). A clear difference in uptake of [^{18}F]FDS by *Candida glabrata* was shown (66.54 ± 224.67 Bq/10^6 CFU) when compared with the other two strains of *C. albicans* analyzed (ATCC 10231 = 21496.06 ± 10684.79; clinical strain = 5846.24 ± 924.90 Bq/10^6 CFU; Figure 4A). [^{18}F]FDS is therefore useful to discriminate between yeasts with positive sorbitol assimilation (i.e., *C. albicans*) and those unable to assimilate sorbitol (i.e., *C. glabrata*; Kurtzman and Fell, 1998). This result could improve the diagnosis of disseminated/invasive *Candida albicans* infections (especially in the liver, CNS, eye, and other sterile locations) using [^{18}F]FDS-PET. We obtained higher uptakes (Bq/10^6 CFU) in *C. albicans* than *E. coli* ATCC 29213, as was the case in a recently published study (Kim et al., 2022). In another study however, the results showed that [^{3}H]sorbitol uptake was 10-fold lower in *C. albicans* than in *E. coli* at 120 min (Lai et al., 2022). This difference in uptake probably depends on the units used for normalization. A universal indicator to normalize both bacterial and fungal biomass is challenging because of differences in growth and cell size (fungi are much larger than bacterial cells). *In vitro* uptake may be underestimated when normalized to the amount of protein (Kim et al., 2022). This discrepancy could probably be resolved in further experiments, by testing *in vivo* uptake in an animal model of acute mixed infections with *C. albicans* and *E. coli* (normalized to final CFU/g per tissue).

The [^{18}F]FDS PET images clearly differentiated between inflammation and *E. coli* myositis infection although *postmortem* biodistribution studies found no uptake (%ID/g) differences between hindlimbs (Figures 5A,C). This diagnostic imaging with class-specific bacterial and yeast probes could be of interest when clinicians have a definite etiology of the infection. Even so, it is difficult to differentiate between all types of bacteria and microorganisms with probes because of the large number of different species. [^{18}F]FDS is a GN-specific probe with a low limit of detection (5.5 $\log_{10}$ CFU/g) and so can diagnose

chronic infections with Enterobacterales. Its previous translation to humans (Yao et al., 2016; Zhu et al., 2016; Ordonez et al., 2021) supports safe use of this technology in chronic infections. The limitation of our results is that [^{18}F]FDS may not differentiate between bacteria and yeasts and so adequate clinical information is needed. It would be interesting to develop animal models (with yeasts or mixed infections with bacteria and yeasts) to check and compare [^{18}F]FDS-PET signals. To avoid negative results in specific detection of Enterobacterales and *C. albicans*, sequential use of other radiotracers could be considered to broaden the range of pathogens identified. In addition, [^{18}F]FDS imaging could improve the monitoring of prolonged treatment in deep-seated Enterobacterales infections, as antimicrobial therapy may fail due to the impaired drug penetration or acquisition of antimicrobial resistance.

4.3. New synthesis of [^{18}F]FPABA: An approach to an imaging probe for all bacterial and yeast species

The proposed synthesis pathway to obtain [^{18}F]FPABA offers a promising solution due to its various advantages, which include the ease of obtaining the radiosynthetic precursor, the simple intermediate steps using everyday laboratory reagents, all highly soluble in water. The simplicity of the pathway also facilitates synthesis on different automated radiosynthesizers if a semipreparative radio-HPLC system is available. Further improvements in synthesis, yet unexplored, may be able to increase the yield while maintaining the radiochemical purity of the final product above 97%. [^{18}F]FPABA appears to be a better radiotracer than [^{11}C]PABA, not only because of the longer half-life of the radionuclide (110 min for fluorine-18 vs. just 20 min for carbon-11), but probably also because of the *in vivo* metabolism of the radiotracer, which could complicate image interpretation in the carbon-11 tracer. The accumulation of sulfonamide-like chemicals in the cell depends to a significant extent on the degree of ionization in the cytoplasm and the surrounding medium (Zarfl et al., 2008). Zarfl et al. point out that no accumulation occurs in the cell if the external pH exceeds the intracellular pH. A lower pH amplifies microorganisms that can accumulate because most bacteria have an intracellular pH of around 7 (*E. coli* = 7.6).

In vitro uptake of [^{18}F]FPABA was tested in all bacterial and yeast strains (Figure 3C). [^{18}F]FPABA appears to be a better probe for all bacteria and yeasts for diagnosis of infection, with higher *in vitro* uptake than [^{18}F]FDS. Previous *in vitro* studies have examined *S. aureus* and *E. coli* with [^{18}F]FPABA and [^{11}C]PABA (Zhang et al., 2018; Ordonez et al., 2022). *Pseudomonas aeruginosa* and *Mycobacterium tuberculosis* were assessed only with ^{3}H (Ordonez et al., 2017), but no other species were tested. We obtained the same promising results in Enterobacterales, *S. aureus*, and *P. aeruginosa*. New data were obtained for *C. acnes*, yeast, *S. epidermidis*, and Enterobacterales. Unlike [^{18}F]FDG and [^{18}F]FDS, *P. aeruginosa* incorporates [^{18}F]FPABA (Figure 4C), which makes this probe of interest in nosocomial infections. Although the innovative ^{68}Ga- and [^{18}F]FIAU-radiolabeled siderophores showed potential in models for bacteria-specific imaging with *P. aeruginosa* (Petrik et al., 2021), they fell short when translated to human clinical trials (Zhu et al., 2016; Cho et al., 2020).

Different *in vitro* uptakes were obtained in strains of the same species (*S. aureus* and *S. epidermidis*), as was found in other studies performed with [^{18}F]FPABA and *S. aureus* (Zhang et al., 2018). DHPS has different expression levels in the same bacterial species, which may explain the different results observed (Wang et al., 2021). Alterations in this enzyme, one of the mechanisms of bacterial resistance, correlate with the low effectiveness of sulfonamides in some species or strains. These resistance mechanisms or concomitant treatment prior to image acquisition may affect [^{18}F]FPABA activity. In addition, AbgT transporters are exporters of PABA and interspecies variation may have an impact (Delmar and Yu, 2016). Furthermore, bacteria are capable of *de novo* PABA synthesis from chorismate and glutamine (Dosselaere and Vanderleyden, 2001). Therefore, future studies should evaluate possible signal variation in PABA PET imaging.

To the best of our knowledge, this is the first study of *in vitro* uptake of [^{18}F]FDG, [^{18}F]FDS, and [^{18}F]FPABA in yeasts. Our results showed [^{18}F]FPABA uptake in the yeasts tested and suggest that it is a promising future tool in fungal diagnostics. We suspect that these results of *in vitro* uptake are because DHFR (dihydrofolate reductase), an enzyme essential for folate-dependent pathways in fungi, is a valid antifungal target in *C. albicans* (DeJarnette et al., 2020). The DHFR enzyme is the step subsequent to PABA incorporation into DHPS. In addition, DHPS inhibitors such as sulfamethoxazole are an effective treatment for *Pneumocystis* pneumonia (caused by the fungus *Pneumocystis jirovecii*). Although folate biosynthesis pathways and enzymes have been characterized in both bacteria and plants, they are not well studied or characterized in yeasts. Our results confirm that yeast requires *in vitro* uptake of PABA and that [^{18}F]FPABA could be used as a probe for yeasts in PET imaging.

[^{18}F]FPABA PET, performed on mouse models of *E. coli* and *S. aureus* myositis, clearly differentiated between inflammation and infection and showed no uptake in the inflamed limb (Figures 5A, 6A). The SUVr values of [^{18}F]FPABA were lower than expected (Figures 5B, 6B) because the bone showed uptake and was difficult to avoid when VOIs were drawn on the image. In *post-mortem* biodistribution studies, Zhang et al. observed that [^{18}F]FPABA accumulated in the tibia at different rates (at 30, 60, and 120 min) with high ID%/g values, which might explain why some of the bone was seen on images and the SUV was less sensitive (Zhang et al., 2018). Our interpretation however was limited to visual analysis and current advances in artificial intelligence can certainly improve our image data (Schwenck et al., 2022). However, the post-mortem analysis between hindlimbs with infection (*S. aureus* and *E. coli*) and inflammation was statistically significant, and clearly demonstrated detection of infection (Figures 5C, 6C).

The mean bacterial load in acute *S. aureus* and *E. coli* myositis in our experiments (Supplementary Table S5) was around 7 $\log_{10}$ CFU/g, and [^{18}F]FPABA localized all these infections. This bacterial load is low compared to acute infections, where the CFU/mL is 8 $\log_{10}$ or more (Davey and Barza, 1987; König et al., 1998). However, the infection load for chronic or bloodstream infections is even lower (Kang et al., 2014). [^{18}F]FPABA uptake remains high regardless of the growth phase (Zhang et al., 2018) and testing this probe on lower bacterial loads in chronic infections and implant-associated biofilms could be of interest in the future. PET imaging with [^{11}C]PABA on a rabbit model of *S. aureus* prosthetic implant infection obtained a good discrimination ratio (target-to-nontarget tissue) of 3.17 (Ordonez et al., 2022). The main problem in that study was that the image was obtained 7 days after infection and with bacterial loads of 7-$\log_{10}$ CFU, similar to acute infection (without the decreased sensitivity associated with low bacterial load). [^{18}F]FPABA uptake into other typical implant-associated microorganisms, such as *C. acnes,* was *in vitro* in our study and it would be interesting to test them on *in vivo* models. It could be an improvement over microbiological tests that are long (14 days) and require complicated incubation atmospheres (microaerophilic/anaerobic; Schäfer et al., 2008).

5. Conclusion

[^{18}F]FDG is actively incorporated by most bacteria and yeasts. Nevertheless, non-lactose fermenters (i.e., *P. aeruginosa* and *S. maltophilia*) show no uptake *in vitro* and further in-depth studies are needed to clarify this aspect, as the metabolic basis is unknown. In the future, animal models and clinical studies should focus on non-lactose fermenters to check the diagnosis of infection using [^{18}F]FDG PET, even if the signal depends on other factors (such as inflammation, sensitivity, PET camera resolution, surrounding tissue, or target-to-normal tissue ratio).

[^{18}F]FDS is metabolized by Enterobacterales and is able to differentiate yeasts that assimilate sorbitol (i.e., *Candida albicans*) from those that do not (i.e., *Candida glabrata*). [^{18}F]FDS PET imaging could therefore be useful when there are appropriate clinical data focused on Enterobacterales infection (i.e., hepatobiliary infections, intestinal focus) or IFIs caused by *C. albicans*. Murine models of acute *E. coli* infection show nonspecific uptake of [^{18}F]FDG due to sterile inflammation, but no inflammation with [^{18}F]FDS.

[^{18}F]FPABA appears to be a potential probe for imaging infections as all tested bacteria and yeasts showed [^{18}F]FPABA uptake, even fastidious microorganisms (such as *C. acnes*). [^{18}F]FPABA was the only probe tested that showed *in vitro* uptake of *P. aeruginosa,* unlike [^{18}F]FDG and [^{18}F]FDS. Therefore, it is crucial to know why uptake of [^{18}F]FPABA is different in some bacterial species and to expand studies to correlate this with the biological characteristics of the different microorganisms. Further investigation in both *in vitro* and *in vivo* experiments is needed to select the best PET imaging probes for *P. aeruginosa*.

In acute myositis, both GP and GN bacteria incorporate [^{18}F]FPABA.

The limitations of our study that should be addressed in the future include testing microorganisms that affect immunocompromised patients (i.e., *Aspergillus, P. jirovecii*), *in vivo* models with yeast species, *Corynebacterium* spp. and chronic infections. Future studies on chronic infections with low numbers of bacteria and yeast using [^{18}F]FPABA could also be very interesting to further broaden the potential clinical applications of this radiotracer.

Data availability statement

The original contributions presented in the study are included in the article/Supplementary material; further inquiries can be directed to the corresponding author.

Ethics statement

The animal study was reviewed and approved by Ethics Committee for Animal Experimentation of the University of Navarra (protocol no. 103-17).

Author contributions

MR, JS, MC, and IP designed and analyzed the data. MC and IP coordinated the study. JS, RR, FP, KP, JLl, and IP synthesized [18F]FDS and designed the [18F]FPABA synthesis. MR, JS, and MC performed the *in vitro* experiments. MR, ME, and FC-T conducted the animal experiments and microbiological studies. MC analyzed the animal images. MR, MC, JLe, FC-T, JD, and IP provided critical comments on this project. MR, JS, MC, and IP wrote the initial draft, and all coauthors edited the manuscript. All authors contributed to the article and approved the submitted version.

Funding

This work was funded by research project PI17/00873 from the Spanish Ministry of Health. Part of the work was supported by MCIN/AEI/10.13039/501100011033 (PID2020-117656RB-I00).

Acknowledgments

We thank the staff of the PET-GMP laboratory for their help in the synthesis of radiotracers and the Clinical Microbiology and Parasitology Service, specifically Ana Ramos for expert technical assistance. We would like to thank Janet Dawson for her help in proofreading and editing the final English version of the manuscript. Parts of this work were previously presented at the 29th European Congress of Clinical Microbiology and Infectious Diseases and the 32nd and 35th Annual Congress of the European Association of Nuclear Medicine.

Conflict of interest

The authors declare that the research was conducted in the absence of any commercial or financial relationships that could be construed as a potential conflict of interest.

Publisher's note

All claims expressed in this article are solely those of the authors and do not necessarily represent those of their affiliated organizations, or those of the publisher, the editors and the reviewers. Any product that may be evaluated in this article, or claim that may be made by its manufacturer, is not guaranteed or endorsed by the publisher.

Supplementary material

The Supplementary material for this article can be found online at: https://www.frontiersin.org/articles/10.3389/fmicb.2023.1094929/full#supplementary-material

References

Ankrah, A. O., Creemers-Schild, D., de Keizer, B., Klein, H. C., Dierckx, R. A. J. O., Kwee, T. C., et al. (2021). The added value of [18 f]fdg pet/ct in the management of invasive fungal infections. *Diagnostics* 11, 1–13. doi: 10.3390/diagnostics11010137

Auletta, S., Varani, M., Horvat, R., Galli, F., Signore, A., and Hess, S. (2019). PET radiopharmaceuticals for specific bacteria imaging: a systematic review. *J. Clin. Med.* 8. doi: 10.3390/jcm8020197

Bermingham, A., and Derrick, J. P. (2002). The folic acid biosynthesis pathway in bacteria: evaluation of potential for antibacterial drug discovery. *BioEssays* 24, 637–648. doi: 10.1002/bies.10114

Chakfé, N., Diener, H., Lejay, A., Assadian, O., Berard, X., Caillon, J., et al. (2020). Editor's choice—European Society for Vascular Surgery (ESVS) 2020 clinical practice guidelines on the management of vascular graft and endograft infections. *Eur. J. Vas. Endovasc. Surg.* 59, 339–384. doi: 10.1016/j.ejvs.2019.10.016

Cho, S. Y., Rowe, S. P., Jain, S. K., Schon, L. C., Yung, R. C., Nayfeh, T. A., et al. (2020). Evaluation of musculoskeletal and pulmonary bacterial infections with [124I]FIAU PET/CT. *Mol. Imaging* 19, 153601212093687–153601212093689. doi: 10.1177/1536012120936876

Cordaro, C. (1976). Genetics of the bacterial phosphoenolpyruvate: glycose phosphotransferase system. *Annu. Rev. Genet.* 10, 341–359. doi: 10.1146/annurev.ge.10.120176.002013

Davey, P. G., and Barza, M. (1987). The inoculum effect with gram-negative bacteria in vitro and in vivo. *J. Antimicrob. Chemother.* 20, 639–644. doi: 10.1093/jac/20.5.639

DeJarnette, C., Luna-Tapia, A., Estredge, L. R., and Palmer, G. E. (2020). Dihydrofolate Reductase is a valid target for antifungal development in the human pathogen Candida albicans. *mSphere* 5. doi: 10.1128/msphere.00374-20

Delmar, J. A., and Yu, E. W. (2016). The AbgT family: a novel class of antimetabolite transporters. *Protein Sci.* 25, 322–337. doi: 10.1002/pro.2820

Dosselaere, F., and Vanderleyden, J. (2001). A metabolic node in action: chorismate-utilizing enzymes in microorganisms. *Crit. Rev. Microbiol.* 27, 75–131. doi: 10.1080/20014091096710

Dubois, B., Feldman, H. H., Jacova, C., Hampel, H., Molinuevo, J. L., Blennow, K., et al. (2014). Advancing research diagnostic criteria for Alzheimer's disease: the IWG-2 criteria. *Lancet Neurol.* 13, 614–629. doi: 10.1016/S1474-4422(14)70090-0

Erba, P. A., and Slart, R. H. J. A. (2020). Radiolabeled-white blood cell imaging in cardiac device-related infective endocarditis: worth all the effort? *JACC Cardiovasc. Imaging* 13, 1752–1754. doi: 10.1016/j.jcmg.2020.02.033

Góralska, K., Blaszkowska, J., and Dzikowiec, M. (2018). Neuroinfections caused by fungi. *Infection* 46, 443–459. doi: 10.1007/s15010-018-1152-2

Guedj, E., Varrone, A., Boellaard, R., Albert, N. L., Barthel, H., van Berckel, B., et al. (2022). EANM procedure guidelines for brain PET imaging using [18F]FDG, version 3. *Eur. J. Nucl. Med. Mol. Imaging* 49, 632–651. doi: 10.1007/s00259-021-05603-w

Habib, G., Lancellotti, P., Antunes, M. J., Bongiorni, M. G., Casalta, J. P., del Zotti, F., et al. (2015). 2015 ESC Guidelines for the management of infective endocarditis: the task force for the Management of Infective Endocarditis of the European Society of Cardiology (ESC). Endorsed by: European Association for Cardio-Thoracic Surgery (EACTS), the European. *Eur. Heart J.* 36, 3075–3128. doi: 10.1093/eurheartj/ehv319

Haidar, G., and Singh, N. (2022). Fever of unknown origin. *N. Engl. J. Med.* 386, 463–477. doi: 10.1056/NEJMra2111003

Hall, G. S., Pratt-Rippin, K., Meisler, D. M., Washington, J. A., Roussel, T. J., and Miller, D. (1994). Growth curve for Propionibacterium acnes. *Curr. Eye Res.* 13, 465–466. doi: 10.3109/02713689408999875

Heuker, M., Sijbesma, J. W. A., Aguilar Suárez, R., de Jong, J. R., Boersma, H. H., Luurtsema, G., et al. (2017). In vitro imaging of bacteria using 18F-fluorodeoxyglucose micro positron emission tomography. *Sci. Rep.* 7, 4973–4979. doi: 10.1038/s41598-017-05403-z

Jenks, J. D., Cornely, O. A., Chen, S. C. A., Thompson, G. R. III, and Hoenigl, M. (2020). Breakthrough invasive fungal infections: who is at risk? *Mycoses* 63, 1021–1032. doi: 10.1111/myc.13148

Kang, D. K., Ali, M. M., Zhang, K., Huang, S. S., Peterson, E., Digman, M. A., et al. (2014). Rapid detection of single bacteria in unprocessed blood using integrated comprehensive droplet digital detection. *Nat. Commun.* 5, 1–10. doi: 10.1038/ncomms6427

Kawamura, J., Ueno, K., Taimura, E., Matsuba, T., Imoto, Y., Jinguji, M., et al. (2021). Case report: (18)F-FDG PET-CT for diagnosing prosthetic device-related infection in an infant with CHD. *Front. Pediatr.* 9:584741. doi: 10.3389/fped.2021.584741

Kim, D. Y., Pyo, A., Ji, S., You, S. H., Kim, S. E., Lim, D., et al. (2022). In vivo imaging of invasive aspergillosis with 18F-fluorodeoxysorbitol positron emission tomography. *Nat. Commun.* 13, 1–11. doi: 10.1038/s41467-022-29553-5

König, C., Simmen, H. P., and Blaser, J. (1998). Bacterial concentrations in pus and infected peritoneal fluid - implications for bactericidal activity of antibiotics. *J. Antimicrob. Chemother.* 42, 227–232. doi: 10.1093/jac/42.2.227

Kurtzman, C. P., and Fell, J. W. (Eds.) (1998). "Summary of species characteristics" in *The Yeasts. 4th Edn.* ed (Amsterdam: Elsevier), 915–947.

Kwee, T. C., Kwee, R. M., and Alavi, A. (2008). FDG-PET for diagnosing prosthetic joint infection: systematic review and metaanalysis. *Eur. J. Nucl. Med. Mol. Imaging* 35, 2122–2132. doi: 10.1007/s00259-008-0887-x

Lai, J., Shah, S., Knight, R., Martinez-Orengo, N., Patel, R., Mitchell, A., et al. (2022). Evaluation of 2-[18F]-Fluorodeoxysorbitol PET imaging in preclinical models of Aspergillus infection. *J. Fungi* 8. doi: 10.3390/jof8010025

Lauri, C., Signore, A., Glaudemans, A. W. J. M., Treglia, G., Gheysens, O., Slart, R. H. J. A., et al. (2022). Evidence-based guideline of the European Association of Nuclear Medicine (EANM) on imaging infection in vascular grafts. *Eur. J. Nucl. Med. Mol. Imaging* 49, 3430–3451. doi: 10.1007/s00259-022-05769-x

Lengeler, J. (1975). Nature and properties of hexitol transport systems in Escherichia coli. *J. Bacteriol.* 124, 39–47. doi: 10.1128/jb.124.1.39-47.1975

Li, Y., Daryaee, F., Yoon, G. E., Noh, D., Smith-Jones, P. M., Si, Y., et al. (2020). Positron emission tomography imaging of Staphylococcus aureus infection using a nitro-Prodrug analogue of 2-[18F]F-p-Aminobenzoic acid. *ACS Infect. Dis.* 6, 2249–2259. doi: 10.1021/acsinfecdis.0c00374

Li, Z.-B., Wu, Z., Cao, Q., Dick, D. W., Tseng, J. R., Gambhir, S. S., et al. (2008). The synthesis of 18F-FDS and its potential application in molecular imaging. *Mol. Imaging Biol.* 10, 92–98. doi: 10.1007/s11307-007-0125-0

Li, J., Zheng, H., Fodah, R., Warawa, J. M., Ng, C. K., et al. (2017). Validation of 2-^{18}F-fluorodeoxysorbitol (^{18}F-FDS) as a potential radiopharmaceutical for imaging bacterial infection in the lung. *J. Nucl. Med.* 59:195420. doi: 10.2967/jnumed.117.195420

Mahmood, M., Kendi, A. T., Ajmal, S., Farid, S., O'Horo, J. C., Chareonthaitawee, P., et al. (2019). Meta-analysis of 18F-FDG PET/CT in the diagnosis of infective endocarditis. *J. Nucl. Cardiol.* 26, 922–935. doi: 10.1007/s12350-017-1092-8

Morens, D. M., and Fauci, A. S. (2020). Emerging pandemic diseases: how we got to COVID-19. *Cells* 183:837. doi: 10.1016/j.cell.2020.10.022

Ordonez, A. A., Parker, M. F. L., Miller, R. J., Plyku, D., Ruiz-Bedoya, C. A., Tucker, E. W., et al. (2022). 11C-Para-aminobenzoic acid PET imaging of S. aureus and MRSA infection in preclinical models and humans. *JCI Insight* 7, 1–11. doi: 10.1172/jci.insight.154117

Ordonez, A. A., Weinstein, E. A., Bambarger, L. E., Saini, V., Chang, Y. S., DeMarco, V. P., et al. (2017). A systematic approach for developing bacteria-specific imaging tracers. *J. Nucl. Med.* 58, 144–150. doi: 10.2967/jnumed.116.181792

Ordonez, A. A., Wintaco, L. M., Mota, F., Restrepo, A. F., Ruiz-Bedoya, C. A., Reyes, C. F., et al. (2021). Imaging Enterobacterales infections in patients using pathogen-specific positron emission tomography. *Sci. Transl. Med.* 13. doi: 10.1126/scitranslmed.abe9805

Petrik, M., Umlaufova, E., Raclavsky, V., Palyzova, A., Havlicek, V., Pfister, J., et al. (2021). (68)Ga-labelled desferrioxamine-B for bacterial infection imaging. *Eur. J. Nucl. Med. Mol. Imaging* 48, 372–382. doi: 10.1007/s00259-020-04948-y

Rowe, S. P., and Pomper, M. G. (2021). Molecular imaging in oncology: current impact and future directions. *CA Cancer J. Clin.* 72, 333–352. doi: 10.3322/caac.21713

Schäfer, P., Fink, B., Sandow, D., Margull, A., Berger, I., and Frommelt, L. (2008). Prolonged bacterial culture to identify late periprosthetic joint infection: a promising strategy. *Clin. Infect. Dis.* 47, 1403–1409. doi: 10.1086/592973

Schwenck, J., Kneilling, M., Riksen, N. P., la Fougère, C., Mulder, D. J., Slart, R. J. H. A., et al. (2022). A role for artificial intelligence in molecular imaging of infection and inflammation. *Eur. J. Hybrid Imag.* 6, 17–16. doi: 10.1186/s41824-022-00138-1

Wang, R., Li, K., Yu, J., Deng, J., and Chen, Y. (2021). Mutations of folC cause increased susceptibility to sulfamethoxazole in mycobacterium tuberculosis. *Sci. Rep.* 11, 1352–1311. doi: 10.1038/s41598-020-80213-4

Weinstein, E. A., Ordonez, A. A., DeMarco, V., Murawski, A. M., Pokkali, S., MacDonald, E., et al. (2014). Imaging enterobacteriaceae infection in vivo with 18F-fluorodeoxysorbitol positron emission tomography. *Sci. Transl. Med.* 6:259ra146. doi: 10.1126/scitranslmed.3009815

Yao, S., Xing, H., Zhu, W., Wu, Z., Zhang, Y., Ma, Y., et al. (2016). Infection imaging with 18F-FDS and first-in-human evaluation. *Nucl. Med. Biol.* 43, 206–214. doi: 10.1016/j.nucmedbio.2015.11.008

Zarfl, C., Matthies, M., and Klasmeier, J. (2008). A mechanistical model for the uptake of sulfonamides by bacteria. *Chemosphere* 70, 753–760. doi: 10.1016/j.chemosphere.2007.07.045

Zhang, Z., Ordonez, A. A., Wang, H., Li, Y., Gogarty, K. R., Weinstein, E. A., et al. (2018). Positron emission tomography imaging with 2-[18F]F- p-Aminobenzoic acid detects Staphylococcus aureus infections and monitors drug response. *ACS Infect. Dis.* 4, 1635–1644. doi: 10.1021/acsinfecdis.8b00182

Zhu, W., Yao, S., Xing, H., Zhang, H., Tai, Y. C., Zhang, Y., et al. (2016). Biodistribution and radiation Dosimetry of the Enterobacteriaceae -specific imaging probe [18 F] Fluorodeoxysorbitol determined by PET/CT in healthy human volunteers. *Mol. Imaging Biol.* 18, 782–787. doi: 10.1007/s11307-016-0946-9

Frontiers in Microbiology

Explores the habitable world and the potential of microbial life

The largest and most cited microbiology journal which advances our understanding of the role microbes play in addressing global challenges such as healthcare, food security, and climate change.

Discover the latest Research Topics

See more →

Frontiers

Avenue du Tribunal-Fédéral 34
1005 Lausanne, Switzerland
frontiersin.org

Contact us

+41 (0)21 510 17 00
frontiersin.org/about/contact